Canadian
Journal of Chemistry

ORGANIC DEUTERIUM COMPOUNDS

XXI. SYNTHESIS OF DEUTERATED AZOBISMETHANE[1]

A. T. MORSE,[2] T. F. MASSIAH,[2] AND L. C. LEITCH

ABSTRACT

Deuterated azobismethane was synthesized in the conventional way from dimethyl sulphate and hydrazine.

The principal sources of methyl radicals for photochemical investigations are acetone, dimethyl mercury, and azomethane. Deuteromethyl radicals are similarly obtained from the corresponding deuterated compounds, of which only acetone-d_6 and bistrideuteromethyl-mercury have been reported (2). It seemed of interest to prepare deuteroazobismethane, since it is the only convenient way of obtaining methyl-d_3 radicals for certain work.

With the exception of 2,2'-azobispropane-2,2'-d_2, which was reported by us a few years ago (8), deuterated azoalkanes are unknown. The synthesis of azoalkanes from aldehydes or ketones via the azines and 1,2-dialkylhydrazines described in that paper is not applicable to the preparation of azomethane or deuteroazomethane because condensation of formaldehyde and hydrazine hydrate gives rise to polymers rather than the azine. Furthermore, formaldehyde-d_2, which is required in the present instance, is very difficult to prepare (1). Initially, lithium aluminum hydride reduction of 1,2-diacylhydrazines was found to be unsuccessful. This was also experienced by Hinman (6). However, we were led to reinvestigate this reaction by the appearance of a paper by Stewart (10) on the facile preparation of formic-d acid which readily yields 1,2-diformyl-d_2 hydrazine. Eventually, 1,2-dimethylhydrazine was obtained in 50% yield when 1,2-diformylhydrazine was reduced with a large excess of LiAlH$_4$ in dioxane as a solvent. However, the excessive cost of lithium aluminum deuteride precludes the use of the method for preparing more than very small quantities of azomethane-d_6.

As methyl-d_3 iodide is now readily available (9), methylation of 1,2-dibenzoylhydrazine was attempted with methyl iodide instead of dimethyl sulphate, but no methylation took place under a variety of conditions. Consequently, the method of Folpmers (3) and Hatt (5) remained the only practical route to azomethane-d_6:
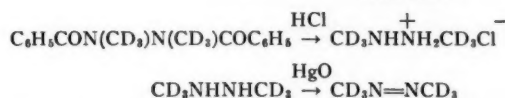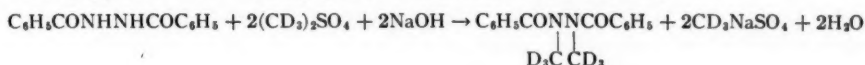
$$C_6H_5CONHNHCOC_6H_5 + 2(CD_3)_2SO_4 + 2NaOH \rightarrow C_6H_5CONNCOC_6H_5 + 2CD_3NaSO_4 + 2H_2O$$
$$\underset{D_3C \quad CD_3}{|\quad|}$$

$$C_6H_5CON(CD_3)N(CD_3)COC_6H_5 \xrightarrow{HCl} CD_3\overset{+}{N}HNH_2CD_3\overset{-}{Cl}$$

$$CD_3NHNHCD_3 \xrightarrow{HgO} CD_3N{=}NCD_3$$

In our first experiments with dimethyl-d_6 sulphate the ester was prepared from methyl-d_3 alcohol and chlorosulphonic acid. This method was somewhat inconvenient because methyl-d_3 alcohol had to be prepared from the bromide. Recent work from this laboratory on the preparation of deuterated esters from methyl-d_3 bromide and silver salts of the acids (7) held out the promise that dimethyl-d_3 sulphate might be prepared from methyl-d_3 bromide and silver sulphate. These reactants did in fact give the inorganic ester in 90% yields. From the investigations of Gragorov (4) on the mobility of radicals it would appear that deuterated dimethyl sulphate could also be prepared by exchanging methyl-d_3 iodide with normal dimethyl sulphate or preferably a homologous sulphate ester. This method is probably less convenient than the one described.

The succeeding steps in the synthesis of azomethane-d_6 paralleled those used to prepare the light compound (8) and call for no special comments.

<div align="center">EXPERIMENTAL</div>

Dimethyl-d_6 Sulphate

(a) *By direct esterification of methyl-d_3 alcohol.*—To chlorosulphonic acid (665 g; 6.0 moles), cooled to $-15°$ C in a 1-liter flask fitted with a dropping funnel, a reflux condenser, and a magnetic stirrer, methyl-d_3 alcohol (175 g; 5.0 moles) was added dropwise while maintaining the temperature below $0°$ C. After the addition of alcohol had been completed the reaction mixture was fractionated under reduced pressure in a Vigreux column. The yield of dimethyl-d_6 sulphate, b.p. 69 to 71° C/11 mm, n_D^{25} 1.3858, was 309 g (90%).

(b) *From methyl-d_3 bromide and silver sulphate.*—Methyl-d_3 bromide was prepared as described in a previous paper of this series (9). Silver sulphate (31.0 g; 0.1 mole) was ground to a fine powder in a mortar and placed in a heavy-walled glass tube which was then constricted near the top to facilitate sealing later. Methyl-d_3 bromide (21.0 g; 0.22 mole) was condensed into the tube on a vacuum manifold. The sealed tube was then heated for 4 to 5 hours at 100° C. The contents of the cold tube was washed out with ether into a gravity funnel. The silver iodide on the funnel was washed several times with small portions of ether. The combined ether extracts were freed of solvent and the residue was distilled in a Späth bulb from an air bath at 50° C under 0.1 mm on the vacuum line. The yield of product, n_D^{20} 1.3851, was 10.6 g (85%). The index of refraction of normal dimethyl sulphate is 1.3860.

sym-Dimethyl-d_6 Dibenzoylhydrazine

To a stirred suspension of 40 g (0.165 mole) 1,2-dibenzoylhydrazine in 300 ml of 2% sodium hydroxide solution heated to 80° C were added dropwise and simultaneously from two dropping funnels, 65 ml (0.65 mole) of dimethyl-d_6 sulphate and 125 ml of 50% aqueous sodium hydroxide solution. After it was stirred for an additional hour at 80° C the reaction mixture was set aside to crystallize in the refrigerator. The crystalline solid which had separated was collected on a funnel and dissolved in 50 ml of chloroform. The solution was dried over magnesium sulphate and treated with 100 ml of a 50% mixture of ether and pentane. After the mixture had been allowed to stand at 0° C in the refrigerator for several hours the crystals were filtered off and washed with pentane. Yield: 23 g (24.4%), m.p. 85–86° C.

1,2-Dimethyl-d_6-hydrazine

The dibenzoyldimethyl-d_6-hydrazine obtained above (23.0 g; 0.085 mole) was heated under reflux for 3 hours with 95 ml of 35% concentrated hydrochloric acid. The reaction

mixture was steam-distilled to remove benzoic acid and then evaporated to dryness in a flash evaporator. The residue of crude 1,2-dimethyl-d_6-hydrazine monohydrochloride was dissolved in 40 ml of water and added slowly with stirring to 100 ml of 50% aqueous sodium hydroxide. The base liberated was purified and freed of water by distillation on the vacuum line through a U-tube filled with potassium hydroxide pellets. Yield: 5.3 g, n_D^{24} 1.4188 (95.5%).

Bisazomethane-d_6

A solution of 1,2-dimethyl-d_6-hydrazine (5.3 g; 0.08 mole) in 50 ml of water was added to a stirred suspension of 22.0 g (0.11 mole) of yellow mercuric oxide in 40 ml of water in a flask with a reflux condenser to which was attached a spiral trap cooled to $-78°$ C in a bath of acetone and solid carbon dioxide. After addition of the base was completed the reaction mixture was slowly heated to reflux. The apparatus was swept with a slow stream of nitrogen. The yield of azomethane-d_6 which analyzed 99.3 atom % deuterium by mass spectrometry was 3.2 g (62.2%).

1,2-Dimethylhydrazine

1,2-Diformylhydrazine (22.0 g; 0.25 mole) was extracted in a Soxhlet by a refluxing solution of 66 g (2.0 mole) of lithium aluminum hydride in 1 liter of dioxane. After 24 hours the hydride was decomposed by careful addition of water. Inorganic hydroxides were removed by centrifugation. The filtrate was acidified and evaporated to dryness in a flash evaporator. The residue was dissolved in the minimum amount of water and the solution added to an excess of 50% alkali. The supernatant layer of insoluble 1,2-dimethylhydrazine was distilled off on a vacuum manifold. Yield: 7.5 g (50%). It was converted into azomethane by oxidation with mercuric oxide as described in ref. (8). The azo compound was identified by mass analysis.

ACKNOWLEDGMENTS

REFERENCES

1. BANNARD, R. A., MORSE, A. T., and LEITCH, L. C. Can. J. Chem. **31**, 351 (1953).
2. BEVEGE, E. E., RENAUD, R., and LEITCH, L. C. Can. J. Chem. **31**, 1259 (1953).
3. FOLPMERS, M. T. Rec. trav. chim. **34**, 34 (1915).
4. GRAGOROV, I. P. Doklady Akad. Nauk S.S.S.R. **99**, 101 (1954).
5. HATT, H. H. Organic syntheses, coll. vol. II. John Wiley & Sons, Ltd., New York. 1944. p. 208.
6. HINMAN, R. L. J. Am. Chem. Soc. **78**, 1645 (1956).
7. ISABELLE, M. E. and LEITCH, L. C. Can. J. Chem. **36**, 440 (1957).
8. RENAUD, R. and LEITCH, L. C. Can. J. Chem. **32**, 545 (1954).
9. RENAUD, R. and LEITCH, L. C. Can. J. Chem. **34**, 179 (1956).
10. STEWART, R. Can. J. Chem. **35**, 766 (1957).

POTATO X VIRUS

PART II. PREPARATION AND PROPERTIES OF PURIFIED, NON-AGGREGATED VIRUS FROM TOBACCO[1]

M. E. REICHMANN

ABSTRACT

When sap from tobacco, infected with potato X virus, was dialyzed against 0.05 M and then against 0.005 M sodium citrate, no aggregation of the virus was detected after ultracentrifugation. Flow birefringence measurements were made to compare virus preparations obtained by ultracentrifugation of untreated sap and of sap that had been treated with various buffers. Only versene and citrate were found to prevent aggregation. The influence of pH in the range 5.7–7.3 was very slight. Possible explanations of this effect are discussed.

Nitrogen and phosphorus content and the sedimentation constant of the purified, non-aggregated virus are reported.

INTRODUCTION

An investigation of size and size distribution of viruses in solution requires that special precautions be taken, during the process of isolation and purification, not to change these characteristics. Even in the case of the most studied virus, the tobacco mosaic virus, few authors emphasize this point (1) and only recently has the preparation of purified uniform tobacco mosaic virus been described (2).

The irreversible end-to-end aggregation of potato X virus in the process of purification is a well-known phenomenon (3, 4, 5). In a previous publication from this laboratory the size and size distribution of potato X virus in tobacco sap was reported (6). For more accurate studies a purified preparation was needed. This paper describes conditions under which this virus can be isolated without alteration in its state of aggregation. Preliminary conclusions concerning the nature of the aggregation processes are drawn from some of the properties of this preparation.

EXPERIMENTAL

Purification

The potato X virus and the conditions under which it was grown in tobacco have been described previously (6). Freshly frozen tobacco leaves were squeezed with a mortar and pestle. The sap was centrifuged at 4000 r.p.m. for 30 minutes. The brown supernatant was dialyzed overnight against a large volume of 0.05 M sodium citrate. The dialysis bags were then transferred to a large volume of 0.005 M sodium citrate and the dialysis continued for another 10 hours. The sap was then centrifuged at 4000 r.p.m. for 20 minutes and the supernatant was ultracentrifuged at 75,000$\times g$ for 90 minutes. The pellet was water-clear with a brown core in the center. After decantation the pellet was resuspended in 0.005 M sodium citrate. It dissolved readily except for the brown core which was insoluble. The insoluble material was removed by slow centrifugation and the supernatant was submitted to two additional cycles of ultracentrifugation and slow centrifugation in 0.005 M sodium citrate. The final pellet obtained was water-clear and dissolved readily with only traces of insoluble material. In contrast, virus material prepared from sap that had not been treated with sodium citrate was slower to dissolve and the amounts of insoluble material in each step were larger.

Flow Birefringence Measurements

The extinction angles χ were measured at different velocity gradients G in a small flow birefringence apparatus manufactured by Rao Instrument Company, Brooklyn, New York (7). Comparisons between different samples were made in a concentration range of 0.08 to 0.02% virus in 0.005 M sodium citrate. The extinction angles were found independent of virus concentration in this range. In Fig. 1 typical extinction angles vs. gradient measurements are shown for virus in sap, virus purified as described above, and virus isolated from untreated sap by one ultracentrifugation. The low extinction angles of the latter sample confirm findings reported in the literature that the virus aggregates under these conditions (3, 4, 5). Similar results were obtained whether the virus was resuspended in distilled water or in 0.005 M citrate. Moreover, each ultracentrifugation – slow centrifugation cycle increased the amount of aggregated material.
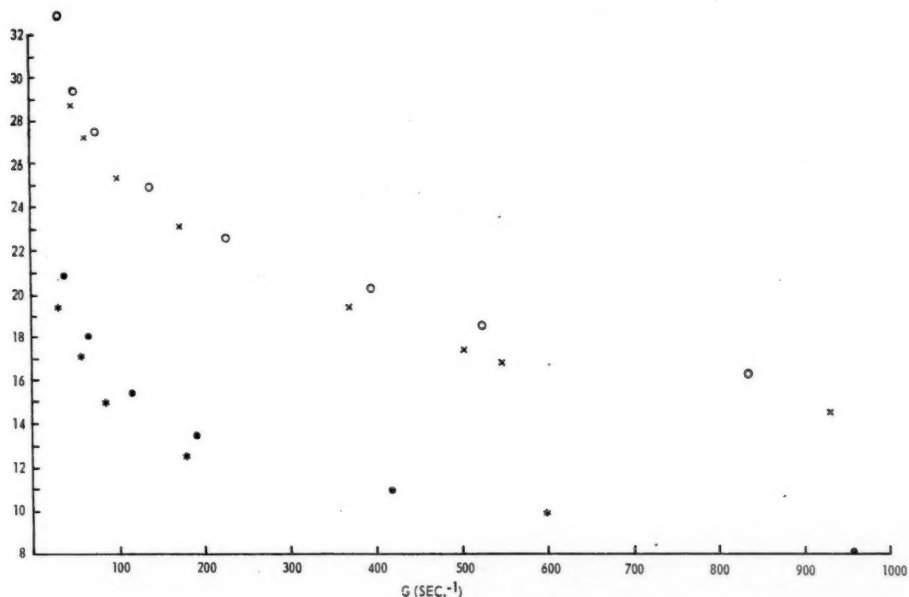
FIG. 1.   Extinction angle χ vs. gradient G plot: ✕, virus in sap; ●, once ultracentrifuged and dissolved in 0.005 M sodium citrate; *, once ultracentrifuged and dissolved in distilled water; ○, ultracentrifuged after citrate treatment.

On the other hand, virus obtained from citrate-treated sap showed virtually no change in the χ vs. G curve. The small shift towards higher extinction angles was probably a result of minor losses of aggregated material in the process of ultracentrifugation.

In Fig. 2, δ, the phase difference in degrees, divided by the concentration c (in per cent virus) is plotted for the purified non-aggregated material. The downward curvature in this plot indicates the rigid nature of the particle. This is in agreement with similar earlier measurements of the virus in tobacco sap (6).

The Effect of pH and Ionic Strength

To speed up the purification procedure several short cuts were attempted. One aliquot of a sap was dialyzed against 0.05 M sodium citrate and a second aliquot was dialyzed

directly against 0.005 M sodium citrate. Both samples showed an increase in aggregation after ultracentrifugation. To test the effect of pH, citrate buffer at pH 5.7 was used. Other ions were also tested. The results are summarized in Tables I and II.
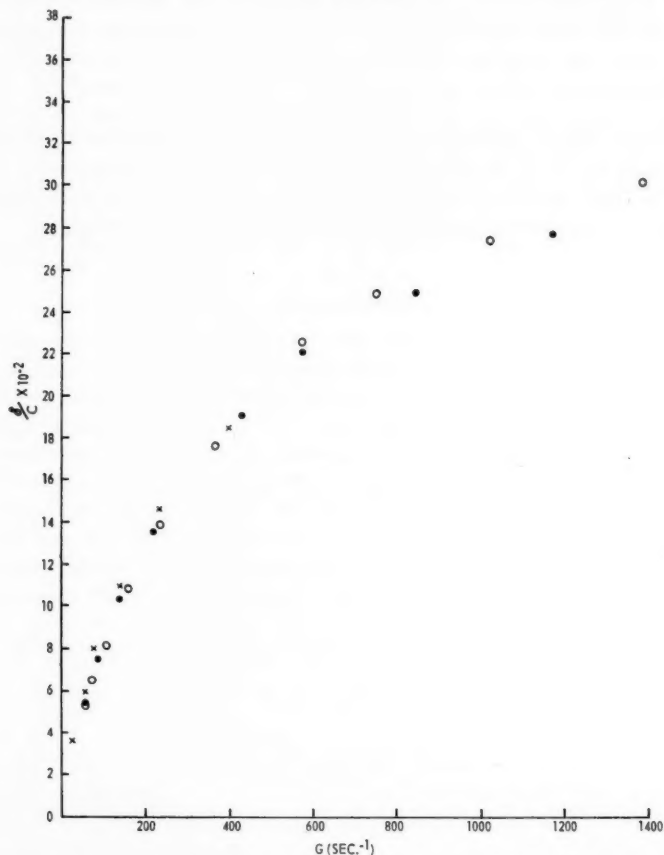
FIG. 2.   Amount of birefringence divided by concentration, plotted against velocity gradient. Purified non-aggregated virus in 0.005 M sodium citrate.

The purified non-aggregated virus was insoluble in water in the complete absence of electrolytes. When thoroughly dialyzed against distilled water, the virus solution became turbid and upon centrifugation at 4000 r.p.m. for 20 minutes practically all the virus was in the pellet. This pellet could be redissolved in 0.005 M sodium citrate. Flow birefringence measurements indicated that no aggregation occurred in this process.

Nitrogen and Phosphorus Content

Kjeldahl nitrogen was determined using essentially the procedure of Miller and Miller (8). The theoretical curves and experimental data were determined on a Beckman DU spectrophotometer at 480 mμ, in a concentration range of 0.06 to 0.12 mg of nitrogen. Phosphorus content was determined by the method of Michelson (9). The virus concentration was obtained from dry weights at 100° C in a vacuum oven by subtracting

TABLE I

The influence of various ions and of pH on the tendency of potato X virus to aggregate
after ultracentrifugation

Dialysis of sap	Solvent after ultracentrifugation	Aggregation
0.05 M Na citrate followed by 0.005 M Na citrate	0.005 M Na citrate	−
0.05 M Na citrate	0.05 M Na citrate	+
	0.005 M Na citrate	+ + −
0.005 M Na citrate	0.005 M Na citrate	+
0.05 M citrate buffer, pH 5.7, followed by 0.005 M of same buffer	0.005 M citrate buffer, pH 5.7	+ −
0.05 M versene, pH 7.2, followed by 0.005 M of same buffer	0.005 M versene, pH 7.2	−
0.05 M K phosphate buffer, pH 7.2, followed by 0.005 M of same buffer	0.005 M K phosphate buffer, pH 7.2	+
0.005 M K phosphate buffer, pH 7.2	0.005 M K phosphate buffer, pH 7.2	+
0.05 M NaCl, pH 7.2 (adjusted with NaOH), followed by 0.005 M of same buffer	0.005 M NaCl, pH 7.2 (adjusted with NaOH)	+

NOTE: −, No change.
   +, Low extinction angles (approximately like points ● in Fig. 1).
 + + −, Slight lowering of extinction angles (by 3° at 250 sec⁻¹).
   + −, Very slight lowering of extinction angles (by 1° at 250 sec⁻¹).

TABLE II

The influence of various ions on the tendency of purified potato X to aggregate after
ultracentrifugation

Dialysis of purified non-aggregated virus	Solvent after ultracentrifugation	Aggregation
0.005 M NaCl, pH 7.2 (adjusted with NaOH)	0.005 M NaCl, pH 7.2 (adjusted with NaOH)	−
0.005 M phosphate, pH 7.2	0.005 M phosphate, pH 7.2	−
0.1 M phosphate, pH 5.7	0.1 M phosphate, pH 5.7	+

NOTE: −, No change.
   +, Lower extinction angles (see points ● in Fig. 1).

the dry weight of the citrate solvent. The nitrogen and phosphorus values were
15.7±0.4% and 0.59±0.02% respectively. These data are in good agreement with the
values found by Loring (4).

Serology

Antisera were prepared by injecting the citrate-treated, three times ultracentrifuged
preparation into rabbits. These sera were compared by means of the complement fixation
serological technique (10, 11) with sera prepared from four times ultracentrifuged – slow
centrifuged aggregated material. In addition to antibodies against virus, traces of
antibodies against normal plant proteins were detected in all sera. However, the virus,
given cyclic centrifugation only, produced considerably more of these antibodies than
the citrate-treated virus.

Ultraviolet Absorption

An attempt was made to determine the extinction coefficient at 260 mμ. It was found
that in 0.005 M sodium citrate Beer's law was not followed in a virus concentration
range of 0.01 to 0.045% indicating interactions of the chromophoric groups. The same
was true when higher sodium citrate concentrations or 0.05–0.1 M phosphate buffer at

pH 7.2 were used. At pH 5.7 in 0.1 M phosphate, however, the extinction coefficient was independent of concentration. An average value of 26.8 g virus/100 ml cm was derived.

The ultraviolet absorption spectrum under these conditions showed a minimum at 245 mμ and a broad maximum at 260 mμ. The ratio of the 260/280 mμ absorptions was 1.20. After correction for scattering from measurements at 320 to 410 mμ (12) this ratio became 1.19. On the other hand, virus prepared by four cycles of ultracentrifugation – slow centrifugation from sap untreated with sodium citrate had a 260/280 mμ ratio of 1.30 when corrected for scattering.

Sedimentation

The sedimentation coefficient of the non-aggregated purified preparation was determined in 0.1 M phosphate buffer, pH 5.7, in a virus concentration range 0.25–0.02%. Photographs were taken at 4-minute intervals in a Spinco Model E Analytical Ultracentrifuge at 25,980 r.p.m. The sedimentation coefficients were converted to corresponding values at 20° C in water. The least-squares line derived from the data followed the equation $1/S_{20} \times 10^{10} = 8.49 + 4.58\ c$ giving a sedimentation coefficient S_{20} of 117.7 Svedbergs at zero concentration. Similar studies at pH 7.1 reported in the literature gave the value 123.5 Svedbergs (5). As stated in reference (5) the preparation contained a small amount of material that sedimented very rapidly. With the preparations described in this paper, however, there was no indication of the presence of material other than that contained in the major peak. Figure 3 represents the ultracentrifuge patterns of a 0.25% and 0.02% solution respectively.
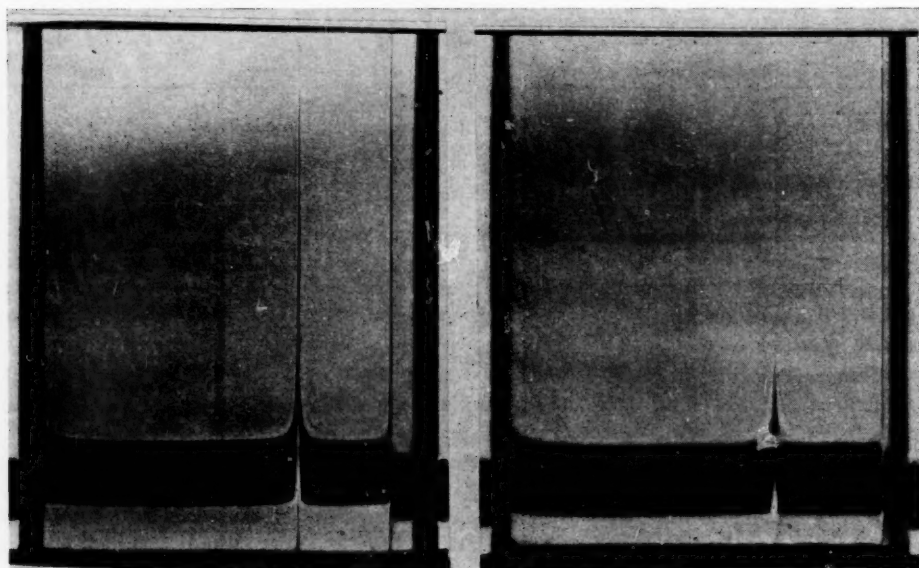
Fig. 3. Sedimentation pattern of purified non-aggregated virus in 0.1 M phosphate, pH 5.7. Virus concentrations 0.25% and 0.02% bar angles 70 and 55° respectively. Sedimentation from right to left.

DISCUSSION

The data in Table I indicate that when potato X virus in tobacco sap was exposed to 0.05 M sodium citrate, some of its structural features connected with its tendency to aggregate end-to-end irreversibly were altered. Once this change had taken place the

virus only aggregated when ultracentrifuged at high ionic strength. The influence of pH in the range 5.7–7.4 was very small. Versene buffer at pH 7.2 under the same conditions had a similar effect, while potassium phosphate and sodium chloride were not active. The data in Table II furnished further evidence indicating irreversible changes in the virus structure. In contrast to the untreated virus, the preparation purified with citrate did not aggregate when ultracentrifuged after "exhaustive" dialysis against 0.005 M phosphate or sodium chloride at pH 7.2. At higher salt concentrations, however, aggregation occurred.

Recently a more critical attitude to the degree of purity in tobacco mosaic virus preparations has revealed that treatment with citrate and other ions alters the composition of these preparations (13, 14, 15, 16). Thus Ginoza et al. (13) were able to prepare colorless pellets of a group of strains of T.M.V. after citrate, versene, and phosphate treatments, while the untreated virus when ultracentrifuged always gave amber-colored pellets. This color was found to be associated with small nucleoprotein molecules that were split off the virus during these procedures. The amount of nucleoprotein removed increased with increasing phosphate concentration and at higher temperatures. Pirie (15) also reported the release of labile phosphorus-containing compounds when T.M.V. was exposed to citrate.

It is possible that the tendency of potato X virus to aggregate is linked with the presence of phosphorus-containing or other compounds that are removed when potato X virus is treated with 0.05 M citrate or versene at 5° C. The action of such compounds could be either limited to the facilitation of a close approach of virus particles, similar to the non-specific action of electrolytes, or could be of a more specific nature. The change in the 260/280 mμ absorption ratio cannot be taken as evidence for the splitting of such compounds. It merely indicates that the surrounding of the chromophoric groups has changed under the influence of citrate.

The possibility of heavy metals participating in the aggregation processes cannot be ruled out. The chelating properties of citrate and versene would lead to considerations similar to those made in connection with preparations of colorless T.M.V. pellets (13).*

Finally, the chemical purity of the preparation described in this paper should be considered. The complement fixation experiments indicate that a higher degree of purity has been achieved than in samples prepared by techniques described in the literature. The author is well aware, however, that it may be subject to the same criticism as T.M.V. preparations obtained by ultracentrifugation (15, 17, 18). As stated in the introduction, the main concern of this study was to preserve the size and size distribution intact. Methods offered by critics of the degree of purity of virus preparations unfortunately change these properties in the case of most viruses. Consequently, to the author's knowledge no method is available at the present time which would completely satisfy both the criteria of chemical purity and the requirements for physicochemical studies.

REFERENCES

1. WATANABE, I. and KAWADE, Y.   Bull. Chem. Soc. Japan, **26**, 294 (1953).
2. BEODTKER, H. and SIMMONS, N. S.   J. Am. Chem. Soc. **80**, 2550 (1958).
3. BAWDEN, F. C.   Plant viruses and virus diseases. Chronica Botanica Company, Waltham, Mass. 1950.
4. LORING, H. S.   J. Biol. Chem. **126**, 455 (1938).
5. LAUFFER, M. A. and CARTWRIGHT, T. E.   Arch. Biochem. Biophys. **38**, 371 (1952).
6. REICHMANN, M. E.   Can. J. Chem. **36**, 1603 (1958).

*In one of our preparations the tobacco leaves were squeezed in a stainless steel Carver press basket. The sap in this preparation darkened very rapidly on standing, indicating the presence of traces of metals from the press. The citrate-treated, purified virus when dialyzed against 0.1 M phosphate buffer at pH 5.7 aggregated and most of it came out of solution. This behavior was never observed in preparations squeezed by a mortar and pestle.

7. EDSALL, J. T., RICH, A., and GOLDSTEIN, M.   Rev. Sci. Instr. **23**, 695 (1952).
8. MILLER, G. L. and MILLER, E. E.   Anal. Chem. **20**, 481 (1948).
9. MICHELSON, O. B.   Anal. Chem. **29**, 60 (1957).
10. BROOKSBY, J. B.   The technique of complement fixation in foot-and-mouth disease research. A.R.C. Rept. Ser. London, No. 12 (1952).
11. WRIGHT, N. W. and STACE-SMITH, R.   To be published.
12. ENGLANDER, S. W. and EPSTEIN, H. T.   Arch. Biochem. Biophys. **68**, 144 (1957).
13. GINOZA, W., ATKINSON, E. D., and WILDMAN, S. G.   Science, **119**, 269 (1954).
14. SIEGAL, A. and WILDMAN, S. G.   Phytopathology, **44**, 277 (1954).
15. PIRIE, N. W.   J. Biol. Chem. **63**, 316 (1956).
16. MATTHEWS, R. E. F. and SMITH, J. O.   Nature, **180**, 375 (1957).
17. PIRIE, N. W.   Exptl. Cell Research, (Suppl.) **1**, 193 (1949).
18. PIRIE, N. W.   Advances in Virus Research, **4**, 159 (1957).

THE N- AND C-TERMINAL END GROUPS OF HAIR KERATIN[1]

M. F. Kerr and C. Godin

ABSTRACT

The N-terminal and the C-terminal residues of human and horse hair and partially reduced hair have been determined. Aspartic acid, glutamic acid, glycine, serine, threonine, alanine, and valine were identified as N-terminal groups. Aspartic acid, glutamic acid, glycine, serine, threonine, and alanine were identified as C-terminal groups. These are the same N-terminal and C-terminal amino acids as have been found previously for wool and feather keratin.

INTRODUCTION

The purpose of the following work was to establish a procedure which would serve to differentiate among the hair keratins of different species of animals, including man. At present a visual microscopic procedure is used in practically all forensic work involving hair. For most cases this is sufficient, particularly if negative results will suffice. In some cases, however, the microscope is simply inadequate in providing the information required by the examiner.

Recently, the N-terminal and the C-terminal residues of wool keratin were determined (1, 2, 3, 4, 5, 6). Complex mixtures of end groups were found and it was hoped that some qualitative differences could be established between the hair keratins of different species using these methods. This paper reports the identification of N-terminal and C-terminal residues in human and horse hair.

EXPERIMENTAL

Hair.—The human hair was obtained from the "N" Division, R.C.M.P. Barracks, and was exclusively male. The horse hair was obtained from the "N" Division, R.C.M.P. Stables, and was exclusively tail hair. To degrease the hair it was extracted in a Soxhlet for 2 hours each with acetone and ether and then air-dried. Finely ground hair was obtained by grinding the hair in liquid nitrogen in a porcelain mortar.

Dinitrophenylation.—Finely ground hair (0.5 g) was suspended in water (12 ml) containing sodium bicarbonate (0.5 g). Ethanol (25 ml) containing 1-fluoro-2,4-dinitro-benzene (FDNB) (0.86 g) was added and the mixture was shaken for 48 hours at 40° C (2). The hair was then isolated by filtration, washed with water, alcohol, and ether. When partly reduced keratin was dinitrophenylated, the mixture was first extracted with ether, then acidified. The insoluble dinitrophenyl-proteins (DNP-proteins) were centrifuged down and washed with water, alcohol, and ether.

Hydrazinolysis.—The method described by Niu and Fraenkel-Conrat (7) was used.

Hydrolysis.—The DNP-proteins were hydrolyzed in 6 N HCl in sealed tubes for 24 hours at 100° C.

Chromatography.—The DNP-amino acids were spotted on Whatman paper No. 3 MM buffered at pH 6. The chromatograms were developed with *tert*-amyl alcohol saturated with pH 6 phthalate buffer (8). Each spot obtained was run again after elution from the paper. The same paper was used for the second run but the phthalate buffer alone was used as solvent. In the buffer alone the R_f values are different from those obtained in *tert*-amyl alcohol.

Reduction.—Hair keratin was partly reduced with sodium thioglycolate (9). Hair (0.5 g) was suspended in water (25 ml) containing sodium hydroxide (4 g). Thioglycolic

acid (2.5 ml) was added. The mixture was shaken at room temperature for a given period of time (3 to 5 hours). The residue was then filtered off and the keratin precipitated by careful acidification with acetic acid or dilute hydrochloric acid. The acidification was followed with a pH meter; a first protein fraction (black solid) came out between pH 8 and pH 7 and a second fraction (white solid) between pH 4 and pH 1.

RESULTS

Hair.—The N-terminal amino acids obtained from human and horse hair by the dinitrophenyl method were aspartic acid, glutamic acid, glycine, serine, threonine, alanine, and valine. Using the hydrazinolysis method for the determination of C-terminal groups in proteins, six C-terminal residues were detected in human and horse hair. They were identified by paper chromatography after transformation into DNP-derivatives. They were shown to be aspartic acid, glutamic acid, glycine, serine, threonine, and alanine.

Partly Reduced Keratin.—Treatment with alkaline thioglycolate for 3 hours transforms keratin into a protein mixture containing 25% of its sulphur as cysteine (9). When the reduction was allowed to proceed for 3 to 5 hours, the protein fractions obtained by acidification to pH 8–7 and pH 4–1 had the same N-terminal and C-terminal groups as intact hair.

DISCUSSION

Human hair and horse hair have the same seven N-terminal groups and the same six C-terminal groups. The same amino acids are also found as N-terminal and C-terminal residues of wool keratin (1–6). The same seven N-terminal groups have also been found recently in feather keratin (10). No attempt was made to do a quantitative estimation of end groups because it was shown recently that the results of quantitative determination in wool are not very reliable (4), at least not reliable enough to establish species differences with certitude. Crude wool keratin was also shown recently to have the same N-terminal groups as intact wool (4). It is therefore not surprising that partly reduced hair keratin has the same N-terminal and C-terminal groups as intact hair.

As no qualitative differences are found between keratin terminal groups in four species —man, horse, sheep, and fowl—this method was not investigated any further as a means of distinguishing between the hair keratins of different species.

REFERENCES

1. BLACKBURN, S. Biochem. J. **47**, 443 (1950).
2. MIDDLEBROOK, W. R. Biochim. et Biophys. Acta, **7**, 547 (1951).
3. ALEXANDER, P. and SMITH, L. F. Proc. Intern. Wool Textile Research Conf. Australia, Vol. B, p. B-56 (1956).
4. THOMPSON, E. O. P. Australian J. Biol. Sci. **10**, 225 (1957).
5. BLACKBURN, S. and LEE, G. R. J. Textile Inst. **45**, T487 (1954).
6. BRADBURY, J. H. Biochem. J. **68**, 482 (1958).
7. NIU, C-I. and FRAENKEL-CONRAT, H. J. Am. Chem. Soc. **77**, 5882 (1955).
8. BLACKBURN, S. and LOWTHER, A. G. Biochem. J. **48**, 126 (1951).
9. GODDARD, D. R. and MICHAELIS, L. J. Biol. Chem. **112**, 361 (1935).
10. WOODIN, A. M. Biochem. J. **63**, 576 (1956).

A NOTE ON THE ELECTRICAL CONDUCTANCES OF DIELECTRIC FLUIDS IN ULTRASONIC FIELDS[1]

N. BERKOWITZ

ABSTRACT

The electrical conductances of ethyl bromide, n-propyl bromide, n-butyl bromide, methanol, and ethanol in ultrasonic fields have been measured at frequencies between 250 kc/s and 2 Mc/s and intensities between 0.7 and 24 w/cm². Measurements were made at room temperature, using a simple d-c. technique. It is shown that a *simple* transient increase in conductance, such as has previously been observed by Seidl, may be confined to unassociated fluids and that it can occasionally give way to a much more complex—and not as yet fully understood—behavior pattern.

When a dielectric liquid (such as hexane or toluene) is placed in an ultrasonic field, a marked transient change in its electrical conductance K is induced. As soon as irradiation is begun, a sharp (and often virtually instantaneous) rise in K, followed by a relatively slow approach to a new equilibrium conductance, is observed; and when the acoustic field is removed, K will more or less rapidly return to its original value (1, 2). The plot of K vs. time t (at constant frequency f and intensity I) will, in other words, take the form illustrated in Fig. 1. Meyer (1) has interpreted these phenomena by assuming transfer of adsorbed impurities from the electrodes into the liquid, while Seidl (2), working with toluene, hexane, and carbon tetrachloride, rejects Meyer's explanation and postulates, instead, an acoustic splitting of "complex ions" and a consequent increase either in the number or in the mobility of the charge carriers.
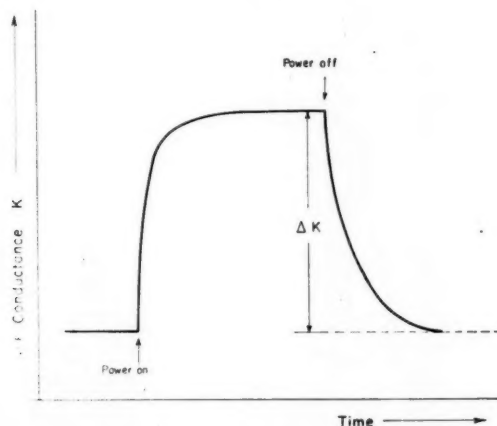
FIG. 1. General variation of conductance with time of irradiation (after Seidl).

Measurements made in this laboratory tend, broadly, to support Seidl's thesis: desorption of impurities—or a simple temperature effect that would accrue from acoustic heating of the liquid under test— appear quite insufficient to account for the experimental observations (and, indeed, to be generally irreconcilable with them). Both processes are, for instance, inconsistent with the very rapid initial rise in K and with its almost equally

rapid fall when the ultrasonic field is switched off; and ΔK is always far greater than can be accounted for by the relatively small temperature rise in the test fluid during irradiation (cf. Seidl). On the other hand, the available evidence now suggests that "complex ion" splitting represents only one of several phenomena. If the range of fluids under examination is extended, and if measurements of K are made at several frequencies and intensities, seemingly more complex changes than those exemplified by Fig. 1 are occasionally recorded. Pronounced differences can, in particular, be noted in the responses of associated and unassociated liquids; and under certain conditions, ultrasonic irradiation appears to cause a *fall* rather than an increase in the conductance.* The purpose of this note is to report data illustrating these statements.

In the study here under review, a Mullard E.7562 generator, coupled to an oscillating ($\sim$15 cm^2) quartz crystal mounted in a sealed transducer housing, was used to produce ultrasonic waves in the frequency range 250 kc/s to 2 Mc/s. Maximum intensities of the tuned beams varied from about 2.3 w/cm^2 at 250 kc/s to nearly 35 w/cm^2 at 2 Mc/s. The conductivity cell was blown of thin pyrex glass and fitted with two platinum plate electrodes disposed at 90° to the acoustic wave front; a 1.5-volt potential was applied to these electrodes from a (frequently checked) dry cell. Resistances were measured by connecting cell and battery in series to a Leeds & Northrup d-c. bridge and a Pye "Scalamp" galvanometer. No attempt was made to determine the cell constant and
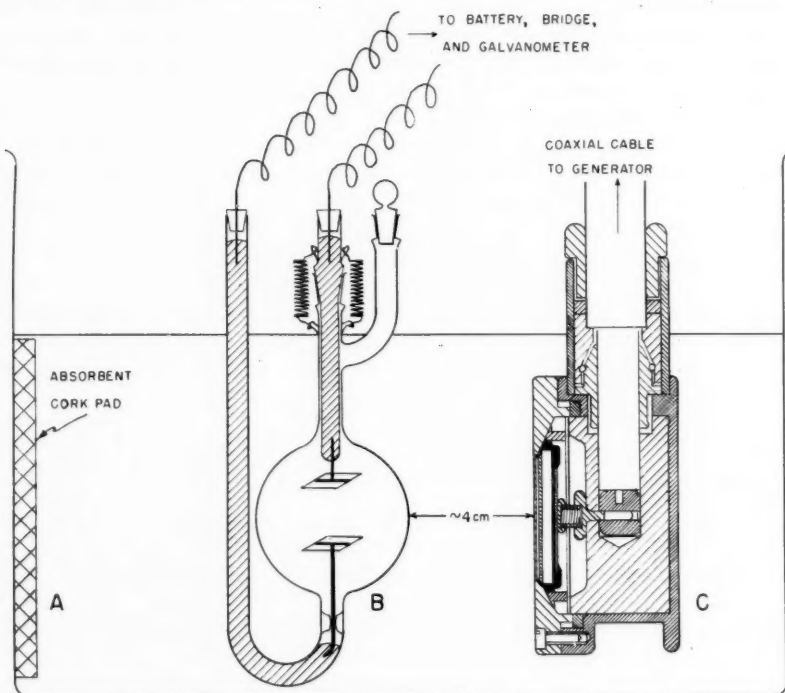
FIG. 2.   Diagram of apparatus (not to scale):
A: constant-temperature bath; B: conductivity cell; C: transducer.

*It should be noted that this phenomenon further militates against attributing the observed change in K—or any substantial part of this change—to a temperature rise in the liquid under test.

to convert the measured resistances to absolute resistivities; and similarly, no attempt was made, at this time, to investigate the variation of the measured response with the cell/crystal distance. Since large changes in K during ultrasonic irradiation did not apparently require a particularly critical adjustment of the assembly (or, for that matter, a critical design of the cell), it was deemed adequate to select an arbitrary cell/crystal distance (*ca.* 4 cm) and to maintain this constant throughout the investigations. Spurious conductance changes (such as might arise from impurities) were minimized by employing pure liquids and by conditioning the cell for several hours with the particular liquid under test. (The conditioning aliquot was removed and the cell freshly filled immediately prior to a measurement.) Further, in order to eliminate back e.m.f.'s, measurements of K in the ultrasonic field were only begun after the external potential had been applied to the test sample for at least 30 minutes and the conductance had attained a constant value. Both cell and transducer were immersed in a constant-temperature bath controlled to within $\pm 0.02°$ C. The assembly is shown diagrammatically in Fig. 2.

Liquids chosen for study were (*a*) a homologous series of unassociated fluids (comprising ethyl, *n*-propyl, and *n*-butyl bromide, all obtained from the Matheson Company Inc. with "reagent grade" purity), and (*b*) two highly associated fluids (methyl and ethyl alcohol).* The latter were purified by careful drying and subsequent double redistillation. In the case of (*a*), K was always measured at $25 \pm 0.02°$ C and in the case of (*b*), at $35 \pm 0.02°$ C. In the diagrams shown below, all experimental data are expressed as conductances (in reciprocal ohms). The degree of reproducibility can be gauged from the duplicates that are shown in several instances.

Plots of K/t for the three unassociated dielectrics (EtBr, *n*-PrBr, *n*-BuBr) are reproduced in Figs. 3 and 4. They follow closely upon the course of Seidl's curves (cf. Fig. 1)—a course here designated as Type A—but they differ from them in some quantitative aspects. Thus, at $f = 250$ kc/s and $I = 2.3$ w/cm², ΔK is in all three instances of the order of 10% (as compared with 31% and 47% reported by Seidl for CCl₄ and hexane respectively); and the return of K to its initial value after the field has been switched off occurs over a rather shorter period (*ca.* 5 minutes as compared with 20 minutes for
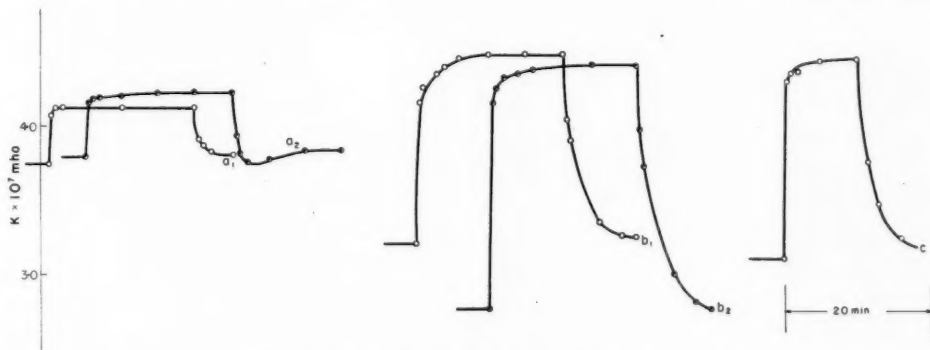
FIG. 3. a_1, a_2: Ethyl bromide; $f = 250$ kc/s, $I \sim 2.3$ w/cm².
b_1, b_2: Ethyl bromide; $f = 1$ Mc/s, $I \sim 12.4$ w/cm².
c: Ethyl bromide; $f = 2$ Mc/s, $I \sim 24$ w/cm².

Because Seidl concentrated on non-polar or very weakly polar dielectrics, attention in the present study was focused upon relatively strongly polar ones.
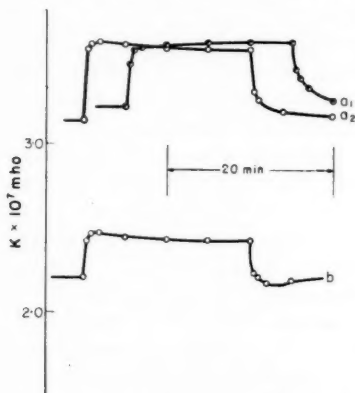
FIG. 4. a_1, a_2: n-Propyl bromide; $f = 250$ kc/s, $I \sim 2.3$ w/cm².
         b: n-Butyl bromide; $f = 250$ kc/s, $I \sim 2.3$ w/cm².

CCl₄). These differences, however, are almost certainly merely a consequence of different experimental conditions. For example, the rate of fall in K after termination of irradiation will depend upon the rate of cooling of the liquid to bath temperature and upon acoustic reverberation within the cell; and ΔK itself may be expected to depend upon the frequency and/or intensity (i.e. upon parameters not mentioned in Seidl's paper). This latter dependence is, in fact, clearly shown in Fig. 3: for ethyl bromide, ΔK increases from roughly 10% at $f = 250$ kc/s and $I = 2.3$ w/cm² to nearly 50% at $f = 1$ Mc/s and $I = 12.4$ w/cm². The fact that no further increase in ΔK is observed when irradiating at $f = 2$ Mc/s and $I = 24$ w/cm² suggests, however, that there is a more or less definite limiting value that cannot be appreciably exceeded. In Seidl's terms, it may correspond to *complete* splitting of complex ions and, hence, to maximum mobility of the resultant simple charge carriers. Significantly, ΔK was unaffected by molecular size or by the extent of cavitation (which could be varied by dissolving variable quantities of pure nitrogen in the outgassed liquid).

In the case of the two alcohols, however, much more profound departures from Seidl's data are noted. With methanol, the general behavior is still reminiscent of that of the bromides; but ΔK at 250 kc/s and $I = 2.3$ w/cm² now amounts to nearly 50% (instead of 10% as recorded with the bromides under the same conditions), and K tends to *fall* slightly after rapid attainment of its maximum value (cf. Fig. 5—a form designated as Type B). It should here be pointed out that this fall cannot be associated with a back e.m.f., since termination of the irradiation is accompanied by a rapid return of the conductance *to its original value, not to a lower one.* This is particularly well exemplified by curve d of Fig. 5; the same curve, incidentally, suggests that ΔK_{max} lies close to 50% reached at $f = 250$ kc/s, $I = 2.3$ w/cm².

Finally, with ethanol, neither Type A nor Type B K/t curves are found. At $f = 250$ kc/s and $I < 1$ w/cm² as well as at $f = 1$ Mc/s and $I = 12.4$ w/cm², K *falls* under the influence of ultrasonic irradiation ($-\Delta K$ amounting to about 9 and 15% respectively); at $f = 1$ Mc/s, recovery of K requires inordinately long periods of time (25–30 minutes); and an upward change of the conductance during irradiation is only observed at $f = 250$ kc/s and $I = 1.4$ and 2.3 w/cm². Even in this range, the *initial* response to irradiation is a reduction (cf. Figs. 6 and 7).
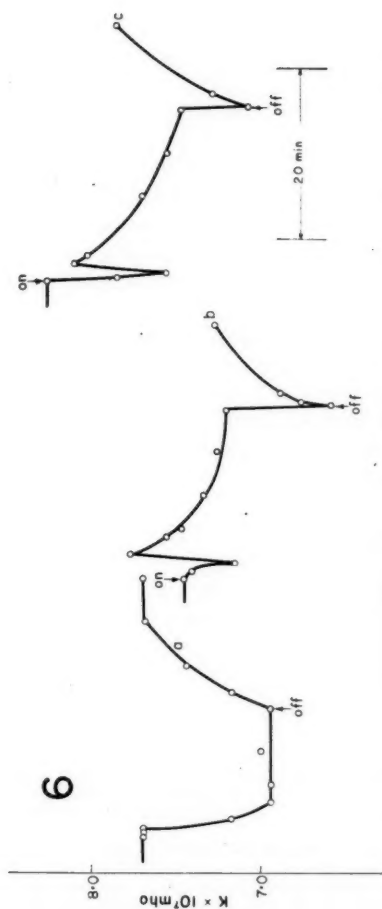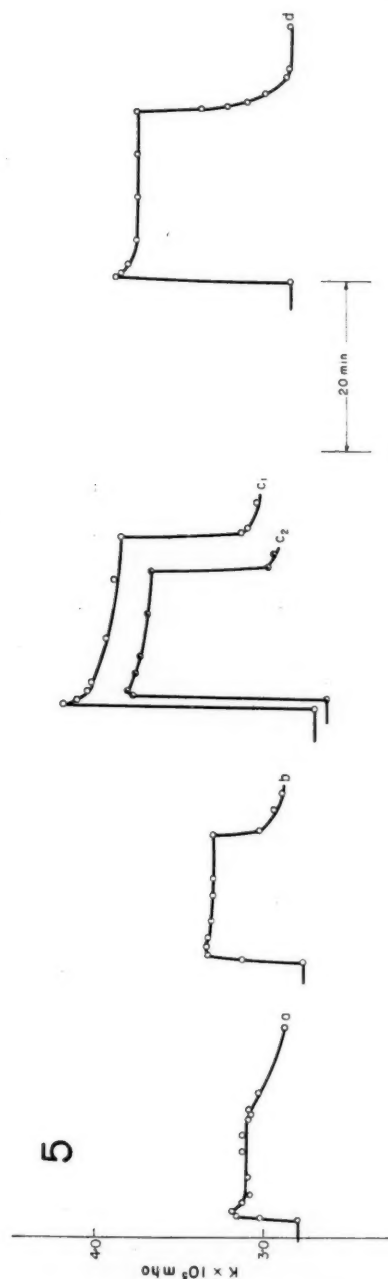
FIG. 5. a: Methanol; $f = 250$ kc/s, $I \sim 0.7$ w/cm².
b: Methanol; $f = 250$ kc/s, $I \sim 1.4$ w/cm².
c_1, c_2: Methanol; $f = 250$ kc/s, $I \sim 2.3$ w/cm².
d: Methanol; $f = 1$ Mc/s, $I \sim 12.4$ w/cm².

FIG. 6. a: Ethanol; $f = 250$ kc/s, $I \sim 0.7$ w/cm².
b: Ethanol; $f = 250$ kc/s, $I \sim 1.4$ w/cm².
c: Ethanol; $f = 250$ kc/s, $I \sim 2.3$ w/cm².
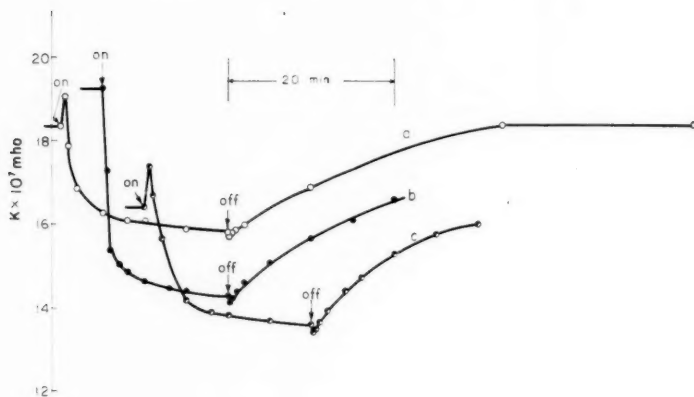
FIG. 7. a, b, c: Ethanol; $f = 1$ Mc/s, $I \sim 12.4$ cm^2.

To account for the observations made with methanol, only a slight modification of
Seidl's hypothesis appears to be necessary: if the initial upward change of K is once
again (as in the case of unassociated fluids) ascribed to disruption of complex ions (or
better, to disruption of associated complexes), the subsequent slight fall of the con-
ductance can be attributed to the re-establishment of some form of equilibrium between
associated and non-associated charge carriers. But in the case of ethyl alcohol, the experi-
mental data indicate a much more complex pattern of events. The nature of these events
remains, at this stage, necessarily speculative and it is therefore not proposed to discuss
them here. Two notable features of the K/t curves obtained at $f = 250$ kc/s and $I = 1.4–$
2.3 w/cm^2 (Fig. 6, curves b and c) might, however, usefully be noted. First, the rise in
conductance after the 2nd or 3rd minute of irradiation was in all cases accompanied
by a sudden onset of cavitation. As long as the liquid was not cavitating, K continued
to fall towards an equilibrium value similar to that shown in Fig. 6a.* Secondly, the form
of curve (excluding the initial portion) is strongly reminiscent of the dielectric relaxation
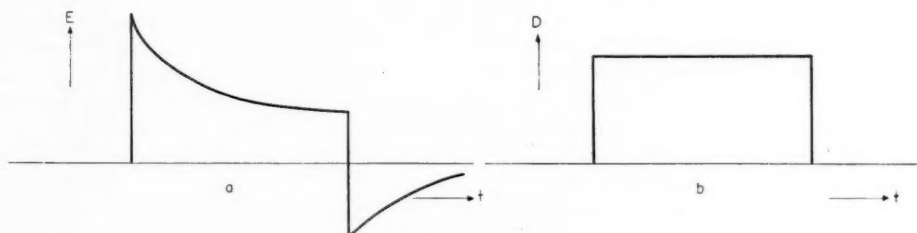
FIG. 8.   Dielectric relaxation under prescribed D (after Böttcher).
               a: Variation of electrical field with time.
               b: Variation of dielectric displacement with time.

*In the case of the bromides and methyl alcohol, there was no apparent connection between an upward change
of K and cavitation. For example, at f = 250 kc/s and I = 0.75 w/cm^2, the conductance of methanol increased
despite complete absence of visible cavitation; and with the bromides, ΔK was found to be independent of the
extent of cavitation. In the light of these observations, one is tempted to suggest that cavitation (insofar as it
can occur at all) and an upward change in the conductance are two events following upon a single cause, e.g. an
energy build-up in the liquid to a critical threshold value.

curves discussed by Böttcher (3); the particular case considered by him involves a polar dielectric between the plates of an ideal condenser to which a uniform static field is applied and in which one is concerned with the time variation of the resultant electrical field E. (This variation, and the corresponding variation of the dielectric displacement D, are shown as curves a and b in Fig. 8.)

REFERENCES

1. MEYER, M.   Z. Physik, **102**, 279 (1936).
2. SEIDL, F.   Z. Physik, **116**, 359 (1940).
3. BÖTTCHER, C. J. F.   Discussions Faraday Soc. No. **23**, 7 (1957).

DETERMINATION OF URANIUM IN FLOTATION CONCENTRATES
AND IN LEACH LIQUORS BY X-RAY FLUORESCENCE[1]

G. L. Smithson, R. L. Eager, and A. B. VanCleave

ABSTRACT

X-Ray fluorescence has been applied to the analysis of flotation concentrates obtained from pegmatitic uranium ores occurring in Northern Saskatchewan. Approximate uranium analyses can be obtained by direct measurement on flotation concentrates but more accurate results are obtained by using an internal standard such as strontium or yttrium. The time required for an analysis, as compared to that of conventional chemical or fluorimetric methods, is considerably reduced and flotation pilot plant operations can therefore be more effectively controlled. The method has been extended to include the analysis of sulphate leach liquors obtained from the leaching of pegmatitic ores and their flotation concentrates. Organic phases obtained in liquid – liquid extraction studies can also be rapidly analyzed for uranium by X-ray fluorescence.

INTRODUCTION

The application of X-ray fluorescence to quantitative analysis for uranium has been the subject of studies by Cope (1), Pish and Huffman (2), and Kehl and Russell (3). It has generally been found desirable to use internal standards such as strontium, molybdenum, yttrium, or bromine to avoid matrix effects. Claisse (4) has suggested a fusion method by which accurate X-ray fluorescence analysis can be done without an internal standard. The fusion method involves dilution of the sample with the flux, thus decreasing the limit of detection.

The authors have been interested in developing rapid and reasonably accurate methods for the determination of uranium in flotation concentrates collected from the low grade pegmatitic ores of Northern Saskatchewan (5). Uranium analyses on sulphate leach liquors and on aqueous and other liquid phases resulting from liquid – liquid extraction studies are also of interest. The conventional chemical methods and the widely used fluorimetric method (6) of uranium analysis are very time consuming and of little value in the control of a flotation pilot plant. The possibility of applying X-ray fluorescence to this problem has therefore been investigated.

EXPERIMENTAL

Equipment

A General Electric XRD-5D/F X-ray spectrometer equipped with a Machlett AEG 50 tungsten target tube, a lithium fluoride crystal, a 0.010-inch Soller slit, and a No. 2 SPG (Krypton) proportional counter tube was used. The X-ray tube was operated at 50 KVP and 50 ma. In charting spectra the following settings were normally employed: scanning speed 0.2 deg/min; chart speed 6 in./hr; time constant 8; full-scale pen deflections of 200, 1000, or 2000 c.p.s. Bakelite sample holders with $22 \times 22 \times 3$ mm recesses were used for solid samples.

The grinding and mixing of solid samples was done in a motor-driven mullite mortar and pestle.

ANALYSIS OF FLOTATION CONCENTRATES WITHOUT AN INTERNAL STANDARD

Since the matrix minerals and the average particle size in the flotation concentrate from a particular pegmatitic ore were believed to be reasonably uniform, an attempt was made to apply X-ray fluorescence analysis to the concentrates without any pretreatment other than drying. Typical results are shown by the lower line in Fig. 1 in which the intensity of the U L_{α_1} line (as determined from chart recording) is shown plotted against the per cent of U_3O_8 (as determined fluorimetrically (6)) in the sample. The positions of the straight lines in Fig. 1 were determined by the method of least squares. The scatter
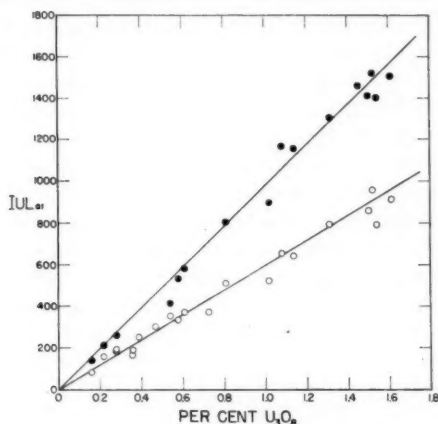
FIG. 1.   Calibrations for the determination of U_3O_8 in flotation concentrates without using an internal standard.

○ Dry samples direct from flotation plant.
● Dry samples from flotation plant ground for 30 minutes in a mechanical mortar.
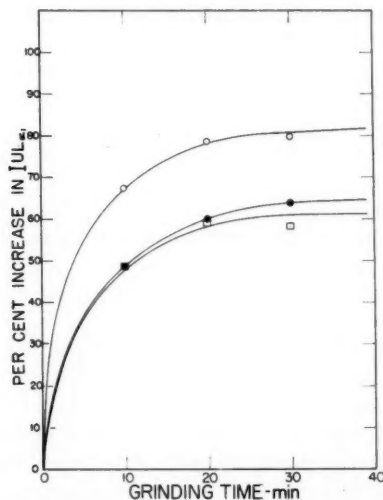
FIG. 2.   The effect of mortar grinding time on the intensity of the U L_{α_1} line in three samples of flotation concentrate.

of the experimental points about the lower line is partly due to errors inherent in both the fluorimetric and X-ray fluorescence methods, and partly due to variations in particle size of the samples. Some measure of the effect of particle size variation is shown by the results given in Figs. 1 and 2. The intensity of the U L_{α_1} line was observed to increase as the particle size was reduced,* finally reaching a constant level after about 30 minutes of grinding of the sample in a mortar. The top line in Fig. 1 could be used as a calibration curve to determine the per cent U_3O_8 in flotation concentrates from the particular ore used, provided that the particle size of the samples had been sufficiently reduced either in the grinding circuit of the pilot plant or by subsequent treatment in a mortar. Calibrations lying anywhere between the two lines shown in Fig. 1 could be obtained for the particular ore depending on the degree of comminution of the sample. Standards would have to be set up for each ore for a particular set of grinding conditions. Obviously, this would not be a very satisfactory procedure if a number of ores were being treated under a variety of pilot plant conditions. However, if a large number of analyses were required on flotation concentrates from a given ore, and the grinding circuit remained unchanged, it would be possible to apply X-ray fluorescence methods directly to the concentrate samples without further preparation. The results obtained would not be as reliable as those that can be obtained by employing a suitable internal standard. The main advantage would be in obtaining an approximate result in the minimum of time.

The per cent deviation from the mean intensity of the U L_{α_1} line produced by removing samples from the sample holder and repacking them, varied from 0.2 to 2.4%. Such fluctuations are considered to be within the accuracy of the X-ray technique.

ANALYSIS OF FLOTATION CONCENTRATES USING AN INTERNAL STANDARD

Uranium Determination

If uranium analyses of flotation concentrates collected by a variety of methods or of ores from a variety of sources are required, the addition of a suitable internal standard is desirable. Since no significant amounts of strontium have been detected in the Saskatchewan pegmatites under study, it has been convenient to use it as an internal standard for solid samples.

The procedure adopted for adding the internal standard to solid samples is as follows:

(*a*) A 3-g sample of dry flotation concentrate is poured into a watch glass to form a cone-shaped mass.

(*b*) A crater is formed in the cone by pressing the bottom of a small test tube down on the apex of the cone.

(*c*) One milliliter of absolute ethanol is added to the crater. (The dry flotation concentrates are hydrophobic. The ethanol facilitates the spreading of the aqueous solution of the standard through the sample.)

(*d*) One milliliter of aqueous $Sr(NO_3)_2$ solution containing 10 mg of Sr per milliliter is added to the crater.

(*e*) The sample is dried for 30 minutes under a heat lamp, transferred to the mullite mortar, and ground for 30 minutes.

A portion of the sample prepared as above is packed into a sample holder and the significant part of the X-ray spectrum either recorded or determined by setting the spectrogoniometer at 2θ angles as listed in Table I and counting for 100 seconds. The background count at the position of the peak is interpolated from the background counts on either side of the peak.

The original flotation concentrates were approximately 90% minus 270 mesh. Grinding for 30 minutes reduces the sample to approximately 90% minus 400 mesh.

TABLE I
2θ Angle settings for LiF crystal

| Matrix | Desired constituent | | | | | | Internal standard | | | | | | |
| | U | | | Fe | | | Sr | | Y | | | Br | |
	B.G.[a]	P.[b]	B.G.	B.G.	P.	B.G.	B.G.	P.	B.G.	P.	B.G.	P.	B.G.
Solid		26.14	27.10	55.00	57.50	60.00	24.60	25.18					
Aqueous solution	25.40	26.14	27.40	55.00	57.50	60.00			23.20	23.82	24.40		
Aqueous solution } Organic solution	25.30	26.14	29.00									29.96	34.50

[a] B.G.—Background count.
[b] P.—Peak position.
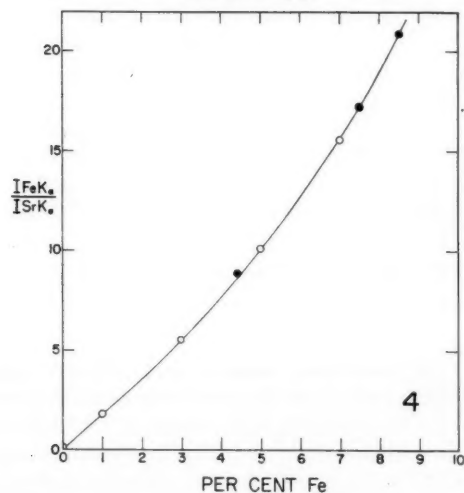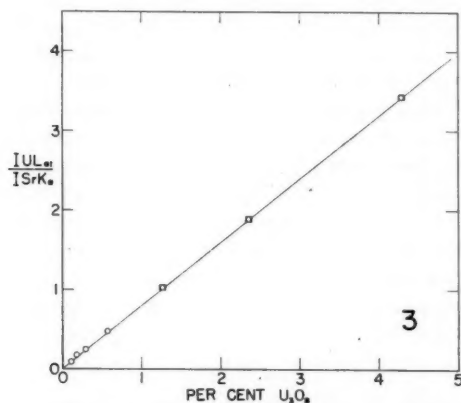
Fig. 3.   Calibration for the determination of U_3O_8 in solids with strontium as internal standard.
○ Chart-recording method.   □ Direct-count method.
Fig. 4.   Calibration for the approximate determination of iron in solids by reference to strontium internal standard.   ○ Synthetic mixtures.   ● Analyzed flotation concentrates.

The samples used for calibration (Fig. 3) were obtained from the Department of Mines and Resources, Ottawa, and the New Brunswick Laboratory of A.E.C., New Brunswick, N.J., together with two samples analyzed chemically (7) by the authors. Although these samples contained a variety of uranium minerals in differing matrices, the experimental points, whether determined from chart recordings or by counting at the specified angles, occur within experimental error on the straight line shown in Fig. 3. Although this method of analysis requires more time than would be the case if no internal standard was used, it yields more accurate and reliable results. Using the chart-recording technique, a single operator can analyze about 24 samples in an 8-hour day. Since samples of flotation concentrate can be fairly rapidly dried, analytical results can be transmitted to the pilot plant operator much more rapidly than is the case when the ultraviolet fluorimetric method is used.

The reproducibility of the method of using strontium as an internal standard was tested by repeating the procedure for adding the standard on 10 separate portions of a given sample. The ratio $I(U\ L_{\alpha_1})/I(Sr\ K_\alpha)$ was determined for each preparation both from the chart recording and by counting at fixed positions. The mean intensity ratios and the standard deviations were 0.649 ± 0.015 and 0.670 ± 0.020 for the direct-count and chart-recording methods respectively. The standard deviations for the two methods indicate an overlap in the ratio values. As expected, the results calculated from chart recordings are less precise than those obtained by direct counting.

Table II shows a comparison of analytical results on three flotation concentrate samples as determined by chemical analysis, fluorimetric analysis, and by X-ray fluorescence analysis using strontium as an internal standard. The agreement between the results for the three methods is well within their estimated limits of accuracy. The approximate relative time required for an analysis by each of these methods was estimated on the assumption that a single operator worked full time on a routine basis.

TABLE II

Comparison of results from different analytical methods

	% U_3O_8		
Sample	Chemical	Fluorimetric	X-Ray fluorescence
F 18 C$_1$	0.91	0.97	0.89
F 22 C$_1$	1.56	1.60	1.61
F 23 C$_1$	2.15	2.19	2.13
Approx. relative time required for analysis	5	2.5	1
Estimated max. % error	±2	±10	±5

Iron Determination

There is a tendency for acid-consuming minerals, such as iron oxides and other minerals containing iron, to be collected along with uranium minerals in the flotation of pegmatitic ores (5). A knowledge of the approximate iron content of uranium ore flotation concentrates is therefore useful in assessing the value of various collectors and systems of flotation. A good estimate of the iron content of these flotation concentrates can be made by referring the intensity of the Fe K_α line to that of the internal standard used to determine the uranium content. A calibration curve used for this purpose is shown in Fig. 4.

The samples used for calibration were (*a*) synthetic mixtures prepared by mixing iron ores of known iron content with quartz and (*b*) flotation concentrates which had been chemically analyzed for their iron content by the authors. The failure of the calibration curve to go through the origin is due to the occurrence of a small peak for this element inherent in the X-ray equipment (see also Fig. 6).

ANALYSIS OF SULPHATE LEACH LIQUORS

Uranium Determination

The X-ray fluorescence technique has also been applied to the analysis of pregnant leach solutions resulting from the leaching of uranium ores or their flotation concentrates with sulphuric acid. The design of the sample holder for liquids is similar to that described by Pish and Huffman (2) except that a polyethylene washer is used and the cell is covered with a piece of 0.0005-inch mylar film. It has been found necessary to replace the mylar film each time that the sample is changed to avoid effects due to uranium adsorption. Liquids are transferred to and from the sample holder by means of a hypodermic syringe equipped with a curved-tip stainless steel needle.

Although strontium is a convenient internal standard to use with solid samples, it is not suitable for use with solutions which contain sulphate ions. An alternative standard, yttrium, has been found to be quite satisfactory for use with sulphate leach liquors. The pegmatitic ores under investigation contain only trace amounts of rare earths and there is no evidence for the presence of yttrium in the ore or sulphate leach solutions. In the event that significant amounts of rare earths were present in the ore, another internal standard such as bromine could be selected. The calibration for the determination of uranium in aqueous solution shown in Fig. 5 was set up by diluting a standard solution of uranyl nitrate and using yttrium nitrate as the internal standard. Aqueous solution samples are prepared for analysis by adding 0.50 ml of stock yttrium nitrate solution (10 mg of yttrium per milliliter) to a 10-ml volumetric flask and diluting to volume with the solution containing dissolved uranium. Relative intensities determined from chart recordings and by direct counting (see Table II for spectrometer settings) were found to agree within estimated experimental error.

The greater precision of the direct-counting method, as compared to that of the chart-recording method of determining relative intensities for samples in the same concentration range, is shown in Table III. The data in Table III also indicate the decrease in precision that occurs in the chart-recording method when the concentration of U_3O_8 in the sample drops below 1 mg/ml. The per cent standard deviation of the intensity ratio determined by direct count for samples containing more than 1 mg/ml of U_3O_8 would undoubtedly be less than the $\pm 2.2\%$ shown for the chart-recording method. Concentrations as low as 0.1 mg U_3O_8 per milliliter can readily be determined by this method.

TABLE III

Comparison of percentage standard deviations in $I(U\,L_{\alpha_1})/I(Y\,K_\alpha)$ determined by chart-recording and by direct-counting methods

Method	No. determinations	Concn. range U_3O_8 in mg/ml	% Standard deviation
Chart record	30	1.0–10	± 2.2
Chart record	15	0.5–1.0	± 10.9
Direct count	15	0.5–1.0	± 3.8
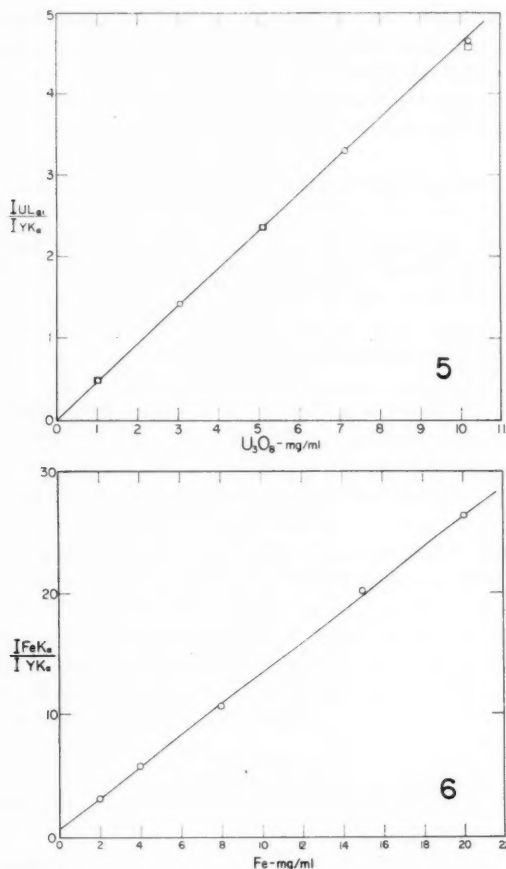
FIG. 5. Calibration for the determination of U_3O_8 in aqueous solutions using yttrium as an internal standard. O Direct-count method.   □ Chart-recording method.
FIG. 6. Calibration for the approximate determination of dissolved iron in aqueous solutions by reference to yttrium internal standard.

No special precautions were taken to provide for additional heat exchangers to prevent temperature changes in the liquid samples during irradiation.

Since the concentration of dissolved iron in sulphate leach liquors varies considerably, the effect of adding varying amounts of iron on the observed $I(U\ L_{a_1})/I(Y\ K_a)$ ratio was studied. Experiments were done in which the iron content of the solutions was varied from 2 to 20 mg/ml. Although the intensities of both the U L_{a_1} and Y K_a lines were decreased as the iron concentration in the solution was increased, the ratio of their intensities was found to be constant within experimental error. This analytical method for uranium can therefore be applied to the analysis of pregnant leach liquors with confidence.

Iron Determination

It is often useful to have at least an approximate idea of the dissolved iron content

in uranium ore leach liquors. Yttrium would not normally be used as an internal standard for iron because of the considerable difference in the wave lengths of their K_α lines. However, since yttrium is already present in the sample for the uranium analysis, a good approximation of the iron content can be made by reference to it. An example of a calibration curve used for such determinations is shown in Fig. 6 (see comment regarding Fig. 4).

Determination of Uranium in an Organic Solvent

In the course of liquid – liquid extraction studies of the recovery of uranium from pregnant leach solutions, many uranium analyses of both aqueous and organic phases are required. Although the ultraviolet fluorimetric method of uranium analysis is usually the most satisfactory one to use in determining the normally small concentrations of uranium remaining in the aqueous phase, it is often cumbersome and inaccurate when applied to the loaded organic phase. If the fluorimetric method is used for the analysis of the organic phase it is generally necessary to back-extract the uranium to an aqueous phase (8), a step which often reduces the accuracy of the determination. An X-ray fluorescence analysis method applied directly to the loaded organic phase does not suffer from this difficulty. Since inorganic substances such as strontium and yttrium are generally not very soluble in the organic liquids that extract uranium, some other internal standard has to be chosen. Bromine in the form of bromobenzene has been suggested for this purpose (2).

Calibrations for the use of bromine as an internal standard are shown in Fig. 7 for both aqueous solutions of uranyl sulphate and for uranium in 0.1 M solutions of tri(iso)-octyl amine in kerosene containing 2.5 volume per cent of n-decyl alcohol. The calibration for aqueous solutions shown in Fig. 7 was obtained by adding 0.50 ml of sodium bromide solution (10 mg Br per milliliter) to a 10-ml volumetric flask and diluting to volume with standard uranyl sulphate solution. The organic solution calibration was obtained by successively extracting 50 ml of standard uranyl sulphate solution (pH adjusted to 1.5 with sulphuric acid) with five 20-ml portions of a 0.1 M solution of tri(iso)octyl amine in kerosene containing 2.5 volume per cent of n-decyl alcohol. (A fluorimetric analysis of the raffinate showed that at least 99.4% of the uranium had
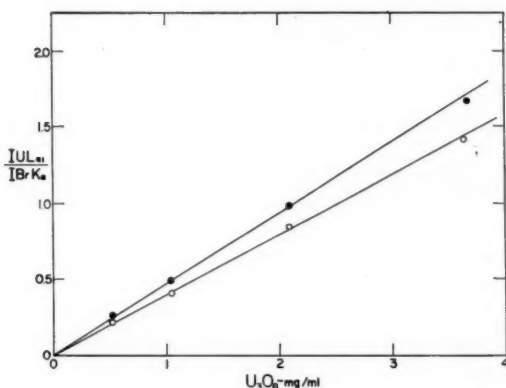
FIG. 7.   Calibrations for the determination of U_3O_8 in aqueous and kerosene solutions with bromine as internal standard.
⬤Aqueous solutions.   ⭘0.1 M tri(iso)octyl amine in kerosene solution.

been extracted to the organic phase.) The organic extracts were combined and a 9.5-ml aliquot taken for analysis along with 0.50 ml of a solution of analyzed bromobenzene in kerosene (10 mg Br per milliliter). As long as the concentration of dissolved uranium (expressed as U_3O_8 equivalent) exceeds 0.1 mg/ml, this method of analyzing aqueous or organic phases is very satisfactory and requires much less time than other standard analytical methods. However, it is necessary to have a calibration for each organic diluent used, as the reflection of X-rays is dependent on the density of the medium (9).

CONCLUSIONS

X-Ray fluorescence analysis greatly reduces the time required for the analysis of flotation concentrates accumulating from pilot plant studies on uranium ores. It is possible to do uranium analyses directly on concentrate samples from a given ore that has been subjected to a standard treatment but, if reliable and more accurate results are required, the addition of an internal standard such as strontium or yttrium and further comminution of the sample is necessary. An approximate analysis for iron in an ore or concentrate can be made by reference to the internal standard used for uranium. The lowest concentration of uranium that can conveniently be determined by X-ray fluorescence analysis of solids is about 0.02% U_3O_8.

Uranium analyses and approximate iron analyses can also very conveniently be done on sulphate leach liquors containing uranium by X-ray fluorescence with reference to a yttrium internal standard. The use of bromine as an internal standard for the determination of uranium in organic solvents is quite satisfactory. The low limit for the accurate determination of uranium in solution is about 0.1 mg of U_3O_8 per milliliter.

X-Ray fluorescence could probably readily be adapted to continuous control analysis in commercial uranium mills.

ACKNOWLEDGMENTS

REFERENCES

1. COPE, J. H.   Norelco Reptr. 3, 41 (1956).
2. PISH, G. and HUFFMAN, A. A.   Anal. Chem. 27, 1875 (1955).
3. KEHL, L. W. and RUSSEL, R. G.   Anal. Chem. 28, 1350 (1956).
4. CLAISSE, F.   Quebec Dept. of Mines, Prelim. Rept. No. 327 (1956).
5. VANCLEAVE, A. B. and EAGER, R. L.   Proc. Second Intern. Conf. Peaceful Uses Atomic Energy, A/CONF. 15/P/230 (1958).
6. CENTANNI, F. A., ROSS, A. M., and DE SESA, M. A.   Anal. Chem. 28, 1651 (1956).
7. NEW BRUNSWICK LABORATORY.   Manual of analytical methods for the determination of uranium and thorium in their ores. 15 (1955).
8. THOMPSON, R. B.   M.Sc. Thesis, University of Saskatchewan. 1957.
9. KOKOTAILO, G. T. and DAMON, G. F.   Anal. Chem. 25, 1185 (1953).

URONIC ACIDS FROM WHITE SPRUCE (PICEA GLAUCA (MOENCH) VOSS)[1]

G. A. ADAMS

ABSTRACT

Acid hydrolysis of extractive-free white spruce wood produced a number of neutral and acidic sugars and oligosaccharides. The acidic components were isolated and three of these were shown to be 4-O-methyl-D-glucuronic acid, 2-O-(4-O-methyl-α-D-glucopyranosyluronic acid)-D-xylose, and tentatively O-(4-O-methyl-α-D-glucopyranosyluronic acid)-(1 → 2)-O-β-D-xylopyranosyl-(1 → 4)-D-xylopyranose.

Investigations of the hemicelluloses of white spruce (*Picea glauca*) have yielded an arabogalactan (1) and a glucomannan (2). Since neither of these fractions contained more than a trace of uronic acids, it seemed likely that the acid components were associated with the xylan portion of the wood. The present communication is concerned with the composition and identification of three uronic acid components isolated from spruce wood by partial hydrolysis.

The uronic acids were obtained by acid hydrolysis of extractive-free white spruce wood and separated from the neutral sugars by adsorption on an anion exchange resin. Further separation of the recovered uronic acid components yielded several fractions of which three (I, II, and III) were identified.

Chromatographic evidence, methoxyl content, and equivalent weight tentatively identified fraction I as 4-O-methyl-D-glucuronic acid. Conversion of the acid to its methyl ester methyl glycoside and reduction with lithium aluminum hydride yielded 4-O-methyl-D-glucose, which was characterized as crystalline 4-O-methyl-D-glucose phenylosazone.

Hydrolysis of fraction II and chromatographic examination of the hydrolyzate indicated the presence of D-xylose and 4-O-methyl-D-glucuronic acid. Reduction of the ester glycoside gave the corresponding disaccharide glycoside which on hydrolysis yielded crystalline D-xylose and 4-O-methyl-D-glucose, the latter being identified as its crystalline phenylosazone. The point of attachment of the 4-O-methyl-D-glucuronic acid to the D-xylose residue was determined by methylation studies. The aldobiouronic acid methyl ester, methyl glycoside, was converted to methyl-O-(4-O-methyl-D-gluco-pyranosyl)-D-xyloside by reduction with lithium aluminum hydride and the product was then fully methylated. On hydrolysis it yielded 3,4-di-O-methyl-D-xylose and 2,3,4,6-tetra-O-methyl-D-glucose thus proving that the acid was attached glycosidically to $C_{(2)}$ of the xylose residue. Recent evidence has established that the glycosidic bond in this aldobiouronic acid is in the α configuration (3). These findings showed that the aldobiouronic acid was 2-O-(4-O-methyl-α-D-glucopyranosyluronic acid)-D-xylopyranose.

The aldotriouronic acid (fraction III) was composed of 4-O-methyl-D-glucuronic acid and D-xylose and had $[\alpha]_D^{25}$ +59°. It could not be obtained in crystalline form. The attachment of the 4-O-methyl-D-glucuronic acid and the xylose units to one another was determined by methylation studies. The aldotriouronic acid was converted to its corresponding methyl ester methyl glycoside by treatment with 1% methanolic hydrogen chloride at room temperature. Reduction with lithium aluminum hydride provided the

glycoside of the trisaccharide which was methylated with methyl iodide and silver oxide. Hydrolysis of the fully methylated trisaccharide yielded approximately equimolecular quantities of 2,3,4,6-tetra-O-methyl-D-glucose, 2,3-di-O-methyl-D-xylose, and 3,4-di-O-methyl-D-xylose. The lower rotation of the aldotriouronic acid ($+59°$) as compared to that of the aldobiouronic acid ($+97°$) indicated that the xylobiose moiety in the former had a negative rotation and its glycosidic linkage was β. The foregoing findings established the aldotriouronic acid tentatively as O-(4-O-methyl-α-D-glucopyranosyluronic acid)-$(1 \rightarrow 2)$-O-β-D-xylopyranosyl-$(1 \rightarrow 4)$-D-xylopyranose.

The aldobiouronic acid, 2-O-(4-O-methyl-α-D-glucopyranosyluronic acid)-D-xylose, is the most common uronic component of wood. Its presence was first suggested in oak wood (4) and in 1952 it was identified in aspen wood (5). Since that time it has been found in all woods examined for it including both coniferous (6–13) and deciduous species (14–21).

Aldotriouronic acids containing 4-O-methyl-D-glucuronic acid and D-xylose have been isolated from aspen wood (17) in crystalline form and from Monterey pine (22), although the structures have not been reported. The aldotriouronic acid, O-(4-O-methyl-α-D-glucopyranosyluronic acid)-$(1 \rightarrow 2)$-O-β-D-xylopyranosyl-$(1 \rightarrow 4)$-D-xylose, has been obtained in crystalline form from western hemlock (23) and jute (24). The present aldotriouronic acid of white spruce, although not obtained in crystalline form, has a chemical structure identical with the crystalline uronic acids of western hemlock and jute.

It was pointed out in an earlier publication (25) that the presence of a methyl ether substituent on $C_{(4)}$ of the glucuronic acid is associated with glycosidic attachment to $C_{(2)}$ of the xylose unit. Recently Brasch and Wise have isolated 3-O-α-(4-O-methyl-D-glucuronosyl)-D-xylose from Monterey pine (13) and have suggested that it may be a component of other woods; however, careful examination of the hydrolyzate from white spruce has not revealed the presence of this component.

EXPERIMENTAL

All specific rotations were equilibrium values unless otherwise stated and melting points are corrected.

Paper Chromatography

Chromatographic separations were carried out by the descending method on Whatman No. 1 paper using the following solvents: (A) ethyl acetate:pyridine:water (2:1:2); (B) ethyl acetate:acetic acid:formic acid:water (19:3:1:4); and (C) ethanol:benzene:water (47:200:15). A 3% solution of p-anisidine hydrochloride in ethanol was used as the spray reagent.

Preparation of Uronic Acids

White spruce wood (*Picea glauca* (Moench) Voss) was reduced to shavings and rendered extractive-free as previously described (26). The wood (500 g) was heated with 0.5 N sulphuric acid (7000 ml) at a temperature of 94° C until the reducing power became constant (9 hours). The hot solution of sugars and sugar acids was recovered by filtration through a sintered glass filter (porosity C) and the wood residue was washed free of acid. The hydrolyzate and washings were brought to pH 6.0 by careful addition of barium hydroxide and barium carbonate. The barium sulphate was removed by filtration and the solution and washings were passed through a column of Amberlite IR-120 resin to remove cations. The uronic acid components were then absorbed on a column of Dowex 1-X⁴ (acetate form) (30×180 mm). The column was washed with water until the eluate gave a negative anthrone test for sugars. Electrophoretic examination of the

washings on paper in 0.025 N sodium bicarbonate solution showed no trace of uronic acids. The uronic acid components were eluted from the column by 0.1 N formic acid and were collected by an automatic fraction collector in 200 tubes (13 ml in each tube). Chromatographic examination of the recovered fractions in solvent B showed that only minor separation of four major components had been achieved. The major fraction (tubes 41–80) contained 74% of the material put on the column. Further separation of this fraction was carried out on a cellulose column (30 mm × 450 mm) using solvent B. Four main fractions were obtained having R_x values (movement relative to that of xylose) as follows: 0.49, 0.64, 0.93, 1.16. Paper chromatographic examination (solvent B) showed that one fraction (R_x 0.49) was a mixture of two components. The eluting solvent was partly removed by evaporation at 40° C under reduced pressure and the aqueous solution of the residual uronic acid extracted thoroughly with ether to remove formic acid. Freeze drying of the aqueous solution yielded the uronic acids as white porous solids. Three fractions having the following properties were recovered: fraction I (0.222 g); R_x 1.16 (solvent B); $[\alpha]_D^{25}$ +48.6°; methoxyl 14.9; acid equivalent 205 (calculated for $C_7H_{12}O_7$, methoxyl 14.9%; acid equivalent 208). Fraction II (0.816 g); R_x 0.93 (solvent B); $[\alpha]_D^{25}$ +97°; methoxyl 9.4%; acid equivalent 340 (calculated for $C_{12}H_{20}O_{11}$, methoxyl 9.1%; acid equivalent 340). Fraction III (0.988 g); R_x 0.64 (solvent B); $[\alpha]_D^{25}$ +59°; methoxyl 6.1%; acid equivalent 510 (calculated for $C_{17}H_{28}O_{16}$, methoxyl 6.54%; acid equivalent 472).

Hydrolysis Products of Uronic Acid Fractions

Samples of fractions II and III (approximately 10 mg each) were heated in sealed tubes with 4 ml of methanolic hydrogen chloride (8%) for 10 hours at 80° C. After removal of solvent, hydrolysis was continued with N hydrochloric acid for 12 hours at 100° C. Chromatograms of the hydrolyzates in solvent A and B showed the presence of D-xylose and 4-O-methyl-D-glucuronic acid. On the basis of chromatographic comparison in solvent B with a known reference, fraction I was identified tentatively as 4-O-methyl-D-glucuronic acid.

Examination of the Uronic Acid Fractions

4-O-Methyl-D-glucuronic Acid (Fraction I)

The acid (113 mg) was converted to its methyl ester methyl glycoside by heating in a sealed glass tube with 15 ml of methanolic hydrogen chloride (3%) for 10 hours at 80° C. The product (123 mg) was dissolved in dry tetrahydrofuran (25 ml) and the solution was added dropwise over a period of 1 hour to a stirred suspension of lithium aluminum hydride (500 mg) in tetrahydrofuran (25 ml). The reaction mixture was refluxed gently for 1 hour, cooled, and the unused lithium aluminum hydride was decomposed by addition of ethyl acetate and finally water. After filtration, concentration, and deionization by Amberlite IR-120 and Amberlite IR-4B the glycoside of the monosaccharide was recovered (112 mg). Hydrolysis by 0.5 N hydrochloric acid (6 ml) in a sealed glass tube at 100° C for 8 hours yielded 4-O-methyl-D-glucose, as shown by chromatographic examination of the neutralized hydrolyzate in solvent A.

The phenylosazone of 4-O-methyl-D-glucose was prepared by heating the sugar (88 mg) with water (2.0 ml), acetic acid (0.3 ml), and phenylhydrazine (0.5 ml) for 1 hour at 90° C. The recovered 4-O-methyl-D-glucose phenylosazone was recrystallized from benzene and had a m.p. and mixed m.p. of 158–159° C (27).

2-O-(4-O-Methyl-α-D-glucopyranosyluronic Acid)-D-xylose (Fraction II)

Identification of the constituents of the aldobiouronic acid was made as follows: the aldobiouronic acid (370 mg) was converted to the methyl ester methyl glycoside (390

mg) and reduced by lithium aluminum hydride to the glycoside of its corresponding disaccharide (398 mg) by the methods described above. Hydrolysis with 0.5 N hydrochloric acid yielded a syrup (383 mg) which on chromatographic examination in solvent A was found to contain D-xylose and 4-O-methyl-D-glucose. A portion of the mixture (250 mg) was separated on a Celite column (28) (35 mm × 160 mm) using butanol saturated with water as the eluting solvent. Xylose (89 mg) was obtained in crystalline form and on recrystallization from methanol had a m.p. and mixed m.p. of 142–143° and $[\alpha]_D^{25}$ +19.2° (c, 1.7% in water). The syrupy 4-O-methyl-D-glucose (115 mg), $[\alpha]_D^{25}$ +60.1 (c, 2.3% in water) methoxyl 15.6% (calculated for $C_7H_{14}O_6$, methoxyl 16.0%), was converted to its crystalline phenylosazone. The 4-O-methyl-D-glucose phenylosazone on recrystallization from 25% aqueous acetone solution had a m.p. of 158–159° C.

Conversion of Aldobiouronic Acid to Disaccharide

The aldobiouronic acid (896 mg) was converted to its methyl glycoside methyl ester by refluxing with 2% methanolic hydrogen chloride (30 ml) for 8 hours. The methyl ester methyl glycoside (924 mg) in tetrahydrofuran solution (25 ml) was reduced by lithium aluminum hydride (1 g) to the glycoside of the neutral disaccharide (842 mg) $[\alpha]_D^{25}$ +95° (c, 1.29% in water).

Methylation of the Glycoside of 4-O-Methyl-D-glucosyl-D-xylose

The disaccharide (842 mg) was dissolved in 20% sodium hydroxide (10 ml) and methylated by the simultaneous dropwise addition of 45% sodium hydroxide and dimethyl sulphate 30 ml; two additional methylations were carried out prior to the recovery of the product. The reaction mixture was heated at 95° for 1 hour, cooled, acidified with sulphuric acid to pH 5.0, and extracted with chloroform. Evaporation of the chloroform yielded a syrup (805 mg). The infrared spectrum of this product indicated that a small amount of free hydroxyl groups was still present. One methylation with Purdie's reagents, methyl iodide (25 ml) and silver oxide (10 g), yielded a syrup (798 mg) having no free hydroxyl groups as shown by its infrared spectrum. Anal. Calc. for $C_{18}H_{34}O_{10}$: OCH_3, 52.9%. Found: OCH_3, 51.9%.

Hydrolysis of Methyl-2-O-(2,3,4,6-tetra-O-methyl-D-glucopyranosyl)-3,4-di-O-methyl-D-xyloside and Recovery of Methylated Sugars

The methylated disaccharide (798 mg) was dissolved in 8% methanolic hydrogen chloride (25 ml) and refluxed gently for 18 hours. Solvent was removed and the hydrolysis was continued in 0.5 N hydrochloric acid (20 ml) for 9 hours at 100° C. The hydrolyzate was neutralized with silver carbonate, deionized by Amberlite IR-120 resin and Amberlite IR-4B resin, and concentrated in vacuo to a clear syrup (584 mg). Chromatographic examination of the syrup in solvent C revealed two spots similar in mobility and color reaction to 3,4-di-O-methyl-D-xylose and 2,3,4,6-tetra-O-methyl-D-glucose. The sugars were separated on a Celite column (30 mm × 350 mm) using butanol saturated with water to give 3,4-di-O-methyl-D-xylose (120 mg) and 2,3,4,6-tetra-O-methyl-D-glucose (281 mg).

Identification of 3,4-Di-O-methyl-D-xylose

The clear syrup had $[\alpha]_D^{25}$ +21±1° (c, 1.0% in water); methoxyl content calculated for $C_7H_{14}O_5$: 34.8%; found: OCH_3, 34.8%. Chromatographic examination in solvent C showed that the syrup had the same R_g value (0.38) as 3,4-di-O-methyl-D-xylose and was easily distinguished from the 2,3- and 2,4-isomers (R_g values 0.31 and 0.27 respectively). Electrophoresis (29) in borate buffer using the same reference sugars showed

that the unknown sugar had the same mobility as 3,4-di-O-methyl-D-xylose. The sugar (71 mg) water (1.5 ml) containing barium carbonate (65 mg) was oxidized in the dark with bromine (0.6 ml) for 48 hours. The bromine was removed by aeration, and the solution was extracted continuously with chloroform for 48 hours. The syrup which was recovered from the chloroform extract was distilled, boiling point (bath temp.) 120–150° (0.02–0.018 mm), and on seeding with 3,4-di-O-methyl-D-xylono-δ-lactone, crystallization occurred. Recrystallization from ether solution to which a few drops of hexane were added yielded 3,4-di-O-methyl-D-xylono-δ-lactone, m.p. and mixed m.p. 66–67° C, $[\alpha]_D^{25}$ $-22°\pm1°$ (c, 1.0 in water) (30).

Identification of 2,3,4,6-Tetra-O-methyl-D-glucose

The clear syrup recovered from the Celite column crystallized on seeding with 2,3,4,6-tetra-O-methyl-D-glucose. Recrystallization from ether – petroleum ether solution gave needles having m.p. and mixed m.p. 94–96° C and $[\alpha]_D^{25}$ $+84°\pm2°$ (c, 1.07 in water). A methanolic solution of the sugar (52 mg) was refluxed with aniline (25.4 mg) for 2 hours to give crystalline 2,3,4,6-tetra-O-methyl-N-phenyl-D-glucosylamine which on recrystallization from hexane had m.p. and mixed m.p. 134–136° C, $[\alpha]_D^{25}$ $+239°\pm1°$ (c, 1% in chloroform) (31).

Characterization of O-4-O-Methyl-α-D-glucopyranosyluronic Acid-(1 → 2)-O-β-D-xylo-pyranosyl-(1 → 4)-D-xylose (Fraction III)

Attempts to crystallize the aldotriouronic acid were unsuccessful. The acid (500 mg) was converted to its methyl glycoside methyl ester by reacting with 1% methanolic chloride (10 ml) at room temperature. Within 5 hours the specific rotation had become constant and the solution no longer reduced Fehling's solution. Chromatographic examination in solvent C showed only one component and hence no hydrolysis had occurred. The methyl ester methyl glycoside (481 mg) was reacted with diazomethane in methanol solution to assure esterification of all carboxyl groups. Reduction with lithium aluminum hydride in tetrahydrofuran solution yielded the glycoside of the neutral trisaccharide (493 mg).

Methylation of Methyl[O-4-O-methyl-α-D-glucopyranosyl-(1 → 2)-O-β-D-xylopyranosyl-(1 → 4)]-D-xyloside

The trisaccharide (493 mg) was dissolved in methanol (10 ml) and methylated with methyl iodide (30 ml) and silver oxide (6 g) by refluxing 20 hours. After the third methylation the product was completely soluble in methyl iodide. Five methylations yielded a brownish syrup (315 mg) having no free hydroxyl groups as shown by its infrared spectrum. Anal. Calc. for $C_{25}H_{46}O_{14}$: OCH₃, 48.9. Found: OCH₃, 46.8; $[\alpha]_D^{25}$ $+52.9°$ (c, 1% in methanol).

Hydrolysis of Methyl[O-2,3,4,6-tetra-O-methyl-α-D-glucopyranosyl-(1 → 2)-O-β-3,4-di-O-methyl-D-xylosyl-(1 → 4)]-2,3-di-O-methyl-D-xyloside

The methylated trisaccharide (300 mg) was dissolved in 8% methanolic hydrogen chloride and refluxed for 12 hours; after removal of the solvents, the hydrolysis was completed by heating in 0.5 N hydrochloric acid for 8 hours. Recovery after neutralization with Amberlite IR-4B yielded a clear syrup (230 mg). Chromatographic examination in solvent C showed the presence of three sugars which corresponded in color reaction and rate of movement to authentic samples of 2,3-di-O-methyl-D-xylose, 3,4-di-O-methyl-D-xylose, and 2,3,4,6-tetra-O-methyl-D-glucose. The methylated sugars were separated on sheets of Whatman No. 1 filter paper using solvent C. Elution of the paper

strips with methanol yielded solutions of the crude syrups which were filtered and then dried to constant weight. Yields: 2,3,4,6-tetra-O-methyl-D-glucose, 69.8 mg; 3,4-di-O-methyl-D-xylose, 48.3 mg; and 2,3-di-O-methyl-D-xylose, 42.6 mg.

Identification of Component Sugars

3,4-Di-O-methyl-D-xylose.—The colorless syrup had $[\alpha]_D^{25}$ +22.2° (c, 1.20% in methanol) and the R_g values in solvent C were identical with those of an authentic sample of 3,4-di-O-methyl-D-xylose. Anal. Calc. for $C_7H_{14}O_5$: OCH_3, 34.8. Found: OCH_3, 34.4. Bromine oxidation as described above yielded crystalline 3,4-di-O-methyl-D-xylono-δ-lactone, m.p. 66–67° C, $[\alpha]_D^{25}$ −21° (c, 1% in water).

2,3-Di-O-methyl-D-xylose.—This sugar had $[\alpha]_D^{25}$ +20.8° (c, 1.06% in methanol). Anal. Calc. for $C_7H_{14}O_5$: OCH_3, 34.8. Found: OCH_3, 34.6. The R_g value in solvent C was identical with that of 2,3-di-O-methyl-D-xylose. Conversion to the anilide provided crystalline 2,3-di-O-methyl-N-phenyl-D-xylosylamine, m.p. and mixed m.p. 123–124° C and $[\alpha]_D^{25}$ +188 (c, 0.5% in ethyl acetate) (32).

2,3,4,6-Tetra-O-methyl-D-glucose.—The rate of movement of this sugar on paper strips in solvent C was the same as that of an authentic sample of 2,3,4,6-tetra-O-methyl-D-glucose. Refluxing with aniline in methanolic solution provided the characteristic crystalline 2,3,4,6-tetra-O-methyl-N-phenyl-D-glycosylamine which on recrystallization from hexane had a m.p. and mixed m.p. of 134–136° C, $[\alpha]_D^{25}$ +235±1° (c, 1.1% in chloroform).

ACKNOWLEDGMENT

REFERENCES

1. ADAMS, G. A.   Can. J. Chem. **36**, 755 (1958).
2. TIMELL, T. E. and TYMINSKI, A.   Tappi, **40**, 519 (1957).
3. GORIN, P. A. J. and PERLIN, A. S.   Can. J. Chem. **36**, 999 (1958).
4. O'DWYER, M. H.   Biochem. J. **28**, 2116 (1934).
5. JONES, J. K. N. and WISE, L. E.   J. Chem. Soc. 2750 (1952).
6. GORROD, A. R. N. and JONES, J. K. N.   J. Chem. Soc. 2522 (1954).
7. BALL, D. H., JONES, J. K. N., NICHOLSON, W. H., and PAINTER, T. J.   Tappi, **39**, 438 (1956).
8. JONES, J. K. N. and PAINTER, T. J.   J. Chem. Soc. 669 (1957).
9. ASPINALL, G. O. and McKAY, J. E.   J. Chem. Soc. 1059 (1958).
10. DUTTON, G. G. S. and SMITH, F.   J. Am. Chem. Soc. **78**, 2505 (1957).
11. HAMILTON, J. K. and THOMPSON, N. S.   J. Am. Chem. Soc. **79**, 6464 (1957).
12. ASPINALL, G. O. and CARTER, M. E.   J. Chem. Soc. 3744 (1956).
13. BRASCH, D. J. and WISE, L. E.   Tappi, **39**, 768 (1956).
14. GILLHAM, J. K. and TIMELL, T. E.   Can. J. Chem. **36**, 410 (1958).
15. JONES, J. K. N. and WISE, L. E.   J. Chem. Soc. 2750, 3389 (1952).
16. JONES, J. K. N., MERLER, E., and WISE, L. E.   Can. J. Chem. **35**, 634 (1956).
17. MILKS, J. E. and PURVES, C. B.   J. Am. Chem. Soc. **78**, 3738 (1956).
18. ASPINALL, G. O., HIRST, E. L., and MAHOMED, R. S.   J. Chem. Soc. 1734 (1954).
19. ADAMS, G. A.   Can. J. Chem. **35**, 556 (1957).
20. GLAUDEMANS, C. P. J. and TIMELL, T. E.   J. Am. Chem. Soc. **80**, 941 (1958).
21. SAARNIO, J., WATHEM, K., and GUSTAFSSON, C.   Acta Chem. Scand. **8**, 825 (1954).
22. BRASCH, D. J. and WISE, G. E.   Tappi, **39**, 581 (1956).
23. HAMILTON, J. K. and THOMPSON, N. S.   J. Am. Chem. Soc. **79**, 6464 (1957).
24. SRIVASTAVA, H. C. and ADAMS, G. A.   (In press).
25. ADAMS, G. A. and BISHOP, C. T.   J. Am. Chem. Soc. **78**, 2842 (1956).
26. ADAMS, G. A.   Tappi, **40**, 721 (1957).
27. SMITH, F.   J. Chem. Soc. 2646 (1951).
28. LEMIEUX, R. U., BISHOP, C. T., and PELLETIER, G. E.   Can. J. Chem. **34**, 1365 (1956).
29. CONSDEN, R. and STANIER, W. M.   Nature, **169**, 783 (1952).
30. JAMES, S. P. and SMITH, F.   J. Chem. Soc. 739 (1945).
31. IRVINE, J. C. and MOODIE, A. M.   J. Chem. Soc. **93**, 95 (1908).
32. EHRENTHAL, I., RAFIQUE, M. C., and SMITH, F.   J. Am. Chem. Soc. **74**, 1341 (1952).

PHOTOCHEMICAL SEPARATION OF MERCURY ISOTOPES

II. THE REACTION OF Hg^{202}6($^3P_1$) ATOMS, PHOTOEXCITED IN NATURAL MERCURY VAPOR, WITH WATER VAPOR AND OTHER HgO-FORMING SUBSTRATES[1]

R. Pertel[2] and H. E. Gunning[3]

ABSTRACT

An investigation has been made of the reaction of Hg^{202}($^3P_1$) atoms, photoexcited in natural mercury vapor, with several HgO-forming substrates, including water vapor, nitrous oxide, and oxygen. The reactions were carried out under flow conditions at room temperature. Emphasis has been placed on the Hg^{202} content of the HgO product. Enrichment in Hg^{202} would be evidence of the primary formation of a mercury compound.

In the reactions with nitrous oxide and oxygen, it was found that the HgO product contained the normal abundance of Hg^{202}. With water vapor, a product containing up to 35% Hg^{202} was obtained, compared to the normal abundance of 29.8%. The addition of 1,3-butadiene to the water vapor substrate was found to have a marked effect on the enrichment in Hg^{202} in the HgO product. A product containing 85% Hg^{202} was recovered when the substrate contained 21 mole % of added butadiene. A systematic study of the effect of butadiene concentration on the enrichment reaction showed that the Hg^{202} content remains constant for butadiene concentrations exceeding approximately 10 mole %. The water–butadiene reaction is recommended as a simple method for preparing Hg^{202} from natural mercury.

The factors influencing the enrichment process are discussed, together with the significance of the results with respect to the mechanisms of decomposition of the molecules studied.

INTRODUCTION

In the mercury-6($^3P_1$)-photosensitized decomposition of certain gaseous oxygen-containing compounds, HgO is formed as a product of the reaction. Important among such substrates are water vapor, oxygen, and nitrous oxide. Through the technique of monoisotopic photosensitization, it is possible to obtain information on the extent to which a mercury compound is formed in the primary process. Thus, in the water reaction, if a single isotope specie, Hg^i, is photoexcited in the natural mercury vapor (Hg^N) present in the reaction cell, it is possible to distinguish between primary processes of the type:

$$\text{Hg}^i 6(^3P_1) + \text{HOH} \rightarrow \text{Hg}^i \text{OH} + \text{H} \qquad [1]$$

and

$$\text{Hg}^i 6(^3P_1) + \text{HOH} \rightarrow \text{H} + \text{OH} + \text{Hg}^i 6(^1S_0), \qquad [2]$$
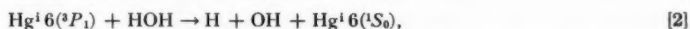
since reaction [1] could lead to the formation of an HgO enriched in the exciting isotope.

The reaction of Hg^{198}6($^3P_1$) atoms, in Hg^N, with HOH–N$_2$ mixtures has been studied previously (1). The HgO was found to contain 15% Hg^{198}, compared to the natural abundance of 10.0%. The photoexcitation of Hg^{198}6($^3P_1$) atoms in Hg^N is complicated by the juxtaposition of the 201b of Hg^{201} in the h.f.s. of Hg^N. Some excitation of Hg^{201}6($^3P_1$) atoms in Hg^N would be expected in irradiation with an Hg^{198} source. The experimental and theoretical aspects of the photoexcitation of single mercury isotopes in Hg^N has been discussed in an earlier study (2).

Zellikoff, Aschenbrand, and Wyckoff (3) have made a preliminary study of the reaction of Hg^{202}6($^3P_1$) atoms, in Hg^N, with HOH–N$_2$ mixtures. At low substrate pressures the HgO product was found to contain 35% Hg^{202}, compared to the natural abundance of 29.8%.

In the present investigation, major emphasis has been placed on the reaction of Hg^{202}6($^3P_1$) atoms with water vapor. Certain of our preliminary findings have already

been published (4, 5). Experimental conditions have been sought which yield maximum enrichment in Hg^{202} in the HgO product of the reaction. In addition to the information on reaction mechanism which can be obtained from such a study, it was hoped that the reaction could be developed into a simple method for proliferating mercury isotopes.

Preliminary data are also reported on the reaction of $Hg^{202}6(^3P_1)$ atoms with O_2 and N_2O, in order to assess the importance of primary HgO formation in these reactions.

The details of the investigation follow.

EXPERIMENTAL

The reactions were carried out under flow conditions, at room temperature, in a high-vacuum system. The reaction cell consisted of a 5-coil helix, fashioned of 12 mm O.D. optical quartz. The cell was attached to the flow system by standard tapers. For the light source, a quartz electrodeless discharge was used, 8 mm O.D., 150 mm in length, containing a few milligrams of 98.3% Hg^{202}. The discharge was sustained with a Baird Microwave Exciter, operating at a wavelength of 12.2 cm. The lamp was maintained at 25.0° C by being enclosed in a jacket of Vycor 7910 glass, through which thermostatted distilled water was circulated. The lamp-water jacket assembly was axially disposed within the coils of the spiral reaction cell. The microwave reflector was placed a few centimeters from the reaction cell.

Flow rates were measured with calibrated, U-shaped manometers containing dibutyl phthalate. The flow rates were expressed in milliliters per minute at 25° C and 760 mm pressure. Hoke high-vacuum needle valves served to control the flow rate.

Efficient mercury vapor saturation of the substrate gases was achieved by allowing the gases to pass through an operating, umbrella-type, mercury diffusion pump. The partial pressure of mercury vapor in the gas stream was controlled by circulating thermostatted water through the jacket of the mercury diffusion pump.

Small Emil Greiner vernier manometers were used to measure pressures in the reaction zone.

In the water reaction, difficulty was encountered in maintaining a constant pressure of water vapor under flow conditions. This problem was partially solved by installing a water reflux assembly with two 60-cm Graham Coil condensers in series, with a spray trap at the top of the reflux unit, connecting to the flow system. The vapor pressure of water in the stream was controlled by circulating water from a thermostat through the condenser jackets.

The gases used were the highest purity grades obtainable from the Mathieson Company. The nitrous oxide and butadiene were further purified by trap-to-trap distillation. When gas mixtures were used, the mole ratio was controlled by separate flow control units. Samples of the gas mixtures were analyzed by low temperature distillation.

The HgO deposits were removed from the cell by solution in hydrochloric acid. The mercury was recovered from the neutralized solution by deposition on gold wire. The fraction of Hg^{202} in the recovered mercury was determined, by Resonance Radiation Absorbiometry. The method has been described elsewhere (6).

RESULTS

Calibration of Isotope Analysis Unit

The analytical unit was repeatedly calibrated, during the course of the investigation, by determining the absorption of the radiation from the Hg^{202} source by a sample of

Hg^N in the absorption cell. Aminco, style F, calibrated, fused quartz absorption cells with path length of 0.1003 cm were used throughout the study. The temperature of the Hg^N in the absorption cell was varied from 10° C to 40° C in the calibration runs. The mercury vapor pressure data used were those of Busey and Giauque (7), as in the original investigation on the analytical method (6). The natural abundance of Hg^{202} was taken to be 29.80% (8). The validity of the calibration is dependent upon the shape of the emission line from the Hg^{202} source. There must be negligible overlap of the emission line on absorption contours adjacent to that of Hg^{202}. In order to check this point, AEC-enriched samples, containing up to 98.5% Hg^{202}, were analyzed, using the afore-mentioned method of calibration. The deviation from the mass spectrometric values on the samples did not exceed 2%.

Nitrous Oxide

Data obtained over the pressure range 2–102 mm are shown in Table I. For these runs the mean percentage of Hg^{202} in the oxide is 29.8±0.9%. These data would suggest that HgO is not formed in the primary process in the nitrous oxide reaction. It should be emphasized, however, that failure to find enrichment in the exciting isotope in the HgO is not unequivocal proof that primary formation of HgO is absent. This matter will be discussed in a later section of this paper.

TABLE I

Hg^{202} enrichment in the HgO product of the reaction of Hg$^{202}6(^3P_1)$ atoms in Hg^N with nitrous oxide under flow conditions

Pressure, mm	Temp., °C	Flow rate ml/min at 25° and 760 mm	% Hg^{202} in HgO
2.2	29	80	29.0
21.1	34	47.2	30.3
26.0	28	36	29.3
100	30	50	28.8
102	29	—	31.6
		Average	29.8±0.9

At reaction pressures less than one millimeter the apparent percentage of Hg^{202} in the HgO product was found to vary from 21.5% to 27.8%. The most reasonable explanation of these subnormal values is that there was insufficient mercury from the HgO product to achieve equilibrium vapor pressure in the absorption cell. The product yield was observed to be small at low pressures, owing, presumably, to incomplete quenching.

Oxygen

The enrichment data for dry oxygen and oxygen–nitrogen mixtures are shown in Table II. Copious HgO formation was observed at all pressures studied. No problem was therefore encountered in obtaining sufficient material for analysis.

From the data in Table II, it is apparent that there is no evidence for Hg^{202} enrichment in the HgO product of the reaction of Hg$^{202}6(^3P_1)$ with oxygen and oxygen–nitrogen mixtures. The mean value of 30.2±1.2 can be considered, within the experimental error, as normal abundance. There is, therefore, no evidence for primary HgO formation from these data.

TABLE II

Hg^{202} enrichment in the HgO product of the reaction of Hg$^{202}6(^3P_1)$ atoms in Hg^N with oxygen and oxygen–nitrogen mixtures

Pressure, mm	Temp., °C	Comp. mole %		Flow rate ml/min at 25° and 760 mm	% Hg^{202} in HgO
		O$_2$	N$_2$		
6.8	30	100	0	22.8	30.1
14.7	30	100	0	36.8	29.7
23.0	28	100	0	140.8	30.3
24.6	32	100	0	74.5	31.5
0.015	27	21	79	—	31.9
9.5	28	24.2	75.8	26.2	31.3
13.7	30	30.6	69.4	43.3	28.6
14.8	27	51.4	48.6	63.3	28.1
				Average	30.2±1.2

Water Vapor

In the initial work on the reaction of water vapor with Hg$^{202}6(^3P_1)$ atoms, a number of exploratory runs were made in order to test various hypotheses, and to confirm the findings of the previous study (3). In all runs, the total pressure was kept low, in order to avoid broadening effects in absorption (2).

In these preliminary runs, the flow rates varied appreciably during the course of a run, and the rates given are averaged values. Both nitrogen and helium were used as carrier gases, in order to ascertain whether the ability of nitrogen to induce 6($^3P_0$) atom formation in mercury would be significant in the enrichment process.

Several runs were made in which gases were added to suppress the secondary formation of Hg^{N}O. Thus NO was added to combine with free oxygen atoms, since the latter are capable of forming Hg^{N}O with the Hg^N in the gas stream.

Isobutane was used as the carrier gas in one series, as a possible method of reducing the concentration of H atoms and OH radicals in the reaction zone, by abstraction reactions of the type:

$$H + C_4H_{10} \rightarrow H_2 + C_4H_9, \qquad [3]$$

$$OH + C_4H_{10} \rightarrow HOH + C_4H_9. \qquad [4]$$

Unfortunately the addition of isobutane to the stream resulted in a rapid reduction of the HgO product to Hg, and hence insufficient product was recovered for analysis.

Data representative of a large number of runs are given in Table III.

TABLE III

Hg^{202} enrichment in the HgO product of the reaction of Hg$^{202}6(^3P_1)$ atoms in Hg^N with water vapor

Pressure, mm	Temp., °C	Comp. mole %		Flow rate ml/min at 25° C and 760 mm	% Hg^{202} in HgO
		HOH	Carrier		
8.9	28	100	0	20	34.7
10.2	26	100	0	15	32.1
11.4	29	50	50 (He)	33	31.3
13.3	33	50	50 (N$_2$)	42	33.5
15.4	32	50	50 (N$_2$)	53	30.7
9.0	26	28	72*	24	30.3

*Carrier gas contained 29% N$_2$ and 43% NO.

As can be seen from Table III, the percentage of Hg^{202} in the HgO product varied from 30–35%. Carrier gases were not found to play an advantageous role. Later in this paper data will be presented which suggest that the variation in the isotopic abundance of Hg^{202} in the HgO product is intimately associated with the method of recovering mercury from the product. Our findings at this stage of the investigation were in general agreement with those of Zelikoff, Aschenbrand, and Wyckoff (3).

Since it appeared probable that the enrichment in Hg^{202} arose from the formation of $Hg^{202}OH$, from reaction [1] the failure to obtain pure $Hg^{202}O$ could be due to the secondary formation of $Hg^{N}OH$ by interaction of OH radicals formed in [2], with the Hg^{N} always present in the reaction zone:

$$Hg^{N} + OH + M \rightarrow Hg^{N}OH + M. \qquad [5]$$
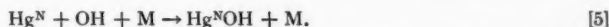
It is conceivable that reaction [1] is the only primary process under which conditions the degradation of the $Hg^{202}OH$ could arise from exchange reactions of the type:

$$Hg^{202}OH + Hg^{N} \rightarrow Hg^{N}OH + Hg^{202}. \qquad [6]$$
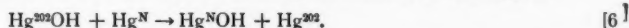
Butadiene would be expected to react rapidly with OH radicals, and also possibly with $Hg^{202}OH$, since the latter should have free-radical character. Studies were therefore undertaken with water–butadiene mixtures as a possible means for suppressing the isotopically degradative reactions [5] and [6]. The remarkable effect of the addition of butadiene to the reaction stream is shown in Table IV for runs of 90-minute duration.

From Table IV, it can be seen that the addition of butadiene to the gas stream has resulted in a marked increase in the Hg^{202} content of the HgO product. During these runs, it was observed that a thin film of polymer formed on the walls of the spiral cell. The mercury-6($^3P_1$)-sensitized decomposition of 1,3-butadiene was investigated by Gunning and Steacie (9). These authors showed that butadiene does not polymerize under flow conditions, since free radicals are not formed in the primary process. The presence of butadiene polymer would therefore be evidence, in our study, of the formation of free radicals in the water decomposition.

TABLE IV

Hg^{202} enrichment in the HgO product of the reaction of $Hg^{202}6(^3P_1)$ atoms in Hg^{N} with water vapor – 1,3-butadiene mixtures

Pressure, mm	Temp., °C	Comp. mole %		Flow rate ml/min at 25° C and 760 mm	% Hg^{202} in HgO
		HOH	C_4H_6		
5.3	25	96	4	12.2	78
5.1	25	94	6	21.8	84
9.8	30	93	7	51.5	72
8.5	24	93	7	22.4	75
8.4	27	79	21	34.8	85
17.1	28	75	25	69.7	70
8.5	28	46	54	45.3	66
8.6	24		~100*	21.5	32.5
11.7	27	45	10†	60.8	75

*There may have been a trace of moisture in the butadiene.
†45% Nitrogen added, 45-minute exposure.

In a reaction of this type, there are many variables which require systematic study: i.e. flow rate, pressure, reaction temperature, water-to-butadiene ratio, product-recovery methods, etc. These studies will form the basis of further investigations. In the apparatus

used in this study, it was difficult to vary flow rate and reaction pressure independently. A series of runs of 120-minute duration were carried out, however, in which the reaction pressure was held constant at 3.7 ± 1.0 mm at low flow rates, while the water-to-butadiene ratio was varied. The results of these runs are summarized in Table V.

From Table V it can be seen that at constant pressure, low flow rate, and butadiene concentrations exceeding 10 mole %, the percentage of Hg^{202} appears to reach a constant value, independent of butadiene concentration, of $75\pm3\%$. A major experimental difficulty in this investigation was the maintenance of a constant partial pressure of water vapor over the course of a run. In obtaining the data for Table V, great care was taken to maintain a constant pressure of water vapor during each run. This accounts, in large measure, for the greater consistency in the enrichment values obtained, in comparison with those given in Table IV. Furthermore, in comparing the data of Tables IV and V, it should be borne in mind that the former are values for runs of 90-minute duration, while the latter are for runs of 120-minute duration. In general, it was found that prolonging the exposure time decreased the enrichment.

TABLE V

Hg^{202} enrichment in the HgO product of the reaction of $Hg^{202}6(^3P_1)$ atoms of Hg^N with water vapor – 1,3-butadiene mixtures as a function of the butadiene concentration
(Total pressure 3.7 ± 1.0 mm)

Temp.	Comp. mole %		Flow rate ml/min at 25° C and 760 mm	% Hg^{202} in HgO
	HOH	C_4H_6		
27	96	4	10.6	58
25	93.5	6.5	7.7	72
27	90	10	8.5	77
25	87.5	12.5	8.6	76
32	86	14	16.2	64
24	79	21	12.2	63
27	73	27	11.0	73
25	71.5	28.5	7.5	77
20	48.1	51.9	5.3	76

A variable which was appreciated relatively late in the investigation was the degradative effect of product-recovery techniques on the percentage of Hg^{202} in the recovered mercury. In an earlier paper (5), data were presented which showed that Hg^{202++} ions will be isotopically degraded when the solution is in contact with a globule of Hg^N. The exchange occurs presumably between dissolved Hg^N and Hg^{202++}. The $Hg^{202}O$ deposited in the reaction cell has chemisorbed upon it a layer of Hg^N. This adsorbed layer is extremely difficult to remove. A number of experiments were performed in which the cell, after reaction, was exhaustively evacuated through a trap containing liquid nitrogen, in an attempt to drive off the adsorbed Hg^N. This procedure had little effect upon the percentage of Hg^{202} in the product.

The kinetics of the exchange reaction between dissolved Hg^N and Hg^{202++} ion will require detailed study. It is fairly clear, however, at this stage, that the rate of exchange decreases with decreasing concentration of the hydrochloric acid used to dissolve the HgO from the reaction cell. The effect of acid concentration is illustrated by the following data: three runs were made with a substrate containing $5.5\pm1.5\%$ butadiene. Acid concentrations of 12.0 M, 6.0 M, and 2.5 M were used in recovering the HgO product. The analyses of the recovered mercury samples gave, for the percentage of Hg^{202}, 72, 78,

and 84 respectively. There appeared to be little effect on the Hg^{202} enrichment when acid concentrations less than 2.5 M were employed. For the runs reported in Table V, 0.16 M hydrochloric acid was used to dissolve the HgO product from the cell.

DISCUSSION

Nitrous Oxide and Oxygen Reactions

The failure to obtain an HgO product, enriched in Hg^{202}, in the nitrous oxide and oxygen reactions, would suggest that a mercury compound is not formed in the primary process. However, even with the pure water vapor reaction, the enrichment is small, butadiene being required to suppress the isotopically degradative processes operative. The oxygen and nitrous oxide reactions will require further study, in the presence of free-radical acceptor addends, before unequivocal statements can be made concerning the primary formation of mercury compounds.

Water Vapor Reaction

As a positive result of this investigation, it has been shown that in the flow reaction between $Hg^{202}6(^3P_1)$ atoms in Hg^N and mixtures of water vapor and 1,3-butadiene, the HgO product of the reaction is highly enriched in Hg^{202}. The reaction recommends itself as a simple method for preparing Hg^{202} from natural mercury.

In the reaction with pure water vapor, the Hg^{202} content of the HgO product was not found to exceed 35%, in agreement with an earlier study (3). From the kinetic standpoint, it can be conservatively stated that some fraction of the primary interaction between $Hg^{202}6(^3P_1)$ atoms and HOH molecules leads to the formation of a mercury compound. The role of butadiene in increasing the Hg^{202} content of the oxide can be explained, at this stage of our knowledge, on two bases:

(a) There are two primary processes—reactions [1] and [2]. The butadiene serves to clean up OH radicals, formed in [2], thereby suppressing the formation of Hg^NO by reaction [5].

(b) Reaction [1] is the only primary process operative and the failure to obtain pure $Hg^{202}O$, from water substrate alone, is attributable to exchange reactions, similar to [6], occurring in the gas phase or on the wall. Here the butadiene could suppress exchange degradation by combining with the quasi-free radical $Hg^{202}OH$.

It should be pointed out that $Hg^{202}OH$ is not necessarily the initial mercury compound formed. The primary step could be

$$Hg^{202}6(^3P_1) + HOH \rightarrow Hg^{202}H + OH. \qquad [7]$$
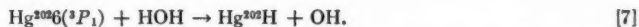
The unstable species HgH has been adduced many times to explain the preference of Hg $6(^3P_1)$ atoms for C–H bond scission in hydrocarbon reactions. The problem has been thoroughly discussed by Steacie (10). The low heat of formation of HgH (8.5 kcal) would argue against its surviving sufficiently long to form a stable product in the water reaction.

Investigations are now in progress in the laboratories of one of us (H.E.G.) which should yield further information on the kinetics of the water reaction. In addition to systematic studies of the effects of the various reaction parameters on the Hg^{202} content of the HgO product, the quantum yield of $Hg^{202}O$ formation is being investigated. Quantum yield measurements are difficult in water vapor – butadiene mixtures, owing to the high quenching cross section of butadiene. The situation is further complicated by the fact that water vapor converts Hg $6(^3P_1)$ atoms to the $6(^3P_0)$ state at least as efficiently

as nitrogen. Finally, information is being obtained on the nature of the polymer formed in the reaction with water–butadiene mixtures. The presence of Hg–C bonds in the polymer would be evidence of interaction of butadiene with mercurial free radicals.

REFERENCES

1. BILLINGS, B. H., HITCHCOCK, W. J., and ZELIKOFF, M.   J. Chem. Phys. **21**, 1762 (1953).
2. OSBORNE, K. R., McDONALD, C. C., and GUNNING, H. E.   J. Chem. Phys. **26**, 124 (1957).
3. ZELIKOFF, M., ASCHENBRAND, L. M., and WYCKOFF, P. H.   J. Chem. Phys. **21**, 376 (1953).
4. PERTEL, R. and GUNNING, H. E.   J. Chem. Phys. **26**, 219 (1957).
5. GUNNING, H. E.   Can. J. Chem. **36**, 89 (1958).
6. OSBORN, K. R. and GUNNING, H. E.   J. Opt. Soc. Am. **45**, 552 (1955).
7. BUSEY, R. H. and GIAUQUE, W. F.   J. Am. Chem. Soc. **75**, 806 (1953).
8. NIER, A. O.   Phys. Rev. **79**, 450 (1950).
9. GUNNING, H. E. and STEACIE, E. W. R.   J. Chem. Phys. **12**, 484 (1944).
10. STEACIE, E. W. R.   Atomic and free radical reactions. Reinhold Publishing Corp., New York. 1954. pp. 414 ff.

FUSED HETEROCYCLICS

PART III. SYNTHESIS OF QUINOLINO-(2':3':3:4)-QUINOLINE[1]

RAGINI ANET[2]

ABSTRACT

Quinolino-(2':3':3:4)-quinoline has been synthesized from 3-aminoquinoline-4-carboxylic acid via 4'-hydroxyquinolino-(2':3':3:4)-quinoline.

Quinolinoquinolines containing fused pyridine rings were of interest in connection with the structure of calycanine (1). In Part II of this series (2) the synthesis of quinolino-(2:3:3':2')-quinoline was reported. The synthesis of an angular isomer, quinolino-(2':3':3:4)-quinoline, is now described.
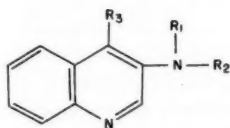
I, $R_1 = R_2 = H$; $R_3 = COOH$
II, $R_1 = Ph$; $R_2 = H$; $R_3 = COOH$
III, $R_1 = R_2 = Ph$; $R_3 = COOH$
IV, $R_1 = Ph$; $R_2 = R_3 = H$
V, $R_1 = R_2 = Ph$; $R_3 = H$
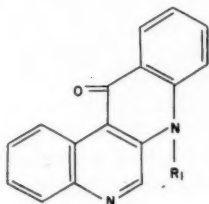
VII, $R_1 = Ph$

VI, $X = OH$
VIII, $X = Cl$

IX, X = (4-CH₃-phenyl-SO₂-NH—NH)
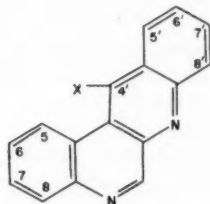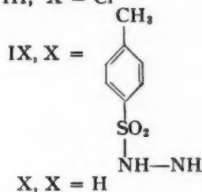
X, $X = H$

Although the base itself (X) has not been synthesized previously, 4'-hydroxy derivatives with substituents in the 2-, 6'-, 7'-, and 8'-positions have been prepared by the cyclization of appropriately substituted 3-arylaminoquinoline-4-carboxylic acids (3, 4, and 5). This method, in its essentials, was followed for the synthesis of 4'-hydroxy-quinolino-(2':3':3:4)-quinoline.

The preparation of 3-phenylaminoquinoline-4-carboxylic acid (II) was carried out by the extension of the arylation reaction described in Part II (2). When 3-aminoquinoline-4-carboxylic acid (I) (6) was treated with iodobenzene and copper catalyst, a mixture of 3-phenylamino- and 3-(diphenylamino)-quinoline-4-carboxylic acids (II and III respectively) was obtained. As in the case of the corresponding quinaldine acid (2), the monosubstituted acid could not be obtained exclusively. The acids were separated by fractional crystallization and decarboxylated to the corresponding bases 3-phenylamino- and 3-(diphenylamino)-quinolines (IV and V), which were characterized as their picrates.

The mixture of acids obtained in the arylation reaction was cyclized with phosphoryl

chloride, and the intermediate chloro derivatives hydrolyzed to give 4'-hydroxyquinolino-(2':3':3:4)-quinoline (VI) and 4'-keto-1'-phenyldihydroquinolino-(2':3':3:4)-quinoline (VII). The cyclized products were separated readily as they had markedly different solubilities in organic solvents. The 4'-hydroxy derivative (VI) gave a typical acridone-like fluorescence in presence of alkali (7) and was characterized as its picrate; whereas the 4'-keto compound was non-fluorescent and did not give any crystalline salts.

The reduction of the 4'-hydroxy derivative to the unsubstituted quinolinoquinoline with zinc dust did not prove successful. However, by using the method of Albert and Royer (8) for the conversion of acridone into acridine, the desired compound (X) was obtained. The 4'-hydroxy derivative (VI) was refluxed with phosphoryl chloride to give the 4'-chloro compound (VII) which was sensitive to hydrolysis with acid, but could be stored satisfactorily over potassium hydroxide *in vacuo*. It was characterized as the picrate. On treatment of the chloro derivative with *p*-toluenesulphonylhydrazide (8) in chloroform, the 4'-*p*-tosylhydrazidoquinolino-(2':3':3:4)-quinoline (IX) was obtained as the hydrochloride. Attempts to prepare the free base from its hydrochloride were unsuccessful and led to considerable decomposition. It was found that the reaction of the chloro derivative with *p*-tosylhydrazide was slower than in the case of the acridine derivative (8). The 4'-hydrazido hydrochloride was treated with 1 *N* sodium hydroxide in ethylene glycol to give a mixture of the 4'-hydroxy derivative (VI) and the desired quinolino-(2':3':3:4)-quinoline (X) which were readily separated by chromatography over alumina. The quinolinoquinoline crystallized from methanol in cream-colored needles m.p. 179°–180° C. Its ultraviolet absorption spectrum is recorded in Fig. 1.
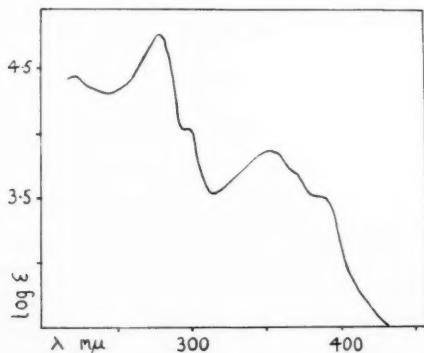
FIG. 1. Ultraviolet absorption spectrum of quinolino-(2':3':3:4)-quinoline in methanol.

EXPERIMENTAL

All melting points are uncorrected. Analyses by Drs. Weiler and Strauss, Oxford.

3-Phenylaminoquinoline-4-carboxylic Acid (II)

3-Aminoquinoline-4-carboxylic acid (I, 6.35 g) (6), 10 g (7.35 ml) iodobenzene, 9 g anhydrous potassium carbonate, and 0.8 g copper catalyst (Naturkupfer C) were refluxed in a mixture of 20 ml benzyl alcohol and 40 ml cyclohexanol for 3 hours with strict exclusion of moisture. The reaction mixture was cooled, diluted with 50 ml water, and steam-distilled to remove the alcohols. The solution was filtered hot into dilute acetic acid and allowed to stand at room temperature for 6–8 hours. The orange precipitate (9.2 g, m.p. 224°–232° C, with decomposition) was dried, and crystallized from a 1:1 mixture

of chloroform–methanol. Lemon-yellow feathery needles of the 3-phenylamino acid (II), m.p. 243°–244° C (decomp.), were obtained after several crystallizations. Found: C, 72.1; H, 4.8; N, 10.9. Calc. for $C_{16}H_{12}N_2O_2$: C, 72.7; H, 4.5; N, 10.6%. The acid was sparingly soluble in water, benzene, ether, and alcohol. Its solutions in alkali were colorless.

3-Phenylaminoquinoline (IV)

The acid (II, 1.2 g) was heated at 250° C for 1 hour. The acid melted with decomposition and after the first few minutes, some of the base started to sublime into the air condenser attached to the flask. After decarboxylation was complete, the contents of the flask were allowed to cool and were extracted with methanolic hydrochloric acid. The acid solution was poured into an excess of aqueous potassium hydroxide, and the aqueous solution extracted with ether. Evaporation of the ether extract after charcoal treatment gave an oil (0.9 g), which solidified on refrigeration. Crystallization from dilute methanol gave the base (IV) as needles, m.p. 121°–123° C. Found: C, 81.9; H, 5.45; N, 12.4. Calc. for $C_{15}H_{12}N_2$: C, 81.8; H, 5.45; N, 12.4%. The base was very soluble in organic solvents and its solutions exhibited a strong blue fluorescence in ultraviolet light.

The *picrate* prepared in methanol gave orange needles, m.p. 189°–190° C with decomposition. Found: N, 15.4. Calc. for $C_{21}H_{15}N_5O_7$: N, 15.6%.

3-(Diphenylamino)-quinoline-4-carboxylic Acid (III)

A suspension of 1.5 g of 3-amino acid (I) in 25 ml benzyl alcohol was refluxed with 2.0 g anhydrous potassium carbonate, 0.2 g. Naturkupfer C and 2.3 g (1.7 ml) iodobenzene for 6 hours. The reaction was worked up as in the case of the 3-phenylamino acid (II) described above when 1.95 g of a bright yellow solid, m.p. 255°–264° C, was obtained. This was washed with acetone and crystallized from chloroform–methanol in stout yellow rods, m.p. 270°–272° C with decomposition. Found: C, 77.5; H, 4.8; N, 8.1. Calc. for $C_{22}H_{16}N_2O_2$: C, 77.6; H, 4.8; N, 8.2%. The acid was sparingly soluble in most organic solvents but was readily soluble in aqueous alkali to give colorless solutions. It was insoluble in dilute mineral acids but dissolved in concentrated hydrochloric acid on prolonged boiling.

3-(Diphenylamino)-quinoline (V)

The acid (III, 1.5 g) was decarboxylated at 270° C for 1 hour. On working up the reaction as in the case of the 3-phenylamino compound (IV), an oil (1.0 g), solidifying on refrigeration was obtained (m.p. 155°–164° C with previous softening). Repeated crystallizations from dilute methanol or other organic solvents failed to raise the melting point and the base was therefore purified by sublimation at 180° C under reduced pressure (20 mm). Crystallization of the sublimate from dilute methanol gave colorless needles, m.p. 162°–164° C. Found: C, 84.7; H, 5.4; N, 9.7. Calc. for $C_{21}H_{16}N_2$: C, 85.1; H, 5.4; N, 9.4%. The base was very soluble in organic solvents to give yellowish solutions with a vivid blue fluorescence.

The *picrate* prepared from equimolecular quantities of the base and picric acid in benzene–methanol formed orange needles, m.p. 205°–206° C with decomposition. Found: C, 61.9; H, 3.7; N, 13.6. Calc. for $C_{27}H_{19}N_5O_7$: C, 61.7; H, 3.7; N, 13.3%.

4'-Hydroxyquinolino-(2':3':3:4)-quinoline (VI)

Five grams of the crude 3-phenylamino acid (II) were refluxed with 12.5 ml phosphoryl chloride under anhydrous conditions. A vigorous reaction set in at 60°–65° C and heating was interrupted till it was over. The refluxing was continued for 90 minutes the bath temperature being maintained at 110–120° C. Phosphoryl chloride was removed under

reduced pressure, care being taken that the bath temperature did not exceed 100° C. The dark residue, after removal of the acid chloride, was heated on the steam bath with 300 ml 1 N hydrochloric acid for 2 hours, filtered, and poured into excess ammonium hydroxide. After 16 hours at room temperature the dark solid was filtered, dried, and extracted with hot chloroform to remove the 4′-keto compound (vide infra) formed from the disubstituted acid (III). The residue was extracted with hot ethanol (charcoal) and the 4′-hydroxy derivative obtained by evaporation of the ethanol was crystallized from dilute acetic acid in yellow needles, m.p. 360° C. Found (sample dried at 100° C under 2 mm): C, 72.9; H, 4.6. Calc. for $C_{16}H_{10}N_2.H_2O$: C, 72.7; H, 4.5. Found (sample dried at 250° C under 0.5 mm): C, 74.9; H, 4.6. Calc. for $C_{16}H_{10}N_2O.H_2O$: C, 75.0; H, 4.3%. Attempts to remove the last 0.5 molecule of water of crystallization were unsuccessful even after repeated sublimation and extensive drying. The 4′-hydroxy compound was sparingly soluble in ether, benzene, and chloroform but readily so in ethanol and ethyl acetate. Its alcoholic solutions were non-fluorescent but gave a vivid green fluorescence in presence of a pellet of potassium hydroxide.

The *picrate* formed by refluxing (VI) with picric acid in ethanol for 4 hours gave needles, m.p. 255°–258° C. Found: C, 55.9; H, 3.1; N, 14.8. Calc. for $C_{22}H_{13}N_5O_8$: C, 55.6; H, 2.7; N, 14.8%.

4′-Keto-1′-phenyldihydroquinolino-(2′:3′:3:4)-quinoline (VII)

Diphenylamino acid (III, 0.8 g) was refluxed with 5 ml phosphoryl chloride and the reaction worked up as above. The 4′-keto derivative (VII) was obtained from the chloroform extract as a dark solid (0.6 g). Treatment with charcoal and crystallization from methanol gave pale yellow needles, m.p. 282°–284° C. Found: C, 81.8; H, 4.4; N, 8.7. Calc. for $C_{22}H_{14}N_2O$: C, 82.0; H, 4.4; N, 8.7%.

4′-Chloroquinolino-(2′:3′:3:4)-quinoline (VIII)

4′-Hydroxy compound (VI, 1.5 g) was refluxed with 20 ml phosphoryl chloride under anhydrous conditions for 6 hours. After removal of the acid chloride under reduced pressure, the orange-colored solid was added to a vigorously stirred 5% aqueous ammonium hydroxide containing crushed ice. The solution was kept alkaline to phenolphthalein by adding more ammonia if necessary. After 30 minutes the solution was centrifuged and the cream-colored solid dried in a vacuum desiccator over potassium hydroxide. Extraction of the dry solid with benzene containing a pellet of potassium hydroxide gave the 4′-chloro compound which crystallized from petroleum ether (b.p. 40°–60° C) in colorless prismatic needles, m.p. 191°–192° C. Found: C, 73.0; H, 3.8; Cl, 13.1. Calc. for $C_{16}H_9N_2Cl$: C, 72.6; H, 3.4; Cl, 13.4%.

The *picrate* formed in benzene gave orange needles, p. 209°–210° C with decomposition. Found: C, 54.0; H, 2.6. Calc. for $C_{22}H_{12}N_5O_7Cl$: C, 53.5; H, 2.4%.

4′-p-Tosylhydrazidoquinolino-(2′:3′:3:4)-quinoline Hydrochloride (IX)

The 4′-chloro compound (VIII, 0.18 g) was dissolved in the minimum quantity of chloroform and added to a saturated solution of 0.17 g p-tosylhydrazide (8) in the same solvent. After 48 hours at room temperature, the solution turned pale yellow but no solid separated. The chloroform was removed on the steam bath and fresh chloroform added to the reaction mixture which was left at room temperature for a further 72 hours. (It was found that a fast stream of hydrogen chloride when passed through the solution after the initial 48 hours gave the hydrochloride of (VIII) in one experiment.) After the completion of the reaction, the red solid was filtered from the chloroform, dried, and

crystallized from methanol containing a drop of hydrochloric acid in red needles which did not melt but decomposed at 320° C. Found: C, 61.5; H, 4.2. Calc. for $C_{23}H_{19}N_4SO_2Cl$: C, 61.3; H, 4.2%.

Quinolino-(2':3':3:4)-quinoline (X)

One half gram of (IX) was heated on the steam bath with 10 ml 1 N sodium hydroxide in ethylene glycol (4 g sodium hydroxide dissolved in a mixture of 70 ml ethylene glycol and 30 ml water) for 3 hours. The solution turned crimson and lumps of a precipitate were formed which were broken up from time to time with a glass rod. Evolution of gas began after the first few minutes and continued for 2 hours, when the solution became clear. It was then diluted with 20 ml water and refrigerated overnight. The flocculent precipitate that had separated was filtered after 24 hours, taken up in 1 N hydrochloric acid, and reprecipitated with ammonia. The base was taken up in ethyl acetate and chromatographed over alumina, when the quinolinoquinoline (X) separated as a strongly fluorescent band in ultraviolet light. Elution with ethyl acetate gave (X) which crystallized from methanol in needles, m.p. 179°–180° C. Found: C, 83.1; H, 4.5. Calc. for $C_{16}H_{10}N_2$: C, 83.5; H, 4.4%. The base was readily soluble in ethyl acetate, alcohol chloroform, and ether. It dissolved in mineral acids to give non-fluorescent solutions

REFERENCES

1. ROBINSON, R. and TEUBER, H. J.   Chem. & Ind. 783 (1954).
2. ANET, R.   Can. J. Chem. **36**, 1449 (1958).
3. DIESBACH, H. DE and MOSER, E.   Helv. Chim. Acta, **20**, 132 (1937).
4. DIESBACH, H. DE and KLEMENT, O.   Helv. Chim. Acta, **24**, 166 (1941).
5. COLONNA, M. and DAL MONTE-CASONI, D.   Gazz. chim. ital. **78**, 793 (1948).
6. COLONNA, M.   Boll. sci. fac. chim. ind. univ. Bologna, 89 (1941); Chem. Abstr. **37**, 3096 (1943).
7. ALBERT, A.   The acridines. Edward Arnold & Co., London. 1951.
8. ALBERT, A. and ROYER, R.   J. Chem. Soc. 1148 (1949).

THE INTERACTION OF FRIEDEL–CRAFTS CATALYSTS WITH ORGANIC MOLECULES

I. THE CH₃COCl:AlCl₃ SYSTEM[1]

DENYS COOK[2]

ABSTRACT

An infrared study of the liquid complex of aluminum chloride with acetyl chloride has been undertaken. The results indicate that the pure liquid complex is not a simple mixture, but consists of (1) the donor–acceptor complex $CH_3\overset{\underset{\displaystyle |}{Cl}}{C}\!=\!O \ldots AlCl_3$ and (2) the ions $[CH_3CO]^+$ and $[AlCl_4]^-$. A solution of the liquid complex in a solvent of high dielectric constant like nitrobenzene ($\epsilon = 36.1$) contains both these species, but in a low dielectric constant solvent like chloroform ($\epsilon = 5.05$) only (1) is present. The carbon–chlorine bond in (1) is modified. The mechanism of Friedel–Crafts ketone synthesis is briefly examined in the light of these results.

A variety of metallic halides have been used as catalysts in the Friedel–Crafts ketone synthesis. The most widely used of these is $AlCl_3$, but others, such as BF_3, $AlBr_3$, $SbCl_3$, $SbCl_5$, $FeCl_3$, $TiCl_4$, $SnCl_4$, and $ZnCl_2$ etc., have all been used. All these halides have in common the function of Lewis acids, due either to electron deficiency, or to hybridization changes to give complex ions.

Numerous examples exist in the literature of complexes formed from such Lewis acids and various donors. The characteristics of the donor molecule are usually those of well-directed lone-pair electrons. Thus compounds like R_2O, $R_2C\!=\!O$, RCN, R_3N, RNO_2 etc. can all form more or less stable complexes with Lewis acids, the electron deficiency of the latter being satisfied by sharing the lone-pair electrons of the donor group. Some of the Lewis acids can function as acceptors in a slightly different way. Thus NaCl and $AlCl_3$ form the compound $NaAlCl_4$, which has been shown to consist of Na^+ and $[AlCl_4]^-$ ions (1, 2).

The presence of two functional groups in an acyl halide, namely a carbonyl donor group and an ionizable chlorine atom, suggests that two types of intermediates may be possible in the Friedel–Crafts ketone synthesis: (a) the ions $[CH_3CO]^+$ and $[AlCl_4]^-$, and (b) the donor–acceptor complex formed between the carbonyl–oxygen lone-pair electrons and the vacant orbital of the $AlCl_3$, as suggested by Pfeiffer (3). An extension of (b) proposed by Dilthey (4) involved loss of a Cl^- from the donor–acceptor complex to give a complex ion.

It is the purpose of this paper, from the spectroscopic evidence presented, to show that the donor–acceptor complex as in (b) is present in solution in solvents of low dielectric constant, but that in the pure complex or in its solution in solvents of high dielectric constant ions such as in (a) are present as well as the donor–acceptor complex.

After the experimental work described here was completed, two papers by Susz and Wuhrmann (5, 6) appeared on the infrared spectra of the complexes $CH_3COF:BF_3$ and $CH_3COCl:AlCl_3$. These gave the first clear indication of the presence of the $[CH_3CO]^+$ ion. The present work corroborates their findings but important differences exist which are detailed below.

EXPERIMENTAL

Aluminum chloride was purified by vacuum sublimation of reagent grade $AlCl_3$ in the apparatus shown in Fig. 1a. The $AlCl_3$ was sublimed from the bulb to the cold finger and then transferred to the seal-off tube with continuous pumping. A known quantity, 4.729 g, was then transferred to the reaction tube (which had been flamed and then cooled with dry nitrogen) in Fig. 1b which was sealed off as quickly as possible. The molar equivalent of CH_3COCl, 2.77 g, was distilled onto the $AlCl_3$ at liquid nitrogen temperatures. On warming to room temperature the $AlCl_3$ gradually went into solution, though slight heat was necessary to make the last traces dissolve, giving a homogeneous light brown solution. Excessive heat which would favor decomposition was avoided. Even so some slight decomposition occurred as HCl was found in the gas phase. Infrared examination of the gas phase showed the evolved gases to be chiefly HCl and CH_3COCl, and mass spectrometry confirmed this but also indicated the presence of further unidentified fragments of mass 45, 60, 73, and 87. The total volume of gas evolved was computed from the pressure and an estimate of the volume of the apparatus. Assuming only the two components mentioned above to be significant, the weight of these products lost from the reaction tube was 0.072 g HCl and 0.157 g CH_3COCl. These represent maximum values, since the unidentified products would lower these figures.
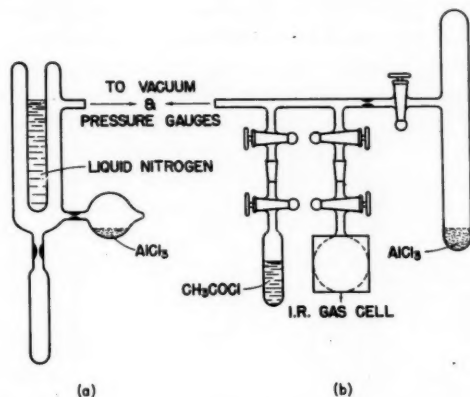
FIG. 1. (a) $AlCl_3$ sublimation apparatus. (b) Apparatus for preparation of complex.

The reaction tube was transferred to a dry box which contained a bed of silica gel, and which had been well flushed with dry nitrogen for a few hours before. After it had been left standing for at least two hours in the dry box the reaction tube was opened, and the various cells made up for spectroscopic analysis.

A double beam rock salt spectrometer was used to record the spectra in the region of 4000 cm^{-1} to 625 cm^{-1}. From 625 cm^{-1} to 350 cm^{-1} a modified Perkin–Elmer 12C spectrometer with CsBr optics was used. The standard bands in a thin film of polystyrene were used for calibration.

RESULTS

The principal bands of the various spectra are shown in Table I together with those of pure acetyl chloride. Figure 2 shows the spectrum of the pure liquid complex.

FIG. 2. Spectrum of pure liquid complex. Capillary film between NaCl plates.

TABLE I

Principal bands in the spectra

Assignment	CH_3COCl*	This work	Susz and Wuhrmann	$C_6H_5NO_2$†	$CHCl_3$‡	CS_2‡
		CH₃COCl: AlCl₃		CH₃COCl: AlCl₃ in solution in:		
ν CH₃, a''	3012 w§	2941 m	2950 m			
ν CH₃, a'	2960	2874 m				
ν [CH₃CO]⁺		2307 s	2305 vs			
		2203 vs	2200 w, sh	2193 vs		
ν C=O, a'	1808 vs	1779 m		1805 vs	1793 w	1802 w
				1681 m		
ν C=O ... AlCl₃		1637 vs	1639 m	1642 vs	1660 m	
					1613 m	
		1567 s	1560 w		1558 w	
δ CH₃, a''	1433 m	1497 s	1485 m		1479 m	
δ CH₃, a''?	1418 m					
δ CH₃, a'	1370 s	1379 s, b			1389 w	
	1357 s	1348 s			1340 w	
		1321 s	1312 s			
		1305 s				
		1236 m				
		1159 m	1154 w		1156 m	
		1117 m				
		1018 m, sh				
ν C—C, a'	1103 vs	1006 s	1000 vs		1099 w	1095 w
δ CH₃, a''?	1028 s					
δ CH₃, a'	952 vs	969 m			952 w	952 vw
		716 m	719 s			
		662 m, sh				
		649 m			625 m	
ν C—X, a'	539 s					
		540 s, b			540 s	
		485 s, b	500 s		500 m	
δ C—X, a'	436 s					
or		390 s			370 s	
δ CCO, a'	352 m					

*These values agree well with those of J. C. Evans and H. J. Bernstein, Can. J. Chem. **34**, 1083 (1956), whose notation is followed.
†About 0.5 cc liquid complex in about 5 cc $C_6H_5NO_2$.
‡Saturated solution.
§w = weak, m = medium, s = strong, v = very, b = broad, sh = shoulder.

DISCUSSION

The strongest band in the spectrum of the pure liquid complex is at 1637 cm⁻¹. On account of its intensity it is likely that this is a carbonyl group vibration, and it seems logical to assign this band to the C=O vibration in the complex I:

$$CH_3—C \overset{O ... AlCl_3}{\underset{Cl}{}} \qquad I$$

Since $\nu_{C=O}$ for acetyl chloride is 1807 cm^{-1} in the liquid, this band in the complex is lowered by 170 cm^{-1}. Shifts in $\nu_{C=O}$ of comparable magnitude have been observed by Susz and Cooke (7) in the equimolar complex of benzophenone and AlCl$_3$. In the complex $\nu_{C=O}$ was 1525 cm^{-1} and in pure benzophenone it was 1650 cm^{-1}, a shift of 125 cm^{-1}.

Susz and Wuhrmann tentatively assigned the 1639 cm^{-1} band to the C=C vibration in CH$_2$=C(Cl)—O—AlCl$_2$ which they thought might have been present in small amounts in their complex, and the 1567 cm^{-1} band to the perturbed carbonyl vibration. The high intensity of the 1637 cm^{-1} band would seem to rule out this interpretation, since such a C=C vibration would be expected to be quite weak. It is much more likely that their band at 1639 cm^{-1} was due to a small amount of the complex I which could very well have been present in their complex.

Two strong bands are located at 2307 cm^{-1} and 2203 cm^{-1}. These two bands are in the region of triple bond stretching frequencies and their presence in the spectrum is of unusual interest. They constitute the grounds for suspecting the presence of the ion [CH$_3$CO]$^+$ in the complex. This ion should be linear (it is isoelectronic with CH$_3$CN). Variations in carbonyl stretching frequencies are due, in part, to the electronegativity of the group, or groups, attached to the carbonyl group (8). The positive charge on the carbon atom of the carbonyl group should have a very strong electron-withdrawing effect. This would, therefore, raise the carbonyl frequency by a large amount. The band at 2307 cm^{-1} is thought to be compatible with such a structure. Alternatively the structure may be described in terms of resonance, where the actual structure is a hybrid of the forms CH$_3$C$^+$=O and CH$_3$C≡O$^+$. The bond order of the carbonyl group would be between 2 and 3, and the carbonyl frequency much higher than an ordinary ketone.

This is in harmony with the findings of Susz and Wuhrmann (5), who observed a very strong band at 2305 cm^{-1}. In contrast, the band at 2200 cm^{-1}, which they report to be of weak intensity, is very strong. This band could have two possible causes. It may be due to the complex ion II, as proposed by Dilthey, or an ion pair of the form III

[CH$_3$CO]$^+$ ... AlCl$_3$ $\mathrm{CH_3{-}\overset{+}{C}}{\diagup}^{\mathrm{O}}$ $\left[\begin{array}{c}\mathrm{Cl}\\\diagdown\\\mathrm{AlCl_3}\end{array}\right]^-$
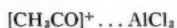
II   ·III

in which there is little interaction between the Cl atom and the central C atom. In support of II the lowering of $\nu_{C=O}$ from 2307 cm^{-1} in [CH$_3$CO]$^+$ to 2203 cm^{-1} in [CH$_3$CO]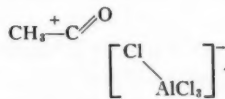$^+$ ...AlCl$_3$ seems to be in accord with other data on the lowering of $\nu_{C=O}$ of carbonyl compounds in complexes with strong Lewis acids. However, it might be argued that III seems more probable, since the cation [CH$_3$CO]$^+$, by virtue of its electron deficiency, might not be able to form a donor–acceptor complex with a Lewis acid. Evidence presented later in this paper tends to support III as a better interpretation of the 2203 cm^{-1} band.

The main differences between the spectra of Susz and Wuhrmann and the present work can be ascribed to the different physical state of the respective complexes. Susz and Wuhrmann worked exclusively with the solid complex, whereas the complex reported here was a viscous liquid. The solid would be disposed to allow the maximum contribution from the ionic species, but in the liquid state such long-range order would break down leading to the presence of both the ions [CH$_3$CO]$^+$ and [AlCl$_4$]$^-$, and the donor–acceptor complex I, with the latter probably predominating.

The band at 2941 cm^{-1} is assigned to the antisymmetrical CH stretching frequency, the other sharp band at 2874 cm^{-1} being the symmetrical CH stretching vibration. The lowered CH$_3$ stretching frequencies in the complex, 2941 and 2874 cm^{-1} (compared with 3012 and 2960 cm^{-1} in acetyl chloride), are compatible with the ionic structure [CH$_3$CO]$^+$, since hyperconjugation (H$^+$CH$_2$=C=O etc.) in the ion should produce such shifts. Two strong bands 1379 cm^{-1} and 1348 cm^{-1} are probably associated with the CH deformation frequencies of the CH$_3$—C group.

In the low frequency region one significant feature emerges. This is the disappearance of the bands at 436 cm^{-1} and 593 cm^{-1} associated with the C—Cl bond. The formation of the ion [CH$_3$CO]$^+$ would naturally result in the absence of these bands. However, the formation of the complex I would modify them. Three alternatives can be considered: (1) In the complex I all the group frequencies may be altered so that, even though the C—Cl bond still has the same force constant, its frequency is shifted. (2) The force constant is increased leading to a band at higher frequency. (3) The force constant is lowered leading to a lower frequency. Of these (2) can be ruled out, since there is no band in this region of sufficient intensity to be considered a C—Cl fundamental. Since many of the other bands are found in approximately the proper region this would tend to discount (1), and leave (3) as the probable reason for the disappearance of the two bands. Since the low frequency cutoff of CsBr is about 320 to 350 cm^{-1} it is not possible to observe bands with lower frequencies.

If the cation [CH$_3$CO]$^+$ is present then there should be signs in the spectrum of [AlCl$_4$]$^-$. Little is known of the spectroscopic behavior of this anion in the infrared. Gerding and co-workers (2) have investigated some systems containing AlCl$_3$ by Raman spectroscopy. In the system Na$^+$ + [AlCl$_4$]$^-$ they found the following frequencies: $\nu_1 = 349$, $\nu_2 = 146$, $\nu_3 = 575$, and $\nu_4 = 180$ cm^{-1}. For liquid NO$^+$ + [AlCl$_4$]$^-$ they found $\nu_1 = 349$, $\nu_2 = 136$, $\nu_3 = 450$–539 very broad, $\nu_4 = 182$ cm. However, for solid NO$^+$ + [AlCl$_4$]$^-$ ν_3 seemed to be a composite band with peaks at 460, 470, and 549 cm^{-1}. Of these Raman frequencies only ν_3, and ν_4 should be infrared active, and because of wavelength limitations only ν_3 visible.

In the CH$_3$COCl: AlCl$_3$ complex two broad strong bands at 485 and 540 cm^{-1} are observed. It is not possible to ascribe these to any specific vibration, but their presence suggests the structures [AlCl$_4$]$^-$ or Cl$_3$Al. . .O. The spectrum of AlCl$_3$ dissolved in acetone contains these bands and here the complex can only be formed between the O lone-pair electrons and the AlCl$_3$.

Preliminary experiments had indicated the presence of the 2203 cm^{-1} band in mixtures prepared without taking extensive precautions to exclude air. This band at 2203 cm^{-1} was at that time thought to be due to the [CH$_3$CO]$^+$ ion, but the possibility remained that it could be due to a ketene-like structure, possibly as a result of dehydrohalogenation of the acyl halide. Ketenes have bands considerably higher in frequency than ordinary carbonyl bands. On account of the volatility of such compounds (ketene b.p. −56° C) it would be expected that some of it should be present in the vapor phase. However, no bands in the appropriate region were found in the infrared spectrum of the evolved vapors, nor did analysis by mass spectrometer reveal any ketene. The possibility of any ketene-like compound being present in the liquid complex is therefore very remote.

The behavior of the complex alone should be compared with the results obtained by dissolving the complex in various solvents. Frequently nitrobenzene is used as solvent in Friedel–Crafts ketone synthesis. The bands in the spectrum of the complex in nitrobenzene, in which it dissolves completely to give a yellow solution, are shown in Table I.

Some similarities exist between these bands and those of the complex alone. The band at 2193 cm^{-1} (cf. 2203 cm^{-1} in the pure complex) is present, as is the band at 1642 cm^{-1} (cf. 1637 cm^{-1} in the pure complex). The band at 1805 cm^{-1} is more intense than that (1779 cm^{-1}) in the pure complex. The band at 2307 cm^{-1} has completely disappeared. These changes can be explained by a partial dissociation of the complex I to give essentially free CH$_3$COCl (the band at 1805 cm^{-1}). The AlCl$_3$ released can interact with the excess nitrobenzene (to form the complex C$_6$H$_5$NO$_2$.AlCl$_3$ which is soluble in excess nitrobenzene), or complex with the [CH$_3$CO]$^+$. The former seems more likely, since it is probable that nitrobenzene is a better donor than the [CH$_3$CO]$^+$ ion. The absence of the 2307 cm^{-1} band and the strong 2193 cm^{-1} band suggests that the [CH$_3$CO]$^+$ is present as the ion pair III.

The liquid complex is only slightly soluble in CHCl$_3$. Most of it remains as an oily layer at the bottom of the tube, but the CHCl$_3$ layer turns a pink color which gradually fades with time. Table I lists the bands observed in the latter layer. Apart from the chloroform bands the strongest band is at 1660 cm^{-1}. It is assumed that this is the same band as that at 1637 cm^{-1} in the complex and in C$_6$H$_5$NO$_2$ solution. This band is apparently doubled with another subsidiary peak at 1613 cm^{-1}. The weaker band at 1793 cm^{-1} is undoubtedly due to CH$_3$COCl interacting with CHCl$_3$. It is significant that no bands are observed in the 4.5 μ region. The two bands at 436 cm^{-1} and 493 cm^{-1} associated with the C—Cl bond in CH$_3$COCl are either weak or absent, while those at 500 and 540 cm^{-1} are due to the complex I, as observed earlier.

In solution in CS$_2$ the only bands present are reasonably well accounted for by CH$_3$COCl.

The foregoing provides strong evidence that the pure complex contains the [CH$_3$CO]$^+$ ion, which is currently accepted as being an intermediate in the Friedel–Crafts ketone synthesis. In solvents of high dielectric constant like nitrobenzene ($\epsilon = 36.1$) the same conclusion holds. In solvents of low dielectric constant like chloroform ($\epsilon = 5.05$) no ions have been detected *in solution*, and the CH$_3$COCl and AlCl$_3$ exist in the form of the donor–acceptor complex I. In this complex the C—Cl bond is thought to be weakened. This would have the effect of lowering the activation energy of the reaction between the complex and an aromatic hydrocarbon to form a ketone, and facilitate reaction. Two important experimental conditions would be fulfilled on this view. Firstly, the yield of ketone would be proportional to the amount of AlCl$_3$ used, and secondly, the AlCl$_3$ would be complexed with the carbonyl group throughout the reaction. It should be reiterated, however, that the pure liquid complex is not completely soluble in CHCl$_3$, but forms a lower insoluble layer. Reaction at the surface of this layer could still take place via an ionic intermediate.

REFERENCES

1. BAENZIGER, N. C.   Acta. Cryst. **4**, 216 (1951).
2. GERDING, H. and HOUTGRAAF, H.   Rec. trav. chim. **72**, 21 (1953).
3. PFEIFFER, P.   Organische molekulverbindungen. 2nd ed. von Ferdinard Enke. 1927. p. 409.
4. DILTHEY, W.   Ber. **71**, 1350 (1938).
5. SUSZ, B. P. and WUHRMANN, J. J.   Helv. Chim. Acta, **40**, 722 (1957).
6. SUSZ, B. P. and WUHRMANN, J. J.   Helv. Chim. Acta, **40**, 971 (1957).
7. SUSZ, B. P. and COOKE, I.   Helv. Chim. Acta, **37**, 1273 (1954).
8. COOK, D.   J. Am. Chem. Soc. **80**, 49 (1958).

THE ADSORPTION OF KRYPTON ON GRAPHITE ABOVE AND BELOW THE TRIPLE POINT[1]

H. L. McDermot and B. E. Lawton

ABSTRACT

The adsorption of krypton on graphite has been measured above and below its Triple Point. Above the Triple Point, a smooth isotherm was found which showed two types of hysteresis. In contrast, the isotherm measured below the Triple Point displayed two discontinuities. The surface area of this graphite measured by means of the krypton isotherm was found to be in agreement with that previously measured by nitrogen adsorption.

INTRODUCTION

The adsorption of krypton by artificial graphite has been studied as part of a program directed toward a study of these graphites. The adsorption of krypton by a substance closely related to graphite (P33 carbon black graphitized at 2700° C) has been studied by Singleton and Halsey (10); Amberg, Spencer, and Beebe (1); Clark (4); and Ross and Winkler (9). In every instance stepwise isotherms were obtained at 77° K. The reversibility of the isotherm was demonstrated by Clark. Heats of adsorption measured by Amberg, Spencer, and Beebe were found to show a maximum at a coverage close to the monolayer. A second smaller maximum coincided with the completion of the second layer. The stepwise isotherms, coupled with the heat curve, are strong evidence that the surface of this graphitized black was homogeneous. Ross and Winkler conducted measurements down to low pressures and presented isotherms which displayed discontinuities characteristic of two-dimensional phase changes. They made measurements at 77° and 90° K and showed that the vertical discontinuity signifying two-dimensional liquefactions occurred at 77° but not at 90° K. The two-dimensional critical temperature was estimated to be 82° K. The measurements reported here were undertaken to investigate further the rather unusual hysteresis effects reported previously for artificial graphites manufactured by Acheson Co. Previous papers in this series (6, 7) have presented evidence of two types of hysteresis occurring on the adsorption of oxygen, nitrogen, and argon (6, 7) by artificial graphites at liquid air temperatures. These measurements have now been extended to krypton and sulphur dioxide (8). Those with krypton were done above and below the Triple Point. Two types of hysteresis have been reported with the artificial graphites: the normal type of hysteresis due to pores occurring at high relative pressures and a second type extending down to low relative pressures which has been termed "swelling hysteresis". This type of hysteresis has also been demonstrated for the adsorption of nitrogen by the carbon black "Spheron 6" at 77° K and for the adsorption of diethyl ether by charcoal (2, 7).

EXPERIMENTAL AND RESULTS

The graphite used in these experiments was a purified Acheson graphite designated by us as GF-3. Its properties have been given before (7, 11).

The krypton was obtained from the Matheson Co. and used without further purification.

Isotherms were measured at 119° K and 78° K. Before each isotherm was measured, the sample was evacuated for at least 12 hours at 200° C. The isotherm at 119° K was
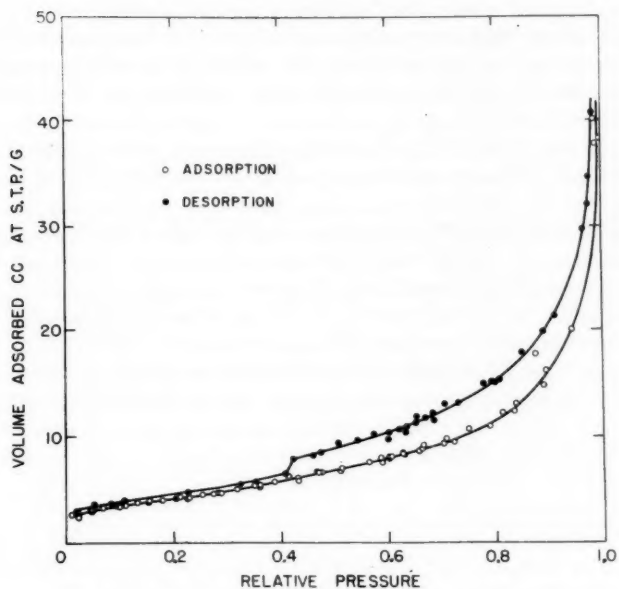
FIG. 1.   The adsorption of krypton by graphite at 119° K.
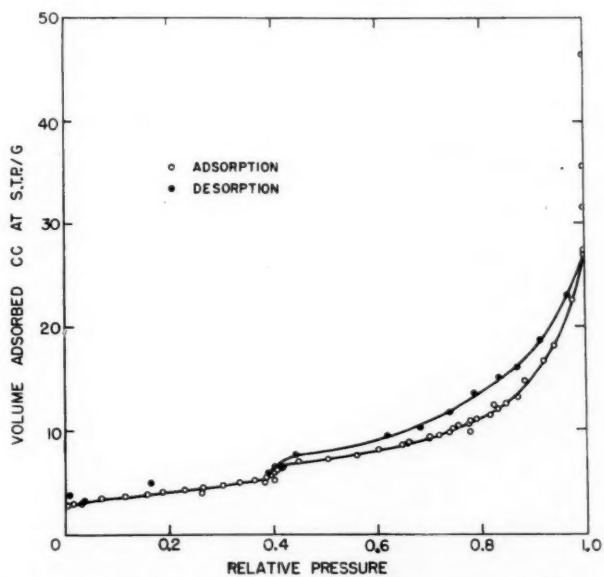
FIG. 2.   The adsorption of krypton by graphite at 78° K.

measured with a standard volumetric adsorption apparatus. The constant-temperature bath consisted of Dewar flask containing Freon 12, which was cooled externally by a liquid nitrogen bath and heated internally by means of a nichrome heater. Control was effected by means of a krypton vapor pressure thermometer. The temperature was maintained at 119.4° K to better than a tenth of a degree. The isotherm at 78° K was measured using an open bath of liquid nitrogen. Pressures were measured by means of a McLeod gauge. Low pressures were corrected for thermal transpiration by the formula of Liang (5).

The isotherms at 119° and 78° K are presented in Figs. 1 and 2 respectively. It is clear that the isotherm at 119° K is smooth and displays pore hysteresis and swelling hysteresis. Although swelling hysteresis was observed above the Triple Point of krypton, it was found impossible to demonstrate it at 78° K, below the Triple Point, owing to difficulties in desorption at low pressures. The few points obtained by warming the sample were not conclusive. The 78° K isotherm is presented because it gives evidence of two discontinuities for adsorption on a heterogeneous surface in contrast to those discussed in the Introduction which were observed with a homogeneous carbon surface. One discontinuity observed at a relative pressure of 0.4 is shown in Fig. 2, while the second found at a pressure of 1.7 μ is shown in Fig. 3.

DISCUSSION

The hysteresis loop shown in Fig. 1 is similar in shape to those previously reported for argon, oxygen, and nitrogen (6). It is interesting that the isotherm resembles closely the argon isotherm (6) on another artificial graphite despite the fact that the diameter of the krypton is about 17% greater than that of the argon. Figure 2 gives the isotherm
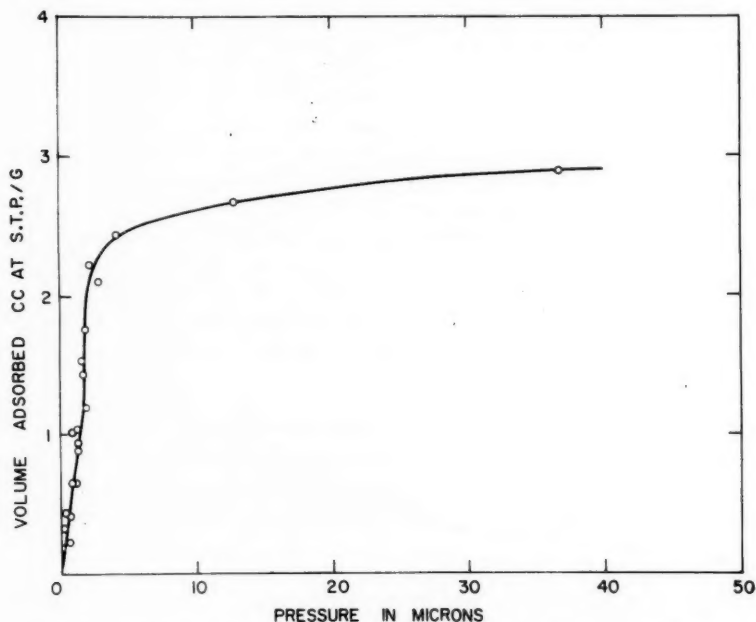
FIG. 3.   The adsorption of krypton by graphite at 78° K (low pressure region).

at 78° K below the Triple Point of krypton. The isotherm is quite different from that measured above the Triple Point. The hysteresis loop is differently shaped and it shows a marked discontinuity at a relative pressure of 0.4. A second discontinuity shown in Fig. 3 was found at a pressure of 1.7 μ. This type of discontinuity, which is generally interpreted as a two-dimensional condensation, is usually seen only with homogeneous surfaces. The surface of this graphite is known to be heterogeneous (11), hence this phenomenon can be explained in these terms only if one postulates that the surface contains homogeneous regions of widely different surface energies. Thus it might be imagined that two-dimensional condensation occurs on a homogeneous region of high surface energy, while little adsorption occurs at other sites. The second discontinuity occurs at the completion of two monolayers. It may conceivably signal the point at which a solid lattice starts to form in the pores.

The surface area of the graphite was estimated from the isotherm at 78° K using the B.E.T. equation and the value of 19.5 Å² (3) for the area of the krypton molecule. The area was found to be 17.4 m²/g, in good agreement with the area of 18.4 m²/g previously reported (6) using nitrogen as the adsorbate.

REFERENCES

1. AMBERG, C. H., SPENCER, W. B., and BEEBE, R. A.   Can. J. Chem. 33, 305 (1955).
2. ARNELL, J. C. and McDERMOT, H. L.   Proc. Second Intern. Congr. Surface Activity, II, 113 (1957).
3. BEEBE, R. A., BECKWITH, J. B., and HONIG, J. M.   J. Am. Chem. Soc. 67, 1554 (1945).
4. CLARK, H.   J. Phys. Chem. 59, 1068 (1955).
5. LIANG, S.   J. Appl. Phys. 22, 148 (1951).
6. McDERMOT, H. L. and ARNELL, J. C.   Can. J. Chem. 33, 913 (1955).
7. McDERMOT, H. L. and LAWTON, B. E.   Can. J. Chem. 34, 769 (1956).
8. McDERMOT, H. L.   Unpublished.
9. ROSS, S. and WINKLER, W.   J. Colloid Sci. 10, 330 (1955).
10. SINGLETON, J. H. and HALSEY, C. D.   J. Phys. Chem. 58, 1011 (1954).
11. WILSON, L. G. and McDERMOT, H. L.   Can. J. Chem. 35, 15 (1957).

FORMATION OF AN ORGANOCHROMIUM COMPOUND IN THE REDUCTION OF CHLOROFORM BY CHROMOUS PERCHLORATE[1]

F. A. L. ANET

ABSTRACT

The reduction of chloroform by chromous perchlorate in aqueous solution gave chloropentaaquochromium(III) perchlorate and dichloromethylpentaaquochromium(III) perchlorate in equimolecular amounts.

Anet and Leblanc (1) reported that the reduction of benzyl chloride by chromous perchlorate gave an organochromium ion of the structure $Cr(H_2O)_5CH_2Ph^{++}$(I). This method of preparing organochromium compounds could not be extended to simple alkyl halides for these were resistant to reduction under the conditions used. Other halides, e.g. phenacyl chloride, were reduced (1), but did not give organometallic compounds. The present communication deals with the formation of an organochromium compound in the reduction of chloroform by chromous perchlorate.

Whereas methyl chloride and methylene chloride were not reduced by chromous perchlorate at room temperature, chloroform was reduced in a few minutes, and carbon tetrachloride in a few seconds. In both cases where reduction took place, as observed by a change in color from blue (Cr^{++}) to red, it was immediately apparent that the chromous ion was not being oxidized solely to either $Cr(H_2O)_6^{+++}$ (pale blue-violet) or $Cr(H_2O)_5Cl^{++}$ (green), or to a mixture of the two ions. The red solution obtained from carbon tetrachloride decomposed to a green solution in a few seconds, and was not examined further. However, the red solution obtained in the reduction of (excess) chloroform appeared to be unchanged after a few hours, even in the presence of air. The products in this solution were therefore investigated.

The solution, which was actually grayish-red in color, contained no free chloride ion, for addition of silver nitrate did not give a precipitate. Since it was suspected that there was more than one chromium species present, separation of the components from the red solution by extraction with butanol was tried. This failed, although the procedure had been successful (1) in separating the products from the reduction of benzyl chloride. A separation into two components was achieved by ion-exchange chromatography of the solution on Dowex 50-X4 resin and elution with M perchloric acid. The first fraction eluted was green in color and its visible absorption spectrum and reactions showed that it contained the ion $Cr(H_2O)_5Cl^{++}$. The second fraction was pinkish-red and appeared to contain only a single colored ion, as shown by the constancy of its absorption spectrum (λ_{max} 395 mμ and 510 mμ) as it was being eluted. Analysis of this fraction (*vide infra*) showed that the color was due to an organochromium ion of the structure $Cr(H_2O)_5$-$CHCl_2^{++}$.

The method of analysis previously (1) used with I was not applicable, as no reaction took place on addition of mercuric chloride to the red fraction. When the red fraction was heated, chloride ions were liberated and a reducing solution was produced. Accordingly, it was heated with silver perchlorate and potassium permanganate. Silver chloride was precipitated along with manganese dioxide, but addition of hydrogen peroxide left only the former, which was collected and weighed. The carbon dioxide which was evolved during the oxidation was swept out by nitrogen and determined as barium

carbonate. Finally, chromium was determined spectrophotometrically in the solution left after filtration of the silver chloride. These results gave a ratio of Cr: C: Cl very close to 1: 1: 2. The amount of potassium permanganate consumed was determined in separate experiments and corresponded to the oxidation of $Cr(H_2O)_5CHCl_2^{++}$ to Cr^{+++}, Cl^-, H_2O, and CO_2.

The position of elution of the red fraction strongly suggested that the colored ion had two positive charges, for King and Dismukes (2) have found that the minimum concentrations of perchloric acid required to easily elute chromium species of charges $+1$, $+2$, and $+3$ from Dowex 50 resin are 0.1 M, 1 M, and 5 M respectively.

The amounts of chromium present in the green and red fractions above were equal, and accounted for all the chromous perchlorate used in the reduction.

These results can be explained most simply if the red fraction contains the ion $Cr(H_2O)_5CHCl_2^{++}$(II), analogous in structure to $Cr(H_2O)_5CH_2Ph^{++}$ obtained from benzyl chloride (1), and formed as follows:

$$CHCl_3 + 2Cr^{++} + 10H_2O \rightarrow Cr(H_2O)_5Cl^{++} + Cr(H_2O)_5CHCl_2^{++}.$$
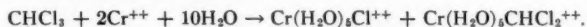
The ion II may be described as an octahedral complex of chromium(III) with five water molecules and the dichloromethyl anion as ligands. The stability of this organochromium ion, like that of I, is due to the substitution-inertness of chromium(III) complexes (3). Thus the chromium–carbon bond behaves like a covalent bond with little polar character.

The reactions of II were rather different from those of I previously studied (1). Whereas I underwent decomposition on heating to give bibenzyl, presumably via benzyl radicals, II did not give tetrachloroethane, or its reduction product, dichloroethylene (since chromous ions would be formed as well). Instead, chloride ions were liberated but no volatile organic compound was formed. This reaction is at present under investigation. Unlike I, II did not react with oxygen, sulphur dioxide, or mercuric chloride, nor was it reduced by hydrogen in the presence of a palladium catalyst. Attempts to obtain sparingly soluble salts of II were not successful.

Taube and Myers (4) have found that chromous perchlorate reduced $Co(NH_3)_5Cl^{++}$ as follows:

$$Co(NH_3)_5Cl^{++} + Cr^{++} + 5H_2O \rightarrow Cr(H_2O)_5Cl^{++} + Co^{++} + 5NH_3.$$

In this one-electron reduction, no free chloride ion was liberated, and it was shown that the reduction took place by direct transfer of a chlorine atom from cobalt to chromium. If it is assumed that the first step in the reduction of chloroform proceeds in a similar fashion, with transfer of a chlorine atom from carbon to chromium, then dichloromethyl radicals will be formed,

$$CHCl_3 + Cr^{++} + 5H_2O \rightarrow Cr(H_2O)_5Cl^{++} + \cdot CHCl_2.$$
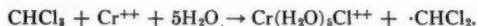
These radicals can either dimerize or react with chromous ion to give an organochromium ion as follows:

$$\cdot CHCl_2 + Cr^{++} + 5H_2O \rightarrow Cr(H_2O)_5CHCl_2^{++}.$$
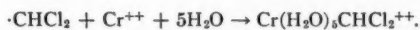
If this reaction is fast, no dimerization will take place.

Thus the mechanism is consistent with the observed facts that no chloride ion was produced and that an equal amount of II and $Cr(H_2O)_5Cl^{++}$ were formed.* It is also

*It was stated in our communication (1) on the reduction of benzyl chloride with chromous perchlorate that the inorganic chromium species formed were $Cr(H_2O)_6^{+++}$ (mainly) and $Cr(H_2O)_5Cl^{++}$. It seems, however, that the $Cr(H_2O)_6^{+++}$ was formed as a result of the decomposition of $Cr(H_2O)_5CH_2Ph^{++}$, for under suitable conditions we have now found that no chloride ion is liberated during the reduction.

in agreement with the fact that carbon tetrachloride was reduced most easily and methyl chloride least easily, for it is known (5) that chlorine substitution stabilizes the methyl free radical. Further work on the mechanism of these reductions is in progress.

EXPERIMENTAL

Preparation of Chromous Perchlorate Solution

Chromous perchlorate was prepared by the electrolytic reduction of chromic perchlorate containing perchloric acid at a mercury cathode. A carbon anode separated from the cathode by a porous porcelain pot was used. The chromic perchlorate was prepared (6) by reduction of reagent grade chromium trioxide with formic acid in dilute perchloric acid and was recrystallized from a small amount of dilute perchloric acid. The reagent was prepared, stored, and used under an atmosphere of nitrogen, purified by bubbling through two solutions of chromous chloride containing amalgamated zinc followed by a water wash. As found recently by Schug and King (6), this reagent is stable for some months, unlike that prepared by zinc–amalgam reduction. Various strengths of the reagent from $0.2\ M$ to $0.5\ M$ Cr^{++} in perchloric acid of concentration $0.2\ M$ to $1\ M$ were prepared.

Reduction of Chloroform with Chromous Perchlorate

Water (1 l) was freed of oxygen and then shaken with chloroform (10 ml). Chromous perchlorate (500 ml, $0.2\ M$) solution was added in an atmosphere of nitrogen and the solution allowed to stand 2 to 3 hours at room temperature. The grayish-red solution gave no precipitate with silver nitrate solution at room temperature. A portion (100 ml) of this solution was placed on a column (15 cm $\times$ 2 cm) of Dowex 50-X4 (200–400 mesh) in the hydrogen form and the column eluted with M perchloric acid at the rate of 1–2 drops per second. A green fraction (100 ml) was soon eluted, followed by a colorless solution (150 ml), and then by a red fraction (110 ml). The green fraction had the same visible absorption as described for $Cr(H_2O)_5Cl^{++}$ by Elving and Zemel (7). It gave no precipitate with silver nitrate in the cold, but on heating, silver chloride was gradually precipitated leaving a bluish-violet solution of $Cr(H_2O)_6^{+++}$. The chromium content of the green fraction was determined by direct spectrophotometric measurement in a 1-cm cell, taking $\epsilon = 17.8$ for $Cr(H_2O)_5Cl^{++}$ at λ_{max} 605 mμ (7).

Analysis of Dichloromethylpentaaquochromium(III) Perchlorate Solution

For analysis a quantity of the red fraction above was heated to boiling for 5 minutes with excess (about twofold) of silver perchlorate and potassium permanganate solutions. The cooled solution was treated with hydrogen peroxide to dissolve the manganese dioxide, and the silver chloride filtered off on a sintered glass crucible. The filtrate was made up to a definite volume and its absorbance at 575 mμ measured in a 5-cm cell. For $Cr(H_2O)_6^{+++}$ ϵ was taken as 13.9 at λ_{max} 575 mμ (7). The consumption of potassium permanganate was determined in separate experiments carried out as above except that instead of adding hydrogen peroxide a known quantity of ferrous ammonium sulphate was added, sufficient to react with the excess potassium permanganate and manganese dioxide. The excess ferrous salt was then back-titrated with 0.1 N KMnO$_4$.

A number of analyses were carried out on samples from the same reduction and from different reductions; a typical value obtained for the Cr: C: Cl ratio was 1.00: 1.02: 2.06.

Reactions of Dichloromethylpentaaquochromium(III) Perchlorate Solutions

Solutions in dilute perchloric acid were stable for several hours at room temperature,

and many days at 0°. When the solutions were heated the red color gradually disappeared and the solution became greenish-blue and contained large amounts of chloride ion.

REFERENCES

1. ANET, F. A. L. and LEBLANC, E.   J. Am. Chem. Soc. **79**, 2649 (1957).
2. KING, E. L. and DISMUKES, E. B.   J. Am. Chem. Soc. **74**, 1674 (1952).
3. TAUBE, H.   Chem. Revs. **50**, 69 (1952).
4. TAUBE, H. and MYERS, H.   J. Am. Chem. Soc. **76**, 2103 (1954).
5. STEACIE, E. W. R.   Atomic and free radical reactions. Vol. 1. 2nd ed. Reinhold Publishing Corporation, New York. 1954. p. 96.
6. SCHUG, K. and KING, E. L.   J. Am. Chem. Soc. **80**, 1089 (1958).
7. ELVING, P. J. and ZEMEL, F.   J. Am. Chem. Soc. **79**, 1281 (1957).

THE KINETICS OF THE DECAY OF NITROGEN ATOMS AS DETERMINED FROM CHEMICAL MEASUREMENTS OF ATOM CONCENTRATIONS AS A FUNCTION OF PRESSURE[1]

Roger Kelly[2] and C. A. Winkler

ABSTRACT

A method is described for studying both the surface and homogeneous decay of N atoms in which the atom concentration reaching a reaction vessel after a period of decay is measured as a function of pressure by HCN production from ethylene or ethane under conditions of complete consumption of the atoms and complete initial dissociation of the nitrogen. The results indicated that the surface decay proceeded by a first-order mechanism between 55° C and 400° C, with the collision efficiency for an Na_2HPO_4 surface essentially constant at 2.75×10^{-4}. The activation energy of surface decay was 1.0 kcal mole^{-1} and the concentration of surface species 1.9×10^{14} cm^{-2}. It was concluded that the surface decay probably leads directly to molecules in the ground state.

Depending on the temperature and whether or not N_2 and N were considered equivalent as third bodies, the rate constant of the homogeneous decay varied from 1.09×10^{-33} to 13.2×10^{-33} cc^2 molecule^{-2} sec^{-1}. The homogeneous decay therefore appears to have a positive temperature coefficient and to be of only secondary importance below about 2 mm pressure under the prevailing conditions. The similarity of *one-half* the rate constant of homogeneous decay at 25° C (0.55×10^{-33} to 0.97×10^{-33}) to the rate constant of afterglow emission obtained by Berkowitz *et al.* (2×10^{-33}) suggests that *all* homogeneous decay gives rise to afterglow via the $^5\Sigma$ state.

Of the numerous studies on atom decay that have been published, perhaps the most conclusive have been those of Smith (1) and Linnett and Marsden (2, 3) on the surface decay of H and O atoms respectively. In both cases, atom concentrations in a side arm attached to a discharge tube were measured with a thermocouple probe. Since complications due to flow were eliminated, the mathematical analysis of the results was fairly simple, and it was possible to show that first-order surface decay with a collision efficiency in the range 10^{-3} to 10^{-5} was the dominant mode of decay at the pressures and temperatures used. The homogeneous decay of H atoms has also received considerable attention (e.g. 4).

Studies on the decay of active nitrogen and therefore on the recombination of the N(^4S) atoms which are its major constituent (5, 6) have, on the other hand, generally been qualitative. In fact, the only rate constant for N atom decay that has apparently been published is that for the emission of afterglow in homogeneous decay (6), while, in the case of the surface decay, even the order itself has not been settled beyond question. The main facts known about N atoms are thus the following. They decay in part on surfaces and in part homogeneously (7). The surface decay is nonluminous, i.e. the afterglow does not intensify in the neighborhood of surfaces (7), and probably first-order (7, 8, 9). Part or all of the homogeneous decay is accompanied by the emission of yellow-orange afterglow (7), the intensity of which is proportional to [active nitrogen]^2 [inert gas] (10, 6). (The work cited did *not* determine whether the inert gas could include the active nitrogen itself.) The rate constant of afterglow emission is 2×10^{-33} cc^2 molecule^{-2} sec^{-1} (6) and the mechanism probably involves an $N_2(^5\Sigma)$ intermediary (6, 11).

The present work was undertaken to confirm the order of the surface decay of N atoms, and to obtain rate constants for both the surface and homogeneous decay.

EXPERIMENTAL

Choice of Method

The measurement of N atom concentrations is complicated by the fact that, though active nitrogen contains the ^4S atom as a major constituent, there is still a possibility that excited molecules are present (12, 13, 14, 15, 16), if only in low vibrational levels of the ground state. Virtually any excited form would, of course, be deactivated on a metal surface (14), so that measurements of the activity using a thermocouple probe (cf. 1, 2, 3) would be of uncertain significance. On the other hand, the production of HCN from ethylene under conditions of complete consumption ("cleanup") of active nitrogen (high ethylene flowrates and elevated temperatures), a mode of measurement frequently used in past work (e.g. 17, 18), would likely reflect the *atom* concentration alone owing to the high activation energy to be expected in most reactions involving excited nitrogen molecules (13).[3] HCN production also has the advantages that it is not subject to mechanical failure and, since negligibly small quantities of other nitrogen-containing compounds are formed (20, 21), it provides an absolute value of the atom concentration. Production of HCN from ethylene was therefore chosen to measure the N atom concentration and the results were checked using ethane.

Apparatus

The use of chemical measurement of the atom concentrations meant that a fast-flow system of the type employed by Winkler and co-workers (see, in particular, 21, 22, 23) rather than the much simpler diffusion system of Smith (1) or static system of Rayleigh (7) had to be used (Fig. 1).

Dry, oxygen-free nitrogen[4] at atmospheric pressure was introduced at A and passed through a needle reduction valve B and a capillary flowmeter C. In the discharge tube D the nitrogen was subjected to a rapid condensed discharge. (Internal electrodes which had been machined from solid aluminum were used. They were about 60 cm apart, and were each 7.0 cm long, 1.8 cm O.D., and 7/16 inch I.D.; two setscrews were used to affix them to lengths of 0.060-inch diameter tungsten wire.) The resulting atom-containing mixture was then passed through a tube E, which will be called the "decay tube". In most of the work the decay tube had a volume of 281 cc, a length of 31.7 cm, and an I.D. of 3.36 cm (see, however, series 2). The large volume served to increase the time of decay and therefore (i) to lower the N atom concentration sufficiently, even under conditions of complete initial dissociation, for cleanup to be readily achieved, and (ii) to make the effect of dissociation on the decay time less marked (Appendix C). The large diameter served (i) to reduce the pressure gradient in the decay tube (Appendix A), and (ii) to reduce the rate constant of surface decay. A cylindrical, electrically heated furnace was built around the decay tube to determine the effects of temperature on the rate constants. At the lower end of the decay tube was a constriction 2.0 cm long and 0.60 cm I.D. which served (i) to terminate the region of decay sharply and independently of pressure (i.e. the reaction flame was invariably located just below the constriction), (ii) to enable independent heating and poisoning of the decay tube and reaction vessel, and (iii) to prevent back-diffusion of the reactant from the reaction vessel. The decay tube was followed by a 300-cc spherical reaction vessel F into which the reactant could be injected

[3]*Direct evidence to this effect appears to have been obtained in a study of the reaction of active nitrogen with nitric oxide (19). However, even if the excited molecules could react to give HCN, such HCN production would be automatically eliminated by the use of limiting slopes as described in a following section, provided the excited molecules were formed only by homogeneous atom decay.*

[4]*The method of purification is that described in references (21) and (23) rather than (22), i.e. passing the nitrogen over heated copper and through a liquid-air trap.*
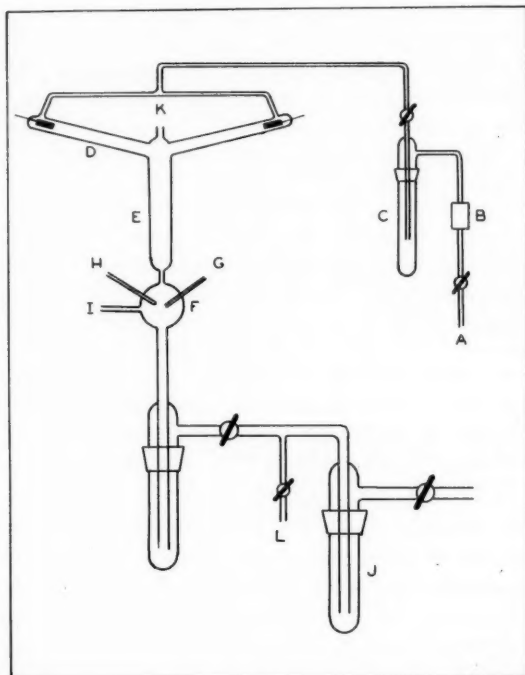
FIG. 1. Apparatus.

through jet G. (The arrangement for metering in the reactants has been described else-where (21).) The reaction vessel was surrounded by a second furnace, the temperature of which was measured by a thermocouple in the well H; a McLeod gauge was attached at I. From the reaction vessel the gas mixture was led through a trap J surrounded by liquid air, and thence to a pump. The Wrede gauge outlet K was present only during the experiments of series 4.

In the majority of the experiments the discharge tube, decay tube, and reaction vessel were poisoned by drawing up a 20% aqueous solution of Na_2HPO_4. This poison was used, rather than the more efficient HPO_3, since it did not react with ammonia and was unusually stable and reproducible. In a few experiments of series 6 the poison on the reaction vessel alone was changed to KCl; however, KCl could not be used in the discharge tube nor on any heated surface, since the active nitrogen then reacted with it, creating an intense reddish-orange glow.

Power was supplied from a 220-v a-c. source, transformed first with a 2400-w, 220-v variac and then with an 1897-w, 110 → 4820-v transformer, and finally rectified with two Raytheon 866A tubes in parallel. The weakest element in the circuit was the variac, which burned out several times. For most of the work the secondary circuit had a resis-tance of 1250 ohms and a capacitance of either 4 μf (for pressures <1.7 mm) or 2 μf (for pressures >1.7 mm, <4 mm). If the variac were adjusted to give a flashrate of 60 per second (except in the pressure range 1.2 to 1.7 mm, when 30 to 40 per second was ade-quate), complete dissociation of the nitrogen could be brought about. (This is treated in detail in a following section.)

HCN production was determined by titrating the recovered HCN with $AgNO_3$ (24) after it had been distilled at $-23°$ C from the trap (previously coated with solid CCl_4) into a removable unit attached at L and containing about 15 cc of frozen water (cf. 25). A sufficient amount of product to enable convenient analysis was generally obtained with reaction times of 100 seconds.

THEORY

To derive decay equations, i.e. equations which will relate the atom concentrations measured in the reaction vessel to the rate constants for decay, it is necessary to know the rate-controlling step in each mode of decay. These steps may be summarized as follows:

radiative decay $\qquad\qquad\qquad\qquad$ $N + N \rightarrow N_2 + h\nu$,

homogeneous decay $\qquad\qquad\qquad$ $N + N + M \xrightarrow{k_2} N_2^* + M$,

where M is a third body and N_2^* an unspecified excited molecule;

first-order surface decay $\qquad\qquad$ $N + N \cdot surface \xrightarrow{k_1} N_2 + surface$,

and second-order surface decay $\qquad$ $N + N + surface \xrightarrow{k_3} N_2 + surface$.
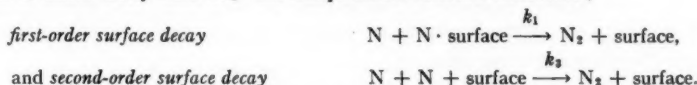
The constants k_1, k_2, and k_3 will be defined to give the rate of atom destruction directly, without a factor of two.

Before proceeding further it will be necessary to introduce certain simplifications. Radiative decay will be neglected altogether, in general because stabilizing radiation is seldom observed in the recombination of atoms and free radicals, in particular because the nitrogen afterglow, which might be identified with such radiation, is neither continuous (26, p. 400) nor diffuse (26, p. 414), and obeys termolecular kinetics. For homogeneous decay only extreme cases of third-body efficiency will be treated. In the one case, which in the present work turns out to correspond to a lower limit of k_2, N_2 and N will be considered to be equivalent as third bodies for N atom recombination, so that [M] becomes simply the total observed pressure P. In the other, which corresponds to an upper limit of k_2, the efficiency of N as a third body will be considered to be much less than that of N_2, so that [M] becomes $(P-[N])$.[5] The two orders of surface decay will be assumed to be mutually exclusive. In terms of the mechanisms of surface decay to be discussed later this situation should prevail at temperatures or atom concentrations where the number per cm^2 of surface species (C_s in equation [10]) either approaches its maximum (i.e. monolayer) value to yield first-order surface decay, or becomes proportional to the atom concentration, corresponding to second-order surface decay.

Depending on the order of the surface decay and the relative efficiencies of N_2 and N as third bodies, four differential equations of decay are thus possible:

[1] $\qquad\qquad\qquad d[N]/dt = -k_1[N] - k_2[N]^2 P$,

[2] $\qquad\qquad\qquad\qquad\quad = -k_1[N] - k_2[N]^2(P-[N])$,

[3] $\qquad\qquad\qquad\qquad\quad = -k_3[N]^2 - k_2[N]^2 P$,

[4] $\qquad\qquad\qquad\qquad\quad = -k_3[N]^2 - k_2[N]^2(P-[N])$.

[5]In the event that evidence was obtained that the efficiency of N was greater than that of N_2, the case where [M] = [N] would have to be considered instead. This case cannot, of course, be eliminated a priori, since according to the mechanism of homogeneous decay proposed by Berkowitz et al. (6) the main function of the third body is to induce an electronic transition.

The significance of each is obvious. If $[N]_0$ is the value of $[N]$ at $t = 0$, the solutions of equations [1] and [3] are, respectively,

[5] $$P/[N] = e^{k_1 t}P/[N]_0 + (e^{k_1 t}-1)k_2 P^2/k_1$$

and

[6] $$1/[N]-1/[N]_0 = (k_3+k_2 P)t.$$

Though an exact solution to equation [2] can also be obtained, it is not readily used for interpreting experimental data unless $[N]_0 = P$ and $[N] \ll P$. Then

$$\ln P/[N]-k_1 t \approx (k_2 P/\sqrt{q})\ln \frac{1+k_2 P/\sqrt{q}}{1-k_2 P/\sqrt{q}},$$

where $q = k_2^2 P^2+4k_1 k_2$. If, in addition, $k_2 P \ll 2\sqrt{k_1 k_2}$, an even simpler form arises,

[7] $$1/(\ln P/[N]-k_1 t) \approx \tfrac{1}{2}+2k_1/k_2 P^2.$$

Equation [7] is obviously valid only at low pressures and also requires a prior knowledge of $k_1 t$ obtained from equation [5]. Since the surface decay will be shown to be first order, equation [4] will not be further considered except to note that at not too low pressures its solution reduces to equation [6].

In interpreting experimental data in terms of equations [5] to [7], the data obtained at low pressures must be weighted more heavily than those at high pressures. For example, in plots of $P/[N]$ versus P^2, the limiting slopes as $P \to 0$ would be derived rather than slopes of best fit. The reasons are the following: (i) Equations [1] to [7] actually presume a number of conditions respecting diffusion, the time of decay, etc., such that the equations are more valid at low pressures (see Appendix A). (ii) Equation [7] is *inherently* valid only at low pressures. (iii) If excited molecules are present, there is a possibility that their reactivity will be superimposed upon that of the atoms; however, if they are formed only by the homogeneous decay of the atoms, their concentration necessarily falls off rapidly as the pressure is decreased.

Though equations [5] to [7] can in general be applied to studies in which any one of $[N]_0$, time, or pressure is varied, pressure variation alone is used in the present work. However, it is then necessary that the initial dissociation be complete, i.e. $[N]_0 = P$, since otherwise $[N]_0$ becomes an unknown function of P. Additional reasons why complete dissociation is desirable are that a precise control of the flashrate is then not necessary, equation [7] is inherently valid only under such conditions, and it becomes possible to distinguish unambiguously the different orders of surface decay simply by comparing the low-pressure asymptote of a graph of $[N]$ versus P with the line corresponding to the maximum possible atom flowrate, i.e. $2[N_2]$ versus P. The asymptote would coincide with this line if the surface decay were second order, but would have a much reduced slope $(Pe^{-k_1 t})$ if it were first order. These relations hold irrespective of the relative efficiencies of N_2 and N as third bodies. (While the striking feature of Smith's method was a similar clear-cut distinction of reaction order, it should be pointed out that the present method, in contrast to that of Smith, enables the evaluation of rate constants for homogeneous decay. It is not sufficiently sensitive, however, to determine the relative efficiencies of N_2 and N as third bodies.)

An additional relation that will be required is that for obtaining the collision efficiency or "recombination coefficient" from a rate constant for first-order surface decay. For a cylindrical decay tube of radius r_0 it is given by (27)

[8] $$\gamma = (2r_0/\bar{c})(k_1/2),$$

where $\bar{c}$ is the mean kinetic velocity. If γ is known, the activation energy of surface decay (E_1) and the number per cm² of surface species (C_s) can also be obtained using absolute rate theory (28, 27):

[9] $$E_1 = -Rd(\ln \gamma T)/d(1/T)$$

and

[10] $$C_s = 2\pi mkT\gamma/h^2 e^{-E_1/RT},$$

where T is the absolute temperature and k the Boltzmann constant. Equations [9] and [10] should be valid for any mechanism of surface decay which assumes an *immobile* surface layer.

The use of $k_1/2$ rather than k_1 in equation [8] represents a departure from the original treatment (27), but is likely more correct. Thus, considering a given surface site, each instance of decay will be followed by an instance of surface-layer formation. Since dissociation or bond stretching are not involved in the formation of a surface layer of atoms, the activation energy should be zero (28) and the process correspondingly rapid. The result is that the observed rate of decay will be double that due to the activated process described by equations [8] to [10]. Conversely, the use of an uncorrected rate constant in equation [8] as in previous publications (e.g. 1, 2, 3, 27) would make γ *high* by a factor of two.

<div align="center">RESULTS</div>

Conditions of Cleanup

A cleanup of N atoms is achieved only at high reactant flowrates and above a certain temperature. For the reactants used in the present work the minimum temperatures (about 300° C) were readily obtained from published data (21). Since minimum flowrates, on the other hand, depend on the atom concentration, on the reaction temperature, and on factors peculiar to each apparatus, the results of past work could not be used. It was therefore necessary to determine, at a series of atom concentrations, the minimum flowrate applicable with each reactant and reaction temperature. The data obtained in these preliminary experiments will not be given, though it will be understood that in all experiments to be described plateau flowrates of reactant were used.

Extent of Initial Dissociation

The first four series of experiments were designed to determine if complete initial dissociation, i.e. $[N]_0 = P$, could be brought about without overtaxing the electronic components. In all cases the decay tube and reaction vessel were unheated. In *series 1* the amount of HCN formed from ethylene at 0.80 mm pressure and a capacitance of 4 μf was determined as a function of primary voltage (variac setting) and thence flashrate. Discharge was observed to start at 35 v, while the HCN production remained constant from 45 to 70 v.

The apparatus used in *series 2* differed in having a much smaller decay tube: 14.0 by 1.55 cm, volume = 26 cc. Accordingly, the time of decay was much shortened and the data should have indicated more directly the variation of $[N]_0$. However, a cleanup of N atoms was difficult to achieve, so that the destruction of ammonia, which is apparently due to excited molecules present in the active nitrogen in small amounts (12, 13, 16), was measured instead. (The amount of ammonia destroyed was determined as the difference between pressure–volume measurements of the amount drawn from the storage vessel and the amount recovered.) The results, obtained as a function of pressure, primary voltage,

and capacitance are given in Fig. 2A. It is seen that, as the pressure was increased, the ammonia destruction at each primary voltage and capacitance at first followed a common curve, but finally dropped below as the flashrate decreased to zero. No energy expenditure would bring the reactivity above this common curve.
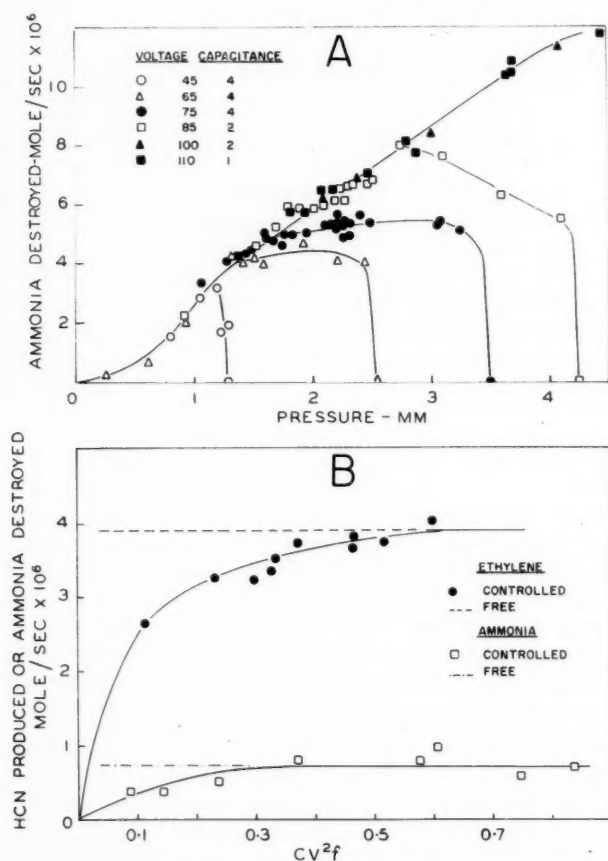
FIG. 2A.   Series 2. Ammonia destruction as a function of pressure, primary voltage, and capacitance (μf).
FIG. 2B.   Series 3. HCN production from ethylene and ammonia destruction as functions of CV^2f and the nature of the discharge.

In *series 3* a more precise energy variation study was conducted at 1.4 mm pressure with the flashrate electronically controlled.[6] The exact amount of energy expended in terms of CV^2f, where C is the capacitance, V the primary voltage, and f the flashrate, could thus be determined. As in series 1 and 2, the reactivities of ethylene and ammonia were readily made independent of energy expenditure (Fig. 2B), and it will be noted that the values then corresponded to those obtained at a similar pressure but under the conditions of series 5 and 6, viz. free discharge and with the circuit described earlier.

[6]*A General Electric FG105 thyratron was incorporated into the high-voltage circuit, a 90-v dry cell being sufficient to keep it non-conducting. The flashrate could then be controlled by shorting out the dry cell with a variable speed, motor-driven, rotary spark gap.*

The observation in the preceding series that reactivities could be made independent of energy expenditure indicates, of course, either that the desired condition of complete initial dissociation was achieved, or else that an equilibrium condition of partial dissociation occurred. Accordingly, in *series 4* a Wrede gauge made of sintered glass (Fisher filter stick of fine porosity) was attached to the discharge tube as indicated in Fig. 1 (K), and then connected to a differential manometer consisting of a nearly horizontal U-tube filled with diffusion-pump oil. The manometer was calibrated against a McLeod gauge. However, some difficulty was encountered using the Wrede gauge, since each reading required at least 20 minutes before the manometer was steady, so that, by the time several readings had been made at the high energy expenditures used, the discharge tube became contaminated with material from the electrodes (cf. 2, p. 496) and $[N]_0/P$ values in the range 0.15 to 0.20 were the highest that could be obtained. In an attempt to counteract this contamination, ethane was injected into the nitrogen stream at a point prior to the discharge tube for a few seconds at the beginning of each experiment. The polymeric material which would be laid down on the walls was expected to restore the apparatus to a condition more nearly like that during normal experiments, and greatly increased $[N]_0/P$ values (in the range 0.55 to 0.60) were in fact observed.

In interpreting the gauge measurements, it must be borne in mind that they represent the *average* atom concentrations in the discharge tube, not those at the instant of discharge. The observed $[N]_0/P$ values should therefore be compared with the maximum average values obtainable at the flashrates used, i.e: with

$$\overline{[N]_0/P} = 1/t \int_0^t ([N]/P)\, dt.$$

Expressing $[N]/P$ in terms of equation [5], and substituting $P = 1.4$ mm (the pressure at which most of the gauge measurements were made), $k_1 = 17.2$, $k_2 = 1.77$ (rate constants applicable at 400° C, from Table II), it is possible to show that the values of $\overline{[N]_0/P}$ corresponding to flashrates of 60 and 30 per second are 0.85 and 0.73. If k_1 is doubled, the values for the same flashrates are 0.70 and 0.58. It is therefore evident that, while the $\overline{[N]_0/P}$ values calculated for high flashrates and for normal values of k_1 are slightly in excess of the gauge measurements, the effect of a moderate increase in the rate constant of surface decay k_1, such as would result if the discharge tube were contaminated from the electrodes, is sufficient to make the values agree quite closely. Complete initial dissociation therefore appears to have been achieved (cf. Armstrong and Winkler (29)). (The $\overline{[N]_0/P}$ values given above are of incidental interest in that they indicate the upper limits of active nitrogen concentration that can be obtained at a given flashrate by shortening the decay tube or increasing the flowrate.)

With the information available in series 1 to 4, the minimum energy expenditures which bring about complete initial dissociation at a given pressure can, in principle, be determined. However, a general statement of conditions which give adequate, but otherwise unspecified, energy expenditures is sufficient for the present purposes: see description of circuit. All subsequent experiments will be understood to be conducted under these conditions.

HCN *Production as a Function of Pressure*

The actual study of the decay of N atoms was now undertaken. With the furnace on the reaction vessel set for about 350° C and the decay tube either unheated (average temperature = 55° C; *series 5*) or at 400° C[7] (*series 6*), the HCN production from ethylene

[7]*When the decay tube was at 400° C it was not necessary to heat the reaction vessel to achieve maximum reactivity with ethylene. This was not true, however, with ethane.*

and ethane was determined as a function of pressure (Fig. 3). The maximum possible N atom flowrates, obtained from the observed relation between nitrogen flowrate and pressure by doubling the flowrate values to take dissociation into account, are also indicated in Fig. 3. The experimental values for the two series were obtained in random order so that any differences would be real and not due to permanent changes in the glass or poison. In some of the experiments of series 6 the poison on the reaction vessel alone was changed to KCl. The fact that the low-pressure asymptotes of the curves for HCN production lead to a pressure slightly greater than zero (0.15 mm) probably has no great significance, since a similar property is evident in the relation between nitrogen flowrate and pressure.

The main conclusions to be drawn from Fig. 3 are the following:

(i) Since the amounts of HCN formed from ethylene and ethane coincide at all pressures investigated, a complete cleanup of N atoms rather than fortuitously similar reactivities *without cleanup* is proved.
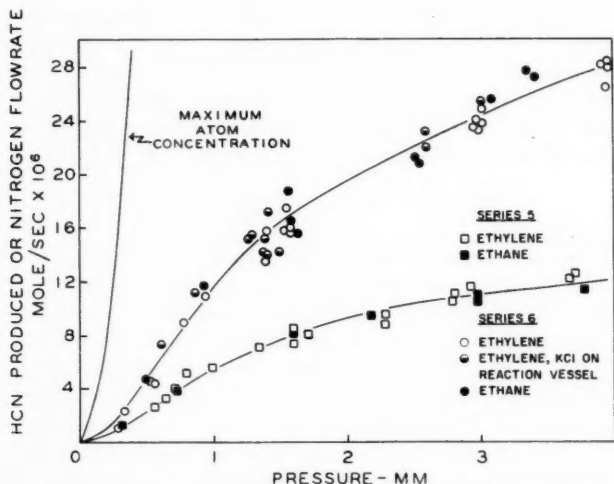
Fig. 3.   Series 5 and 6.   HCN production from ethylene and ethane as a function of pressure at elevated temperatures.

(ii) Since the use of KCl on the reaction vessel has no effect on the results, surface effects may be assumed absent unless, as is unlikely, KCl and Na_2HPO_4 happen to have equivalent poisoning qualities. The absence of surface effects further confirms that cleanup was achieved.

(iii) Heating the decay tube greatly increases the number of N atoms which reach the reaction vessel, though, since the rate constants for decay will be shown to *increase* with temperature, this effect must be due solely to a decreased time of decay (cf. equation [15]).

(iv) Since the low-pressure asymptotes of the curves for HCN production do not coincide with the line giving the maximum possible atom flowrate, the surface decay is shown to be first order and the relevant decay equations are therefore [5] and [7].

(v) The curves for HCN production diverge only slightly from their low-pressure asymptotes up to 2 mm pressure. Surface decay is therefore more important than

homogeneous decay in this pressure region, at least with the poison used and for the given diameter of decay tube.

It was also shown in experiments which will not be described here (*series* 7) that the effect of temperature on decay varies continuously without maxima between the temperatures used in series 5 and 6. All conclusions on N atom decay may therefore be generalized over this range. Such a generalization would not otherwise follow, since, as seen in the H atom study of Smith (1) and in several instances cited by Shuler and Laidler (27, p. 1215), the surface collision efficiency may maximize under certain conditions.

Calculations

As a first step in fitting the data of series 5 and 6 to the relevant decay equations [5] and [7], it was necessary to convert the observed HCN flowrates into partial pressures. This was done by means of the empirical relation between nitrogen flowrate and pressure (part of which is shown in Fig. 3, though with a factor of two), with a suitable correction for dissociation. These relations are discussed in Appendix B and lead to equation [14]. Values of $P/[N]$ calculated from the data of series 5 and 6 by means of this equation are included in Table I.

TABLE I

Data used for the calculation of the rate constants for N atom decay

Pressure, mm	$[N] = HCN$ $\mu m/sec \times 10^6$ (from Fig. 3)	Conversion factor $\mu m/sec \leftrightarrow mm$ (from eq. [14])	$P/[N]$	$1/(\ln P/[N] - k_1 t)$
		Temperature of decay tube: 55° C		
0.5	2.3	.0233	9.32	24.
1.0	5.4	.0190	9.74	11.6
1.5	7.7	.0180	10.8	5.26
2.0	9.3	.0176	12.2	3.22
2.5	10.3	.0174	13.95	2.25
3.0	11.0	.0173	15.75	1.76
3.5	11.6	.0172	17.55	1.48
4.0	12.2	.0172	19.1	1.32
		Temperature of decay tube: 400° C		
0.5	4.6	.0223	4.87	23.
1.0	11.6	.0180	4.79	37.
1.5	16.0	.0171	5.48	6.21
2.0	19.4	.0168	6.14	3.64
2.5	22.2	.0167	6.73	2.72
3.0	24.4	.0166	7.40	2.17
3.5	26.4	.0166	7.97	1.87
4.0	28.0	.0166	8.59	1.64

To obtain k_1, the lower limits of k_2, and certain related quantities, plots of $P/[N]$ versus P^2 in accordance with equation [5] were now made (Figs. 4A and 4B). From the intercepts of the limiting slopes as $P \rightarrow 0$, i.e. $e^{k_1 t}$ (note that the factor $P/[N]_0$ drops out under conditions of complete initial dissociation), the quantity $k_1 t$ was obtained, with k_1 following from equation [17] as derived in Appendix C. The lower limits of k_2 could then be obtained from the limiting slopes themselves, i.e.

$$d(P/[N])/dP^2 = (e^{k_1 t} - 1)k_2/k_1,$$

and values for the collision efficiency (γ), activation energy of surface decay (E_1), and number per cm² of surface species (C_s) from equations [8], [9], and [10] respectively.
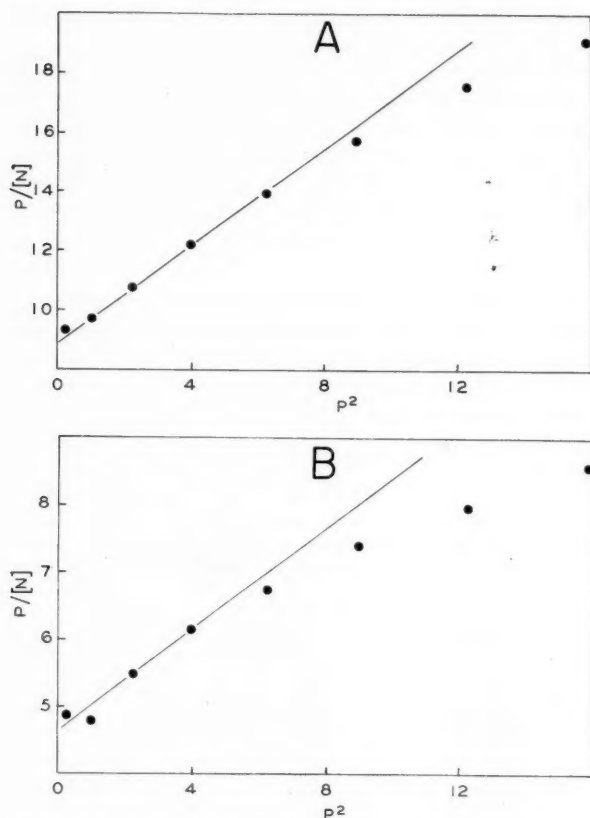
FIG. 4A.   Analysis of the data of series 5 in accordance with equation [5]. (Intercept = 8.9, limiting slope = 0.82 mm^{-2}.)
FIG. 4B.   Analysis of the data of series 6 in accordance with equation [5]. (Intercept = 4.65, limiting slope = 0.375 mm^{-2}.)

Finally, to obtain the upper limits of k_2, plots of $1/(\ln P/[N]-k_1t)$ versus $1/P^2$ in accordance with equation [7] were made (Fig. 4C). (Values of $1/(\ln P/[N]-k_1t)$ were included in Table I.) The upper limits of k_2 followed from the slopes of the lines joining the point $(0, \frac{1}{2})$ with *high* values of $1/P^2$, i.e.

$$\frac{d(1/(\ln P/[N]-k_1t))}{d(1/P^2)} = 2k_1/k_2.$$

The values for the various quantities that were derived are given in Table II.

To evaluate exactly the relative importance of homogeneous and surface decay *under the prevailing conditions*, the following relation was used: mean ratio of homogeneous to surface decay =

$$1/P \int_0^P (k_2/k_1)P[N]d[N] = k_2P^2/2k_1.$$
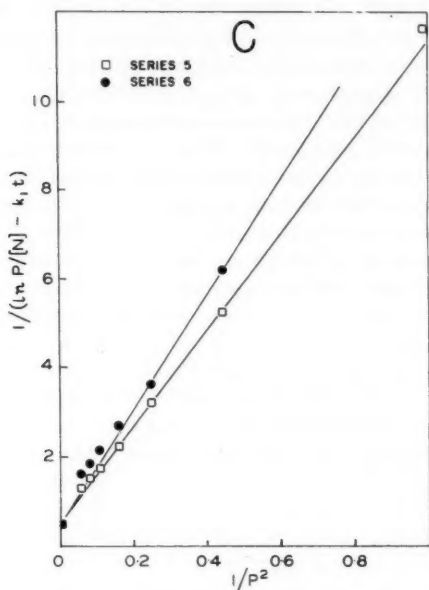
FIG. 4C. Analysis of the data of series 5 and 6 in accordance with equation [7]. (Limiting slopes = 10.90 mm² [series 5], 12.60 mm² [series 6].)

Using $k_1 = 11.1$ and $k_2 = 1.15$ this expression yields 0.052 at 1 mm and 0.83 at 4 mm. The previous conclusion is therefore confirmed that homogeneous decay is of secondary importance below about 2 mm pressure *under the prevailing conditions.*

TABLE II

The rate constants for N atom decay and related quantities

Quantity*	Value at 55° C	Value at 400° C
$k_1 t$	2.19	1.54
k_1	11.1 sec^{-1}	17.2 sec^{-1}
γ	2.65×10^{-4}	2.86×10^{-4}
k_2 (lower limit)	1.15 A	1.77 A
	1.32×10^{-33} B	8.6×10^{-33} B
k_2 (upper limit)	2.04 A	2.73 A
	2.35×10^{-33} B	13.2×10^{-33} B
E_1	1.0 kcal mole^{-1}	
C_s	1.9×10^{14} cm^{-2}	

*k_1, γ, E_1, and C_s apply only to surfaces coated with Na_2HPO_4. The units of k_2 are abbreviated as follows: A $\equiv$ mm^{-2} sec^{-1}, B $\equiv$ cc^2 molecule^{-2} sec^{-1}. Values for k_2, obtained from those at 55° C by using 298° K in the factor to convert mm^{-2} to cc^2 molecule^{-2}, are as follows: $>1.09 \times 10^{-33}$ B, $<1.94 \times 10^{-33}$ B.

DISCUSSION

The Decay of N, H, *and* O *Atoms*

The present work has confirmed that the surface decay of N atoms follows first-order kinetics. While this result was anticipated, it is perhaps significant that close similarities

exist in the behavior of N, H, and O atoms. All exhibit first- rather than second-order surface decay with collision efficiencies (γ) in the range 10^{-3} to 10^{-5}, activation energies (E_1) in the range 1 to 2 kcal mole^{-1}, and values of 10^{14} to 10^{15} cm^{-2} for the concentration of surface species (C_s).[8] It would therefore be expected that the mechanism of the surface decay of N atoms would be the adsorption mechanism which has been so successful in explaining the behavior of H atoms (27). This mechanism proposes that the gas-phase atoms recombine with a layer of atoms adsorbed on the surface (8, 9, 27, 28), the order of the process depending on whether the surface layer is complete or concentration dependent. However, Linnett and Marsden (2, 3) have pointed out that at room temperature O atoms are only weakly adsorbed on glass. To explain the first-order decay they therefore suggested a slightly different mechanism according to which the gas-phase O atoms combine directly with the structural oxygen of the glass or poison, with water of hydration, or with a surface layer of oxide. This mechanism would give second-order kinetics only at temperatures sufficiently high to decompose the surface compound, i.e. at temperatures well in excess of the "desorption" temperature.

Since there seems to be no information available on the adsorption of N atoms on Na_2HPO_4 or related solids, it is not possible to decide with certainty whether the surface layer responsible for the surface decay consisted of adsorbed atoms or a true surface compound (a nitride or nitrate). However, whatever the origin of the layer, it evidently remains intact even at 400° C so that it was valid to assume, in deriving equations [1] to [7], that the two orders of surface decay were not competitive. Furthermore, as stated before, the decision does affect the validity of equations [8] to [10].

The homogeneous decay of N and H atoms is perhaps less comparable than the surface decay, since the rate constants for N atoms (Table II) appear to be an order of magnitude smaller than those for H atoms (Amdur's values of 30×10^{-33} to 61×10^{-33} (4) are typical of a number of H atom studies), in spite of the greater diameter of nitrogen. However, the difference is probably adequately explained by the steric factor shown by Berkowitz et al. (6) to be associated with the transition $N_2(^5\Sigma) + M \rightarrow N_2(B^3\Pi) + M$.

A positive temperature coefficient was observed for the rate constant of N atom homogeneous decay. This was unexpected in view of Rayleigh's (10) observation of a negative temperature coefficient in measurements of afterglow intensity between the temperature of liquid air and 100° C, and it is therefore possible that the results of the present work were subject to a large, systematic error. Perhaps the most likely source of such an error lies in the assumption of complete initial dissociation, since, had $[N]_0/P$ steadily decreased as pressure was increased, the effect would have been easily mistakable for a pressure-dependent mode of decay; however, no pressure dependence in $[N]_0/P$ was observed in the Wrede gauge measurements of series 4. The positive temperature coefficient therefore appears to be real. If the positive temperature coefficient observed by Robinson and Amdur (30) in the decay of H atoms could be attributed not only to the surface decay, but also to the homogeneous decay, the present results for N atoms could be considered to have good precedent.

Details of the Decay Mechanisms

To good approximation, a ^4S atom can combine only into $^1\Sigma_g^+$, $^3\Sigma_u^+$, $^5\Sigma_g^+$, and $^7\Sigma_u^+$ molecular states (6). For nitrogen, the $^7\Sigma$ state is probably higher than the ^4S dissociation

[8]*For H atoms the values of E_1 and C_s are: $E_1 = 0.9$ (30), $C_s = 1.35 \times 10^{15}$ (31, 32, 27), where E_1 applies only to dry surfaces (27). The corresponding values for O atoms can be calculated from the data of Linnett and Marsden as given in Table I of ref. (2) (Fig. 8 of this reference could not be used as it appears to have an error in the ordinate): $\gamma = (1.2/2) \times 10^{-4}$ at 17° C, $\gamma = (3.56/2) \times 10^{-4}$ at 400° C. Hence $E_1 = 2.0$, $C_s = 2.7 \times 10^{14}$. The introduction of a factor of two was justified in an earlier section.*

energy, while the $^5\Sigma$ state is believed to be the precursor of the afterglow (6, 11). There-fore, since it has been observed both by Rayleigh (7) and in the present work[9] that the afterglow intensity remains unchanged in the neighborhood of various surfaces, the *final* molecules formed in surface decay must be in the $A^3\Sigma$ or ground states. A further decision between these two states could perhaps best be made if the long-lived $A^3\Sigma$ molecules (14) could be shown absent from active nitrogen, or, if present, formed only from homogeneous atom decay. Such information is not available, but it is significant that the surface layer responsible for the surface decay remained intact at 400° C. That is, the *transition* molecules formed in surface decay probably exist briefly in close association with the wall, so that complete deactivation to low vibrational levels of the ground state should occur before the molecules separate. It is therefore suggested that the following mechanism accounts for *all* the surface decay (cf. 27):

$$N(^4S) + \text{surface} \rightarrow N(^2S) \cdot \text{surface},$$
$$N(^4S) + N(^2S) \cdot \text{surface} \xrightarrow{k_1} N_2(^y\Sigma) \cdot \text{surface},$$
$$\rightarrow N_2(^1\Sigma) \cdot \text{surface},$$
$$\rightarrow N_2(^1\Sigma) + \text{surface},$$
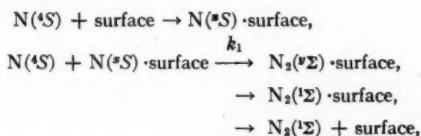
where x and y cannot be specified with certainty due to the proximity of a surface, and $N_2(^y\Sigma)\cdot$ and $N_2(^1\Sigma)\cdot$ are transition molecules.

With homogeneous decay there exists a similar choice of paths and it was, in fact, considered by Berkowitz *et al.* (6) that recombination into the $^5\Sigma$ state with subsequent afterglow emission accounted for only part of the decay. This conclusion was based on a comparison of the rate constant of afterglow emission (2×10^{-33}) with the rate constant for a three-body collision process ($\sim10^{-32}$). However, comparing the former with *one-half*[10] the rate constant of homogeneous decay at 25° C as obtained in the present work (0.55×10^{-33} to 0.97×10^{-33}), it appears that *all* homogeneous decay must give rise to afterglow via the $^5\Sigma$ state, since the constants are essentially equal. This conclusion would be unaltered even if the afterglow constant were *high* by a factor of two or three, so that the following mechanism, which is identical with that proposed by Berkowitz *et al.* (6), may be tentatively assumed to account for *all* the homogeneous decay:[11]

$$\left.\begin{array}{l} 2N(^4S) + M \rightleftharpoons N_2(^5\Sigma) + M \\ N_2(^5\Sigma) + M \longrightarrow N_2(B^3\Pi) + M \end{array}\right\} k_2$$
$$N_2(B^3\Pi) \rightarrow N_2(A^3\Sigma) + h\nu$$
$$N_2(A^3\Sigma) \rightarrow ?.$$
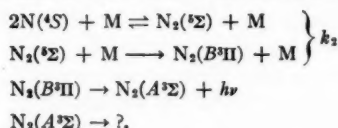
The last step will be considered further in a subsequent paper.

REFERENCES

1. SMITH, W. V. J. Chem. Phys. **11**, 110 (1943).
2. LINNETT, J. W. and MARSDEN, D. G. H. Proc. Roy. Soc. A, **234**, 489 (1956).
3. LINNETT, J. W. and MARSDEN, D. G. H. Proc. Roy. Soc. A, **234**, 504 (1956).
4. AMDUR, I. J. Am. Chem. Soc. **60**, 2347 (1938).
5. JACKSON, D. S. and SCHIFF, H. I. J. Chem. Phys. **23**, 2333 (1955).
6. BERKOWITZ, J., CHUPKA, W. A., and KISTIAKOWSKY, G. B. J. Chem. Phys. **25**, 457 (1956).
7. RAYLEIGH, LORD. Proc. Roy. Soc. A, **151**, 567 (1935).

[9] *The apparatus used was constructed by Dr. A. Fontijn of this Department. It had a window suitable for observing reaction flames.*

[10] *The factor of two arises since two atoms disappear for each photon emitted.*

[11] *Actually, Berkowitz et al. show that this mechanism requires a negative temperature coefficient. A discrepancy therefore exists which must be satisfactorily explained before the mechanism can be adopted without reservation.*

8. BUBEN, N. and SHEKHTER, A.   Acta Physicochim. U.R.S.S. **10**, 371 (1939).
9. SHEKHTER, A.   Acta Physicochim. U.R.S.S. **10**, 379 (1939).
10. RAYLEIGH, LORD.   Proc. Roy. Soc. A, **176**, 1 (1940).
11. KISTIAKOWSKY, G. B. and WARNECK, P.   J. Chem. Phys. **27**, 1417 (1957).
12. FREEMAN, G. R. and WINKLER, C. A.   J. Phys. Chem. **59**, 371 (1955).
13. EVANS, H. G. V. and WINKLER, C. A.   Can. J. Chem. **34**, 1217 (1956).
14. LICHTEN, W.   J. Chem. Phys. **26**, 306 (1957).
15. KAUFMAN, F. and KELSO, J. R.   J. Chem. Phys. **28**, 510 (1958).
16. KISTIAKOWSKY, G. B. and VOLPI, G. G.   J. Chem. Phys. **28**, 665 (1958).
17. FORST, W., EVANS, H. G. V., and WINKLER, C. A.   J. Phys. Chem. **61**, 320 (1957).
18. WILES, D. M. and WINKLER, C. A.   Can. J. Chem. **35**, 1298 (1957).
19. VERBEKE, G. J. O.   Ph.D. Thesis, McGill University, Montreal, Quebec. 1958.
20. VERSTEEG, J. and WINKLER, C. A.   Can. J. Chem. **31**, 1 (1953).
21. GARTAGANIS, P. A. and WINKLER, C. A.   Can. J. Chem. **34**, 1457 (1956).
22. GREENBLATT, J. H. and WINKLER, C. A.   Can. J. Research, B, **27**, 721 (1949).
23. BLADES, H. and WINKLER, C. A.   Can. J. Chem. **29**, 1022 (1951).
24. KOLTHOFF, I. M. and SANDELL, E. B.   Textbook of quantitative inorganic analysis. Revised ed.
     Macmillan & Co., Ltd., London. 1948.
25. ONYSZCHUK, M., BREITMAN, L., and WINKLER, C. A.   Can. J. Chem. **32**, 351 (1954).
26. HERZBERG, G.   Spectra of diatomic molecules. 2nd ed. D. Van Nostrand Company, Inc., New York.
     1950.
27. SHULER, K. E. and LAIDLER, K. J.   J. Chem. Phys. **17**, 1212 (1949).
28. LAIDLER, K. J.   J. Phys. Chem. **53**, 712 (1949).
29. ARMSTRONG, D. A. and WINKLER, C. A.   J. Phys. Chem. **60**, 1100 (1956).
30. ROBINSON, A. L. and AMDUR, I.   J. Am. Chem. Soc. **55**, 2615 (1933).
31. JOHNSON, M. C.   Trans. Faraday Soc. **28**, 162 (1932).
32. LANGMUIR, I.   J. Chem. Soc. 511 (1940).
33. STEINER, W.   Trans. Faraday Soc. **31**, 623 (1935).
34. STEINER, W.   Trans. Faraday Soc. **31**, 962 (1935).
35. BRONWELL, A.   Advanced mathematics in physics and engineering. McGraw-Hill Book Co., Inc.,
     New York. 1953.

APPENDIX A

Assumptions in the Decay Equations

The decay equations assume a number of simplifying conditions beyond the basic ones already discussed. The use of a time-independent pressure, P, requires that there be no significant pressure gradient in the decay tube whether due to flow, heating, or dissociation (valid at all pressures). The use of plots extending over a range of pressure requires that the molar flowrate of nitrogen vary directly with pressure, for only then will the linear velocity of the gas and thence the time of decay (at least in the absence of dissociation) be pressure independent (see Fig. 3; the validity increases with pressure). The effect of dissociation on the time of decay must also be pressure independent (see Appendix C; valid only at low pressures or large decay times). The use of an average temperature for the decay tube in calculating the time of decay (Appendix C) assumes that the temperature of the decay tube is uniform (valid, in particular at higher temperatures). The decay tube must be of uniform diameter so that k_1 and k_3 will be constant.

Axial diffusion, i.e. diffusion in the direction of flow, must transport an insignificant amount of mass compared with the flow. This is borne out by the following calculation: the maximum contribution by diffusion to the flow occurs initially when, at 55° C and a pressure of 2 mm, and with $[N]_0 = P$, it amounts to

$$-D\partial[N]/\partial t \cdot \partial t/\partial x \cdot \pi r_0^2 = 6.6 \ \mu m/sec,$$

where $D = \bar{c}\lambda/3$, λ is the mean free path, $-\partial[N]/\partial t = (k_1P + k_2P^3)(n\mu/P)$, $n\mu$ is the number of micromoles per cubic centimeter at a pressure P, $\partial t/\partial x = t_0/2 \times 31.7$, t_0 is given by equation [15], 2 is a factor to take dissociation into account, and 31.7 is the length of the decay tube. Since the flow under the same conditions is 218 $\mu m/sec$ (from equation [11]), diffusion can be neglected.[12] This would not necessarily be true at very

---

[12]*Steiner (33) has made a similar calculation to determine if diffusion could be neglected.*

high pressures owing to the greater value of $\partial[N]/\partial t$. Radial diffusion, on the other hand, must eliminate any radial concentration gradient (see Appendix D; valid at low pressures and high temperatures).

APPENDIX B

Conversion of Flowrates to Partial Pressures

It was found that above about 0.30 mm the relation between nitrogen flowrate and pressure (cf. Fig. 3) was approximately linear and could therefore be represented simply by

[11]
$$[N_2]_{\mu m/sec} = 59.0(P-0.15),$$

where $\mu m/sec$ is the abbreviation for micromoles per second and P is in millimeters. The temperature at which the measurements were made was 25 to 30° C. Neglecting the effect of dissociation, a relation applicable to N atoms formed in the nitrogen stream follows as

[12]
$$[N]_{\mu m/sec} = 59.0([N]_{mm}/P)(P-0.15).$$

However, equation [12] must be corrected for the fact that with the apparatus used, dissociation brought about an increased flowrate rather than an increased pressure such that (cf. 33)

[13]
$$\text{flowrate} \propto \frac{P}{P-[N]_{mm}/2}.$$

Substituting for $[N]_{mm}$ in equation [13] the approximate value $[N]_{\mu m/sec}/59.0$ obtained from equation [12], and then using the result as a correction factor for equation [12], one obtains the desired relation:

[14]
$$[N]_{mm} \approx \frac{[N]_{\mu m/sec}(P-[N]_{\mu m/sec}/118)}{59.0(P-0.15)}.$$

APPENDIX C

The Time of Decay

The volume flowrate can be derived directly from equation [11] and has an average value of 1006 cc sec^{-1} at 25° C and in the region 1 to 3 mm pressure. It therefore follows that the average time of flow through the 281 cc decay tube, provided the nitrogen is undissociated, is

[15]
$$t_0 = 0.279 \times 298/T \text{ sec},$$

where T is the average temperature of the decay tube in ° K. The increased flowrates arising from dissociation will reduce the time, so that it is necessary to find a relation between t_0 and the true time of decay t. Let x be distance measured along the decay tube, x_0 the length of the decay tube, and v_0 the linear flowrate in the absence of dissociation. Then, if there is no dissociation, $x_0/v_0 = t_0$, while if there *is* dissociation (cf. equation [13]),

[16]
$$dx/dt = v_0/(1-[N]/2P).$$

Neglecting homogeneous decay, the substitution $[N] \approx Pe^{-k_1 t}$ can now be made and equation [16] integrated, so that, on equating the two expressions for x_0/v_0, one obtains

[17]
$$k_1 \approx \frac{k_1 t + \ln 2 - \tfrac{1}{2}e^{-k_1 t}}{t_0}.$$

Equation [17] is necessarily valid only at low pressures (when homogeneous decay is of secondary importance) or at large decay times (when the entire effect of dissociation becomes less marked).

APPENDIX D

Radial Diffusion

As a result of surface decay it is inevitable that a radial concentration gradient, however slight, will exist, and that the surface decay will therefore be self-inhibiting. However, such an effect has in the past generally been treated with such a rigid application of Fick's laws that a simple method of correcting for radial diffusion has apparently not been obtained (cf. 34). Since the formal approach involves assigning variability to the "shape" of the gradient, it was natural to try an approach in which a constant "shape" was used, in particular a *linear* gradient such that, as seen along a diameter of the system, it appears as an inverted "V".[13] A simple expression for the effect of radial diffusion when the surface decay is first order is then readily obtained.

Equating the rate of decay to the rate of diffusion towards the walls in the manner indicated by Steiner (34), one obtains

[18] $$2 \times \bar{c}[N]'\gamma/4 = -D\partial[N]/\partial r = (\bar{c}\lambda/3r_0)([N]'' - [N]'),$$

where $[N]'$ is the atom concentration at the surface of the decay tube, $[N]''$ is the concentration at the center of the decay tube, and r is the variable corresponding to r_0. The necessity of the factor of two on the left side was indicated in an earlier section. It is readily shown that the average atom concentration in a *cylindrical* system, $\overline{[N]}$, is related to $[N]'$ and $[N]''$ by

[19] $$\overline{[N]} = \tfrac{1}{3}[N]'' + \tfrac{2}{3}[N]'.$$

Combining equations [18] and [19],

$$[N]' = \overline{[N]}/(1 + \gamma r_0/2\lambda),$$

where the term $(1 + \gamma r_0/2\lambda)$ is the desired correction for radial diffusion. The rate constant for surface decay is therefore more correctly given by

$$k_1' = k_1/(1 + \gamma r_0/2\lambda) = k_1/(1 + \alpha P),$$

where k_1 is given by equation [8] and (assuming $\sigma = 3.84 \times 10^{-8}$ cm) $\alpha = 3.16 \times 10^4 \gamma r_0/T$ mm^{-1}.

If similar arguments are applied to a *spherical* system, where

$$\overline{[N]} = \tfrac{1}{4}[N]'' + \tfrac{3}{4}[N]',$$

then $\alpha = 3\gamma r_0/8\lambda = 2.37 \times 10^4 \gamma r_0/T$ mm^{-1}. It can be proved that, provided $\alpha P \ll 1$, no correction is necessary to k_2 in either a cylindrical or spherical system.

The treatment given is general and can be applied to experimental situations other than the present, e.g. static systems. However, it may not be valid for a short-lived species formed in the *interior* of a system, since a very marked pressure effect would be expected if the time for diffusion to the walls were comparable to the life of the species. As far as the present work is concerned, since α would amount to only 0.043 mm^{-1} (for $r_0 = 1.68$ cm, $\gamma = 2.65 \times 10^{-4}$, $T = 328°$ K), the correction for radial diffusion can be neglected, at least at the lower pressures.

[13]*A gradient of this sort appears to have theoretical justification, since it represents the limiting case as Dt gets large, i.e. it applies at high temperatures, low pressures, or when decay is slow. (That a decreasing rate of decay is very approximately equivalent to an increasing value of Dt is evident from the fact that there is no gradient in the absence of decay.) Compare the exact expression for radial diffusion in a cylinder (35, p. 272).*

RADIOLYSIS OF TETRACHLOROETHYLENE[1]

J. W. Sutherland and J. W. T. Spinks

ABSTRACT

When tetrachloroethylene is irradiated with Co^{60} gamma rays in the presence of oxygen or air, the main products are trichloroacetyl chloride, phosgene, and oxalyl chloride. The reaction is a chain reaction. Possible reaction mechanisms are discussed.

INTRODUCTION

Tetrachloroethylene, when irradiated in a two-phase aqueous system or when irradiated with a soluble pH indicator dye, liberates acidic products. The acid yields are high (G_{H^+} values up to 6000), suggesting that a chain mechanism is operative (1, 2). Chain reactions, although highly sensitive, are often greatly influenced by dose rate, temperature, and the presence of trace impurities. In addition, this particular reaction proceeds to some degree under the influence of light (3, 4). These complicating factors, undesirable in chemical dosimetry, can be effectively removed and in some cases totally suppressed by the addition of stabilizing reagents such as ethyl alcohol, resorcinol, and thymol. Although the sensitivity of the system to radiation is thereby markedly reduced (G value about 30), the use of stabilizers has made it possible to use tetrachloroethylene dosimeters which can register doses in the range, 1.0 to 10^6 r and which show excellent reproducibility (1).

The purpose of this study is to arrive at a more fundamental understanding of the chain mechanism in this sytem and to see whether further study of it would be useful in interpreting some of the processes occurring when ionizing radiation interacts with matter, e.g., in providing evidence of track effects (5).

EXPERIMENTAL

Reagent grade Kodak Eastman tetrachloroethylene, stabilized by the addition of 0.5% ethyl alcohol, was used as starting material. The alcohol can be removed by repeated water extractions or by fractional distillation. Pure tetrachloroethylene is prone to decompose under the influence of light and oxygen (3, 4), and thus a large sample of pure material cannot be prepared and stored for any length of time. Since this necessitates preparation of alcohol-free reagent immediately prior to each irradiation run, the following procedure was adopted.

Approximately 50 ml of reagent grade tetrachloroethylene (ethyl alcohol stabilized) was shaken with $CaCl_2$, filtered, and fractionally distilled. The middle fraction, b.p. 120–121° C, was used. Samples which had been treated for 24 hours and 3 days, respectively, were equally sensitive to radiation. Samples which had been extracted for periods of 2 and 12 hours were found less radiation sensitive.

The system irradiated, unless stated otherwise, was a 3-ml sample of pure tetrachloroethylene overlayered with 2 ml of water which had been distilled from alkaline permanganate and then redistilled from an alkaline suspension of manganous hydroxide. Samples were irradiated in glass-stoppered Pyrex tubes (12×100 mm), with gamma radiation from either a 1-curie or a 1000-curie Co^{60} source (6). After irradiation the solution was transferred to a 10-ml Erlenmeyer flask, and two 1-ml portions of wash water added. The acids liberated were titrated against standard base (NaOH) using a

microburette and a 0.1% solution of chlorophenol red as indicator. Samples were titrated to the same color as a blank (pH about 6), which had received identical treatment except for irradiation.

Irradiations were carried out at room temperature.

Dose rates were measured with a ferrous sulphate dosimeter ($G_{Fe^{+++}} = 15.5$) (7).

Infrared spectra were recorded with a Perkin–Elmer double beam infrared spectrophotometer.

RESULTS

In general, titration of the acids formed on irradiation was difficult owing to a pronounced postradiation effect which, however, apparently decreased in magnitude the less acid there was liberated. For example, there was no measurable postradiation effect with a 0.3% hexylresorcinol stabilized, air-equilibrated system (Table I).

TABLE I

Irradiation of air-equilibrated tetrachloroethylene stabilized with 0.3% by weight hexylresorcinol

(Samples, 3 ml stabilized tetrachloroethylene overlayered with 2 ml water; temp., 25° C; mean dose rate = 10 r/minute.)

Dose, kr	Time between irradiation and titration (minutes)	Acid yield, meq $\times 10^{-3}$ per ml	Acid yield, meq $\times 10^{-6}$ per ml TCE per r	G_{H^+} values*
9.22	30	0.20	0.0216	15.1
9.10	50	0.195	0.0214	15.0
9.83	100	0.203	0.0214	15.0
9.55	230	0.207	0.0216	15.1
9.55	325	0.207	0.0216	15.1
10.3	440	0.220	0.0223	15.6
				15.2±0.2

*G values are calculated on the basis that only the energy absorbed by the tetrachloroethylene phase is responsible for the chemical reactions. The factor for converting column 4 to column 5 is 703.

However, with a more sensitive system, e.g., using tetrachloroethylene which had been freed from alcohol and saturated with oxygen prior to irradiation, complete extraction of acid products was more difficult (Table II).

Preliminary experiments were also done in air-equilibrated tetrachloroethylene–water systems. In such systems, reproducibility was apparently achieved by periodic shaking

TABLE II

Irradiation of purified tetrachloroethylene saturated with oxygen

(Samples, 3 ml purified tetrachloroethylene (CaCl$_2$ extracted for 24 hours, redistilled) saturated with O$_2$ prior to irradiation. Acidic products extracted with H$_2$O after irradiation. Temp., 25° C; mean dose rate, 10 r/minute.)

Dose, r	Acid yield at various postreaction times in meq $\times 10^{-3}$/ml TCE				Total yield		
	25 hr	29 hr	47 hr	52 hr	Meq $\times 10^{-3}$ per ml	Meq $\times 10^{-6}$ per ml per r	G_{H^+} values
160	0.042				0.042	0.26	180
323	0.120				0.120	0.34	240
640	12.00	2.85	4.20	0.59	19.60	30.10	21,100
960	19.20	2.77	2.46	0.36	24.80	25.00	17,500
1300	20.30	1.75	2.28	0.22	24.60	19.00	13,300
1620	—	20.7	1.27	0.16	22.10	13.60	9,500

of samples during a 24-hour period before titration. It was also noted that if the samples were titrated immediately following irradiation, a sharp end-point color was reached which rapidly changed to the acidic color on standing. When the sample was left to stand without stirring, an acid aqueous layer formed at the interface of the water and tetrachloroethylene phase. This behavior occurred whether the system was left in the dark or not. Identical treatment of the blank showed no such behavior, even on exposure to sunlight. When bromocresol purple indicator was used, some of the indicator (chlorophenol red is insoluble in the tetrachloroethylene layer) dissolved in the tetrachloroethylene phase and showed a persistently acid reaction. The addition of hexylresorcinol, subsequent to irradiation (even in large amounts), had no inhibiting effect on this behavior, although it would presumably prevent decomposition under the influence of light and temperature. The more acid liberated, the more difficult it was to reach a stable end point. Shaking the solution or stirring it more vigorously produced more acid in the aqueous layer. Samples overlayered with different amounts of water gave similar acid yields.

When water saturated with tetrachloroethylene was irradiated, no detectable acid was liberated in the dose range being studied (0–2000 r).

These observations suggest that the continued acid production after irradiation is a result of gradual extraction of acidic products from the tetrachloroethylene phase, rather than a continuation of a chemical decomposition of the tetrachloroethylene.

Variation of Acid Yield with Absorbed Dose

Experimental data are summarized in Figs. 1, 2, and 3. Data for Fig. 1 were obtained for tetrachloroethylene which had been extracted for about 24 hours with $CaCl_2$ and redistilled before irradiation.

A series of runs at different dose rates was made with a sample of air-equilibrated tetrachloroethylene which had been left for a month overlayered with water. The water was separated, the tetrachloroethylene dried with $CaCl_2$ and redistilled. The results are shown in Figs. 2 and 3.

It is evident that we are now dealing with a more sensitive system. In samples where the tetrachloroethylene was overlayered with water the same limiting value of acid liberated was obtained, viz., about 4 meq $\times 10^{-3}$/ml, but this value was reached at
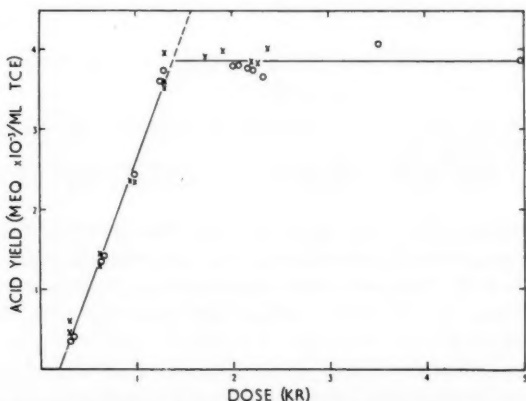
Fig. 1. Acid yield as a function of absorbed dose. Tetrachloroethylene extracted 24 hours with calcium chloride and redistilled. Samples consisted of 3 ml of tetrachloroethylene overlayered with 2 ml of water and air equilibrated. Temperature, 25° C; dose rate, 10 r per minute.
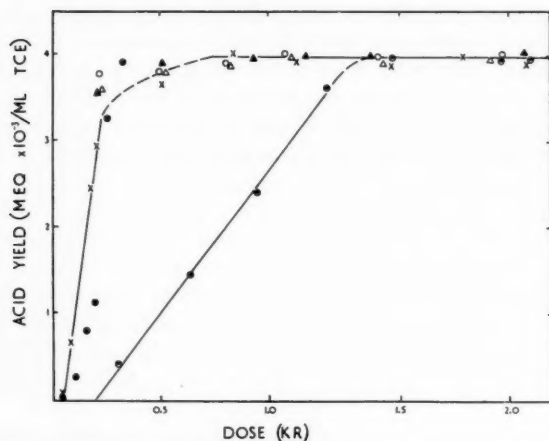
FIG. 2.   Acid yield as a function of adsorbed dose.
⊖Tetrachloroethylene extracted with CaCl₂ for 24 hours and redistilled. Dose rate 10 r per minute.
△, ▲, ○, ●, ✕ Tetrachloroethylene extracted with water for about one month, dried, and redistilled.
● 2.67 r/min; ▲ 10.r/min; ○ 13.0 r/min; △ 26.6 r/min; ✕ 41.9 r/min. All samples were 3 ml of tetra-chloroethylene overlayered with 2 ml of water and air equilibrated.
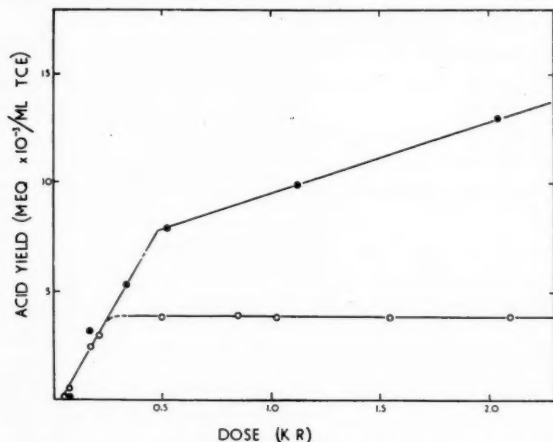
FIG. 3.   Acid yield versus absorbed dose. Tetrachloroethylene extracted with water for about one month.
Dose rate, 41.9 r/min. Temperature, 28° C.
● Samples were 3 ml of air-equilibrated tetrachloroethylene; 2 ml water added after irradiation.
○ Samples were 3 ml of air-equilibrated tetrachloroethylene overlayered with 2 ml of water.

lower doses of the order of 200 r (cf. Fig. 1, 1.4 kr). The probable explanation for the increased rate is that traces of alcohol left by the CaCl₂ method of purification were removed from the system by the water, thus making it more radiation sensitive. The G values are extremely high, e.g., at 41.3 r/minute G_{H^+} is of the order 12,600, over the initial range of absorbed dose.

Figure 3 shows a comparison of the acid yields obtained when tetrachloroethylene alone and tetrachloroethylene overlayered with water, both systems being air equilibrated, are irradiated. When tetrachloroethylene alone is irradiated, there is no limiting value to acid production though the rate of reaction changes after a time. The change in slope

is attributed to progressive exhaustion of the original oxygen present in the solution followed by diffusion of the oxygen from the gas phase into the tetrachloroethylene. This is extremely slow when the tetrachloroethylene is overlayered with water but is fast enough to support an appreciable rate of reaction when the tetrachloroethylene is in direct contact with air.

The induction period is reduced to about 50 r for the more highly purified tetrachloroethylene system.

Studies on the Effect of Oxygen

It is seen that the same limiting value of acid produced is reached in all systems overlayered with water despite their differing sensitivities. These observations suggest that an oxidation reaction is occurring in the tetrachloroethylene phase, the extent of the reaction being determined by the oxygen content of the tetrachloroethylene phase layer. This view was supported by the results of experiments in which the system was flushed, (a) with N_2, and (b) with oxygen, prior to irradiation. (See Table III.)

TABLE III

Effect on acid yield of flushing system with oxygen or nitrogen prior to irradiation

(Samples, 3 ml of tetrachloroethylene overlayered with 2 ml H_2O; dose rate, 10 r/minute; temp., 25° C.)

Pretreatment	Dose, kr	Acid yield, meq $\times 10^{-6}$ per r per ml	G_{H^+} values
(a) Tetrachloroethylene purified by $CaCl_2$ extraction (24 hours), followed by distillation			
Air-saturated	2.17	1.80	1270
	2.16	1.85	1300
N_2-flushed	2.18	0.0038	2.7
	2.12	0.0036	2.7
O_2-flushed	2.15	8.75	6150
	2.10	8.90	6250
(b) Ethyl alcohol stabilized tetrachloroethylene (0.5% EtOH)			
Air-saturated	16.8	0.190	133
	21.0	0.160	112
N_2-flushed	6.9	0.0049	3.4
	7.1	0.0057	4.0

From Fig. 3, the limiting amount of acid produced in an air-saturated sample is 3.94 meq $\times 10^{-3}$ per ml, i.e., 23.7×10^{17} hydrogen ions per milliliter of TCE.

In a subsequent section, the analysis of the radiation products is described. From this, it appears that 2 molecules of acid are formed from each molecule of acid chloride formed, and that the percentages of $(COCl)_2$, $COCl_2$, and CCl_3—$COCl$ are 3–4%, 37–38%, and 59%, respectively.

Hence, 11.85×10^{17} molecules of acid chloride are formed per milliliter of TCE, and using the percentage analysis figures, the total number of acid chloride molecules liberated per milliliter of tetrachloroethylene is 0.35×10^{17} molecules $(COCl)_2 + 4.5 \times 10^{17}$ molecules of $COCl_2$ and 7.0×10^{17} molecules CCl_3COCl.

Therefore, the total number of oxygen molecules required to produce the products is 6.1×10^{17}.

No value for the oxygen content of an air-saturated solution of tetrachloroethylene is available in the literature. However, values for various related compounds, given in International Critical Tables (8), are tabulated below:

Compound	No. oxygen molecules per milliliter of air-saturated compound
CCl_4	1.2×10^{18}
$CHCl_3$	1.1×10^{18}
$C_2H_2Cl_4$	5.5×10^{17}
C_2Cl_4	4.8×10^{17}

together with a value for C_2Cl_4 obtained in a preliminary experiment done in these laboratories. It is in line with the values reported for similar compounds.

The above evidence suggests that the observed break in Figs. 1, 2, and 3 is due to oxygen depletion and that the radiolysis of tetrachloroethylene is essentially an oxidation reaction.

Identification of Reaction Products

Fifty milliliters of purified tetrachloroethylene was irradiated with gamma rays, a slow stream of oxygen being bubbled through to promote the yield of product. The solution was given a dose of about 10^3 r.

The irradiated solution had a pungent odor. On distillation the first 0.5–1 ml distilled at about 118° C (fraction 1). The bulk (fraction 2) distilled at 120–121° C, the boiling point of TCE, and retained to some extent the pungent odor. A residue of about 0.2 ml of a higher boiling fraction (fraction 3) remained. An attempt to find its boiling point resulted in some decomposition.

Infrared spectra were measured of pure tetrachloroethylene, irradiated tetrachloroethylene, and fractions 1, 2, and 3.

Irradiated tetrachloroethylene showed an additional band of low intensity at 1800 cm^{-1}, characteristic of the $C=O$ of an acid chloride (9). Fraction 1 gave a sharper, much enhanced, band at 1810 cm^{-1} and also a strong band at 830 cm^{-1}, the C–Cl region of an acid chloride. In addition, a weak band appeared at 1650 cm^{-1}, which was tentatively ascribed to a $C=C$ linkage. The spectrum of fraction 3 was identified as that of a trichloroacetic acid - tetrachloroethylene mixture.

It was concluded that the main chemical reaction taking place on irradiation of an oxygen–tetrachloroethylene solution was an oxidation to acid chlorides. Part of the acid chloride has been hydrolyzed to trichloroacetic acid, presumably by traces of H_2O which may have been present in the O_2 supply. One of the acid chlorides is trichloroacetyl chloride.

In order to identify any other acid chlorides which may have been present, 50 ml of irradiated tetrachloroethylene was reacted with excess primary amine and the reaction products isolated and identified as far as possible by comparing their melting points and infrared spectra with those of specimens of pure compounds. The method used for the working up of the products of reaction with aniline is shown in Table IV.

The compounds isolated from the reaction in this manner of aniline and p-toluidine respectively were aniline hydrochloride, trichloroacetanilide, N,N'-diphenylurea, oxanilide, and the corresponding p-toluidine derivatives. Unidentified derivatives of aniline and p-toluidine having m.p.'s of 137 and 179° C, respectively, were also obtained. The data available suggest that they were derived from the same compound. For the aniline derivative, empirical formula $C_{16}H_{14-16}N_2O$, infrared spectra indicates N—H, C—H aromatic, C=N, a monosubstituted phenyl ⬡ —X,
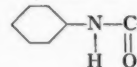
a carbonyl linkage ⬡—N—C— ·Cl is absent.
          H O

TABLE IV

Tetrachloroethylene $+ O_2$

γ-rays

Tetrachloroethylene + irradiation products

+ Aniline

Products

Filtered

Precipitate, m.p. 195° C —————————————— Filtrate evaporated to dryness at room temperature

Digested 5% HCl

—EtOH, fractional recrystallization with addition of H_2O

Filtrate evaporated to give crystals, m.p. 197° C ——————— White precipitate, m.p. 237° C

Hot EtOH

—Small amount crude material, m.p. 137° C

Needles, white, m.p. 238° C

—Yellow crystals, m.p. 137° C

—White crystals, m.p. 97° C

Fractional crystallization from EtOH + H_2O

$+ H_2O$

Final crystals, small plates, m.p. 248° C

One possible formula* is:

$$\text{⟨C₆H₅⟩—N=CH—CH=CH—}\overset{\displaystyle O}{\overset{\|}{C}}\text{—NH—⟨C₆H₅⟩}$$

and it is probable that the precursor is a 4-carbon molecule formed in the radiation reaction.

Identification of Acids Formed on Hydrolysis

The irradiated solution was extracted with water and the water phase separated and evaporated to dryness at room temperature. Crystals were obtained, m.p. 54° C (trichloroacetic acid, m.p. 57–58° C). Evaporation must be at a low temperature, since in hot water or basic solution (10) trichloroacetic acid decomposes in the manner, $CCl_3COOH \rightarrow CO_2 + CHCl_3$.

The crystals, on being shaken with concentrated aqueous ammonia containing Cu_2Cl_2, gave a dark blue color instantly. This is characteristic of trichloroacetic acid (10), though similar behavior is exhibited by dichloroacetic acid. Aqueous hydrolysis of $COCl_2$ and $(COCl)_2$ yields only hydrochloric acid (10). No oxalic acid is formed, although vapor-phase hydrolysis of $(COCl)_2$ is said to yield some.

$$COCl_2 + H_2O \rightarrow CO_2 + 2HCl,$$

$$(COCl)_2 + H_2O \rightarrow CO + 2HCl + CO_2.$$
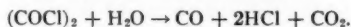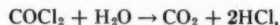
Quantitative Determination of Products

The three main reactions which yield acidic products in the irradiation of TCE are:

Suggested by Dr. R. A. Abramovitch.

$$CCl_3C{<}^O_{Cl} + H_2O \rightarrow CCl_3COOH + HCl, \tag{1}$$

$$COCl_2 + H_2O \rightarrow CO_2 + 2HCl, \tag{2}$$

$$(COCl)_2 + H_2O \rightarrow CO + CO_2 + 2HCl. \tag{3}$$
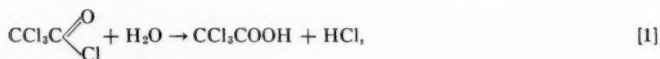
About 30 ml of TCE + 5 ml H_2O (to trap the phosgene) were irradiated for 3 days. A stream of oxygen was bubbled through during the irradiation. The irradiated mixture was extracted three times with water (about 30-ml portions each time) over a period of 24 hours. The water layer was separated and its acid content determined by titrating 5-ml samples with standard alkali to pH 4 using screened methyl orange as indicator. The chloride content of the sample was estimated by titration of 5-ml samples, which had been neutralized by NaOH (phenolphthalein as indicator), with standard $AgNO_3$ solution using dichlorofluorescein as an indicator. The amount of HCl expressed as a percentage of the total acid was 70.5. Hence:

$$\text{acidity due to } CCl_3COOH = 29.5\%,$$
$$\text{acidity due to } CCl_3COCl = 59\%,$$
$$\text{acidity due to } COCl_2 + (COCl)_2 = 41\%.$$

Since CCl_3COCl, $COCl_2$, and $(COCl)_2$ all yield 2 molecules of acid per molecule of acid chloride, the percentages of the acid chloride formed in the irradiation of TCE are 59% CCl_3COCl and 41% $(COCl_2 + (COCl)_2)$.

Determination of $COCl_2$ and $(COCl)_2$ Content

Since these two compounds behave very similarly chemically, it is difficult to estimate the composition of a mixture of them by chemical means. However, under experimental conditions phosgene ($COCl_2$) is a gas, b.p. 8° C, and oxalyl chloride a liquid, b.p. 62° C, and therefore the mixture should be readily separable by refluxing. Approximately 30 ml of TCE was irradiated, with O_2 bubbling through, for 5 days. Ten milliliters of solution was refluxed for 2 hours to distill off the phosgene, the remaining acid chlorides hydrolyzed, and the percentage chloride of the total acid content determined. The value obtained was 51.4%. A second sample, which was refluxed for 45 minutes, gave 52.0%. Taking the HCl content of the solution as 52%, then 96% of the acidity is due to hydrolysis of CCl_3COCl and 4% due to oxalyl chloride. Hence, since originally a sample of irradiated TCE contained 59% trichloroacetyl chloride, the true percentage of oxalyl chloride in a sample of irradiated TCE is $59/96 \times 4 = 3\%$. While no great accuracy is claimed for this figure it does indicate that oxalyl chloride is found in relatively small amounts and that the main reaction products are: CCl_3COCl (59%), $COCl_2$ (37–38%), and $(COCl)_2$ (3–4%). An implicit assumption in these calculations has been that the same fraction of each acid chloride is formed irrespective of dose received.

DISCUSSION

G Values

G_{H^+} values were calculated, assuming that acidic products are formed only as the result of energy absorbed by the tetrachloroethylene phase.

At the water–tetrachloroethylene interface there may be some reaction by H and OH radicals from the radiolysis of water. These reactions may lead to acidic products, but such reactions will probably not produce long chains, and in these circumstances their effect will be negligible.

Because of the influence of oxygen depletion in the solution, and the presence of an apparent induction period, G values are taken from the slopes of the straight lines in Fig. 2. From the analysis figures found for the relative amounts of CCl_3COCl (59%), $COCl_2$ (39%), and $(COCl)_2$ (3%), the following G values can be calculated (Table V).

TABLE V

Tetrachloroethylene extracted with $CaCl_2$ and H_2O

(Samples, 3 ml air-equilibrated tetrachloroethylene overlayered with 2 ml water)

(a) Tetrachloroethylene extracted with $CaCl_2$ (24 hours) redistilled	(b) Tetrachloroethylene extracted with H_2O (about one month), dried over $CaCl_2$, and redistilled
$G_{(H^+)} = 2250$	$G_{(H^+)} = 12,600$
G (acid chloride) $= 1125$	G (acid chloride) $= 6300$
G (CCl_3COCl) $= 660$	G (CCl_3COCl) $= 3700$
G ($COCl_2$) $= 430$	G ($COCl_2$) $= 2400$
G (($COCl)_2$) $= 34$	G (($COCl)_2$) $= 190$
G (C_2Cl_4) $= 910$	G (C_2Cl_4) $= 5000$
G (O_2) $= 570$	G (O_2) $= 3240$

One question arises which the present experimental data cannot settle, viz., is the production of oxalyl chloride a primary oxidation product or is it a secondary product resulting from radiolysis of CCl_3COCl or $COCl_2$?

The large G ($COCl)_2$ value, 190, suggests that $(COCl)_2$ is a primary oxidation product. (N.B. In these calculations of G values we have assumed that we can extrapolate analysis data from a sample which had been given a dose of 1000 kr with O_2 bubbling to the dose range being studied, viz., about 1 kr.) The final concentration of acid chloride reached in the 1000-kr run was 0.16 molar $\equiv 4.3\%$ conversion on a mole basis.

Radical Yields

Radical yields G_R for several organic liquids have been measured. Chapiro *et al.* (11) find values of G_R for CCl_4 and $CHCl_3$ of about 70 and 60, respectively, using the D.P.P.H. method. Schulte (12), using tagged Cl_2 in CCl_4, finds a value for G_R as $\lessgtr 3.5$.

If we assume that G_R for C_2Cl_4 is between 60 and 3.5, and assume each radical initiates a chain reaction leading to acidic products (see later this section) approximate values for kinetic chain lengths can be derived, e.g., for systems (a) and (b) Table V. We have: $G_{H^+} = 2250$, kinetic chain length between 34 and 650; $G_{H^+} = 12600$, kinetic chain length between 210 and 3600.

Tetrachloroethylene Dosimeters

The radiation reaction in a tetrachloroethylene air-equilibrated solution has been shown to be an oxidation reaction, and there will be a limiting value to the dose which can be measured by a dosimeter consisting of tetrachloroethylene overlayered with water. From our results this limiting value will correspond to a maximum value of 3.94 meq $\times10^{-3}$ per ml TCE of acid liberated. A typical value for the rate of acid production in a stabilized two-phase tetrachloroethylene dosimeter is 0.05 meq $\times10^{-6}$ per ml per r (1). Hence, for a system of this particular sensitivity, one would expect that for doses greater than 80 kr, this system would lose its sensitivity (provided no oxygen has diffused into the tetrachloroethylene phase during irradiation).

Our work emphasizes the observation by Taplin (1) that, after exposure of the dosimeter, vigorous shaking over a period of time is required to bring about complete extraction of acidic products.

Effect of Stabilizers

Certain reagents, notably alcohols and phenols, retard the radiation-induced reaction (1). Bailey (3, 4) has found that the photochemical oxidation of perchloroethylene is accelerated by I_2, slightly retarded by quinol, fairly well retarded by butyl-α-isobutyl alcohols, turpentine, benzaldehyde, resorcinol, naphthols, napthylamine, and sulphur, and well retarded by alcohol, ether, thymol, o-toluidine, sodium thiosulphate, and thiourea. He observes that in certain cases, e.g., quinol, benzaldehyde, resorcinol, diphenylamine, napthylamine, and the naphthols, the retarding agent caused development of color. This is interesting, since such reactions might be easily followed spectrophotometrically and might help in elucidating the chain propagating reactions or in development of a method of finding the radical yield in tetrachloroethylene.

Oxidation Reaction

The main reactions occurring in the radiolysis of tetrachloroethylene can be summarized thus:

$$C_2Cl_4 + \tfrac{1}{2}O_2 \rightarrow CCl_3COCl, \qquad [a]$$

$$C_2Cl_4 + O_2 \rightarrow 2COCl_2, \qquad [b]$$

$$C_2Cl_4 + O_2 \rightarrow (COCl)_2 + 2Cl. \qquad [c]$$

Reaction [c] is non-stoichiometric, there being a loss of 2 atoms of chlorine. This may appear in the system as molecular Cl_2 or C_2Cl_6. Such compounds have not been looked for, but other workers (13) have detected molecular Cl_2.
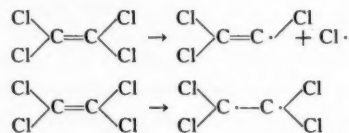
Reaction Mechanism

In the present system the oxygen concentration is about 0.002 molal and if it is assumed that the ease of ionization of O_2 and C_2Cl_4 is about the same, and that there is no preferential transfer of ionization or excitation energy to the O_2 molecules, then ionization and excitation will be mainly confined to the C_2Cl_4 molecules.

Both ionic and molecular species will be in a variety of excited states. The nature of the secondary processes ultimately leading to chemical reaction is still obscure, although theoretical evidence has been advanced showing that in a liquid charge neutralization occurs before the ions can react chemically (14, 15, 16). Ion molecule type reactions have also been proposed. Iodine scavenger studies (17) have shown that molecular decomposition processes occur in organic systems.

However, the chain characteristics of the oxidation reactions are such that initiation and propagation must be by free radicals. Molecular products can be assumed to be of negligible importance. These radicals probably arise from dissociation of excited molecules.

Because of its simplicity, changes in the excited tetrachloroethylene molecule are limited to rather few possibilities, e.g.

$$\mathrm{Cl}_2\mathrm{C}{=}\mathrm{CCl}_2 \rightarrow \mathrm{Cl}_2\mathrm{C}{=}\mathrm{C}\mathrm{Cl} + \mathrm{Cl}\cdot$$

$$\mathrm{Cl}_2\mathrm{C}{=}\mathrm{CCl}_2 \rightarrow \mathrm{Cl}_2\mathrm{C}{-}\mathrm{C}\cdot\mathrm{Cl}_2$$

The formation of a diradical will be energetically more improbable, and hence as a result of the primary act we would anticipate the production of $Cl\cdot$ and $C_2Cl_3\cdot$ radicals.

Important in any radiation scheme is the spatial distribution of such radicals. Chapiro (5) has recently discussed the distribution of free radicals and is of the opinion that the over-all spatial distribution of free radicals is similar but not identical with the distribution of the ions.

In the radiolysis of C_2Cl_4, Cl and C_2Cl_3 radicals will be produced. Some of these radicals will recombine and react with each other yielding molecular products, possibly Cl_2 and C_4Cl_6 (hexachlorobutadiene). The yield of these products will be influenced by the rate of diffusion of radicals, the velocity constants of their reactions, and the presence and efficacy of any scavenger molecules present.

It is interesting to note that in a N_2-saturated system a value of G_{H^+} of ~ 4 was obtained (Table III), whether pure tetrachloroethylene or stabilized tetrachloroethylene was used.

Thus we would anticipate that, in a tetrachloroethylene solution overlayered with water, acids will continue to be produced after exhaustion of the dissolved oxygen. However, the rate will be so low that it is not measurable under our conditions up to an absorbed dose of 20 kr.

With gamma radiation, where the clusters are widely separated, there will be little chance of radical–radical reactions from different tracks, and hence there will be a finite number of radicals escaping into the solvent from the clusters for a fixed amount of radiation absorbed.

These radicals can then interact with solvent molecules, C_2Cl_4, and solute molecules, O_2. The ensuing reactions will again be governed by: (a) rate of diffusion of radicals, (b) velocity constants of the reaction, and (c) concentration of solute and solvent molecules.
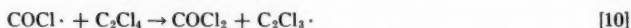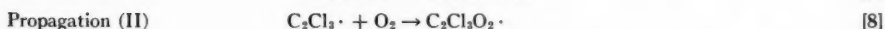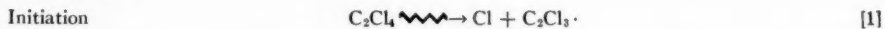
Pertinent to this work are the studies by Schumacher (18, 19) and co-workers, and Dickinson and co-workers (20, 21, 22) on the photochemical chlorine sensitized oxidation of tetrachloroethylene. The products of the oxidation reaction, isolated by them, were CCl_3COCl and $COCl_2$. The reaction was studied in the gas phase and in CCl_4 as solvent (21). Dickinson and Leermakers (20, 21) show that the products of oxidation, CCl_3COCl and $COCl_2$, undergo little or no further oxidation on prolonged exposure to light. In CCl_4 solution the rate of oxidation of C_2Cl_4 is independent of $[O_2]$ (provided the latter is not too low), proportional to the first power of the light intensity, and dependent on the chlorine concentration but only to the extent that the amount of chlorine affects the rate of energy absorption. The reaction rate varies to some extent with the tetrachloroethylene concentration and the temperature. A quantum yield of 1–2.5 moles of C_2Cl_4 oxidized per einstein is found.

In the gas phase (22), the rate of reaction has no strong dependence on the partial pressures of Cl_2, O_2, and C_2Cl_4. However, the reaction is much faster and quantum yields of 200–500 were found.

Schumacher (19) has also studied this reaction in the vapor phase and finds that approximately 80% of tetrachloroethylene is converted to CCl_3COCl and 20% to $COCl_2$, in agreement with Dickinson's figures. The phosgene content of the reaction product slowly increases with temperature. The over-all temperature coefficient is unity and the total pressure has little effect on the rate of reaction. The addition of alcohol strongly retards the reaction. With pure tetrachloroethylene he finds a quantum efficiency of 230 molecules of tetrachloroethylene per quantum at a temperature of 60° C and at 100 mm Cl_2, 200 mm O_2, and an absorbed intensity of 1.6×10^{12} hv/sec cc.

Possible Reaction Mechanisms in the Radiolysis of Air-equilibrated Tetrachloroethylene

From the foregoing one can postulate that the following chain mechanism is occurring in our system:

Initiation $C_2Cl_4 \rightsquigarrow Cl + C_2Cl_3 \cdot$ [1]

Propagation (I) $Cl + C_2Cl_4 \rightarrow C_2Cl_5 \cdot$ [2]

$C_2Cl_5 \cdot + O_2 \rightarrow C_2Cl_4O_2 \cdot$ [3]

$C_2Cl_5O_2 \cdot \rightarrow CCl_3COCl + ClO$ [4a]

or $\rightarrow 2COCl_2 + Cl$ [4b]

$ClO + C_2Cl_4 \rightarrow CCl_3COCl + Cl$ [5a]

or $\rightarrow COCl_2 + CCl_3 \cdot$ [5b]

$CCl_3 \cdot + O_2 \rightarrow CCl_3O_2 \cdot$ [6]

$CCl_3O_2 \cdot \rightarrow COCl_2 + Cl$ [7]

Propagation (II) $C_2Cl_3 \cdot + O_2 \rightarrow C_2Cl_3O_2 \cdot$ [8]

$C_2Cl_3O_2 \cdot \rightarrow COCl_2 + COCl \cdot$ [9a]

or $\rightarrow (COCl)_2 + Cl$ [9b]

$COCl \cdot + C_2Cl_4 \rightarrow COCl_2 + C_2Cl_3 \cdot$ [10]

Chain termination is probably by mutual destruction of radicals. Propagation step [2] can account for increased phosgene to trichloroacetyl chloride ratio found in the radiolysis reaction.

Other equally plausible mechanisms can be advanced based on the formation of epoxides (23, 24) or of the ClOO radical (cf. (25)). Further work in the absence of oxygen and using E.P.R. techniques might help to establish the mechanism.

REFERENCES

1. TAPLIN, G. V. Radiation dosimetry. *Edited by* G. J. Hine and G. L. Brownell. Academic Press Inc., New York. 1956. Chap. 8.
2. SIGOLOFF, S. C. Nucleonics, **16** (No. 10), 54 (1956).
3. BAILEY, K. C. J. Chem. Soc. 767 (1939).
4. BAILEY, K. C. and HICKSON, W. S. E. J. Chem. Soc. 145 (1941).
5. CHAPIRO, A. Radiation Research, **6**, 11 (1957).
6. HUMMEL, R. W., VAN CLEAVE, A. B., and SPINKS, J. W. T. Can. J. Chem. **31**, 1203 (1953).
7. WEISS, J., ALLEN, A. O., and SCHARZ, H. A. Intern. Conf. Peaceful Uses Atomic Energy, **14**, 179 (1956).
8. INTERNATIONAL CRITICAL TABLES. Vol. 3. McGraw-Hill Book Co., Inc., New York. 1928.
9. BELLAMY, J. J. The infra-red spectra of complex molecules. Methuen & Co. Ltd., London. 1954.
10. HUNTRESS, E. M. Organic chlorine compounds. John Wiley & Sons, Inc., New York. 1950.
11. PREVOT-BERNAS, A., CHAPIRO, A., COUNSIN, C., LAIDLER, T., and MAGAT, M. Discussions Faraday Soc. **12**, 98, 129 (1952).
12. SCHULTE, J. W. J. Am. Chem. Soc. **79**, 4643 (1957).
13. SCHULTE, J. W., SUTTLE, J. F., and WILHELM, R. J. Am. Chem. Soc. **75**, 2222 (1953).
14. COLLINSON, E. and SWALLOW, A. J. Chem. Revs. **56**, 471 (1956).
15. BURTON, M., MAGEE, J. L., and SAMUEL, A. H. J. Chem. Phys. **20**, 760 (1952).
16. SAMUEL, A. H. and MAGEE, J. L. J. Chem. Phys. **21**, 1080 (1953).
17. McCAULEY, C. E. and SCHULER, R. H. J. Am. Chem. Soc. **79**, 4008 (1957).
18. SCHUMACHER, H. J. Z. Elektrochem. **42**, 522 (1936).
19. SCHOTT, C. and SCHUMACHER, H. J. Z. physik. Chem. B, **49**, 107 (1941); Chem. Abstr. **38**, 3551 (1944).
20. DICKINSON, R. C. and LEERMAKERS, J. A. J. Am. Chem. Soc. **54**, 3852 (1932).
21. DICKINSON, R. C. and LEERMAKERS, J. A. J. Am. Chem. Soc. **54**, 4648 (1932).
22. DICKINSON, R. C. and CARRICO, J. L. J. Am. Chem. Soc. **56**, 1473 (1934).
23. MAYO, F. R., MILLER, A. A., and RUSSEL, G. A. J. Am. Chem. Soc. In press.
24. TWIGG, G. H. Chem. Eng. Sci. Suppl. **3**, 5 (1954).
25. PORTER, G. and WRIGHT, F. J. Discussions Faraday Soc. **14**, 23 (1953).

THE HEAT AND ENTROPY OF ASSOCIATION OF THE COMPLEX IONS FORMED BY EDTA WITH THE LANTHANIDE ELEMENTS IN AQUEOUS SOLUTION[1]

R. H. BETTS AND OLIVE F. DAHLINGER

ABSTRACT

A radio tracer method has been used to measure the heat and entropy of association of all the lanthanide ions (except promethium) with the chelating agent EDTA. Entropy terms are largely responsible for the remarkable stability of these complex ions. The results suggest, but do not prove, that a change in configuration of the complex occurs after gadolinium (element 64).

INTRODUCTION

All of the trivalent lanthanide ions in aqueous solution form very robust 1:1 complexes with the chelating agent ethylenediamine tetraacetic acid (EDTA). Wheelwright *et al.* (1) found the association constant K for the complex in 0.1 M potassium chloride to increase with atomic number, rising from 5×10^{14} for lanthanum (element 57) to 1.2×10^{19} for lutetium (element 71). The *average* difference between association constants for successive members of this group is 2.4. However a "plateau" occurs in the region Eu–Gd, for which $K_{Eu} = 4.9 \times 10^{16}$ and $K_{Gd} = 5 \times 10^{16}$. Beyond gadolinium, the interval between the association constants opens out again.

These authors suggest, as an explanation for this plateau, that the progressively smaller radii of the lanthanide ions in the series from La to Lu imposes increasing steric hindrance on the interaction between EDTA and the ion; they also suggest that for the series La to Gd, EDTA exerts its maximum chelating effect, all six groups (four carboxyls and two amino nitrogens) being co-ordinated to the metal ion. After Gd, only five of the chelating groups can fit around the central ion, leaving 1 molecule of water still attached. The evidence of Moeller *et al.* (2), however, suggests that Nd^{3+} is probably penta-co-ordinated by EDTA rather than 6 co-ordinated. A change in co-ordination after Gd would then be from penta-co-ordination to tetra-co-ordination, rather than from 6- to 5- as proposed by Wheelwright.

If such changes in co-ordination occurred, then on the basis of Cobble's discussion of the entropy of complex ions (3), one might expect significant differences in the entropy of formation of the complex ions of the two groups. The only experimental information available relating to the heat and entropy changes in these systems is given in an earlier paper from this laboratory (4). It was shown there that the difference in the heats of reaction for the systems

$$La^{3+} + X^{-4} \rightleftharpoons LaX^- \qquad [1]$$

and

$$Nd^{3+} + X^{-4} \rightleftharpoons NdX^- \qquad [2]$$

was zero (X^{-4} represents the fully ionized form of EDTA). Moreover, the differences in the entropies of formation of LaX^- and NdX^- appeared to be satisfactorily related to the differences in the partial molal entropies of the hydrated cations.

The present paper records the application of a radiochemical technique, described in ref. 4, to measurements of the relative stability, as a function of temperature, of the complex ions of EDTA with all the lanthanide elements except element 61. The object of the measurements was to provide further quantitative data on those factors which determine differences in stability among the members of this group of elements. In particular, heat and entropy changes which occur on formation of the complexes have been evaluated. The results also provide an independent confirmation of earlier isothermal measurements of the stability of these complex ions (1).

The method used depends on measurement of the position of equilibrium in the system:
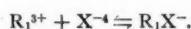
$$R_1X^- + R_2{}^{3+} \rightleftharpoons R_2X^- + R_1{}^{3+} \qquad \qquad [3]$$

where R_1 and R_2 represent different lanthanides. The equilibrium constant $K_{1,2}$ for reaction [3] is

$$K_{1,2} = (R_2X^-)(R_1{}^{3+})/(R_1X^-)(R_2{}^{3+}).$$

The association constant K_1 for formation of the complex ion R_1X^- may be written as:

$$K_1 = (R_1X^-)/(R_1{}^{3+})(X^{-4})$$

corresponding to the equilibrium:

$$R_1{}^{3+} + X^{-4} \rightleftharpoons R_1X^-.$$

A similar relation can be written for the association constant K_2 for the formation of R_2X^-. Clearly, $K_{1,2} = K_2/K_1$; measurement of the position of equilibrium in reaction [3] gives therefore the *ratio* of the stability constants for the formation of the two complex ions concerned. Similarly, the thermodynamic quantities $\Delta F^\circ_{1,2}$, $\Delta H^\circ_{1,2}$, and $\Delta S^\circ_{1,2}$ of reaction [3] are simply related to the corresponding quantities for the formation of the complex ions. Thus, for element 1:

$$\Delta F^\circ_1 = -RT \ln K_1 = \Delta H^\circ_1 - T\Delta S^\circ_1;$$

for the element 2:

$$\Delta F^\circ_2 = -RT \ln K_2 = \Delta H^\circ_2 - T\Delta S^\circ_2,$$
$$\Delta F^\circ_{1,2} = -RT \ln K_{1,2} = -RT \ln K_2/K_1 = (\Delta H^\circ_2 - \Delta H^\circ_1) - T(\Delta S^\circ_2 - \Delta S^\circ_1),$$

whence

$$\Delta F^\circ_{1,2} = \Delta F^\circ_2 - \Delta F^\circ_1,$$
$$\Delta H^\circ_{1,2} = \Delta H^\circ_2 - \Delta H^\circ_1,$$

and

$$\Delta S^\circ_{1,2} = \Delta S^\circ_2 - \Delta S^\circ_1.$$

Evidently the enthalpy and free energy of formation for a single lanthanide–EDTA system can be calculated from the equilibria including two lanthanides, provided these quantities are available for one of them. The results in this paper have been normalized using the value of −21,890 calories, for ΔF_{Nd}, from the results of Wheelwright *et al.* (1). Their value was measured at 20° C, but has been adjusted to 25° using $\Delta H_{Nd} = -800$ cal/mole, a value obtained in this present work. For our single normalizing value of ΔH, we are indebted to Dr. R. W. Attree of these laboratories. Using a Tian–Calvet calorimeter recently described (5) reaction [1] above was found to be exothermic, $\Delta H_{La} = -800 \pm 20$ cal per mole. As will be seen below the discussion of the results depends primarily on the *differences* among the lanthanides, so that errors associated with the normalizing values ΔF_{Nd} and ΔH_{La} will have no serious consequences.

EXPERIMENTAL

Materials

The lanthanide chlorides, with the exception of cerium, were prepared by dissolving a weighed amount of oven-dried (110° C) oxide in a slight excess of hydrochloric acid. The excess acid was removed by several evaporations to near dryness, after which the material was made up to a known volume in water. The oxide formula was taken to be R_2O_3 for all of the lanthanides except for praeseodymium (Pr_6O_{11}) and terbium (Tb_4O_7). Cerium chloride was prepared by dissolving CeO_2 in a mixture of sulphuric acid and hydrogen peroxide. The trivalent hydroxide was then precipitated with ammonia, washed several times, and then redissolved in hydrochloric acid. The resulting solution was taken to near dryness several times, and finally dissolved in a known volume of water.

The oxides of La, Pr, Nd, Sm, Eu, Gd, Tb, Ho, Er, and Tm were purchased from Lindsay Chemical; the analyses supplied indicated a chemical purity of 99.8% or better. The cerium was Johnson–Matthey "spec-pure" CeO_2. Dy, Yb, and Lu were provided as 99.8% pure oxides by courtesy of the Ames Laboratory of the U.S.A.E.C.

The solutions prepared in this way were used, except for Nd, without further standardization. The Nd stock solution was standardized by titrating aliquots with versene (the disodium salt of EDTA) in the presence of calcium, using eriochrome black T as an indicator for the end point. This method, which is adopted from a procedure described by Cheng *et al.* (6), uses calcium carbonate as a primary standard.

EDTA was purified by recrystallization of the acid H_4X from a water solution of the disodium salt. The insoluble acid was washed, dried at 105° C, and samples assayed in the presence of excess calcium chloride by titration with standard sodium hydroxide. The pH was monitored with a Beckman model G glass electrode assembly. An aqueous stock solution of EDTA, fully neutralized with potassium hydroxide, was prepared from this purified and standardized material.

The radio tracers used in the analytical scheme (see below) were 11.6-day Nd[147], Yb[169,175] (30-day and 4.2-day), and 72-day Tb[160]. These were prepared by neutron irradiation in the NRX reactor of the corresponding pure oxides. The steps taken to establish the radiochemical purity of the neodymium and ytterbium activities have been described previously (4, 7). The radioactive decay of Tb[160] was followed for 7 months (three half-lives) and showed no indication of extraneous radio nuclides. A half-life of 72.8 ± 0.1 days was observed. Values of 72.3-day (8) and 73.0-day (9) have been recorded in the literature.

Procedure

Solutions for which equilibrium measurements were made were 0.10 M in potassium chloride and 0.01 M in ammonium acetate. The KCl was added to maintain the solutions at constant ionic strength, and also to make the results directly comparable with those of Wheelwright *et al.* (1). Ammonium acetate was added to ensure that all comparable experiments were made at the same pH (5.3 ± 0.1). Doubly distilled water was used throughout this investigation.

Solutions were prepared containing known amounts of two lanthanides, together with a known concentration of K_4X. Conditions were so chosen that the concentration of the chelating agent (2×10^{-4} M) was never more than 50% of the sum of the concentrations of the two lanthanides present ($4-12\times10^{-4}$ M). Under these conditions, all of the EDTA was present at equilibrium either as R_1X^- or R_2X^-; the concentrations of the species H_4X, H_3X^-, .../X^{-4} etc. being negligible in comparison.

TABLE I

Summary of equilibrium constants at various temperatures

Lanthanide pair	0°	25.7°	35.2°	ΔH, cal/mole	$K_{25°}$
Series A. Comparisons with terbium					
(TbX)(Sm)/(Tb)(SmX)	4.25	6.53	7.08		
	4.20	6.20	6.59	+2300	6.16±0.10
	4.38	6.43	6.93	(130)	
(TbX)(Eu)/(Tb)(EuX)	3.34	4.36	4.57	+1660	4.51±0.10
	3.43	4.74	5.04	(190)	
	3.66	4.80	5.06		
(TbX)(Gd)/(Tb)(GdX)	2.38	3.64	2.97		
	2.80	3.29	3.45	+1070	3.15±0.13
	2.72	3.18	3.17	(330)	
(TbX)(Dy)/(Tb)(DyX)	.344	.326	.355	0	
	.320	.338	.326	(190)	0.344±.008
	.351	.366	.360		
(TbX)(Ho)/(Tb)(HoX)	.175	.186	.183		
	.183	.190	.200	+250	
	.180	.190	.182	(120)	.187±.003
(TbX)(Er)/(Tb)(ErX)	.083	.084	.090		
	.090	.092	.091	0	
	.090	.088	.085	(150)	0.088±.002
Series B. Comparisons with neodymium					
(NdX)(La)/(Nd)(LaX)	7.4*	7.2*	7.2*	0	7.2±0.1
(NdX)(Ce)/(Nd)(CeX)	4.16	3.78	3.92	−330	
	4.31	4.11	3.86	(140)	4.01±0.06
	(4.62)	4.05	4.10		
(NdX)(Pr)/(Nd)(PrX)	1.96	1.84	2.00		
	1.99	1.91	1.91	0	
	(2.24)	2.04	1.97	(150)	1.95±0.03
(NdX)(Sm)/(Nd)(SmX)	.332	.342	.332		
	.327	.335	.335	0	
	(.309)	.326	.336	(60)	0.333±0.002
Series C. Comparisons with ytterbium					
(YbX)(Ho)/(Yb)(HoX)	7.69	8.28	8.50		
	8.29	8.34	8.37	+230	
	(9.16)	8.29	8.25	(100)	8.28±0.09
(YbX)(Er)/(Yb)(ErX)	4.66	4.56	4.72		
	4.96	4.50	4.57	−340	
	4.85	4.20	4.36	(160)	4.54±0.09
(YbX)(Tm)/(Yb)(TmX)	2.37	2.23	2.28		
	2.43	2.14	2.21	−360	
	2.32	2.14	2.19	(110)	2.23±0.03
(YbX)(Lu)/(Yb)(LuX)	.634	.703	.755		
	.672	.709	.771	+680	
	.655	.692	.772	(110)	.720±.010

Values of the equilibrium constants enclosed in parentheses were not used in the calculations. The probable errors in the ΔH values in column five are indicated by parentheses.

*Data for the La–Nd system from ref. 4.

The appropriate tracer was prepared as an aqueous solution of RCl_3, and added to each equilibrium solution concurrently with the other components of the systems.

Three aliquots were taken from each solution, one of which was allowed to reach equilibrium at 0° C, the second at 25.7° C, and the third at 35.2° C. After equilibrium had been reached (as judged by analysis on successive days*), three samples for each

*In some cases, particularly those involving the heavier lanthanides at 0° C, equilibrium was attained only after several weeks. This is not unexpected, since earlier work (4) has shown that the rate of dissociation of RX^- ions in aqueous solution at pH 5.3 is very slow.

temperature were taken for determination of the position of equilibrium (see below). Each lanthanide pair was studied at three different values of the ratio R_1Cl_3/R_2Cl_3 (1:1, 2.5:1, and 5:1), so that in all nine measurements of the position of equilibrium (three sets in triplicate) were obtained at each temperature for each pair of elements examined. Altogether about 300 such measurements were made in the present study.

The pH of the equilibrium systems was measured in every case, and was found to be 5.3 ± 0.1.

The position of equilibrium in each system was calculated from the distribution of a radioactive tracer for one of the lanthanide ions between the forms R^{3+}_{aq} and RX^-. The cationic form is held quantitatively on a short Dowex 50 cation resin column, while the form RX^-, being anionic, passes through to the effluent. The relative amounts of the element R in the anionic or cationic form were calculated from the radioactivity in the effluent relative to that in the original solution. Further details of this technique, and of the methods of radioassay used are given in ref. 4.

Tb^{160} was used in the first series of experiments, in which the lanthanides Sm, Eu, Gd, Dy, Ho, and Er were compared with Tb. Nd^{147} was used in the second series, in which Nd was compared with La, Ce, Pr, and Sm. $Yb^{169,175}$ was used as the tracer in the last series, involving comparisons of Ho, Er, Tm, and Lu with Yb.

TABLE II

Comparison of association constants for formation of lanthanide–EDTA complex ions

$T = 25.0°$ C $\qquad\qquad\qquad\qquad\qquad$ $\mu = 0.1$ (KCl)

R	This work	Ref. 1	R	This work	Ref. 1
La	1.56×10^{15}	0.51×10^{15}	Tb	207×10^{15}	190×10^{15}
Ce	2.79	2.4	Dy	602	390
Pr	5.74	5.5	Ho	1107	500
Nd	(11.2)	(11.2)	Er	2350	1000
Sm	33.6	35	Tm	4450	4100
Eu	45.9	49	Yb	9920	5000
Gd	65.7	50	Lu	13800	12000

RESULTS

The experimental results are summarized in Table I. The first column in the table identifies the lanthanide pair, and defines the form of the equilibrium constant. The second, third, and fourth columns list the experimental values at 0° C, 25.7° C, and 35.2° C, respectively, of the equilibrium constant defined in column one. Three values for each temperature are recorded, and represent the results of separate experiments for different concentration ratios of the lanthanide pair. The fifth column gives the value of the enthalpy change (ΔH) for the equilibrium. These values of ΔH are calculated in each case by a least squares fit of the data to the relation:

[4] $$\log K = -(\Delta H/2.303 \, RT) + \text{constant}.$$

Least squares analyses were also used to calculate the probable errors in the ΔH terms; the appropriate uncertainties are given in parentheses in column 5. The final column gives the value of K at 25.0° C, calculated from the appropriate form of equation [4] above. The probable errors indicated for K in this column were also calculated by least squares analyses.

Thermodynamic Quantities for Each Lanthanide–EDTA System

The results of Table I have been normalized to yield values for changes in the free energy ($\Delta F°$), entropy ($\Delta S°$), and enthalpy ($\Delta H°$) involved for each lanthanide–EDTA system.

(a) Normalization of the $\Delta F°$ Terms

The value of 1.12×10^{16} for the equilibrium constant for the NdX–Nd system at 25° C has been taken from the work of Wheelwright *et al.* (1). Thus the value of K_{La}, from the results in Table I, is therefore

$$1.12 \times 10^{16}/7.2 = 1.56 \times 10^{15},$$

while that for K_{Sm} is

$$1.12 \times 10^{16}/0.333 = 3.36 \times 10^{16}.$$

The result for Tb is then calculated from that for Sm, and the values for Eu, Gd, Dy, Ho, and Er are then calculated relative to Tb. The value for K_{Yb} is calculated by comparison with both K_{Ho} and K_{Er} and finally the values of K_{Tm} and K_{Lu} are calculated relative to that of K_{Yb}. The results of these comparisons are shown in Table II. Column two of Table III gives the same results expressed in calories per mole at 25.0° C. The free energy change $\Delta F°$ has been calculated from the relation $\Delta F° = -RT \ln K$.

(b) Normalization of the $\Delta H°$ Terms

The reaction: $La^{3+} + X^{-4} \leftrightarrows LaX^-$ is found to be exothermic (see Introduction) and $\Delta H_{La} = -800$ cal per mole. The equilibrium constant for the La–Nd system is independent of temperature and therefore ΔH_{Nd} is also -800 cal per mole. Equilibria in the systems Nd–Pr and Nd–Sm are also temperature independent, and this implies that $\Delta H_{La} = \Delta H_{Pr} = \Delta H_{Nd} = \Delta H_{Sm} = -800$ cal per mole.

The value of ΔH for the Tb–Sm system is $+2300$ cal per mole, which leads to a value of $+1500$ cal per mole for the Tb system. (See the appropriate equations in the Introduction, where $\Delta H°_2 = -800$ cal, $\Delta H°_{1,2} = +2300$ cal, and $\Delta H°_1 = (2300 - 800) = +1500$ cal per mole.)

Proceeding in this way, the value of ΔH for each lanthanide–EDTA system was calculated; the results are listed in column three of Table III.

TABLE III

Thermodynamic quantities for the formation of lanthanide–EDTA complex ions at 25° C

Lanthanide	$\Delta F°$, cal/mole	$\Delta H°$, cal/mole	$\Delta S°$, cal/mole/° C
La	−20,720	− 800*	66.8
Ce	−21,070	− 470	69.1
Pr	−21,490	− 800	69.4
Nd	−21,890*	− 800	70.7
Sm	−22,540	− 800	72.9
Eu	−22,720	− 160	75.7
Gd	−22,940	+ 430	78.4
Tb	−23,620	+1500	84.3
Dy	−24,250	+1500	86.3
Ho	−24,610	+1250	86.7
Er	−25,060	+1500	89.1
Tm	−25,440	+1580	90.6
Yb	−25,910	+1320	91.3
Lu	−26,110	+ 640	89.7

*Normalizing values (see text).

The entropy change accompanying complex formation was calculated directly from the relation

$$\Delta F^\circ = \Delta H^\circ - T\Delta S^\circ, \text{ for } T = 298.1^\circ \text{ K.}$$

These values are given in column four of Table III.

Precision of the Derived Results

Table I shows that the probable error in the enthalpy change for each lanthanide pair lies between 60 and 330 calories, the average uncertainty in this quantity being ± 150 calories. The equilibrium constants listed in Table I appear to be precise to $\pm 2\%$. However, the method of intercomparison used to deduce the thermodynamic quantities for each lanthanide–EDTA system inevitably causes a carry-over and multiplication of these errors. Assuming a coefficient of variation of $\pm 2\%$ in every ratio given in Table I, then (relative to K_{Nd}, for which no error need be assigned) K_{Sm} is in doubt by $\pm 3\%$, as are the values for K_{La}, K_{Ce}, and K_{Pr}. The Tb value relative to K_{Sm} is precise to $\pm 2\%$, but relative to K_{Nd}, it is precise to $\sqrt{(3^2+2^2)} \cong \pm 4\%$. The further stages of intercomparison give rise to a maximum uncertainty in the values of K_{Lu} and K_{Tm}, *relative to K_{Nd}*, of $\pm 6\%$.

The uncertainty in ΔF°, relative to ΔF° for Nd, then varies from ± 10 cal per mole for La, to ± 35 cal per mole for Lu and Tm.

The uncertainty of ± 150 cal per mole for each value of ΔH listed in Table I leads in a similar way to a maximum uncertainty of ± 370 cal for ΔH°_{Lu}, again relative to the value of -800 cal per mole for the normalizing value of ΔH°_{La}. The relative uncertainty between ΔH values for adjacent lanthanides is about ± 210 cal per mole.

These errors in both ΔF° and ΔH° are reflected in the precision of the ΔS° terms; the values for this quantity listed in the last column of Table III are thought to be precise to ± 2.0 e.u.

DISCUSSION

A comparison of the present results at 25° C with those of Wheelwright *et al.* (1) is shown in Table II. The two sets of data have been normalized to give agreement at K_{Nd}. In addition, the earlier results have been adjusted to 25° C from 20° C, using the appropriate ΔH values listed in Table III. The largest adjustments required (5.7%) are in the K values for Tb to Yb, inclusive.

The errors quoted for the K values in ref. 1 vary from a minimum of $\pm 15\%$, in the region from La to Sm, and gradually increase to reach $\pm 250\%$ at Lu. Generally speaking, with the possible exception of the values for K_{La}, the two sets of data are in reasonable agreement. However, the present results are thought to be considerably more precise than the previously published measurements.

The results in Table III show very clearly that the remarkable stability of these complex ions is due almost entirely to the large increase in the entropy of the system when the complex is formed. The differences in stability among the complex ions are also in large measure due to the entropy terms, although in some cases, both ΔH and ΔS terms contribute appreciably in this respect.

The results in Table III may be used, with reservations, to calculate the *relative* partial molal entropies of the complex ions themselves. For this purpose it is convenient to consider the relation between the observed entropy change, ΔS°, and the conventional partial molal entropies, $\bar{S}^\circ$, of the species concerned. Thus for the reaction:

$$R^{3+}{}_{aq}+X^{-4} \rightleftharpoons RX^-$$

$$\Delta S^\circ = \bar{S}^\circ{}_{RX^-} - \bar{S}^\circ{}_{R^{3+}} - \bar{S}^\circ{}_{X^{-4}},$$

and
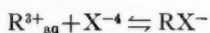
[5] $$(\Delta S^\circ + \bar{S}^\circ{}_{R^{3+}}) = \bar{S}^\circ{}_{RX^-} - \bar{S}^\circ{}_{X^{-4}}.$$

For a series of lanthanide–EDTA systems, the left hand side of equation [5] provides a *relative* measure of $\bar{S}^\circ{}_{RX^-}$, since the term $\bar{S}^\circ{}_{X^{-4}}$ is common. To make such comparisons, it is necessary to know the appropriate value of $\bar{S}^\circ{}_{R^{3+}}$, in addition to the experimental quantity ΔS°. Unfortunately, no experimentally based values of $\bar{S}^\circ{}_{R^{3+}}$ are available, and it is necessary to calculate these quantities for semiempirical formulae.

The two most generally accepted equations for calculation of $\bar{S}^\circ$ terms for aqueous ions are due to Powell and Latimer (10) and, more recently, to Laidler (11). Both equations provide a good fit to a large assembly of experimental information. In the following, both formulae are used to calculate the partial molal entropies of the lanthanide cations. The fundamental parameter required by both equations is the radius of the ion. The recent measurements of Dauben and Templeton (12) are particularly suitable in this connection, since as these authors observe, the radii have been estimated with sufficient precision to permit meaningful comparison of the properties of the lanthanides which depend on this parameter.

Table IV summarizes the results of these calculations. The data in columns 2 and 3 depend on the Powell–Latimer equation, while the last two columns are derived from the Laidler equation. The latter treatment gives results for $\bar{S}^\circ$ which are slightly more

TABLE IV

Relative partial molal entropy of the complex ions RX⁻

R	Ref. 10		Ref. 11	
	$-\bar{S}^\circ{}_{R^{3+}}$	$(\Delta S^\circ + \bar{S}^\circ{}_{R^{3+}})$	$-\bar{S}^\circ{}_{R^{3+}}$	$(\Delta S^\circ + \bar{S}^\circ{}_{R^{3+}})$
La	34.7	32.1	39.2	27.6
Ce	36.3	32.8	41.3	27.8
Pr	37.5	31.9	43.0	26.4
Nd	38.5	32.2	44.5	26.2
Sm	40.3	32.6	47.1	25.8
Eu	41.1	34.6	48.4	27.3
Gd	41.8	36.6	49.5	28.9
Tb	42.7	41.6	50.9	33.4
Dy	43.6	42.7	52.3	34.0
Ho	44.5	42.2	53.8	32.9
Er	45.3	43.8	55.2	33.9
Tm	46.1	44.5	56.5	34.1
Yb	46.8	44.5	57.7	33.6
Lu	47.5	42.2	58.8	30.9

Values of ΔS° from Table III.
Units are cal/mole/° C at 25° C.

negative than the corresponding values calculated from ref. (10). However, the results for either equation, when combined with the experimental entropy change ΔS° shown in Table III, gives results which are qualitatively compatible.

The relative entropy of the complex ion RX⁻ (as expressed by the quantity ($\Delta S^\circ + \bar{S}^\circ{}_{R^{3+}}$) in Table IV) is essentially constant for the lanthanides La to Gd; after Gd, a second group of constant values is apparent, which differ significantly from the first group. A quantitative statement of this result is shown in Table V.

TABLE V

Average values for the relative entropies of the
complex ions RX$^-$

Elements	$(\Delta S° + \bar{S}°_{R^{3+}})$ cal/mole/° C	
	Ref. 10	Ref. 11
La to Gd	33.3±1.4	27.1±0.9
Tb to Lu	43.1±1.1	33.3±0.7
Difference	9.8±1.8	6.2±1.1

The difference between the entropies of the complex ions of the two groups is from 6 to 10 e.u., depending on which equation is used to evaluate the terms in $\bar{S}°_{R^{3+}}$. The constancy of the values in each group is particularly striking; in only two cases (Lu and Gd) does an individual value of $(\Delta S° + \bar{S}°_{R^{3+}})$ differ from the average value of the subgroup by more than the estimated uncertainty attached to the quantity $\Delta S°$.

Clearly, the results shown in Table V depend very critically on the validity of the calculations of the terms in $\bar{S}°_{R^{3+}}$. In this connection, no allowance has been made for possible contributions to the entropy of the lanthanide ions arising from the term $R \ln p$, when p is the multiplicity of the ground state of the ion (10). These reservations must be borne in mind during the discussion which follows.

The entropy of a simple hydrated ion is determined primarily by its charge and radius, while the entropies of complex ions have additional contributions arising from structural factors (3). The constancy of the entropies within each of the two groups of complex ions (La to Gd, and Tb to Lu) would therefore appear to indicate the close similarity in structure and radius of the individual ions comprising each subgroup. Moreover, the trend with atomic number that is evident in the terms $\bar{S}_{R^{3+}}$ has largely disappeared when the corresponding ions RX$^-$ are compared. This is thought to be a consequence of the reduction of charge (from $+3$ to -1); in addition the ionic charge is spread over a relatively large structure. The radius of the individual ions RX$^-$ in each subgroup appears to be determined mainly by the EDTA part of the ion and the slight differences in the radii of the central ion are evidently smoothed out. As a result, the lanthanide contraction, the effect of which is evident in the entropies of the hydrated ions, is no longer reflected in the individual members of each subgroup of the complex ions.

On the other hand, the entropies of the two groups of complex ions differ by 6 to 10 e.u. An unreasonably large change in the radius would have to be postulated to account for a change of this magnitude in the entropy of a singly charged ion in solution. It appears likely therefore that a change in configuration occurs after Gd, as suggested by Wheelwright et al. (1). However, it is not possible from entropy considerations alone to state with precision the exact nature of the structural changes that may be involved. The following comments must therefore be considered as speculative, and are put forward to indicate that reasonable changes in structure will account for the observed entropy differences.

If the central ion is co-ordinated to five chelating groups in the EDTA molecule (2), then one of the nitrogen atoms participates in two 5-membered rings in the chelate structure. One ring involves the sequence N–C–C–N–R, and the other N–C–C–O–R. The opening of this N–R bond gives rise to a tetra-co-ordinate structure, and would lead to an entropy gain of $\smile$28 e.u. (14 e.u. for each ring involved (3)). The co-ordination

position freed on the central ion would then be occupied by a water molecule, leading to an entropy decrease of ⌣17 e.u. (3). The net result is that the entropy of the less highly organized complex would be approximately $28 - 17 = 11$ e.u. more positive than that of the fully co-ordinated species, in reasonable agreement with the experimental result.

SUMMARY AND CONCLUSION

The complex ions formed by the lanthanide ions with EDTA owe their exceptional stability to the large positive increase in entropy which occurs when the complex ion is formed. Two subgroups (La to Gd, and Tb to Lu) can be distinguished on the basis of the entropy changes involved. The differences between the two subgroups can be accounted for by plausible changes in the structure of the complex ions of the two groups. Within each subgroup, the differences in the partial molal entropy of the hydrated ions account very largely for the successive gradation in the association constants. The partial molal entropies of the individual complex ions is constant within experimental error in each of the two groups.

ACKNOWLEDGMENTS

REFERENCES

1. WHEELWRIGHT, E. J., SPEDDING, F. H., and SCHWARZENBACH, G.   J. Am. Chem. Soc. **75**, 4196 (1953).
2. MOELLER, T., MOSS, F. A. J., and MARSHALL, R. H.   J. Am. Chem. Soc. **77**, 3182 (1955).
3. COBBLE, J. W.   J. Chem. Phys. **21**, 1451 (1953).
4. BETTS, R. H., DAHLINGER, O. F., and MUNRO, D. M.   UNESCO Conf. on Radioisotopes, Paris, Sept. 1957. The Pergamon Press, Ltd., London. 1958. Paper No. 212.
5. ATTREE, R. W., CUSHING, R. L., LADD, J. A., and PIERONI, J. J.   Rev. Sci. Instr. **29**, 491 (1958).
6. CHENG, K. L., KURTZ, T., and BRAY, R. H.   Anal. Chem. **24**, 1640 (1952).
7. BETTS, R. H., DAHLINGER, O. F., and MUNRO, D. M.   Can. J. Phys. **36**, 73 (1958).
8. KESHISHIAN, V., KRUSE, H. W., KLOTZ, R. J., and FOWLER, C. M.   Phys. Rev. **96**, 1050 (1954).
9. THIRY, H.   Bull. soc. roy. sci. Liège, **26**, 29 (1957).
10. POWELL, R. E. and LATIMER, W. M.   J. Chem. Phys. **19**, 1139 (1951).
11. LAIDLER, K. J.   Can. J. Chem. **34**, 1107 (1956).
12. TEMPLETON, D. H. and DAUBEN, C. H.   J. Am. Chem. Soc. **76**, 5237 (1954).

# ISOMERIC 5-(SUBSTITUTED)AMINOTHIATRIAZOLE AND 1-SUBSTITUTED-TETRAZOLINETHIONES[1]

Eugene Lieber[2] and J. Ramachandran

ABSTRACT

The reaction of organic isothiocyanates with sodium azide in ethanol and water has been investigated. Water is shown to be the more advantageous solvent for this reaction giving higher yields and initially purer 1-substituted-tetrazoline-5-thiones. A series of these latter compounds was made by this procedure. The yield of product appears to be dependent on the electrical properties of the substituent of the isothiocyanate, the yields decreasing as the electron-donating properties increase. A series of new 4-substituted-thiosemicarbazides has been prepared and converted by diazotization to the corresponding 5-(substituted)amino-thiatriazoles. A theory to account for the differences in the mode of reaction of hydrazoic acid and azide ion is presented and discussed. The basic conversion of 5-(substituted)amino-thiatriazoles to 1-substituted-tetrazolinethiones may involve a simple dearrangement–rearrangement mechanism complicated by side reactions. A summary of known isomeric 5-(substituted)aminothiatriazoles and 1-substituted-tetrazolinethiones is presented.

INTRODUCTION

Recently, Lieber, Pillai, and Hites (1) have shown that the reaction of 4-substituted-thiosemicarbazides (I) as well as the reaction of alkyl- or aryl-isothiocyanates (II), with hydrazoic acid, leads to identical 5-(substituted)amino-1,2,3,4-thiatriazoles (III). Oliveri-Mandala (2) had previously assigned a thiocarbamyl azide structure (V) to the reaction product of compound II with hydrazoic acid. The resolution of this problem is similar to that discussed by Lieber and co-workers (3, 4) for the reaction of azide ion with carbon disulphide, which was shown to be thiatriazolinethione (VI), rather than the
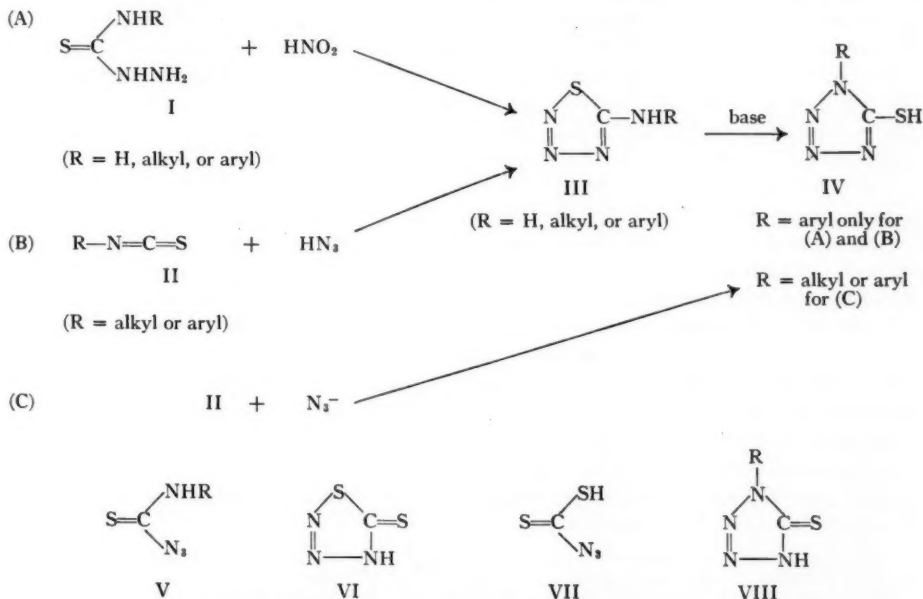
[1]*Manuscript received August 18, 1958.*
Contribution from the Department of Chemistry of DePaul University, Chicago, Illinois.
[2]*To whom all requests for additional information should be addressed.*

Can. J. Chem. Vol. 37 (1959)

acyclic azidodithiocarbonic acid (VII) (5). On the other hand, Stolle (6) had previously shown that the reaction of azide ion (sodium azide) with II leads to the formation of 1-substituted-tetrazole-5-thiols (IV, R = alkyl or aryl), the end products of the reaction (B) (isomerization of III with base for R = aryl substituents only (1)). More recently, Lieber and co-workers (7) have shown, by infrared absorption spectroscopy, that IV exists in the *thione form*, VIII, and, hence, is more properly termed 1-substituted-tetrazolinethiones. The interesting divergence in the mode of reaction of hydrazoic acid and azide ion, as illustrated by (B) and (C), prompted an investigation of the effect of solvent on the behavior of azide ion with organic isothiocyanates, since it was considered that the type of product produced, III or IV, would be dependent on the reactive intermediates involved, which in turn would be influenced by the solvent used. The influence of solvent should be particularly noted for azide ion owing to its initially charged character, in contrast to hydrazoic acid. Stolle (6) carried out the reaction with azide ion in boiling ethanol, whereas Oliveri-Mandala (2) used an ethereal solution of hydrazoic acid. Lieber and co-workers (1) showed that the reaction with hydrazoic acid can be carried out equally well in either ethanol or water, reaction (B), the 5-(substituted) amino-1,2,3,4-thiatriazole (III) being obtained in each case, and identical with the initial product of reaction (A).

The present communication relates to a study of reaction (C), particularly with the effect of solvents on the yields and purity of the reaction product,[3] IV, and extends the number of isomeric 5-(substituted)aminothiatriazoles, III, reported previously (1).

EXPERIMENTAL[4, 5]

Organic isothiocyanates, RNCS.—The organic isothiocyanates described previously (1) were used in the present study. Additional isothiocyanates prepared were R = *p*-nitrophenyl-; 2,4-dichlorophenyl-; *p*-dimethylaminophenyl-; and *p*-fluorophenyl-; by the reaction of the corresponding amine hydrochloride with thiophosgene.[6] The *p*-fluorophenylamine was made by the sequence: *p*-nitraniline; *p*-nitrophenyl diazonium fluoborate (8) (yield 90%, m.p. 156° (decomp.)); *p*-nitrofluorobenzene (8) (yield 33%, m.p. 27°); *p*-fluoroaniline (9) (yield 45%, b.p. 182–187° at 748 mm). The following data gives in sequence R, % yield, m.p. or b.p., and references: *p*-nitrophenyl, 90, m.p. 113° (10); 2,4-dichlorophenyl, 94, m.p. 39–40° (11); *p*-dimethylaminophenyl, 90, m.p. 70° (12); *p*-fluorophenyl, 63, b.p. 222–226° at 740 mm (10).

4-Substituted-thiosemicarbazides (Table I).—These were prepared as previously described (1). With the exception of the *p*-fluorophenyl-derivative, all of the 4-substituted-thiosemicarbazides described in Table I are new compounds. The melting point of the *p*-fluorophenyl-derivative obtained in this research does not agree with that previously reported. While a well-defined white crystalline product was obtained for the *p*-dimethyl-aminophenyl-derivative, an acceptable analysis could not be obtained, although its diazotization (see below, Table II) gave a correctly defined thiatriazole.

Syntheses of thiatriazoles (Table II).—These were prepared by suspending the 4-substituted-thiosemicarbazide in 10% hydrochloric acid and diazotizing according to the method described by Lieber and co-workers (1). The resulting precipitates were purified by recrystallization from aqueous acetone.

TABLE I

4-Substituted-thiosemicarbazides and benzylidene derivatives

R =	% Yield	M.p., °C[a]	Formula	% C Calc.	% C Found	% H Calc.	% H Found	% N Calc.	% N Found	% S Calc.	% S Found
			RNHC(S)NHNH$_2$								
4-O$_2$NC$_6$H$_4$[b]	90	190	C$_7$H$_8$N$_4$O$_2$S	39.62	39.58	3.77	3.50	26.41	26.80	15.09	14.91
2,4-Cl$_2$C$_6$H$_3$[b,c]	95	174	C$_7$H$_7$Cl$_2$N$_3$S	35.59	35.56	3.00	3.20	17.79	17.40	13.56	13.40
4-FC$_6$H$_4$	84	177–178[d]	C$_7$H$_8$FN$_3$S	45.38	45.31	4.38	4.50	22.68	22.20		
4-(CH$_3$)$_2$NC$_6$H$_4$[e]	100	192	C$_9$H$_{14}$N$_4$S	51.40	57.23	6.71	6.97	26.64	21.90	15.25	14.2
			RNHC(S)NHN=CHC$_6$H$_5$								
4-O$_2$NC$_6$H$_4$[b]	93	215–216	C$_{14}$H$_{12}$N$_4$O$_2$S	56.00	55.76	4.00	4.02	18.67	18.80	10.67	10.57
2,4-Cl$_2$C$_6$H$_3$[b,f]	—	218	C$_{14}$H$_{11}$Cl$_2$N$_3$S	51.85	51.82	3.40	3.19	12.96	12.90	9.87	9.22
4-FC$_6$H$_5$[b]	—	195–196	C$_{14}$H$_{12}$FN$_3$S					15.39	15.20		

NOTES: [a] With decomposition. [b] New compounds. [c] Calc.: Cl, 30.40. Found: Cl, 30.09. [d] BuvHoi (13) reports a melting point of 189°. [e] This is a new compound; the analysis represents the best obtainable after repeated purifications and analysis. [f] Calc.: Cl, 21.91. Found: Cl, 21.90.
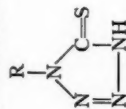
TABLE II

5-Arylamino-1,2,3,4-thiatriazoles
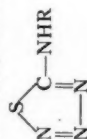
R =	% Yield	M.p., °C	Formula	Analysis							
				% C Calc.	% C Found	% H Calc.	% H Found	% N Calc.	% N Found	% S Calc.	% S Found
4-NO$_2$C$_6$H$_4$*	90	152–153	C$_7$H$_5$N$_5$O$_2$S	37.67	37.71	2.24	2.31	31.39	31.20	14.35	14.40
2,4-Cl$_2$C$_6$H$_3$*,[a]	85	140	C$_7$H$_4$Cl$_2$N$_4$S	34.01	34.17	1.62	1.83	22.68	22.20	12.95	13.15
4-FC$_6$H$_4$*	75	127–128	C$_7$H$_5$FN$_4$S	42.86	42.41	2.51	2.71	28.57	28.90	16.32	16.40
4-(CH$_3$)$_2$NC$_6$H$_4$	88	140	C$_9$H$_{11}$N$_5$S	48.85	48.95	5.01	4.74	31.65	32.00	14.49	14.45

[a] Calculated: Cl, 28.75%. Found: Cl, 29.00%.
* New compound.

TABLE III

### 1-Substituted tetrazoline-5-thiones

$$\begin{array}{c} R \\ | \\ N{-}C{=}S \\ \| \quad | \\ N{-}N{-}NH \end{array}$$

R =	% Yield	M.p., °C Found	M.p., °C Rept.	Formula	% C Calc.	% C Found	% H Calc.	% H Found	% N Calc.	% N Found	% S Calc.	% S Found
C_6H_5ᵃ	96	150	150									
2,4-$Cl_2C_6H_3$*ᵃ,ᵇ	97	130–131	—	$C_7H_4Cl_2N_4S$	34.01	34.09	1.62	1.56	22.68	22.78	12.95	12.91
2-$CH_3C_6H_4$ᵈ	92	123	123									
4-$CH_3C_6H_4$ᵈ	82	153	150									
4-$NO_2C_6H_4$*ᵃ	80	148	—	$C_7H_5N_5O_2S$	37.67	37.65	2.24	2.34	31.39	31.40	14.35	14.35
4-FC_6H_4*ᵃ	78	154–155	—	$C_7H_5FN_4S$	42.86	42.89	2.55	2.61	28.57	28.20	16.33	16.10
4-$(CH_3)_2NC_6H_4$*ᵃ	73	180	—	$C_9H_{11}N_5S$	48.87	48.90	4.98	5.07	31.75	31.40	14.47	14.46
$C_6H_5CH_2$ᶜ	48	144	144									
CH_3*ᶜ,ᵉ	52	125–126	126	$C_2H_4N_4S$	20.68	20.84	3.47	3.43	48.24	48.20	27.61	27.80
C_2H_5*ᶜ,ᵉ	46	50	—	$C_3H_6N_4S$	27.68	27.80	4.65	4.52	43.04	43.50	24.63	24.50
$CH_2{=}CH{-}CH_2$ᵈ,ᵉ	88	69	69	$C_4H_6N_4S$							22.55	22.30

*New compound. ᵃRefluxed for 6 hours. ᵇCalculated for $C_7H_4Cl_2N_4S$: Cl, 28.80%. Found: Cl, 28.75%. ᶜRefluxed for 8 hours. ᵈStirred at room temperature for 3 hours. ᵉWorked up by alternate procedure.

1-Substituted-tetrazoline-5-thiones (*Table III*).—The following general procedure was adopted. A mixture of 0.05 mole of the isothiocyanate and 0.075 mole of sodium azide dissolved in 100 cc of water was refluxed for a period ranging from 4 to 8 hours. The mixture was then cooled and filtered from any insoluble material present. The filtrate was then extracted twice with ether to remove any unreacted isothiocyanate present. The aqueous layer was cooled and acidified with concentrated hydrochloric acid to pH 3 (Congo red paper end point). If the product precipitated out at this stage (as was usually the case), it was filtered and washed with water. An alternative procedure (designated in Table III by the superscript *) was employed if the product did not precipitate subsequent to acidifying to Congo red paper. The acidified solution was extracted with ether and the ether extract washed with a little ice-cold water. The ether extract was then dried, filtered from the drying agent, and the ether carefully removed on a steam bath. The product which remains as a residue was purified. The purification was effected in the case of the 1-aryl tetrazoline-5-thiones by recrystallization from ethanol and a mixture of chloroform and petroleum ether was employed in the case of the 1-alkyl derivatives.

The reaction of n-heptyl isothiocyanate and n-butyl isothiocyanate with sodium azide.— The products obtained were oils which decomposed on distillation and consequently could not be purified. In the case of the *n*-heptyl isothiocyanate, 70% of the isothiocyanate was recovered unchanged after refluxing for 10 hours. In the reaction of *n*-butyl isothiocyanate with sodium azide, 50% of the isothiocyanate was recovered after refluxing for 10 hours.

The reaction of sodium azide with p-nitrophenyl isothiocyanate.—An insoluble orange-red precipitate was obtained. This was found to melt at 172–174°. The melting point identified the substance to be 1,3-di-(*p*-nitrophenyl)-thiourea:
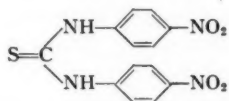
as the reported (15) m.p. is 175°.

The reaction of phenyl isothiocyanate with sodium azide.—This reaction was studied under different conditions. The results are summarized in Table IV, where the experimental conditions are also given.

Reaction of 5-methylamino-1,2,3,4-thiatriazole with sodium azide.—Sodium azide, 2.6 g (0.04 mole), dissolved in 100 cc of water was refluxed with 2 g (0.02 mole) of 5-methylamino-1,2,3,4-thiatriazole for 4 hours. The reaction mixture was cooled and the yellow

TABLE IV

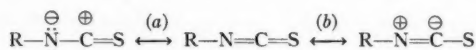Reaction of sodium azide with phenyl isothiocyanate in different solvents

Solvent	No. moles of sodium azide used	Time of refluxing (hours)	Yield of 1-phenyl tetrazoline-5-thione (%)	Melting point of crude product (° C)
95% Ethanol[a]	1.5	7	60	140–143
50% Ethanol	1.5	4	68	146–148
Water	1.5	4	96	150[a]
Water	1.0	4	88	150[a]

[a]The melting point of pure 1-phenyl tetrazoline-5-thione is 150° C.

material that had precipitated was filtered. The filtrate was acidified, extracted with ether, washed, and dried. The ether was then removed by distillation and the white crystalline residue washed with petroleum ether and filtered. Yield, 0.3 g (15%), m.p. 124–126°; no depression of mixed melting point with an authentic (1) sample of 1-methyltetrazoline-5-thione.
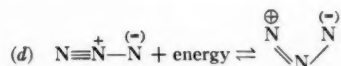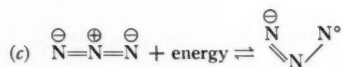
DISCUSSION

Water was used as the solvent for the synthesis of the 1-substituted-tetrazoline-5-thiones summarized in Table III. It will be noted that the yield of product is approximately doubled as one proceeds from the 1-alkyl- to the 1-aryl-derivatives. This trend in yield suggests that resonance interaction is important for the activation of the organic isothiocyanate. This is reasonable, since competitive conjugation is possible in the isothiocyanates as indicated below:

$$\overset{\ominus}{R-N}\overset{\oplus}{-}C{=}S \overset{(a)}{\longleftrightarrow} R-N{=}C{=}S \overset{(b)}{\longleftrightarrow} R-\overset{\oplus}{N}{=}\overset{\ominus}{C}-S$$

When R is an aryl group resonance interaction by process (a) is predominant, facilitating the creation of an electron-deficient carbon atom; whereas if R is an alkyl group resonance interaction by process (a) is inhibited and activation is then probably achieved by process (b). It is evident that this latter activation will be considerably less than in process (a), primarily as a result of the smaller difference in electronegativities of carbon and sulphur and, secondly, because of the electron-releasing properties of alkyl groups. The reaction may be considered as a nucleophilic attack of the azide ion on the electron-deficient carbon atom of the isothiocyano-group, followed by ring closure to the tetrazole by donating of electrons to an electron-deficient nitrogen atom of the azido-moiety. This suggests two conceivable pathways by which the reaction may proceed on this basis, the driving force being the considerable resonance stabilization of the tetrazolinethione anion, (1). While thus far only the activation of the isothiocyanate has been discussed, it must be considered that the activation of the azide ion is also an important step in the process. The observation that the yields and purity of 1-substituted-tetrazoline-5-thiones are improved considerably when the solvent is changed from alcohol to water suggests that the activation of the azide ion is of importance. While the solvent thus appears to be of considerable importance, the interpretation of the data is made difficult by the occurrence of side reactions.

The propensity of hydrazoic acid or azide ion to react with reagents leading to the formation of tetrazoles or 1,2,3-triazoles (16) necessitates the concept of a reactive intermediate for the azido-moiety which departs from the rigid linearity of this group in order that ring closure be effected. This concept suggests the necessity for the activation of the azide ion by the following processes:

$$(c) \quad \overset{\ominus}{N}{=}\overset{\oplus}{N}{=}\overset{\ominus}{N} + \text{energy} \rightleftharpoons \overset{\overset{\ominus}{N}\quad N°}{\diagdown_N\diagup}$$

$$(d) \quad N{\equiv}\overset{+}{N}{-}\overset{(-)}{N} + \text{energy} \rightleftharpoons \overset{\overset{\oplus}{N}\quad \overset{(-)}{N}}{\diagdown_N\diagup}$$

The advantage of this theory is that the activated structures produced by either (*c*) or (*d*) (or both) is not restricted by any criterion of linearity. The departure from linearity can be assumed to take place after the initial attack of the azide ion. On the other hand there is a great deal of attraction to the alternative assumption that *both the isothiocyano- and azido-moieties are activated prior to condensation*. This latter assumption then leads to the process in which the tetrazole ring is the result of a simple neutralization of charges, illustrated for one case as follows:

X
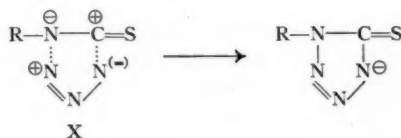
Similar reactive intermediates to that of X can be considered for the other resonance forms of the isothiocyano- and azido-groups.

The trend in the yields of the 1-aryl tetrazoline-5-thiones also lends support to the idea that resonance interaction of the isothiocyano group with the aromatic ring influences the activation of the isothiocyanate. Thus, the dimethylamino-, fluoro-, and methyl-groups in the para position of the aryl ring lower the yields (Table III) to a small extent, since the resonance interaction, in these cases, tends to suppress activation of the isothiocyano group by process (*a*), with probably increase of process (*b*). On the other hand, ortho substituents in the aromatic ring of the isothiocyanate increases the yields to a small extent probably because of steric inhibition of resonance. The above considerations lead to the expectation that the maximum yield of 1-substituted-tetrazoline-5-thione would be obtained by reaction of *p*-nitrophenyl isothiocyanate owing to the relatively greater electron-withdrawing ability of the nitro group. The apparent fall in yield is due to a side reaction involving the hydrolysis of the isothiocyanate to *p*-nitraniline, which is subsequently converted to 1,3-di(*p*-nitrophenyl)-thiourea. Dyson and Browne (10) have demonstrated that the solvolytic (in ethanol) attack on substituted-aryl-isothiocyanates increases as the electron-withdrawing ability of the substituent increases. This factor readily explains the lower yields of 1-substituted-tetrazoline-5-thiones when ethanol is used as solvent (Table IV), where as in water the solvolytic attack is reduced *owing to a higher degree of activation of the azide ion in water as contrasted with ethanol.*

The difference in the types of products formed when hydrazoic acid is used remains to be explained. It is suggested that the tetrazole ring closure is blocked as a result of the protonation of the organic isothiocyanate due to an initial acid–base reaction:

$$RNCS + HN_3 \rightarrow (R-NH-\overset{+}{C}=S)N_3^-.$$
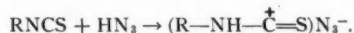
The subsequent step involving a neutralization of charges which may be indicated as follows:


XI
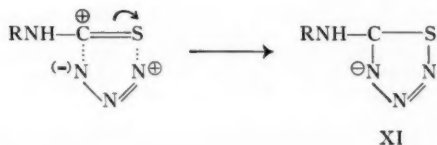
the protonation of the nitrogen preventing ring closure at that point, since such a ring closure would produce a *high energy* form of the isomeric structure:

$$R-\overset{\oplus}{N}H-C=S$$
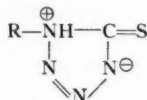
The process thus proceeds by a path producing the product of minimum energy, the anion XI.

In the previous investigation (1) on the chemistry of 5-(substituted)amino-1,2,3,4-thiatriazoles, it was noted that their isomerization with base to give the 1-substituted-tetrazoline-5-thione could be effected only with the 5-arylaminothiatriazoles (III, R = aryl). The yields in this reaction ranged from 22 to 37% and 1,3-diaryl thioureas were formed as by-products. Azide ion was identified among the degradation products. Organic isothiocyanates were also identified (either *per se* or as the 1,3-diaryl thiourea). The present investigation accordingly suggests that the mechanism of the base isomerization of III to IV may simply involve a dearrangement–rearrangement:

$$III \rightarrow RNCS + N_3^- \rightarrow IV.$$
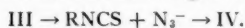
However, the speculations are complicated by the observations (1) that III simultaneously undergoes an internal oxidation–reduction to form elemental sulphur, nitrogen, and cyanamid derivatives. The observation that a 15% yield of 1-methyltetrazoline-5-thione (IV, R = CH_3) was obtained by refluxing 5-methylamino-1,2,3,4-thiatriazole with sodium azide is of considerable interest in that it suggests that the yields obtained in the base isomerization of III to IV is dependent upon the base strength. The latter factor will determine the rate at which the isothiocyanate *undergoes hydrolysis rather than recombination* to IV.[7] It is also interesting to note that when *n*-heptyl isothiocyanate was refluxed with sodium azide in water, 75% of the isothiocyanate was recovered unchanged after 10 hours. The apparent inertness of *n*-heptyl isothiocyanate to react with azide ion[8] may be accounted for by a too high electron density on the carbon of the isothiocyano group due to the electron-donating character of the heptyl radical. Under the same conditions, 50% of *n*-butyl isothiocyanate was recovered unchanged.

A summary of the known isomeric 5-(substituted)amino-1,2,3,4-thiatriazoles and 1-substituted-tetrazoline-5-thiones are presented in Table V together with their uncorrected melting points. It is unlikely that a correlation can be found, since both types of structures are thermally unstable. It is interesting to note that a third structural isomer can be readily made by the reaction of organic thiocyanates with azide ion, in which 5-mercaptotetrazoles are formed (17):
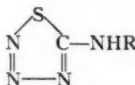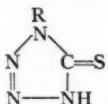
$$RSCN + NaN_3 \xrightarrow{H^+}$$
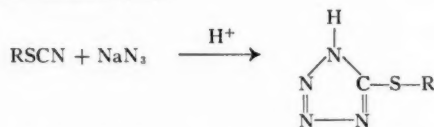
[7]*In unpublished data from the authors' laboratory, III (R = C_6H_5) (1 mole) was refluxed for 30 minutes in aqueous media with 2 mole proportion of the respective bases: (a) sodium carbonate; (b) sodium bicarbonate; (c) ammonium hydroxide; and (d) sodium acetate. The data following represents the percentage yields of IV (R = C_6H_5) and 1,3-diphenyl thiourea isolated: (a) (44) (20); (b) (58) (4); (c) (25) (62); (d) (7) (none). In only the latter case, 80% of unchanged III (R = C_6H_5) was recovered. This phase of the investigation is being continued.*

[8]*Further unpublished work from the authors' laboratory has found that attempts to base isomerize III (R = n-(C_7H_{15}) yields only n-heptyl isothiocyanate, azide ion, and n-heptyl urea; the latter product offering evidence for the internal oxidation–reduction disruption of the molecule.*

This reaction is under investigation and will be subsequently reported upon.

TABLE V

Summary of isomeric 5-(substituted)aminothiatriazoles and
1-substituted-tetrazoline-5-thiones

	Melting point, ° C	
R =	$\underset{N-N}{\overset{S}{N}}$ C—NHR	$\underset{N-NH}{\overset{R}{N}}$ C=S
CH_3	93–96	125–126
C_2H_5	66–67	50
$n\text{-}C_4H_9$	40–41	oil[b]
$n\text{-}C_7H_{15}$	75–75.5	oil[b]
$CH_2{=}CHCH_2$	53–53.5	69
$C_6H_5CH_2$	80.5–81	144
C_6H_5	142–143	150
$2\text{-}CH_3C_6H_4$	114–115	121–123
$4\text{-}CH_3C_6H_4$	142–144	153
$4\text{-}ClC_6H_4$	147–148	156–157
$2,4\text{-}ClC_6H_3$	140	130–131
$4\text{-}FC_6H_4$	127–128	154–155
$4\text{-}O_2NC_6H_4$	152–153	148
$4\text{-}(CH_3)_2NC_6H_4$	140	180
$(CH_3)_2{}^a$	49–51	—

NOTE: [a]5-Dimethylamino-1,2,3,4-thiatriazole.
[b]Composition as yet unconfirmed.

ACKNOWLEDGMENTS

REFERENCES

1. LIEBER, E., PILLAI, C. N., and HITES, R. D. Can. J. Chem. **35**, 832 (1957).
2. OLIVERI-MANDALA, E. Gazz. chim. ital. **43**, I, 304 (1913); **44**, I, 670 (1914); **51**, II, 195 (1921).
3. LIEBER, E., PILLAI, C. N., RAMACHANDRAN, J., and HITES, R. D. J. Org. Chem. **22**, 1750 (1957).
4. LIEBER, E., OFTEDAHL, E., GRENDA, S., and HITES, R. D. Chem. & Ind. 893 (1958).
5. AUDRIETH, L. F. Chem. Revs. **15**, 169 (1934).
6. STOLLE, R. (a) J. prakt. Chem. **124**, 261 (1930); (b) J. prakt. Chem. **133**, 60 (1932); (c) Ber. **63**, 670 (1930).
7. LIEBER, E., RAO, C. N. R., PILLAI, C. N., RAMACHANDRAN, J., and HITES, R. D. Can. J. Chem. **36**, 801 (1958).
8. SCHIEMANN, G. and PILLERSKY, R. Ber. **62**, 3040 (1929).
9. WILKINSON, J. H. and FINAR, I. L. J. Chem. Soc. 759 (1947).
10. DYSON, G. M. and BROWNE, D. W. J. Chem. Soc. 3285 (1931).
11. DYSON, G. M., GEORGE, H. J., and HUNTER, R. F. J. Chem. Soc. 3041 (1926).
12. DYSON, G. M., GEORGE, H. J., and HUNTER, R. F. J. Chem. Soc. 442 (1927).
13. BUV-HOI, No. Ph., XUONO, No. D., and NAM, No. H. J. Chem. Soc. 2160 (1956).
14. KENDALL, J. D. U. S. Patent No. 2,386,869. Oct. 16, 1945; C. A. **40**, 611.
15. DYSON, G. M. J. Chem. Soc. 174 (1934).
16. (a) BENSON, F. R. and SAVELL, W. L. Chem. Revs. **46**, 1 (1950). (b) BENSON, F. R. Chem. Revs. **41**, 1 (1947). (c) HUISGEN, R. and UGI, I. Chem. Ber. **90**, 2914 (1957). (d) UGI, I. and HUISGEN, R. Chem. Ber. **91**, 531 (1958).
17. FINNEGAN, W. G., HENRY, R. A., and LOFQUIST, R. J. Am. Chem. Soc. **80**, 3908 (1958).

# THE CONDENSATION OF 3-AMINO-5-PYRAZOLONES WITH ALDEHYDES SYNTHESES OF 5-PYRAZOLONOGUANIDINES[1]

PAUL E. GAGNON, JEAN L. BOIVIN,[2] AND JOSEPH ZAUHAR[3]

ABSTRACT

3-Amino-5-pyrazolones did not react with guanidine in aqueous solution, but with aldehydes in the presence of piperidine, the amino group was removed in some cases. 5-Pyrazolonoguanidines were synthesized by the direct fusion of 3-amino-5-pyrazolones and dicyandiamide. The infrared spectra of the pyrazolone derivatives prepared are briefly discussed.

INTRODUCTION

Previous investigations by Nencki and Sieber (1) have shown that the amino function of α-amino acids could interreact with guanidine carbonate to yield guanidoaliphatic acids. It was expected that 3-amino-5-pyrazolones (2, 3, 4, 5, 6, 7) and 3-amino-1-phenyl-5-pyrazolone (8) would behave similarly towards guanidine or guanidine carbonate when heated in aqueous solution. However, in all the experiments made, the starting materials were recovered, no evidence of condensation being detected. This was attributed to the prototropic shift occurring in 3-amino-5-pyrazolones and its 4-substituted derivatives which can exhibit 10 possible tautomeric structures (5) of which configurations I, II, and III contribute to their stability towards guanidine.
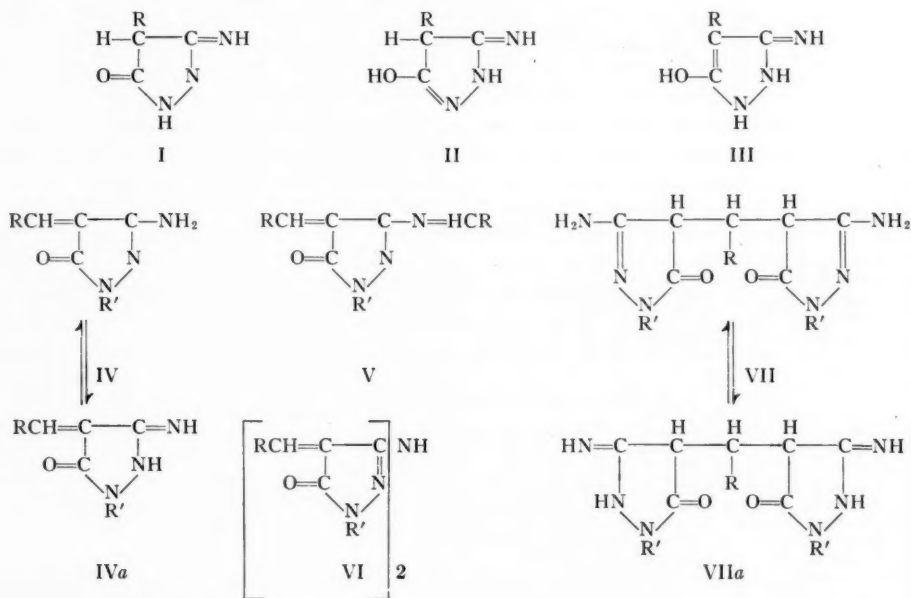
Since the amino group of 3-amino-5-pyrazolones did not react with guanidine, the behavior of pyrazolones towards aldehydes was studied in order to determine the stability of the amino groups.

Theoretically, condensation between 3-amino-5-pyrazolones and aldehydes in a basic medium would be expected to yield pyrazolones IV, IVa, V, VI, VII, and VIIa.

In formula IV the amino group is stabilized by the tautomeric form IVa and consequently, no reaction would be expected. Configuration V would result from the condensation of 1 mole of pyrazolone and 2 moles of aldehydes. The formation of a Schiff base in position 3 would give evidence of the existence of a free amino group. If 3-amino-5-pyrazolones reacted with 1 mole of aldehyde, 1 mole of ammonia being liberated in the process, pyrazolone VI would be formed. This type of condensation would justify the existence of a free amino group in position 3, the condensation occurring in a similar manner with α-amino acids and guanidine. Graham, Reckhow, and Weissberger (9) have shown that such a condensation was possible between 3-amino-1-phenyl-5-pyrazolone and ethylamine. A mixture of 3-ethylamino-1-phenyl-5-pyrazolone and 3,3-imino-bis(1-phenyl-5-pyrazolone) was obtained, the latter being the principal product of the reaction. Condensation of type VII would indicate that the stability of the amino group is probably due to the prototropic shift giving the tautomeric form VIIa.

RESULTS AND DISCUSSION

3-Amino-5-pyrazolone, Benzaldehyde, and Phenylacetaldehyde

When a mixture of benzaldehyde and 3-amino-5-pyrazolone, in a molar ratio of 3 : 1 respectively, was refluxed in the presence of piperidine, the reaction proceeded according to the following equation:
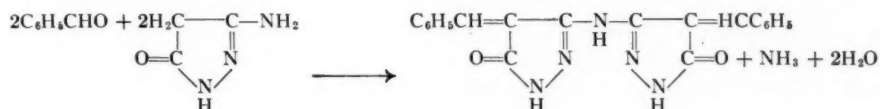
The compound isolated was slightly soluble in bases, insoluble in acids, and gave a negative test with ferric chloride, indicating no actual or potential enolic group.

With phenylacetaldehyde under similar conditions, the reaction was quite different. The amino group was not eliminated but reacted with the aldehyde.
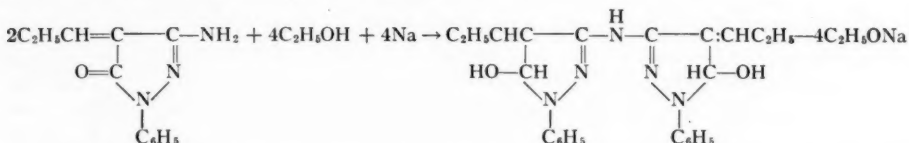

The compound which was isolated indicated that an active amino group, similar to those of primary amines, was present in position 3.

3-Amino-1-phenyl-5-pyrazolone and Aldehydes

3-Amino-1-phenyl-5-pyrazolone was also condensed with five aldehydes under similar conditions as in the foregoing experiments. The results obtained are recorded in Table I. Acetaldehyde condensed with only the methylene group of the pyrazolone and similar results were obtained with propionaldehyde indicating that under the above conditions,

the amino group was not reactive. Previous investigations by Knorr (10) have shown that 3-methyl-1-phenyl-5-pyrazolone, when treated with sodium ethylate, was not transformed into the corresponding hydroxy compound. However, in the present work, when the propylidene derivative was treated with sodium and ethyl alcohol, not only the corresponding hydroxy compound was formed but also ammonia was evolved to yield 3,3'-imino-bis(4-propylidene-1-phenyl-5-pyrazalin-5-ol).

$$2C_2H_5CH{=}C{-}\!\!\!-\!\!\!-C{-}NH_2 + 4C_2H_5OH + 4Na \rightarrow C_2H_5CHC{-}\!\!\!-\!\!\!-C{-}N{-}C{-}\!\!\!-\!\!\!-C{:}CHC_2H_5{-}4C_2H_5ONa$$

The equation indicates that the amino and not the imino structure of the pyrazolone was the predominant tautomeric form, the amino group being susceptible to elimination, n-valeraldehyde, on the other hand, condensed with both the methylene and the amino group. According to the elemental analyses and molecular weight determinations, both a monomer and a dimer having the same empirical formula $C_{19}H_{25}ON_3$ were isolated.

When benzaldehyde and the pyrazolone were condensed in a solution of benzene without piperidine, reaction occurred only with the methylene group. No ammonia was eliminated and the compound formed could be reduced to the corresponding pyrazalin-5-ol. On the other hand, in the presence of piperidine, benzaldehyde condensed with the methylene group and 1 mole of ammonia was eliminated from 2 moles of the intermediate product to yield 3,3'-imino-bis(4-benzylidene-1-phenyl-5-pyrazolone). A dimer with the same empirical formula, $C_{32}H_{23}O_2N_5$, was also isolated. With p-methoxybenzaldehyde in the presence of piperidine, condensation occurred with the methylene group, and 1 mole of ammonia was eliminated from 2 moles of the intermediate to give 3,3'-imino-bis(4-p-methoxybenzylidene-1-phenyl-5-pyrazolone). The corresponding pyrazalin-5-ol was easily obtained by reduction with sodium and ethyl alcohol. All the above compounds gave negative tests with ferric chloride, indicating the absence of an enolic group. No evidence for compounds having the structure VII could be found in the present work.

The condensation products of 3-amino-5-pyrazolones with aldehydes clearly indicate that the amino group in position 3 does not always exhibit the same stability and can be removed in some cases under appropriate conditions.
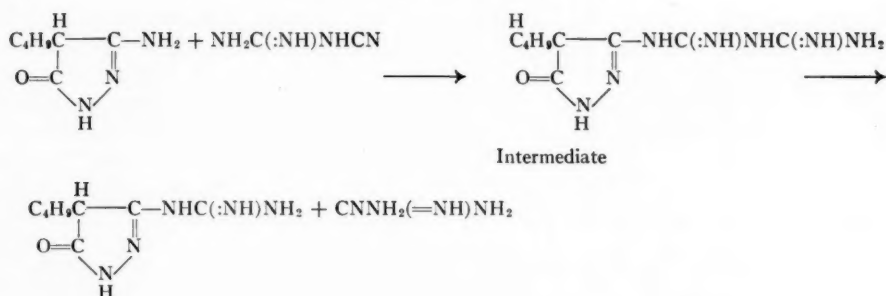
5-Pyrazolonoguanidines

4-Butyl-, 4-amyl-, and 4-benzyl-3-amino-5-pyrazolones, when heated with dicyandiamide, yielded the corresponding 5-pyrazolonoguanidines. For instance, 4-butyl-3-amino-5-pyrazolone and dicyandiamide heated at 150° C yielded 4-butyl-5-pyrazolonoguanidine. The biguanide intermediate probably formed at 150° C decomposed to the 5-pyrazolonoguanidine.

The guanidine derivative isolated was soluble in acids and bases and gave a positive test with ferric chloride for an enolic structure.

With 4-amyl-3-amino-5-pyrazolone, the reaction was carried at 180° C, since fusion was complete at a much higher temperature than in the case of 4-butyl-3-amino-5-pyrazolone. The reaction took place through the formation of a biguanide intermediate which decomposed at 180° C to give N,N'-bis(4-amyl-5-pyrazolono)-guanidine and ammonia. With 4-benzyl-3-amino-5-pyrazolone, the result was similar to that obtained with 4-amyl-3-amino-5-pyrazolone. The above compounds were soluble in bases and insoluble in acids and gave a positive test with ferric chloride.

TABLE I

3-Amino-1-phenyl-5-pyrazolone and aldehydes

Aldehydes RCHO R =	Products	Solvent	M.p. °C	Yield	Formula	Molecular weight Calc.	Molecular weight Found (Rast)	Analysis Calc. C	H	N	Analysis Found C	H	N	Solubility Acids	Bases
CH3—	CH3CH:C———C—NH2 / OC—N(C6H5)—N	Ethanol	225–226	95.7	C11H11ON3	201	184 and 215	65.53	5.47	20.80	65.1	5.6	20.5	Slight	Insoluble
C2H5—	C2H5CH:C———C—NH2 / OC—N(C6H5)—N	Ethanol	184–186	56.1	C12H13ON3	215	232 and 256	67.00	6.10	19.60	67.2	6.0	19.0	Slight	Insoluble
C4H9—	C4H9CH:C———C—N:CH / OC—N(C6H5)—N C4H9	Methanol or benzene	165–167	51.0	C19H25ON3	311	301 and 319	73.30	8.04	13.41	73.5	7.9	13.2	Insoluble	soluble
	+ Dimer	Ethanol	241–243	18.0	(C19H25ON3)2	622	604 and 670	73.30	8.04	13.41	73.6	8.2	13.1	Insoluble	soluble
C6H5—	C6H5CH:C———C—NH2 / OC—N(C6H5)—N	Methanol	231–233	84.5	C16H13ON3	263	256 and 261	72.98	4.98	15.96	70.8	5.1	16.0	Slight	Insoluble
C6H5—	(C6H5CH:C———C)2=NH / OC—N(C6H5)—N + Dimer	Dioxane	242–244	34.1	C32H23O2N5	509	Insoluble in camphor	75.42	4.54	13.75	75.9	5.0	13.6	Insoluble	soluble
		Methanol	260–261	17.2	(C32H23O2N5)2	1018	940 and 1050	75.42	4.54	13.75	75.8	4.7	13.4	Insoluble	soluble
C6H5— OCH3	(C6H5CH:C———C)2=NH / OCH3, OC—N(C6H5)—N	Acetic acid	253–254	89.1	C34H27O4N5	569	Insoluble in camphor	71.69	4.77	12.29	71.7	5.2	11.7	Insoluble	soluble

$$C_4H_9C\!\!-\!\!C\!\!-\!\!NH_2 + NH_2C(:NH)NHCN \longrightarrow C_4H_9C\!\!-\!\!C\!\!-\!\!NHC(:NH)NHC(:NH)NH_2 \longrightarrow$$

Intermediate

$$C_4H_9C\!\!-\!\!C\!\!-\!\!NHC(:NH)NH_2 + CNNH_2(=\!NH)NH_2$$

Infrared Absorption Spectra

The infrared absorption spectra were obtained with a Perkin–Elmer Model 21, double beam self-recording spectrophotometer and the bands corresponding to the 16 compounds studied are recorded in Table II. With most of the pyrazolones investigated, three absorption bands at 3400, 3300, and 3100 wave numbers were obtained and are attributed to the NH stretching vibrations of these compounds. However, these absorption bands are absent in the spectra of 4-phenylethylidene-3-iminophenyl-ethylidene-5-pyrazolone and 4-pentylidene-3-iminopentylidene-1-phenyl-5-pyrazolone where the

TABLE II

Infrared absorption spectra

Compound No.	Absorption bands in wave numbers									
1		3300	3225	1710	1690	1610	1590	1490		725	695
2						1600	1555		763	715	700
3		3300	3150		1680	1630	1590	1490	755	715	690
4	3400	3300	3150		1680	1625	1590	1490	760	710	685
5		3300			1670		1580	1480	760	740	685
6					1670	1600	1585	1500	760	720	690
7			3100	1700	1670	1620	1585	1500	750	720	690
8	3400	3300	3100		1680	1605	1550	1480	745	720	700
9	3400	3300	3100		1680	1600	1550	1480	750		700
10			3150		1690	1620	1585	1480	750	720	690
11		3250		1700	1680	1620	1590	1490	750	725	695
12			3150		1670	1600	1590	1490	750	720	685
13		3270	3110		1685	1600	1585	1490	750	720	690
14	3400	3270	3100		1640		1580	1490	760	720	690
15		3280	3100		1620				760	720	685
16	3300	3280	3100		1610			1490	760	720	695

1. 3,3'-Imino-bis(4-benzylidene-5-pyrazolone).
2. 4-Phenylethylidene-3-iminophenylethylidene-5-pyrazolone.
3. 4-Ethylidene-3-amino-1-phenyl-5-pyrazolone.
4. 4-Propylidene-3-amino-1-phenyl-5-pyrazolone.
5. 3,3'-Imino-bis(4-propylidene-1-phenyl-5-hydroxypyrazolone).
6. 4-Pentylidene-3-iminopentylidene-1-phenyl-5-pyrazolone.
7. Dimer of 4-pentylidene-3-iminopentylidene-1-phenyl-5-pyrazolone.
8. 4-Benzylidene-3-amino-1-phenyl-5-pyrazolone.
9. 4-Benzylidene-3-amino-1-phenyl-5-pyrazalin-5-ol.
10. 3,3'-Imino-bis(4-benzylidene-1-phenyl-5-pyrazolone).
11. Dimer of 3,3'-imino-bis(4-benzylidene-1-phenyl-5-pyrazolone).
12. 3,3'-Imino-bis(4-p-methoxybenzylidene-1-phenyl-5-pyrazolone).
13. 3,3'-Imino-bis(4-p-methoxybenzylidene-1-phenyl-5-pyrazalin-5-ol).
14. (4-Butyl-5-pyrazolono)-guanidine.
15. N,N'-bis(4-amyl-5-pyrazolono)-guanidine.
16. N,N'-bis(4-benzyl-5-pyrazolono)-guanidine.

hydrogen has been substituted by a benzyl and butyl group respectively. The ketonic function was exhibited in the range of 1620 to 1690 wave numbers by all the compounds but the spectra of 3,3'-imino-bis(4-propylidene-1-phenyl-5-pyrazalin-5-ol) and 3,3'-imino-bis(4-p-methoxybenzylidene-1-phenyl-5-pyrazalin-5-ol) failed to show their hydroxyl function.

An analogy found in these spectra and attributed to the over-all molecule is the three absorption bands in the range of 750 to 720 and 690 wave numbers.

EXPERIMENTAL*

3-Amino-5-pyrazolone and Benzaldehyde

3,3'-Imino-bis(4-benzylidene-5-pyrazolone).—Benzaldehyde (0.56 mole) was introduced into a flask containing cooled ethanol (200 ml), piperidine (4 ml), and 3-amino-5-pyrazolone (0.20 mole) and the resulting mixture refluxed. 3-Amino-5-pyrazolone slowly passed into solution, during which time ammonia was liberated, and after refluxing for 24 hours, the reaction was complete. The resulting reddish-brown solution was then filtered, the filtrate was evaporated to one-half of its original volume, and left to stand in a cool place. The white product which separated from the solution after it had been left standing for 24 hours was filtered, washed with ethanol, and dried. The compound 3,3'-imino-bis(4-benzylidene-5-pyrazolone) was recrystallized from ethanol. It was insoluble in acids and slightly soluble in bases and gave a negative test with ferric chloride, m.p. 252–253° C. Yield, 17%. Calc. for $C_{20}H_{15}O_2N_5$: C, 67.20; H, 4.23; N, 19.60%. Found: C, 67.6; H, 4.1; N, 19.3%.

3-Amino-5-pyrazolone and Phenylacetaldehyde

4-Phenylethylidene-3-iminophenylethylidene-5-pyrazolone.—To a cooled mixture of 3-amino-5-pyrazolone (0.20 mole) in ethanol (715 ml) and piperidine (4 ml), phenylacetaldehyde (50%, 134.4 g, 0.56 mole) was slowly added, and the mixture refluxed for 24 hours and treated as in the preceding experiment. A white solid separated from the concentrated solution when it was left standing. The crude product was filtered, washed with ethanol, and dried. 4-Phenylethylidene-3-iminophenylethylidene-5-pyrazolone, which crystallized from methanol in plate-like crystals, was insoluble in acids and slightly soluble in bases. It gave a negative test with ferric chloride and could not be reduced with sodium in ethanol, m.p. 264–266° C. Yield, 30%. Calc. for $C_{19}H_{17}ON_3$: C, 75.21; H, 5.65; N, 13.85%. Found: C, 75.7; H, 5.4; N, 13.9%.

3-Amino-1-phenyl-5-pyrazolone and Aldehydes

3-Amino-1-phenyl-5-pyrazolone.—To a cooled mixture of aldehyde (0.14 mole), ethanol (50 ml), and piperidine (2 ml) was added 3-amino-1-phenyl-5-pyrazolone (0.06 mole). The mixture was refluxed for 24 hours and the alcoholic solution was then evaporated under reduced pressure to one-half of its original volume, and upon cooling, the crude material separated from the solution. The products isolated together with their recrystallizing solvents, melting points, yields, molecular weights, analyses, and solubility tests are given in Table I. All the compounds isolated gave negative tests with ferric chloride.

Benzaldehyde

4-Benzylidene-3-amino-1-phenyl-5-pyrazolone.—To a cooled solution of benzaldehyde (0.34 mole) in benzene (800 ml) was added 3-amino-1-phenyl-5-pyrazolone (0.11 mole).

*All melting points are uncorrected.

The reaction mixture was refluxed for 24 hours, after which time a white solid precipitated from the solution. The product was cooled, filtered, and washed with ethanol. The crude product was extracted with methanol (375 ml), the extract was filtered and evaporated to one-half of its original volume, and then left to crystallize overnight in the refrigerator. 4-Benzylidene-3-amino-1-phenyl-5-pyrazolone crystallized out in clustered colorless needles. The compound was soluble in hot ethanol, soluble in acids, and insoluble in bases. No coloration was obtained with ferric chloride, m.p. 231–233° C. Yield, 85%. Calc. for $C_{16}H_{13}ON_3$: C, 72.98; H, 4.98%. Found: C, 72.8; H, 5.1; N, 16.0%.

Reduction of 5-Pyrazolones with Sodium and Absolute Ethanol

3,3′-Imino-bis(4-propylidene-1-phenyl-5-hydroxypyrazolone).—A suspension of 4-propylidene-3-amino-1-phenyl-5-pyrazolone (0.01 mole) in absolute ethanol was prepared in a 3-necked flask fitted with a condenser. To the mixture were added clean pieces of sodium (0.07 mole) at such a rate that vigorous refluxing was continuous. The mixture was then refluxed for 1½ hours to assure that all the sodium had reacted, and during this time, ammonia was evolved. The ethanol was then removed by evaporation under reduced pressure. The resulting yellow sludge was dissolved in water (40 ml) and the solution filtered. The filtrate was neutralized with acetic acid (50%), whereupon a red amorphous product precipitated immediately. The reduced compound, 3,3′-imino-bis(4-propylidene-1-phenyl-5-pyrazalin-5-ol), was separated by filtration, washed with water, and dried. The crude product crystallized from methanol in red cubical crystals. 3,3′-Imino-bis(4-propylidene-1-phenyl-5-pyrazolone) was found insoluble in water, acids, and ether, and slightly soluble in bases. A negative test was obtained with ferric chloride, m.p. 215–217° C. Yield, 82%. Calc. for $C_{24}H_{27}O_2N_5$: C, 69.0; H, 6.52; N, 16.78%. Found: C, 70.0; H, 6.4; N, 16.6%.

4-Benzylidene-3-amino-1-phenyl-5-pyrazalin-5-ol. — 4-Benzylidene-3-amino-1-phenyl-5-pyrazolone (0.01 mole) in absolute ethanol (125 ml) was reduced with sodium (0.17 mole) as in the foregoing experiment. The reduced compound, 4-benzylidene-3-amino-1-phenyl-5-pyrazalin-5-ol, was recrystallized from methanol and isolated as colorless needles; it was soluble in acids and bases and insoluble in ether. A negative test was obtained with ferric chloride; the compound had a tendency to decompose in air, m.p. 197–199° C. Yield, 58%. Calc. for $C_{16}H_{15}ON_3$: C, 72.43; H, 5.70; N, 15.84%. Found: C, 72.0; H, 5.2; N, 15.2%.

3,3′-Imino-bis(4-p-methoxybenzylidene-1-phenyl-5-pyrazalin-5-ol.—A suspension of 3,3′-imino-bis(4-p-methoxybenzylidene-1-phenyl-5-pyrazolone (0.02 mole) and ethanol (300 ml) was treated with sodium (0.38 mole) so that refluxing was continuous and the reaction mixture was then treated as in the preceding experiments. The crude product obtained recrystallized from benzene gave a colorless compound, m.p. 170–172° C. Yield, 38%. Calc. for $C_{34}H_{31}O_4N_5$: C, 71.19; H, 5.45; N, 12.21%. Found: C, 70.5; H, 5.6; N, 11.8%.

5-Pyrazolonoguanidines

N,N′-bis(4-substituted-5-pyrazolono)-guanidines. — 4-Substituted-3-amino-5-pyrazolone (0.03 mole) was fused with dicyandiamide (0.02 mole), with stirring. The mixture began to melt at 90° C, during which time a slight exothermic reaction occurred and ammonia was liberated. The temperature of the melt was then raised to 180° C and kept there for 3 hours. The molten mass was then cooled, extracted with ethanol, and precipitated with a large quantity of water. The guanidine derivative was then recrystallized several times from an ethanol–water mixture. The compound was soluble in acetone and bases,

and insoluble in acids. A positive test for an enolic group was obtained with ferric chloride. The guanidine derivatives isolated were: N,N'-bis(4-amyl-5-pyrazolono)-guanidine, m.p. 197–199° C. Yield, 86%. Calc. for $C_{17}H_{29}O_2N_7$: C, 56.20; H, 7.99; N, 27.0%. Found: C, 55.9; H, 7.8; N, 27.4%. Molecular weight: Calc. 363. Found (Rast method): 382 and 395. N,N'-bis(4-benzyl-5-pyrazolono)-guanidine, m.p. 258–261° C. Yield, 75%. Calc. for $C_{21}H_{21}O_2N_7$: C, 62.53; H, 5.21; N, 24.30%. Found: C, 62.3; H, 5.0; N, 23.6%. Molecular weight: Calc. 403. Found (Rast method): 419 and 427.

4-Butyl-5-pyrazolonoguanidine.—4-Butyl-3-amino-5-pyrazolone (0.03 mole) was fused with dicyandiamide (0.02 mole), with stirring. The mixture began to melt at 85° C, and the temperature was slowly raised to 150° C and held at that temperature for 3 hours. The melt was then treated as in the preceding experiments. The crude 4-butyl-5-pyrazolono-guanidine was then recrystallized from an ethanol–water mixture. The compound was soluble in acetone, acids, and bases and gave a positive test with ferric chloride, m.p. 239–241° C. Yield, 57%. Calc. for $C_8H_{15}ON_5$: C, 48.73; H, 7.61; N, 35.53%. Found: C, 48.4; H, 7.6; N, 35.5%. Molecular weight: Calc. 197. Found (Rast method): 210 and 221.

REFERENCES

1. NENCKI, M. and SIEBER, N.   J. prakt. Chem. **17**, 478 (1878).
2. CONRAD, M. and ZART, M.   Ber. **39**, 2282 (1906).
3. HEPNER, B. and FAJERSZTEJN, S.   Bull. soc. chim. France, **4**, 854 (1937).
4. GAGNON, P. E., SAVARD, K., GAUDRY, R., and RICHARDSON, M.   Can. J. Research, B, **25**, 28 (1947).
5. GAGNON, P. E., BOIVIN, J. L., and JONES, R. N.   Can. J. Research, B, **27**, 190 (1949).
6. GAGNON, P. E., BOIVIN, J. L., and GIGUÈRE, J.   Can. J. Chem. **29**, 328 (1951).
7. GAGNON, P. E., NOLIN, B., and JONES, R. N.   Can. J. Chem. **29**, 843 (1951).
8. WEISSBERGER, A. and PORTER, H. D.   J. Am. Chem. Soc. **64**, 2133 (1942).
9. GRAHAM, B., RECKHOW, W., and WEISSBERGER, A.   J. Am. Chem. Soc. **76**, 3993 (1954).
10. KNORR, L.   Ann. **238**, 147 (1887).

NOTES

## SYNTHESIS OF ALKYL 1-PHENYL-5-CHLORO-1,2,3-TRIAZOLE-4-CARBOXYLATE

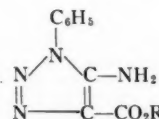Eugene Lieber,* T. S. Chao, and C. N. R. Rao

INTRODUCTION

The ability to exchange the chlorine in position 5 of the *vic*-triazoles by nucleophilic substitution makes it a desirable intermediate in synthetic work in this field. Dimroth (1), and later Dutt (2), reported on the preparation of I and II by the reaction of the esters of 1-phenyl-5-hydroxy-1,2,3-triazole-4-carboxylate (3), III, with phosphorus pentachloride and by the diazotization of the hydrochloride of the ester of 1-phenyl-5-amino-1,2,3-triazole-4-carboxylate (1), IV; in the latter synthesis Dimroth (1) gave no details of procedure nor yield of product. The phosphorus method is also sketchily described, the literature (1, 2) implying that it
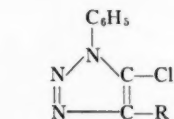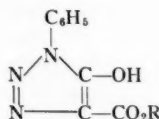
I (R = CO₂C₂H₅)
II (R = CO₂CH₃)   III (R = CH₃; or, C₂H₅)   IV (R = CH₃; or, C₂H₅)

merely involves heating IV and phosphorus pentachloride together. In our hands the yields obtained with the phosphorus pentachloride method were found to be dependent on the care taken to maintain anhydrous conditions and the rates of phosphorus pentachloride addition. As triazoles of the general structure I and II were required for previous studies (4, 5, 6), detailed experimental procedures were worked out starting from the intermediates III and IV and are reported upon in the present communication. The diazotization procedure offers an advantage in that the required intermediate IV can be made more easily and in higher yields than III (4) and in turn gives comparable conversions to the required 5-chloro-compounds (I, II). The experimental section presents typical preparations involving both the phosphorus pentachloride and diazotization methods, respectively.

EXPERIMENTAL†,‡

Methyl 1-Phenyl-5-chloro-1,2,3-triazole-4-carboxylate (II)

Phosphorus pentachloride procedure.—A 500-ml, 3-necked flask was equipped with a stirrer and a reflux condenser. To the third neck was connected a 125-ml Erlenmeyer flask connected by a short piece of ½-in.-diameter Tygon tubing through 16 mm glass tubing from the necks of the Erlenmeyer flask and reaction flask respectively. The Tygon connector was of sufficient length to permit the Erlenmeyer flask to rest on its bottom when not in use as described below. The complete setup was flame-dried and cooled to room temperature under a nitrogen atmosphere. The reaction flask was then charged with 65.7 g (0.3 mole) of *methyl 1-phenyl-5-hydroxy-1,2,3-triazole-4-carboxylate* (II, R = CH₃) (3), which had been dried in a vacuum desiccator over Drierite for 2 days.

*To whom all inquiries for additional information should be addressed.
†Melting points were taken on a Fisher–Johns heating block and are corrected.
‡Microanalyses by Dr. C. Weiler and Dr. F. B. Strauss, Oxford, England.

Seventy-four grams (0.33 mole) of PCl_5 was placed in the Erlenmeyer flask. The reaction flask was heated in a water bath to 70° and kept at 65–70° during the reaction. By raising the Erlenmeyer flask containing the PCl_5 to a slightly inverted position and gently tapping its wall, PCl_5 was caused to flow slowly and intermittently into the reaction flask. The progress of the reaction was indicated by the HCl evolution and was controlled accordingly, completing the addition of PCl_5 in about 90 minutes, after which time the reaction mixture was heated in a gently boiling water bath for 4 hours in order to complete the reaction. After being cooled to room temperature the system was connected to a water pump through a $CaCl_2$ tower and a dry-ice trap. The dissolved HCl was first removed, after which the $POCl_3$ was distilled off at 31–32° at 47 mm. The last traces of $POCl_3$ were removed by distilling at 1–2 mm, using a well-protected oil pump. The residue solidified into a brown mass while being stirred with a glass rod. The suspension was poured into 500 ml of water and filtered. The solid was suction dried and weighed 44 g, m.p. 80–82°. The filtrate was separated into two layers. The ether layer was washed with water, dried, and evaporated under vacuum recovering 4 g additional product. Purification was effected by recrystallization from methanol; yield, 41 g (57.4%), white needles, m.p. 87° (1). Anal. Calc. for $C_{10}H_8ClN_3O_2$: C, 50.52; H, 3.40; N, 17.70; Cl, 14.92. Found: C, 50.57; H, 3.48; N, 17.60; Cl, 14.82. The mother liquor was in the form of a dark red thick oil which failed to crystallize.

Ethyl 1-Phenyl-5-chloro-1,2,3-triazole-4-carboxylate (I)

Diazotization procedure.—A mixture of 250 ml of absolute ethanol and 23.2 g (0.1 mole) of *ethyl 1-phenyl-5-amino-1,2,3-triazole-4-carboxylate* (1, 4) was placed in a 1-l. 3-necked flask equipped with a stirrer, dropping funnel, and a gas inlet tube, all exits were protected with drying tubes. The mixture was cooled to 0–5° with stirring, whereupon a slow stream of *dry* HCl gas was slowly bubbled through the mixture until the suspended solid went into solution. Seventeen grams (0.1 mole) of freshly prepared isoamyl nitrite (7) was then added rapidly and the reactants stirred at 0–5° for 48 hours. It was then poured into 500 ml of ice water with vigorous stirring. A fine orange-colored precipitate was obtained. It was filtered, suction dried, and dissolved in 50 ml of boiling methanol. After evaporation *in vacuo*, 12 g (47%) of deeply yellow-colored needle-like crystals was obtained. Recrystallization from methanol containing a small amount of water gave pale yellow needles, m.p. 79°. Dutt (2) reported a m.p. 80–81°. Anal. Calc. for $C_{11}H_{10}ClN_3O_2$: C, 52.50; H, 4.01; Cl, 14.09; N, 16.70. Found: C, 52.24; H, 4.10; Cl, 13.90; N, 17.00. The mother liquor, after evaporation of all of the solvent, gave about five grams of a red viscous oil which could not be crystallized.

1. DIMROTH, O. Ann. **364**, 183 (1909).
2. DUTT, P. K. J. Chem. Soc. 265 (1923).
3. DIMROTH, O. Ann. **335**, 1 (1904).
4. LIEBER, E., CHAO, T. S., and RAO, C. N. R. J. Org. Chem. **22**, 654 (1957).
5. LIEBER, E., RAO, C. N. R., and CHAO, T. S. J. Am. Chem. Soc. **79**, 5962 (1957).
6. LIEBER, E., RAO, C. N. R., and CHAO, T. S. Current Sci. (India), **26**, 14 (1957).
7. NOYES, W. A. Org. Syntheses, Coll. Vol. II, 109 (1943).

Symposium on Charge Transfer Processes

A REPORT ON A SYMPOSIUM HELD BY THE PHYSICAL CHEMISTRY DIVISION OF THE CHEMICAL INSTITUTE OF CANADA[1]

B. E. CONWAY

INTRODUCTION

A symposium on Charge Transfer Processes both in the homogeneous solution phase and at electrode interfaces was held at the Chemistry Department of the University of Toronto on 4th and 5th September, 1958. The meeting was sponsored by the Chemical Institute of Canada, supported by the National Research Council, and organized under the chairmanship of B. E. Conway (University of Ottawa). Twenty-seven invited papers were presented, the majority of which had been preprinted and circulated to participants prior to the meeting. The sessions were devoted to ten-minute presentations of these papers together with periods of discussion on related groups of papers. A number of the invited papers are being published in the present issue of the Canadian Journal of Chemistry. In this paper a general account of the meeting is given together with reports on the main matters which arose in discussion and the conclusions arising therefrom.

Although individual papers on some aspects of Charge Transfer Processes have been presented at various meetings in North America and Europe, it is some time since a meeting specifically on this topic has been held. The last general meetings held specifically on electrochemical charge transfer processes were the Faraday Society Discussion in 1947 and the Bunsengesellschaft meeting at Goslar in 1951. Since these meetings, there have been considerable advances made in the field both in homogeneous and heterogeneous processes. In the present symposium an attempt was made to bring together contributions from those interested in homogeneous and also heterogeneous processes, since similar problems are encountered in both of these types of charge transfer processes; thus, the degree of solvent reorganization which occurs in the charge transfer step, the nature of the electron transfer process, specific effects of aquo- and non-aquo-ligand interaction with the ions involved are problems common to both the fields of homogeneous and heterogeneous processes. For the latter type of reactions, adsorption of reactants and solvent, the effect of electrode field on the reaction kinetics and adsorption of reactants and the electronic character of the metal (e.g. s, p, or d-band character) must also be considered. Papers were therefore also invited on adsorption at electrodes and the nature of the double layer at electrode interfaces. The somewhat specialized fields of so-called "charge-transfer spectra" and "charge-transfer complexes" were considered to be outside the scope of the present meeting.

HOMOGENEOUS PROCESSES

Despite their familiarity in classical inorganic solution chemistry, the detailed mechanism of a number of apparently simple redox reactions involving simple and complex inorganic ions has not until relatively recently been examined or understood. The first four papers of the symposium dealt with theoretical and experimental results obtained with such systems.

[1]*Manuscript received July 10, 1958.*
Contribution from the Department of Chemistry, University of Ottawa, Ottawa, Canada.

Can. J. Chem. Vol. 37 (1959)

120

Electron Transfer Reactions between Ions in Solution

H. Taube (University of Chicago), in giving the opening paper on "Bridging and Simple Ligand Effects in Electron Transfer Reactions", stressed the role of changes which must occur in the co-ordination sphere of the ions when the transfer of the electron(s) occurs. Two types of transition states are to be distinguished: (i) the outer sphere activated complex in which both of the ions concerned in the redox reaction are relatively inert to ligand substitution (e.g. as determined by isotopic exchange experiments) and in which the inner co-ordination spheres hence cannot suffer appreciable interpenetration; (ii) the bridged activated complex in which a ligand, often anionic, is shared between the metal ions, so that a change in the first co-ordination sphere of at least one of the partners of the redox pair must occur. Examples of redox pairs involved in the first type of reaction are $Fe(CN)_6^{-3,-4}$, $IrCl_6^{-2,-3}$, $Mo(CN)_8^{-3,-4}$, $Fe(dipy)_3^{+3,+2}$, $Os(o\text{-phen})_3^{+3,+2}$, $MnO_4^{-1,-2}$; in the second type of case the redox reaction between $(NH_3)_5CoCl^{++}$ with Cr^{++} was discussed. $CrCl^{++}$ is formed as a product and not $Cr(H_2O)_6^{+++}$ in this reaction, thus suggesting that a Cr—Cl bond is involved in the activated state. A variety of other anions which may take part in the formation of bridged transition states were listed, and kinetic data were presented in cases involving reactions between Cr^{++} and $Cr(III)$ complexes. The role of conjugation when organic ligands are involved in the reaction between Cr^{++} and $Co(III)$ complexes was examined. It was pointed out that, although the reaction mechanisms are known in a number of selected cases, the subject of inorganic redox reactions must be regarded as still being in an unsatisfactory state of development so long as relatively common reactions such as those between Fe^{++}–Fe^{+++} and Fe^{++} and $Ce(IV)$ are not understood with regard to their detailed mechanism.

In regard to the Fe^{++}–Fe^{+++} case, K. J. Laidler (University of Ottawa) presented some interesting theoretical considerations concerning the mechanism and free energy of activation of this reaction. The reaction between Fe^{++} and Fe^{+++} was considered to be diffusion controlled, the approach of the ions being hindered by their electrostatic repulsion, which was estimated taking into account the dielectric saturation in the solvent near to the ions. As the ions are brought together the electrostatic repulsion rapidly increases but the probability of electron tunneling between the ions increases at the same time. An optimum separation of the ions exists for which the redox reaction has a maximum rate or minimum free energy of activation $\Delta G^{\ddagger}$. The value of $\Delta G^{\ddagger}$ calculated is in good agreement with that derived from experimental data.

The applicability of the Franck–Condon principle to the electron transfer and solvent redistribution which occurs in electron transfer reactions such as that between Fe^{++}–Fe^{+++} ions, was vigorously discussed by R. A. Marcus (Brooklyn Polytechnic Institute) and K. J. Laidler. It was felt that since the electron transfer must occur by a relatively rapid tunneling step, the solvent distribution about the ions could be regarded as essentially remaining static during the electron transfer. This is what had been assumed in the calculations.

The principle of equivalence change in redox systems was dealt with in a paper by J. Halpern (University of British Columbia). A number of oxidizing and reducing reagents are known where stable oxidation states differ by two electron equivalents, e.g. $Tl(I)$–$Tl(III)$; $Sn(II)$–$Sn(IV)$. The mechanism of the reactions in which such redox pairs react with 1-equivalent reductants or oxidants, e.g. $Fe(II)$–$Fe(III)$ or $Ce(III)$–$Ce(IV)$, is of interest. The principle of equivalence change (Schaffer (1)) states that such reactions are generally slow compared with analogous reactions between 1-equivalent reductants

and 1-equivalent oxidants or between 2:2 equivalent systems. The equivalence principle was examined by Halpern with reference to the kinetics of three types of reaction: (i) electron transfer reactions between two metal ions; (ii) oxidation of metal ions by molecular oxygen; and (iii) reduction of metal ions by molecular hydrogen. It was concluded that the principle has only limited applicability to the reactions studied and that other factors are involved in determining the kinetics, viz. formation of intermediate complexes between the oxidant and reductant, participation of chain reactions. Some reactions are complicated in that they proceed by simultaneous bimolecular and termolecular paths, the latter being favored by lower activation energies.

A general theoretical paper by R. A. Marcus (Brooklyn Polytechnic Institute) "On the Theory of Electrochemical and Chemical Electron Transfer Processes" brought together some of the problems common to the fields of homogeneous and heterogeneous charge transfer reactions. The solvent configuration about the reacting ions was considered gradually to change during the reaction to a configuration characteristic of the final state of the reaction; at the same time the electronic configuration was regarded as undergoing a corresponding change, following the molecular redistribution adiabatically. This view was disputed by K. J. Laidler, who regarded the electron tunneling as fast and preceding the molecular rearrangement of the solvent. The role of image forces in heterogeneous reactions was given some qualitative examination in the light of recent calculations of Sachs and Dexter (2). It must be pointed out, however, that a problem of some magnitude still exists. Thus in electrode processes and in ionic adsorption, it appears that the effect of the image potential is surprisingly small; thus the absence of any significant specific adsorption of NaF and of simple cations at the electrocapillary maximum of Hg is unexpected. In the double layer the water molecules in the first coordination sphere about the ions will have a low dielectric constant (cf. (6); see (3), and K. J. Laidler, this symposium), so that the image potential might be expected to be not less than three or four kilocalories. It was pointed out by R. A. Marcus that the attraction of the ions to the interface may lower the entropy of solvation of the ions. However, this would not be in the direction which would cancel the effect of the electrostatic image interaction. It appears that this matter requires some further examination.

Proton Transfer Reactions

In recent years, considerable interest has been shown in the mechanism of proton transport in solutions and in hydrogen bonded solids. Two papers concerning this topic were presented: one on the "Limiting Conductance of Lyonium and Lyate Ions" by M. Kilpatrick (Illinois Institute of Technology) and the second on "Some Considerations on the Role of Proton Tunneling in Certain Charge Transfer Processes" by B. E. Conway (University of Ottawa). M. Kilpatrick presented data for the ratio of equivalent conductances of HCl–DCl mixtures to that of KCl in H_2O–D_2O solutions and also for the ratio of conductance of $HClO_4$–$KClO_4$ and HCl–KCl in H_2O–H_2O_2 and H_2O–CH_3OH mixtures, respectively. In H_2O–H_2O_2 solutions the anomalous proton conductance is partially eliminated; in H_2O–D_2O mixtures it is diminished at intermediate concentrations of D_2O. Preferential solvation effects are important in determining the anomalous proton conductance in solutions of acids in mixed solvents. The conductance behavior of a number of interesting non-aqueous systems was discussed.

The conductance of solid D_2O had been measured under conditions of rigorous purification by B. E. Conway in order to obtain an estimate of the isotopic ratio of equivalent conductance of H^+/D^+ in their respective pure ices. A value of about 1.6 was obtained for this ratio. The proton tunneling theory previously given (4) was re-examined using

a quantal energy distribution and it was shown that an isotopic ratio of conductance of H^+ to that of D^+ in H_2O and D_2O ices, respectively, of 1.1 could be derived and a better value of the absolute mobility of H^+ in H_2O ice obtained. Classically, an isotopic ratio of conductance in the ices should be about nine.

The electrochemical behavior which would arise if proton tunneling occurred at electrodes was also examined and criteria were proposed for recognition of the effect. At intermediate overpotentials the Tafel equation is still obeyed but has an anomalously high slope which is dependent upon the isotopic mass. High separation factors do not necessarily arise in H^+/D^+ tunneling. Values comparable with those deduced classically (*ca.* 3 to 10) should arise at moderate cathodic overpotentials. It was pointed out that except in ice, the proton tunneling mechanism is not unambiguously demonstrable experimentally yet is theoretically indicated in a number of reactions. R. A. Marcus suggested that this could be because energy levels in initial and final states of the reaction were not available at comparable energies except in the case of proton transfer in ice where the initial and final states of the reaction are identical. J. E. B. Randles (University of Birmingham) pointed out that in the case examined by B. E. Conway for electrodes, some suitable levels should become available as the electrode potential was varied. Similarly, B. E. Conway referred to the *o, p*-hydrogen conversion case as one where the necessary levels should be available yet proton tunneling was not clearly indicated as the mechanism (5) of this reaction.

HETEROGENEOUS PROCESSES

Electrolytic Metal Deposition

Three papers on metal deposition were presented. The first by J. O'M. Bockris and W. Mehl (University of Pennsylvania) was concerned with the determination of the rate-determining step(s) in the electrolytic deposition of silver. A galvanostatic method had been employed in which the overpotential build-up lines at constant current density were interpreted with the aid of kinetic equations deduced for various limiting conditions corresponding to (i) slow ionic transfer of Ag^+ to the metal surface; (ii) comparably slow transfer and surface diffusion of adsorbed ions or atoms; and (iii) slow surface diffusion alone. The results indicated that path (iii) was rate-determining at low current densities whilst (i) was rate determining at high current densities. A useful comparison of expressions used in crystal growth from the vapor phase, with corresponding ones arising in electrolytic metal deposition was presented.

The kind of information which can be deduced from a study of radioisotope exchange reactions between ions and their corresponding metals was examined by C. V. King (New York University). The roles of the exchange current, adsorption of ions, local cell electrolysis and corrosion, and self-diffusion in the metal were discussed. It was shown that, in general, the exchange current cannot unambiguously be measured by the radiotracer method unless conditions are unusually favorable. Some results were presented which demonstrated the importance of internal self-diffusion as a factor to which too little attention had been paid in previous work.
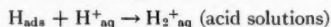
The mechanism of growth of electrolytic metal whiskers was described by D. A. Vermilyea (General Electric Company) in terms of the theory of crystal growth. Incorporation of organic additives into the growing whiskers was likely and poisoning of the non-growing crystal faces was indicated below a certain critical current density, i_c. An estimate of i_c made theoretically was in quite good agreement with that found experimentally for silver whisker formation from $AgNO_3$ solutions.

Some discussion of these papers centered around the question of the nature of the
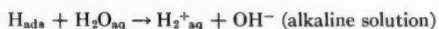
adsorbed entity resulting from the first ionic transfer stage in metal deposition and the mechanism by which a whisker begins its growth from a non-dendritic surface. It is probable that the adsorbed species which undergo surface diffusion across planar crystal faces to growing edges are not completely neutral atoms. Some appreciable ionic character in the bond between the adsorbed species and the bulk metal is probably preserved, e.g. as with H atoms adsorbed at metals where the surface dipole moment is considerable. Ionic transfer directly from the double layer to growing edges or kinks is unlikely as is indicated theoretically (6) on general energetic grounds.

The Hydrogen Evolution Reaction

Three papers were read on various aspects of the cathodic hydrogen evolution reaction. D. J. G. Ives (Birkbeck College, University of London) described some anomalies in the behavior of gold electrodes with respect to rest potentials and kinetics of the hydrogen evolution reaction, when the electrodes had been thermally deactivated at 800° C. The rest potentials were positive and overpotentials increased during polarization. The behavior was similar to that observed with poisoned platinum electrodes. The desorption of adsorbed H as molecule ions through the mechanisms

$$H_{ads} + H^+_{aq} \rightarrow H_2^+_{aq} \text{ (acid solutions)}$$

and

$$H_{ads} + H_2O_{aq} \rightarrow H_2^+_{aq} + OH^- \text{ (alkaline solution)}$$

was considered. It was shown that such processes are energetically not unlikely if it can be assumed that H_2^+ has a heat of hydration of at least -221 kcal mole^{-1}. The molecular dimensions and electron distribution in H_2^+ are not inconsistent with such a solvation energy. The desorption mechanism involving H_2^+ was suggested as a possible explanation for "reduction at a distance" claimed by Kobosew and Nekrassov (7) and again demonstrated by Poltorak (8). It was suggested that H_2 molecule production could occur in the solution by dissociation and recombination of the H atoms with liberation of the protons. Protons from the solution would thus only be involved as "carriers" in this desorption and H_2 production mechanism.

Electrolytic hydrogen production at single and polycrystalline silver electrodes was considered by A. Antoniou and F. E. W. Wetmore (University of Toronto), who reported new experimental data over a range of temperatures for polarization of silver in 1 M H_2SO_{4aq}. Tafel lines having an inflection were observed thus confirming qualitatively the previous work on silver (9); the Tafel slopes were approximately 0.059 (i.e., $2.3RT/F$) and 0.112 (i.e., 2.3 $(2RT/F)$). The apparent heat of activation was 18.8 kcal for low current densities and 14.3 kcal mole^{-1} for higher current densities. The lower slope of 0.059 could be explained in terms of slow surface migration of H atoms to recombination sites or on the basis of a first order H atom recombination step (10). At high current densities $\nu/\beta = 4$ (where ν is the stoichiometric number and β the symmetry factor taken as 0.5) so that a slow H^+ ion discharge reaction is indicated as the rate-determining step. It was pointed out by R. Parsons (University of Bristol) in discussion that a previous explanation (11) of the change of slope in terms of the change of the ψ_1* potential, as the electrode potential passes through the potential of zero charge of the metal, could not explain the magnitude of the change of Tafel slope observed. B. E. Conway emphasized that a similar effect would also be expected at other metals, e.g. Pb, Cu, Ni, where the potential of zero charge is within the range of potentials accessible in cathodic overpotential studies. The fact that inflections in Tafel lines are not observed for these

ψ_1 is the potential of the outer Helmholtz plane.

metals lends support to Parson's comment. Moreover, it is only for silver that the potential of zero charge is positive to the hydrogen reversible potential, i.e. outside the range of cathodic overpotentials examined. The somewhat unique polarization behavior of silver therefore appears to reflect a genuine change of rate-determining mechanism with change of electrode potential (see also (12)).

The nature of the Pd–H system and the mechanism of hydrogen transport through the metal have been problems of interest for some years. Technological interest in these phenomena has arisen on account of the effect of dissolved H on the mechanical properties of certain metals, e.g. iron. S. Schuldiner and J. P. Hoare (U.S. Naval Research Laboratory) reported some interesting experiments on the transport of hydrogen through Pd and Pt bielectrodes and through Pd-clad electrodes in the form of sandwiches with the Pd as the outside metal. Studies were made by measuring the current–potential or potential behavior on both sides of diaphragm electrodes. Transport of hydrogen in an *atom* concentration gradient (i.e. using the β-phase of the Pd–H system) occurs with Pd and Pd-clad Fe only. Under a proton concentration gradient, hydrogen transfer occurs readily through Pd but not through Pt unless this is sandwiched between Pd. Transfer also occurs through sandwiched Fe. No transport of hydrogen either as protons or atoms occurs through Au or Ni. The latter result is surprising and occasioned some discussion, since under other conditions Ni dissolves hydrogen and the time variation of overpotential at Ni in ultrapurified solutions is believed to be due to uptake of H into the metal with consequent change in the electronic properties of the metal.

Other Electrochemical Reduction Processes

Three papers were devoted to heterogeneous reduction reactions other than those involved in the deposition of metals or hydrogen. J. E. B. Randles (University of Birmingham) described methods of calculating kinetic parameters of fairly fast redox reactions, from current potential curves obtained with rotating electrodes or stationary electrodes in stirred solutions or with dropping mercury electrodes. A comparison between the results obtained by means of the steady state current–potential relationship and by a-c. impedance measurements for the V^{2+}/V^{3+} reaction at the dropping mercury electrode was made. Satisfactory agreement between the kinetic parameters obtained by means of the two methods is found if in the interpretation of the current–potential curves due allowance is made for concentration polarization effects. This was achieved in the case of the expanding mercury drop at which the slow V^{++}/V^{+++} electrochemical reaction was occurring, by using Koutecky's analysis of the diffusion problem for this case. A mathematical and numerical analysis was given.

In the case of the reduction of chloraquo–Cr(III) ions at the dropping mercury electrode, P. J. Elving (University of Michigan) and B. Zemel (Shell Development) showed that the polarographic waves for Cr(III) species in various concentrations of perchloric acid, hydrochloric acid, and neutral salts were best interpreted by assuming two concurrent mechanisms for the electron transfer process: (i) the direct transfer of an electron to the Cr(III) ion from the electrode at the interface of the drop and (ii) the transfer of an electron to the Cr(III) ion from a Cr(II) ion produced at the interface. Only in the case of $[CrCl_2(H_2O)_4]^+$ ions in 12 M HCl is the direct electron transfer mechanism dominant.

Some problems in electrochemical reduction and cathodic preparation of certain organic compounds of pharmacological and biochemical interest were discussed by M. J. Allen (C.I.B.A. Pharmaceutical Products) and apparatus used in controlled potential electrolysis was described.

Anodic Electrode Processes

The development of the field of anodic processes has in general lagged behind that of cathodic processes mainly on account of the greater complexity of problems involved. This is due, for example, to the variety of surface oxide species which can be formed anodically on certain metals, the resistance of the surface films, and the time variation of electrode potential during formation of the films and during oxygen evolution on them. Two papers were given on the anodic passivation of iron; in the first paper by Snavely and Hackerman (University of Texas) a study of passivation at iron was made by determining the charge corresponding to the amount of iron dissolved in solution compared with the charge required to reach passivation in an anodic polarization of the iron. The number of coulombs found to be involved in the formation of the passive layer corresponding to a film of Fe_2O_3 15 Å thick if the electrode surface were planar was 0.002 cm^{-2}. A Flade arrest is not observed in anodic decay traces unless a potential of at least 1.2 v (E_H) is reached during the anodic charging. The passive layer is thus probably incomplete below this potential. The charge corresponding to the Flade arrest is equivalent to only about 10% of the passive layer.

The mechanism of formation and the properties of passive films on iron were discussed by M. Cohen (National Research Council). The reactions of water with iron under the following conditions were described: in the absence of oxygen and additives; in the absence of oxygen but in the presence of additives (oxidizing anions, e.g. nitrite, chromate, tungstate, molybdate); in the presence of oxygen; in the presence of oxygen plus oxidizing ions; and in the presence of oxygen and non-oxidizing buffering ions. Film-stripping techniques have shown that the films are mainly anhydrous ferric oxides. The thickness and chemical nature of the films formed under various conditions were reported.

L. Young (British Columbia Research Council) considered the growth of anodic oxide films, mainly from a theoretical standpoint; a number of models were considered for the formation and growth of oxide films. The roles of movement by metal ions, by oxygen, by lattice vacancies or interstitial ions, and the creation of defects by the applied field were examined.

Electrochemical processes at the nickel – nickel oxide electrode were examined by B. E. Conway and P. Bourgault (University of Ottawa) particularly with respect to the mechanism of the self-discharge and oxygen evolution which occurs on open circuit after charging the electrode. The open-circuit decay occurs by mixed anodic and cathodic processes, the rates of which are limited by the rate of evolution of oxygen at anodic sites. The potential on open circuit is determined by the quasi-equilibrium between the reduced and oxidized forms of the nickel oxide present at a given potential, the rate constants of the redox reactions between these species being large compared with that of the oxygen evolution process. Rates of self-discharge were determined as a function of KOH and H_2O activity and it was shown that two consecutive processes were involved in the decay, one having a Tafel slope of 2.3 $\frac{2}{3}(RT/F)$ and the other 2.3 $\frac{2}{5}(RT/F)$ (or 2.3 $\frac{1}{3}(RT/F)$). The rate of the process which was more dependent upon potential was also more dependent on KOH activity. The rates of both processes were increased by increasing KOH activity but decreased by increasing H_2O activity thus confirming the rate-controlling process as the oxygen evolution reaction. Mechanisms of anodic oxygen evolution which could explain the experimental results were proposed. In discussion of these papers, R. Parsons pointed out that under the limiting conditions for which rate laws for complex anodic processes have been previously calculated by the Christiansen method (13), this method was not in fact always necessary, since the same results could be obtained by

use of a simpler direct procedure using "quasi-equilibrium" steady-state concentrations of reacting intermediates for steps prior to the rate-determining step in a series of consecutive reactions.

Adsorption at Electrode Interfaces and the Double Layer

The last six papers of the symposium were concerned with the properties of the double layer and with adsorption in relation to electrode processes. In a paper by A. Frumkin *et al.* (Academy of Sciences, Moscow) some interesting effects of specifically adsorbed anions on the rate of electroreduction of $S_2O_8^{-2}$ ions at the negatively charged mercury electrode were reported. At a given potential and for a given cation the rate of reduction is increased in the order $Cl^- < Br^- < I^-$. The acceleration of the electroreduction, e.g. by I^-, depends on the nature of the cation, increasing in the sequence $Na^+ < K^+ < Cs^+$. It is concluded that the ψ_1 potential which determines, in part, the kinetics of the reaction is a fluctuating one influenced locally by the proximity of cations and anions, and is not the usually considered average ψ_1 potential in the double layer. In this way the specific effect of cations can be explained. The adsorption of anions at the negatively charged mercury electrode depends to a considerable extent on the formation of cationic "bridges".

Some general considerations on the correlation between the double-layer structure and electrode kinetics were presented by M. Breiter and P. Delahay (Louisiana State University). Experimental results on the reduction of IO_3^-, CH_3NO_2, and discharge of $[Cd(CN)_4]^{2-}$ were considered in terms of the double-layer structure and specific adsorption at the electrode. R. S. Hansen (Iowa State College) described some results on the frequency dependence of the double-layer capacity at mercury and deduced relaxation times, τ, for the water in the double layer as low as 10^{-2} seconds. Since this was very much higher than τ values for H_2O bound in ice (10^{-6} seconds) it was felt that the results and their interpretation might require further examination. R. Parsons presented a rigorous thermodynamic analysis for calculation of heats and entropies of adsorption of ionic species from electrocapillary data obtained at various temperatures, and showed results for adsorption of KI at mercury. E. Blomgren and J. O'M. Bockris (University of Pennsylvania) described electrocapillary data obtained for adsorption of HCl and aromatic amine hydrochlorides at mercury and deduced the components of charge in the double layer as a function of electrode potential. J. M. Los and C. K. Tompkins (University of New Brunswick) reported results obtained for the adsorption of methylene blue on mercury, determined by allowing many drops of mercury to come into equilibrium with the solution, and then to fall off into a common pool in a separate vessel, the solution in which was subsequently analyzed. The adsorption followed a Langmuir type of isotherm. B. E. Conway and R. G. Barradas in discussion reported some determinations of adsorption of organic ions and molecules at *solid* metal electrodes of Cu, Ni, and Ag using a direct spectrophotometric method. Isosteric heats of adsorption had been derived for acridine in aqueous solution at copper.

REFERENCES

1. Shaffer, P. A.   J. Am. Chem. Soc. **55**, 2169 (1933). J. Phys. Chem. **40**, 1021 (1936).
2. Sachs, R. G. and Dexter, D. L.   J. Appl. Phys. **21**, 1304 (1950).
3. Webb, J. C.   J. Am. Chem. Soc. **48**, 2589 (1926).
4. Conway, B. E., Bockris, J. O'M., and Linton, H.   J. Chem. Phys. **24**, 834 (1956).
5. Bell, R. P.   Proc. Roy. Soc. (London), A, **139**, 466 (1933).
6. Conway, B. E. and Bockris, J. O'M.   Proc. Roy. Soc. (London) (In press).
7. Kobosew, N. V. and Nekrassov, N. I.   Z. Elektrochem. **36**, 529 (1930).
8. Poltorak, O. M.   Zhur. Fiz. Khim. **27**, 599 (1953).
9. Bockris, J. O'M. and Conway, B. E.   Trans. Faraday Soc. **48**, 724 (1952).
10. Laidler, K. J.   J. Phys. & Colloid Chem. **53**, 712 (1949).
11. Bockris, J. O'M., Ammar, I. A., and Huq, A. K.   J. Phys. Chem. **61**, 879 (1957).
12. Conway, B. E. and Bourgault, P. L.   Can. J. Chem. **37** (1959) (This issue).
13. Bockris, J. O'M.   J. Chem. Phys. **24**, 817 (1956).

BRIDGING AND NON-BRIDGING LIGAND EFFECTS IN REDOX
REACTIONS OF METAL IONS[1]

HENRY TAUBE

In this paper we shall be concerned with a description of the processes which are involved in the transfer of an electron from one metal ion center to another in solution, emphasizing in the description the changes in the first co-ordination spheres. Two distinct types of activated complexes have been characterized for these reactions, which throughout this article will be called the "outer sphere" activated complex and the "bridged" activated complex. In the outer sphere activated complex, the number and identity of the groups comprising the first co-ordination sphere remains unaltered on electron transfer; in the bridged activated complex, a common group is shared by the metal ions, so that a change in the first co-ordination sphere of at least one of the partners accompanies the formation of the activated complex. Other types of activated complexes have been suggested for redox reactions of metal ions, but for none of the others has as direct a demonstration of the characteristic features been possible as for the two which have been described above. This remark applies also to the hydrogen atom transfer formulation (1, 2, 3) (or its variations) according to which it is proposed that the redox process is brought about by the transfer of a hydrogen atom from the first co-ordination sphere of a hydrated reducing cation to that of the oxidizing cation. Although such a mechanism may apply in some cases, there is no proof that it operates in the systems for which it has been proposed.

A property of the ions in the system undergoing reaction which is significant in determining the reaction mechanism, and in permitting classification of the reaction type, is the ease with which they undergo substitution. Only when certain conditions are fulfilled with respect to the substitution lability of the redox partners has it been possible to draw fairly definite conclusions as to the nature of the activated complexes. The majority of the systems do not meet the rather special requirements which the substitution labilities compared to rates of electron transfer must fulfill, and for them the evidence as to mechanism type thus far advanced remains indirect.

The differences in the activated complexes recognized by the classification which has been made are not trivial. It is obvious that for the outer sphere types, the readjustments which accompany electron transfer may take place largely in the solvent and in the ion atmospheres. Such effects exist outside the first co-ordination sphere also for bridged activated complexes, although in certain cases they may be much reduced in intensity, but in addition, important chemistry in the first co-ordination spheres must be recognized as taking place. For reactions involving activated complexes which differ so markedly in structure as the two outlined, it is difficult at the present stage of development to propose a single simple theory of reaction rates which embraces both. Rather, it appears essential first to delineate experimentally each type of mechanism, and to try to assess the importance of the factors that affect the rate by each kind of reaction path. In this area as in others concerned with reaction mechanisms, it is in general not a question of either/ or, and contributions to the over-all rate by rival paths must in general be acknowledged.

The emphasis which is placed on the bridged activated complex in this paper in no sense implies that this kind of mechanism is considered more important—in fact, the development of the subject will show that definite proof of the operation of the mechanism involving bridged activated complexes is restricted thus far to only a small number of different central cations. However, the mechanisms involving the bridged activated complex have associated with them interesting chemistry in large variety, and are worthy of consideration for their own sake, so that no apology for the present lack of generality is due. Further, it is likely that the most fruitful way to attack the systems which do not readily lend themselves to direct tests of mechanism will be from ground thoroughly prepared by understanding systems of known mechanisms.

A brief outline of observations and problems in the field of mechanisms involving outer sphere activated complexes is offered, and following this, a more detailed discussion of the bridged activated complex.

THE OUTER SPHERE ACTIVATED COMPLEX

In many redox reactions, reactant and product complex ions are substitution inert, or at least submit to substitution much less rapidly than to electron transfer. If in addition the species concerned are co-ordinatively saturated, it can reasonably be supposed that there is no interpenetration of the co-ordination spheres on electron transfer. The conclusion that an outer sphere activated complex operates for such systems is for the most part based on evidence no more direct than that outlined, yet some of the systems in question are so extremely inert to substitution that there is little doubt that an outer sphere activated complex is all that is accessible to the systems. Thus redox reactions or exchange reactions involving only species drawn from among the following and their like: $Fe(CN)_6^{-3,-4}$, $IrCl_6^{-2,-3}$, $Mo(CN)_8^{-3,-4}$, $Fe(dip)_3^{+3,+2}$, $Os(o\text{-phen})_3^{+3,+2}$, $MnO_4^{-1,-2}$ almost certainly take place without interpenetration of, or dislocations in, the first co-ordination spheres of the reactant ions. Substitution in the first co-ordination spheres of these ions is slow (for the manganese oxy-ions, this is true only in alkaline solution), and it is doubtful that any useful labilization of the ligands takes place on close approach of the reactants (this is particularly true when the products resulting on electron transfer are also substitution inert). For the $MnO_4^- - MnO_4^=$ electron exchange reaction, which is the one which has been most thoroughly studied (4), it is known that the co-ordination spheres are not disrupted on electron transfer. This follows from Symons' observation (5) that the reduction of MnO_4^- to $MnO_4^=$ in alkaline solution takes place preserving the oxygen-isotopic composition of the complex ions.

It is a feature of all the systems mentioned above that not only is the co-ordination sphere not reorganized on electron transfer, but in fact there is little change in the dimensions of the molecules when the indicated change in electronic charge takes place. For these systems, electron exchange takes place rapidly (specific rates at 25° of the order of 10^{-3} mole^{-1} sec^{-1} and higher) (6). Whether the conditions that the geometry remains unchanged when electron transfer takes place is sufficient to ensure that the process be rapid is not at all certain, however. The ions referred to are also of such nature that the d electrons are probably not localized on the central metal ions, and for them, Marcus's (7) assumption that they be considered conducting spheres may well be justified. However, for a pair of fully ammonated ions, which then present a shell of protons on their exterior and which satisfy the geometric requirements, the rates may well be slower by several powers of 10. Such a system may be hard to find, for the property of the ligands which brings d electrons to the exterior of the complex ion is also the property that ensures that little change in dimensions takes place on electron transfer.

It is by no means a necessary condition for the operation of the outer sphere mechanism that there be little change in dimensions of the ions, for if the ligands are chosen to be unfavorable to the formation of the bridged activated complex, electron transfer through the intact co-ordination spheres may still be the easier route to products. Thus the electron exchange between $Co(en)_3^{++}$ and $Co(en)_3^{+++}$ (8) presumably must occur by the outer sphere mechanism, for although $Co(en)_3^{++}$ is substitution labile, $Co(en)_3^{+++}$ is not, and the groups on the co-ordinated nitrogens prevent the formation of a bridged activated complex. The $Co(en)_3^{++}$–$Co(en)_3^{+++}$ reaction is much slower ($k \sim 10^{-3}$ mole^{-1} sec^{-1} at 25°) than the others of this class mentioned above. This is a result in part at least of the cost in energy for making the substantial change in the dimensions of the ions prior to electron transfer, which is necessary to bring about the matching of the energy of the electron at the two sites. As already mentioned, the difference in specific properties of en as compared to o-phen, for example, may also be a factor but it is impossible at the present time to evaluate its importance.

Some of the features of interest in the reactions which proceed by outer sphere activated complexes have been referred to already, as for example, the influence on the rates of the geometrical requirements and the properties of the ligands. Of interest also are the dielectric properties of the reaction medium, which are dealt with in Marcus's theory (9), and salt effects, which are delineated partially in the experiments by Sheppard and Wahl (4). An important problem which remains to be settled is the average separation of the ions in the activated complexes for electron transfer: the experimental solution of this problem is by no means obvious.

THE BRIDGED ACTIVATED COMPLEX

Introduction

For a system in which the oxidizing agent is substitution inert, the reducing agent is labile to substitution, but the product formed on its oxidation is inert to substitution, a direct demonstration of a bridged structure for the activated complex can be made by simple analysis of reaction products. The significance of the conditions imposed on the substitution properties is most easily developed by using a specific example. The reaction of $(NH_3)_5CoCl^{++}$ with Cr^{++} has been found to take place forming as product not $Cr(H_2O)_6^{+++}$ but $CrCl^{++}$ (9) (in addition to Co^{++} and NH_4^+ as other products). Cr^{+++} is very slow to undergo substitution, thus $CrCl^{++}$ can not have been formed from Cr^{+++} and Cl^-. This conclusion is reinforced by repeating the experiment in the presence of radioactive Cl^-; it is found that substantially no radioactivity gets into the $CrCl^{++}$ (10). The formation of $CrCl^{++}$ proves a Cr–Cl bond in the activated complex; the property of the oxidizing agent $Co(NH_3)_5Cl^{++}$ as being substitution inert ensures that a Co–Cl bond is maintained, and the property of Cr^{++}_{aq} as being substitution labile provides for the formation of the bridged structure.

Most of the work in this field has been done with Co(III) complexes as oxidizing agents and Cr^{++}_{aq} as reducing agent. Cr^{++}_{aq} appears to be unique among the pure aquo-ions under ordinary conditions in having the combination of properties required to establish the operation of the bridged activated complex. If interest is not restricted to pure aquo-ions, Co(II) can also be mentioned as a reducing agent which can be similarly exploited. In the presence of NH_3 and numerous other ligands, Co(II), although itself labile to substitution, becomes substitution inert on oxidation. As oxidizing agents that lend themselves to the type of experiment outlined, we have a wider choice, including most Co(III) complexes, Cr(III) complexes, Pt(IV) complexes (though here a complication enters because the stable product is 2 e^- removed), Ir(IV) complexes, Ru(IV)

complexes, and some complexes of Fe(III). It is possible that at lower temperatures, such as become accessible when CH_3OH is solvent, many more oxidizing agents and reducing agents will show the necessary relation of rates of substitution to rate of electron transfer to make a direct test of mechanism possible for them. Before these general remarks are concluded, attention should be drawn explicitly to the remarkable feature of inorganic cations that a change in oxidation number by one unit can cause enormous changes in substitution lability. Thus, the replacement of water in $Cr(H_2O)_6^{+++}$ by solvent water takes place at $25°$ with a half time of the order of 30 hours. The similar exchange for Cr^{++}_{aq} is so rapid that it has not been measured and $t_{\frac{1}{2}}$ is likely of the order of 10^{-5} seconds. To add interest to the situation, Cr(IV) is again probably very labile to substitution (12, 13).

For the remainder of this section, experimental results on features of the bridged activated complex will be presented, and any discussion of the implications of these observations for other systems will be deferred.

Variety of Bridging Groups

Complexes of the type $(NH_3)_5Co^{III}L$ can be prepared with a great variety of ligands L. Experiments using oxidizing agents of this class and Cr^{++} as reducing agent have demonstrated group transfer from Co to Cr for L = F^-, Cl^-, Br^-, I^-, CNS^-, N_3^-, $SO_4^=$, $PO_4^=$, $P_2O_7^=$, and a variety of carboxylic acids, results for which will be discussed in some detail in the next subsection. Of special interest are experiments on the transfer of H_2O and OH^-, as relating to redox reactions of aquo-cations. A definitive result has been obtained for L = OH^-, showing that transfer is complete for this ion; the experiments with L = H_2O are inconclusive but some transfer at least by this path is indicated (14). With L = NO_3^-, net transfer to chromium is not observed. Many of the ligands mentioned have also been shown to transfer when Cr(III) complexes act as oxidizing agents (15).

Relative Rates for Various Bridging Groups

A rate comparison which has an obvious qualitative interpretation is that for the reactions of Cr^{++} with $Co(NH_3)_6^{+++}$ and with $Co(NH_3)_5OH_2^{+++}$, the reaction with the aquo-ion is more rapid by a factor of at least one hundred. The significant difference between the two oxidizing agents is that only with the aquo-ion is a pair of electrons exposed to make a bridged complex readily accessible. The totally ammonated complex may in fact react by making use of an outer sphere activated complex.

Other rate comparisons which will be offered are somewhat more subtle. Thus it is not obvious what progression in rates should be observed for the series of halo complexes. Kinetic experiments on reactions of the two types

$$(NH_3)_5Cr\,X^{++} + Cr^{++} + 5H^+ = Cr^{++} + 5NH_4 + Cr^{++}$$

and

$$(H_2O)_5Cr^*\,X^{++} + Cr^{++} = Cr^{*+++} + (H_2O)_5Cr\,X^{++}$$
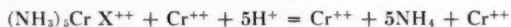
agree that rates increase progressively from X = F^- to X = I^-. It should be noted that in each class of reaction, the rates are first order in chromic complex, first order in chromic ion, and independent of (H^+). The data for these reactions and other similar ones are summarized in Table I.

A comparison of special interest displayed in this table is that of the rate of reaction of Cr^{++} with CrN_3^{++} and $CrNCS^{++}$. Ball and King (15) make the point that attack by Cr^{++} at the atom bearing the Cr^{+++} is impossible for steric reasons, and that attack

TABLE I

The rates of reaction of Cr^{++} with various $Cr(III)$ complexes

Oxidant	k, mole^{-1} sec^{-1}	Temp.	$\Delta H^{\ddagger}$	$\Delta S^{\ddagger}$	Ref.
CrF^{++}	2.6×10^{-2}	27	13.7	-20	15
$CrCl^{++}$	$8.3 \pm 2, 9.1 \pm 1$	0	—	—	16, 15
$CrBr^{++}$	> 60	0	—	—	15
$CrNCS^{++}$	1.8×10^{-4}	27	—	—	15
CrN_3^{++}	>1.2	0	—	—	15
$(NH_3)_5CrF^{++}$	2.7×10^{-4}	25	13.4	-30	17
$(NH_3)_5CrCl^{++}$	5.1×10^{-2}	25	11.1	-23	17
$(NH_3)_5CrBr^{++}$	3.2×10^{-1}	25	8.5	-33	17
$(NH_3)_5CrI^{++}$	5.5 ± 1.5	25	—	—	17
$t\text{-}CrCl_2^+$	$\sim 2 \times 10^3$	25	—	—	10

takes place at the remote end of the ligand. The slower rate for NCS^- compared to N_3^- can be attributed to this, that remote attack by Cr^{++} on NCS^- forms products different from the reactants, and in a less stable form, so that the energy requirements of the over-all process must be added to the pure kinetic requirements in determining the rate.

The results of experiments done by Sebera and Taube (18) on carboxylic acids as electron mediators are summarized in Table II. These experiments are still in progress, and a large number of experiments of obvious interest still remain to be done.

TABLE II

Carboxylic acids as electron mediators in the reaction of $(NH_3)_5Co^{III} L$ with Cr^{++} ($\mu = 1.00, 25°$ C)

L	k, mole^{-1} sec^{-1}	$\Delta H^{\ddagger}$	$\Delta S^{\ddagger}$	Ref.
$CH_3CO_2^-$	0.15			19
$CH_3(CH_2)_2CO_2^-$	0.08			19
$CH_3CH{=}CHCO_2^-$	0.18			19
$HO_2CCH_2CH_2CO_2^-$	0.19	3.0	-50	18
$^-O_2CCH_2CH_2CO_2^-$	1			18
Trans-				
$HO_2CCH{=}CHCO_2^-$	1.13	7.5	-33	18
$Cis\text{-}HO_2CCH{=}CHCO_2^-$	>200			18
o-Phthalic	0.076	5.1	-47	18
m-Phthalic	0.093	2.6	-56	18
p-Phthalic	~ 40			18
Oxalate	>200			19

One comparison of interest is that of the rate for fumaric acid as ligand with that for succinic acid. The latter reacts at a specific rate much like those at which monocarboxylic acids react. Thus for all of this group including succinic acid attack by Cr^{++} at the carboxyl adjacent to the Co(III) is indicated. To explain the higher rate for fumaric acid it is suggested that when it is the bridging group, attack by Cr^{++} takes place at the end remote from the Co(III). This mechanism is possible because fumarate can offer a conjugated system of double bonds for electron transfer. The higher rates come about because the Cr^{++} is not required to approach as closely to the Co(III) center as is the case when succinate is bridging group. An extraordinary result, not included in the table, and consistent with this interpretation is that the rate of electron transfer when fumaric acid is bridging group, is strongly accelerated by acid. The function of the additional proton may be to improve the conjugation between the Co(III) and Cr(II) centers.

By associating with the carbonyl oxygen adjacent to Co(III), it brings about the necessary redistribution of the electrons, as indicated in the formulation below of the activated complex.

$$\left[\begin{array}{c} (H_3N)_5\,Co\,O \quad\quad H \quad\quad\quad O\,Cr \\ \diagdown C-C=C-C \diagup \\ HO \quad\quad H \quad\quad OH \end{array} \right]^{+4}$$
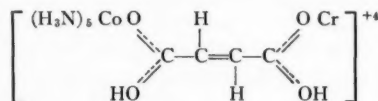
These general conclusions are supported by the observations made with the isomers of phthalic acid. Conjugation is not possible for the ortho or meta acid (but for different reasons) and the rates are slow. For the para isomer conjugation is possible and the rates are very high; furthermore, with this isomer but not the others, acceleration by acid is observed.

The high rate for the maleate complex is not understood by the considerations outlined thus far. The maleate complex reacts more rapidly than does the fumarate complex, although the geometry prevents effective conjugation, and it reacts much more rapidly than the o-phthalic complex which has similar geometry. An hypothesis which is reasonable in the light of these comparisons and which furthermore accommodates the observations that of all the ligands mentioned maleate is the most easily reduced by Cr^{++} is that when maleate is the ligand we are dealing not with electron transfer *through* the ligand, but *to* the ligand. A similar mechanism may operate for oxalate, which is also easily reduced by Cr^{++}. Isotopic fractionation experiments can differentiate the mechanisms proposed on the one hand for fumarate and on the other for maleate, but these have not been done, and they will in fact be rather difficult to do.

The Reaction of $(NH_3)_5CoOH_2^{+++}$ with Cr^{++}

This reaction is especially featured because of its relation to the important class of redox reactions between aquo-ions. It differs from most other reactions of its class in admitting much more incisive tests of mechanism than are usually possible. One of these which provided proof that reaction takes place by transfer of oxygen has already been mentioned.

In common with other redox reactions of aquo-cations which have been studied, the reaction in acidic medium proceeds by two parallel paths differing in the dependence on (H^+). The rate law for this reaction may be represented by the equation:

$$-d(Cr^{++})/dt = k_1(Cr^{++})[(NH_3)_5CoH_2O^{+++}]+k_2'(Cr^{++})[(NH_3)_5CrOH_2^{+++}]/(H^+)$$

The kinetic data on this system, including experiments with D_2O as solvent are shown in Table III (20). It should be noted that the second term on the right of the equation above can be cast in the equivalent form:

$$k_2(Cr^{++})[(NH_3)_5CoOH^{++}],$$

where $k_2 = k_2'/K_D$ and K_D is a dissociation constant of $(NH_3)_5CoOH_2^{+++}$ under the specific experimental conditions (21).

TABLE III

Kinetics of the reaction of Cr^{++} with $(NH_3)_5CoOH_2^{+++}$ (at $\mu = 1.0$, temp. 20° second as unit of time)

Solvent	k_1	k_2'	k_2	E_1	E_2	$\Delta S_1^{\ddagger}$	$\Delta S_2^{\ddagger}$
H_2O	0.50	1.58	1.5×10^6	3.3	4.8	−48	−15
D_2O	0.13	0.40					

Of interest in the kinetic data is the large change in specific rate caused by the loss of the proton from the aquo-ion, and the low values of the activation energies. These points will not be developed further here, but should not be dismissed without mentioning that a case for the existence, not merely of a binuclear activated complex, but of a binuclear intermediate can be based on the low values of E observed here and in other cases as well. Of significance equal to that of the oxygen-tracer experiments are experiments on oxygen-isotope fractionation in the reaction (14). These experiments have shown that $(NH_3)_5CoO^{16}H^{++}$ reacts more rapidly than the ion having O^{18} in the OH group by a factor of 1.03_5. This is a relatively large kinetic oxygen isotope effect, and it shows that the Co–O bond is greatly weakened in the activated complex. Thus the OH$^-$ is not to be regarded merely as a means of binding Co(III) and Cr(II) together, but in fact an important event in the transfer of the electron is the stretching of the Co–OH bond, and presumably the simultaneous shortening of the Cr–OH bond. The question of other bond dislocations in the activated complex will be dealt with in the next subsection.

The measurement of the effect on the rate of electron transfer caused by the change from H_2O to D_2O as solvent has been suggested as a means of distinguishing the "hydrogen atom transfer" mechanism from other mechanisms. The significance of the H_2O–D_2O experiments in the present system is that they test the magnitude of the effect for a reaction which does not involve hydrogen atom transfer, but which by one path at least proceeds by transfer of OH. The remarkable result is that a large H–D isotope effect is found, a decrease in k_1 and k_2' of almost a factor of 4 in changing from H_2O to D_2O as solvent. The effect on k_2' must be factored into the effect on k_2 and K_D. The H_2O–D_2O effect on K_D has been measured as 1.5 (21) (K_D in H_2O compared to K_D in D_2O), thus a healthy kinetic isotope effect in k_2 of 2.6 is still left. The origin of this large isotope effect is in the hydrogen-containing bridging group (the specific rate for the reaction $(NH_3)_5CrCl^{++} + Cr^{++}$ decreases by only a factor of 1.3 in changing to D_2O as solvent). It means presumably that the H–O bond is substantially stretched in the activated complex. Possibly the complex adopts a linear arrangement of Co–O–Cr centers, and the p-electrons of oxygen are used to contribute to the bonding. The two paths for the reaction may be quite similar except that when the aquo-ion reacts, both hydrogens in water are removed in the activated complex, but when the hydroxy complex reacts, one is removed by an equilibrium process preceding the rate-controlling step and one in the activated complex. Rather similar H–D isotope effects are to be expected on this basis, as is observed.

Effects of Non-bridging Ligands

This important subject will be dealt with only briefly, because little in the way of systematic work on this feature of these reactions has been done. The existence of important ligand effects, short of bridging ligand effects is, of course, to be expected and is easily demonstrated. Thus, when the reaction of $(NH_3)_5CoOH_2^{+++}$ with Cr^{++} proceeds in the presence of pyrophosphate ion, it takes place much more rapidly than when pyrophosphate is omitted, and pyrophosphate is incorporated into the chromic product (19). The inertia of the Co(III) complex to substitution ensures that the pyrophosphate does not act as a bridging group, yet it does get into the activated complex, presumably by replacing water molecules on Cr^{++}. That a bridging group is involved is proved by the experiment using $(NH_3)_5CoCl^{++}$ as oxidizing agent. When this is done, both Cl and pyrophosphate are incorporated into the chromic complex.

Groups differ widely also in their capacity to influence rates in non-bridging positions.

Pyrophosphate, $SO_4^=$, and Cl^- decrease in effect in this order; the effect of Cl^- is so small that in 0.1 M solution, its influence on the rate of the reaction of $(NH_3)_5$ to OH_2^{+++} with Cr^{++} is not detected.

The non-bridging ligand effects can conveniently be studied by working with a series of Co(III) complexes containing a common bridging group. Such studies have not been carried far, and only a single problem in this field has been given some attention. Orgel (22) has discussed the reaction of Cr^{++} with Co(III) complexes, and has suggested that the electron gained by Co(III) is accommodated in the d_z^2 orbital. This orbital is made available by removing not only the bridging ligand from the cobalt, but also the group *trans* to it. This interesting suggestion finds support in the observation that *trans* $Co(en)_2Cl_2^+$ is reduced *more* rapidly by V^{++}_{aq} or Fe^{++}_{aq} than is the *cis* form (23). It has been tested by observing the fractionation of nitrogen in NH_3 when *cis*- and *trans*-$NH_3(en)_2CoCl^{++}$ react with Cr^{++}. These experiments have shown (24) that there is no significant N-isotope fractionation either when NH_3 is *cis* or when it is *trans* to the Cl bridging group. This experimental result, if sustained, would show that the principal bond dislocations of the Co(III) center take place at the bridging group and would suggest that the primary product of the reaction is a penta-co-ordinated Co(III) complex which retains the configuration of the parent complex, but which has in place of the bridging group a single electron. The result cannot be considered general even for all Co(III) complexes and the ion $NH_3(dip)_2CoCl^{++}$ might in fact show a strong *trans* effect on electron transfer.

CONCLUSION

Not all aspects of interest in the field of reactions proceeding by the bridged activated complex have been discussed nor even referred to, but perhaps a sufficient number of results were reviewed to indicate the nature of the problems and the nature of the experiments which can be done to elucidate mechanisms. Most of the techniques used unfortunately do not apply to the redox reactions of ions when both partners are substitution labile. However much is written concerning the outer sphere and bridged activated complexes the subject of redox reactions of metal ions remains in an unsatisfactory state when a reaction as much studied as the $Fe^{++}-Fe^{+++}$ electron exchange is not understood nor a reaction as much applied as the $Fe^{++}-Ce(IV)$ reaction. It is to be hoped that experimental techniques will be introduced which will yield conclusions for these systems as direct as some of those possible for specially selected systems. Failing to discover such techniques an indirect attack must be used, to develop thoroughly an understanding of the field in which mechanisms can be established, to develop the experimental observations in the field of the labile systems, and to bring to bear on these observations the principles which have been established for systems of known mechanisms.

An illustration of this kind of approach which will serve better perhaps to expose its limitations than to reveal its capacities is the following: from the fact that Cl^- does not markedly accelerate the reaction of $(NH_3)_5CoOH_2^{+++}$ with Cr^{++}, that $CrCl^{++}$ is not formed in this reaction, and that Cl^- does markedly accelerate the reaction of Fe^{+++} with Cr^{++} forming $CrCl^{++}$, we argue that in the activated complex for the latter process both Fe^{+++} and Cr^{++} make a bond to Cl^- (i.e., the difference in the kinetic behavior of the two systems is understood by invoking the difference in substitution lability of the two oxidizing agents). Thus the reaction of Fe^{+++} with Cr^{++} accelerated by a variety of ligands can be brought into the field of the bridged activated complexes. There is a close similarity (9) of the rates at which Fe^{++} reacts with Fe(III) complexes to the rates at

which Cr^{++} reacts with the same complexes and therefore similar mechanisms are indicated. These considerations thus lead to the conclusion that the Fe^{++}–$Fe(III)$ exchange reactions also proceed by bridged activated complexes. Considerations of this kind are hardly satisfactory however, because they do not expose the contributions of minor, but nevertheless interesting, rival paths, nor is a sufficiently convincing case for the mechanism by the major paths made.

A field for experiment which may improve our understanding of the redox process under discussion is in the reactions of reducing agents having differing electronic structures with a series of substitution-inert complexes. Thus, some interesting conclusions are indicated by results recently obtained (23) using V^{++} as reducing agent when these results are considered in the context of those already obtained with Cr^{++}. A large number of Co(III) complexes show the same order of reactivity with V^{++} as they do with Cr^{++}, but the contrast in rates is much less. The reaction of $(NH_3)_5CoOH_2^{+++}$ is abnormally rapid, however, and shows some unusual salt effects. We believe at present that V^{++} reacts by both kinds of mechanism. When a suitable bridging group is present, the bridged activated complex is still formed. But when the aquo-ion or the hexammino-ion is used the outer sphere activated complex predominates as providing the reaction path. The differences in V^{++} and Cr^{++} are to be understood as resulting from the differences in electronic structure, V^{++} having only the three lower lying d-orbitals populated but Cr^{++} having one electron more. Eu^{++} will also be of interest in these studies as will Fe^{++} (its reactivity can be enormously increased by suitable complexing).

Another area which promises to be fruitful is the reduction of Co(III) and, if possible, Cr(III) complexes by reaction through outer sphere activated complexes. This can be done by using $Cr(dip)_3^{++}$ or $V(dip)_3^{++}$ as reducing agent. The reaction of $Co(NH_3)_6^{+++}$ with $Cr(dip)_3^{++}$ in fact proceeds so rapidly that we (23) have not succeeded in measuring its rate, in marked contrast to the slow rate when Cr^{++}_{aq} is used. Rate comparison for the same series of Co(III) complex being reduced by both mechanisms should prove to be very instructive, and instructive also in comparison with rates of reduction of the same complexes at electrodes.

REFERENCES

1. DODSON, R. W. and DAVIDSON, N.   J. Phys. Chem. **56**, 866 (1952).
2. HUDIS, J. and DODSON, R. W.   J. Am. Chem. Soc. **78**, 911 (1956).
3. REYNOLDS, W. L. and LUMRY, R. W.   J. Chem. Phys. **23**, 2460 (1955).
4. SHEPPARD, J. C. and WAHL, A. C.   J. Am. Chem. Soc. **79**, 1020 (1957).
5. SYMONS, M. C. R.   J. Chem. Soc. 3676 (1954).
6. WAHL, A. C. and DECK, C. D.   J. Am. Chem. Soc. **76**, 4054 (1954). EICHLER, B. and WAHL, A. C.   J. Am. Chem. Soc. **80**, 4145 (1958). GEORGE, P. and IRVINE, D. H.   J. Chem. Soc. 587 (1954).
7. MARCUS, R. A.   J. Chem. Phys. **24**, 966 (1956).
8. LEWIS, W. B., CORYELL, C. D., and IRVINE, J.   J. Chem. Soc. Suppl. Issue, **2**, S386 (1949).
9. TAUBE, H., MYERS, H., and RICH, R. L.   J. Am. Chem. Soc. **75**, 4118 (1953).
10. TAUBE, H. and MYERS, H.   J. Am. Chem. Soc. **76**, 2103 (1954).
11. HUNT, J. P. and TAUBE, H.   J. Chem. Phys. **19**, 602 (1951).
12. TAUBE, H.   Chem. Revs. **50**, 69 (1952).
13. OGARD, A. E. and TAUBE, H.   J. Phys. Chem. **62**, 357 (1958).
14. MURMANN, R. K., TAUBE, H., and POSEY, F. A.   J. Am. Chem. Soc. **79**, 262 (1957).
15. BALL, D. L. and KING, E. L.   J. Am. Chem. Soc. **80**, 1091 (1958).
16. TAUBE, H. and KING, B. L.   J. Am. Chem. Soc. **76**, 4053 (1954).
17. OGARD, A. E. and TAUBE, H.   J. Am. Chem. Soc. **80**, 1084 (1958).
18. SEBERA, D. R. and TAUBE, H.   To be published.
19. TAUBE, H.   J. Am. Chem. Soc. **77**, 4481 (1955).
20. ZWICKEL, A. and TAUBE, H.   To be published.
21. BEARCROFT, D. J. and TAUBE, H.   To be published.
22. ORGEL, L. E.   Inst. intern. chim. Solvay, Xe Conseil chim. 289 (1956).
23. ZWICKEL, A. and TAUBE, H.   Unpublished observations.
24. SCHUG, K. and TAUBE, H.   These results should be regarded as tentative. The experiments reported are of good quality but further checking is necessary before the result is published.

SOME THEORETICAL ASPECTS OF ELECTRON-TRANSFER
PROCESSES IN AQUEOUS SOLUTION[1]

Keith J. Laidler

ABSTRACT

A theoretical treatment has been developed for the rates of electron-transfer reactions in aqueous solution, with particular reference to the ferric–ferrous system. The reactions are considered to be diffusion-controlled processes, the approach of the ions being hindered by the electrostatic repulsion between them. Calculations have been made of the free energy of the diffusion process and for the repulsion, account being taken of the variation in dielectric constant with the electric field. The form of the potential-energy barrier between the ions is calculated for various separations, and the transmission coefficient calculated using the quantum-mechanical expression corresponding to a rectangular barrier. The total free energy of activation for the reaction, which is the sum of the contributions due to diffusion, repulsion, and tunnelling, is found to pass through a minimum at a separation of about 4 Å. The calculated free energy of activation for the reaction is 15.4 kcal, in good agreement with the experimental value of 16.8 kcal. The energy and entropy of activation for the reaction are also briefly discussed.

INTRODUCTION

During the past few years a considerable number of kinetic studies have been concerned with electron-transfer processes between ions in different valency states. A well-known process of this type is that between ferric and ferrous ions in aqueous solution,

$$Fe^{++} + Fe^{+++} \rightarrow Fe^{+++} + Fe^{++}.$$

Although many complexities exist, the evidence indicates that in some cases these reactions occur by a simple transfer of an electron from one ion to another. This is possibly true of the ferric–ferrous reaction, and Silverman and Dodson (1) have determined values of 9.9 kcal and -25 e.u. for the energy and entropy of activation of the process.

This paper is concerned with the theory of simple electron-transfer reactions, and for the most part deals quantitatively with the factors influencing the rate of the Fe^{++}–Fe^{+++} reaction. Several previous theoretical discussions of these reactions have been presented, notably by Libby (2), Weiss (3), Eyring and co-workers (4, 5), and by Marcus (6e). In the case of the latter two treatments, an attempt was made to calculate the free energies of activation (ΔF^*) of a number of reactions, including the Fe^{++}–Fe^{+++} one. The quantitative agreement with experiment was not, however, completely satisfactory. The experimental ΔF^* for the Fe^{++}–Fe^{+++} system is 16.8 kcal at 25° C: Eyring et al. obtain agreement only by arbitrarily adding a term of 8.1 kcal, while Marcus (6a) calculated a value of 9.8 kcal.* It has appeared to the present writer that this lack of good agreement could be attributed to failure to take into consideration certain important factors which must influence the rate. In particular it would seem that neither Eyring nor Marcus treated in sufficient detail the collisions (or, more correctly, *encounters*) between the reacting ions.

In the present work an attempt has been made to bring about some improvement, particularly with respect to the two points noted above. If in the present paper a somewhat critical view appears to have been taken of the preceding theoretical treatments

this has been done entirely to clarify the main points, and not to deprecate the earlier work which contains many valuable features and upon which the present work relies very heavily.

THE FREQUENCY OF IONIC ENCOUNTERS

In what follows it will be concluded, on the basis of the experimental evidence, that there does occur a direct transfer of an electron from the ferric to the ferrous ion. The electron-transfer process will be seen later to occur by quantum-mechanical tunnelling, and is much more probable when the ions are close together. The very close approach of the ions is obviously rendered unlikely by the electrostatic repulsions. A compromise is therefore struck, the most likely transfers occurring (as will be seen) when the ions are about 4 Å apart.

In the treatment of Eyring *et al.* (4) the rate of encounter has been taken as equal to the term kT/h multiplied by the factor $\exp(-\Delta F^*_{rep}/RT)$, where ΔF^*_{rep} is the free energy of repulsion between the two ions. This, however, cannot be correct, since it does not take proper account of the variation in the frequency of encounter with the separation of the ions, σ, in the activated state. The distance σ does appear in the ΔF^*_{rep} term, but it should also appear in the pre-exponential term; quite apart from electrostatic effects an encounter with a large σ is intrinsically more probable than one with a small σ, and intuitively one would expect the pre-exponential term to be proportional to σ.

A more satisfactory treatment of the frequency with which the ions come within a distance of σ of one another is provided by the theory of diffusion-controlled reactions, a theory that has been developed to explain the coagulation of colloids (7, 8), the rates of quenching of fluorescence in solution (9), and more recently the rates of certain enzyme-catalyzed reactions (10). The theory is briefly as follows. According to Smoluchowski (7), in the absence of electrostatic interactions the frequency of approach of two molecules to within a distance of σ cm is given by

$$[1] \qquad Z = 2\pi(D_1+D_2)n_1n_2\sigma,$$

where n_1 and n_2 are the numbers of the two types of molecules in unit volume and D_1 and D_2 are the diffusion constants. Bradley (11), however, argues that Smoluchowski's equation is too large by a factor of 12, and instead proposes

$$[2] \qquad Z = \tfrac{1}{6}\pi(D_1+D_2)n_1n_2\sigma.$$

This expression is equivalent to the following expression for the rate constant:

$$[3] \qquad k = \tfrac{1}{6}(\pi N/1000)D_{12}\sigma \text{ liter mole}^{-1}\text{ sec}^{-1},$$

where $D_{12} = D_1+D_2$. The above equations are arrived at by integration of the appropriate differential equations for diffusion.

When the reacting species are ions the electrostatic interactions have to be taken into account in the setting up of the differential equations. This has been done by Debye (9), who found that the reaction rate in the case of a free energy of repulsion equal to ΔF^{**}_{rep} must now be divided by the integral

$$[4] \qquad 1/f = \sigma \int_{\sigma}^{\infty} \Delta F^{**}_{rep}/kT \, \frac{dr}{r^2}.$$

The repulsive free energy is given for the case of constant dielectric constant ϵ by

[5] $\Delta F^{**}{}_{\text{rep}} = z_1 z_2 e^2 / \epsilon k T r,$

where e is the electronic charge and z_1 and z_2 the valencies of the ions. When ϵ is independent of σ the reciprocal of the integral becomes

[6] $f = (z_1 z_2 e^2 / \epsilon k T \sigma)(e^{z_1 z_2 e^2 / \epsilon k T \sigma} - 1)^{-1}.$

When z_1 and z_2 are of the same sign, as for the reactions under consideration, the exponential term is always much larger than unity, so that

[7] $f = (z_1 z_2 e^2 / \epsilon k T \sigma)\, e^{-z_1 z_2 e^2 / \epsilon k T \sigma}$

[8]   = $(\Delta F^{**}{}_{\text{rep}} / k T)\, e^{-\Delta F^{**}{}_{\text{rep}} / k T}.$

The expression for the rate constant for the encounter is therefore

[9] $k_{\text{enc}} = \tfrac{1}{6}(\pi N / 1000)\, D_{12} \sigma\, (\Delta F^{**}{}_{\text{rep}} / k T)\, e^{-\Delta F^{**}{}_{\text{rep}} / k T}$

with $\Delta F^{**}{}_{\text{rep}}$ given by eq. [5].

Since the experimental results are usually quoted in terms of a conventional free energy of activation, defined by

[10] $k = (\mathbf{k} T / h)\, e^{-\Delta F^{*}{}_{\text{exp}} / R T},$

it is convenient to express k_{enc} in the same form, namely as

[11] $k_{\text{enc}} = (\mathbf{k} T / h)\, e^{-\Delta F^{*}{}_{\text{diff}} / R T}\, e^{-\Delta F^{*}{}_{\text{rep}} / R T},$

where $\Delta F^{*}{}_{\text{diff}}$ relates to the diffusion process only and $\Delta F^{*}{}_{\text{rep}}$ to the repulsive term f. The term $\Delta F^{*}{}_{\text{diff}}$ depends slightly upon the value taken for D_{12}. There is not a large variation in the diffusion constants for ions, and a value of 1.2×10^5 cm^2 sec^{-1} has been taken as typical of the diffusion constant of ions such as Fe^{++} and Fe^{+++}. With $D = 2.4 \times 10^5$ it is then readily calculated that at a temperature of 25.0° C,

[12] $\Delta F^{*}{}_{\text{diff}} = 1.358 \log_{10} 8.203 \times 10^4 / \sigma.$

In the same way it is found that since

[13] $e^{-\Delta F^{*}{}_{\text{rep}} / R T} = (\Delta F^{**}{}_{\text{rep}} / R T)\, e^{-\Delta F^{**}{}_{\text{rep}} / R T},$

[14] $\Delta F^{*}{}_{\text{rep}} = \Delta F^{**}{}_{\text{rep}} - 2.303 R T \log_{10} \Delta F^{**}{}_{\text{rep}} / R T.$

THE FREE ENERGY OF ACTIVATION DUE TO ELECTROSTATIC REPULSION

The exact treatment of electrostatic repulsion presents a problem of very considerable difficulty. If the solvent were a continuous dielectric having a dielectric constant ϵ that is independent of the field strength, the free energy $\Delta F^{**}{}_{\text{rep}}$ corresponding to a separation of σ would be given by eq. [5] with r equal to σ; $\Delta F^{*}{}_{\text{rep}}$ could then be readily calculated using eq. [14]. The true $\Delta F^{*}{}_{\text{rep}}$ values are, however, at all distances somewhat greater than calculated in this way, since the dielectric constant in the neighborhood of the ions is actually less than the macroscopic value. This effect has a significant effect on the calculated free energies of activation, as will be seen later.

The dielectric behavior of water in the near neighborhood of ions has recently been treated by Laidler and Pegis (12), whose work will now be extended to give an approximate treatment of electrostatic repulsive energies. According to Kirkwood (13), Booth (14), and Grahame (15) the variation of the differential dielectric constant ϵ_d with the field strength E is given extremely closely by the expression

[15] $$\epsilon_d = dD/dE = [(\epsilon_0-n^2)/(1+bE^2)]+n^2,$$

where D is the electric displacement, ϵ_0 the dielectric constant at zero field strength (taken as 78.5 for water at 25.0° C), n is the optical refractive index ($n^2 = 1.78$), and b is a quantity the value of which is given by Booth's theory. In the present calculations a value of 1.08×10^{-8} e.s.u.$^{-2}$ has been taken for b, since this value agrees closely with Booth's theory and with the experimental results obtained by Malsch (16).

Equation [15] integrates to

[16] $$D = n^2E+[(\epsilon_0-n^2)/b^{\frac{1}{2}}]\ \tan^{-1} b^{\frac{1}{2}}E$$

and since the electric displacement D at a distance r from an ion of valency z is ze/r^2 we have

[17] $$n^2E+[(\epsilon_0-n^2)/b^{\frac{1}{2}}]\ \tan^{-1} b^{\frac{1}{2}}E = ze/r^2.$$

Although E cannot be expressed explicitly as a function of r, eq. [17] can be used to prepare curves showing the variation; such curves are shown in Fig. 1 for $z = 1, 2, 3$, and 4. By interpolation, values of E can therefore be obtained corresponding to various values of r, and eq. [15] can then be used to calculate the differential dielectric constant at various distances from the ion. Such plots are shown in Fig. 2, from which it is seen that for a ferric ion, for example, the dielectric constant has the low value of 1.78 up to a distance of about 3 Å, after which the value rises fairly steeply. Even at a distance of 10 Å, however, the value is significantly below the limiting value of 78.5.
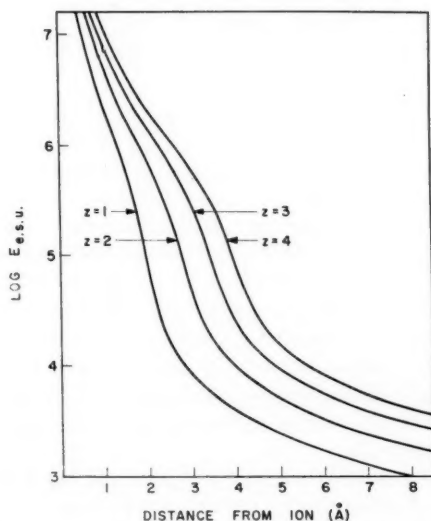
FIG. 1. Plots of the logarithm of the field strength, in electrostatic units (dynes), against the distance from the ion, for ions of valencies equal to 1, 2, 3, and 4.

The difficulty of calculating the repulsive free energy between two ions such as the ferric and ferrous ions arises from the fact that each ion produces a field, so that there is a considerable superposition of fields when the ions are close together. This superposition affects the dielectric constant, which in turn affects the individual fields. There appears
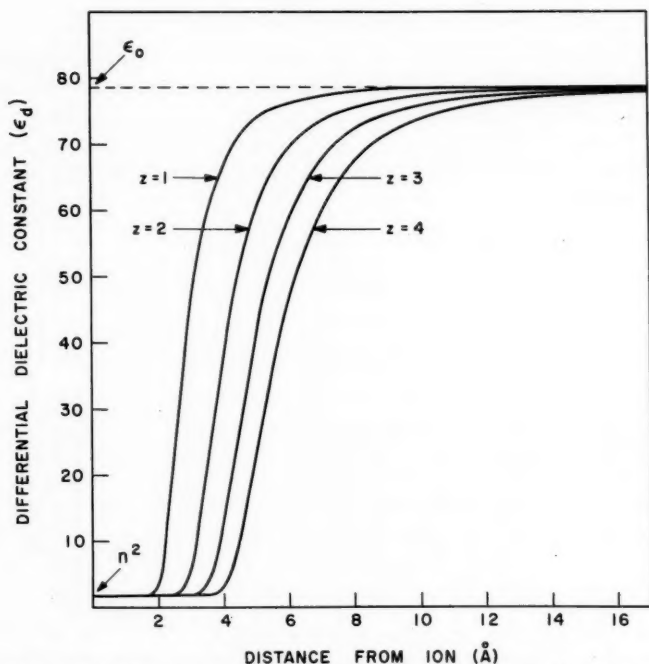
FIG. 2.   Plots of the differential dielectric constant against the distance from the ion, for ions of valencies equal to 1, 2, 3, and 4.

to be no simple way of treating this problem, and the only exact procedure seems to be to bring the ions together in a vacuum and then to calculate the energy residing in the dielectric. Mathematically this problem has so far proved intractable and a simpler procedure has therefore been employed.

The method adopted was to calculate the field at a distance r from the ferric ion, and to assume that the force acting on the ferrous ion is equal to this field multiplied by the charge on the ferrous ion. This procedure would, of course, be strictly correct if instead of the ferrous ion one were considering a test charge sufficiently small as not to affect the field of the ferric ion. Owing to the mutual interference of fields there will, however, be some error in the case of a large charge such as the ferrous ion. The procedure employed will, however, undoubtedly give a repulsive energy that is a significantly better approximation than that given by assuming the dielectric constant to be 78.5, and will probably not be far from the truth.

The procedure used is as follows. From the $z = 3$ curve in Fig. 1 it is possible to evaluate numerically the area under the curve from $r = \infty$ to r equal to any desired value σ. This area is a measure of the work required to bring a unit charge from infinity to σ. Multiplication by the charge on the ferrous ion then gives a value for the work, i.e. of ΔF^{**}_{rep}, required to bring the ferrous ion from infinity to a distance of σ. Figure 3 shows another plot of E against σ, and also gives ΔF^{**}_{rep} plotted against σ. Included on the figure are the curves that are calculated on the assumption that there is no dielectric saturation, i.e. that ϵ remains 78.5 at all distances. The difference between the two cases is seen to be negligible at distances greater than about 5 Å, but to be extremely

great at smaller distances. Neglect of the saturation effect would therefore lead to considerable error, in that the ions would be permitted to approach much more closely than they are actually able to do.
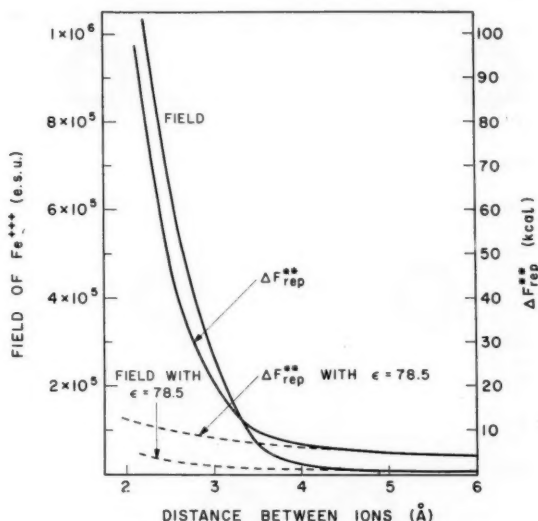
FIG. 3.   Plots of the field due to a ferric ion (left-hand scale), and of the free energy of repulsion between a ferric ion and a ferrous ion (right-hand scale) against the distance. The dotted curves are calculated on the assumption of a dielectric constant of 78.5, the full curves for a dielectric constant that varies with field strength according to equation [15].

QUANTUM-MECHANICAL TUNNELLING

Inspection of Fig. 3 shows that the two ions cannot approach to within a distance of 3 Å without a considerable expenditure of free energy. Calculations of the work of electron transfer show that except at distances shorter than 3 Å the energy barrier for the transfer of an electron is more than 200 kcal in height. It therefore follows that the transfer must occur by quantum-mechanical tunnelling, and it is readily found that for the types of energy barriers involved the tunnelling rates are sufficiently large to permit reaction to proceed by this mechanism.

The first problem is the calculation of the potential-energy barrier. Here the main point that must be taken into consideration is that the rates of electron tunnelling are so large that there is insufficient time for the reorganization of neighboring solvent molecules. In other words, after the electron has left the ferrous ion the surrounding solvent molecules remain oriented in the same manner even though the ion has now become a ferric ion. The field around the newly formed ferric ion must therefore be calculated on the basis of a charge of $3e$ on the ion, but with a ferrous-type ionic atmosphere. This can simply be done by calculating the field due to a ferrous ion in its ferrous-type atmosphere and multiplying the result by $3/2$.

The calculations of the barriers have therefore been carried out in this way, and the assumption of superposition of fields has again been made. The procedure has been to calculate, using the methods of the preceding section, the field round the newly formed ferric ion, with its ferrous-like atmosphere, and also that round the ferric ion
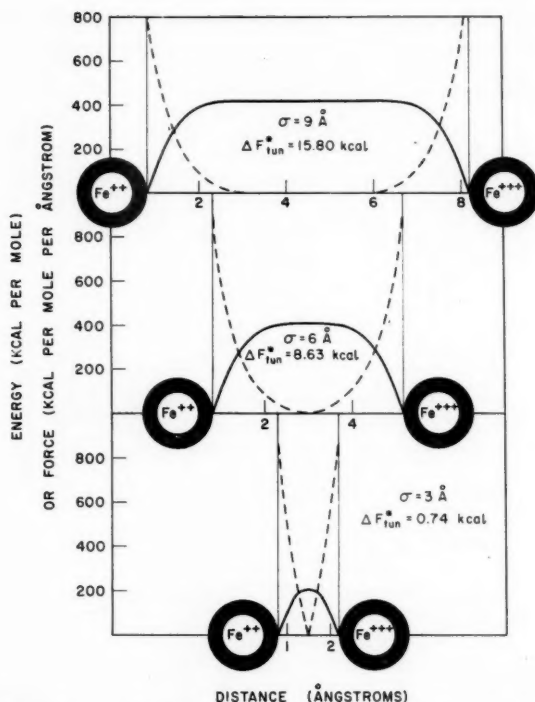
FIG. 4. Plots of force between ferric and ferrous ions against their separation (dotted curves) and of the potential-energy barrier (full curves). The ferric ion produced when the electron leaves the ferrous ion is in a ferrous-like atmosphere; this causes a slight asymmetry in the potential-energy barriers.

which the electron is approaching; this has a normal ferric-type atmosphere. For a given value of σ the two fields can be superimposed, and a curve can therefore be plotted for the force on the electron at various positions. By graphical integration the energy can then be calculated, and the barrier plotted. Figure 4 shows, for separations of 3, 6, and 9 Å, the plots of force and energy. In making these calculations the radius of the ferric ion was taken as 0.8375 Å, which is the crystal radius of 0.67 Å multiplied by the factor 1.25, as suggested by Couture and Laidler (17) and by Laidler and Pegis (12). It is to be noted that the energy curves in Fig. 4 rise and fall fairly steeply; this is because, during the first and last parts of its progress, the electron is moving through a region where the dielectric constant is small and where the forces are therefore strong.

The expression for the probability of tunnelling takes simple forms for barriers that are triangular or rectangular. The barriers for the present system are closer to rectangles than to triangles, and the approximation will be made of treating them as rectangular; the transmission coefficient is then (18)

[18] $$\kappa = 4e^{-2\gamma\alpha}[2\alpha\gamma/(\alpha^2+\gamma^2)]^2,$$

where

[19] $$\alpha = 2\pi\sqrt{(2mW)}/h$$

and

[20] $$\gamma = 2\pi\sqrt{[2m(V_0-W)]}/h,$$

m is the mass of the electron, V_0 the height of the barrier, and W is the kinetic energy of the electron prior to tunnelling. Following Marcus, Zwolinski, and Eyring (4) a value of 77.18 kcal per mole has been taken for W.

The values of κ calculated for the three separations of 3 Å, 6 Å, and 9 Å are shown in Fig. 4. The transmission coefficient can formally be expressed as

[21] $$\kappa = e^{-\Delta F^*_{tun} F/RT},$$

and the ΔF^*_{tun} values calculated in this way are shown in Fig. 4; additional values are included in Table I.

TABLE I

Free energies of activation for the Fe^{++}–Fe^{+++} exchange at various ionic separations

Separation (Å)	ΔF^{**}_{rep}	ΔF^*_{rep}	ΔF^*_{diff}	ΔF^*_{tun}	ΔF^*_{calc}
2.5	48.34	45.73	6.20	0.11	52.04
3.0	20.70	18.60	6.02	0.74	25.36
3.5	9.65	8.00	6.00	2.40	16.40
4.0	6.88	5.43	5.80	3.60	14.83
4.5	5.64	4.30	5.75	4.85	14.90
5.0	5.07	3.80	5.71	6.10	15.60
6.0	4.23	3.07	5.61	8.63	17.31
7.0	3.62	2.55	5.50	11.00	19.05
8.0	3.17	2.18	5.40	13.40	20.98
9.0	2.81	1.89	5.38	15.80	23.07

Weighed average of ΔF^*_{calc} = 15.4 kcal.

THE OVER-ALL FREE ENERGY OF ACTIVATION

The results of the various calculations are summarized in Table I for a range of values of σ. Included in this table are the ΔF^*_{diff} values calculated using eq. [12], the ΔF^*_{rep} values calculated using eq. [14] from the ΔF^{**}_{rep} values shown in Fig. 3, and the ΔF^*_{tun} values calculated in the manner described in the preceding section. Since according to the definitions of the three quantities the over-all rate of reaction corresponding to a given σ is given by

[22] $$k = (\mathbf{k}T/h)\ e^{-\Delta F^*_{diff}/RT}\ e^{-\Delta F^*_{rep}/RT}\ e^{-\Delta F^*_{tun}/RT},$$

the calculated ΔF^*_{calc} is the sum of ΔF^*_{diff}, ΔF^*_{rep}, and ΔF^*_{tun}, and is shown in the last column of the table. The values are shown plotted against σ in Fig. 5.

It is seen from the plot of ΔF^*_{calc} that the value passes through a minimum of about 14.8 kcal at a separation of about 4 Å. This value does not, however, quite represent the over-all free energy of activation, which will actually be a value averaged over all values of σ. The average ΔF^*_{calc} is given by

[23] $$\Delta F^*_{calc} = \frac{\int_{14.8}^{\infty} \Delta F^*_{calc}\ e^{-\Delta F^*_{calc}/RT}\ d\Delta F^*_{calc}}{\int_{14.8}^{\infty} e^{-\Delta F^*_{calc}/RT}\ d\Delta F^*_{calc}},$$

the value of which is found to be 15.4 kcal.

In view of the approximation involved, particularly in the treatment of the superposition of fields, the agreement between this calculated value and the experimental value of 16.8 kcal is quite satisfactory. The agreement is much better than that given by earlier treatments, a fact that is to be attributed to the following factors:
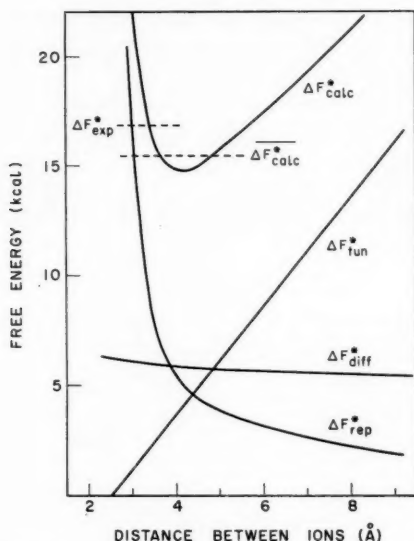
FIG. 5. Plots of the various free-energy terms against the distance between the ions. The upper curve represents the sum of the three contributions, and the lower horizontal line shows the calculated weighted-average free energy of activation, to be compared with the observed value shown by the upper horizontal line.

(1) The present treatment of the reaction as a diffusion-controlled one. The value of ΔF^*_{diff} at 4 Å is seen to have a value of nearly 6 kcal; no corresponding term appears in the earlier treatments.

(2) The more careful consideration devoted, in the present work, to the effects of dielectric saturation. Neglect of these effects allows the ions to approach much more closely than 4 Å, and the resulting ΔF^*_{calc} is less by more than a kilocalorie.

The reason that the present treatment gives a value of ΔF^*_{calc} that is too low is probably due to the fact that the treatment of repulsive effects somewhat underestimates the value of ΔF^*_{rep}. It does not seem likely that the calculated values of ΔF^*_{diff} and ΔF^*_{tun} can be much in error. It is to be noted that the present way of looking at the problem, particularly of treating the energy barriers, leaves no place for the "rearrangement" free energy considered by Eyring et al., this factor having been included in the present treatment of the repulsive energy and the potential-energy barrier.

ENERGIES AND ENTROPIES OF ACTIVATION

The calculation of energies and entropies of activation is always more difficult than that of free energies of activation, since the energies and entropies depend in a more intimate way on the various structural factors. It is, however, of interest to see to what extent the present treatment offers an interpretation of the experimental values of $E = 9.9$ kcal and $\Delta S^* = -25$ e.u. We will consider separately the three terms involved, namely diffusion, tunnelling, and repulsion. Since the average ΔF^* corresponds approximately to a value of σ equal to 5.0 Å, the figures to be quoted below will be related to this separation.

Activation energies for the viscous flow of water (19) and for diffusion processes in water (20) are usually close to 4.0 kcal at 25° C. Since at $\sigma = 5.0$ Å, $\Delta F^*_{diff} = 5.7$ kcal, it follows that $\Delta S^*_{diff} = -5.7$ e.u.

The transmission coefficient is proportional to $\exp[k(V_0 - W)^{\frac{1}{2}}]$ and V_0 and W are practically temperature independent (since most of the work of transferring the electron is done through the dielectrically saturated layer). The free energy of activation for tunnelling, equal to 6.1 kcal, therefore corresponds entirely to an apparent entropy of activation, so that

$$E_{tun} = 0 \text{ and } \Delta S^*_{tun} = -20.3 \text{ e.u.}$$

Since the heats and entropies for repulsion are very difficult to estimate in a reliable manner they have been obtained by difference, and are shown as starred values in the table below:

	ΔF^*	E	ΔS^*
Diffusion	5.7	4.0	-5.7
Tunnelling	6.1	0	-20.3
Repulsion	5.0*	5.9*	3.0*,†
Experimental values	16.8	9.9	-25

†The apparent discrepancy in the ΔS^* values is due to the fact that in the calculation of ΔS^*_{exp} the pre-exponential factor is taken as ekT/h rather than kT/h.

The very elementary theory of the entropy of activation for repulsion, with $\epsilon = 78.5$ and $\partial \ln \epsilon / \partial T = -0.0046$, gives,

$$\Delta S^*_{rep} = -18.8(z_1 z_2 / \sigma) = -22.6 \text{ e.u.,}$$

which is very far from the derived value of 3.0 e.u. The entropy of activation will, however, be very markedly increased when there is initially almost complete saturation in the vicinity of both of the reacting ions. It is found, for example, that entropies of activation for reactions between ions of the same sign are frequently larger than predicted by the elementary theory. The reason for these effects may well be that, in order for the ions to approach closely, water molecules must be "unfrozen"; such a process will require energy and will result in an increase in entropy.

REFERENCES

1. SILVERMAN, J. and DODSON, R. W. J. Phys. Chem. 56, 846 (1952).
2. LIBBY, W. F. J. Phys. Chem. 56, 863 (1952).
3. WEISS, J. Proc. Roy. Soc. A, 222, 128 (1954).
4. MARCUS, R. J., ZWOLINSKI, B. J., and EYRING, H. J. Phys. Chem. 58, 432 (1954).
5. ZWOLINSKI, B. J., MARCUS, R. J., and EYRING, H. Chem. Revs. 55, 157 (1955).
6. MARCUS, R. A. (a) J. Chem. Phys. 26, 867 (1957). (b) Trans. N.Y. Acad. Sci. 19, 423 (1957).
7. SMOLUCHOWSKI, M. V. Z. physik. Chem. 92, 129 (1917).
8. VERWEY, E. J. and OVERBEEK, J. Th. G. Theory of the stability of lyophobic colloids. Elsevier Press, Inc., N.Y. 1948.
9. DEBYE, P. Trans. Electrochem. Soc. 82, 265 (1942).
10. ALBERTY, R. A. and HAMMES, G. G. J. Phys. Chem. 62, 154 (1958).
11. BRADLEY, R. S. Trans. Chem. Soc. 1910 (1934).
12. LAIDLER, K. J. and PEGIS, C. Proc. Roy. Soc. A, 241, 80 (1957).
13. KIRKWOOD, J. G. J. Chem. Phys. 7, 911 (1939).
14. BOOTH, F. J. Chem. Phys. 19, 391, 1327, 1615 (1951).
15. GRAHAME, D. C. J. Chem. Phys. 21, 1054 (1953).
16. MALSCH, J. Physik. Z. 29, 770 (1928); 30, 837 (1929).
17. COUTURE, A. M. and LAIDLER, K. J. Can. J. Chem. 34, 1209 (1956).
18. MOTT, N. F. and SNEDDON, I. N. Wave mechanics and its applications. The Clarendon Press, Oxford. 1948. pp. 15-17.
19. EWELL, R. H. and EYRING, H. J. Chem. Phys. 5, 726 (1937).
20. SCHEFFER, J. D. R. and SCHEFFER, F. E. C. Proc. Acad. Sci. Amsterdam, 19, 148 (1916).

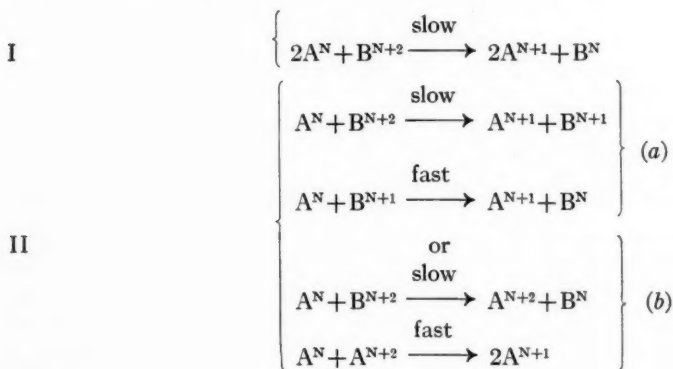# THE PRINCIPLE OF EQUIVALENCE CHANGE IN OXIDATION–REDUCTION REACTIONS[1]

J. HALPERN

ABSTRACT

The principle of equivalence change predicts that oxidation–reduction reactions between 1-equivalent oxidants and 2-equivalent reductants (or vice versa) will, in general, be slow, since they must proceed either through termolecular paths or through the formation of unstable intermediates. In this paper, the kinetics and mechanisms of a number of reactions of this type are examined and an attempt is made to assess the validity of the considerations on which this principle is based. Among the reactions considered are (1) electron transfer between metal ions; (2) oxidation of metal ions by oxygen; and (3) reduction of metal ions by hydrogen. In each of these cases it is found that the principle of equivalence change has only limited validity and that a number of other factors are important in determining the relative rates and mechanisms of reactions of different equivalence type. Among these are the formation of stabilized intermediate complexes between oxidant and reductant and the possibility of unstable intermediates acting as carriers in chain reactions. In reactions of thallium(I) or thallium(III) with 1-equivalent metal ions, thallium(II) is formed as an intermediate. Some of these reactions are not as slow as expected, apparently because of favorable entropies of activation. Several of the reactions examined proceed simultaneously through bimolecular and termolecular paths, the latter being favored because of lower activation energies.

INTRODUCTION

A large number of oxidizing and reducing agents are known whose stable oxidation states differ by two electron equivalents (e.g., Tl(I)–Tl(III), Sn(II)–Sn(IV), H_2–$2H^+$, O_2–H_2O_2) and the question arises of how these react with 1-equivalent reductants or oxidants (e.g., Fe(II)–Fe(III), Ce(III)–Ce(IV), etc.). The principle of equivalence change, due to Shaffer (1, 2, 3), states that such reactions are, in general, slow compared to reactions between 1-equivalent oxidants and 1-equivalent reductants or between 2-equivalent oxidants and 2-equivalent reductants. This principle can be interpreted in the following way: Two general types of mechanisms can be conceived for a reaction between a 1-equivalent reductant, A, with stable oxidation states N and N+1, and a 2-equivalent oxidant, B, with stable oxidation states N and N+2.

$$
\text{I} \quad \left\{ \begin{array}{c} \text{slow} \\ 2A^N + B^{N+2} \longrightarrow 2A^{N+1} + B^N \end{array} \right.
$$

$$
\text{II} \quad \left\{ \begin{array}{c} \left. \begin{array}{c} \text{slow} \\ A^N + B^{N+2} \longrightarrow A^{N+1} + B^{N+1} \\ \text{fast} \\ A^N + B^{N+1} \longrightarrow A^{N+1} + B^N \end{array} \right\} \ (a) \\[2em] \left. \begin{array}{c} \text{or} \\ \text{slow} \\ A^N + B^{N+2} \longrightarrow A^{N+2} + B^N \\ \text{fast} \\ A^N + A^{N+2} \longrightarrow 2A^{N+1} \end{array} \right\} \ (b) \end{array} \right.
$$

It is anticipated that reactions proceeding by the first type of mechanism will be slow because they involve a termolecular step, while reactions of the second type will be slow because of the high activation energy associated with the formation of the unstable intermediate, B^{N+1} or A^{N+2}. It also follows that such reactions should be susceptible to catalysis by species, X, which have three oxidation states, N, N+1, and N+2, with suitably disposed potentials through a mechanism of the type:

$$
\text{III} \quad
\begin{cases}
A^N + X^{N+2} \longrightarrow A^{N+1} + X^{N+1} \\
A^N + X^{N+1} \longrightarrow A^{N+1} + X^N \\
X^N + B^{N+2} \longrightarrow X^{N+2} + B^N
\end{cases}
$$
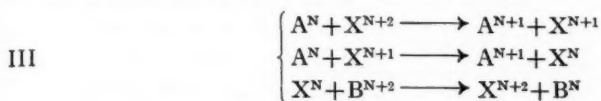
Recent studies on the kinetics and mechanisms of a variety of inorganic oxidation–reduction reactions make possible for the first time a detailed assessment of the validity of these considerations. This is attempted in the present paper with particular reference to three relatively simple types of reactions, (1) electron transfer between metal ions; (2) oxidation of metal ions by molecular oxygen; and (3) reduction of metal ions by molecular hydrogen. The principles which emerge from a consideration of these systems appear capable of extension to reactions of more complex species.

1-EQUIVALENT AND 2-EQUIVALENT OXIDANTS AND REDUCTANTS

The inherent tendencies of different oxidizing agents to undergo 1-equivalent or 2-equivalent reduction are revealed by differences in the products that are obtained when they react with certain reducing agents, notably hydrazine (4, 5) and sulphurous acid (6). In the case of sulphurous acid, 1-equivalent oxidation favors the formation of dithionate, while 2-equivalent oxidation results exclusively in the formation of sulphate, according to the mechanisms:

$$
SO_3^{2-} \xrightarrow{-e} SO_3^- \longrightarrow \tfrac{1}{2}S_2O_6^{2-},
$$

$$
SO_3^{2-} \xrightarrow{-2e} SO_3(SO_4^{2-}).
$$
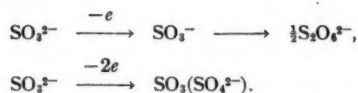
The following classification of oxidants, due to Higginson and Marshall (6), is based on this criterion:

1-Equivalent	2-Equivalent	1,2-Equivalent
Ce(IV)	Tl(III)	$Cr_2O_7^{2-}$
Co(III)	H_2O_2	MnO_4^-
Fe(III)	I_2, Br_2, Cl_2	$PtCl_6^{4-}$
Mn(III)	IO_3^-, BrO_3^-	VO_2^+
OH	BrO^-, ClO^-	

Many oxidants can be unambiguously classified as being of the 1- or 2-equivalent type; a few which give intermediate stoichiometry are denoted as 1,2-equivalent.

The occurrence of 2-equivalent steps in oxidation–reduction reactions is now well recognized and Michaelis's hypothesis that all such reactions proceed by successive univalent steps (7) must be considered as without general validity. This conclusion is relevant to the present discussion, since this hypothesis, if valid, would remove the most obvious basis for the principle of equivalence change.

ELECTRON-TRANSFER REACTIONS BETWEEN METAL IONS

A significant test of the principle of equivalence change should be provided by comparing the kinetics of an oxidation–reduction reaction between a 1-equivalent and a 2-equivalent metal ion, with the kinetics of the isotopic exchange reactions between the two valence states of each ion. The data summarized in Table I permit three such comparisons, i.e., for the Fe^{2+}–Tl^{3+}, Tl^+–Co^{3+}, and Tl^+–Ce^{4+} reactions.

TABLE I

Electron-transfer reactions between metal ions

Reaction	Equivalence type	k (25°), l mole^{-1} sec^{-1}	E, kcal	$\Delta S^{\ddagger}$ e.u.	Reference
Fe^{2+}–Fe^{3+}	1–1	4	9.9	−25	8
Co^{2+}–Co^{3+}	1–1	0.75(0°)	—	—	9
Ce^{3+}–Ce^{4+}	1–1	2×10^{-2}	7.7	−40	10
Tl^+–Tl^{3+}	2–2	4×10^{-5}	17.6	−21	11
Fe^{2+}–Tl^{3+}	1–2	2×10^{-2}	18	−7	12
Tl^+–Co^{3+}	2–1	3×10^{-3}	26.4	+22	13
Tl^+–Ce^{4+}	2–1	Very slow	—	—	14

Both the Fe^{2+}–Tl^{3+} and Tl^+–Co^{3+} reactions have been shown to proceed through type II mechanisms, involving one-electron transfer steps with the formation of $Tl(II)$ as an intermediate (13, 15). In line with the principle of equivalence change, the activation energy of each of these reactions appears to be higher than the activation energies of both the corresponding isotopic electron-exchange reactions; presumably this reflects the formation of the unstable $Tl(II)$ species. However, the rates of these reactions are not lower than, but in both cases intermediate between, those of the corresponding exchange reactions, i.e., $k_{Tl^+-Tl^{3+}} < k_{Fe^{2+}-Tl^{3+}} < k_{Fe^{2+}-Fe^{3+}}$. This is because in each case the mixed reaction is favored by a more positive entropy of activation.

Until data are obtained for more systems, it is not possible to conclude whether this is a general feature of such reactions, but there are grounds for anticipating that this may prove to be the case. These are provided by the recognition that one of the principal contributing factors to the instability of intermediate valence states of metal ions in solution is a low hydration energy; usually this is because the ion is "abnormally" large having, as in the case of Tl^{2+}, only a single electron in its outer shell. However, for the same reason the entropy of hydration of the ion will tend to be more positive than those of stable ions of similar charge (e.g., Tl^{2+} vs. Hg^{2+}). A reaction involving the formation of such an ion would therefore be expected to require considerable energy but to be favored by an abnormally positive entropy. If, as often tends to be the case, the charge distribution of the activated complex approaches that of the products, a similar trend would be reflected in the energies and entropies of activation.

The increase in entropy of activation (relative to the exchange reactions) is more pronounced for the Tl^+–Co^{3+}, than for the Fe^{2+}–Tl^{3+} reaction, and this may be due to the influence of an additional factor. The rate-determining step of this reaction,

$$Tl^+ + Co^{3+} \longrightarrow Tl^{2+} + Co^{2+}$$

involves a change in the ionic charges in the direction of charge equalization (more uniform spreading out of the charge). This is generally accompanied by a decrease in the electrostriction of the surrounding solvent and hence by an increase in entropy. The entropy of activation should also be shifted toward more positive values. This effect should not be apparent in the Fe^{2+}–Tl^{3+} reaction, whose rate-determining step,

$$Fe^{2+} + Tl^{3+} \longrightarrow Fe^{3+} + Tl^{2+}$$

involves no change in charge type, nor in the isotopic exchange reactions which are, of course, symmetrical.

In contrast to the other two systems and more clearly in line with the principle of equivalence change, the $Tl^+–Ce^{4+}$ reaction appears to be much slower than either the $Tl^+–Tl^{3+}$ or $Ce^{3+}–Ce^{4+}$ exchange reaction. It is not possible to draw any detailed conclusions from this, since there is some uncertainty about the mechanism of oxidation of Tl^+ by Ce^{4+}. Preliminary kinetic measurements (14) suggest that this proceeds not by direct reaction between the ions but by a mechanism, such as

$$CeOH^{3+} \rightleftharpoons Ce^{3+} + OH,$$
$$Tl^+ + OH \rightarrow Tl^{2+} + OH^-,$$
$$Tl^{2+} + Ce^{4+} \rightarrow Tl^{3+} + Ce^{3+}.$$
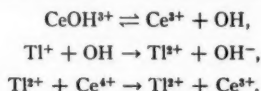
The possibility that the first step of this mechanism also constitutes a path of $Ce^{3+}–Ce^{4+}$ exchange cannot be dismissed.

Catalysis of the $Tl^+–Ce^{4+}$ reaction by Mn^{2+} (1) and by halide ions (16) has been reported and attributed to a type III mechanism.

The above reactions have been discussed without reference to the question of whether they occur by actual electron transfer between the metal ions or by some other mechanism, e.g., H-atom transfer between the hydration shells of the ions. There is still some uncertainty about this question (17), but the considerations which have been invoked here would be applicable in either case.

OXIDATION OF METAL IONS BY MOLECULAR OXYGEN

The first stable reduction product of oxygen is hydrogen peroxide, and it can therefore be considered as a 2-equivalent oxidizing agent. Kinetic data for the oxidation of several metal ions by oxygen are summarized in Table II.

TABLE II
Oxidation of metal ions by oxygen

Reaction	Kinetics	E (kcal)	$\Delta S^{\ddagger}$ (e.u.)	Reference
Fe(II) → Fe(III)	$k[O_2][Fe(II)]^2$	17.4	−15	18
Pu(III) → Pu(IV)	$k[O_2][Pu(III)]^2$	19	+11.2*	19
V(III) → V(IV)	$k[O_2][V(III)]$	20.1	+6†	20
U(IV) → U(VI)	$k[O_2][U(IV)]$	22	—	21

*The high apparent entropy of activation may be due to considerable charge neutralization in the activated complex, since the kinetics suggest that 2–3 sulphate ions participate in the rate-determining step.
†Calculated on the assumption that the reacting species is VOH^{2+}; this is suggested by the pH dependence of the rate.

Fe(II) is a 1-equivalent reductant and its oxidation by oxygen, as evidenced by the third-order kinetics, appears to proceed by a type I mechanism. This is also the case for the oxidation of Pu(III) to Pu(IV), despite the fact that the +5 state of Pu is relatively stable and hence a 2-equivalent oxidation of Pu(III) is feasible. On the other hand, the oxidation of V(III) to V(IV) is a second-order reaction and probably proceeds by a type II mechanism; possible intermediates are V(V) and HO_2. This reaction is very susceptible to catalysis by cupric salts, probably through a mechanism of the type

$$V(III) + Cu(II) \xrightarrow{\text{slow}} V(IV) + Cu(I),$$
$$Cu(I) + O_2 \xrightarrow{\text{fast}} Cu(II).$$
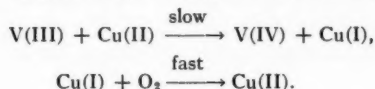
It is of interest that the activation energies for the oxidation of these three metal ions are similar.

Despite the fact that U(IV) is a 2-equivalent reductant, its oxidation to U(VI) by O_2 is not accomplished in a single 2-equivalent step. It has been shown (21) that this reaction occurs by a chain mechanism involving the 1-equivalent steps

$$U(V) + O_2 \rightarrow U(VI) + HO_2,$$

$$U(IV) + HO_2 \rightarrow U(V) + H_2O_2.$$
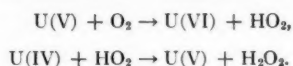
This mechanism involves the formation of the unstable intermediates HO_2 and U(V), but is favored over the direct 2-equivalent oxidation, because of the "amplification factor" introduced by the chain reaction. While this also applies to a number of other reactions between 2-equivalent oxidants and reductants (e.g., the oxidation of SO_3^- by O_2) these do not include any examples of reaction between two metal ions. Thus, the Tl(I)–Tl(III) exchange and the oxidation of U(IV) by Tl(III) (22), which could, in principle, occur by analogous mechanisms, appear to be simple bimolecular reactions.

REDUCTION OF METAL IONS BY MOLECULAR HYDROGEN

Molecular hydrogen reacts homogeneously with a number of metal ions in aqueous solution, reducing them to metallic form or to compounds of lower valence (23). The kinetics of the primary steps in these reactions are summarized in Table III.

TABLE III

Reduction of metal ions by hydrogen

Ion	Kinetics	E (kcal)	$\Delta S^{\ddagger}$ (e.u.)	Reference
Cu^{2+}	$k[H_2][Cu^{2+}]$	26.6	−10	24
Hg^{2+}	$k[H_2][Hg^{2+}]$	18.1	−12	25
Hg_2^{2+}	$k[H_2][Hg_2^{2+}]$	20.4	−10	25
Ag^+ { (I)	$k[H_2][Ag^+]$	24.0	−6	26
(II)	$k[H_2][Ag^+]^2$	14.7	−25	26
MnO_4^-	$k[H_2][MnO_4^-]$	14.7	−17	27
$Ag^+ + MnO_4^{-*}$	$k[H_2][Ag^+][MnO_4^-]$	9.3	−26	27

*Ag^+—Catalyzed reaction between MnO_4^- and H_2.

Since the formation of H atoms (or H_2^+ ions) in aqueous solution is energetically very unfavorable, hydrogen might be expected to behave as a 2-equivalent reductant in these reactions.

The reactions of hydrogen with Hg^{++}, Hg_2^{++}, and MnO_4^- are consistent with this. For example, the mechanism of the reduction of Hg^{2+} to Hg_2^{2+} is probably

$$Hg^{2+} + H_2 \xrightarrow{\text{slow}} Hg + 2H^+,$$

$$Hg + Hg^{2+} \xrightarrow{\text{fast}} Hg_2^{2+}.$$
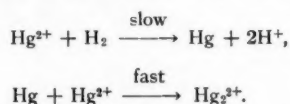
This mechanism is plausible on energetic as well as kinetic grounds, since the proposed rate-determining step, in which a Hg atom is formed, is exothermic by 27 kcal (23). Similar considerations apply to the reduction of Hg_2^{2+} and of MnO_4^-. In each of these cases the rate-determining step appears to be a 2-equivalent reduction, leading to the formation of Hg_2 and Mn(V), respectively, as intermediates.

From the standpoint of the principle of equivalence change, the homogeneous bi-molecular reactions of H_2 with Cu^{2+} and with Ag^+ are, however, surprising. Cu^{2+} is a 1-equivalent oxidant and either type II mechanism would involve a rate-determining step

$$Cu^{2+} + H_2 \rightarrow Cu^+ + H^+ + H \qquad (\Delta H° \sim 54 \text{ kcal})$$

or

$$Cu^{2+} + H_2 \rightarrow Cu + 2H^+ \qquad (\Delta H° \sim 66 \text{ kcal}),$$
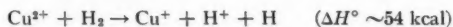
which is energetically inconsistent with the observed activation energy of 26 kcal. The mechanism of the reduction of Cu^{2+} to Cu^+ by H_2 has actually been shown (28) to be

$$Cu^{2+} + H_2 \overset{k}{\rightleftharpoons} CuH^+ + H^+,$$

$$CuH^+ + Cu^{2+} \rightarrow 2Cu^+ + H^+.$$
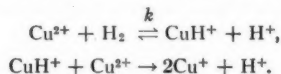
It is thus apparent that in reactions such as this, where the oxidant and reductant form an intermediate complex which is stabilized by covalent bonding, the principle of equivalence change offers little guidance as to the probable kinetics and mechanism.

The reduction of Ag^+ by H_2 also appears to proceed through the formation of covalently bonded hydride intermediates. It is of interest that two paths are observed for this reaction, in which the rate-determining steps involve the heterolytic and homolytic splitting of hydrogen, respectively,

$$Ag^+ + H_2 \rightarrow AgH + H^+,$$

$$2Ag^+ + H_2 \rightarrow 2AgH^+.$$
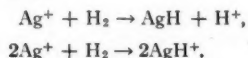
Despite the fact that the latter reaction is termolecular, it is favored relative to the alternative bimolecular path, by its lower activation energy (14.7 vs. 24 kcal) and predominates at lower temperatures. Similarly the marked susceptibility of the reduction of MnO_4^- by H_2, to catalysis by Ag^+, is due to a termolecular rate-determining step,

$$Ag^+ + MnO_4^- + H_2 \rightarrow AgH + MnO_4^{2-} + H^+,$$
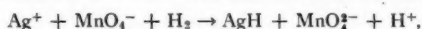
which competes with the bimolecular uncatalyzed reaction because of its lower activation energy (9.3 vs. 14.7 kcal).

These observations prompt some comment on the question of the relative probabilities of bimolecular and termolecular reactions in general. Some measure of this is provided by the difference in entropy of activation for the two types of processes. In solution, this difference is normally only about 10 e.u., corresponding to a factor of about 100 in the rate constant. This is the equivalent of a difference in activation energy of only about 3000 cal at 25°. Even at reactant concentrations as low as 0.001 M an activation energy difference of about 7000 cal will equalize the rates. Since variations of activation energy of this order, even among closely related reactions in solution, are fairly common the widespread emphasis which is encountered in the literature on kinetics on the improbability of termolecular reactions is somewhat misleading. This is particularly relevant to reactions of the type considered here, in which the presence of alternative bimolecular and termolecular paths (the latter having a lower activation energy) is an intrinsic feature.

REFERENCES

1. SHAFFER, P. A. J. Am. Chem. Soc. **55**, 2169 (1933); J. Phys. Chem. **40**, 1021 (1936); Cold Spring Harbor Symposia Quant. Biol. **1**, 50 (1939).
2. REMICK, A. E. J. Am. Chem. Soc. **69**, 94 (1947).
3. WESTHEIMER, F. H. *In* The mechanism of enzyme action. *Edited by* W. D. McElroy and B. Glass. John Hopkins Press, Baltimore, Md. 1954. p. 321.
4. KIRK, R. E. and BROWNE, A. W. J. Am. Chem. Soc. **50**, 337 (1928).

5. HIGGINSON, W. C. E., SUTTON, D., and WRIGHT, P. J. Chem. Soc. 282, 1402 (1953); 1551 (1955).
6. HIGGINSON, W. C. E. and MARSHALL, J. W. J. Chem. Soc. 447 (1958).
7. MICHAELIS, L. Trans. Electrochem. Soc. 71, 107 (1937); Cold Spring Harbor Symposia Quant. Biol. 7, 33 (1939).
8. SILVERMAN, J. and DODSON, R. W. J. Phys. Chem. 56, 846 (1952).
9. BONNER, N. A. and HUNT, J. P. J. Am. Chem. Soc. 74, 1866 (1952).
10. GRYDER, J. W. and DODSON, R. W. J. Am. Chem. Soc. 73, 2890 (1951).
11. PRESTWOOD, R. and WAHL, A. C. J. Am. Chem. Soc. 71, 3137 (1949).
12. JOHNSON, C. E. J. Am. Chem. Soc. 74, 959 (1952).
13. ASHURST, K. G. and HIGGINSON, W. C. E. J. Chem. Soc. 343 (1956).
14. ARMSTRONG, A. M. and HALPERN, J. Unpublished results.
15. ASHURST, K. G. and HIGGINSON, W. C. E. J. Chem. Soc. 3044 (1953).
16. DUKE, F. R. and BORCHERS, C. E. J. Am. Chem. Soc. 75, 5186 (1955).
17. BASOLO, F. and PEARSON, R. G. In Mechanisms of inorganic reactions. Chap. 8. John Wiley & Sons, Inc., New York. 1958.
18. GEORGE, P. J. Chem. Soc. 4349 (1954).
19. BAKER, F. B. and NELSON, T. W. J. Phys. Chem. 61, 381 (1957).
20. RAMSEY, J. B., SUGIMOTO, R., and DEVORKIN, H. J. Am. Chem. Soc. 63, 3480 (1941).
21. HALPERN, J. and SMITH, J. G. Can. J. Chem. 34, 1419 (1956).
22. HARKNESS, A. and HALPERN, J. Unpublished results.
23. HALPERN, J. Quart. Revs. 10, 463 (1956); Advances in Catalysis, 9, 302 (1957).
24. PETERS, E. and HALPERN, J. J. Phys. Chem. 59, 793 (1955).
25. KORINEK, G. J. and HALPERN, J. J. Phys. Chem. 60, 285 (1956).
26. WEBSTER, A. H. and HALPERN, J. J. Phys. Chem. 61, 1239, 1245 (1957).
27. WEBSTER, A. H. and HALPERN, J. Trans. Faraday Soc. 53, 51 (1957).
28. HALPERN, J., MACGREGOR, E. R., and PETERS, E. J. Phys. Chem. 60, 1455 (1956).

ON THE THEORY OF ELECTROCHEMICAL AND CHEMICAL ELECTRON TRANSFER PROCESSES[1]

R. A. MARCUS

ABSTRACT

Kinetic studies of simple electron transfer systems in solution and at electrodes have revealed a number of interesting and simplifying features. The chemical reactions also represent one of the very few cases in kinetics where it has been possible to make reasonable calculations of the absolute rate constant without introducing adjustable parameters or arbitrary assumptions. Because of their comparative simplicity, these processes also serve as a useful kinetic tool for investigating ion–solvent–electrode interactions.

In the present paper the writer's recent theoretical investigations are summarized and used to interpret data obtained from both solution and electrode studies. Various phenomena are discussed in the light of this theory and several predictions of behavior are made. The topics considered include effects of changing the overpotential or the standard free energy of reaction, the ionic structure, temperature, salt concentration, solvent, and electrode material. Both the parallelism between chemical and electrochemical transfers and the role played by the electrostatic image in the latter case are discussed. A classification of reactants is employed throughout, based in part on differences in the theoretical treatment.

INTRODUCTION

In 1952 Libby (19) interpreted the behavior of some isotopic exchange electron transfer reactions in terms of the Franck–Condon principle, a suggestion which served to stimulate much further experimental and theoretical work. About the same time, Randles (31) discussed the rates of simple electron transfer electrode processes in terms of related concepts. This work was followed several years later by Rudolph J. Marcus, Zwolinski, and Eyring's investigation of an electron tunnelling mechanism for electron transfer (28) and by Taube's evidence that a bridge-activated complex may serve as an intermediate in some cases (38). Each of these stimulating contributions was qualitative (19, 31, 38) or semiempirical in nature (28).

More recently the writer has formulated a quantitative theory of electron transfers in solution (20) and at electrodes (26). It is free from arbitrary assumptions and adjustable parameters. In its present form it was devised for *simple* electron transfer reactions in which no rupture or formation of chemical bonds occurs in the transfer step.

THEORY

The basic assumption of the theory is that only a weak electronic interaction of the two reacting species is required for a simple electron transfer process to occur. The reactants may be ions or molecules and, in the electrode system, the electrode and an ion or molecule. Several deductions may be made quantum mechanically from this basic assumption:

(1) The electronic configuration and therefore the charge distribution of the activated complex are inordinately sensitive to the atomic configuration of the medium (as well as to that of the reactants). In this respect and in its consequent mode of treatment it is apparently unique among activated complexes, but it has much in common with the "polaron" (30), the F-center (30), and the "solvated electron".

(2) During the course of a reactive encounter, the atomic configuration of the entire

system gradually changes from one characteristic of the reactants to one characteristic of the products. At the same time the electronic configuration undergoes a corresponding change, following this atomic configurational change adiabatically (27).

(3) As in any reaction, the activated complex can possess one of many possible atomic configurations of positions and momenta, but in the present case the configuration must satisfy a severe energy restriction (20). In *this* atomic configuration, a hypothetical system possessing the electronic wave function (and therefore the ionic charges) of the reactants must have the same energy as that of a hypothetical system possessing the electronic wave function of the products in the same configuration.

An infinite number of atomic configurations can satisfy this energy condition, but only a group of these contribute to the macroscopic or "thermodynamic" properties of the activated complex, namely those which minimize its free energy of formation from the reactants.

In setting up an expression for the reaction rate, the atomic configuration of the system outside the co-ordination shell of each reactant was treated as forming a continuous dielectric medium (20, 26). The configuration of the co-ordination shells themselves was expressed in terms of structural properties such as bond force constants and lengths, using statistical mechanics (22). Special methods involving "nonequilibrium" electrostatic considerations were developed for solving the minimization of free-energy problem subject to the energy restriction (21, 25). The group of atomic configurations constituting the activated complex could not be in electrostatic equilibrium with both hypothetical charge distributions at the same time.

On the basis of theoretical considerations it seems appropriate to classify the reactants somewhat loosely into three groups. Class I consists of those species for which the co-ordination shell of the oxidized form has essentially the same interatomic distances as does that of the reduced form. Class II consists of those in which the bonds of one form have become slightly stretched or compressed compared with the other form. Class III consists of those in which large stretching or compression has occurred.

Examples of Class I include (35) $MnO_4^--MnO_4^{-2}$ and probably $Fe(CN)_6^{-3}-Fe(CN)_6^{-4}$. Examples of Class II include many hydrated metal cations such as $Fe(H_2O)_6^{+3}-Fe(H_2O)_6^{+2}$, and those of Class III include (3, 6) $Co(NH_3)_6^{+3}-Co(NH_3)_6^{+2}$ and $Cr(H_2O)_6^{+3}-Cr(H_2O)_6^{+2}$.

The equations given below were derived for reactants of Class I. Some modifications appropriate to the other classes are noted.

THEORETICAL EQUATIONS

Using as a reaction co-ordinate either a solvent polarization co-ordinate or a movement of either reacting ion relative to the solvent, the following relation can be deduced for both solution and electrode–electron transfer rate constants (20, 26):

[1] $$k = A' e^{-\Delta F^*/RT}$$

where ΔF^* is defined below and where A' is of the order of 10^{15} cc mole^{-1} sec^{-1} and 5×10^4 cm sec^{-1} for solution and electrode processes, respectively.* Defining the activation energy, E_a, in the usual way as $-\partial \ln k/\partial(1/RT)$ and neglecting the minor temperature dependence of A' we find:

*The exact value of A' is under current study. It depends both on the detailed nature of the reaction co-ordinate and on the value of the collision frequency of two uncharged species. Derivations of a high value (10, 20) for the bimolecular collision frequency in solution can be shown to be overestimates for the system under consideration.

[2] $$k = A\ e^{-E_a/RT}$$

where

[3] $$E_a = \Delta F^* + T\Delta S^*$$

[4] $$A = A'\ e^{\Delta S^*/RT}$$

[5] $$\Delta S^* = -\partial\Delta F^*/\partial T.$$

ΔF^* represents the change in free energy of ion–ion and ion–solvent interactions accompanying the formation of the activated complex from the reactants:

[6]

solution

$$\Delta F^* = w^* + m^2\lambda$$

[7] $$-(2m+1)\lambda = \Delta F^0 + w - w^*$$

[8]

electrode

$$\Delta F^* = w^* + m^2\lambda/2$$

[9] $$-(2m+1)\lambda/2 = -ne\eta_a + w - w^*$$

[10] $$\lambda = n^2e^2(1/a - 1/r)\ (1/D_{op} - 1/D_s).$$

The following symbols are employed in these equations:

w^*, w = Work required to bring the two reactants together and the two products together, respectively, from infinity to the positions they would occupy in the activated complex. For the electrode system, w^* and w denote the work required to transport the reactant and the product to the electrode, respectively.

m, λ = Defined by equations [7], [9], and [10].

n = Number of electrons transferred from one reactant to the other (i.e., from a reactant to the electrode, for the electrode case).

e = Unit of electronic charge.

a = Ionic radius (including region occupied by co-ordination shell). If the radii of the two ionic reactants differ, and have values a_1 and a_2, then $2/a = (1/a_1) + (1/a_2)$.

r = Interionic distance in the activated complex or, for the electrode case, twice the distance from the electrode to the center of the ion.

D_{op} = Square of the refractive index.

D_s = Static dielectric constant.

$\Delta F^\circ = -RT \ln K$, K being the equilibrium constant for the reaction at the given salt concentration. ΔF° will be called the "standard" free energy of reaction.

η_a = Activation overpotential (zero for equilibrium at the given salt concentration).

INTERPRETATION OF THE EQUATIONS

Experimentally, various properties of the electron transfer rate constants of both processes can be measured: their dependence on standard free energy or activation overpotential; their dependence on ionic structure; the extent of parallelism between both rate constants for a series of reactants; the frequency factor and activation energy; the dependence of rate constants on added salts, on the solvent medium, and on the electrode material and surface contamination. The equations will be examined with these features in mind.

The theoretical equations of the two processes are closely related. Typically in each

case, ΔF^* decreases with increasing a, decreasing ne, decreasing r, increasing D_{op}, decreasing D_s (except for the latter's effect, more important perhaps, on w^* and w), and increasingly negative $\Delta F°$ or $-ne \eta_a$. This behavior has a simple physical interpretation related to the ease with which the energy restriction discussed earlier can be satisfied (23, 24).

For example, ion–solvent interactions decrease with increasing ionic radius a, so that there would be a smaller energy difference between the two hypothetical charge distributions in the original atomic configuration of the reactants and therefore a smaller reorganization would be needed to equalize the two energies. Similarly, the smaller the charge transferred, ne, or the smaller the distance between the reactants (or between the ion and its electrostatic image in the electrode), the less the medium can discriminate energywise between the two hypothetical charge distributions and therefore the less the reorganization needed for energy equalization. A larger optical dielectric constant, D_{op}, serves to partially neutralize the electrostatic fields of the charges and therefore to reduce their energy difference for a given atomic configuration. The more D_s approaches D_{op}, the smaller the dipolar contribution to the electrical polarization of the medium and the less the necessary rearrangement of the atoms (at least for zero $\Delta F°$ or zero η_a).

The RHS of equations [7] and [9] has an interesting interpretation. The effective driving force of the reaction is not really the free energy difference ($\Delta F°$ or $-ne \eta_a$) between reactants and products when the reacting species are far apart but rather when they are in the positions they occupy in the activated complex. These quantities are simply the $\Delta F°+w-w^*$ and $-ne \eta_a+w-w^*$ of equations [7] and [9]. By lowering the free energy of the final state of the system relative to that of the initial state, these terms reduce the amount of necessary reorganization of atomic configuration of the initial state in order to satisfy the energy restriction (24).

One difference between the two sets of equations is that λ in equations [6] and [7] for the homogeneous system has become $\lambda/2$ for the electrode system. This difference can be attributed to the absence of one half of the dielectric medium in the electrode case. (Effectively, the charge is transferred from the ion to its electrostatic image, and the metal surface bisects the line drawn between the two.)

The theoretical expressions for ΔF^* and ΔS^* of Classes II and III naturally would contain additional terms. Interesting suggestions concerning these classes have been made by several groups (e.g., 1, 3, 6, 9, 14, 29).

INTERPRETATION OF THE DATA

The data will be discussed from the point of view of the various factors influencing the reaction rate.

"Standard" Free Energy Change or Activation Overpotential

The influence of this factor alone on the rate constant, holding the other factors essentially constant, is more easily investigated for the electrode process. When w and w^* are sufficiently small, it can be deduced from equations [1], [8], and [9] that the transfer coefficient—$\partial \ln k/\partial (ne \eta_a)$—is 0.5, a value found in a number of simple electron transfer processes (11, 14, 33). Complexation of the reacting species with added salt can change this coefficient (11) but equation [8] does not apply to such systems.

The quantitative effect of $\Delta F°$ on the homogeneous bimolecular rate constants has been measured experimentally for some nonspherical reactants (4, 5). While ion–solvent interactions in these systems (oxidation of hydroquinone-like compounds) were not as simple as assumed in equation [6] and an atom transfer mechanism could not be ruled out, reasonable agreement with the experimental rate constants was found (24).

Ionic Structure

The effect of ion size on the rates of homogeneous reactions is most conveniently studied using isotopic exchange reactions whose reactants merely exchange their charges, for then ΔF° and $w^* - w$ are both zero, and m of equation [6] is simply $\frac{1}{2}$. The factor of ion size has been extensively investigated by Wahl and co-workers (8, 35, 39, 40). The rates of large ions, probably of Class I, were found to be much larger than those of the smaller ions, $MnO_4^{-1,-2}$ and $Fe(CN)_6^{-3,-4}$. Again, the latter two systems had comparable rates in spite of the greater Coulombic repulsion in the second case, perhaps because of the larger size of the iron cyanide ion (4.5 vs. 2.9 Å). Rather good agreement was obtained between experimental and calculated rate constants using the theoretical equations, taking into consideration the absence of adjustable parameters (16).

The cobalt–nitrogen bonded complexes probably are members of Class III (3, 6) and the rates are therefore extremely slow. The marked increase in rate (3, 18) in the sequence $Co(NH_3)_6^{+3,+2}$, $Co(en)_3^{+3,+2}$, and $Co(phen)_3^{+3,+2}$ may be partly a reflection of increasing ionic size, and partly a reflection of ligand field (29) effects.

The ferrous–ferric system is probably of Class II, and its rate (36) is correspondingly much less than that of the MnO_4^- or $Fe(CN)_6^{-3}$ systems. Nevertheless, its rate greatly exceeds that (1) of $Cr(H_2O)_6^{+3,+2}$, a probable member of Class III (3). Reasonable agreement between calculated and experimental results for the $Fe(H_2O)_6^{+3,+2}$ was found by adapting the theory to Class II reactants (22). Thus far, there is no experimental evidence which definitely establishes either an electron or an atom transfer mechanism for these homogeneous isotopic exchange reactions of hydrated cations. The general parallelism of various rates in the two processes discussed below suggests, however, a common electron transfer mechanism.

Parallelism Between Rates in Solution and at Electrodes

When similar mechanisms are operative, the theoretical equations suggest a close parallelism between the rates of the two processes, particularly when ΔF° and η_a are zero and the work terms are small. The parallelism becomes very close, therefore, when the rates of isotopic exchange reactions are compared with the corresponding electrochemical exchange currents.

The distance of closest approach for the electrode case will depend on the surface contamination and on the strength of metal–solvent binding. Let us write, therefore, $r = 2a + 2b$ for this system and $r = 2a$ for the homogeneous system. When the work terms are negligible, we obtain

[11] $$\Delta F^*{}_{\text{solution}} = \lambda_s^2/4, \quad \Delta F^*{}_{\text{electrode}} = \lambda_e^2/8$$

where

[12] $$\lambda_e/\lambda_s = (1 + 2b/a)/(1 + b/a).$$

The chemical and electrochemical electron transfer rates of the systems (3, 32, 36, 39) $Cr(H_2O)_6^{+3,+2}$, $Fe(H_2O)_6^{+3,+2}$, and $Fe(CN)_6^{-3,-4}$ both increase in the order given as do those of the systems (15, 16, 18) $Co(NH_3)_6^{+3,+2}$ and $Co(en)_3^{+3,+2}$. The absolute rates of various electrochemical processes (32) are in the general range expected from the values of the chemical rate constants, but further work is desirable, both theoretically on Class II and Class III systems as well as experimentally on salt effects and hydrolysis effects.

Frequency Factor and Activation Energy

While some application (24) of the theory has been made to the hydroquinone oxidations referred to earlier, the frequency factors, A, of the simpler isotopic exchange

reactions have been much more revealing. For the latter systems, ΔF^* equals $w^* + \lambda/4$. Correspondingly, ΔS^* is the sum of two terms. The first, $-\partial w^*/\partial T$, is the usual entropy change which results when two ions are brought together. The second, $-(d\lambda/dT)/4$, is the entropy of formation of the "nonequilibrium" atomic configurations from the equilibrium ones at the same r in order to satisfy the energy restriction. Its value may be computed from equation [10]. It proves to be very small for reactants of Class I.

Application of the theoretical equations to Class I reactants by the writer led to good agreement between experimental and calculated frequency factors for the $MnO_4^{-1,-2}$ system and (within a factor of 50) for the $Fe(CN)_6^{-3,-4}$ system, the latter system having an extremely small frequency factor (40).† These results suggest that the probability of adiabatic reaction may be of the order of unity, at least for these systems. The frequency factors of Class I reactants provide the most direct measure of this probability factor.

Many of the hydrated metal cations, which are mainly of Class II, tend to hydrolyze and form other complexes easily. In a careful investigation Silverman and Dodson (36) unravelled the rate constant of the $Fe^{+3,+2}$ system from those involving $FeOH^{+2}$ and others. The frequency factor was very small. If $-\partial w^*/\partial T$ is fairly small at the high ionic strengths (high acidity) needed to minimize hydrolysis, this low A-value indicates an additional negative contribution to ΔS^*.

Recently, Baker, Basolo, and Neumann (3) have reported a most interesting result of a very high frequency factor, 5×10^{16} cc mole^{-1} sec^{-1}, for a Class III system, $Co(phen)_3^{+3,+2}$. One simple extension of the present theory for Class I systems to those of Class III can provide an explanation of this possible behavior if the following reaction has an appreciably positive entropy change:

$$Co(phen)_3^{+3} + M(phen)_3^{+2} = Co(phen)_3^{+2} + M(phen)_3^{+3},$$

where $M(phen)_3^{+2}$ is some reactant of Class I or II, such as $Fe(phen)_3^{+2}$. No entropy data appear to have been reported for this process. A similarly high frequency factor has been reported for another Class III system (2a), $Cr(H_2O)_6^{+3,+2}$, but this reaction may be complicated by hydrolysis effects.

The frequency factors of the electrochemical systems have not been measured in the same detail. However, in a recent study, Randles and Somerton (32) found them to be typically in the range 3×10^2 to 3×10^4 cm sec^{-1}. The reactants were primarily hydrated metal cations and so were mostly of Class II. In one system, $Cr(CN)_6^{-3,-4}$, a rather low frequency factor (10 cm sec^{-1}) was found. The electrostatic repulsion between ion and electrode was estimated to be large for this system, and the low A-value was attributed to a small transition probability factor because of the increased r. However, we see from equation [10] that there is also an image term present. This term would tend to favor small r's. An alternative explanation for the A-value could be given on the basis of the usual sign of $-\partial w^*/\partial T$. When two reactants of like sign approach each other, the enhanced electrostatic field polarizes the solvent more strongly and causes a negative ΔS^*. A different region for testing the appropriateness of assuming simple Coulombic interactions and their consequent effects on ΔS^* is suggested in the concluding section.

Activation energies for several electrochemical electron transfers have been measured (32). While these results cannot be precisely compared with those of the isotopic exchange reactions (36, 40), partly because there was no detailed examination of hydrolysis and

†*The data were extrapolated to infinite dilution, taking cognizance of the comparative insensitivity of the theoretical activation energy to salt effects.*

salt effects, the results tentatively indicate the activation energies of the electrode reactions to be more than one-half those of the corresponding exchange processes. Should this result prove to be generally true (at least for Class I and Class II reactants) one possible interpretation would be that the distance between the ion in the activated complex and its electrical image exceeds twice the ionic radius (cf. equations [10] and [11]). An independent, approximate estimate of this distance may be obtainable from an experiment suggested in the concluding section.

Salt Effects

Using a rough model for ionic interactions the w and w^* terms were calculated by the writer for several Class I reactions and compared with the data of Wahl and co-workers (35, 40). Fair agreement was obtained using no adjustable parameters.

No detailed study of salt effects for simple electron transfers at electrodes appears to have been reported. Therefore it is not yet possible to adequately test the usual assumption (one not made here) that the work required to transport an ion from the body of the solution to the electrode, w^* or w, equals the ionic charge multiplied by the difference of potential at the initial and final positions of the ion, these potentials being computed in the absence of the ion. This assumption is clearly valid when the ionic charge is so small that it does not perturb the configuration of the remaining ions. It is also clearly invalid at the point of zero electrode charge. At this point, the work term estimated on the basis of the above assumption is zero, whereas it actually equals the free energy of interaction of the ion with the image. For infinite dilution, the latter term is $-q^2/2D_s r$, q being the ionic charge, while for dilute salt solutions, an approximate (unpublished) estimate of it is $(-q^2/2D_s r) \exp(-\kappa r)$, κ being the usual Debye κ.

Solvent Effects

Solvent effects for simple electron transfers will occur, according to the theory, whenever there is a change in dielectric constant, refractive index, ionic radius, or standard free energy of reaction. Changes in composition of the co-ordination shell, which may include the solvent, naturally alter a, $\Delta F°$, and the ease of intramolecular compression or stretching. In addition, there are effects which were not incorporated in the theory, effects such as changes in ion-pairing, selective solvation of solvent mixtures, and a change of the mechanism itself. A possible example of selective solvation (7) has been described (2).

Heavy water has been used as a solvent in several studies (e.g., 13, 37). Hudis and Dodson (13) have demonstrated the importance, when hydrolyzed species and other complexes are present, of determining the various equilibrium constants so that meaningful electron transfer rate constants for the different species can be obtained and solvent effects evaluated. The rate constant for $Fe^{+3,+2}$ was smaller by a factor of 2 in D_2O (13), while that of $NpO_2^{+2,+1}$ was smaller by a somewhat smaller factor (37). A qualitative interpretation of the solvent effects can be given in terms of atom transfer (13, 37) or electron transfer (23) theories. Thus far, however, comparative studies in the two solvents do not permit either mechanism to be distinguished from the other. This situation results from the fact that ions have different solvation energies in the two media (17), so that water does not behave as an inert solvent.

The rate of the $Co(NH_3)_6^{+3,+2}$ reaction appears to be faster in liquid ammonia (12) than in water, where it was immeasurably slow (18). The activation energy was high, being in the range found for two other Class III compounds (2a, 3). Possible explanations

for the solvent effect include a change of mechanism, such as a dissociation (12) or possibly a hydrolyzed intermediate, $Co(NH_3)_5NH_2^{+2}$. However, the effect of pH on the reaction rate is not known.

Effects of Electrode Material

A dependence of rate constant on electrode material will occur if there is any change in surface contamination (32) and possible metal–solvent binding, or if electrode charge density at a given η_a changes sufficiently to alter w^* or w. The rate constants measured for one system with several solid electrodes underwent no great variation (within a factor of 10) but were much smaller than that found for a mercury electrode (32).

The Image Force Law and Its Implications

The role of the electrostatic image has been generally ignored in electrochemical theories. A recent investigation (34) of the quantum limitations of the image force law for a vacuum is reassuring. It has been applied by the writer to dielectric media and to electrochemical theory.

The effect of this image is to partially neutralize the field of the ion and to reduce, thereby, the configurational rearrangement free energy needed to satisfy the energy restriction. It is noteworthy that its calculated effect remains, even at salt concentrations sufficiently large as to make w^* and w negligible. This is because it is impossible for the ionic atmosphere in the activated complex to neutralize the ion–image interactions of the two different hypothetical charge distributions at the same time. A compromise configuration results. A similar behavior exists in the homogeneous case, where the $1/r$ term remains even if w^* and w are zero.

At the point of zero electrode charge there is a net, shielded Coulombic attraction between the ion and its image, which is quite large for very dilute solutions. According to the theory a positive ΔS^* would result, since the attraction lowers the entropy of the solvation. A measurement of the frequency factor in this region would permit a determination of this ΔS^*.

If this prediction is verified for Class I reactants, it will be interesting to compare ΔS^* with the theoretical estimates.

ACKNOWLEDGMENTS

REFERENCES

1. ADAMSON, A. W. and VORRES, K. S.   J. Inorg. & Nuclear Chem. **3**, 206 (1956).
2. AMIS, E. S.   J. Chem. Phys. **26**, 880 (1957).
2a. ANDERSON, A. and BONNER, N. A.   J. Am. Chem. Soc. **78**, 3826 (1954).
3. BAKER, B. R., BASOLO, F., and NEUMANN, H. M.   Paper presented at the Symposium on Mechanisms of Inorganic Reactions in Solution. Northwestern University, Chicago, Ill. 1958.
4. BAXENDALE, J. H. and HARDY, H. R.   Trans. Faraday Soc. **50**, 808 (1954).
5. BAXENDALE, J. H. and LEWIN, S.   Trans. Faraday Soc. **42**, 126 (1946).
6. BROWN, H. C.   J. Phys. Chem. **56**, 868 (1952).
7. COHEN, D., SULLIVAN, J. C., AMIS, E. S., and HINDMAN, J. C.   J. Am. Chem. Soc. **78**, 1543 (1956).
8. EICHLER, E. and WAHL, A. C.   Private communication.
9. FRIEDMAN, H. L., HUNT, J. P., PLANE, R. A., and TAUBE, H.   J. Am. Chem. Soc. **73**, 4028 (1951).
10. FROST, A. A. and PEARSON, R. G.   Kinetics and mechanism. John Wiley & Sons. Inc., New York. 1953. p. 118.
11. GERISCHER, H.   Z. Elektrochem. **54**, 366 (1950).
12. GROSSMAN, J. J. and GARNER, C. S.   J. Chem. Phys. **28**, 268 (1958).
13. HUDIS, J. and DODSON, R. W.   J. Am. Chem. Soc. **78**, 1911 (1956).
14. HUSH, N. S.   J. Chem. Phys. **28**, 962 (1958).
15. LAITINEN, H. A. and GRIEB, M. W.   J. Am. Chem. Soc. **77**, 5201 (1954).

16. LAITINEN, H. A. and KIVALO, P.   J. Am. Chem. Soc. **75**, 2198 (1953).
17. LANGE, E. and MARTIN, J.   Z. Elektrochem. **42**, 662 (1936).
18. LEWIS, W. B., CORYELL, C. D., and IRVINE, J. W.   J. Chem. Soc., Suppl. Issue, **2**, S386 (1949).
19. LIBBY, W. F.   J. Phys. Chem. **56**, 863 (1952).
20. MARCUS, R. A.   J. Chem. Phys. **24**, 966 (1956).
21. MARCUS, R. A.   J. Chem. Phys. **24**, 979 (1956).
22. MARCUS, R. A.   Paper presented at the Southeast Chemical Conference, American Chemical Society, Memphis, Tenn. 1956; cf. Trans. N.Y. Acad. Sci. **19**, 423 (1957).
23. MARCUS, R. A.   J. Chem. Phys. **26**, 867 (1957).
24. MARCUS, R. A.   J. Chem. Phys. **26**, 872 (1957).
25. MARCUS, R. A.   O.N.R. Technical Report No. 11, Project NR-051-331 (1957).
26. MARCUS, R. A.   O.N.R. Technical Report No. 12, Project NR-051-331 (1957). Paper presented at 132nd National Meeting of the American Chemical Society, New York City, N.Y. 1957.
27. MARCUS, R. A.   Unpublished lectures. 1957.
28. MARCUS, R. J., ZWOLINSKI, B. J., and EYRING, H.   J. Phys. Chem. **58**, 432 (1952).
29. ORGEL, L. E.   Report to X⁰ Inst. intern. Chim. Solvay, Conseil chim. 289 (1956).
30. PEKAR, S. I.   Untersuchungen über die Elektronentheorie der Kristalle, Akademische Verlagsgesellschaft M.B.H., Berlin. 1953.
31. RANDLES, J. E. B.   Trans. Faraday Soc. **48**, 828 (1952).
32. RANDLES, J. E. B. and SOMERTON, K. W.   Trans. Faraday Soc. **48**, 937 (1952).
33. RUBIN, H. and COLLINS, F. C.   J. Phys. Chem. **58**, 958 (1954).
34. SACHS, R. G. and DEXTER, D. L.   J. Appl. Phys. **21**, 1304 (1950).
35. SHEPPARD, J. C. and WAHL, A. C.   J. Am. Chem. Soc. **79**, 1020 (1957).
36. SILVERMAN, J. and DODSON, R. W.   J. Phys. Chem. **56**, 846 (1952).
37. SULLIVAN, J. C., COHEN, D., and HINDMAN, J. C.   J. Am. Chem. Soc. **79**, 3672 (1957).
38. TAUBE, H. and MYERS, H.   J. Am. Chem. Soc. **76**, 2103 (1954).
39. WAHL, A. C. and DECK, C. P.   J. Am. Chem. Soc. **76**, 4054 (1954).
40. WAHL, A. C.   Private communication.

ON THE EQUIVALENT REDOX POTENTIAL OF AQUEOUS SOLUTIONS UNDER IONIZING RADIATION[1]

I. H. S. HENDERSON, E. G. LOVERING, R. L. HAINES, AND E. J. CASEY

ABSTRACT

A study of the electrochemical behavior of aqueous solutions irradiated by Co^{60} γ- and 50–300-kv X-rays is being carried out. Results are presented which show that aqueous solutions of various electrolytes over a pH range of 0.0 to 14.0 attain a steady-state potential under irradiation.

This steady-state potential, whose existence was postulated by Dainton and Collinson (who called it the equivalent redox potential), has been determined to be −0.85 v with respect to a hydrogen electrode in the same solution. This value is a property of water and is independent of pH, solute, temperature and radiation energy, and intensity within the ranges investigated.

Electrodes under irradiation sometimes show potentials different from the potential of the bulk electrolyte. This is considered to be a result of selective adsorption of one or more primary or secondary radiation products. These transient phenomena depend upon source intensity and solute concentration and disappear when irradiation is stopped.

INTRODUCTION

There is much indirect evidence that among the primary products formed during gamma- or X-irradiation of water and aqueous solutions are hydrogen atoms and hydroxyl radicals. These species undergo further reaction to produce hydrogen molecules and hydrogen peroxide as well as oxidation or reduction products which are characteristic of the solute. Ions such as ceric, iodate, nitrate, and permanganate are reduced; while others, such as ferrous, iodide, nitrite, sulphite, and oxalate are oxidized. Allen (1) suggested that prolonged irradiation should lead ultimately to an equilibrium concentration ratio of a redox system. This idea was further developed by Dainton and Collinson (2), who proposed in 1950 that a solution under irradiation attained an equivalent redox potential (ERP) when the rate of oxidation equalled the rate of reduction in the solution. This ERP was assumed to be a characteristic of the solvent and hence independent of the nature and, within limits, the amount of solute. From a consideration of the normal electrode potentials of a number of systems whose behavior under irradiation had been investigated, Dainton and Collinson estimated the ERP for X-, γ-, and α-irradiation to be in the neighborhood of −0.95 v, and that increasing acidity displaced the ERP to even more negative values and that there was an increasing tendency toward oxidation in acid media. These authors argued further that, since on thermodynamic grounds the potential expected from an equimolar solution of H and OH would be somewhat positive, there was a possibility that the highly oxidizing species OH^+ was also present. Its fate was suggested to be $OH^+ + OH^- = H_2O_2$. (Hydrogen molecule ions may also be present as secondary intermediate products.) The effect of oxygen on the ERP was not considered in detail, but from work of Amphlett (3) on ferrous o-phenothroline they suggested (2) that the effect of oxygen, and hence HO_2, on the ERP was small.

A survey of the literature reveals that there have been few attempts to follow the course of radiation-induced chemical reactions by measurement of the potential changes in solution during and after irradiation. Veselovsky (4) has reviewed some of his own and other Russian work in this field, and has concluded that the concept of the equivalent

redox potential was invalid because it ignored the kinetic behavior of electrochemical processes determining the steady-state potentials of the solution. His argument was based essentially on the observations that (a) platinum electrodes in γ-irradiated aqueous solutions of sulphuric acid, particularly in the presence of oxalate, showed a potential corresponding to that of the hydrogen electrode and (b) that electrodes such as a silver electrode in oxygen-saturated solution showed potentials approaching that of the oxygen electrode and in oxygen-free solutions showed a potential from 0.5 to 0.6 v more noble than a hydrogen electrode in the same solution. Under his conditions, the steady-state potentials measured were those due to individual radical species in the presence of excess oxidizing or reducing agent, and hence these observations have no direct bearing on the Dainton–Collinson ERP concept, which referred to the steady state obtained when the rates of oxidation and reduction processes in the bulk solution were equal.

Mendvedovsky et al. (5) used platinum electrodes in irradiated solutions of 0.8 N sulphuric acid containing ferrous and ferric sulphates to follow potential changes in the solution. Ferrous sulphate was oxidized during irradiation until the ratio of ferrous sulphate to ferric sulphate was steady at approximately 0.02. Similar results were obtained in perchloric acid solution and it was concluded that the potential measured was a property only of the final ratio of ferric ion to ferrous ion, and not a direct effect of radiation on the electrodes.

In a recent technical note, Clark (6) has reported the effect of Co^{60} γ-irradiation on the potential behavior of platinum and stainless steel electrodes in 0.1 N sulphuric acid under atmospheres of hydrogen, nitrogen, and air. Measurements were made at 85° C using Ag/Ag_2SO_4 reference electrodes. Under irradiation, the Pt electrode potential rapidly approached the hydrogen potential. When irradiation was interrupted, the potential decreased to −0.85 v with respect to the hydrogen electrode. In an experiment carried out under hydrogen, a trace of potassium bromide was added to the electrolyte. The electrode continued to show the hydrogen potential until the hydrogen flow was interrupted, after which the potential of the solution decreased to approximately −0.78 v with respect to the hydrogen electrode in the same solution. When irradiation was discontinued, the potential decreased further to at least −0.82 v.

Because of the apparent uncertainty (3) concerning the existence and the properties of the ERP, it was decided that part of our study of the electrochemical properties of aqueous solutions under irradiation should include an investigation of this concept.

EXPERIMENTAL METHOD

Glass cells containing test solutions were irradiated using a 300-curie Co^{60} source at a distance of approximately 20 cm, or using a 50- to 300-kv, 3-kw X-ray machine. The maximum energies absorbed were approximately 6×10^{13} ev cm^{-3} sec^{-1} and 6×10^{14} ev cm^{-3} sec^{-1} respectively. Each cell had appropriate electrode assemblies so that the potential of the solution could be followed during irradiation.

Potentials were measured using a General Radio type 1230A Electrometer-Amplifier with input resistance settings of 10^{10} ohms or higher.

The solutions were made up using conductivity water and reagent grade chemicals. The acid used was redistilled reagent grade sulphuric acid. Supporting electrolyte solutions for certain experiments were pre-electrolyzed under an argon atmosphere after being placed in the cells. A small weighed amount of "redox indicator" reagent was added directly to the electrolyte in the test flasks. The materials used for this purpose were potassium iodide, potassium iodate, iron, thallium, and cerous sulphate at concentrations of 10^{-4} to 10^{-3} molar.

Argon was deoxygenated by passage over Cu at 700° C and Ti at 800–900° C in a purification train. Stirring was achieved either by magnetic stirrers rotated at about 300 r.p.m., or by vibrating stirrers operated by 60 cycle a-c. Irradiations were carried out at room temperature.

Figure 1 is the photograph of a 100-ml cell which was a round bottom flask having a number of ground glass outlets through which were inserted reference electrodes, polarizing electrodes, and gas inlet tubes. The internal indicator electrode was a piece of Pt gauze, and the external reference was Hg/Hg_2SO_4 for cells containing sulphuric acid as supporting electrolyte, $Pb/PbSO_4$ for cells containing sodium sulphate with pH < 10, and Hg/HgO for solutions with pH > 10. The reference electrodes were connected to the cell solutions by salt bridges filled with supporting electrolyte of the same concentration as in the reference electrode and cell. The data of Hamer (7) and Harned and Hamer (8) were used to determine the potentials of the Hg/Hg_2SO_4 and $Pb/PbSO_4$
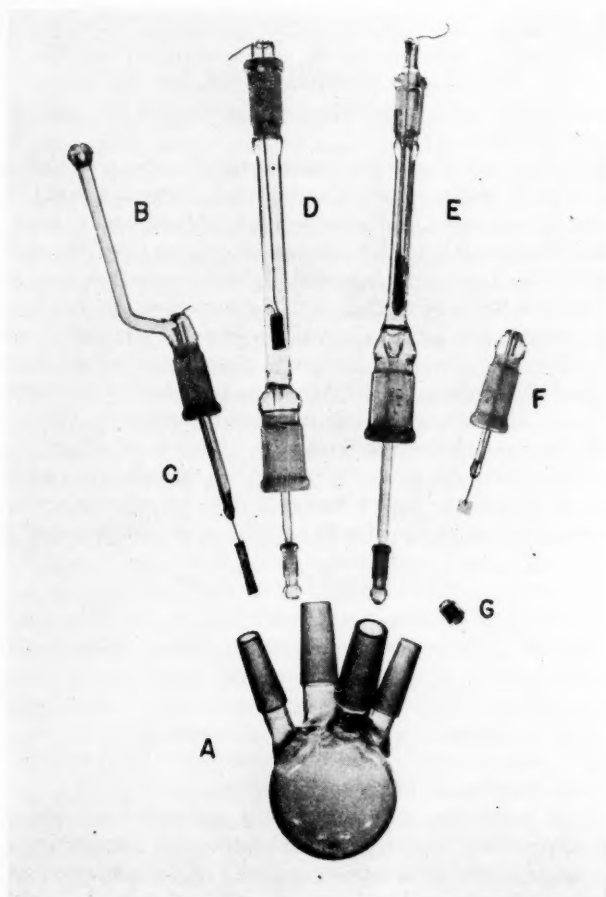
FIG. 1. Photograph of cell. A—100-ml cell; B—argon inlet; C—internal polarizing electrode; D—external polarizing electrode; E—reference electrode (Hg/Hg_2SO_4); F—internal reference electrode (Pt); G—magnetic stirring bar.

electrodes, and that of Akerlof and Bender (10) for the Hg/HgO electrode in alkaline solutions. The potential of each electrode was checked periodically against a hydrogen electrode in the same solution.

<div align="center">RESULTS AND DISCUSSION</div>

The Steady State ERP

Under the experimental conditions of the present work, radiation had no effect on the reference electrodes, probably because (*a*) the concentration changes brought about by irradiation were small by comparison with the amount of redox material in the reference electrodes, and (*b*) the reference electrodes were exposed to radiation of much lower intensity than that experienced by the test cells.

The iodine redox indicator system in sulphuric acid, sodium sulphate, and potassium hydroxide was found to be the most convenient in the present work over the pH range investigated because of the absence of insoluble products at high pH.

In general, each electrolyte when irradiated showed a definite and reproducible potential, whose value (referred to the normal hydrogen electrode) was to a first approximation a function only of the hydrogen ion activity of the electrolyte, and was independent of the supporting electrolyte and indicator redox system. However, in several cases to be discussed later, transient potential behavior occurred during the first few minutes of the irradiation or after irradiation was stopped. In the iodine-containing electrolytes these transients were found to be the smallest. They were absent at high pH, but were present at low pH in sufficient degree to introduce an uncertainty of ± 0.03 v in the values of the ERP.

Table I gives the final steady-state values obtained during irradiation of several
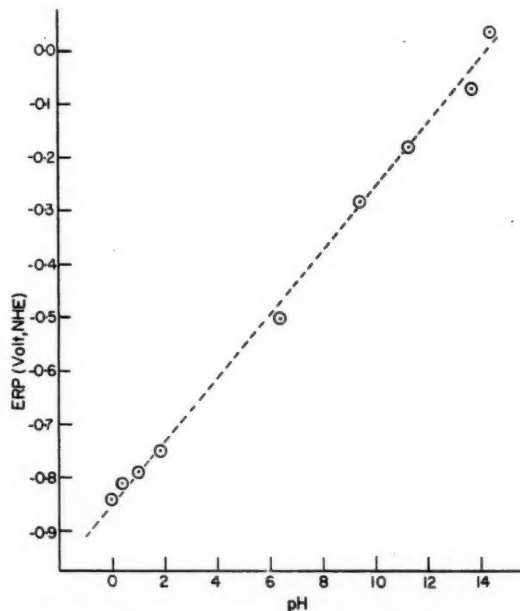
FIG. 2. Plot of equivalent redox potential referred to normal hydrogen electrode vs. pH. Slope of line 0.059 v/pH unit.

TABLE I

Equivalent redox potential of several electrolytes under ionizing X-radiation

Solution No.	Indicator conc., moles/liter	Carrier electrolyte and conc.	Reference type	ERP vs. ref.* (measured)	pH (measured)	ERP vs. H_2†	ERP vs. NHE (calc.)
1	$KI(10^{-4}\ M)$	$H_2SO_4(1.0\ M)$	Hg/Hg_2SO_4	-0.17	-0.13	-0.84	-0.84
2	$Ce_2(SO_4)_3(10^{-3}\ M)$	$H_2SO_4(0.5\ M)$	Hg/Hg_2SO_4	-0.14	0.37	-0.83	-0.81
3	$Tl(10^{-4}\ M)$	$H_2SO_4(0.5\ M)$	Hg/Hg_2SO_4	-0.17	0.37	-0.86	-0.84
4	None added	$H_2SO_4(0.4\ M)$	Hg/Hg_2SO_4	-0.14	0.50	-0.83	-0.81
5	$Fe(5\times10^{-4}\ M)$	$H_2SO_4(0.4\ M)$	Hg/Hg_2SO_4	-0.18	0.50	-0.87	-0.85
6	$KI(10^{-3}\ M)$	$H_2SO_4(0.4\ M)$	Hg/Hg_2SO_4	-0.14	0.50	-0.87	-0.81
7	$As_2O_3(10^{-3}\ M)$	$H_2SO_4(0.4\ M)$	Hg/Hg_2SO_4	-0.14	0.50	-0.83	-0.81
8	$KIO_3(6\times10^{-4}\ M)$	$H_2SO_4(0.1\ M)$	$Pb/PbSO_4$	-1.09	0.90	-0.85	-0.81
9	$KI(2.5\times10^{-4}\ M)$	$H_2SO_4(0.1\ M)$	Hg/Hg_2SO_4	-0.09	0.90	-0.85	-0.77
10	$KI(5\times10^{-4}\ M)$	$H_2SO_4(0.01\ M)$	Hg/Hg_2SO_4	-0.07	2.09	-0.86	-0.75
11	$KI(5\times10^{-4}\ M)$	$KCl(0.2\ M$ with Na-K-phosphates	H_2/H^+	-0.876	6.4	-0.876	-0.50
12	$KI(5\times10^{-4}\ M)$	$Na_2SO_4(1.0\ M)$	$Pb/PbSO_4$	-0.63	9.47	-0.84	-0.28
13	$KI(8\times10^{-4}\ M)$	$Na_2SO_4(0.01\ M)$	$Pb/PbSO_4$	-0.48	11.35	-0.85	-0.18
14	$Ce_2(SO_4)_3(10^{-4}\ M)$	$KOH(1.0\ M)$	Hg/HgO	-0.03	13.9	-0.89	-0.065
15	$KI(10^{-4}\ M)$	$NaOH(1.4\ M)$	H_2/H^+	-0.879		-0.879	
16	$KI(5\times10^{-4}\ M)$	$HC_2H_3O_2(0.2\ M)$	$Hg/Hg_2(C_2H_3O_2)_2$		Extensive transients		No steady value
17	$Fe(10^{-3}\ M)$	$HNO_3(1.0\ M)$	H_2/H^+		No steady value		

*Minus signs are used when ERP is the more noble electrode.

†Hydrogen electrode in the same solution.

electrolytes. The values for solutions containing iodine and iron are listed as measured; thallium, cerium, and pure acid values listed have been corrected for transient potential behavior. The mean values at each pH are plotted in Fig. 2 as ERP (referred to the normal hydrogen electrode, NHE) vs. pH with a line of calculated slope 0.059 drawn through the points. Hence, the value of the ERP was consistently 0.85 v more noble than the hydrogen electrode in the same solution or 0.38 v less noble than the oxygen electrode.

The steady-state values were found to be independent of the intensity and maximum energy of the radiation within the limits of the available equipment.

The Approach to the ERP

The steady-state potentials obtained in these experiments were attained after a period of irradiation which varied with (a) redox indicator concentration, (b) source intensity, and (c) the number of coulombs by which the system had been oxidized or reduced away from the ERP prior to irradiation.

Figure 3, a plot of potential vs. time for iodine in 1.0 M sulphuric acid, shows the typical behavior of solutions in approaching the steady-state value. In the example shown, the solution was reduced with respect to the ERP before irradiation began. The effect of the radiation was to oxidize the solution to a potential of -0.84 v. The value remained constant when the irradiation was stopped, as shown by the regions labelled "open-circuit". After the solution had been oxidized with respect to the ERP by passage of current, irradiation reduced the solution until it again showed a potential of -0.84 v.

The redox reactions taking place as the system approached the ERP were followed by continuous measurement of potential during the irradiation, but the experimental conditions reported here were not conducive to a straightforward analysis of the reaction kinetics. The type of curve obtained for E vs. time was a function of redox indicator concentration, the standard electrode potential of the redox system, and the intensity
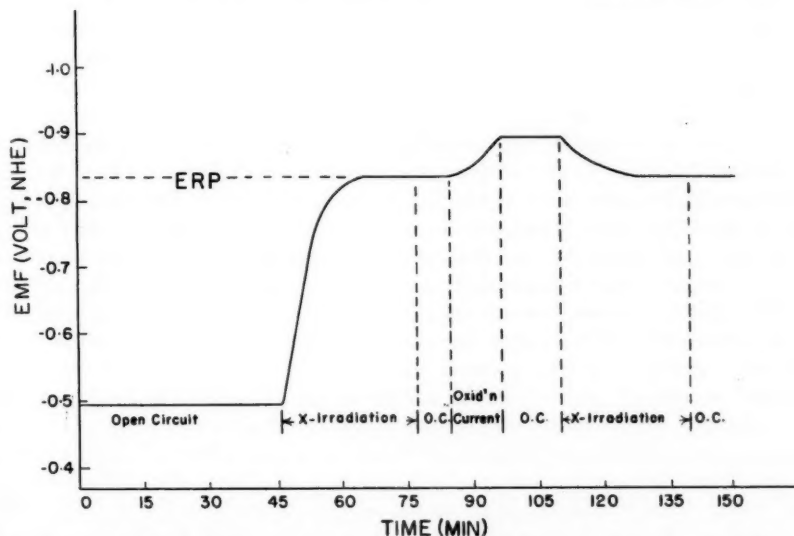
FIG. 3.   Potential vs. time curve showing approach to steady state during irradiation for solution (i) reduced and (ii) oxidized with respect to the steady-state value.

and energy of the radiation. The presence of trace impurities such as oxygen had a marked effect on the shape of the potential–time curves. The same steady-state value (within ± 0.005 v for a given solution) was reached whether the solution had been previously oxidized or reduced with respect to the steady-state value, and the potential remained constant for a period of minutes to hours after irradiation ceased. In this respect the results differed from those of Clark (6). However, ERP's estimated from his results at 85° are in good agreement with the present results at 25° C. This indicates that there is no marked temperature coefficient for the ERP, a result consistent with the behavior of free radical reactions.

The potentials listed in Table I as ERP values were not characteristic of the electrode metal under irradiation. In general, the potentials shown by the electrode when a steady state had been attained during irradiation did not change on interruption of the irradiation, and fresh Pt or Au electrodes inserted into the cell after irradiation showed the same potentials as the irradiated electrodes. In one experiment, carried out in potassium hydroxide solution, in which cerium oxides were deposited on a nickel electrode, both the nickel electrode and a platinum electrode in the same solution attained the same steady-state potential. It appeared that prolonged irradiation of platinum electrodes in sulphuric acid solution made the electrode more noble by as much as 0.03 v with respect to a fresh platinum electrode. This effect was not reproducible. Whenever it was observed, the ERP value was taken as the potential shown by fresh electrodes, since the irradiated electrodes after a cleaning in hot concentrated nitric acid solution and flaming to yellow heat showed the same potential as did the fresh electrodes. (This could not be attributed to an overvoltage effect on the electrodes because for all measurements the input resistance of the electrometer was at least 10^{10} ohms, whereas polarization was not observed unless the electrometer input resistance was less than 10^7 ohms.)

Transient Phenomena

With carefully pre-electrolyzed and deoxygenated strong acids containing iodide, a change in the potential of the indicator electrode to a value different from that of the bulk electrolyte was observed when irradiation began. Upon cessation of irradiation the potential quickly (within 3 minutes) assumed the potential of the electrolyte. This phenomenon could be attributed to the preferential adsorption of hydrogen atoms on the platinum electrode which made the electrode show a potential more "hydrogen-like" than the potential of the solution during irradiation. This effect, which was reproducible, was more pronounced with greater source intensities and in the absence of solutes with which hydrogen atoms could react before becoming adsorbed on the electrode. It is interesting to note that, since oxygen is an effective trap for hydrogen atoms via the formation of HO_2, the effect was not observed unless great care was taken to exclude oxygen, or at least until sufficient energy had been absorbed by the solutions to remove oxygen as HO_2. The transient potential behavior observed by Clark (6), obtained with much higher γ-intensities than used in the present work, could also be interpreted as due to hydrogen atom or hydrogen molecule adsorption, even in experiments carried out in cells exposed to the air, since it is probable that the radiation intensity was high enough for hydrogen atoms to remove oxygen from the system as HO_2 more rapidly than oxygen could redissolve in the solution. When there was sufficient oxygen present to react with all the hydrogen atoms during irradiation, platinum electrodes showed a transient potential a few millivolts more noble than that of the solution. This effect was attributable in part to the action of HO_2 radicals on the electrode, and confirms an observation made by Veselovsky.

In the present work, the indicator ions were usually present in sufficient concentration to be potential determining at and near the ERP; that is, the hydrogen or hydrogen atom concentration was not great enough to produce a direct effect on the potential of the platinum electrode. Attempts to measure the ERP of ultrapure water or sulphuric acid would be expected to show transient potentials during irradiation, even though irradiation leads to a steady-state hydrogen peroxide concentration (9), because of the relatively large adsorbability of hydrogen atoms on the platinum surface. Thus Zalkind *et al.* (11), during irradiation of oxygen-free solutions of acid and alkali, have observed potentials as high as 0.95 v between platinum and gold electrodes in the same solution. The effect was attributed to the selective adsorption of hydrogen on platinum and hydroxyl radicals on gold.

General Considerations

The relationship between ERP and the hydrogen and oxygen electrodes indicates that this potential is a characteristic of water and its hydrogen ion concentration only, and is not affected by source intensity or energy. Thus the results of the present investigation are in general agreement with the theory proposed by Dainton and Collinson, and demonstrate its essential correctness, although their estimated value for the ERP (-0.95 v) is more noble by about 0.1 v than the experimental value reported here. In agreement with Dainton and Collinson, it is not anticipated that the ERP of solutions exposed to α- or β-radiation would be very different from the value observed for γ- and X-radiation. However, if α- and β-emitters were present in the solution during measurement, it is expected that the very high local radical density produced would give rise to even larger transient effects than those observed with γ- and X-rays.

The ERP may be expected to change from the value of -0.85 v reported here when the activity of the water is appreciably decreased. In this case the ERP would be a function of the solute and its concentration. The ERP may also be expected to be a function of the ratio of the volume of solution to the area of catalytic surface for combination of radicals, since this would interfere with the steady-state radical concentrations (cf. ref. 4 concerning production of hydrogen peroxide during irradiation of suspensions of zinc oxide).

Veselovsky has pointed out that the application of electrochemical techniques can be a useful tool in the study of a number of problems in radiation chemistry. As an example of this, he has estimated the influence of oxalate on the rate of production of hydrogen atoms (the "G" value) during irradiation of aqueous sulphuric acid. The results which have been obtained in the present work indicate that solvent and solute effects on both the "G" values for primary and secondary products and on the ERP, as well as the influence of radiation on solids (electrodes) in contact with aqueous solution, may also be investigated electrochemically. The major advantage of these techniques over other kinetic methods employed in radiation chemistry is that they permit the investigator to follow and to monitor continuously the chemical changes taking place during irradiation.

REFERENCES

1. ALLEN, A. O. J. Phys. & Colloid Chem. **52**, 479 (1948).
2. DAINTON, F. S. and COLLINSON, E. Ann. Rev. Phys. Chem. **2**, 99 (1951).
3. AMPHLETT, C. B. Nature, **165**, 977 (1950); **171**, 690 (1953); Trans. Faraday Soc., Radiation Chem. 144 (1952).
4. VESELOVSKY, V. I. Proc. Intern. Conf. Peaceful Uses Atomic Energy, Geneva, **7**, 599 (1956). ZALKIND, Ts.I. and VESELOVSKY, V.I. Sbornik Rabot Radiatsionnoi Khim, Akad. Nauk, S.S.S.R. 66 (1955).
5. MENDVEDOVSKY, V. I., BAKH, N. A., and ZHURAVSKAYA, E. V. Sbornik Rabot Radiatsionnoi Khim, Akad. Nauk, S.S.S.R. 71 (1955).
6. CLARK, W. E. J. Electrochem. Soc. **105**, 483 (1958).

7. Hamer, W. J.   J. Am. Chem. Soc. 57, 9 (1935).
8. Harned, H. S. and Hamer, W. J.   J. Am. Chem. Soc. 57, 33 (1935).
9. Hochanadel, C. J.   J. Phys. Chem. 56, 587 (1952). See also ref. 4.
10. Akerlof, G. C. and Bender, P.   J. Am. Chem. Soc. 70, 2366 (1948).
11. Zalkind, Ts.I., Veselovsky, V. I., and Gochaliev, G. Z. All-union Conference on the Application
    of Radioactive and Stable Isotopes and Radiation in the National Economy and Science, Session
    on Radiation Chemistry. Moscow, March 25 to April 2, 1957.

LIMITING CONDUCTANCE OF LYONIUM AND LYATE IONS[1]

Martin Kilpatrick

ABSTRACT

The problem of proton mobility has been considered in H_2O–CH_3OH, H_2O–D_2O, and H_2O–H_2O_2 solvents from the current viewpoint of the mechanism of proton mobility for aqueous solutions. Mixed solvents are more complicated in that one must consider the relative basicity and acidity of the species competing for the protons. It is concluded that for dilute solutions of $HClO_4$, where water is replaced by hydrogen peroxide, the decrease in equivalent conductance relative to that of KCl in the same solvent mixture is due to the partial elimination of the proton transfer process.

For highly acidic non-aqueous solvents of high dielectric constants such as HF, HCN, and HCOOH, the problem of the weakness of the usual "strong" acids of aqueous solution makes a direct determination of the limiting equivalent conductances difficult. In the case of anhydrous hydrogen fluoride the available experimental evidence indicates that the limiting conductance of the lyonium ion is approximately the same as that of the potassium ion but the lyate ion has a higher limiting conductance than other stable anions.

The higher proton mobility in ice leads one to expect that hydrogen-bonded systems may be found where the conductivity may approach that of electronic semiconductors.

In a paper presented before the 111th meeting of the Electrochemical Society in May, 1957, and to be published elsewhere (1), the author showed that the limiting equivalent conductance of perchloric acid relative to that of potassium perchlorate decreased as the water was replaced by hydrogen peroxide. The experimental results (2) are presented in Fig. 1 together with some more recent results (3) for 0.01 M HCl relative to 0.01 M KCl when water is replaced by methyl alcohol and some earlier work on the replacement of H_2O by D_2O (4). The conclusion was drawn that the change in structure of the solvent decreased the conductance by proton transfer.

Thomas and Maass (5) offer an alternative explanation on the basis of the reduction of the number of ions in the solution owing to a decrease in the degree of dissociation of the acid. They confirm the experimental results of Shanley et al. (2) for sulphuric acid and report additional data for HNO_3 and HF in H_2O–H_2O_2 mixtures at higher concentrations of acid.

The generally accepted view for water is that in addition to 1 water molecule associated with the proton there are 3 molecules of water hydrogen bonded to the hydroxonium ion (6). This cluster forms the inner hydration shell with an outer shell held more loosely by hydrogen bonding. The inner-shell hydrogen bonds are strengthened by dipole interaction and will be less subject to disorder from thermal motion. Within the inner sphere, proton jumps take place readily while transfer of protons beyond this depends on reorientation of the water molecules. From the fact that the number of hydrogen bonds decreases with increasing temperature while the extra mobility increases, Krogh-Moe (7) concludes that the rate cannot be proportional to the mean number of hydrogen bonds. That the model is only a qualitative one has been pointed by Samoilov (8), who points out that the tetrahedral arrangement in ice is partially washed out by the thermal motion. The X-ray diffraction studies show the number of nearest neighbors to be 4.6 at 30° (9).

A mixed solvent will be more complex than a solvent composed of one species and one must deal with strong electrolytes and consider at least three effects. The two solvent

species will compete for the proton to form the lyonium ion; there will also be competition for the inner hydration sphere and orientation of both species at the periphery of the inner hydration shell. For low mole fractions of alcohol, the lyonium ions will be hydronium ions and we might conclude that the interference with the proton transfer process occurs first in the outer hydration zone. As the mole fraction of alcohol increases, some water is replaced by alcohol in the inner zone and the lyonium ions are partially alcohol-solvated protons. The increase beyond 90% alcohol is due to proton transfers via alcohol molecules. In this case HCl does show indications of being a weak acid in alcohol but this is not true of perchloric acid.

In the case of the replacement of water by hydrogen peroxide, while it is true that acids become weaker due to the more acidic nature of hydrogen peroxide, perchloric acid at low concentration is a strong electrolyte (10) and at the high dielectric constant of the solvent there should not be ion pairs. The first effect should be in the outer shell and at very high mole fractions of H_2O_2 the lyonium ion will become protons solvated with H_2O_2. It is not impossible that in pure anhydrous H_2O_2 we might have chain transfer via proton jumps between H_2O_2 molecules but these will have to be practically in the absence of water. In other words the curve in Fig. 1 may rise steeply beyond 99%.
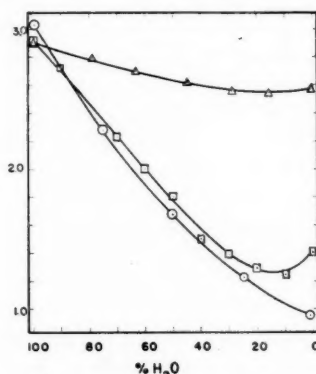
FIG. 1.   Ratio of equivalent conductances:
△ H_2O-D_2O; $\Lambda^{.01}_{HCl+DCl}/\Lambda^{.01}_{KCl}$
○ $H_2O-H_2O_2$; $\Lambda^{\circ}_{HClO_4}/\Lambda^{\circ}_{KClO_4}$
□ H_2O-CH_3OH; $\Lambda^{.01}_{HCl}/\Lambda^{.01}_{KCl}$

In the case of the H_2O-D_2O mixtures the D_2O will have a good fraction of the protons at equal mole fractions but even here the non-linearity above the viscosity effect shows that there is some interference in the proton and deuteron transfers. The fraction of protons on H_2O and D_2O could be determined by nuclear magnetic resonance measurements.

Figure 2 shows the ratio of $\Lambda^{\circ}_{KOH}/\Lambda^{\circ}_{KCl}$ for water peroxide solvents and $\Lambda_{KOH}/\Lambda_{KCl}$ at 0.01 molar concentration for water – methyl alcohol. Here the curves are quite different, the addition of methyl alcohol decreasing the proton transfer via the water molecule and showing no appreciable minimum, although there are methoxide ions present at the high alcohol side (11). In the case of hydrogen peroxide – water solvents the hydroxyl ions react with the hydrogen peroxide to form hydroperoxide ions and the lyate ions, hydroxyl and hydroperoxide have both water and hydrogen peroxide in the inner solvation shell.
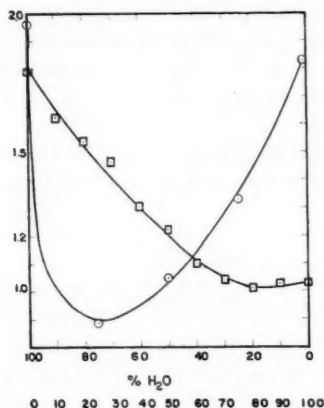
FIG. 2.   Ratio of equivalent conductances:
○ H_2O—H_2O_2; $\Lambda^\circ_{KOH}/\Lambda^\circ_{KClO_4}$
□ H_2O–CH_3OH; $\Lambda^{-01}_{KOH}/\Lambda^{-01}_{KCl}$

The ratio $\Lambda^\circ_{HCl}/\Lambda^\circ_{KCl}$ from the data of Barak and Hartley (12) at 25° C gives 0.98 instead of 1.03 (Fig. 2); so we conclude there is no minimum in the curve and there is no increase in the limiting conductance of the methoxide ion in methyl alcohol. Gurney (13) explains this fact by pointing out that although proton jumps do take place, that owing to the removal of the dipole moment on addition of a proton, such proton jumps take place equally well in the direction of the field as against the field.

LIMITING EQUIVALENT CONDUCTANCES IN NON-AQUEOUS SOLUTIONS

In ammonia the lyonium and lyate ions are the ammonium and amide ions.

$$NH_3 + NH_3 \rightleftharpoons NH_4^+ + NH_2^-$$
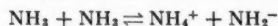
The ions show no abnormal electrical mobility and Gurney (13) accepts the Hückel explanation on the basis that the ammonium ion has no dipole moment. There is no experimental evidence for abnormal limiting conductance in the solvents hydrazine, pyridine, hydroxylamine, and other amines.

In the highly acidic solvents both the sulphuric acid cation and anion show abnormal conductance (13). In anhydrous hydrogen fluoride the fluoride ion has been shown to have a higher mobility than the borofluoride and antimony hexafluoride ions but there is no evidence that the solvated proton shows abnormal electrical conductance (14). The problem in determining the limiting conductance in this solvent is that the strong acids of aqueous solution are weak electrolytes in anhydrous hydrogen fluoride.

The measurements were based on the fluoride ion accepting property of antimony pentafluoride to form the stable SbF_6^- anion. Conductance measurements showed $Na^+ SbF_6^-$ to be a strong electrolyte and the equivalent conductance of $H_2^+F SbF_6^-$ was shown to be less than that of the sodium salt, leading to the conclusion that $l^\circ_{H_2^+F} < l^\circ_{Na^+}$. The success of these experiments depended on the exclusion of water, as H_2O would compete with HF for the protons and SbF_6^- would be converted to an hydroxy acid (15). If these experiments are reliable we have a case where the anion of the solvent may be chain conducting but the cation has no abnormal conductance.

Liquid hydrogen cyanide is another high dielectric solvent where the "strong" acids of aqueous solution are weak. Other cations and anions show equivalent conductances

which are three or four times higher than the corresponding ions in water (16). The problem of the limiting conductance of the lyonium ion could probably be attacked in analogous fashion to that used for HF. The ion product is 2×10^{-19} (17), and reasoning by analogy from aqueous solution (18) the $[Cu(CN)_2]^-$ anion is quite stable.

$$HCN + HCN \rightleftharpoons H^+ \cdot HCN + CN^-$$
$$+$$
$$CuCN$$
$$\downarrow$$
$$[Cu(CN)_2]^-$$
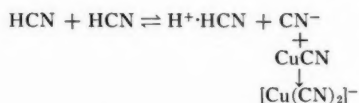
A comparison of Λ° for $NaCu(CN)_2$ and Λ° for a solution of CuCN in anhydrous hydrocyanic acid should decide the ratio $l^\circ_{H^+}/l^\circ_{Na^+}$. Mercuric cyanide might be more suitable than cuprous cyanide provided it was sufficiently soluble. The solubilities of non-ionic cyanides in anhydrous hydrocyanic acid are not accurately known. There is no evidence of abnormal conductance of lyonium or lyate ions in acetonitrile.

The carboxylic acids with the exception of formic acids are solvents of low dielectric constant. Potentiometric studies in formic acid (dielectric constant 58 at 16° C) (19) indicate the "strong" acids of water are weak electrolytes. Like sulphuric acid, the auto-protolysis of formic acid is so high that the solvent conductance makes conductivity studies of acids difficult to interpret (20). Formamide (21) and dimethyl formamide (22) are high dielectric solvents but show no abnormal conductance.

PROTON CONDUCTANCE IN SOLIDS

Bjerrum (23) reviews the dielectric properties and conductance of ice and calculates the energy of activation for proton jumps to be 2.5 kcal for H_3^+O and 4.7 kcal for HO^-, which corresponds to an over-all E for the equivalent conductance of 3.1 at 0° which is lower than the experimental value. More recent measurements (24) for polycrystalline ice yield a value of 3.9 kcal at $-15°$ C compared to Bjerrum's calculated value of 2.5. These calculations are based on equivalent conductances $\Lambda^\circ = 298$ with $l^\circ_{H^+} = 215$ and $l^\circ_{HO^-} = 83$ at 0° C. Very recently Conway and Bockris (25) emphasized that the conclusions of Bradley (26) and Owston (27) based on specific conductance are on an unsound basis and they recomputed the absolute mobilities and concluded the rate-determining step in ice is proton tunneling but in water the rate-determining step is controlled by the rotation of the water molecules. This conclusion brings their findings into qualitative agreement with the earlier results of Eigen (28), who determined experimentally both the ion product and the proton mobility. Eigen finds that the protonic mobility is appreciably higher in ice than in water but that a small amount of fluoride markedly reduces the conductivity. Ice crystallized from a solution of caesium fluoride has been found to have H–F incorporated in the lattice (29). Certain polyhydric alcohols show a marked change in conductivity with temperature below their melting points and a proton transfer, and molecular rotation mechanism has been proposed (30).

The structures of HF and HCN (31, 32) in the solid state are both known to be linear chains but no conductance measurements have been reported on the solids. The high proton mobility in ice indicates that $H—O \cdots H$ bonds are involved but this phenomenon should also apply to $H—N \cdots H$ bonds.

Polyvalent metal ions form polynuclear complexes in aqueous solution, and the structures are often held together by oxygen or hydrogen bridges (33). In the corrosion of metals the nature of the solid films is similar to the species found in solution, and proton

mobility along the hydrogen bonds may be the rate-determining step. There have also been some studies of the conductance of hydrocarbon films (34) which indicate that some organic compounds are semiconducting.

ACKNOWLEDGMENT

REFERENCES

1. KILPATRICK, M.   J. Electrochem. Soc. **104**, 73C (1957).
2. SHANLEY, E. S., ROTH, E. W., NICHOLS, G. M., and KILPATRICK, M.   J. Am. Chem. Soc. **78**, 5190 (1956).
3. ERDY-GRUZ, T., KUGLER, E., and REICH, A.   Acta Chim. Acad. Sci. Hung. **13**, 439 (1958).
4. BAKER, W. M. and LaMER, V. K.   J. Chem. Phys. **3**, 406 (1935).
5. THOMAS, D. K. and MAASS, O.   Can. J. Chem. **36**, 744 (1958).
6. ACKERMAN, T.   Discussions Faraday Soc. **24**, 180 (1957).
7. KROGH-MOE, J.   Acta Chem. Scand. **10**, 331 (1956).
8. SAMOILOV, O. YA.   Zhur. Fiz. Khim. **3**, 537 (1957).
9. MORGAN, J. and WARREN, B. E.   J. Chem. Phys. **6**, 666 (1938).
10. MITCHELL, A. G. and WYNNE-JONES, W. F. K.   Trans. Faraday Soc. **51**, 1690 (1955).
11. KOSKIKALLIO, J.   Suomen Kemistilehti, B, **30**, 111 (1957).
12. BARAK, M. and HARTLEY, H.   Z. physik. Chem. **165**, 290 (1933).
13. GURNEY, R. W.   Ionic processes in solution. McGraw-Hill Book Co., Inc., New York and London. 1953. p. 77.
14. KILPATRICK, M. and LEWIS, T. J.   J. Am. Chem. Soc. **78**, 5186 (1956).
15. SCHREWELIUS, N.   Dissertation. Stockholm. 1943.
16. COATES, J. E. and TAYLOR, E. G.   J. Chem. Soc. 1245, 1495 (1936).
17. JANDER, G. and GRUTTNER, B.   Chem. Ber. **81**, 102 (1948).
18. VLADIMIROVA, M. G. and KALOVSKII, I. A.   Zhur. Priklad. Khim. **23**, 580 (1950).
19. SHKODIN, A. M., IZMAILOV, N. A., and DZYUBA, N. P.   J. Gen. Chem. U.S.S.R. **23**, 25 (1953).
20. HAMMETT, L. P. and DIETZ, N., JR.   J. Am. Chem. Soc. **52**, 4795 (1930).
21. DAWSON, L. R., NEWHALL, T. M., and McCREARY, W. J.   J. Am. Chem. Soc. **76**, 6024 (1954).
22. DAWSON, L. R., GOLBEN, M., LEADER, G. R., and ZIMMERMAN, H. K., JR.   J. Electrochem. Soc. **99**, 28 (1952).
23. BJERRUM, N.   Kgl. Danske Videnskab. Selskab, Mat. fys. Medd. **27**, No. 1, 56 (1951).
24. SPERNOL, A.   Z. Elektrochem. **59**, 31 (1955).
25. CONWAY, B. E. and BOCKRIS, J. O'M.   J. Chem. Phys. **28**, 354 (1958).
26. BRADLEY, R. S.   Trans. Faraday Soc. **53**, 687 (1957).
27. OWSTON, P. G.   Quart. Revs. **5**, 344 (1951).
28. EIGEN, M.   J. Electrochem. Soc. **104**, 72C (1957).
29. BRILL, R. and ENDER, H.   Nature, **176**, 925 (1955).
30. KAKUICHI, Y.   Research Inst. Appl. Elec., Hokkaido Univ., Monograph Ser. **4**, 75 (1954).
31. DULMAGE, W. S. and LIPSCOMB, W. N.   Acta Cryst. **4**, 330 (1954).
32. HORNIG, D. F.   Discussions Faraday Soc. **9**, 115 (1950).
33. BIEDERMAN, G., KILPATRICK, M., POKRAS, L., and SILLÉN, L. G.   Acta Chem. Scand. **10**, 1327 (1956).
34. NORTHRUP, D. C. and SIMPSON, O.   Proc. Roy. Soc. (London), A, **234**, 124 (1956).

SOME CONSIDERATIONS ON THE ROLE OF PROTON TUNNELING IN CERTAIN CHARGE TRANSFER PROCESSES[1]

B. E. CONWAY

ABSTRACT

Quantum mechanical tunneling of H atoms in certain reactions can have a rate comparable with that of the corresponding classical reaction. Proton tunneling appears to be the mechanism of proton transport in ice. Further studies of this mechanism have been made by determination of the a-c. and d-c. conductance of D_2O (and H_2O) ice under rigorous conditions of purification. Pre-electrolysis techniques have been applied to the ultrapurification of the D_2O and H_2O used for the conductance determinations. Isotopic ratios of conductance in solid H_2O and D_2O are obtained and discussed in terms of the mechanism of H^+ or D^+ transport in the solid and liquid substances. The theory of proton tunneling previously given is improved by using a quantal distribution function in the calculation of tunneling rates and better agreement with experiment is then obtained. The theoretical isotopic ratio of conductances by the tunneling mechanism in the ices is similar to that found experimentally and smaller than that predicted classically.

Since the proton tunneling theory is quantitatively successful in the case of conductance of ice, its examination for other electrochemical processes involving H is necessary. A favorable case for investigation is the electrochemical hydrogen evolution reaction for which the barrier height for tunneling can be varied. Tunneling probabilities are calculated for proton and deuteron discharge at mercury from acid solutions using the theory of Eckart. At intermediate overpotentials the Tafel equation is still obeyed; at low overpotentials a linear current–potential relation is found as in the classical theory. H/D separation factors are calculated for the tunneling mechanism and it is shown that at intermediate and high overpotentials, tunneling leads to values of the separation factor comparable with those deduced classically. Only at low electrochemical rates of H or D production are high separation factors predicted. The tunneling mechanism, however, is distinguishable from the classical mechanism by a new criterion: the Tafel slopes for the tunneling process would be considerably larger (0.2–0.3) than those arising classically (0.12) for a simple discharge mechanism assuming a symmetry factor of 0.5. It is concluded that in certain cases proton tunneling may occur simultaneously with the classical reaction in electrochemical proton discharge and lead to anomalous Tafel 'b' values which are sometimes observed experimentally.

INTRODUCTION

The possibility of quantum mechanical effects arising from tunneling was recognized by Wigner (1) and Bell (2) as a factor to be considered in the kinetics of chemical reactions involving H or D. Several attempts to find experimental support for this effect have been made and some evidence has been given for quantum mechanical tunneling of H ions or atoms in the following reactions: (i) the ortho-para hydrogen conversion (2, 3); (ii) the rate-determining proton transfer step in the bromination of 2-carbethoxy-cyclopentanone (4); and (iii) in the proton conductance of water and ice (5, 6). In the latter case, the tunneling process is the only one which can account for the high mobility of protons in ice. In the first two cases it appears that only participation of the quantum mechanical process in the net reaction occurs, i.e., quantum and classical processes can occur at comparable rates. However, in proton mobility in ice and water, the quantum mechanical process appears to be considerably faster and hence preferred, although in *liquid* water the over-all rate is limited by water dipole rotation (5).

Further tests of the quantum mechanical mechanism should be possible in the case of conductance of ice by determination of the specific conductance, and hence mobility, of deuterons in heavy ice. Measurements of the specific conductance of ice prepared from 99.8% D_2O have been carried out and estimates of the ionic mobility of D^+ in D_2O ice are made.

Tunneling effects in heterogeneous proton transfer reactions, e.g., in the electrolytic hydrogen evolution reaction may be expected, since in the case of the proton transfer conductance of water and ice such effects occur. The electrochemical kinetic behavior, which would arise if quantum mechanical penetration of the potential barrier at an electrode took place, is deduced and criteria for recognition of the effect are presented.

EXPERIMENTAL

Conductance determinations have been made on D_2O ice (and H_2O ice) and the corresponding liquids by the a-c. and d-c. methods. Alternating-current measurements were made by means of a shielded Wheatstone bridge with capacitative and ohmic components; the a-c. source was a Hewlett–Packard precision oscillator. Direct-current measurements were made on the same bridge but with only ohmic components using a Leeds and Northrup galvanometer of sensitivity 4.5×10^{-9} amp/mm. The cell is shown in Fig. 1 and was mounted in a heavy brass cylinder in order to provide electromagnetic shielding and a region of thermal inertia around the cell. Palladium electrodes were used (cf. 7). The apparatus was maintained at various temperatures constant to 0.05° C in a refrigerated thermostat.

Water was distilled five times: (i) from a Barnstead still; (ii) from alkaline permanganate; (iii) through a column of glass beads heated to 450° C, through which hydrogen
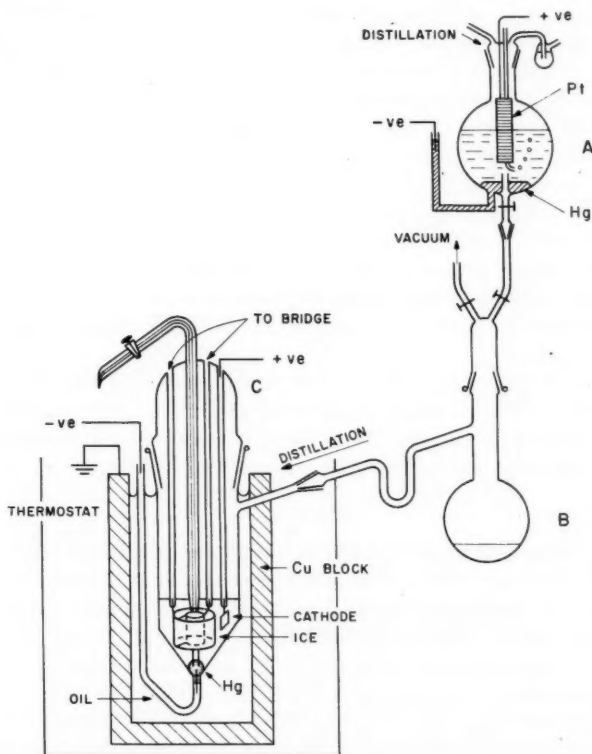
FIG. 1. D_2O distillation, purification, and conductance apparatus.

(free from CO_2 and purified by passage through two liquid air traps) was passed; (iv) again in H_2 in another vessel; and (v) in a fused silica still *in vacuo* under conditions of smooth evaporation from a still water surface. Fifteen milliliters of water was then passed over into the silica conductance vessel in order to wash it and then removed through a capillary tube. Further distillation was then carried out *in vacuo* and another 15 ml of water passed into the cell. This water was then frozen by dipping the lower end of the cell into a bath at $-20°$ C (cf. 7). After several freezing and melting cycles *in vacuo*, ice as clear as liquid water was obtained and no flaws, cracks, or bubbles were visible. After clear ice was obtained, the cell was placed in the thermostat and allowed to stand for some days in order to anneal the ice. Melting, evacuation, and freezing cycles were continued until no further change in conductance occurred.

In previous determinations (7, 8) of the conductance of ice, the conductance of the water used for the preparation of the ice was about fifty times that (9) corresponding to the equilibrium concentrations of H_3O^+ and OH^- ions. The significance of the conductance values thus determined may hence be somewhat limited, since the impurities present in the water may, particularly if acidic, contribute to the conductance in the ice. At the same time, the impurities, if slightly soluble in the ice, create defects in the crystal which could change the behavior of the ice. Such impurities have, for example, a marked effect on the dielectric properties of ice (10).

In the present work, electrolytic purification of the water using a mercury cathode has been carried out, in addition to multiple distillation. Electrolytic purification of "pure solvents" was first used in conductance studies by Jaffé (11) and Schroeder (12), who found that considerable diminution of conductance of ordinarily purified solvents could be achieved by this procedure. Water from stage (iii) (see above) was distilled from stage (iv) into the vessel A in Fig. 1, containing mercury which had been anodically purified, dried, and redistilled in a Hewlett still. After 48 hours' electrolysis at 500 v with the mercury cathodic, the liquid was run out into the silica vessel B. Stage (v) distillation was then carried out. A further electrolysis could be carried out at the mercury drop in the cell C (Fig. 1), but this made no significant difference to the specific conductance of the water prior to freezing, which was between 3 and 5 $\times 10^{-7}$ mho cm^{-1}.

Deuterium oxide (99.8%) was purified by distillation, as above, using steps (iv) with N_2 to (v) and subjected to electrolytic purification as described; measurements were made as in the case of water.

Determinations of the cell constant were made at $25.00\pm0.02°$ C by means of the Jones and Bradshaw (13) standard solutions of KCl. The resistance of the empty cell under vacuum, and that of the leads in the circuit, was about 100 times greater than that of the cell containing ice, and could only be measured with difficulty.

RESULTS

After several cycles of freezing and melting *in vacuo* the resistance of the D_2O ice reached an approximately constant value. The value was checked by melting the ice and returning the liquid to the silica still and repeating the operation. The a-c. resistance (1000 c.p.s.) measured at $-2.0°$ C varied between 2.30×10^6 and 2.74×10^6, whilst the corresponding d-c. values varied from 16.4×10^6 to 19.6×10^6 ohms. The cell constant was 24.8 so that the specific conductances (κ) were $1.6\pm0.5\times10^{-8}$ mho cm^{-1} for 1000 c.p.s. a-c. and $2.2\pm0.6\times10^{-9}$ mho cm^{-1} for d-c. The corresponding values for H_2O ice were $3.5\pm0.5\times10^{-8}$ and $5.2\pm0.7\times10^{-9}$ mho cm^{-1}. The latter value falls near to that given by Bradley (7) for H_2O ice at $-2.0°$ C viz. $10^{-8.24}$ mho cm^{-1}. There is some spread in the

present results but it is comparable with that (0.14 in $\log_{10} \kappa$) found in previous determinations (7). The determinations reported here lead to an isotopic ratio of specific conductance of $\kappa_{H_2O \text{ ice}}/\kappa_{D_2O \text{ ice}} = 2.2$ for a-c. measurements (1000 c.p.s.) and 2.4 for for d-c. measurements.

The a-c. values of conductance are frequency dependent as shown in Fig. 2. The d-c. measurements are time dependent as found previously with H_2O ice (7, 14). The values at "zero time" are recorded above and a typical time dependence is shown in Fig. 3; the effect probably arises from build-up of a space charge near the electrodes when the field is applied. This is probably the cause of the frequency dependence of the a-c. conductance and with this in mind we have plotted in Fig. 2 the a-c. conductance as a function of the square root of the reciprocal frequency; the relationship is not, however, linear, as might be expected if there were a concentration polarization of charge carriers when the field was applied. More complex effects are probably involved. Consideration of the significance of the results will therefore be limited to the "zero time" d-c. values.
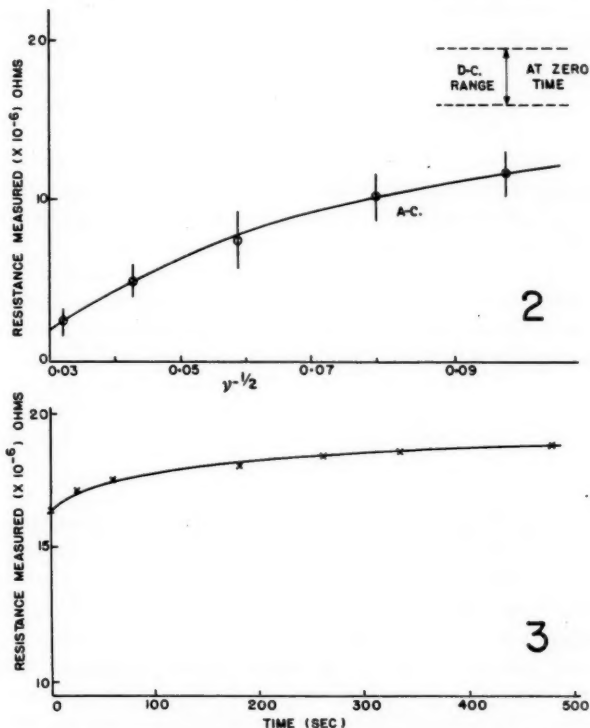
FIG. 2. Comparison of a-c. and d-c. resistance of D_2O ice.
FIG. 3. Typical time variation of d-c. resistance of D_2O ice.

DISCUSSION

1. *Proton and Deuteron Mobility and Tunneling in Ice*

The above measurements on specific conductance cannot be directly interpreted in terms of ionic mobility and hence of ionic transport mechanisms until values (cf. 15) of

the concentration of D_3O^+ and OD^- ions in the ice are available. In H_2O ice the concentration of the corresponding protium species is known (15) and leads to a proton mobility of 1.9×10^{-1} cm^2 sec^{-1} v^{-1}. The theoretical rate of quantum mechanical tunneling of protons in an unperturbed ice structure (i.e., with all H bonds linear and no librational motion) has been calculated (5, 6) using the theory of Eckart (16) for the permeability and a value of 7×10^{-1} cm^2 sec^{-1} v^{-1} for the tunneling rate has been obtained. In the theory previously given (5) we have used, following Bell (2), the expression

$$[1] \qquad N = \frac{N_0}{kT} \int_0^\infty P_w \, e^{-w/kT} dw$$

in order to calculate the integral tunneling probability, where N is the number of penetrations of the barrier out of N_0 presentations of the particle at the barrier per second, w is the total energy of the particle, and P_w is the quantum mechanical tunneling probability for the particle of energy w, calculated from the theory of Eckart (16). For the OH bond, the vibrational half quantum is about 5 kcal mole^{-1}, so that it would be more correct to use a quantal distribution rather than the classical distribution function in equation [1]. Quantally, the total tunneling rate should then be written

$$[2] \qquad N = N_0 \frac{\sum_0^\infty \left(P_w \cdot p \, e^{-(n+\frac{1}{2})h\nu_0/kT} \right)}{\sum_0^\infty p \cdot e^{-(n+\frac{1}{2})h\nu_0/kT}},$$

where n is the vibrational quantum number, ν_0 the ground state vibrational frequency of the OH or OD bond in H_3O^+ or D_3O^+, and p is the quantum weight assumed equal to unity. Since for the OH or OD vibration, $h\nu_0 \gg kT$, the value of N is closely approximated by the value of the *r.h.s* of equation [1] for $n = 0$, other terms contributing negligibly. If we identify N_0 with the frequency of presentations of the particle H or D at the barrier (cf. 2), the rate of tunneling between an H_3O^+ ion and a favorably oriented H_2O molecule follows from the theory previously given as

$$[3] \qquad v = \nu\delta \frac{\phi_x}{kT} \frac{\sum_0^\infty \left(P_w \cdot p \cdot e^{-(n+\frac{1}{2})h\nu_0/kT} \right)}{\sum_0^\infty p \cdot e^{-(n+\frac{1}{2})h\nu_0/kT}}.$$

When $n = 0$ and the particles predominantly approach the barrier with an energy $\frac{1}{2}h\nu_0$, P_w has the values 0.87 for H and 0.60 for D. In equation [3], ν is stretching frequency of the OH or OD bond in H_3O^+ or D_3O^+ undergoing dissociation, δ is the distance (2.8 Å) the proton is transferred per jump, and ϕ_x is the mean change of electrical energy of the particle per jump when unit field is applied; it has the value 1.53×10^{-20} erg (5). In an unperturbed structure with all $OH \cdots O$ hydrogen bonds stationary and colinear, v would give the proton mobility. However, the ice is thermally perturbed in so far as each molecule executes librational oscillations in the lattice. Following the argument of Bernal and Fowler (17), the proton transfer rate will be modified from that given by v on account of the necessity that each OH bond be in a suitable orientation to that of the $2p_z$ partially hybridized lone pair orbitals on the oxygen atom of a neighboring water molecule, before transfer can occur. We have previously shown (5) that orientations*

---

*The orientation requirement discussed here is not the same as the reorientation involved when a proton migrates through liquid water. The molecules in ice are already the "correct way round" for proton transfer to occur, but their librative oscillations restrict proton tunneling since favorable mutual orientations of neighbors in their librational excursions only occur part of the time (17).

of H_3O^+ and neighboring H_2O molecules, mutually favorable for proton transfer by tunneling, occur with a probability of about $\frac{1}{9}$. Owing to the lower zero point librational energy of D_2O in D_2O ice, the librational excursions in the deuterium case will be smaller and the molecule will spend more of its time in orientations favorable to D^+ transfer. This is equivalent to the situation in liquid D_2O, which has a more ordered structure on account of the lower librational zero point energy than in liquid water. Calculations show that in the case of deuteron transfer in D_2O ice the probability factor for mutually favorable orientations is about $\frac{1}{7}$. Using these factors, the mobilities of H^+ and D^+ in their respective ices may now be calculated from equation [3], taking $\nu_{OH} = 1.12 \times 10^{14}$ sec^{-1} and $\nu_{OD} = (1.12/\sqrt{2}) \times 10^{14}$ sec^{-1}. The mobilities, u, are then

$$u_{H^+} = 0.11 \text{ and } u_{D^+} = 0.07 \text{ cm}^2 \text{ sec}^{-1} \text{ v}^{-1}.$$

From considerations based on the experimental value of the over-all specific conductance, u_{H^+} in H_2O–ice has been deduced as 0.19 cm^2 sec^{-1} v^{-1} (6). Use of the quantal distribution in equation [2] thus gives better agreement with experiment than that given by the semiclassical equation [1].

The mobility ratio for the H^+ and D^+ isotopic ions calculated from equation [1] is 6.1. That from equation [3] is only 1.6, i.e., near to that (1.4) for rate-determining rotation of H_2O or D_2O dipoles (5). However, although the isotopic ratios of conductance are now similar for the two mechanisms, the large increase of mobility on going from aqueous acid solutions to pure ice can only be explained in terms of a *transition* from rate-determining dipole rotation (in water) to rate-determining proton tunneling in ice. The dependence of anomalous mobility in alcoholic solutions on the length of the hydrocarbon function (5) has in any case confirmed the dipole rotational mechanism in the case of acid solutions.

It is now of interest to examine if the theory is consistent with the experimental data on the conductance of the heavy ice. We can only make mechanistic interpretations of the results if we can obtain the *mobility* from the experimental conductance. At the present time, we can only proceed further by making the not unreasonable assumption that the *ratio* of ionic products in H_2O ice and D_2O ice is the same as the corresponding ratio for liquid H_2O and D_2O, viz. (at 25° C) $1 \times 10^{-14} : 0.2 \times 10^{-14}$ (18). Some indication that this assumption is not unjustifiable is given by the following considerations: the difference of the heat of ionization of D_2O and H_2O is 0.94 kcal mole^{-1} (19), and it is readily seen that this figure can account for the difference of the ionization constant to within 10%, so that isotopic entropy differences are not significant in determining the *ratio* of ionization constants of D_2O and H_2O. The difference of heat of ionization arises from the different zero-point energies of the species involved. In ice the same situation should hold and the ratio of ionization constants in H_2O and D_2O ices should be approximately equal to the corresponding ratio for the liquid phases if only heat terms are involved.

In ice at $-10°$ C, the concentration of protons is 5×10^{-11} g ion l.$^{-1}$ (15, 6). If we take the ratio of ionization constants as $1 \times 10^{-14}/0.2 \times 10^{-14}$ for H_2O and D_2O, the ratio of proton to deuteron concentrations in H_2O ice and D_2O ice, respectively, will be $(1/0.2)^{\frac{1}{2}}$ i.e., 2.23 : 1. The experimental isotopic d-c. conductance ratio is 5.2/2.2 i.e., 2.35. Hence the ratio of *mobilities** of H^+ and D^+ in their respective ices is about 1.1. The theoretical calculations predict a ratio of 1.6. This must be considered a satisfactory agreement in

---

*The transport numbers of H^+ in H_2O and D^+ in D_2O are approximately equal (viz. 0.64 and 0.66 respectively; see (6) and (34)).

view of the several assumptions made. The measurements clearly support the tunneling
mechanism both for protons and deuterons in ice. The classical mechanism predicts much
lower mobilities (5) and an isotopic ratio of mobilities having the approximate value exp.
$(\Delta_{D-H} \frac{1}{2} h\nu_0)/kT$ i.e., about 9, which is not observed experimentally. In the case of mobilities
of H^+ and D^+ in ice, the isotopic ratio of tunneling rates is hence actually less than that
predicted classically. This is contrary to what has usually been supposed for tunneling
mechanisms.

2. Proton Tunneling at Electrodes

The quantitative success of the proton tunneling theory (5, 6) in the case of proton
conductance in ice suggests that proton tunneling can participate in certain reactions
as is also indicated in other cases (2, 4, 20). It is therefore of interest to examine the
theory in relation to other electrochemical processes involving proton transfer.

Quantum mechanical effects in electrode processes were first considered by Gurney in
1932 (21) with respect to electrons. Bawn and Ogden (22) suggested that tunneling of pro-
tons and deuterons might explain the H/D electrolytic separation factors (s) at various
metals and they deduced a value of s for tunneling of about 100. Such a value was ex-
perimentally observed by Appelby and Ogden (23) but has never been confirmed (24).
On the basis of the theoretical calculations and the more usually observed values of
s (from 3 to 10), it has generally been regarded that tunneling could not participate
to any important extent in the cathodic hydrogen evolution reaction. However, the
calculations of Bawn and Ogden were made on a basis which was not relevant to the
case under consideration; thus the barrier widths which were assumed (1.5, 2.0, and
3.0 Å) are too large and no consideration of the effect of applied potential, which modifies
the height of the potential energy barrier and hence the probability of tunneling, was
made. For the proton transfer reaction

$$H_3O^+ + M + e \rightarrow H_2O + MH_{ads},$$

e.g., at a mercury electrode, the barrier height at the potential of zero charge is about
18 kcal mole^{-1} (25). The barrier width is calculated (cf. 25, 26) from the OH bond length
in the hydroxonium ion, the radius of the hydroxonium ion (assumed approximately equal
to that of water), and the HgH bond length (27). The width is found (25) to be between
0.55 and 0.50 Å. Such a width is consistent with the probable thickness of the double
layer at mercury in acid solutions. For the calculation of the above figures, the "width"
is taken to be the distance of the proton about to be discharged in the H_3O^+ ion from
the position of the H atom adsorbed on the electrode surface. A barrier of width of 0.50–
0.55 Å leads to a theoretical (25) classical heat of activation similar to that observed
experimentally (28). The barrier width assumed by Bawn and Ogden is thus about four
times too large and, since the tunneling probability is very sensitive to dimensional
parameters of the barrier, the value of s calculated is likely to be in error. It is therefore
desirable to calculate the tunneling probabilities for protons and deuterons for the more
realistic barrier dimensions given above and as a function of electrode potential.

A barrier having a form similar to that arising from the intersection of two Morse
curves may be expressed by the function

[4] $V_{(x)} = A e^{2\pi x/l}/(1 + e^{2\pi x/l}) + B e^{2\pi x/l}/(1 + e^{2\pi x/l})^2,$

where $V_{(x)}$ is the potential energy at a distance x along the reaction co-ordinate for a
barrier having a width of $2l$, A is the difference of potential energy between the final and
initial states, and B is $4E^{\ddagger}$, where $E^{\ddagger}$ is the energy of activation, i.e., the value of V at the
maximum of the curve, referred to $V = 0$ at $x = -l$.

The solution of the Schroedinger equation when $V_{(x)}$ is given by equation [4] leads (16) to the permeability or probability of tunneling, P_w, as

[5]
$$P_w = \frac{\cosh 2\pi(\alpha+\beta) - \cosh 2\pi(\alpha-\beta)}{\cosh 2\pi(\alpha+\beta) + \cosh \pi \dfrac{(B-c)^{\frac{1}{2}}}{c}},$$

where $c = h^2/2ml^2$, $\alpha = l/h(2mw)^{\frac{1}{2}}$, $\beta = l/h[2m(w-A)]^{\frac{1}{2}}$, m is the mass of the particle undergoing tunneling, and h is Planck's constant. w is the total energy of the particle approaching the barrier. The total number of particles penetrating the barrier per second is then given (2) by equations [1] or [2].

For tunneling at the mercury electrode interface we place $E^{\pm}$ equal to $E_0{}^{\pm}+\beta\Delta\phi F$, where β is the symmetry factor taken equal to 0.5, $\Delta\phi$ the rational electrode potential, and $E_0{}^{\pm}$ is the heat of activation at the potential of zero charge (i.e., about 18 kcal mole^{-1}); $2l$ is taken as 0.5 Å and m values are those for H and D ions. The probable value of A for proton transfer at the potential of zero charge is -2.5 kcal mole^{-1} (25). The value of A for deuteron transfer from H_2DO^+ ions differs from that for proton transfer by 1.1 kcal mole^{-1}, on account of isotopic differences of (i) OH and OD bond dissociation energies, (ii) heats of hydration, (iii) H and D ionization potentials, and (iv) heats of adsorption at mercury, as discussed by Conway (29) in calculations of the classical values of s for various reaction mechanisms. $E_0{}^{\pm}$ for deuteron transfer is 1.8 kcal larger than that for proton transfer (29). For various values of $\Delta\phi$, A becomes $A_0+\Delta\phi F$, where A_0 is the change of potential energy in the reaction at the potential of zero charge. The values of w in P_w and in the exponential in equation [1] are also changed to $w' = (w+\Delta\phi . F)$ for various values of w and $\Delta\phi$. P_w is then evaluated for a range of values of w' from 0.2×10^{-14} to 100×10^{-14} erg molecule^{-1} and the integral tunneling probability is obtained from equation [1]. The tunneling functions $P_{w'} e^{-w'/kT}$, from which N is evaluated, are shown in Figs. 4, 5, and 6 for five electrode potentials, three temperatures, and for the isotopes ${}_1^1H$ and ${}_1^2D$. In distinction to tunneling through a nuclear potential energy barrier, proton and deuteron tunneling rates are temperature dependent, since the distribution of energies of particles approaching the barrier is temperature dependent and the permeability for a given impact is a function of the total energy of the particle. The apparent energy of activation for a given barrier height is, however, lower than the corresponding classical value (2).

For the electrochemical reaction considered, the main points of interest are the dependence of the tunneling rate upon electrode potential and upon isotopic mass. It is seen from Fig. 7 that the dependence of tunneling probability upon isotopic mass is potential dependent. The values of the separation factor defined by

$$s = (C_D/C_H)_{soln} \cdot v_H/v_D,$$

where C refers to isotopic concentrations in the solution and v_H/v_D is the ratio of rates of discharge of the isotopic ions, may be calculated from the tunneling probabilities together with the ratio of concentrations of H_3O^+ and H_2DO^+ (e.g., in 0.1 N aqueous acid solutions) and the isotopic abundance ratio (30). $a_{H_3O^+}/a_{H_2DO^+}$ has been calculated previously (29) for this case and has a value of 2.6×10^2 in 0.1 N acid solution. Values of s, as a function of electrode potential, are given in Table I.

The separation factor calculated classically is almost independent of potential and has a value of 2.9 (29) for proton discharge at mercury (the experimental value is 3.1 ± 0.2). In isotopic separation work involving the usual analysis of evolved gases, current densities of at least 10^{-3} amp cm^{-2} are required in order to obtain workable rates of gas evolution.
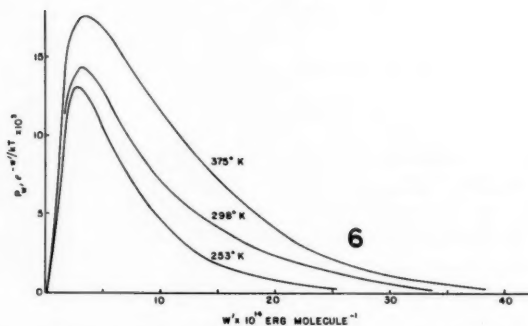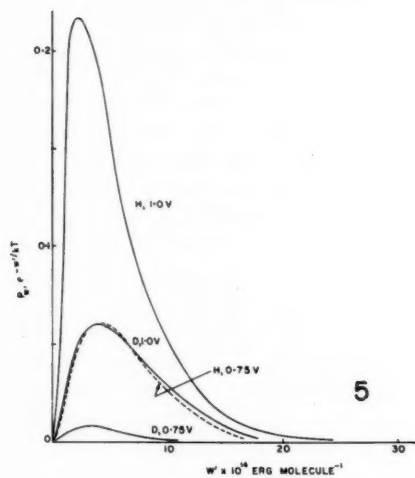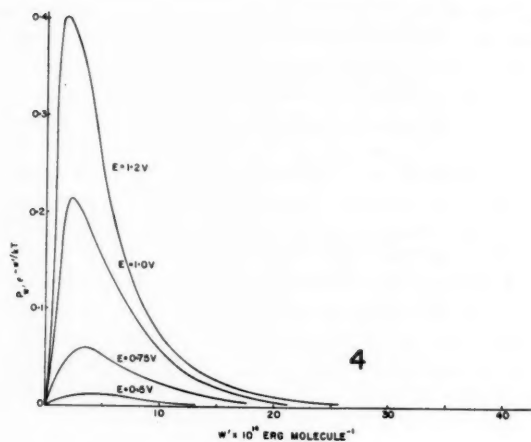
FIG. 4.   Potential dependence of the tunneling function (for H at 298° K).
FIG. 5.   Isotopic dependence of the tunneling function at 298° K.
FIG. 6.   Temperature dependence of the tunneling function (for H at $E = 0.5$ v).

TABLE I

Isotopic separation factors arising if proton or deuteron tunneling occurs

$\Delta\phi$ v	0	0.25	0.50	0.75
s	12.40	5.0	1.6	0.7

The electrode potential at mercury is hence about -1 v (with respect to a hydrogen electrode in the same solution) for such a rate of evolution of gases. The value of s arising from the tunneling mechanism (Table I) is then comparable in magnitude with that calculated for classical transfer. The high values previously predicted (22) are misleading, since the relevant barrier dimensions were not used. Tunneling cannot therefore be excluded as a possible process in electrolytic proton transfer by reference to values of the separation factor, previously indicated as very high if tunneling occurred.

It is possible, however, to propose a new criterion for occurrence of tunneling in electrochemical proton transfer. Fig. 7 shows the logarithm of the integral tunneling probability (to which the electrochemical proton transfer rate is proportional) as a function of electrode potential for proton and deuteron transfer at mercury.
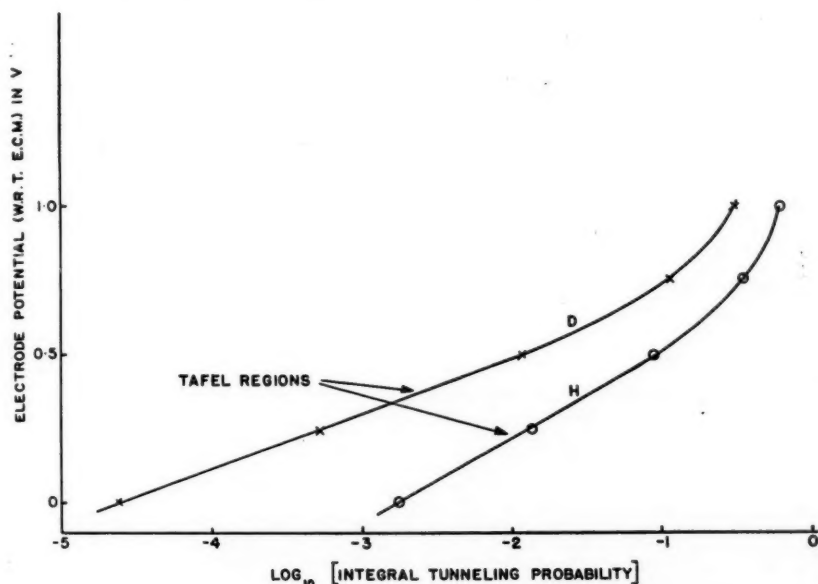
FIG. 7.   Tunneling probability and electrode potential.

At intermediate electrode potentials, a linear $\Delta\phi - \log$ (rate) law is obeyed, i.e., the Tafel equation holds as in classical proton transfer at an electrode. At very low overpotentials Ohm's law is obeyed (5) and hence a linear $\Delta\phi -$ (rate) law is followed, again as in the classical theory. At high electrode potentials there is some tendency for the tunneling rate to approach a limiting value. In the potential range where the behavior is approximated by the Tafel equation, the slope of the $\Delta\phi - \log$ (rate) relationship (Fig. 7) has, however, a value of about 0.25 for proton discharge and 0.17 for deuteron discharge. The

values of these slopes would hence be diagnostic for tunneling transfer, since slopes as high as this do not follow from any mechanism yet proposed for the hydrogen evolution reaction assuming the symmetry factor to be about 0.5. In impure solutions, e.g., at Pb or Hg electrodes, Tafel slopes as high as 0.3 have been observed (33), which are difficult to explain on any of the previously discussed mechanisms (32) of the hydrogen evolution reaction unless unusual values of the symmetry factor are assumed. In impure solutions, the normal barrier height is probably raised as a result of poisoning of adsorption sites for H. Under these conditions the relative participation of proton tunneling compared with classical proton transfer may be enhanced, and hence higher Tafel slopes could arise; some participation of tunneling in the hydrogen evolution reaction at rhodium may account for the anomalous continuously increasing Tafel slope, with increasing overpotential observed for this metal (33). As in the generalized calculations of Bell (2), the tunneling probability calculated here for electrochemical proton transfer is actually larger than the corresponding classical probability, particularly at high cathodic potentials. Use of a quantal distribution in equation [1] instead of the classical one does not materially change the anomaly. In all proton transfer reactions hitherto considered with respect to quantum mechanical effects, only for the case of proton transfer in ice where the potential energy barrier is much lower than in the present case, is the expected tunneling rate actually observed. In the present, and in other cases examined by Bell (2, 4, 20), the experimental kinetic behavior indicates that participation of the classical process in relation to the quantal one is unexpectedly high and constitutes an anomaly of some theoretical interest. Participation of the tunneling process should be more easily observed in relation to the classical process at low temperatures, e.g., in cathodic hydrogen evolution from alcoholic HCl at $-110°$ C. Experiments are in progress to examine this possibility.

REFERENCES

1. WIGNER, E.   Z. physik. Chem. B, **19**, 203 (1933).
2. BELL, R. P.   Proc. Roy. Soc. (London), A, **139**, 466 (1933).
3. PELZER, H. and WIGNER, E.   Z. physik. Chem. B, **15**, 445 (1932).
4. BELL, R. P., FENDLEY, J. A., and HULETT, J. R.   Proc. Roy. Soc. (London), A, **235**, 453 (1950).
5. CONWAY, B. E., BOCKRIS, J. O'M., and LINTON, H.   J. Chem. Phys. **24**, 834 (1956).
6. CONWAY, B. E. and BOCKRIS, J. O'M.   J. Chem. Phys. **28**, 354 (1958).
7. BRADLEY, R. S.   Trans. Faraday Soc. **53**, 687 (1957).
8. JOHNSTONE, M.   Proc. Trans. Nova Scotian Inst. Sci. **13**, 126 (1912).
9. KOHLRAUSCH, F. and HEYDWEILER, A.   Z. physik. Chem. **14**, 317 (1894).
10. SMYTHE, C. P. and HITCHCOCK, J.   J. Am. Chem. Soc. **54**, 4631 (1932).
11. JAFFÉ, G.   Ann. Phys. **28**, 326 (1909).
12. SCHROEDER, J.   Ann. Phys. **29**, 125 (1909).
13. JONES, G. and BRADSHAW, B. C.   J. Am. Chem. Soc. **55**, 1780 (1933).
14. GRÄNICHER, H. C., JACCARD, C., SCHERRER, P., and STEINMANN, A.   Discussions Faraday Soc. **23**, 50 (1957).
15. EIGEN, M. and MAEYER, L.   Z. Elektrochem. **60**, 1037 (1956).
16. ECKART, C.   Phys. Rev. **35**, 1303 (1930).
17. BERNAL, J. D. and FOWLER, R. H.   J. Chem. Phys. **1**, 515 (1933).
18. ABEL, E., BRATU, E., and REDLICH, O.   Z. physik. Chem. **173**, 353 (1935).
19. LANGE, E.   Z. Elektrochem. **44**, 43 (1938).
20. BELL, R. P.   Proc. Roy. Soc. (London), A, **148**, 241 (1935).
21. GURNEY, R. W.   Proc. Roy. Soc. (London), A, **134**, 137 (1932).
22. BAWN, C. E. H. and OGDEN, G.   Trans. Faraday Soc. **30**, 432 (1934).
23. APPELBY, M. P. and OGDEN, G.   J. Chem. Soc. 163 (1936).
24. WALTON, M. F. and WOLFENDON, J. H.   Trans. Faraday Soc. **34**, 436 (1938).

25. PARSONS, R. and BOCKRIS, J. O'M.   Trans. Faraday Soc. **47**, 914 (1951).
26. CONWAY, B. E., BOCKRIS, J. O'M., and LOVROCEK, B.   Proc. Comité intern. thermodynam. et cinét. electrochim. 207 (1954).
27. HERZBERG, G.   Molecular spectra and molecular structure. Vol. I. D. Van Nostrand Company, Inc., New York. 1950. p. 501.
28. BOCKRIS, J. O'M. and PARSONS, R.   Trans. Faraday Soc. **45**, 916 (1949).
29. CONWAY, B. E.   Proc. Roy. Soc. (London), A, **247**, 400 (1958).
30. MATTAUCH, J.   Nuclear physics tables. Interscience Publishers, Inc., New York. 1946.
31. PENTLAND, N., BOCKRIS, J. O'M., and SHELDON, E.   J. Electrochem. Soc. **104**, 182 (1957).
32. BOCKRIS, J. O'M.   Modern aspects of electrochemistry. Academic Press, Inc., New York. 1954. Chap. IV.
33. HICKLING, A. and SALT, F. W.   Trans. Faraday Soc. **36**, 1226 (1940). See also BOCKRIS, J. O'M. and CONWAY, B. E.   Trans. Faraday Soc. **45**, 989 (1949).
34. GIERER, A.   Z. Naturforsch. **5**, 581 (1950).

ON THE MECHANISM OF ELECTROLYTIC DEPOSITION AND DISSOLUTION OF SILVER[1]

WOLFGANG MEHL AND JOHN O'M. BOCKRIS

INTRODUCTION

The mechanism of crystal growth has been an object of study for many years. Beginning with Gibbs (1), major contributions have been made by Volmer (2), Kossel (3), Stranski (4), Becker and Döring (5), Frenkel (6), and Frank (7). From this work it was concluded that the first step in crystal growth is "adsorption" on the surface, whereafter "adatoms" (2) diffuse to steps and along steps to kinks, where they are incorporated into the lattice, after which repetition of these steps ("repeatable step") brings about the incorporation of a kink atom into the lattice (cf. Fig. 1 and Conway and Bockris (21)).
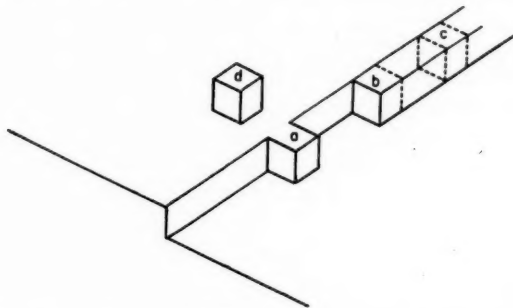
FIG. 1. Schematic view of metal–solution interface depicting (a) atom at edge, (b) kink, (c) atom in edge, (d) adion.

After all the stepped surfaces have been used up, two-dimensional nucleation was expected in the earlier theory (1, 2, 3, 4, 5, 6) to occur on surfaces of low index, which implied that some degree of supersaturation was necessary for the continuation of the growth process. Experiments show, however, that usually crystals can grow indefinitely without a large degree of supersaturation of the surface. This discrepancy arises because the model for crystal growth, sketched above, applies to the growth of a perfect crystal, but most real crystals contain imperfections which provide the steps necessary for growth.

Frank *et al.* (7) have studied the influence of imperfections, mainly screw dislocations, on the growth mechanism. Screw dislocations were found to provide a practically inexhaustible source of steps which turn at higher supersaturations into spirals, forming growth pyramids on the surface.

The equations deduced by Frank (7, 8) can also be used for a discussion of electrolytic crystal growth if the parameters are appropriately changed, but it is necessary to keep in mind that the energetic properties of a metal surface in contact with an electrolytic solution differ essentially from those of a surface in contact with its vapor. Thus, in a solution there exists at the metal surface an electrical double layer, with a field strength of about 10^7 v cm^{-1}; ions from the solution phase are adsorbed on the surface, etc. (13).

For electrolytic crystal growth an important difference to growth of crystals from the gas phase is also that an activation energy has to be overcome to make it possible for the metal ions to cross the electrical double layer and to strip off the solvation sheath (21).

It is the electric field at the metal–solution interface which gives rise to two possible extreme idealizations for models of electrolytic crystal growth (9).

In model A nearly all the electrode surface is active for the process of transferring ions from the solution to the electrode (transfer reaction). The particles on the surface carry probably a partial charge and are therefore best termed adions (21). The consecutive process to that of transfer is surface diffusion of adions to the growth positions on the surface, the final step being incorporation of adions into the lattice. In addition, at higher concentration of adions, nucleation on the surface may occur.

In model B the ions from the solution transfer directly to growing points on the surface (active centers).

Little informative work has been hitherto possible on electrolytic crystal growth, mainly because of experimental difficulties. Metal surfaces readily adsorb impurities, possibly at the active centers important for the crystal growth process. Because of this sensitivity to impurities, one of the main experimental difficulties in such work is keeping a small metal area (of the order of 0.01–1 sq. cm in area) in contact with solution but free of adsorbed impurities. A further intrinsic difficulty is that of carrying out significant measurements whilst the electrode surface remains essentially constant, i.e., observations of the rate of the reaction of a given potential must be made rapidly.

Because of these experimental difficulties only qualitative discussions of electrolytic crystal growth have been possible until now (9, 10). But experiences gained in the preparation of electrodes for studies of the hydrogen evolution reaction (11) and in the development of improved electronic measuring techniques (12) seemed to make worth while an experimental study of the kinetics of electrolytic metal deposition and dissolution.

At silver electrodes, Gerischer et al. (14) observed a deviation from the current–potential relationship to be expected if a rate-determining transfer reaction occurs (a similar observation was recorded by Mattson (15) for copper deposition on copper). These workers found that the exchange current for the system Ag/Ag^+ is independent of the concentration of silver ions in the solutions which appeared to indicate a rate-determining crystallization process for the over-all metal deposition.* Kaischew and co-workers (16) showed by microscopic studies that growth spirals are formed on the silver surface during deposition, thus supporting the applicability of Frank's theory of crystal growth by means of dislocation to electrolytic crystal growth.

It is the aim of the present work to find out: (1) which is the general path (i.e. that of model A or η model B) by which the ions pass from their initial state of hydration in the solution to their final state in the lattice and vice versa, and (2) which step in this path is rate-determining under given sets of conditions.

METHOD OF INVESTIGATION: THE GALVANOSTATIC METHOD

1. Introduction

In the study of the mechanism of crystal growth from the gas phase, the rate of crystal growth is studied as a function of the degree of supersaturation of the vapor. The corresponding measurement here is that of the rate of growth as a function of potential.

*Gerischer has also recently carried out, independently of the present workers, potentiostatic (24) and galvanostatic (25) measurements on silver dissolution, and comes to conclusions similar to those described here (cf. Mehl and Bockris (28)). Different i_0 values recorded in the work of this author, compared with those recorded here, depend upon the quite different methods of preparation of the electrode surfaces used.

If one tries to obtain this i–η relationship under conditions of long-time (minutes) polarization, changes of the electrode surface with time due to the deposition or dissolution process itself, or adsorption of residual impurities, even from highly purified solutions, may make interpretation difficult. Consequently, short-time (milliseconds) polarization is preferable, and the galvanostatic (constant current) method (17) was chosen for the present investigation. Another advantage of this method compared with long-time measurements is that it enables additional evidence concerning the deposition mechanism to be obtained from the potential–time function.

The electrodes are in contact with the solution for minutes (between the time the protecting bulb around the electrodes is broken and that at which the sweep is taken). Therefore, extreme purification of solutions was carried out.

2. Double Layer Charging and Transfer

If a constant current density, i, is switched onto an electrode, this current divides itself into two components. The first one, i_C, is used for charging the electrical double layer at the electrode–solution interface; the second part, i_F, brings about transfer of ions across the double layer from the solution to the electrode surface. The current density, i_C, rapidly decreases with time, during the galvanostatic charging process, which means that i_F increases with time, because

$$[1] \qquad\qquad i = i_C + i_F$$

is constant. If i_F is controlled exclusively by the transfer reaction, then:*

$$[2] \qquad i = Cd\eta/dt + i_0(e^{-\beta\eta\ zF/RT} - e^{(1-\beta)\eta\ zF/RT}),$$

where C = the double layer capacity; i_0 = the exchange current density for the transfer controlled reaction; $0 < \beta < 1$; R, T, and F have their usual significance; and z is the valency of the cation in solution.

A general solution of this equation with the assumption that the double layer capacity is independent of potential was given by Rojter, Juza, and Polujan (17). The η–i relationship thus obtained is complicated and therefore difficult to verify by experiment. For small overpotentials, $\alpha\eta\ zF/RT < 1$, and the solution of equation [2] is, again assuming C independent of potential,

$$[3] \qquad\qquad \eta_t = \eta_\infty(1 - e^{-t/\tau_1})$$

with η_∞ = steady state overpotential,

$$[4] \qquad\qquad \tau = (RT/zFi_0)C.$$

Equation [3] is only an approximation as the double layer capacity changes during the charging process with time so that an exact separation of i_F and i_C is not possible (18). This means that for the analysis of electrode reactions with help of the $\eta(t)$ functions, only such reactions are detectable which have a relaxation time of $\tau > \tau_1$.

3. Electrolytic Resistance of Solution

The ohmic potential drop between reference electrode and measurement electrode can easily be determined because it appears in the $\eta(t)$ function as a jump parallel to the potential axis (see Fig. 5).

*It is assumed that the maximum supply of ions from the bulk of the solution to the double layer (by diffusion and electrolytic transport) far exceeds that required for deposition.

4. Transfer and Surface Diffusion of Ions

In the following considerations, constant Faradaic current $(t \gg \tau_1)$ is assumed. If the surface diffusion coefficient for adions on the metal surface is sufficiently small, so that this process is important for the rate of the over-all process, the surface concentration of adions increases during polarization to a value above that of the surface concentration corresponding to equilibrium, and becomes less than this value during dissolution. In this section the discussion will be limited to the consideration of low overpotential, i.e., a small degree of supersaturation.

Assuming that the adions cause only a small reduction of the free surface area for the transfer reaction and neglecting concentration polarization in the solution, the potential–time function is:

$$[5] \qquad (i_F)_t = i_0[e^{-\beta\eta_t \, zF/RT} - (c_{\eta(t)}/c_0) \, e^{(1-\beta)\eta_t \, zF/RT}]$$

where c_0 is the concentration of adions at equilibrium and $c_{\eta(t)}$ is the concentration of adions at a time t when the overpotential has reached a value of η. For $\eta < RT/\alpha \, zF$ and neglecting second-order terms, one obtains, by expansion of [5] and rearrangement,

$$[6] \qquad -\eta_t = (RT/zF) \, (i/i_0) + (RT/zF) \, (\Delta c_{\eta(t)}/c_0),$$

where

$$\Delta c_{\eta(t)} = c_{\eta(t)} - c_0.$$

Hence, η depends in this case both on i_0 for the transfer reaction and the "concentration overpotential due to surface diffusion".

It is necessary to express $c_{\eta(t)}$ as a function of i and t. Now:

$$[7] \qquad dc/dt = (i_F/zF) - v,$$

where v is the average of the surface diffusion flux of the adions during their passage from the point at which they are transferred to the metal surface and that at which they meet a crystal building point.

Surface diffusion on metal crystals has been dealt with thoroughly by Frank et al. (7) and applied to electrolytic deposition by Vermilyea (10). The present results are consistent with the simple assumption (for $|\eta| \leqslant 5$ mv) that the surface diffusion flux is proportional to the surface supersaturation, $[(c_{\eta(t)}/c_0) - 1]$. Hence:

$$[8] \qquad v = v_0[(c_{\eta(t)}/c_0) - 1]$$

assuming that, near to kinks, the adion concentration remains at equilibrium value, c_0, whilst on crystal planes, where the metal ions are regarded as first being transferred from the solution to the metal surface, the mean surface concentration of adions is $c_{\eta(t)}$. Substituting [8] into [7] and integrating yields

$$[9] \qquad \frac{c_{\eta(t)} - c_0}{c_0} = \frac{\Delta c}{c_0} = \frac{i_F}{zFv_0}(1 - e^{-t/\tau_2})$$

$$[10] \qquad \tau_2 = c_0/v_0.$$

Thus, the steady state value of the increased concentration of adions over that expected for pure transfer control is given $(t = \infty)$ by:

$$[11] \qquad \Delta c/c_0 = i_F/zFv_0.$$

With [9] and [6] the $\eta(t)$ function at small overpotentials, with both surface diffusion

and transfer of ions across the double layer as influencing the value of η_t, and for time $t > \tau_1$, becomes:

$$[12] \qquad -\eta_{(t)} = \frac{RT}{zF}\left[\frac{i_F}{i_0} + \frac{i_F}{v_0 zF}\left(1 - e^{-(v_0/c_0)\,t}\right)\right].$$

For times t, for which $\tau_1 < t < \tau_2$ and with $\tau_2 = c_0/v_0$, from [12]

$$[13a] \qquad -\eta_{(t)} = \frac{RT}{zF}\left(\frac{i_F}{i_0} + \frac{i_F}{c_0 zF}\,t\right)$$

and

$$[13b] \qquad \frac{d\eta_t}{dt} = \frac{RT}{z^2 F^2}\frac{i_F}{c_0}$$

5. Current–Potential Relations in the Steady State

(a) *Transfer is rate-determining.*—The i–η function will then be controlled by:

$$[14] \qquad i_F = i_0(e^{-\beta\eta\, zF/RT} - e^{(1-\beta)\eta\, Fz/RT}).$$

The adion concentration is at its equilibrium value and therefore surface coverage can be neglected (6).

(b) *Transfer and surface diffusion control the role of the over-all reaction.*—With [12] and [11] we get

$$[15]^* \qquad i_F = \frac{e^{-zF\eta/RT} - 1}{(1/i_0)\,e^{-(1-\beta)\eta\, zF/RT} + 1/zFv_0}.$$

(c) *Surface diffusion is rate-determining.*—For

$$zFv_0 < i_0\,e^{(1-\beta)\eta\, zF/RT}$$

there follows,

$$[16] \qquad i_F = zFv_0(e^{-\eta\, zF/RT} - 1).$$

Equations [15] and [16] have been derived under the assumption that v_0 is overpotential-independent. Theoretical work by Frank *et al.* (7) shows, however, that this assumption is incorrect; v_0 increases with increasingly negative overpotential (cf. Discussion).

EXPERIMENTAL

1. Galvanostatic Arrangement (Fig. 2)

The potential source consisted of dry batteries, e.m.f. 90–200 v. Precision resistors (I.R.C.) are represented by R and were arranged in 10 steps, from 1 kilohm to 6.2 meg. The letter O represents a Tektronix oscilloscope, type 531, with type 53/54D plug-in preamplifier. The potential–time curves were photographed with an Exakta camera having a 50-mm lens. Projection of the 35-mm film was made with an enlargement of about ten times to obtain numerical η–t curves. The switch S contained a Western Electric relay, type 175, having a rise time of about 10^{-7} sec[22].

2. Treatment of Solution and Electrodes

The solution was made from A.R. $HClO_4$, which was distilled three times *in vacuo*, the last distillation being into a burette leading directly to the cell. The water was distilled

---

*Equation [15] is valid only under conditions such that the surface coverage with adions is sufficiently low to yield negligible hindrance to the transfer of ions from the solution. In fact, if v_0 is sufficiently low a surface coverage could build up and the first term in [5] should be preceded by a term of the type $1 - \theta_\eta/1 - \theta_0$, where θ_η is the surface coverage at overpotential η. A limiting current could then ensue at sufficiently high overpotentials. But this case is unlikely because of nucleation and a possible increase of v_0 with increasing overpotential.
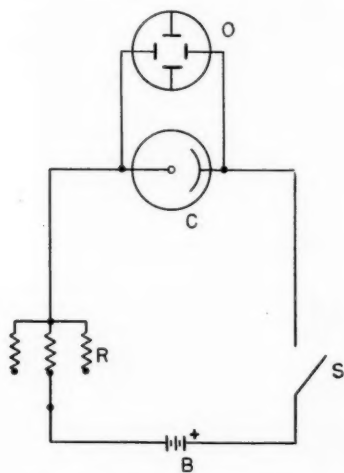
FIG. 2. Galvanostatic arrangement:
B: battery, 90 v; C: measuring cell; O: oscilloscope; S: switch; and R: resistances.

several times and had a final conductance of about 10^{-7} mho cm^{-1}. The AgClO$_4$ ("pure" grade) was recrystallized twice outside the system and twice inside and then introduced into a special cell in which it was subjected to pre-electrolysis for about twenty-four hours with alternating current density of about 3×10^{-1} amp cm^{-2}. The solution was vigorously stirred with carefully purified nitrogen gas, the cathode was of silver, the anode of platinum (vigorous stirring prevented silver needles from growing through the closed tap between cathode and anode compartments).*

The electrodes were prepared by heating a thin (spectroscopically pure) silver wire (0.5 mm diameter) in an atmosphere of purified hydrogen in a quartz tube. A spherical shape was attained by partial melting. Finally, the electrode was sealed in a glass bulb containing only hydrogen, or helium, and the bulb was broken in the solution shortly before measurement. A detailed description of this procedure has been published (19). This method of preparing electrodes is similar in nature to "thermal etching", which has been studied experimentally and theoretically by several authors (20). During the heating process a rearrangement of surface atoms of the polycrystalline surface occurs, to produce facets with simple crystallographic indices; grain boundaries occur as grooves. As the electrodes are being cooled down in a hydrogen stream (high heat conductivity), a relatively high thermal stress would appear in the metal, producing a high concentration of dislocations.

Electron micrographs were taken of the electrodes prepared in this way. They show etch pits with a density of about 10^7 per sq. cm (Fig. 3). According to Hirth and Pound (26, 27), these may be interpreted as due to dislocations with a screw component normal to the surface. Occasionally electrodes indicate surface films of unknown origin (possibly connected with accidental contact between the hot metal and the glass tube during electrode preparation) and results from such electrodes were not further examined.

Other experimental conditions, particularly with regard to purification of gases, etc., were as already described (29).

*The exterior of the pre-electrolysis cell was coated black to exclude light effects. The measurements were carried out under conditions of minimum illumination.
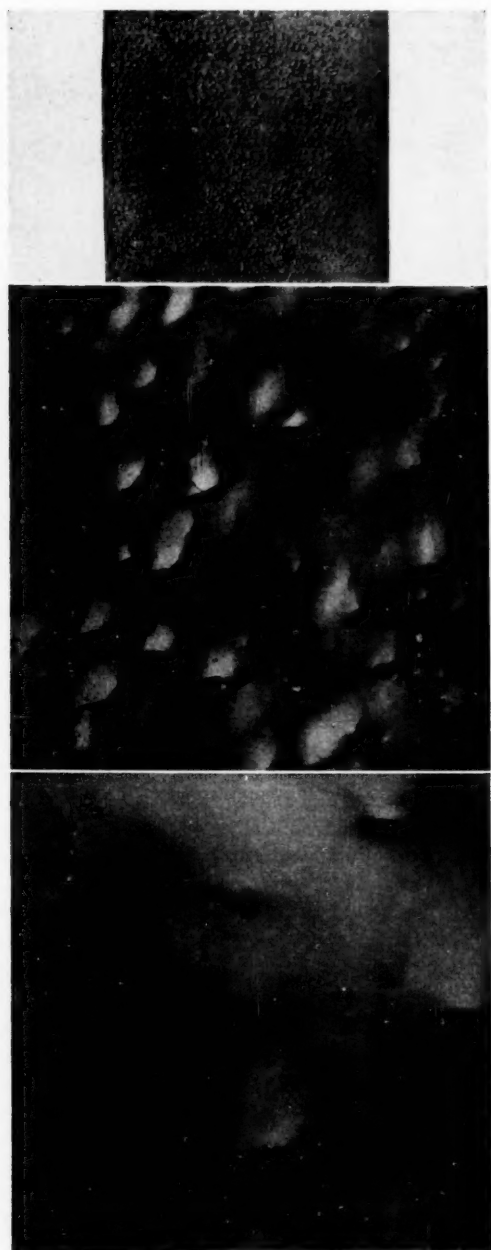
FIG. 3.   Electromicrographs of polycrystalline thermally etched silver surfaces.*
   (a) Etch pits due to dislocation sites
          Magnification 4000 ×
          Magnification 33000 ×
          Magnification 78000 ×
*For footnote see following page.
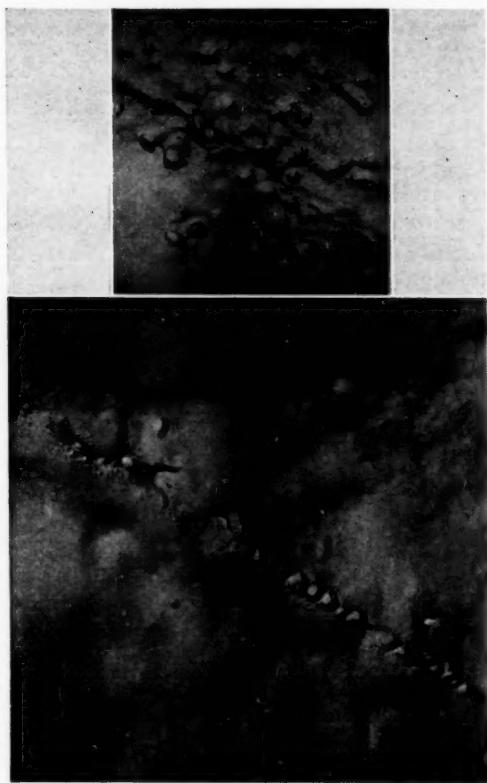
Fig. 3. Electromicrographs of polycrystalline thermally etched silver surfaces.*
(b) Grain boundary with precipitate
Magnification 13000 ✕
Magnification 33000 ✕

*SiO *replicas the contact side of which was shadowed with tungsten oxide. The work was carried out by H. G. Wilsdorf to whom the authors' thanks are due.*

3. Procedure

After one of the four electrodes in the cell had been lowered by means of a sliding fit joint into the solution, the glass bulb surrounding it was broken and the electrode adjusted until it was inside a platinum gauze basket which acted as counterelectrode. The outside resistance R (Fig. 2) was set at a value appropriate for the given current density, and a current impulse given to the electrode. By means of the switch S (22) (Fig. 2) the impulse was restricted to an amount of electricity not more than 10^{-4} coulombs cm^{-2} (i.e., the amount to cover about 1 geometric cm^2). The resulting potential–time curve was photographed.

Such photographs were made at some ten current densities (over the range 3×10^{-4} to 8×10^{-1} amp/cm^2) for each electrode and in each run a maximum of four electrodes were examined. Measurements were made at a variety of concentrations between 10^{-2} and 10^{-1} moles l.$^{-1}$ so that concentration polarization could be avoided. At the end of a series of measurements with increasing current density, some sweeps at lowest current densities were repeated and results, closely similar to those taken earlier, found.
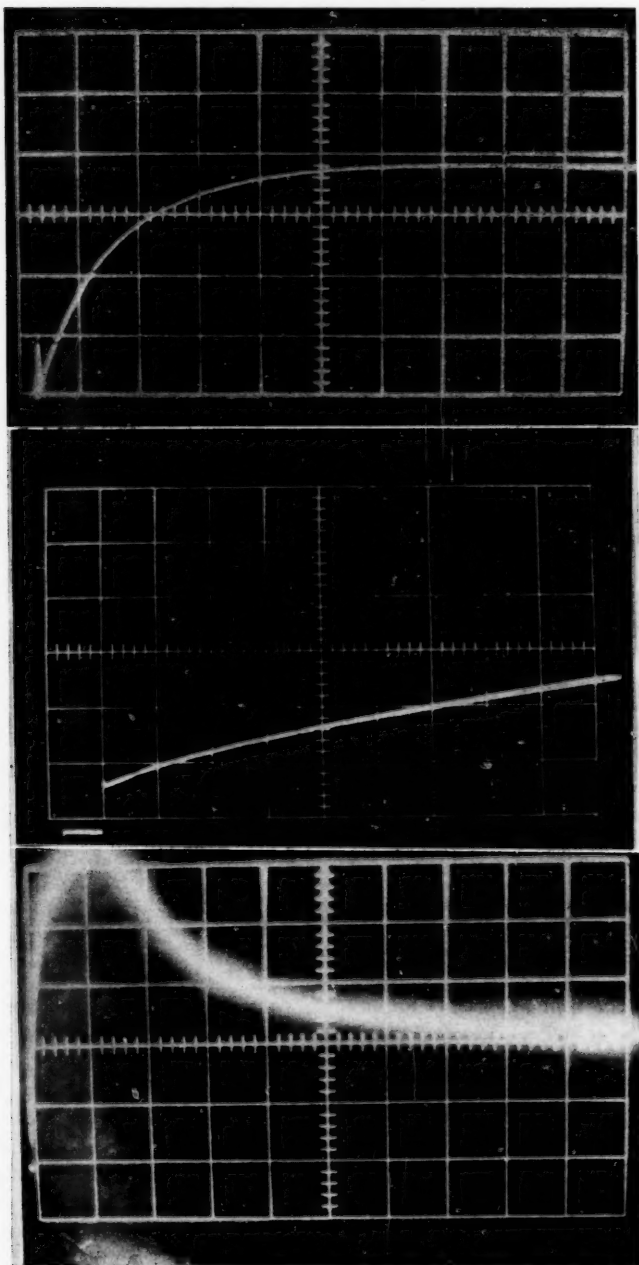
FIG. 4.   (*Top*) Charging curve at low current density: (AgClO$_4$): 2×10^{-1} mole/l.; $i = 2$ ma cm^{-2}; units: t—axis, 2 msec, η—axis, 1 mv.
FIG. 5.   (*Center*) Charging of electrical double layer: $i = 2.5$ ma/cm^2; $t = 10^{-4}$ sec; $\eta = 2$ mv.
FIG. 6.   (*Bottom*) Superpolarization: $i = 500$ ma/cm^2; units: $t = 5\times10^{-3}$ sec; η: 30 mv.

4. Results

Figure 4 shows a typical potential–time curve for the current density 2 ma cm^{-2} at a concentration of 0.2 N AgClO$_4$ in 1 N HClO$_4$ for cathodic polarization. Similar results were obtained for anodic polarization. In Fig. 5, a typical η–t relationship for short times is shown. Figure 6 shows a typical η–t curve measured in unpurified solution, which exhibits the phenomenon of superpolarization.

Figure 7 shows a typical plot of the log i–η_∞ relation for cathodic and anodic polarization, and Fig. 8 a typical linear relation of i to η_∞ at low current densities.
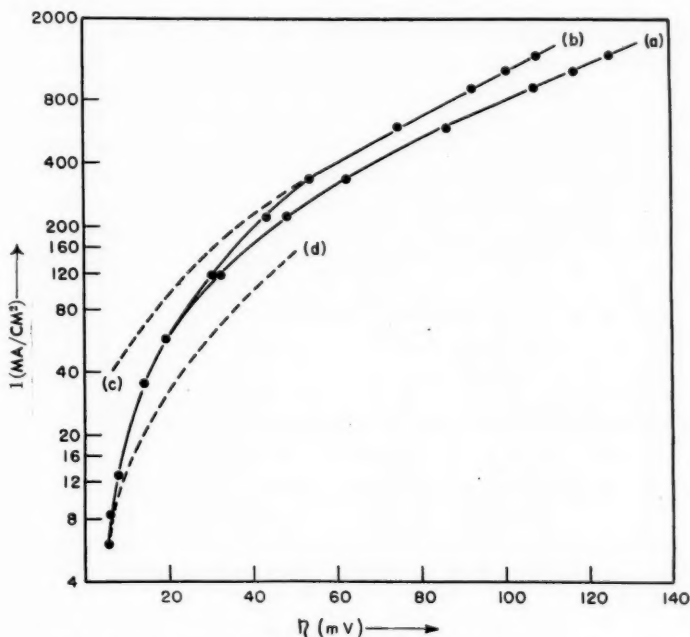
FIG. 7.   Log i–η plot for deposition (a), dissolution (b).
$c_{AgClO_4} = 2 \times 10^{-1}$ mole/l.
(c) Represents (- - - -) slow transfer reaction.
(d) Represents (- - - -) simple diffusion theory.

DISCUSSION

1. Potential–Time Curves

At very short times the current flowing during build-up of potential is used almost exclusively for the charging of the double layer, the capacity of which is therefore given (in the linear $\eta_{(t)}$–t region) by:

[17] $$C = it/\eta_{(t)}.$$

This linear η–t relationship can be expected for times limiting low value of t. With a double-layer capacity of about 20 μ F cm^{-2}, $RT/zFi_0) = 2$ ohm cm^2 and allowing a roughness factor 2, the linear relationship can be expected for times of about $t < 10^{-4}$ second, when $\eta < RT/zF$. In fact, a linear relationship was observed for more than 10^{-3} second with a slope which according to [17] would give an impossible value of 500
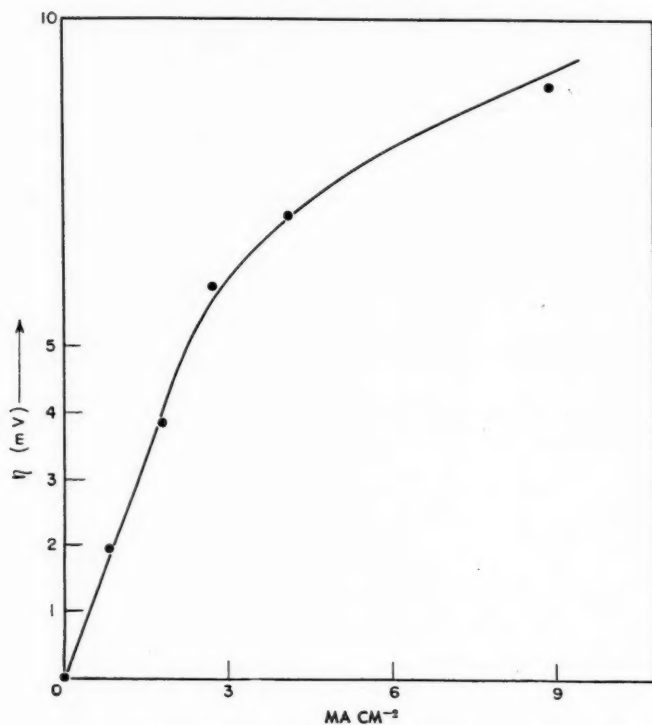
FIG. 8. i–η plot for low current densities. (AgClO$_4$) = 2.10^{-1} mole l.$^{-1}$.

μ F/cm^2 for the double-layer capacity. Similarly, if the transfer step alone were rate-determining, equation [3] shows that the steady state overpotential should be reached at a time of about

[18] $$t = 4\ (RT/zFi_0)C$$

for $\eta < RT/zF$. The actually observed values for this time are more than ten times larger than those predicted.

This slow rise time may be interpreted in terms of the build-up of an adsorption layer of adions, as shown in the next section.*

2. *Potential–Time Relation and the Role of Surface Diffusion*

From [13]:

[19] $$\eta_{(t)} - \eta_\infty = \frac{RT}{zF}\frac{i_F}{zFv_0}\,e^{-(v_0/c_0)\,t}.$$

Also, from [12]:

[20] $$\eta_{t=0} = \frac{RT}{zF}\frac{i_F}{i_0}$$

and

*A slow reaction in the solution cannot be responsible for this behavior because during deposition of metals upon amalgams, behavior may be satisfactorily interpreted in terms of rate-controlling transfer (23).

[21]
$$\eta_{t=0} - \eta_{\infty} = \frac{RT}{zF} \frac{i_F}{zFv_0}.$$

Further, from [12]:

[22]
$$\eta_{\infty} = \frac{RT}{zF}\left(\frac{i_F}{i_0} + \frac{i_F}{zFv_0}\right).$$

Note that in the above equations the double-layer charging has been neglected; they are therefore valid only for times much greater than the rise time of the transfer reaction, i.e., in the systems reported on here, about 10^{-4} seconds (also, it has been assumed that $|\eta| < 5$ mv).

According to [19] $\eta_{t=0}$ can be got by extrapolating a plot of log $(\eta_t - \eta_{\text{st}})$ against t to $t = 0$ (Fig. 9).* The value for i_0 obtained this way [22] can be compared with values obtained by the independent method of extrapolating the linear part of η–log i relation to $\eta = 0$. The values agree to about $\pm 30\%$. If one takes into consideration that the accuracy with which the potential can be determined is $\pm 5\%$ and the overpotential due to transfer (at $|\eta| \leqslant 5$ mv) is about 10% of the total overvoltage, the agreement between the i_0 values obtained in these two independent ways is satisfactory. This agreement confirms the interpretation of the slow rise time of the η–t curve on the basis of slow surface diffusion of adions.
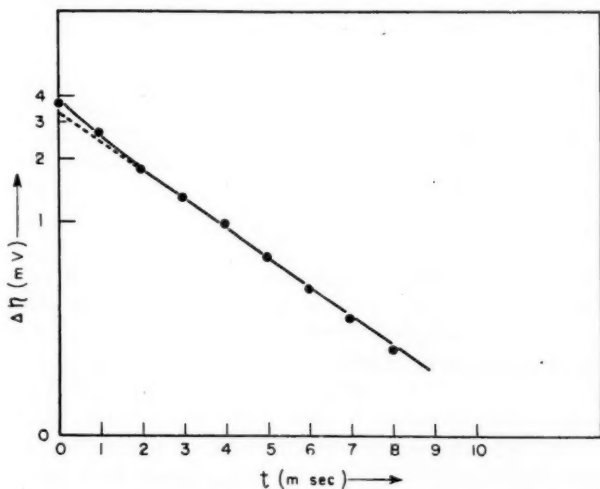
FIG. 9. Separation of total polarization into diffusion and transfer polarization by extrapolation of galvanostatic $\eta(t)$ curves (for parameters, see Fig. 4).

Table I gives values of i_0 obtained by the extrapolation of the Tafel line.† With the known values of i_0, [22] allows the calculation of v_0, values of which are shown in Table I.

3. Concentration of Adions at the Reversible Potential

From [19] we get:

*The $\eta_{t=0}$ referred to is a quantity susceptible only to calculation upon a model such as that suggested. It signifies the potential of the electrode during charging with respect to the corresponding electrode, under conditions such that the double-layer charging is terminated, but before the surface diffusion has had time to affect the concentration of adions over that corresponding to the reversible potential. Correspondingly, $\eta_{t=0}$ depends only upon i_0, and not upon v_0.

†The i_0 values for deposition and dissolution agree well; values of β are almost the same ($\simeq 0.50$) for each process.

[23] $$(d/dt) \ln(\eta_t - \eta_\infty) = -v_0/c_0.$$

From [23] (with v_0 from [21]) and from [13a] directly, the concentration of adions at the reversible potential may be calculated. Both methods lead to the same results. The values obtained this way are presented in Table I.

TABLE I

AgClO$_4$ mole/liter	i_0 amp cm^2	zFv_0 amp/cm^2	c_0 mole/apparent cm^2
2.0×10^{-1}	0.10	1.2×10^{-2}	8×10^{-10}
1.3×10^{-1}	0.08	1.0×10^{-2}	2×10^{-9}
1.0×10^{-1}	0.07	1.4×10^{-2}	4×10^{-10}
0.8×10^{-1}	0.07	1.2×10^{-2}	3×10^{-9}
0.8×10^{-1}	0.07	1.6×10^{-2}	6×10^{-10}
0.6×10^{-1}	0.06	1.2×10^{-2}	1×10^{-9}
0.6×10^{-1}	0.06	1.1×10^{-2}	8×10^{-10}
0.4×10^{-1}	0.05	1.2×10^{-2}	1×10^{-9}
0.2×10^{-1}	0.04	1.5×10^{-2}	6×10^{-10}
0.1×10^{-1}	0.03	1.1×10^{-2}	5×10^{-10}

4. Current–Potential Relation

With the aid of values of v_0 and i_0 calculated as described above, it is possible to evaluate the theoretical $\eta-i$ and $\eta - \log i$ relations for the steady state. These are compared with experiment in Fig. 7.

5. Mechanism of Deposition and Dissolution

As Fig. 7 shows, for silver deposition and dissolution for electrodes prepared by thermal etching, surface diffusion of adions is the principal rate-determining step at low overpotentials, and at high overpotentials the transfer of ions from the solution to the electrode is the rate-determining step. As v_0 does not depend upon the concentration of silver ions in solution (see Table I), the concentration dependence of i_0 is given by:

$$\partial \ln i_0 / \partial \ln \alpha_{Ag} = \beta.$$

It can be predicted from the values for i_0 and v_0 (Table I) that the above statement concerning rate control will be valid down to Ag$^+$ concentrations of about 10^{-4} to 10^{-5} mole l.$^{-1}$. At lower concentrations than these, the transfer step will be rate-controlling at all current densities (for the type of silver surfaces used in the present study).

The path determined for this fundamental example of simple metal deposition corresponds therefore more closely to model A rather than model B (see above).

The transition from rate-determining surface diffusion to rate-determining transfer is due to the decrease of the average distance between growing lines (and hence increase of v_0) with increasing overpotential. The dependence of v_0 upon potential has not yet been subject to a satisfactory theoretical treatment. Provisionally, the following empirical equation may be suggested: $v_0(\eta) = v_0 \, e^{-\eta \, zF/RT}$, whereupon the complete course of the $i-\eta$ relation can thus be described by the equation:

[24] $$i = \frac{e^{-\eta \, zF/RT} - 1}{(1/i_0) \, e^{-(1-\beta)\eta \, zF/RT} + (1/v_0 zF) \, e^{zF\eta/RT}}.$$

For higher overpotentials (24) gives:

[25] $$i = \frac{e^{-\eta \, zF/RT} - 1}{(1/i_0) \, e^{-(1-\beta)\eta \, zF/RT}},$$

and for low cathodic overvoltages:

[26] $$i = zFv_0 \, e^{-\eta \, zF/RT} (e^{-zF \, \eta/RT} - 1).$$

Correspondingly, for crystal growth from the vapor phase, a linear dependence of the rate of growth upon the degree of supersaturation has been found at higher super-saturations (linear law), and a parabolic dependence upon supersaturation at low super-saturations (cf. Frank *et al.* (7)).

The "critical overpotential", which separates the linear and the parabolic law, depends on the ratio i_0/zFv_0 and thus upon the concentration of Ag$^+$ ions in solution (upon which i_0 depends).

It should be noted here that a perfect parabolic law, viz.,

$$i = k(e^{-zF\eta/RT}-1)^2$$

(where k is a constant) can only be expected for a single dislocation and a function such as that reported here for distribution of dislocations on the crystal surface.

6. Equilibrium Concentration of Adions

The equilibrium concentration of adatoms c_{ad} for the system metal–vapor can easily be calculated. With an energy of vaporization for silver of about 65 kcal, it is found that the equilibrium concentration of adions during electrochemical deposition is very much higher than the equilibrium concentration of adatoms during deposition from the vapor phase.

7. Superpolarization

This phenomenon (Fig. 6) occurs at higher overvoltages, 100 mv, and is difficult to study experimentally because of its poor reproducibility. Superpolarization was observed almost exclusively for solutions which had not been well purified so that the phenomenon might well be one of "over-shoot" (24) due to supersaturation of the surface with adions. Vermilyea (10) has discussed this type of phenomenon in terms of dislocation theory (7).

APPENDIX

Certain Terms Used in Electrochemical Crystal Growth Compared with Those Used in Crystal Growth from the Vapor Phase

Burton, Cabrera, and Frank (7) define supersaturation in the vapor by

[1*]
$$\sigma = \alpha - 1; \quad \alpha = p/p_0,$$

where p is the actual vapor pressure and p_0 the saturation value. The supersaturation of adsorbed molecules on the surface is defined by,

[2*]
$$\sigma_s = \alpha_s - 1; \quad \alpha_s = c_s/c_0$$

where c_s and c_0 are the actual and equilibrium concentration of adsorbed molecules respectively.

The "current" from the vapor to the surface is written as

[3*]
$$j = (\alpha - \alpha_s)c_0/\tau_s,$$

where τ_s is the mean life of an adsorbed atom on the surface defined by

[4*]
$$\tau_s = \frac{1}{\nu} \exp(W'_s/RT)$$

where W' = evaporation energy from the surface to the vapor, and ν = frequency factor. In the present theory, the current from the solution to the surface is written (cf. 5) as:

[5*]
$$i = (e^{-zF\eta/RT}-c_s/c_0)i_0\, e^{(1-\beta)\eta\, zF/RT}.$$

Comparison of [3*] and [5*] yields the following analogies:

Comparison of expressions used in crystal growth from vapor phase and by electrolytic means

	Burton, Cabrera, and Frank (7)(vapor phase)	This paper (electrolytic)
Supersaturation in the vapor (solution)	$p/p_0 - 1$	$e^{-zF\,\eta/RT} - 1$
Supersaturation on the surface	$c_s/c_0 - 1$	$c_s/c_0' - 1$
Mean lifetime of adsorbed molecules	τ_s	$(c_0/i_0)\,e^{-(1-\alpha)z\,\eta F/RT}$

REFERENCES

1. GIBBS, J. W.   Collected works. Longmans, Green & Co., Ltd., London. 1928.
2. VOLMER, M.   Kinetik der Phasenbildung. Verlag von Theodor Steinkopff, Dresden und Leipzig. 1939.
3. KOSSEL, W. O.   Nachr. Ges. Wiss. Göttingen, 135 (1927).
4. STRANSKI, J. N.   Z. physik. Chem. **136**, 259 (1928).
5. BECKER, R. and DÖRING, W.   Ann. Physik, Leipzig, **24**, 719 (1935).
6. FRENKEL, I.   J. Phys. Chem. (U.S.S.R), **9**, 392 (1945).
7. FRANK, F. C.   Discussions Faraday Soc. **5**, 48, 67 (1949). CABRERA, N. and BURTON, W. K.   Discussions Faraday Soc. **5**, 33, 40 (1949). BURTON, W. K., CABRERA, N., and FRANK, F. C.   Nature, **163**, 398 (1949). BURTON, W. K., CABRERA, N., and FRANK, F. C.   Phil. Trans. Roy. Soc. London, A, **243**, 299 (1951). FRANK, F. C.   Phil. Mag. **41**, 200 (1950).
8. FORTY, A. J. and FRANK, F. C.   Proc. Roy. Soc. A, **217**, 262 (1953).
9. FISCHER, H.   Elektrolytische Abscheidung und Elektrokristallisation von Metallen. Springer-Verlag, Berlin. 1954.
10. VERMILYEA, D. A.   J. Chem. Phys. **25**, 1254 (1956).
11. BOCKRIS, J. O'M. and CONWAY, B. E.   J. Sci. Instr. **25**, No. 8, 283 (1948).
12. DELAHAY, P.   New instrumental methods in electrochemistry. Interscience Publishers, Inc., New York. 1954.
13. PARSONS, R.   Modern aspects of electrochemistry. *Edited by* J. O'M. Bockris. Academic Press, Inc., New York. 1954. Chap. IV.
14. GERISCHER, H. and VIELSTICH, W.   Z. Elektrochem. **56**, 380 (1952). GERISCHER, H. and VIELSTICH, W. Comité intern. thermodynam. et cinét. électrochim. IV, Réunion. (1952). GERISCHER, H. and TISCHER, R. P.   Z. Elektrochem. **58**, 819 (1954).
15. MATTSON, E. and LINDSTROM, R.   Comité intern. thermodynam. et cinét. électrochim. VI, Réunion. Poitiers. (1954).
16. KAISCHEW, R., MUTAFTSCHIEW, B., and NENOW, D.   Z. physik. Chem. **205**, 341 (1956).
17. ROJTER, W. A., JUZA, W. A., and POLUJAN, E. S.   Acta Physicochim. U.R.S.S. **10**, 389, 845 (1939).
18. BOCKRIS, J. O'M., MEHL, W., CONWAY, B. E., and YOUNG, L.   J. Chem. Phys. **25**, 776 (1956).
19. CONWAY, B. E., BOCKRIS, J. O'M., and MEHL, W.   J. Sci. Instr. **33**, 400 (1956).
20. GWATHMEY, A. T. and BENTON, A. F.   J. Chem. Phys. **8**, 431 (1940). CHALMERS, B., KING, R., and SHUTTLEWORTH, R.   Proc. Roy. Soc. (London), A, **193**, 465 (1948). MULLINS, W.   J. Appl. Phys. **28**, 333 (1957).
21. BOCKRIS, J. O'M. and CONWAY, B. E.   Proc. Roy. Soc. (1958) (In press).
22. MEHL, W., DEVANATHAN, M. A. V., and BOCKRIS, J. O'M.   Rev. Sci. Instr. **29**, 180 (1958).
23. RANDLES, J. E. B. and SOMERTON, K. W.   Trans. Faraday Soc. **48**, 951 (1952).
24. GERISCHER, H. and TISCHER, R. P.   Z. Elektrochem. **61**, 1159 (1957).
25. GERISCHER, H.   Private communication.
26. HIRTH, I. P. and POUND, M. G.   Acta Met. **6**, 1958.
27. HIRTH, I. P. and POUND, M. G.   Meeting of AIME. New York. 1958.
28. MEHL, W. and BOCKRIS, J. O'M.   J. Chem. Phys. **27**, 818 (1957).
29. BOCKRIS, J. O'M. and CONWAY, B. E.   J. Chem. Phys. **28**, 707 (1958).

EXCHANGE BETWEEN METALS AND THEIR IONS IN SOLUTION[1]

Cecil V. King and Nancy E. McKinney

ABSTRACT

The mechanisms by which a metal specimen can acquire radioactivity when immersed in a tracer solution of its own ions are discussed. Consideration is given to the roles of exchange current, adsorption, local cell electrolysis, corrosion, and self-diffusion within the metal. It is shown that exchange current cannot be measured by the tracer method unless conditions are unusually favorable, and that too little attention has been paid to the role of internal diffusion. Some experimental results with silver are presented and the importance of internal diffusion is shown.

INTRODUCTION

A great many articles dealing with metal – metal ion exchange have been published, but the interpretation of experimental results is not entirely satisfactory. The role of diffusion within the metal has been especially puzzling. It is the purpose of this paper to discuss some of the pertinent factors in exchange and to indicate their relative importance. New experimental work with silver is used for illustration.

Exchange Current

A kinetic interpretation of the Nernst equation for "electrode potential"

$$E = RT \ln P/p$$

or its modern equivalent, implies a continual exchange between ions in solution and ions or atoms within the metal phase. The equilibrium exchange rate, when expressed in electrical units, is known as the exchange current i_0. Direct proof of exchange is possible through the use of radioisotopes as tracers, but the tracer method can measure i_0 only under conditions probably never attainable in practice.

1. Assume one face of a metal single crystal to be immersed in a solution of its own ions (with tracer), and that there is no corrosion, no adsorption or electrical double layer formation involving the salt, no local cell electrolysis, no internal diffusion, and no temporary depletion of tracer in the solution next the interface. Exchange can then take place with only one atomic layer on the metal surface, and the rate of activity pickup, extrapolated to zero time, will give the exchange current. Or, an expression could be found for the rate of attainment of radioactive equilibrium, from which the specific exchange rate could be calculated. A value of $i_0 = 5 \times 10^{-8}$ amp/cm² corresponds to exchange of about one atomic layer per hour, but since much re-exchange would occur, radioactive pickup would continue for several hours. For silver, i_0 is reported to be about 10^{-3} amp/cm² (1), and radioactive equilibrium with the surface layer should require only a second or two. This has been found to be the case (2), but the actual rate has not been measured.

2. Exchange current could be measured with the same conditions as above except that self-diffusion in the metal should be much faster than exchange. Nearly all the active atoms entering the surface would diffuse inward rather than re-exchange, and the rate of pickup would give i_0 directly.

The fact is that conditions are never as simple as those discussed above.

Adsorption

Assuming no internal diffusion, but that salt can be firmly adsorbed (through primary attachment of either cation or anion), the rate of attainment of equilibrium could depend on both i_0 and the kinetics of adsorption. In the case of silver–silver salts it is known that adsorption–desorption is a slow process, both from classical and from tracer studies (3, 4). Little is known about adsorption of their own salts on active metals.

If internal diffusion plays a role, then adsorption changes the surface concentration and the activity gradient in the surface layers.

Corrosion

If corrosion products are soluble, the rate and amount of activity pickup by the metal will depend on the exchange current, and whether internal penetration is faster than the metal dissolution. The extreme case has been investigated by dissolving the metal anodically. Matsuura (5) found that the activity acquired by a zinc anode corresponded to about three apparent atomic layers of complete exchange, independent of current density. Gerischer and Tischer found similar results with silver (2). This indicates only that surface exchange is rapid compared to internal diffusion.

If corrosion products are insoluble, activity may be acquired by exchange with the metal and the corrosion products, or by precipitation and adsorption from solution. An extreme case has been found with iron (unpublished results in this laboratory); internal diffusion is inappreciable, i_0 is very small, and there is little activity pickup unless corrosion is quite evident.

Local Cell Electrolysis

There is reason to believe that potential differences, which can cause metal to dissolve at one spot while deposition occurs at another, become negligible after a few hours of immersion. Certain faces of copper single crystals, immersed in $CuSO_4$ solution, undergo recrystallization and the potentials approach an equilibrium value (6). Silver specimens used in exchange experiments have been pre-equilibrated in non-radioactive solutions for periods up to several months (2, 7). Gerischer and Vielstich found no further effect after 24 hours.

Local cell electrolysis which results in solid corrosion products is another matter. The solution becomes alkaline at local cathodes, and radioactive metal can be precipitated as hydrous oxide without any actual exchange. Zinc acquires far more active zinc ion in the presence of air than from deaerated solution, even before an oxide film is visible.

Internal Diffusion

Assuming that corrosion and local cell electrolysis can be eliminated or minimized, then continuing activity pickup, which corresponds to more than adsorption or double layer formation plus complete exchange in one atomic layer, must be due to internal diffusion. Internal diffusion was considered by Gerischer, Vielstich, and Tischer (2) in their work with silver, but was discounted because the calculated diffusion coefficient was several powers of 10 higher than expected. Matsuura (5) found the same difficulty in the case of zinc. We believe that the discrepancies are due to lack of knowledge of the true surface concentration of the diffusing species. The solutions used generally have a concentration of 10^{-4}–10^{-5} moles/cm^3, while the metal contains about 0.1 g-atom/cm^3. Adsorption of a fraction of a monolayer results in a surface concentration much greater than in solution. Adsorption on silver depends on the anion, and can amount to several tenths of a monolayer (8).

In polycrystalline metals grain-boundary diffusion is generally much greater at lower temperatures than lattice diffusion, even though the area of exposed grain boundaries is only a small fraction of the total. Self-diffusion in metals is usually measured by milling thin layers from the surface, after diffusion has taken place from an electrodeposited layer; the activity in each layer is then determined. In diffusion experiments at room temperature much thinner layers must be removed by dissolution in a suitable etching solution.

DIFFUSION EQUATIONS

In the experiments discussed below, it is assumed that the tracer has a constant concentration at the metal surface, which is not strictly true until adsorption equilibrium is reached. This is not the same as in dry diffusion from an electrodeposited layer, where the surface concentration decreases with time. There are two methods of relating the activity pickup and the diffusion coefficient: (1) the total pickup is a function of time, and (2) the activity per unit volume at a given penetration depth after a given time is a function of depth. The equations are analogous to those for heat conduction and are discussed in books on that subject and on diffusion in solids (9); the solutions for *homogeneous* diffusion with the boundary conditions assumed here are described in detail by Darken and Gurry (10).

Total Activity as Function of Time

The activity flux per unit area at the surface (a measure of the number of atoms entering and leaving the metal) is given by:

[1] $$da/dt = a_0 D^{\frac{1}{2}} (\Pi\, t)^{-\frac{1}{2}},$$

where D is the diffusion coefficient (assumed constant). Integration gives

[2] $$a_t = 2a_0 \Pi^{-\frac{1}{2}} (Dt)^{\frac{1}{2}},$$

where a_t is the total activity acquired at time t. This equation is given by Gerischer and Vielstich (2) with the addition of a constant term for the initial rapidly acquired surface activity. If adsorption is slow as it is with silver, or if the surface changes in any way, the surface concentration represented by a_0 will not be constant.

Distribution of Activity in Depth

For homogeneous diffusion with constant a_0, the activity a_x at a given penetration distance x, after a fixed time t, is given, per unit area, by

[3] $$a_x = a_0[1 - \operatorname{erf} x/(4Dt)^{\frac{1}{2}}],$$

where erf refers to the error function. If x can be made small enough and t large enough compared to D, it is convenient to use the expansion

[4] $$\operatorname{erf}(y) = \frac{2}{\Pi^{\frac{1}{2}}}\left(y - \frac{y^3}{3} + \frac{y^5}{5 \times 2!} - \cdots\right)$$

and to neglect the higher terms. This gives

[5] $$a_x = a_0 - a_0 x (\Pi\, Dt)^{-\frac{1}{2}}.$$

If thin layers can be etched from a specimen, the activity per milligram (for example) should be linear with x, or if self-absorption of radiation is negligible, the activity remaining on the specimen should be linear with x. This equation has never been tested so far as we know. Diffusion from a thin deposited layer requires that $\ln a_x$ be linear with x^2.

Grain-boundary Diffusion

Most of the work on exchange from solution has been done with polycrystalline metal specimens. There is no independent theory of grain-boundary diffusion, which is presumably most important at room temperature. Probably equation [2] should apply with an area term depending on grain size inserted. In diffusion from electrodeposited layers, ln a_x is linear with x rather than x^2.

An analysis of the relation between the grain-boundary diffusion coefficient D_b and the volume or lattice diffusion coefficient D_v has been made by Fisher (11), through the analogy with heat flow into thin metal sheets imbedded in a semi-insulating medium. His expression may be put in the following form:

$$[6] \qquad D_b = 2D_v^{\frac{1}{2}}(\log e)^2/\delta(d \log a_x/dx)^2 \, (\Pi t)^{\frac{1}{2}},$$

where e is the logarithm base, δ is the grain-boundary thickness. The equation requires that log a_x be linear with x, as is found in practice.

EXPERIMENTS WITH SILVER

Disks of 99.8% silver, of 5.56 cm^2 area (both sides), were prepared from commercial rolled sheet. Half of the disks were washed in alcohol–ether, immersed for 1 minute in 0.5 M KCN to remove surface compounds, washed, and stored in 0.5 M AgNO$_3$ (inactive) for 1 year. The other disks were annealed at about 700° C for several hours, cooled slowly, etched for 1 minute in dilute KCN–H$_2$O$_2$, washed, and stored in 0.5 M AgNO$_3$ for 8 months. The annealed disks were visibly crystalline and noticeably roughened.

All exchange experiments were carried out in 0.5 M AgNO$_3$ containing Ag^{110} as tracer. Measurement of activity pickup and conversion of counts per minute to gram atoms per cm^2 or apparent atomic layers (of complete exchange) were done in the usual manner.

Disturbing the Specimens

In previous work it has been found that frequent removal of silver coupons for washing and counting results in much more activity pickup than if they are undisturbed for an equal immersion time. This has been ascribed to removal of adsorbed salt from the surface (4, 7) or possibly to slight cold-working of the surface by handling (12). It is now certain that hot-water washing increases the internal diffusion which is obviously responsible for most of the pickup.

Several disks were immersed in the active 0.5 M AgNO$_3$ for periods up to 98 days. Some were removed frequently, washed in cold water, and counted, and these were found to acquire more activity than others which were counted only near the end of the period. The effect of washing in hot water is shown below.

Activity vs. Time

Twelve cold-rolled disks were taken from the storage solution, six were blotted, and six were washed in boiling water. All were immersed in active 0.5 M AgNO$_3$ and kept at room temperature (near 25° C). One of each group was removed each 10 days, washed, and counted. A group of 12 annealed disks was treated in the same way. The activity acquired was plotted vs. the square root of time, as shown in Figs. 1 and 2, as a test of equation [2]. The initial blotting or washing made no apparent difference.

While the points are quite scattered, especially in Fig. 2, it is not inappropriate to draw the straight lines shown, with intercepts of about one day. Gerischer and Tischer have shown that a similar plot, examined over a period of 9 days at 25° C, shows curvature upward during this time, with an intercept at zero time of about three apparent atomic
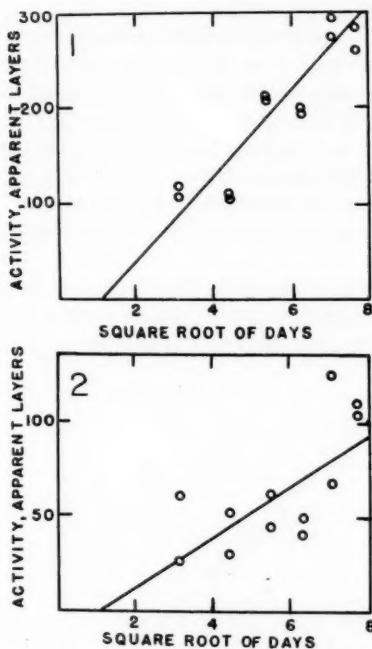
FIG. 1.   Cold-rolled disks.
FIG. 2.   Annealed disks.

layers (the activity acquired in a few seconds). The upward curvature could be due to two factors: (a) the slow establishment of adsorption equilibrium, and (b) diffusion along grain boundaries offers a continually expanding area from which lattice diffusion can take place.

Slopes of the straight lines of Figs. 1 and 2 may be inserted in equation [2] to calculate D. Apparent atomic layers are converted to gram atoms/cm² by multiplying by 19.9 $\times 10^{-10}$, and $a_0 = 5 \times 10^{-4}$ moles/cm³, the solution concentration. This gives

$$\text{cold-rolled coupons:} \quad D = 2.0 \times 10^{-13} \text{ cm}^2/\text{sec};$$
$$\text{annealed coupons:} \quad D = 1.8 \times 10^{-14} \text{ cm}^2/\text{sec}.$$

It is probable that the cold-rolled silver has a larger grain-boundary area and volume than the annealed silver (or its equivalent in broken grains and imperfections) so that this "apparent" diffusion coefficient is larger.

Hoffman and Turnbull (13) have measured both lattice and grain-boundary diffusion in silver in the range 375–500° C by the dry method. For the latter they give the equation

$$D_b = 0.03 \exp(-20200/RT) \text{ cm}^2/\text{sec}.$$

Extrapolation to 25° C gives $D_b = 4 \times 10^{-17}$ cm²/sec. If a_0 were taken as concentrations corresponding to 0.3 and 0.1 atomic layers of adsorbed ion respectively, this value for D would be obtained in the above calculations. Since the roughness factors of the coupons are unknown, and grain size is certainly a factor, further consideration is unwarranted.

Activity vs. Penetration Depth

Although exchange has been reported in most of the literature, in terms of apparent atomic layers of complete exchange, it is evident that exchange occurs to much greater depths. On etching silver coupons which had been immersed for a long time, activity was found to have penetrated as far as 2×10^{-4} cm (about 9000 atomic layers). A solution was prepared which is believed to dissolve silver uniformly: equal parts of (a) 0.5 g KCN in 150 ml water, and (b) 0.9 ml 30% H_2O_2 in 150 ml water.* A 2-minute etch in this mixture dissolved about 0.8 mg from one of the silver disks (840 layers). The disks were weighed after each etch and comparison was made with the total weight loss after a series of etches.

Four cold-rolled and four annealed coupons were immersed in active 0.5 M AgNO₃ and used in testing equation [6]. The results of the etching process are shown in Figs. 3 and 4, where log of activity remaining after each etch is plotted vs. weight lost. The history of
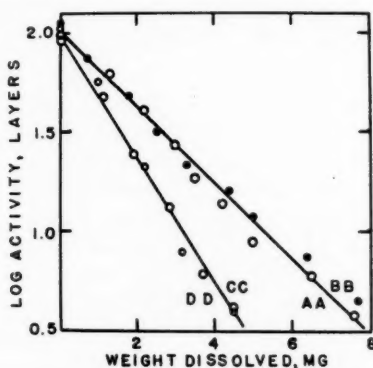
FIG. 3.   Cold-rolled disks.

the disks follows: AA and BB were removed from solution three times, washed in boiling water, counted, and reimmersed; they were washed in boiling water at the end of the period (19 and 23 days); CC and DD were immersed for 20 days, washed in cold water, and stored in a desiccator for 18 days before etching; EE and FF were immersed for 50 days and etched immediately; GG was immersed for 20 days and stored for 30 days; HH was immersed 40 days and stored 10 days before etching. Evidently storage makes little difference, although the surface activity must decrease somewhat by diffusion inward; but washing in hot water is equivalent to using a higher temperature throughout.

The difference between the cold-rolled and the annealed specimens is striking. In the latter case 50–60% of the activity was removed in the first 0.8-mg etch. The grain area exposed to the solution is large, the grain-boundary area small, so that a larger part of the diffusion follows a different law. In any case the slopes of the lines drawn in Fig. 4 were used to calculate D_b.

The value of D_v used was taken from the work of Slifkin, Lazarus, and Tomizuka (14), who made measurements over a wider temperature range than Hoffman and Turnbull. Their equation for the temperature coefficient is:

$$D_v = 0.724 \exp(-45500/RT) \text{ cm}^2/\text{sec}$$

*The best evidence we have that this solution does etch the silver uniformly is the linearity of the plots in Fig. 3.
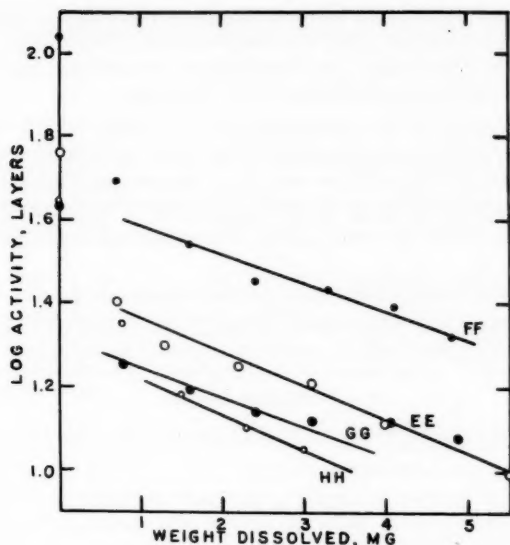
FIG. 4.   Annealed disks.

from which $D_s = 4.4 \times 10^{-34}$ cm^2/sec at 25° C. Fisher (11) suggested that δ, the grain-boundary thickness, be taken as 5×10^{-8} cm, and all other workers have used this figure. Inserting numerical values in equation [6], we obtain

$$D_b = 9 \times 10^{-11}/(\text{slope})^2 t^{\frac{1}{2}} \text{ cm}^2/\text{sec}.$$

In calculating the slope $(= d \log a_x/dx)$, mg silver is multiplied by 1.7×10^{-5} to convert to centimeters for the disks used. The results are given in Table I.

TABLE I

Grain-boundary diffusion coefficients from the Fisher equation

Cold-rolled disks	(Diff. time, sec)$^{\frac{1}{2}}$	Slope $\times 10^{-4}$ cm^{-1}	$D_b \times 10^{21}$ cm^2/sec
AA	1280	1.13	0.55
BB	1420	1.13	0.49
CC	1810	1.84	0.15
DD	1810	1.84	0.15
Annealed disks			
EE	2080	0.48	1.9
FF	2080	0.40	2.7
GG	2080	0.42	2.4
HH	2080	0.48	1.9

DISCUSSION

The fact that the values of D_b in Table I are 4 to 5 orders of magnitude smaller than that calculated from the high-temperature experiments, viz. 4×10^{-17} cm^2/sec, is not surprising in view of the uncertain extrapolations and other factors. If D_s at 25° C is taken from the temperature-coefficient equation of Hoffman and Turnbull, our values of D_b become about 10^{-24} cm^2/sec. The important thing is that continuing exchange *does*

depend on internal diffusion and that measurements *can* be made at room temperature. Gerischer and Tischer commented that the distribution of activity in depth would be useful to know, but that penetration was too shallow for successful measurements. We believe that the etching technique overcomes the difficulty.

Experiments with silver have the advantage that corrosion can be neglected. Similar experiments have been carried out in this laboratory with zinc and cadmium, in solutions which minimize corrosion; they will be described elsewhere. Plots of a_t vs. $t^{\frac{1}{2}}$ curve upward in the initial immersion period as with silver, and D is larger than D_b calculated from dry-diffusion work in the literature. The Fisher method again gives values which are smaller.

Work with single crystals is indicated, and is under way. Since the amount of adsorption on silver is known, equation [2] should apply directly if the surface area can be controlled. With the etching technique it should be possible to apply equation [3] in some form.

ACKNOWLEDGMENT

REFERENCES

1. VIELSTICH, W. and GERISCHER, H.   Z. physik. Chem. **4**, 10 (1955).
2. GERISCHER, H. and VIELSTICH, W.   Z. Elektrochem. **56**, 380 (1952). GERISCHER, H. and TISCHER, R. P.   Z. Elektrochem. **58**, 819 (1954).
3. PROSKURNIN, M. and FRUMKIN, A.   Z. physik. Chem. A, **155**, 29 (1931).
4. KING, C. V. and LEVY, B.   J. Phys. Chem. **59**, 910 (1955).
5. MATSUURA, N.   Sci. Papers Coll. Gen. Educ., Univ. Tokyo, **5**, 97 (1955).
6. TRAGERT, W. E. and ROBERTSON, W. D.   J. Electrochem. Soc. **102**, 86 (1955).
7. KING, C. V. and SIMONSEN, A.   J. Electrochem. Soc. **104**, 194 (1957).
8. KING, C. V. and SCHOCHET, R. K.   J. Phys. Chem. **57**, 895 (1953).
9. CARSLAW, H. S. and JAEGER, J. C.   Conduction of heat in solids. Oxford University Press, London. 1948. BARRER, R. M.   Diffusion in and through solids. Cambridge University Press, London. 1951.
10. DARKEN, L. S. and GURRY, R. W.   Physical chemistry of metals. McGraw-Hill Book Co., Inc., New York. 1953. Chap. 18.
11. FISHER, J. C.   J. Appl. Phys. **22**, 74 (1951).
12. TINGLEY, I. I., HENDERSON, I. H. S., and COFFIN, C. C.   Can. J. Chem. **34**, 14 (1956).
13. HOFFMAN, R. E. and TURNBULL, D.   J. Appl. Phys. **22**, 634 (1951).
14. SLIFKIN, L., LAZARUS, D., and TOMIZUKA, T.   J. Appl. Phys. **23**, 1032 (1952).

SOME ABNORMAL HYDROGEN ELECTRODE REACTIONS

D. J. G. IVES

ABSTRACT

A brief account is given of experiments in which gold electrodes, as a result of thermal deactivation in hydrogen, change from a state in which their behavior in relation to the hydrogen evolution reaction is normal to a state characterized by high positive rest potentials, greatly enhanced overpotentials which increase progressively during current flow, and which decay slowly on open circuit, generating potential–time curves which resemble desorption isotherms.

Conclusions based on these phenomena are supported by the results of experiments with poisoned platinum electrodes, which not only behave similarly but are also shown to retain reducing power for a limited time on open circuit.

It is suggested that electrodeposited hydrogen atoms may sometimes evaporate from an electrode into solution by a mechanism involving the participation of molecule-ions. A recent theoretical treatment of hydrogen overpotential can be extended to allow for the occurrence of such a final reaction step.

Hydrogen overpotential measurements have been made (1) using gold electrodes in the apparatus illustrated in Fig. 1, into which pre-electrolyzed, decinormal hydrochloric acid was delivered by pressure of hydrogen. Further pre-electrolysis of the solution was conducted by means of the ancillary gold electrode in compartment B. The gold test electrode in compartment A, arranged for even distribution of current over the whole of its surface, was supplied by a rapid flow of solution normal to each face by the powerful
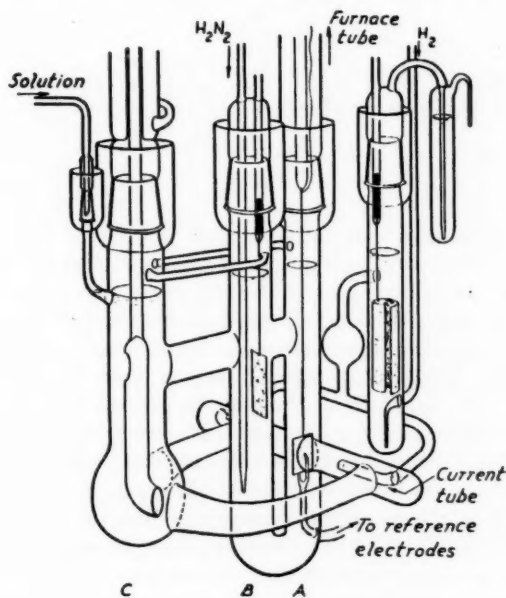
FIG. 1.

centrifugal stirrer C. Except at the highest current densities, all hydrogen produced in the electrode reaction was removed in the dissolved state. Other features of the apparatus are self-explanatory and permit the stringent precautions known to be essential in hydrogen overpotential work to be observed.

Gold electrodes, cleaned by normal chemical methods, showed zero rest potentials with respect to a reversible hydrogen electrode in the same solution. On cathodic polarization, they gave rise to Tafel plots typified by Fig. 2. These plots show slopes consistent with rate-limitation by slow discharge, except where decreasing cathodic polarization allows the back-reaction to assume increasing significance; that the occurrence of a back-reaction must be entertained is shown by, *inter alia*, the effect of sweeping out the cell solution with nitrogen instead of hydrogen.
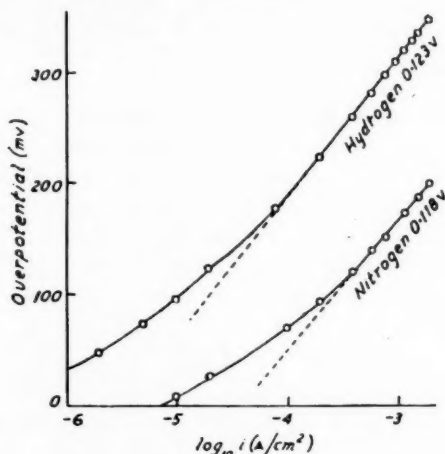
FIG. 2.

This behavior is reasonably normal. The main interest of these experiments arises from the results of withdrawing such a normal electrode from the solution into a silica furnace tube, forming an integral part of the apparatus, and subjecting it to prolonged annealing in hydrogen at temperatures falling from 800° C. On restoration of the cooled electrode to the same solution, its properties were found to be radically changed. It showed a rest potential of about $+400$ mv, complete insensitivity under all conditions to substitution of nitrogen for hydrogen passing through the cell solution, and greatly enhanced cathodic overpotentials which increased steadily with time and generated curved Tafel plots of varying, but excessively high, gradients. The behavior of the electrode on open circuit after cathodization was even more remarkable. On breaking the polarizing circuit, the negative potential of the electrode fell rapidly and linearly with log time to a value between -150 and -200 mv. From this point, the potential decayed more slowly, passing through zero in its progress to the original resting value of $+400$ mv. These changes were slow enough to allow some study to be made of the state of the electrode both before and after its potential passed through zero. Thus, connection via a micro-ammeter to a reversible hydrogen electrode in the same solution caused anodic current to flow at the gold electrode whilst its potential was still negative, but cathodic current passed spontaneously under these same conditions when the gold electrode had attained

positive potentials. In both cases stirring enhanced the current flow, and in both cases the potentials recovered from their displacements towards zero after disconnection. It is thus clearly shown that the potentials through which the electrode passes after cathodic treatment are very well defined, decisively determined by the physical or chemical state of the electrode at each instant. In turn, each state of the electrode must be a function of the stage reached in a slow reaction leading to the final resting state.
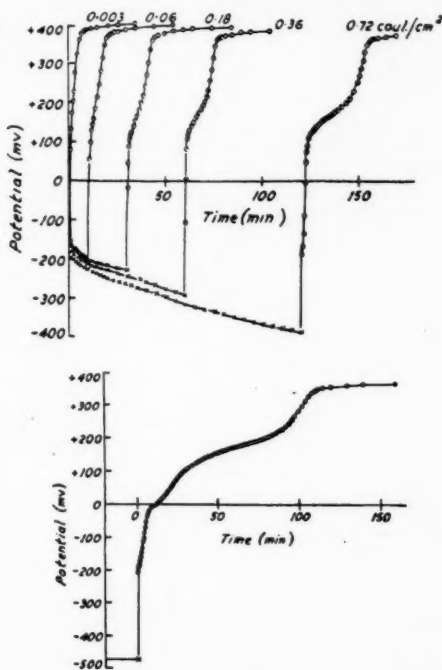
FIG. 3.

Two further facts assist in identifying this reaction. For a given constant current density of cathodization, the course of the open-circuit potential decay which follows depends systematically upon the duration of cathodization. This is illustrated in Fig. 3, where the results of six polarizations at 100 μa cm^{-2} are shown (in the last of these the growth of overpotential, during the cathodization period of 6 hours, is omitted). The form of the open-circuit potential–time curve depends strongly upon the current density in the preceding cathodization *up to a certain current density*, above which there is no such dependence. This is illustrated in Fig. 4, which shows the potential changes following 6-hour cathodizations at three current densities. Attention is drawn to the substantial identity of the curve relating to 20 μa cm^{-2} with that for 100 μa cm^{-2} in Fig. 3. It is believed that this effect is really due to the attainment during polarization of an electrode potential exceeding about -300 mv, when the subsequent potential decay curve assumes the same inflected form, which, for a given electrode, is remarkably reproducible.

There can be little doubt that the main effects of the heat treatment of the gold in hydrogen are the promotion of crystal growth (confirmed by microscopical examination)
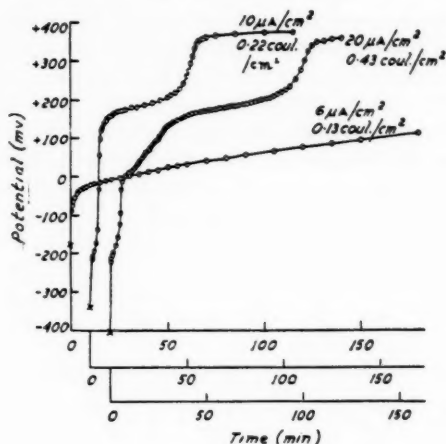
FIG. 4.

and the "burning-out" of catalytically active centers. Certainly, the gold becomes quite indifferent to its gaseous surroundings and is no longer capable of atomizing molecular hydrogen. It follows that it can no longer catalyze the recombination of hydrogen atoms.

The behavior of this thermally deactivated gold as a substrate for the hydrogen evolution reaction is only intelligible in terms of the progressive accumulation of electromotive material during cathodization, and the only material which presents itself is atomic hydrogen. The conclusion is reached that annealed gold forms a "non-equilibrium hydrogen electrode" at which cathodically generated hydrogen atoms pile up and are unable to escape by any *facile* mechanism: combination, evaporation, electrochemical desorption, or ionization. All of the partial processes which are mobile at the reversible hydrogen electrode have become strongly hindered, so that the electrode potential cannot at any stage be determined by a Nernst relation.

In terms of this hypothesis, the sequence of events during cathodization and afterwards is pictured as follows. Hydrogen atoms accumulate at the surface of the electrode at a rate determined by the current density and, normally, the processes by which they leave the surface increase in rate until a steady kinetic state is established. But when these processes are very slow, then at all but the lowest current densities, the accumulation of atoms may become extensive and lead to progressive changes in the properties of the electrode surface, perhaps by the burning-out or saturation of the few remaining active centers. If there is an upper limit to rate of dissipation of hydrogen atoms, not dependent upon potential, *and not kinetically linked with the discharge process*, there will clearly be a critical rate of discharge. For rates of discharge less than this, a kinetic steady state may be established; for higher rates, the accumulation of atoms may proceed unchecked and lead to progressive saturation. Since rate of discharge is a function of electrode potential, this is consistent with the observation that the attainment of a critical potential has a profound effect upon subsequent electrode behavior. The slow and prolonged growth of overpotential, and the dependence of open-circuit potential decay upon the time for which cathodization is continued, coupled with its independence of the current density of cathodization above a certain minimum, strongly suggest that hydrogen atoms penetrate the gold lattice. Gold does not dissolve hydrogen from the

molecular gas phase, but it has recently been shown (2) that an evaporated film of gold takes up gaseous hydrogen atoms quite rapidly; it is believed that a gold cathode which is incapable of catalyzing atom recombination will do the same. If this bulk penetration of the gold can be accepted, then the inflected potential decay curves have a more than superficial relationship to the desorption isotherms (as of hydrogen from palladium) which they so strikingly resemble.

These conclusions have been supported in more detail elsewhere (1), and further discussion must give way to an attempt to meet the obvious demand to demonstrate the alleged heavy, slowly dispersing accumulations of hydrogen atoms at such inactive electrodes.

This has been done with the aid of poisoned platinum electrodes (3) in an apparatus illustrated in Fig. 5, which is largely self-explanatory. The hemispherical platinum "microelectrode" C, cathodized in 0.001 N hydrochloric acid by means of the very large hydrogen electrode A, could be depressed at will against a sintered glass "target" F, which carried a deposit of tungsten trioxide, and through which the cell solution was
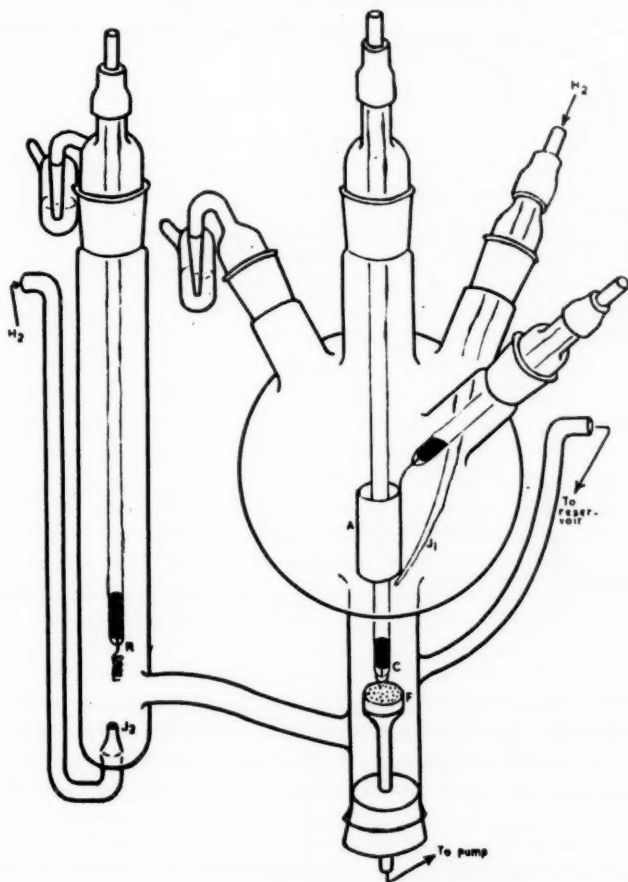
FIG. 5.

continuously drawn. Since poisoned systems were to be studied, rigorous techniques were not employed and the electrodes were studied in three states: (1) ostensibly unpoisoned, (2) poisoned by an electrodeposition of mercury, and (3) additionally poisoned by 10^{-5} mole l^{-1} of mercuric chloride in the cell solution.

The electrodes showed positive rest potentials increasing from 350 to 625 mv with increasing degrees of poisoning (adventitious and deliberate), and very high and erratic overpotentials during cathodic polarization, rising to tens of volts at the maximum current density of about 125 ma cm^{-2}. Even under these extreme conditions, involving blackening and disruption of the electrode surface, the overpotentials remained strongly influenced by poisoning. After cathodization, the negative electrode potentials decayed in a slow and inflected way on open circuit. Provided that a limiting current density had been exceeded in the preceding cathodization, the potential–time curves showed arrests, of length roughly proportional to current density and duration of cathodization; some examples of these curves are shown in Fig. 6.
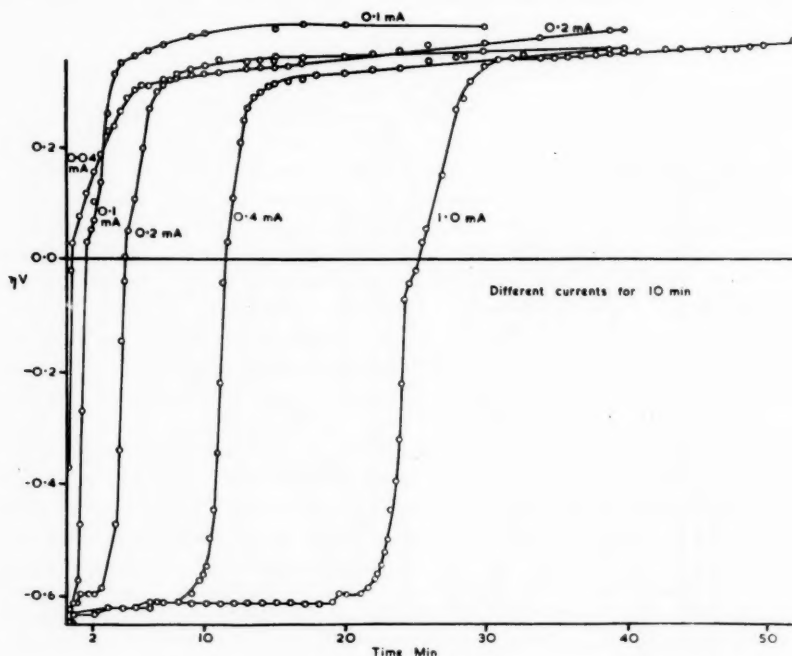
FIG. 6.

A closer correspondence to the behavior of the annealed gold electrodes could hardly be expected, and there can be little doubt that very similar phenomena are involved in the two cases. It was now possible, however, to carry out a chemical test for the presence of a cathodic product with reducing properties, by bringing the cathode into contact with the tungsten trioxide target. Contact established during current flow produced an immediate imprint of tungsten blue, no doubt owing to electronic conduction. For the unpoisoned electrodes, this property vanished instantly the circuit was broken, but it was retained on open circuit by the poisoned electrodes to an extent systematically

related to the duration and current density of cathodization and the degree of poisoning. It was possible to follow the decay of reducing power with time in an approximate way by producing imprints in a standardized manner, and by assessing their depth of color in terms of an arbitrary scale of "color numbers" having a maximum of 10 set by an imprint produced during current flow. It is hoped in due course to improve upon the *ad hoc* device used in this preliminary work. For a standard time of cathodization of 30 minutes at a uniform current density of 25 ma cm^{-2}, the results shown in the following table were obtained.

TABLE I

Decay interval	Electrode state (2)		Electrode state (3)	
	Potential on making contact, mv	Color No.	Potential on making contact, mv.	Color No.
3 seconds	−646	8	−646	10
10 seconds	−646	7	−646	10
30 seconds	−596	4	—	—
1 minute	−546	3	−621	9
5 minutes	−509	2	−621	5
10 minutes	+79	1	−496	3
30 minutes	+159	0	−483	1

It is evident that the residual reducing power was not directly linked with electrode potential, and was in fact often retained when this potential had become positive. It is suggested that these experiments support the conclusion previously drawn.

It may be that this work has some importance as a basis for the view that consideration of the hydrogen evolution reaction has perhaps been too closely confined within the narrow framework of but three reaction steps succinctly denoted by the names Volmer, Tafel, Horiuti (VTH), one or other of which, it is almost universally assumed, must be rate-limiting. One is still invited to accept the gullet-sticking conclusion that at platinum electrodes atom recombination is very fast but is rate-limiting, whilst at mercury it is very slow but is not rate-limiting. The work of the Knorr school (4) has shown the weakness of much of the evidence relating to low overpotential metals and has strongly reinforced the inverse relation established by Bonhöffer (5) between overpotential and catalytic power. This relation has been discounted (6) on the basis of work by Schechter (7) which does not, in the author's view, have any relevance. The fact remains that for eight common metals the sequence of increasing overpotential is the same as the sequence of decreasing catalytic activity, and the chance that these two sequences should occur *un*related to each other is about 1 in 1.6×10^9. But it was the assumption that this obvious relationship required the rate-limiting step in the hydrogen evolution reaction to be atom recombination that was false.

The evidence that slow discharge is rate-controlling at mercury electrodes is strong, but there is no satisfactory evidence at all about the subsequent stages of the reaction at this metal (8, 9). The elegant potentiostatic experiments of Gerischer and Mehl (9) suggest that the mercury surface is bare of hydrogen atoms. What then happens to the atoms that are deposited? It must be admitted that the present position is not altogether satisfactory.

Reconsideration of the work of Kobosew and Nekrassow (10) appears to be desirable for two reasons. A relation was established between hydrogen overpotential at horizontally disposed electrodes of various metals and the degree of reduction of tungsten

trioxide suspended in the electrolyte above the electrodes. The interpretation of this in terms of atomic hydrogen was attacked by the Frumkin school (11), but the resulting polemical exchanges have, in the author's view, been resolved by Poltorak (12), who has convincingly demonstrated "reduction at a distance" (of about 0.5 μ) from a high over-potential cathode, as well as retention of reducing power after cathodization. The present work confirms the latter result, and invites more serious attention to the views of Kobosew. In the earlier paper with Nekrassow (10), he considered both penetration into the metal phase and free evaporation into solution as possible fates for electrodeposited hydrogen atoms, and first introduced, in a rather generalized form, what is now known as electro-chemical desorption and generally associated with the name of Horiuti. He has maintained his views for over twenty years, and his quite recent "adsorption theory of hydrogen overpotential" (13), in spite of certain weaknesses, very adequately explains the opposite effects of poisons on the catalytic and "electrocatalytic" activities of metals.

It appears that more attention is now being given to the role of adsorbed hydrogen atoms in relation to hydrogen overpotential, and one of the most satisfactory discussions is due to Gerischer (14), although still largely confined within the VTH framework. The suggestion is made that his treatment could be extended along the following lines.

There is no lack of evidence that hydrogen atoms can exist in solution for a finite time and no reason to suppose that, generated at an electrode, they need be in equilibrium with the gas phase, need be potential-determining according to a Nernst relation, or are unable ever to leave the electrode by evaporating into the solution. Developments in radiation chemistry have established the molecule-ion, H_2^+, as an intermediate of frequent occurrence, and it is suggested that it may well be concerned in an evaporative process. Coulson has recently emphasized (15) that this entity, one sixth of the size of the hydrogen atom, has its single electron almost exclusively located in regions between the nuclei. The protons are therefore substantially unscreened from the outside, so that the molecule-ion may be expected to behave as if it were two halves of a proton separated by about 1 Å. In this case, its considerable bond energy of 61 kcal mole^{-1} might be expected to be supplemented in aqueous solution by a hydration energy of the same order of magnitude as that of the proton itself (282 kcal g-atom^{-1}). An upper limit to this hydration energy of 255 kcal mole^{-1} has in fact been calculated (16), and it can be shown that a lower limit of 221 kcal mole^{-1} is needed to make the reaction $H + H^+_{hydr.} = H_2^+_{hydr.}$ exothermic. It is considered to be very likely that the hydration energy lies between these limits, or is at least large enough to make the hydrogen molecule-ion an entity very frequently to be reckoned with in aqueous solution in any reaction ostensibly involving hydrogen atoms.

If this can be accepted, a ready means can be seen for the desorption of hydrogen atoms from an electrode at which the absorption energy is not too great. What happens to these atoms when they have diffused, as molecule-ions, some few Angstroms from the electrode surface ceases to be a part of the electrochemical problem! In alkaline solutions, the alternative reaction $H + H_2O = H_2^+_{hydr.} + OH^-_{hydr.}$ may well operate, for it does not seem to be unduly disfavored energetically. Gerischer's calculations may be adapted to this suggestion and, assuming that the standard free energy of hydration of the molecule ion is 50 kcal mole^{-1} less negative than that of the proton, they indicate that for an adsorption energy of hydrogen atoms less than about 30 kcal g-atom^{-1}, an evaporative process involving molecule-ions might well follow a rate-limiting discharge step. It seems appropriate to suggest the name "Kobosew step" for this final stage, which is thought to be operative for high overpotential metals such as mercury.

It is undeniable that the molecule-ion must be a participant, however transitory, in the Horiuti (electrochemical desorption) step. It is therefore tempting to envisage a transition state which could break down in two ways, according to whether desorption or electron transfer were the easier.
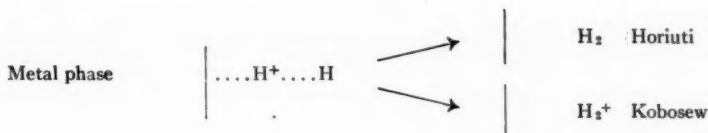
It is clear that the distinction between various proposed mechanisms for the hydrogen evolution reaction depends upon the sequence of acts of discharge, combination, and desorption. The suggestion is now made, in a provocative rather than a didactic spirit, that the usual assumption that desorption must be preceded by, or coupled with, completion of discharge of all the ions involved is not necessarily true.

REFERENCES

1. IVES, D. J. G. and SWAROOPA, S.   J. Chem. Soc. 3489 (1955).
2. TOMPKINS, F. C.   Private communication.
3. GUTT, W. and IVES, D. J. G.   Proc. Chem. Soc. (London), 344 (1957).
4. KNORR, C. A.   Z. Elektrochem. 59, 647 (1955).
5. BONHÖFFER, K. F.   Z. physik. Chem. 113, 199 (1924); Naturwiss. 6, 219 (1927).
6. BOCKRIS, J. O'M.   J. Electrochem. Soc. 99, 366C (1952).
7. SCHECHTER, A.   Acta Physicochim. U.R.S.S. 10, 379 (1939).
8. FRUMKIN, A.   Acta Physicochim. U.R.S.S. 18, 23 (1943).
9. GERISCHER, H. and MEHL, W.   Z. Elektrochem. 59, 1049 (1955).
10. KOBOSEW, N. I. and NEKRASSOW, N.   Z. Elektrochem. 36, 529 (1930).
11. BAGOTSKY, V. S. and JOFA, Z. A.   Compt. rend. acad. sci. U.R.S.S. 53, 439 (1946). FRUMKIN, A. N., JOFA, Z. A., and BAGOTSKY, V. S.   Zhur. Fiz. Khim. 25, 1117 (1951).
12. POLTORAK, O. M.   Zhur. Fiz. Khim. 27, 599 (1953).
13. KOBOSEW, N. I.   Zhur. Fiz. Khim. 26, 112 (1952).
14. GERISCHER, H.   Z. physik. Chem. (Frankfurt), 8, 137 (1956).
15. COULSON, C. A.   J. Chem. Soc. 778 (1956).
16. RIGG, T., STEIN, G., and WEISS, J.   Proc. Roy. Soc. (London), A, 211, 375 (1952). RIGG, T. and WEISS, J.   J. Chem. Phys. 20, 1194 (1952).

CATHODIC POLARIZATION OF SILVER IN SULPHURIC ACID[1]

A. A. ANTONIOU AND F. E. W. WETMORE

ABSTRACT

The hydrogen overpotential on fine silver cathodes has been determined from 2 to 35° and over a current density range from 0.03 to 2000 μa cm^{-2}. Two Tafel slopes were observed, RT/F at low currents, $2RT/F$ at high currents. The stoichiometric number was found to be one and the symmetry factor one-half at low currents. The heat of activation changed from 18.8 kcal at low currents to 14.3 at high currents.

EXPERIMENTAL METHODS

The silver cathodes were of high purity (less than 0.001% impurity) and in the form of single crystal and polycrystalline slabs. After being electropolished the metal was held in a hot hydrogen atmosphere for a few days; a small amount of silver was removed by gentle anodizing. Electrodes so treated were more consistent in their behavior than those not strongly hydrogenated; the latter gave high Tafel slopes, as mentioned by Frumkin (3). Teflon containers exposed only one surface of the slab (110 or 111 plane of the single crystals), of area about 3.5 cm^2.

The anode and the Luggin probe were both hydrogen electrodes. A platinum electrode used for pre-electrolysis could be swung out of the solution when not required. In all the experiments the electrolyte was molar H_2SO_4, made up from triply-distilled reagents. All parts of the cell were maintained under a slightly positive pressure of purified hydrogen.

The cells were mounted in an air bath kept within 0.1° of the desired temperature. A danger in lesser control lies in the variation of the temperature of the probe electrode, which usually has a small heat capacity.

Polarizing currents were kept constant by an electronic regulator. Potential difference between probe and cathode was imposed on a direct-coupled amplifier having an input resistance of 10^{10} ohms; the output could be coupled to either a potentiometer or one of three recording devices. For slow changes an Esterline-Angus recorder (0.5 sec) was convenient; for more rapid changes a Kipp galvanometer (0.01 sec) and drum camera were used; a direct-coupled oscilloscope and fixed camera were used for fast changes. In order that transient fluctuations associated with mechanical contacts could be avoided, rapid build-ups and decays were initiated by a thyratron switch.

RESULTS

Rest-potential

The potential E_r to which the electrode decays after removal of the polarizing current can give information about the purity of the system. The most likely contaminant is oxygen. Experiment has shown that oxygen promotes the corrosion of silver and thus the rest-potential can be viewed as an indicator of the silver ion activity or the equivalent effective concentration of oxygen. For the conditions used here, and at 25°, the partial pressure of oxygen above the electrolyte would correspond to

$$\log p_{O_2}(\text{atm}) = 68E_r - 84.$$

In most of the experiments E_r lay in the range 0.35 to 0.45 volt positive, but in several was substantially less positive. For example, in a particular series the decays occurred within minutes to zero potential and after 8 hours to only 17 mv positive.

Overpotential–Current Relationships

The Tafel plot was found to consist of two distinct linear portions, as exemplified in Fig. 1. Table I gives the slopes, the exchange current densities, and the potential of intersection of the pairs of lines.

The low current slope corresponded closely to RT/F until the electrode had been polarized and allowed to decay many times. The slope then increased, as the time sequences show. It was evident from examination of electrodes used over long periods that some silver had dissolved and been redeposited; a change in the surface was apparent.

TABLE I

Overpotential–current relationships

Date	Temp., °C	Tafel B = 2.3b	i_0, $\mu a\ cm^{-2}$	Tafel B = 2.3b	i_0, $\mu a\ cm^{-2}$	Intersection, mv
		Cell 1, 110 face no. 1				
4.9	25	0.057	0.20			
7.9	15	0.058	0.12			
10.9	34.5	0.056	0.26			
11.9	5.5	0.057	0.026			
26.9	12	0.063	0.21			
30.9	2.5	0.066	0.041	0.122	0.72	180
2.10	2.5	0.075	0.029	0.120	0.35	220
3.10	10	0.073	0.038	0.120	0.43	195
4.10	20	0.067	0.049	0.125	0.93	187
5.10	30	0.065	0.10	0.121	1.6	180
7.10	2	0.081	0.017	0.120	0.11	220
9.10	20	0.074	0.043	0.120	0.49	210
9.11	20	0.095	0.12			
		Cell 3, polycrystalline face				
5.12	20	0.060	0.33	0.112	6.0	160
14.12	20	0.061	0.24	0.111	3.6	160
21.12	7	0.063	0.045	0.115	1.2	200
		Cell 2, 111 face				
8.12	20	0.060	0.24	0.109	4.2	166
14.12	20	0.060	0.36	0.115	6.3	156
		Cell 1, 110 face no. 2				
7.3	26.5	0.069	0.044	0.121	1.2	195
8.3	13.4	0.073	0.012	0.121	0.38	220
11.3	26	0.068	0.044	0.120	1.3	220
12.3	14	0.073	0.012	0.114	0.24	260
19.3	14.5	0.081	0.031	0.116	0.28	250
		Cell 3, 111 face				
30.3	25.5	0.060	0.20	0.117	6.7	190
31.3	25.5	0.058	0.25	0.117	9.4	175
1.4	13	0.058	0.097	0.110	3.3	190
3.4	2	0.061	0.079	0.109	1.6	180
4.4	1.4	0.061	0.042	0.111	1.7	192
5.4	14	0.058	0.10	0.114	3.9	188
6.4	28.3	0.054	0.19	0.120	10.0	178
7.4	27.9	0.052	0.19			
8.4	13	0.055	0.076			
10.4	2.5	0.060	0.039			
18.4	3.7	0.063	0.033	0.107	1.1	220
24.5	5.	0.083	0.030			
7.6	4.4	0.079	0.021			
9.6	4.5	0.080	0.024			
11.6	6.7	0.091	0.054			

The high current slope remained at approximately $2RT/F$ throughout the experiments.

The change from one slope to the other occurred over a small range of current and potential in any particular run. The average potential of intersection was 196 ± 20 mv. The current density of intersection, like the exchange current densities associated with the two linear portions of the Tafel curve, showed considerable scatter, but for each electrode showed a systematic change with temperature. It is clear that these current parameters depend not only on the temperature, but also on the effective surface area, as evidenced by variation of the capacitance of the electrode in the same sense as the variation in i_0.
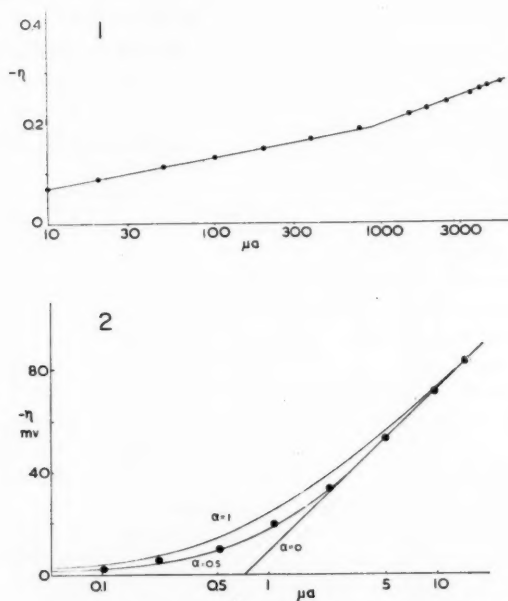
FIG. 1.   Typical overpotential–current relationship.
FIG. 2.   Low current overpotential–current plot.

Symmetry Factor and Stoichiometric Number

The dots of Fig. 2 show the relationship of the overpotential and the current found when decay occurred to zero potential (oxygen practically absent). The bend from linearity indicates clearly that omission of a term for reverse current makes Tafel's equation (shown by the line marked $\alpha = 0$) unsuitable for the range of current below about $10i_0$. Figure 3 shows the plot of the expression

$$i = 2i_0 . \sinh(-\eta/b)$$

proposed earlier (4) as an improvement over Tafel's expression, but premised on symmetry of energy division ($\alpha = 0.5$).

The curves of Fig. 2 express the equations

$$\begin{aligned}
(\text{asymmetric, } \alpha = 1) \quad & i = i_0[\exp(-36.6\eta) - 1] \\
(\text{symmetric, } \alpha = 0.5) \quad & i = i_0[\exp(-36.6\eta) - \exp(36.6\eta)] \\
& = 2i_0 . \sinh(-36.6\eta) \\
(\text{asymmetric, } \alpha = 0) \quad & i = i_0 \exp(-36.6\eta)
\end{aligned}$$

in which the factor 36.6 is the value of $1/b$ found from consideration of the whole range of current below the change of slope of the Tafel plot. The curve indicating symmetry is in close agreement with experiment.

The stoichiometric number has been defined (5) at high overpotentials by

$$\nu = \alpha n F b / RT$$

and at low overpotentials by

$$\nu = -(n F i_0 / RT)(\partial \eta / \partial i)_{\eta \to 0}.$$

As
$$\eta \to 0, \sinh(-\eta/b) \to -\eta/b$$

and
$$-\partial(\eta/b)/\partial i \to \partial \sinh(-\eta/b)/\partial i = 1/2i_0.$$

Hence $\nu = n F b / 2RT$, which is simply the first definition with $\alpha = 0.5$.

Since at low currents b was found to be RT/F and α to be 0.5, the corresponding value of ν is $n/2 = 1$. Owing to the change in slope of the Tafel plot, it is not possible to determine the values of α and ν separately at high currents; all that can be said is that $\nu/\alpha = 4$, to agree with $b = 2RT/F$.
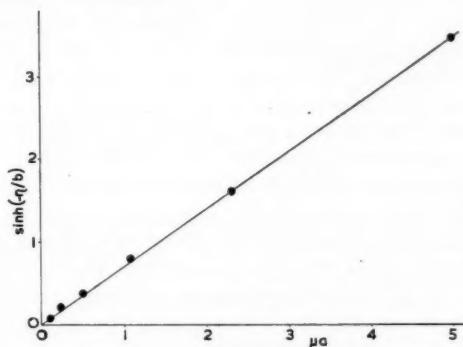
FIG. 3.   Linear function plot.

Temperature Dependence of Overpotential

On varying the temperature at constant current and confirming that the overpotential did return to its original value when the original temperature was re-established, the data of Table II were found.

Diffusion of Hydrogen in Silver

In order to determine whether hydrogen diffuses appreciably through silver, an experiment was carried out with a thin silver foil separating two portions of electrolyte. While one face was polarized at 3 ma cm^{-2}, a probe on the other face showed no change of potential.

Build-up and Decay Curves

The change of potential during polarization and in decay was examined, but not as intensively as the steady state overpotential. There are a few points which may merit mention.

At constant charging current the potential build-up was linear with time and then bent off smoothly to the constant value of overpotential, usually taking longer to reach a steady state than would be expected from the simple expression for build-up (4), and sometimes showing a slight drop after the rapid part of the build-up. In some runs, in

TABLE II

Variation of overpotential with temperature

c.d. $\mu a\ cm^{-2}$	Temp. range, $^\circ$ C	$\Delta\eta/\Delta T$, mv deg^{-1}	Tafel B	ΔH, kcal mole^{-1}	No. of determinations
		Cell 2, polycrystalline			
12.5	13.4–25.7	−2.54	0.060	16.7	2
	5.9–13.4	−3.0	0.060	18.3	1
25	13.0–25.5	−2.7	0.060	17.7	2
	6.2–13.0	−3.0	0.060	18.3	1
125	13–25	−3.8	0.116	12.8	3
	7–13	(−5.5)	0.112	(18.6)	1 (not precise)
250	13–25	−4.2	0.116	14.3	8
	7–13	−4.1	0.112	13.6	8
		Cell 2, 111 face			
15.6	13.4–25.7	−3.1	0.060	20.2	2
	5.9–13.4	−3.2	0.060	19.5	1
31.2	13.0–25.5	−3.1	0.060	20.2	2
	6.2–13.0	−3.3	0.060	20.2	1
156	13–25	−4.3	0.116	14.6	4
	7–13	−4.15	0.112	13.6	3
312	13–25	−4.7	0.116	15.9	7
	7–13	−4.3	0.112	13.9	6

Average ΔH, weighted for number of determinations:
  low currents, 18.8; high currents, 14.3.

which oxygen was known to be present, the initial part of the curve was sigmoid, as would be expected. The apparent capacitance was usually high at very low polarizing currents; capacitances determined through analysis of decay curves did not generally show this same behavior.

Most decays showed linearity of potential in $\log(t+\theta)$ when θ was chosen appropriately (4), but this was not always so for the highest currents. Decay curves taken with the oscilloscope did not show linearity of the potential with time, even initially.

DISCUSSION

Bockris and Conway (2) and Bockris, Ammar, and Huq (1) studied the overpotential on silver in various concentrations of HCl at room temperature. Their results are compared with those found in this work:

	B–C			B–A–H		A–W
	0.1	1.0	5.0	0.1	0.4 N HCl	2 N H$_2$SO$_4$
B, low i	0.09	0.06	0.07	0.057	0.058	0.059
B, high i	0.12	0.13	0.12	0.097	0.101	0.116
Potential of intersection	0.27	0.19	0.28	0.07	0.15	0.20

The present work supports the existence of two distinct Tafel slopes, agrees with the low current slope of B–A–H and the low current stoichiometric number unity, adds that the value of α at low currents is 0.5, and shows a high current slope of $2RT/F$, which lies between the earlier sets. The present work shows that there is a rise in the low current slope as the electrode is worked and that this change may be related to the surface condition; there is no evidence that the change is caused by surface contamination.

Bockris and Conway attributed the existence of two slopes to a phenomenon related to the adsorption of H_3O^+ on the electrode and suggested that the mechanism is probably slow discharge followed by combination.

Bockris, Ammar, and Huq pointed out that the low current slope, RT/F, cannot be explained in terms of simple interpretation of mechanisms already proposed, except by assumption of unrealistic values of α. In order to account for the slope they proposed two explanations. The first of these involves migration of H on the metal surface; they considered it unsatisfactory for silver. Their second and preferred explanation is based on the nearness of the overpotential to the electrocapillary maximum potential and leads to the conclusion that the slope of the Tafel plot can depend on the electrode potential and have the value $2RT/F$ as a maximum. They concluded that electrochemical desorption is the slow step throughout, but did not offer proof that $\nu = 1$ at high currents.

These earlier reports were not in agreement on the low current slope, the high current slope, the variation of the low current slope with concentration, or the potential of intersection. From the second study (B–A–H) there is no indication that the low current slope varies with concentration and it is striking that the present work, at higher acid concentration, shows practically the same value. The considerable variation in the potential of intersection, even in the same solution (0.1 N HCl), raises doubt about the validity of the second explanation (B–A–H) for the change in slope.

Both the sharpness of the break in the Tafel curve and the discontinuity of the heat of activation in going from low to high current point to a change in the nature of the rate-determining step as the current is increased. At high current a slow discharge step with $\alpha = 0.5$ would lead appropriately to $\nu = 2$ and $b = 2RT/F$. At low current $\nu = 1$, which rules out the discharge process as the rate-determining step. The slope, $b = RT/F$, could be attributed to slow surface migration or to another process which is first order with respect to H.

REFERENCES

1. BOCKRIS, J. O'M., AMMAR, I. A., and HUQ, A. K.   J. Phys. Chem. **61**, 879 (1957).
2. BOCKRIS, J. O'M. and CONWAY, B. E.   Trans. Faraday Soc. **48**, 724 (1952).
3. FRUMKIN, A.   Discussions Faraday Soc. **1**, 57 (1947).
4. MORLEY, H. B. and WETMORE, F. E. W.   Can. J. Chem. **34**, 359 (1956).
5. PARSONS, R.   Trans. Faraday Soc. **47**, 1332 (1951).

TRANSPORT OF HYDROGEN THROUGH PALLADIUM-CLAD ELECTRODES

Sigmund Schuldiner and James P. Hoare[2]

ABSTRACT

Electrochemical polarization studies of the transport of hydrogen through Pd, Pt, Pd-clad Pt, Au, Ni, and Fe were conducted under conditions of a concentration gradient of either atoms or protons. Transport of hydrogen through an atom concentration gradient was found for Pd and Pd-clad Fe only. Under a proton concentration gradient, protons migrated readily through Pd, but their transfer through Pt was immeasurable unless the Pt was sandwiched between Pd. Transfer of protons through Fe sandwiched between Pd was also found. Hydrogen atoms evidently did not dissolve to a significant extent in Pt, but if protons are introduced from Pd-clad to Pt they can, under the proper conditions, migrate through Pt. The solution and diffusion of hydrogen atoms and also the migration of protons occurred in Fe. Transport of hydrogen, in any form, through Au and Ni was not detected. Considering the electronic configuration of these metals, it was reasonable that proton migration through Au was negligible; however, it was surprising that protons did not migrate through Ni. Reasons for this anomaly are suggested.

INTRODUCTION

Investigations of the diffusion of atomic hydrogen and deuterium through a β–Pd diaphragm (1, 2, 3) and the migration of protons and deuterons through an α–Pd bielectrode (3, 4) have been reported from the laboratory. For the β–Pd diaphragm a concentration gradient of atomic hydrogen in the palladium cathode arises, whereas for the α–Pd bielectrode there is a migration of protons through the metal under a proton concentration gradient caused by the difference in the electrochemical affinities of the reactions on the cathode and anode sides of the bielectrode.

It was felt that an investigation of the solution and transfer of hydrogen through such metals as Pt, Au, Ni, and Fe could be accomplished by a series of experiments in which these metals would be clad with palladium. The reasons for cladding these metals were twofold. Firstly, by controlling the phase of the palladium–hydrogen alloy (α or β), investigations of the transfer of hydrogen through metals clad with the palladium under conditions of a concentration gradient of either atoms or protons were possible. Secondly, by sandwiching such metals as iron and nickel with palladium, their solution in acid media was prevented. Since the rate of transport of hydrogen through the metals studied was presumably in all cases much slower than for the palladium, the rate would be controlled by these metals. The species of hydrogen which came into contact with these metals at the Pd–metal interface could be controlled also, since the palladium was their only source of hydrogen.

It was also the purpose of this work to try to relate the electronic configuration of the metals studied with the solubility and transfer of hydrogen through them.

EXPERIMENTAL

The experimental techniques and the cell used were the same as reported in references (1, 2, 3, 4). The solution was in all cases highly purified 2 N sulphuric acid. The metal membranes were prepared by cladding the metals on one and/or both sides with palladium. This was done by covering layers of clean metals with sheet titanium, heating red hot with an acetylene torch, and running through a steel roll press with cold rolls. The titanium sheets were then stripped off and the surfaces of the bimetallic sheets were

polished with metallographic paper, followed by cleaning in concentrated nitric acid.

The metal foils used in preparation of the bimetallic specimens were 99.7% palladium, 0.004 inch; 99.99% nickel, 0.002 inch; mild steel, 0.004 inch; 99.97% gold, 0.010 inch; and 99.99% platinum, 0.005 inch thick. The following bimetallic specimens were prepared: Pd: Au, 0.006 inch; Pd: Pt, 0.006 inch; Pd: Pt: Pd, 0.010 inch; Pd: Au: Pd, 0.009 inch; Pd:Ni:Pd, 0.006 inch; and Pd: Fe: Pd, 0.006 inch thick.

For the experiments in which the bimetallic foils were used as cathode diaphragms, purified hydrogen was bubbled through the solutions in both compartments on each side of the diaphragm. The reference electrodes used in each compartment were Pt/H_2 electrodes. The potential drop due to solution resistance on the cathode side was determined simultaneously with the pseudocapacitance test for electrode cleanliness on each side of the membrane by the current interrupter technique (5, 6).

For the experiments in which the bimetallic foils were used as bielectrodes, after the pre-electrolysis and surface activation procedure was finished, solution resistance and cleanliness of electrodes were determined. Then purified hydrogen was bubbled only through the solution in the compartment on the cathode side of the bielectrode, and purified helium was bubbled through the solution in the compartment on the anode side of the bielectrode. When the anode side of the bielectrode consisted of palladium, hydrogen dissolved in this part of the foil was removed by anodic polarization. The removal of hydrogen was indicated by following the anodic charging curve and observing when the anodic potential was several hundred millivolts positive to the potential plateau which resulted from the dissolved hydrogen. This anodic charging was repeated several times at successively reduced applied current densities to assure the removal of most of the hydrogen from the anode side of the bielectrode. The overvoltages on the hydrogen-saturated cathode side were determined against a Pt/H_2 electrode in the same solution. The overvoltages on the helium-stirred anode side were determined against a $(Pd-H)_a/H^+$ electrode (7) in the same solution.

In addition to the experiments with the above materials, pure palladium and pure platinum bielectrodes were compared. These experiments were conducted with hydrogen bubbling through both compartments.

The ambient temperature was $30 \pm 2°$ C. The apparent exposed area of all the electrodes was 0.14 cm^2.

COMPARISON OF A PLATINUM WITH A PALLADIUM BIELECTRODE

A comparison of the overvoltage on a platinum bielectrode with that on a palladium bielectrode of the same dimensions is shown in Fig. 1. Since the catalytic activity of α-palladium is not far removed from that of platinum (4, 8), these curves show the strong influence of the rate of proton migration through the palladium bielectrode. It was previously shown (2) that atomic hydrogen does not diffuse through a platinum diaphragm with a clean surface. Also, a comparison of the anodic polarization curve of the platinum bielectrode, shown in Fig. 1, with the anodic polarization curve for a simple platinum anode indicates that there is not a significant amount of proton migration through the platinum bielectrode. It should be noted that in Fig. 1 the ordinate is given in terms of η', where η' is defined as the difference in potential between the open circuit, reversible electrode potential compared to the polarized electrode potential of the same metal/solution system. This means that the overvoltages on the platinum bielectrode were against a Pt/H_2 electrode in the same solution, and that the overvoltages on the palladium bielectrode were against a $(Pd-H)_a/H^+$ electrode in the same solution.
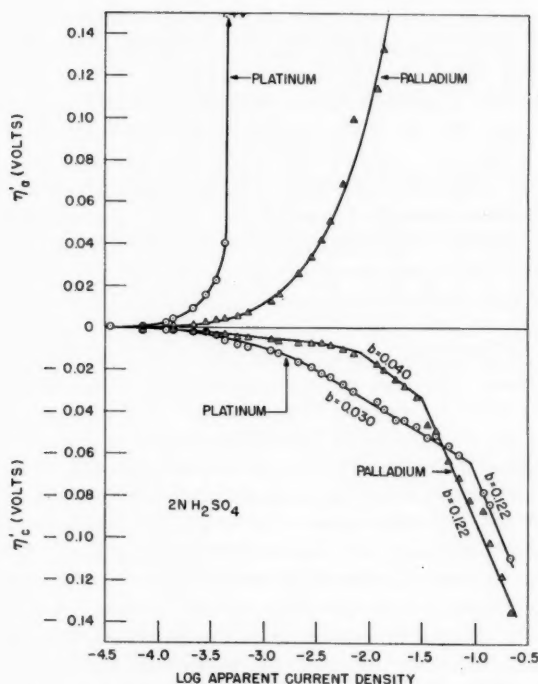
FIG. 1. Comparison of the hydrogen overvoltage on Pd and Pt bielectrodes. Pd and Pt overvoltage values are vs. (Pd–H)$_\alpha$/H$^+$ and Pt/H$_2$ reference electrodes, respectively.

In the low current density range the atomic hydrogen concentration on both sides of the palladium bielectrode changes little, while that on the platinum is rapidly changing. This largely accounts for the difference in overvoltage between the two metals. As the current density is increased on both the platinum and palladium cathode sides, there is a change to a Tafel b-slope of 0.12. In the current density range in which the b-slope on the cathode side is 0.12, most of the anodic reaction on the anode sides of these metal bielectrodes goes into the production of oxygen. As was indicated in previous work (4), it is believed that this change in Tafel slope is caused by the poisoning of the cathode surfaces by oxygen which migrates from the anode side. Kalish and Burshtein (9) have shown that oxygen can diffuse from the interior to the surface of platinum at room temperature. Previous work done at this laboratory (5, 10) has indicated that cathodically polarized platinum in strong sulphuric acid solutions will maintain a Tafel slope of 0.03 to current densities well beyond the value at which the change in slope from 0.03 to 0.12 takes place for the Pt curve in Fig. 1.* Thus for both the platinum and the palladium

*The limiting diffusion current density, i_L, for hydrogen ions in 2 N sulphuric acid solution can be approximated by the equation:

$$\eta_c = 0.059 \log [(i_L - i)/i_L].$$

Using the data for the platinum cathode shown in Fig. 1, at an overvoltage of -0.06 v, the current density is equal to 0.100 amp/cm^2. Applying these values of η_c and i to the above equation, i_L is equal to about 2.8 amp/cm^2. Thus the limiting diffusion current density is well beyond the value at which the change in slope from 0.03 to 0.12 takes place for the Pt curve in Fig. 1.

cathode sides of their respective bielectrodes there is a change in the rate-controlling step from the catalytic combination or electrochemical desorption to a slow hydronium ion discharge. This change takes place at current densities well below the limiting current densities for hydronium ion depletion in the concentration layer on the solution side of the electrodes.

It should be noted that the previous work of the authors on the mechanism of the hydrogen-producing reactions on platinum (5, 10) and palladium (11) have also indicated a change in Tafel slope from 0.03 or 0.04 to 0.12. For these systems it was shown that at the current density at which the change in slope took place there was a depletion of hydronium ions at the interface, and the change in slope was interpreted to mean a change to a slow discharge of water to atomic hydrogen as the rate-controlling step. In other words, in the case of a simple platinum or palladium cathode, the change in slope to 0.12 occurs at a concentration limiting current density because there are not enough hydronium ions at the interface to support the applied current flow. In the case of the cathode side of a platinum or palladium bielectrode, the change in slope appears to be caused by the poisoning of the catalytic surface with oxygen.

Figure 1 further shows that the change in Tafel slope to 0.12 occurs at a significantly lower current density for palladium than for platinum. This is either because the solubility of oxygen in palladium is higher than in platinum or the effects of poisoning by oxygen is much greater for palladium. This is confirmed by the results shown in Fig. 2. Here both electrodes were anodized at 10 ma for a period of 45 minutes. The circuit was broken and both electrodes were allowed to come to their reversible potentials in hydrogen-saturated sulphuric acid solution. As the curves show, the time required for the palladium to reach its open-circuit, steady-state potential was about three times longer than that for the platinum electrode. This was either because the palladium dissolved more oxygen, which took a longer time to remove because of a slow rate of diffusion of the oxygen from the interior to the surface or, if only an equivalent surface layer of oxygen or oxide was formed by both metals, the rate of reduction of the oxygen by hydrogen was slower on the palladium surface. There is also the possibility that these effects are operating simultaneously.
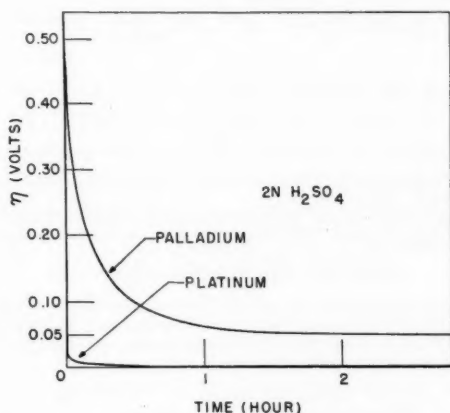
FIG. 2. Comparative rates of reaching reversible, open-circuit potentials on Pd and Pt after anodic polarization. Pt/H_2 reference electrode.

NOBLE METAL ELECTRODES CLAD WITH PALLADIUM ON ONE SIDE

Cathode overvoltage curves for Pd:Pt, Pt:Pd, Pd:Au, and Au:Pd* diaphragms shown in Fig. 3 indicate that in each case the metal exposed to the solution on the polarization, η_p, side of the cell determined the hydrogen-producing mechanism. The absence of overvoltage effects on the diffusion, η_d, sides indicated that hydrogen did not diffuse through any of these combinations.
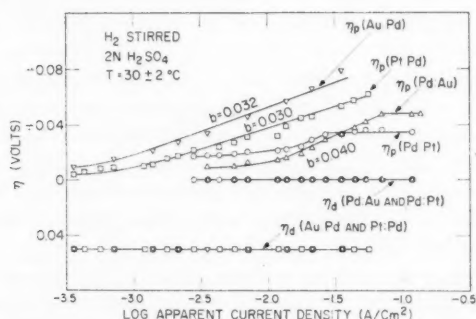
FIG. 3.   Hydrogen overvoltage on polarization and diffusion surfaces of Au and Pt cathode-diaphragms clad on only one side with Pd. Pt/H₂ reference electrode.

In order to determine if protons could migrate through the same palladium-clad noble metal combinations, the electrodes were treated as bielectrodes. On the cathode side of these bielectrodes, the solution was stirred with hydrogen, whereas on the anode side the solution was stirred with helium. By this technique the possibility of the oxidation of molecular hydrogen on the anode side was eliminated and, if hydrogen did migrate through the bielectrode, a depolarization effect should be evident on the anode side. Figure 4 shows the results of these experiments. Because of the complete polarization of the anode curves it can be concluded that proton migration through these metal combinations does not occur significantly. The change from the lower to the 0.12 slope on the cathode overvoltage curves can be interpreted, as above, as due to the migration of oxygen from the anode to the cathode sides with the consequent poisoning of the cathode surface.

METALS SANDWICHED BETWEEN PALLADIUM

Hydrogen overvoltage, η_p, curves for Pd:Fe:Pd, Pd:Ni:Pd, Pd:Au:Pd, and Pd:Pt:Pd cathode diaphragms are shown in Fig. 5. The curves for the polarization sides of the diaphragms are similar to those for palladium (11). As expected, the metal in

Throughout this paper the order of metal foils clad together will be signified by their arrangement from left to right. For the cathode diffusion diaphragms this order will represent the following arrangement in the two-compartment cell:

polarization side: diffusion side.

For example, Pd:Pt means that the palladium was on the polarization side and the platinum was on the diffusion side of the diaphragm. Pd:Pt:Pd means that palladium was on both the polarization and diffusion sides and that platinum was sandwiched in-between. For the bielectrodes, the order from left to right will represent the following arrangement in the two-compartment cell:

cathode: anode.

For example, Pd:Pt means that the palladium was on the cathode side of the bielectrode and the platinum was on the anode side. Pd:Pt:Pd means that palladium was on both the cathode and anode sides and that platinum was sandwiched in-between.
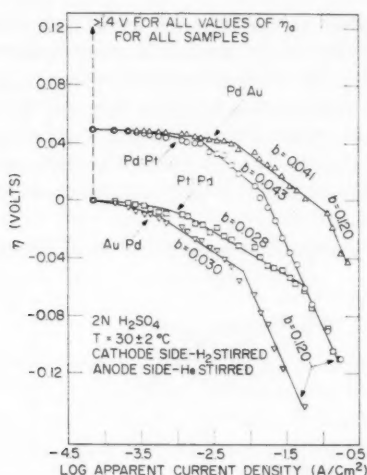
FIG. 4. Hydrogen overvoltage on Au and Pt bielectrodes clad on only one side with Pd. Pt/H$_2$ reference electrode on cathode side; (Pd–H)$_a$/H$^+$ reference electrode on anode side.

the interior does not appear to influence the shape of the overvoltage curves. The differences in the i_0 values and the potentials for the plateaus for these curves are undoubtedly due primarily to the variation in the amount of cold working of each of these sandwiches (2).

Figure 5 shows the diffusion overvoltage, η_d, for the various metal sandwiches. Only for the case of the iron sandwich was there evidence of a significant amount of hydrogen diffusion through the diaphragm. In all cases the potential on the diffusion side at open circuit was equal to 0.05 v. This showed that during the cathodic charging of the palladium with hydrogen on the polarization side not enough hydrogen diffused through the metal in the center to charge the diffusion side to the β-phase. Hence on the polarization sides of these sandwiches the palladium was charged with hydrogen to the β-phase, and on the diffusion side the palladium was in the α-phase. Previous work by the authors (1, 2) has indicated that atomic hydrogen does diffuse through β-palladium. The results shown in Fig. 5 indicate that atomic hydrogen can diffuse through iron also, but not through nickel, platinum, or gold.
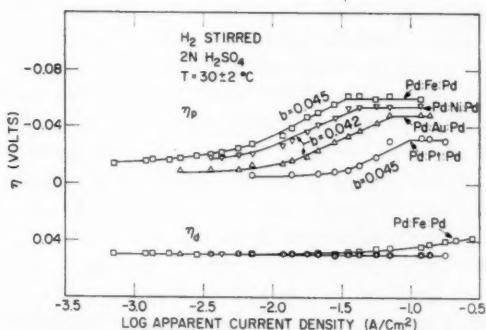
FIG. 5. Hydrogen overvoltage on polarization and diffusion surfaces of cathode-diaphragms consisting of Au, Pt, Ni, and Fe clad on both sides with Pd. Pt/H$_2$ reference electrode.

The metal sandwiches treated as bielectrodes gave the cathodic overvoltage, η_c, curves shown in Fig. 6. These curves are similar to those found for α-palladium bielectrodes (4). The separation of these curves arises from a complicated combination of conditions which include the migration of protons through the membrane, differences in cold working of the sandwiches, area differences, and the rate of oxygen diffusion from the anodic side. Since the primary purpose of this work was to determine the migration of protons through metals other than palladium, a determination of the effects of each of these factors was not made.

The anodic overvoltage, η_a, curves for this series of sandwiches is shown in Fig. 7. In
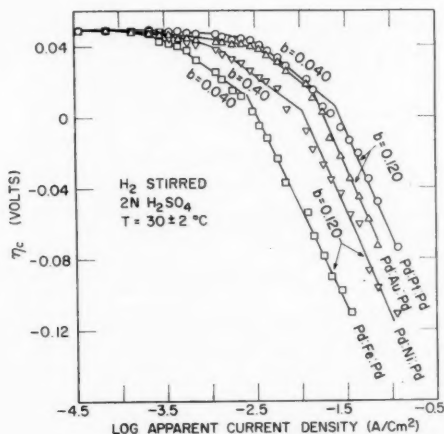
FIG. 6. Hydrogen overvoltage on the cathode surfaces of bielectrodes consisting of Au, Pt, Ni, and Fe clad on both sides with Pd. Pt/H$_2$ reference electrode.
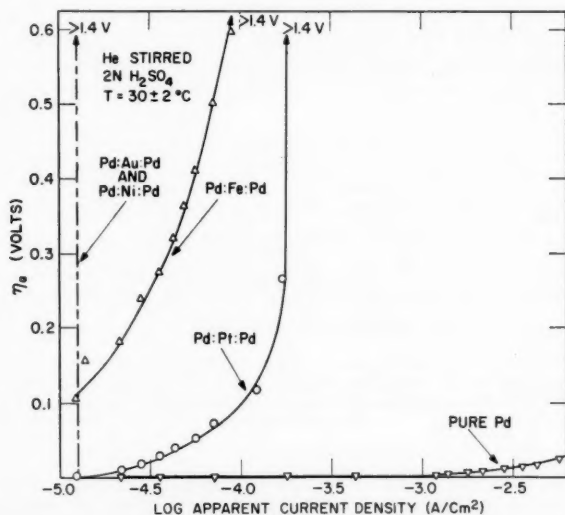
FIG. 7. Hydrogen overvoltage on the anode surfaces of bielectrodes consisting of Au, Pt, Ni, and Fe clad on both sides with Pd. (Pd–H)$_a$/H$^+$ reference electrode.

order to determine the magnitude of the migration of protons through the membranes, the anode was stirred with helium. Hence any depolarization effects on this side would be due to the hydrogen which had migrated from the cathode side. As can be seen in Fig. 7, the platinum sandwich showed the most marked depolarization effect. The iron sandwich showed a depolarization effect also; however, neither gold nor nickel showed any evidence of proton migration through the bielectrode. In Fig. 7 is shown also part of the anodic polarization curve for a pure palladium bielectrode in the same solution (a more complete curve under these conditions is shown in ref. (3)). The comparison of the pure palladium with the platinum and iron sandwiches emphasizes the great differences in rate of proton migration through these specimens.

DISCUSSION

Previous work (1, 2) has shown that when a palladium diaphragm which separates two bodies of solution is made a cathode, hydrogen will be generated on the polarization side. Part of this hydrogen will dissolve in the palladium to form the β-phase. Further solution of hydrogen will set up a concentration gradient of atomic hydrogen* across the diaphragm and the atoms diffusing through the metal will cause an overvoltage effect, η_d, on the diffusion side. When palladium on the cathode side of a bimetallic diaphragm is charged with hydrogen in excess of the β-phase (H/Pd > 0.6), atomic hydrogen will exist in its interior. If this atomic hydrogen can diffuse through Pt, Au, Fe, or Ni clad to palladium, then its effect should be evident as an atomic concentration overvoltage. Such an effect was only found for the Pd : Fe : Pd sandwich and this indicated that atomic hydrogen did diffuse through steel.

If a pure palladium membrane is arranged as a bielectrode, the palladium will be maintained in the α-phase because hydrogen will be removed from the anode side as fast as it will dissolve in the metal on the cathode side (4). It has been shown that this hydrogen migrates through the palladium as protons. Low current density experiments in which the bimetallic membranes were used as bielectrodes would give evidence of the transfer of protons through the metals. If hydrogen, owing to the difference in the electrochemical affinities of the reaction on the cathode and anode sides, migrates through the bielectrode the palladium on the cathode side is maintained in the α-phase and atomic hydrogen virtually does not exist in its interior. Evidence of proton migration through the non-palladium metal would be shown by lowered anodic overvoltages, η_a.

The experimental results with platinum and gold clad on only one side with palladium showed that when the palladium was on the cathode side of the bielectrode there was no evidence of proton diffusion through the membrane. Similarly when the platinum or gold was on the cathode side, proton migration did not occur. However, for the steel and platinum sandwiches there was definite evidence of proton migration through these metals. In the case of platinum there apparently was no proton migration through the Pd : Pt combination because at low current densities the hydrogen would merely dissolve in the palladium until it was charged to the β-phase. The solution or removal of the hydrogen atoms on the Pd–cathode side was evidently much more rapid than the oxidation of hydrogen atoms on the Pt–anode side. The small effect of current density on cathodic overvoltage in the low current density range shown in Fig. 4 is indicative of the charging of the palladium with hydrogen. For the case of the sandwich Pd : Pt : Pd, proton migration through the bielectrode occurred, since, in the low density range, the

*Electrons from these atoms can be considered to occupy the H 1s-band rather than the Pd 4d-band. These electrons in excess of the amount required to fill the d-band of Pd move in a band which is characteristic of the proton lattice.

rate of removal of hydrogen atoms from the palladium cathode side would evidently be the same as the rate of oxidation of hydrogen atoms on the palladium anode side.

Proton migration through palladium, iron, and platinum bielectrodes can be explained on the basis of the holes in the d-bands of these metals. When the hydrogen atom formed on the surface of α–Pd enters the interior of the metal, it donates its electron to the d-band of the palladium and the proton exists in an interstitial position in the Pd lattice. In order for the proton to exist in the platinum or steel lattice, an electron must accompany it, so that electrical neutrality may be maintained. Both platinum and iron have holes in their d-bands so that the addition of electrons will not increase the total energy significantly, since the density of levels in the d-bands of these metals is very large. Hence protons can exist in and migrate through the interior of these metals. On the other hand, gold has a filled d-band and electrons would have to enter the $6s$-band. Since the density of levels in the s-band is very low this would require a large increase in energy. As a result, under the experimental conditions used, protons do not migrate through gold.

From this viewpoint it is expected that protons should migrate through nickel. The experimental evidence does not support this, even at current densities as low as 10^{-7} amp/cm². A partial explanation may lie in the fact that the holes in the d-band of Ni are completely polarized in one spin direction (12), which is not the case for Pd, Pt, or Fe. Since electrons can enter only one half of the d-band in Ni but can enter both halves in Pd, Pt, or Fe, the energy for the solution of the same amount of hydrogen will be increased much more in the case of Ni than in the other metals. This, of course, assumes that for these metals the density of levels is nearly the same for the $3d$-, $4d$-, and $5d$-band. This extra energy appears to be prohibitive to the solution of hydrogen as protons in nickel to an appreciable extent. However, other effects such as differences in solvation energy of the proton may be more important.

CONCLUSIONS

For the β–Pd cathode of a Pd : Pt or Pd : Pt : Pd diaphragm where there is an atomic hydrogen gradient and hydrogen can diffuse through the palladium, diffusion through the platinum was not detected. This indicates that under an atomic hydrogen concentration gradient alone hydrogen atoms will not dissolve in platinum. In the case where a concentration gradient of protons exists across a bielectrode of platinum sandwiched between palladium, protons will migrate through. In this case the protons already exist in the palladium in contact with the platinum. Hence, as is also shown in the case of the Pt : Pd bielectrode, the s-electron of a hydrogen atom does not enter the d-band of platinum spontaneously.

A similar argument can be used for the Pd : Fe : Pd bielectrode. However, for this combination there is some atomic hydrogen diffusion through the steel if a concentration gradient and the s-electrons of hydrogen atoms can enter the d-band of iron spontaneously.

It can be concluded that, under the experimental conditions used, hydrogen can dissolve and migrate only as protons through platinum, whereas it can either migrate as protons or diffuse as atoms through iron or palladium. Neither protons nor hydrogen atoms can be transported through gold or nickel.

ACKNOWLEDGMENTS

SCHULDINER AND HOARE: TRANSPORT OF HYDROGEN 237

REFERENCES

1. SCHULDINER, S. and HOARE, J. P. J. Electrochem. Soc. **103**, 178 (1956).
2. HOARE, J. P. and SCHULDINER, S. J. Electrochem. Soc. **103**, 237 (1956).
3. SCHULDINER, S. and HOARE, J. P. J. Electrochem. Soc. **105**, 278 (1958).
4. HOARE, J. P. and SCHULDINER, S. J. Electrochem. Soc. **104**, 564 (1957).
5. SCHULDINER, S. J. Electrochem. Soc. **99**, 488 (1952).
6. SCHULDINER, S. and HOARE, J. P. J. Chem. Phys. **26**, 1771 (1957).
7. SCHULDINER, S., CASTELLAN, G. W., and HOARE, J. P. J. Chem. Phys. **28**, 16 (1958).
8. SCHULDINER, S. and HOARE, J. P. International colloquium on reference electrodes and structure of the double layer. Paris. October, 1956.
9. KALISH, T. V. and BURSHTEIN, R. K. Doklady Akad. Nauk, S.S.S.R. **88**, 863 (1953).
10. SCHULDINER, S. J. Electrochem. Soc. **101**, 426 (1954).
11. HOARE, J. P. and SCHULDINER, S. J. Electrochem. Soc. **102**, 485 (1955).
12. BOZORTH, R. M. Ferromagnetism. D. Van Nostrand Company, Inc., New York. 1951. Figs. 10–17.

THE DETERMINATION OF KINETIC PARAMETERS OF REDOX REACTIONS FROM CURRENT–POTENTIAL CURVES[1]

J. E. B. RANDLES

ABSTRACT

Methods are suggested for calculating kinetic parameters of moderately rapid redox reactions from current–potential curves obtained with (a) rotating electrodes or stationary electrodes in stirred solutions, (b) dropping mercury electrodes. Experimental results for the V^{2+}/V^{3+} reaction at a dropping mercury electrode are presented and compared with a-c. impedance measurements on the same system. It is found that there is a good agreement between the kinetic parameters obtained by the two methods when the current–potential curves are interpreted with the aid of Koutecký's theory of diffusion to a dropping mercury electrode.

INTRODUCTION

In the investigation of the kinetics of moderately rapid electrode reactions by means of the steady-state current–potential relationship, the necessity of taking account of concentration polarization has been recognized for a long time and a number of theoretical treatments have appeared (1). However, no very satisfactory method of deriving the kinetic parameters for such reactions from the current–potential data has emerged. Simple plots of η (overpotential) against $\log i$ are still commonly used (2), although this is of little value in the region of the reversible potential or when concentration polarization becomes predominant. Frequently very little of the graph approximates to a straight line. Similar remarks apply to the utilization of current–potential curves obtained with a dropping mercury electrode (D.M.E.) when the deviation from the ideal reversible curve is not large.

For reactions too rapid to be satisfactorily investigated by d-c. polarization in the steady state, or quasi steady state (D.M.E.), relaxation methods are employed.* Of these, measurements of the a-c. impedance of an electrode is probably the most useful. The range of application (in terms of rate of electrode reaction) of this method overlaps with that of the d-c. polarization methods and it is of interest to compare the kinetic parameters obtained by the two types of method for the same electrode reaction. This comparison promises to be of most interest when the D.M.E. is used, for two reasons: (a) the reproducibility of the electrode makes an accurate comparison possible, (b) there remains some uncertainty in the theory of the current–potential relationship for this electrode which such a comparison may resolve.

The present paper has two purposes: first to present what the author regards as the most convenient method of calculating kinetic parameters of moderately rapid electrode reactions from current–potential curves, and secondly to compare results so obtained with a D.M.E. with the results of a-c. impedance measurements. The reaction selected for this purpose is the V^{2+}/V^{3+} reaction.

Calculation of Kinetic Parameters From Current–Potential Curves

We shall consider a simple electrode reaction of first order in both the cathodic and anodic directions which may be written

[1] $$(1) + ne^- \rightleftharpoons (2).$$

Substances (1) and (2) are both present in the electrolyte solution or, if the electrode is mercury, (2) may be a metal dissolved in the mercury. Any other molecules such as H_2O or complexing ions which may take part in the reaction are assumed to be present in such large excess that the reaction remains pseudounimolecular in both directions. The modification of the treatment given below to the case when (2) is the metal of the electrode can easily be made.

In practice, free diffusion of ions unaccompanied by migration is ensured by the presence of an excess of an indifferent electrolyte, and this also results in the substances (1) and (2) having activity coefficients independent of their own concentrations. Hence the Nernst equation for the potential E^r, of a reversible electrode becomes

[2] $$E^r = E_f{}^\circ + (RT/nF) \ln(C_1{}^\circ / C_2{}^\circ)$$

where $C_1{}^\circ$ and $C_2{}^\circ$ are the bulk concentration of (1) and (2) and $E_f{}^\circ$ is the 'formal' potential (for $C_1{}^\circ = C_2{}^\circ$). Further, if $k_1{}^r$ and $k_2{}^r$ are the rate constants of the forward (left to right) and reverse directions of reaction [1] at the equilibrium potential E^r, then

[3] $$k_1{}^r\, C_1{}^\circ = k_2{}^r\, C_2{}^\circ.$$

Hence it is easily seen that for two potentials of the electrode E^r and $E^{r\prime}$ (corresponding to different ratios of $C_1{}^\circ$ to $C_2{}^\circ$),

[4] $$E^r - E^{r\prime} = (RT/nF) \ln(k_2{}^r / k_1{}^r)\,(k_1{}^{r\prime} / k_2{}^{r\prime}).$$

For a particular system, having given bulk concentrations $C_1{}^\circ$ and $C_2{}^\circ$, we shall denote by $k_1{}^r$ and $k_2{}^r$ the rate constants at the equilibrium potential and by k_1 and k_2 the rate constants at any other potential E, thus

[5] $$E - E_r = \eta = (RT/nF) \ln(k_2/k_1)\,(k_1{}^r / k_2{}^r)$$

or,

[6] $$k_2/k_1 = (k_2{}^r / k_1{}^r) \exp nf\eta$$

where F/RT is abbreviated to f, and η is the overpotential of the electrode:

Steady-state Diffusion

For steady-state diffusion, using a rotating electrode or stationary electrode in a stirred solution, the Nernst layer treatment of diffusion leads to

[7] $$i = nFD_1(C_1{}^\circ - C_1)/\delta = nFD_2(C_2 - C_2{}^\circ)/\delta$$

where i is the cathodic current density, C_1 and C_2 are the concentrations of (1) and (2) at the electrode surface, D_1 and D_2 are diffusion coefficients, and δ is the thickness of the Nernst layer. Thus, if i_1 and i_2 respectively are the limiting cathodic and anodic diffusion currents (both given positive sign),

[8] $$i_1 = nFD_1C_1{}^\circ/\delta, \qquad i_2 = nFD_2C_2{}^\circ/\delta.$$

From [7] and [8]

[9] $$C_1/C_1{}^\circ = (i_1 - i)/i_1, \qquad C_2/C_2{}^\circ = (i_2 + i)/i_2.$$

The net current density is also given by

[10]
$$i = nF(k_1 C_1 - k_2 C_2)$$

which, using [9], [3], and [6] becomes

[11]
$$i = nFk_1 C_1^\circ \left[\frac{i_1-i}{i_1} - \left(\frac{i_2+i}{i_2} \right) \exp nf\eta \right].$$

By rearrangement we have

[12]
$$-\log_{10} nFk_1 C_1^\circ = \log_{10} \left[\left(\frac{1}{i} - \frac{1}{i_1} \right) - \left(\frac{1}{i} + \frac{1}{i_2} \right) \exp nf\eta \right].$$

Thus, by plotting the right hand side of [12] against $nf\eta$ a nearly straight line should be obtained.

The slope at any point

[13]
$$d(\log_{10} k_1)/d(nf\eta) = -\alpha/2.303$$

gives the cathodic transfer coefficient, α, and the intercept at $nf\eta = 0$ is $\log_{10}(nFC_1^\circ k_1^r)$.

It is advantageous to use $[nf\eta + \ln(C_1^\circ/C_2^\circ)]$ instead of $nf\eta$ as abscissa, since, from equation [2],

$$nf\eta + \ln(C_1^\circ/C_2^\circ) = nf(E - E^r) + nf(E^r - E_f^\circ) = nf(E - E_f^\circ)$$

and this quantity depends only on the potential of the electrode relative to the solution. If also $\log_{10} nFC_1^\circ$ is added to the right hand side of equation [12] before plotting as ordinate, the graphs obtained for any value of C_1° and C_2° should coincide, and the intercept on the axis $nf\eta + \ln(C_1^\circ/C_2^\circ) = 0$ is now $\log_{10} k_s$ where k_s is the standard rate constant of the reaction.*

Dropping Mercury Electrode

The theory of diffusion to a dropping mercury electrode is complicated both by the growth of the drop surface and by the fact that the surface is not planar but spherical. The mathematical difficulties are such that all attempts at an exact solution of the diffusion equations have assumed the electrode reaction to be first order in both directions, as we have already done. A solution of the diffusion equation for an expanding mercury drop electrode and an electrode process involving a slow chemical step was first obtained by Koutecký and Brdička (3). More detailed solutions, specifically for the case of a slow electrochemical step have been given by Smutek (4), Kambara and Tachi (5), and Delahay (6). These workers solved the diffusion equation first for a stationary plane electrode, obtaining expressions for the current density equivalent to

[14]
$$i = nF(k_1 C_1^\circ - k_2 C_2^\circ) \exp Q^2t \, \text{erfc} \, Qt^{\frac{1}{2}},$$

where

[15]
$$Q = (k_1 D_1^{-\frac{1}{2}} + k_2 D_2^{-\frac{1}{2}}),$$

t is the time from the start of the electrolysis, and erfc denotes the complementary error function. This result, for a plane electrode, has to be modified in order to give the current at a dropping mercury electrode. Smutek, and Kambara and Tachi, simply multiplied the whole expression [14] by the area of the drop, while Delahay multiplied also by the Ilkovič (7) factor $(7/3)^{\frac{1}{2}}$. The use of the Ilkovič factor for an expanding drop is certainly

*$k_s = k_1^r = k_2^r$ when $C_1^\circ = C_2^\circ$, see Randles, J. E. B. Discussions Faraday Soc. **1**, 11 (1947) and Delahay, P. New instrumental methods in electrochemistry. Interscience Publishers, Inc., New York. 1954. Chap. 7.

necessary but a consideration of the origin of this factor* shows that the continuous lateral expansion of the diffusion layer, by reducing its thickness, has the same effect as multiplying the diffusion coefficients by $7/3$. Thus the correct way of introducing the Ilkovič factor appears to be to redefine Q thus

$$[16] \qquad Q = (3/7)^{\frac{1}{2}}(k_1 D_1^{-\frac{1}{2}} + k_2 D_2^{-\frac{1}{2}}).$$

This procedure is supported by the fact that it leads to the correct result for the extreme cases, i.e. very slow or very fast electrode reactions, while multiplication of the whole expression [14] by $(7/3)^{\frac{1}{2}}$ leads to an incorrect result for very slow reactions.

An approach distinct from the above was made by Koutecký (18), who solved a diffusion equation appropriate to an expanding electrode but still neglected the curvature of the surface. His results are expressed in terms of a variable χ which is equivalent to $2Qt^{\frac{1}{2}}$ where Q is given by [16]. In later work (9) Koutecký and Cížek have included the effect of the curvature of the surface. Expression [14] and Koutecký's results can be applied with equal ease to the interpretation of polarographic current–potential curves.

It is probably more accurate experimentally, when using a dropping electrode, to measure the instantaneous current at maximum drop size than to measure the average current. Therefore the method of interpreting current–potential curves will be developed for currents measured at maximum drop size. Only minor changes are needed in order to apply it to average currents.

From equation [14] the current at time τ from the start of a new drop ($\tau =$ drop life) is given by

$$[17] \qquad i_\tau = nFA(k_1 C_1{}^\circ - k_2 C_2{}^\circ)\exp Q^2\tau \text{ erfc } Q\tau^{\frac{1}{2}},$$

where A is the surface area of the drop at maximum drop size. Using expressions [3] and [6] which are still valid, [17] becomes

$$[18] \qquad i_\tau = nFA\ k_1 C_1{}^\circ (1 - \exp nf\eta)\exp Q^2\tau \text{ erfc } Q\tau^{\frac{1}{2}}.$$

Now if we denote by i_{τ_1} and i_{τ_2} the limiting cathodic and anodic diffusion currents at maximum drop size, then provided that τ is the same for both

$$[19] \qquad i_{\tau_1}/i_{\tau_2} = C_1{}^\circ D_1{}^{\frac{1}{2}}/C_2{}^\circ D_2{}^{\frac{1}{2}}.$$

Also, with the aid of equations [3], [6], and [19] and using the abbreviation

$$[20] \qquad i_{\tau_1}/i_{\tau_2} = r$$

expression [16] becomes

$$[21] \qquad Q = (3/7)^{\frac{1}{2}}\ k_1 D_1^{-\frac{1}{2}}(1 + r \exp nf\eta).$$

Finally, by using [21] to substitute for k_1 in [18] we reach the equation

$$[22] \qquad i_\tau = nFA\ C_1{}^\circ\left(\frac{7D_1}{3\pi\tau}\right)^{\frac{1}{2}}\left[\frac{1 - \exp nf\eta}{1 + r \exp nf\eta}\right]\theta(Q\tau^{\frac{1}{2}})$$

where

$$[23] \qquad \theta(Q\tau^{\frac{1}{2}}) = \pi^{\frac{1}{2}}Q\tau^{\frac{1}{2}}\exp Q^2\tau \text{ erfc } Q\tau^{\frac{1}{2}}.$$

The function $\theta(Q\tau^{\frac{1}{2}})$ has the property of approaching unity as $Q\tau^{\frac{1}{2}} \to \infty$, i.e. for very rapid electrode reactions. Expression [22] may therefore be written

$$[24] \qquad i_\tau = i_{\tau\infty}\ \theta(Q\tau^{\frac{1}{2}})$$

*See Stackelberg, M.v. Z. Elektrochem. **45**, 466 (1939).

where $i_{r\infty}$ is the value of i_r for an infinitely rapid electrode reaction at the same value of η (i.e. k_1/k_2 unchanged but k_1 and $k_2 \to \infty$). Values of the function $\theta(\chi)$ for a series of values of χ are tabulated in Milner's Polarography (Longmans, Green & Co., Inc., New York and Toronto. 1957. Table 4.1). Koutecký expressed his results in a similar form

[25] $$i_r = i_{r\infty} F(\chi)$$

where $\chi = 2Q\tau^{\frac{1}{2}}$, and he tabulates (10) $F(\chi)$. This table is reproduced by Delahay, P. New instrumental methods in electrochemistry. Interscience Publishers Inc., New York. 1954. Table 4.1.

In order to use equation [24] or [25] it is necessary to find $i_{r\infty}$. It is given by [22] with $\theta(Q_r^{\frac{1}{2}}) = 1$, and may be expressed in terms of either limiting diffusion current. In terms of the cathodic current, i_{r_1},

$$i_{r\infty} = i_{r_1}\left(\frac{1-\exp nf\eta}{1+r\exp nf\eta}\right).$$

The calculation of $i_{r\infty}$ from this expression for each case is laborious and a sufficiently accurate and much simpler method is as follows. The current i_r measured at a series of overpotentials is expressed as a fraction of $\frac{1}{2}(i_{r_1}+i_{r_2})$ (both limiting currents being given positive sign) and plotted against $nf\eta$. Figure 1 shows a typical curve. On this scale the $i_{r\infty}$ curve is that of tanh $-nf\eta/2$ drawn between the limiting current lines and cutting the experimental curve at the point of zero current (see Fig. 1). A template may be used to draw this curve on standard squared graph paper. The results described below were obtained by using a 'Perspex' template on which the full extent of the current axis (i.e. from tanh$-\infty = -1$ to tanh$+\infty = +1$) = 20 cm, and one unit on the $nf\eta$ axis = 2.5 cm. The accuracy of the experimental current measurement would justify a somewhat larger scale.
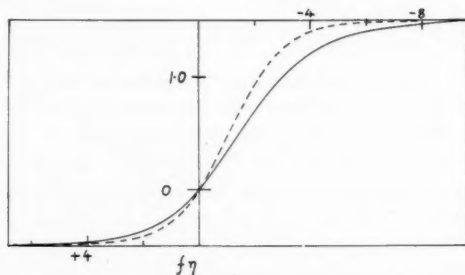
FIG. 1.   Full curve: experimental $2i_r/(i_{r_1}+i_{r_2})$.
Broken curve: $i_{r\infty}$.
Cathodic current plotted above the zero current axis.

The ratio $i_r/i_{r\infty}$ is calculated from the two curves at a series of values of $nf\eta$ corresponding (for reasons which will be apparent later) to selected values of $(nf\eta + \ln r)$. These selected values ranged from -5.2 to $+5.2$ in steps of 0.4, in the calculations to be described below. The fraction $i_r/i_{r\infty}$ is equal to $F(\chi)$ or $\theta(\chi/2)$ and the next step is therefore to read off the corresponding value of $\log(\chi/2)$ from a graph of $F(\chi)$ or $\theta(\chi/2)$ against $\log(\chi/2)$. From equation [22],

$$\log \chi/2 = \log Q\tau^{\frac{1}{2}} = \log(3/7)^{\frac{1}{2}}k_1 D_1^{-\frac{1}{2}}\tau^{\frac{1}{2}}[1+\exp(nf\eta + \ln r)]$$

or

[26] $$\log \chi/2 - \log[1+\exp(nf\eta + \ln r)] = \log_{10}(3\tau/7D_1)^{\frac{1}{2}}k_1.$$

The left hand side of [26] is calculated with the aid of a previously prepared table of values of $\log[1+\exp(nf\eta + \ln r)]$ for the selected values of $(nf\eta + \ln r)$, and is plotted against $(nf\eta + \ln r)$. Since

$$r = i_{r_1}/i_{r_2} = C_1^{\circ}D_1^{\frac{1}{2}}/C_2^{\circ}D_2^{\frac{1}{2}}.$$

Therefore

[27] $$(nf\eta + \ln r) = nf(E-E_f^{\circ})+\tfrac{1}{2}\ln D_1/D_2.$$

Equation [27] shows that the abscissa $(nf\eta + \ln r)$ depends on the potential of the electrode relative to the solution but is independent of C_1°/C_2°. Thus the graphs obtained for any values of C_1° and C_2° should coincide. The slope at any point is

[28] $$d\log_{10} k_1/d(nf\eta) = -\alpha/2.303$$

and the intercept with the line $(nf\eta + \ln r) = \tfrac{1}{2}\ln D_1/D_2$ has the value $\log_{10}(3\tau/7D_1)^{\frac{1}{2}} k_s$.

As will be shown later, these graphs can be compared directly with the results of a-c. measurements.

EXPERIMENTAL

Materials

Solutions were made up in water redistilled in an all-glass still. Perchloric and sulphuric acids were distilled under reduced pressure. A stock solution of VO^{++} in perchloric acid solution was prepared from Analar ammonium vanadate by reduction with SO_2 and boiling out the excess. The solution therefore contained a little $SO_4^{=}$ and NH_4^{+}. The final reduction to a mixture of V^{2+} and V^{3+} was carried out in the electrolysis cell.

Apparatus

The dropping electrode consisted of a short length of capillary tube of 0.045 mm bore, sealed at one end to a length of 1-mm bore tubing which was connected to a mercury reservoir by silicone tubing. The lower end of the capillary was blown out to a small bulb which was drawn to a fine thin-walled tube and cut to a square end (i.d. ~ 0.05 mm, o.d. ~ 0.15 mm, at the tip). This ensures the minimum possible shielding of the mercury drop by the end of the capillary. The dropping electrode was inserted through a ground joint in the cap of the electrolysis cell which also carried an inlet for purified hydrogen, a tube closed by a sintered-glass plug and containing an auxilliary platinum electrode, and a J tube containing mercury which served as a reversible reference electrode. Mercury was introduced into the electrolysis cell from a connection at the lower end. The final reduction of the VO^{++} to a mixture of V^{2+} and V^{3+} was carried out cathodically at the large mercury pool stirred by a stream of hydrogen and with the platinum electrode as anode. The mercury pool also served as second electrode in the d-c. polarization measurements and in the a-c. impedance measurements. The whole electrolysis vessel was surrounded by a thermostatic water jacket.

In the d-c. polarization measurements the current at maximum drop size was measured directly by means of calibrated Cambridge 'spot' galvanometer, internal resistance 50 ohms, of period 2 seconds, slightly under damped. The drop time of the capillary was mechanically controlled at 6.0 seconds (natural drop time ~ 9 seconds). The over-potential was measured between the dropping electrode and the stationary mercury electrode in the J tube. The ohmic potential drop due to the resistance of the capillary and the electrolyte (about 50 ohms) was never greater than 0.3 mv, and was neglected. The capacity current at maximum drop size was also negligible.

The a-c. impedance measurements were carried out by means of an improved version of an apparatus already described (11), details of which will appear in a later publication.

RESULTS AND DISCUSSION

Figure 1 shows an experimental current–potential curve for V^{2+}/V^{3+} in $1\ M\ H_2SO$ together with the i_∞ curve. The temperature was 15.3° C, the total vanadium concentration 0.003 M, and the ratio of the cathodic to anodic limiting currents ($= i_{r_1}/i_{r_2} = r$) was 3.05. Corresponding curves were obtained for the same solution but with $r = 1.06$ and 0.187 respectively. The left hand side of equation [26] calculated for each of the three curves is plotted against ($nf\eta + \ln r$) in the lower part of Fig. 2 using Koutecký's values (10) of $F(\chi)$ modified by his correction for spherical diffusion (see below). The good agreement between the three sets of points is typical of what is obtained if the difference between i_r and i_{r_∞} is as great as, or greater than, that shown in Fig. 1. In the upper part of Fig. 2 are three sets of points calculated from the current–potential curve for $r = 1.06$. The lowest set ($\odot$) was obtained by equating i_r/i_{r_∞} to $\theta(\chi/2)$ (equation [23]). The next set ($\times$) was obtained using Koutecký's tabulated values of $F(\chi)$ and the uppermost set ($+$) by using $F(\chi)$ corrected for spherical diffusion. This correction has been calculated by Koutecký and Čížek (9) and takes the form $\xi.H_c(\chi)$ where ξ depends on the drop time, rate of flow of mercury, and diffusion coefficients of the reactants, and $H_c(\chi)$ is a function
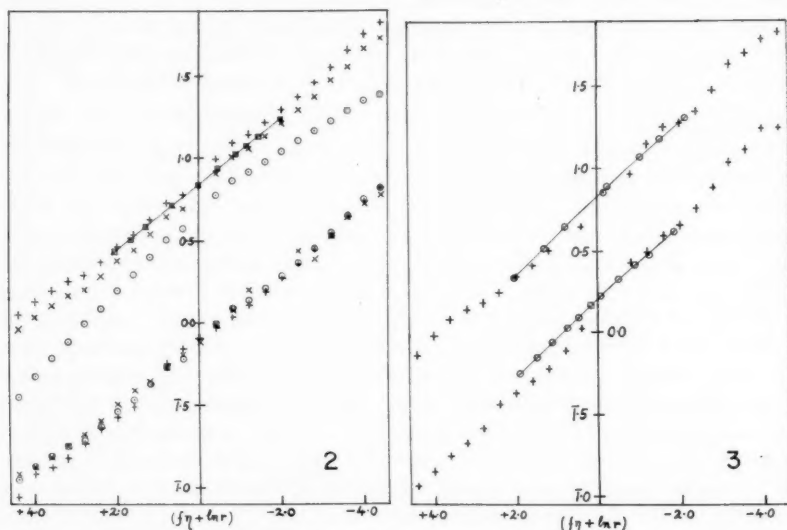
FIG. 2. V^{2+}/V^{3+} in $1\ M\ H_2SO_4$, 15.3° C, L.H.S. of equation [26] plotted as ordinate.
Lower part: $i_r/i_{r_\infty} = F(\chi)$ corrected for spherical diffusion.
$+ - r = 3.05$; $\odot - r = 1.06$; $\times - r = 0.181$.
Upper part: (all points shifted upwards one unit on ordinate scale) $r = 1.06$.
$\odot - i_r/i_{r_\infty} = \theta(\chi/2)$; $\times - i_r/i_{r_\infty} = F(\chi)$.
$+ - i_r/i_{r_\infty} = F(\chi)$ corr. for spherical diffusion.
$\square$ — from a-c. impedance.
FIG. 3. V^{2+}/V^{3+} in $1\ M\ HClO_4$.
$+$ — L.H.S. of equation [26] plotted as ordinate.
$\odot$ — From a-c. impedance.
Lower part: 14.2° C.
Upper part: 25° C (points shifted upwards by 0.5 unit).

of χ which they tabulate. The correction is easily applied by drawing a curve of $F(\chi)-\xi.H_c(\chi)$ against $\log(\chi/2)$, ξ being constant for a given system if τ is constant, and in the present case $\xi = 0.191$. The fourth set of points ($\boxdot$) in the upper part of Fig. 2 was obtained from the a-c. impedance of the same electrode in the same solution but with the total vanadium concentration raised to 0.009 M to improve the accuracy of the measurements. Impedance measurements were made for a range of values of τ. The activation resistance,* R_a, of the electrode is related to the exchange current i_0 by

$$(nFR_a)^{-1} = i_0 = nFA'\ k_1'C_1^{\circ} = nFA'\ k_2'C_2^{\circ}$$

where A' is the area of the drop at the time of the impedance measurement. In practice this measurement was made when the age of the drop was 0.9τ so that the ratio of A' to the maximum area is $(0.9)^{\frac{2}{3}}$. It is thence easily deduced that

[29] $$-\log[nF(0.9)^{\frac{2}{3}}.\ \pi^{\frac{1}{2}}R_a i_{\tau_1}] = \log(3\tau/7D_1)^{\frac{1}{2}}k_1'.$$

The right hand side (R.H.S.) of [29] is identical with the R.H.S. of [26], and hence the L.H.S. of [29] is plotted as the fourth set of points ($\boxdot$) in the upper part of Fig. 2. The other points which agree best with this set are those calculated with the use of Koutecký's $F(\chi)$ corrected for spherical diffusion; the improved agreement resulting from the inclusion of this correction is often more marked than in this example. It is evident that the use of $\theta(\chi/2)$ would give an erroneously low value of the rate constant. None of the lines from the current–potential curves are very straight but those calculated by means of $F(\chi)$ are straighter than those calculated by means of $\theta(\chi/2)$.

In Fig. 3 points calculated from current–potential curves using $F(\chi)$ corrected for spherical diffusion are compared with those calculated from a-c. impedance measurements, for V^{2+}/V^{3+} in 1 M $HClO_4$ at 14.2° C and 25.0° C respectively. There is again good agreement. In both cases the ratio i_{τ_1}/i_{τ_2} was near unity so that the points from the current–potential curves are absent or very uncertain at small values of $(nf\eta + \ln r)$. In Fig. 4 the data from a-c. impedance measurements are plotted on a larger scale. The
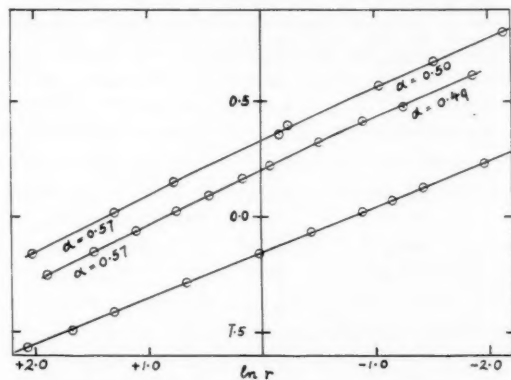
FIG. 4.   L.H.S. of equation [29] plotted as ordinate.
V^{2+}/V^{3+} in: (upper line) 1 M $HClO_4$, 25° C; (middle line) 1 M $HClO_4$, 14.2° C; (lowest line) 1 M H_2SO_4, 15.3° C.

*R_a is equivalent to $R_r - 1/\omega\ C_r$ of earlier papers (Randles, J. E. B.   Discussions Faraday Soc. **1**, 11 (1947).), to R_D of Gerischer, H.   (Z. physik. Chem. **198**, 286 (1951).), and to θ of Grahame, D. C.   (J. Electrochem. Soc. **99**, 370C (1952).). It was calculated by a method similar to that previously described (Laitinen, H. A. and Randles, J. E. B.   Trans. Faraday Soc. **51**, 54 (1954).).

points for the sulphuric acid base solution at $15.3°$ C give a straight line corresponding to $\alpha = 0.455$ and $k_s = 1.39 \times 10^{-3}$ cm sec^{-1}. Those for the perchloric acid base solution give slightly curved lines corresponding to α decreasing from 0.57 to 0.50 ($25°$ C) and from 0.57 to 0.49 ($14.2°$ C) with increasing cathodic potential. However, the evidence is as yet insufficient to confirm that this represents a genuine change in α. The values of k_s are 2.20×10^{-3} and 3.64×10^{-3} cm sec^{-1} respectively corresponding to $\Delta H^{\ddagger} = 7.6$ kcal.

It is concluded from the above results that reliable values of the rate constants and transfer coefficients of redox reactions may be calculated from the current–potential curves obtained with a dropping mercury electrode by means of the Koutecký function $F(\chi)$ corrected for spherical diffusion. With the author's present equipment the method can give an accuracy in the rate constant of $\pm 5\%$ when $k_s \sim 1 \times 10^{-3}$ cm sec^{-1} decreasing to $\pm 30\%$ when $k_s \sim 5 \times 10^{-3}$ cm sec^{-1}. As k_s decreases, the accuracy improves to about $\pm 3\%$, and for $k_s < 2 \times 10^{-4}$ cm sec^{-1} the d-c. polarization method is preferred to the a-c. impedance method, since the accuracy of the latter falls off as k_s decreases below 1×10^{-3} cm sec^{-1}. A disadvantage of the dropping mercury electrode is the occurrence in some circumstances of the interfacial stirring which causes polarographic 'maxima'. This becomes more marked with an increased rate of mercury flow and shorter drop time, which otherwise would be advantageous for measurements on the more rapid reactions.

REFERENCES

1. ESSIN, O. and LOSCHKAREV, M. A. Acta Physicochim. U.R.S.S. **10**, 513 (1939). ESSIN, O. Acta Physicochim. U.R.S.S. **13**, 429 (1942). PETROCELLI, J. V. J. Electrochem. Soc. **98**, 187 (1951). LEWARCOWITZ, E. J. chim. phys. **49**, 557, 564, 573 (1952). DELAHAY, P. New instrumental methods in electrochemistry. Interscience Publishers, Inc., New York. 1954. Chap. 9.
2. TOBIAS, C. W., EISENBERG, M., and WILKE, C. R. J. Electrochem. Soc. **101**, 306 (1954). STERN, M. J. Electrochem. Soc. **104**, 559 (1957).
3. KOUTECKÝ, J. and BRDIČKA, R. Collection Czechoslov. Chem. Communs. **12**, 337 (1947).
4. SMUTEK, M. Chem. Listy, **45**, 241 (1951); Collection Czechoslov. Chem. Communs. **18**, 171 (1953).
5. KAMBARA, T. and TACHI, I. Bull. Chem. Soc. Japan, **25**, 135 (1952).
6. DELAHAY, P. J. Am. Chem. Soc. **75**, 1430 (1953).
7. ILKOVIČ, D. Collection Czechoslov. Chem. Communs. **6**, 498 (1934); J. chim. phys. **35**, 129 (1938).
8. KOUTECKÝ, J. Collection Czechoslov. Chem. Communs. **18**, 597 (1953).
9. KOUTECKÝ, J. and CÍŽEK, J. Collection Czechoslov. Chem. Communs. **21**, 836 (1956).
10. KOUTECKÝ, J. Chem. Listy, **47**, 323 (1953). See also ref. 8, p. 607.
11. RANDLES, J. E. B. Trans. Faraday Soc. **50**, 1246 (1954).

MECHANISMS OF REDUCTION OF CHLOROAQUOCHROMIUM(III) IONS IN ACID MEDIA[1]

PHILIP J. ELVING AND BERNARD ZEMEL

ABSTRACT

The polarographic behavior of the hexaaquochromium(III) and dichlorotetraaquo-chromium(III) ions was observed in the absence of maxima suppressors, and in the presence of various concentrations of perchloric acid, hydrochloric acid, and neutral salt. The polarographic waves obtained for each Cr(III) species in the different media were analyzed by plotting the function $\log[i/(i_d - i)]$ vs. E; the plots generally consist of two straight lines intersecting at about the half-wave potential and can best be explained by assuming two different concurrent mechanisms for the electron transfer process: the direct transfer of an electron to the Cr(III) ion from the electrode at the mercury–solution interface, and the transfer of an electron to Cr(III) from a Cr(II) ion produced at that interface. Only for the dichlorotetraaquochromium(III) ion in 12 M HCl does the direct transfer process appear to be dominant. Polarography of Cr(III) in the latter medium before and after reaction with the medium shows no change in $E_{\frac{1}{2}}$ corresponding to the shift observed in the ultraviolet spectra; this is accounted for by the "catalytic" degradation, i.e., the loss of chloride of the higher chloro complexes due to the rapid anion transfer mechanism for the electron transfer process between halo Cr(III) and Cr(II) ions.

The literature (1) on the polarographic reduction of Cr(III) to Cr(II) indicates the variability of the half-wave potential, $E_{\frac{1}{2}}$, with the natures of the Cr(III) species and of the background electrolyte.

In 0.1 M potassium chloride $E_{\frac{1}{2}}$ of -0.91 v has been reported for the "aged" solution ($1a$, f). Two waves ($E_{\frac{1}{2}} = -0.61$, -0.88 v) were found for the "fresh" green chromic chloride in 0.4 M KCl; the height of the first wave decreased with time and the second increased equivalently ($1b$). In saturated calcium chloride solution, $E_{\frac{1}{2}}$ was reported at -0.55 v ($1e$); however, other workers ($1g$) described two waves of $E_{\frac{1}{2}}$ equal to -0.57 and -0.87 v. With time, the wave at -0.57 v increased in height and that at -0.87 showed an equivalent decrease; on heating to 100° C, the second wave disappeared and reappeared only on dilution. An $E_{\frac{1}{2}}$ of -1.04 v was reported for the violet chromic sulphate and $E_{\frac{1}{2}}$ of -1.25 v for the "green" form in 1.0 M K_2SO_4 ($1h$).

All results reported in the previous paragraph involved the addition of varying amounts of gelatin as a maximum suppressor. Unfortunately, gelatin tends to shift $E_{\frac{1}{2}}$ and to change the wave shape. The extent of these effects is a function of the gelatin concentration and of the type and concentration of background electrolyte ($1e$). The mechanism of maximum suppression is not well understood and, while use of a maximum suppressor may make measurement of a wave easier, its presence generally introduces unknown complications into the electrode process.

In the present study, the polarographic behavior of the two commonly occurring forms of Cr(III), the violet hexaaquo and the dark green dichlorotetraaquo ions, has been investigated in various media in the absence of any maxima suppressor; the Cr(III) concentrations used were low enough that maxima did not interfere. The experimental conditions were such as to permit definite knowledge of the Cr(III) species present, e.g., the supporting electrolytes were usually sufficiently high in acid concentration so as to inhibit formation of hydroxo and condensed species.

DISCUSSION OF OBSERVED POLAROGRAPHIC BEHAVIOR

Selected data to illustrate the discussion are given in Table I.

TABLE I
Half-wave potential and wave slope data for reduction of Cr(III) to Cr(II)

Original species added	Background electrolyte	$-E_{\frac{1}{2}}$ v	Slope of log plot*	
			Before $E_{\frac{1}{2}}$ mv†	After $E_{\frac{1}{2}}$ mv†
$[Cr(H_2O)_6]^{+3}$	0.1 M HClO$_4$	0.80	73 (0.81)	66 (0.89)
	0.5 M HClO$_4$	0.85	76 (0.78)	79 (0.75)
	1.0 M HClO$_4$	0.91	86 (0.69)	102 (0.58)
	1.5 M HClO$_4$	0.92	89 (0.66)	116 (0.51)
	0.1 M HClO$_4$+1.9 M NaClO$_4$	0.89	78 (0.76)	128 (0.48)
	1.9 M NaClO$_4$			
$[CrCl_2(H_2O)_4]^+$	0.1 M KCl	0.57	118 (0.50)	129 (0.46)
	0.1 M HCl	0.55	107 (0.55)	107 (0.55)
	1.0 M HClO$_4$	0.53	139 (0.43)	180 (0.33)
	12 M HCl‡	0.63	54 (1.10)	60 (0.98)
	12 M HCl§	0.63	53 (1.11)	69 (0.86)

*Slope for the plot of $\log[i/(i_d-i)]$ vs. E.

†Value in parentheses corresponds to the slope in millivolts divided into 59.1 mv, i.e., equals the alpha term of equation [2].

‡Data obtained 5 minutes after dissolution of dichlorotetraaquochromium(III) chloride.

§Data obtained after equilibrium was reached.

Hexaaquochromium(III) Ion

The polarography of $[Cr(H_2O)_6]^{+3}$ was investigated using 0.1 to 1.5 M perchloric acid as background electrolyte; in 0.1 M acid the ionic strength was varied by the addition of NaClO$_4$ to an ionic strength of two.

$E_{\frac{1}{2}}$ shifts considerably with the nature and concentration of the background electrolyte. At higher HClO$_4$ concentrations, the hydrogen discharge is superposed on the first (III → II) wave, making it somewhat difficult to evaluate. The waves become increasingly more drawn out with increasing HClO$_4$ concentration and ionic strength; $E_{\frac{1}{2}}$ decreases from −0.80 v in 0.1 M HClO$_4$ to −0.91 in 1.0 M HClO$_4$; this may be due at least in part to an ionic strength effect, since increasing ionic strength at 0.1 M HClO$_4$ shifts $E_{\frac{1}{2}}$ from −0.80 to −0.89 v. Maxima appear when the Cr(III) concentration exceeds 0.8 mM in 0.10 M HClO$_4$. Polarograms for 0.1 to 5.0 mM Cr(III) solutions indicate that above 0.5 mM $E_{\frac{1}{2}}$ becomes slightly more negative with increase in chromium concentration; there is little change below 0.5 mM.

The polarograms were analyzed by plotting $\log[i/(i_d-i)]$ vs. E; $E_{\frac{1}{2}}$, given by intersection of the plot with the zero log axis, was generally identical with that obtained from the polarographic curve by geometrical plotting to within a few millivolts. The plots are unsymmetrical and may best be represented as two straight lines intersecting at or near $E_{\frac{1}{2}}$. The asymmetry increases with both ionic strength and acidity as the slope of the section above the zero log axis decreases more, relatively, than the section preceding $E_{\frac{1}{2}}$. At higher HClO$_4$ concentrations, presence of the hydrogen wave causes a small uncertainty in the i_d value; the value of $E_{\frac{1}{2}}$ is, however, relatively insensitive to this error, the principal effect being a small curvature at high i values.

Dichlorotetraaquochromium(III) Ion

$[Cr(H_2O)_4Cl_2]^+$ was studied in potassium chloride, hydrochloric acid, and perchloric acid solutions. These were prepared immediately before use by dissolving the anhydrous

salt, $[Cr(H_2O)_4Cl_2]Cl$, in a solution containing the proper amount of background electrolyte, and then diluting to the desired concentration. Delay in using the solutions, particularly in perchlorate media, results in a long, ill-defined wave extending to the hydrogen discharge.

As in the case of the hexaaquo ion, the polarographic waves show relatively large shifts in $E_{\frac{1}{2}}$ with changes in concentration and type of supporting electrolyte. The wave shapes are particularly sensitive to the medium used and are considerably more drawn out than in the case for the corresponding $[Cr(H_2O)_6]^{+3}$ waves. Log plots show these waves to be unsymmetrical about $E_{\frac{1}{2}}$ and representable by two intersecting lines.

Chromium(III) in 12 M Hydrochloric Acid

When either the hexaaquo or dichlorotetraaquochromium(III) ions are dissolved in concentrated hydrochloric acid, a slow reaction occurs, as evidenced by a change in the color of the solution. The absorption spectrum, when equilibrium has been established, is independent of the starting material (2). It is, therefore, of considerable interest to observe the effect of this "leveling" process on the polarographic reduction of the species present in solution.

The reaction between the Cr(III) species and 12 M hydrochloric acid, which results in the formation of $[Cr(H_2O)_3Cl_3]^2$, proceeds sufficiently slowly that the polarographic wave obtained within the first 10 minutes after dissolution is merely that for the Cr(III) species added (the wave for the hexaaquo species before appreciable reaction has taken place is cloaked by the hydrogen wave and cannot be deciphered). The wave obtained after equilibrium has been established is then that due to the equilibrium species of Cr(III) in 12 M hydrochloric acid. The waves obtained for either case had an $E_{\frac{1}{2}}$ of -0.60 v, although the wave for the former case appears better formed; the difference in the two waves is best illustrated by the log plot. The Cr(III) to Cr(II) reduction wave for the species present before appreciable reaction has occurred is more symmetrical and its slope is nearer that predicted for a reversible reduction where n equals 1. After reaction with the medium, the wave becomes more asymmetric about $E_{\frac{1}{2}}$; the slope of the section positive to $E_{\frac{1}{2}}$ remains unchanged and that at potentials more negative than $E_{\frac{1}{2}}$ changes.

MECHANISMS OF THE CHROMIUM(III) REDUCTION

In general, ions of the so-called transition groups of the Periodic Table yield irreversible polarographic waves; consequently, their polarography cannot always be straightforwardly interpreted.

For a reversible polarographic wave for reduction of a soluble species to a soluble product, the relationship between current and potential is given by

[1] $$E_{d.e.} = E_{\frac{1}{2}} - [RT/nF] \ln[i/(i_d - i)].$$

For irreversible waves, the same thermodynamic considerations as apply to a reversible wave still hold, but the potential depends also on the rates of the various processes occurring at the mercury drop. By definition, $E_{\frac{1}{2}}$ still is given by the value of $E_{d.e.}$ at the point where $i = i_d/2$, but the simple Heyrovsky–Ilkovic expression of equation [1] no longer holds. Theoretical treatments of the irreversible polarographic wave have been developed (3). The complexity of the process, however, is such that simplifying assumptions must be made and the problem is still far from solved. In the classic treatment developed by Eyring and co-workers (3b), the following equation was obtained by assuming that the properties of an irreversible wave are determined by the rates of diffusion and of electrochemical reduction,

[2] $$E = E_{\frac{1}{2}} - [RT/\alpha nF]\ln[i/(i_d - i)],$$

where α is the transfer coefficient such that the fraction α of the electrode potential favors the reduction at the cathode, and the fraction $(1-\alpha)$ of the potential applies to the reverse process.

If the plot of the log term of equation [2] vs. E is composed of two or more straight-line segments instead of just one straight line, a number of interpretations concerning the electrode processes involved is possible, e.g., the segments are due to successive electrode processes which, although they merge into one wave, have sufficiently different αn product values to produce slope changes in the log i plot (4). Another possibility is that the slope change is due to different, perhaps even concurrent, mechanisms for the electron transfer process with one mechanism predominating in the early part of the wave and the other predominating in the later development of the wave. Other explanations of such multisegmented slopes are possible (5).

Hexaaquo Ion

For the Cr(III)–(II) reduction, $n = 1$, and the slope of the log plot then gives the value for $2.303RT/\alpha F$, i.e., $0.0591/\alpha$ at 25°. The fact that two values for α are obtained from a single polarographic wave for the hexaaquo ion in perchloric acid media may then be interpreted as indicating two different electron transfer processes. The known reactions of the Cr(III)–Cr(II) system lend considerable support to the notions that these consist of the direct transfer of an electron to the Cr(III) species from the electrode at the solution–electrode interface and a second process involving an electron transfer reaction between Cr(III) and Cr(II).

There is evidence for the occurrence of the latter process; an electron exchange

$$Cr^*(III) + Cr(II) = Cr^*(II) + Cr(III) \tag{3}$$
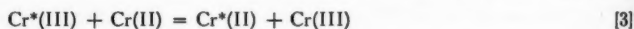
occurs in 1 M perchloric acid with a rate constant of 0.0073 liter mole^{-1} min^{-1} at 25° C (6a). The specific rate of the Cr(III)–Cr(II) electron exchange is likely 0.028 liter mole^{-1} min^{-1} with a water molecule probably being the bridging group in the activated complex (6b). Equation [3], which omits ligands, is therefore a simplified statement of the reaction, since water and hydrogen ions are also involved.

When the polarographic reduction of Cr(III) begins, the Cr(II) concentration in the diffusion layer is negligible, and the Cr(III) is presumably reduced at the electrode interface. As reduction proceeds, the Cr(II) concentration at the interface increases and, at $E_{\frac{1}{2}}$, is essentially equal to that of Cr(III). At potentials more negative than $E_{\frac{1}{2}}$, the [Cr(II)]/[Cr(III)] ratio becomes increasingly greater and there is an increased probability that, instead of the entering Cr(III) being reduced directly at the electrode interface, it may be reduced by a Cr(II) ion at the interface or diffusing from the interface into the diffusion layer. A Cr(II) ion at the mercury–solution interface may thus serve as the electron transfer agent between the incoming Cr(III) ion and the electrode, acquiring another electron from the electrode after it has become a Cr(III) species. The latter electron transfer process may occur before the newly formed Cr(II) ion diffuses away from the original Cr(II) ion, which is fixed at the interface, or possibly even during the electron transfer process between fixed Cr(II) and incoming Cr(III).

In extending the reaction summarized in equation [3] to a reaction which may occur at an electrode interface, the difficulty must be recognized of defining the activated complex concerned, which may or may not involve a water molecule as a bridging group and unknown hydrogen ion dependence.

If the electrolysis of an ion at an electrode is assumed to involve at least two stages

i.e., transfer of the solvated ion from the bulk of the solution to the electrode surface (with more or less loss of the hydration sheath) and subsequent combination of the adsorbed ion with an electron provided by the electrode (7), it is possible that the secondary process outlined in the previous paragraphs, in which the Cr(III) species is already oriented at the interface for the electron transfer process, would have a lower transfer coefficient than the normal direct reduction, so that qualitatively one may account for the two slopes found in the log slope.

If the transfer coefficient is defined as that fraction of the potential "required" to transform an ion from a solution environment to that of the electrode interface, then it is true that the closer an ion is to the interface environment, the lower is the transfer coefficient. It therefore follows that, if a Cr*(II) formed at this surface is oxidized to Cr*(III) by an incoming Cr(III) ion, we have in effect transformed a Cr(III) ion from a position Cr to Cr*, i.e., closer to the interface, so that part of the transformation occurs under this "exchange potential", and only part is facilitated by an applied potential. Consequently the *total* process must have a lower transfer coefficient than one in which there are no exchanges between Cr(III) and Cr*(II).

In order not to have a lower transfer coefficient for the case of Cr(III)–Cr*(II) position exchange, one would have to assume a completely quantum-like jump from solution environment to surface environment without an intermediate state, which seems highly unlikely. To have a higher transfer coefficient would require a new mechanism, e.g., introduction of other ions.

Dichlorotetraaquo Ion

The polarography of the dichlorotetraaquochromium(III) species follows the same general pattern as that observed for the hexaaquo ion. The waves are considerably more drawn out and occur at more positive $E_{\frac{1}{2}}$ values; the log plots show the same asymmetry. However, the situation is complicated by the fact that the Cr(III)–Cr(II) exchange in the chloro complexes is accomplished by an anion transfer mechanism (8), which, omitting complexed water, may be written as

$$Cr^*Cl_2^+ + Cr(II) = Cr^*(II) + CrCl^{++} + Cl^-. \qquad [4]$$
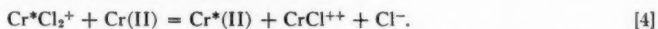
Consequently, one must deal with an alteration in the complex ions as well as with multiple electron transfer processes and space charge effects. Under these circumstances, it is difficult to arrive at any consistent picture without knowing considerably more than is now known about these processes.

One point which should be noted concerning the anion transfer mechanism of equation [4] is the "catalytic" degradation of the higher chloro complexes by the Cr(II) formed in the reduction. The specific rate constant (8) for the reaction of equation [4] at 2° C is 10^4 liters $mole^{-1}$ min^{-1}. It is reasonable to suppose that, in view of the greater lability of the chloride ligands in the higher Cr(III) complexes, the rate for the comparable process for these complexes would be considerably higher. It is then not surprising that $E_{\frac{1}{2}}$ for $[Cr(H_2O)_4Cl_2]^+$ in 12 M hydrochloric acid solution is the same before and after the reaction with the hydrochloric acid, since this catalytic degradation would tend to "level" the complexity of the species involved. Ultraviolet absorption indicates the Cr(III) species finally formed in 12 M HCl to be the trichlorotriaquochromium(III).

EXPERIMENTAL

Preparation, purification, and analysis of the various chromium(III) salts have been described (2). Sodium perchlorate was obtained as a solution of known molarity by titration of sodium hydroxide with a perchloric acid solution.

A Sargent Model XXI Polarograph and a Leeds & Northrup Model E Electro-Chemograph were used in conjunction with a jacketed H-cell (9), maintained at $25 \pm 0.1°$ C, which contained a saturated calomel electrode (S.C.E.) in one arm, separated by a sintered glass disk and KCl–agar plug from the working arm. After runs in perchlorate media, the cell was thoroughly flushed with warm distilled water to remove any precipitated potassium perchlorate from the region near the glass disk.

All $E_{\frac{1}{2}}$ data are referred to the S.C.E.; the iR drop in the cell system was negligible. Some runs were made against a mercury pool electrode in order to ascertain the effect of the agar–KCl bridge; the results were similar to those obtained against the S.C.E.

Oxygen was removed from the test solutions by purging with water-pumped nitrogen which was first deoxygenated by passage through an acid Cr(II) sulphate solution and then equilibrated by passage through some of the test solution; suitable traps were included to prevent contamination. In solutions of high acidity, it was necessary to deoxygenate for extended periods of time before introducing mercury; otherwise, oxygen waves interfered with the polarograms. No maximum suppressors were added.

In order to observe the polarographic wave of the Cr(III) species in 12 M hydrochloric acid before appreciable reaction has taken place, the following procedure was adopted: concentrated hydrochloric acid was placed in the polarographic cell; nitrogen was bubbled through the solution for about 30 minutes; dry $[Cr(H_2O)_4Cl_2]Cl$ or $[Cr(H_2O)_6]Cl_3$, which had been flushed with nitrogen, was then introduced into the solution under a nitrogen cover; the resulting solution was deoxygenated for another 5 to 7 minutes; the polarogram was then taken.

The polarogram of the Cr(III) species existing in 12 M HCl when equilibrium is attained was observed by first dissolving the chromic chloride in the 12 M acid (the form of the complex is immaterial), warming to 90° C to hasten equilibrium, then cooling to room temperature, transferring to the polarographic cell, sweeping with nitrogen for about an hour (from spectrophotometric evidence, reaction is complete within this time), and then taking the polarogram.

ACKNOWLEDGMENT

REFERENCES

1. (a) DAMASSIEUX, M. and HEYROVSKY, J.   J. chim. phys. **26**, 219 (1929). (b) HAMM, R. E. and SHULL, C. M.   J. Am. Chem. Soc. **73**, 1240 (1951). (c) KALOUSEK, M.   Collection Czechoslov. Chem. Communs. **11**, 592 (1939). (d) KOLTHOFF, I. M. and LINGANE, J. J.   Polarography. Vol. II. 2nd ed. Interscience Publishers, Inc., New York. 1952. (e) PECSOK, R. L. and LINGANE, J. J.   J. Am. Chem. Soc. **72**, 189 (1950). (f) PRAJZLER, J.   Collection Czechoslov. Chem. Communs. **3**, 406 (1931). (g) REYNOLDS, G. F., SHALGOSKY, H. I., and WEBBER, T. J.   Anal. Chim. Acta, **8**, 564 (1953). (h) WILLIS, J. B.   J. Proc. Roy. Soc. N. S. Wales, **78**, 239 (1946).
2. ELVING, P. J. and ZEMEL, B.   J. Am. Chem. Soc. **79**, 1281 (1957).
3. (a) DELAHAY, P.   New instrumental methods in electrochemistry. Interscience Publishers, Inc., New York. 1954. (b) EYRING, H., MARKER, L., and KWOH, T. C.   J. Phys. & Colloid Chem. **53**, 1453 (1949). (c) KOUTECKY, J.   Collection Czechoslov. Chem. Communs. **18**, 597 (1953).
4. ELVING, P. J. and OLSON, E. C.   J. Am. Chem. Soc. **79**, 2697 (1957).
5. LAITINEN, H. A., OLDHAM, K. B., and ZIEGLER, W. A.   J. Am. Chem. Soc. **75**, 3048 (1953).
6. (a) ANDERSON, A. and BONNER, N. A.   J. Am. Chem. Soc. **76**, 3826 (1954). (b) PLANE, R. A. and TAUBE, H.   J. Phys. Chem. **56**, 37 (1952).
7. GLASSTONE, S., LAIDLER, K. J., and EYRING, H.   The theory of rate processes. McGraw-Hill Book Co., Inc., New York. 1941. pp. 575–577.
8. TAUBE, H. and MEYERS, H.   J. Am. Chem. Soc. **76**, 2103 (1954).
9. KOMYATHY, J. C., MALLOY, F., and ELVING, P. J.   Anal. Chem. **24**, 431 (1952).

THE INFLUENCE OF SURFACE ACTIVE ANIONS ON THE ELECTROREDUCTION OF THE PERSULPHATE ANION AT NEGATIVE POTENTIALS[1]

A. Frumkin, N. Nikolajeva-Fedorovich, and R. Ivanova

The dependence of the kinetics of electrode processes on the surface layer structure has recently been the subject of a series of investigations. This dependence is especially pronounced if the electrode surface and the reacting particle have charges of the same sign, as in the case of anion electroreduction on a negatively charged surface (1, 2, 3, 4, 5). The phenomena observed under these conditions might be understood if we assume that the rate of the electrode reaction depends not only on the electrode potential, ϕ, but on the potential in that point of the double layer where the center of the particle in the transition state of the reaction is situated too. This local ψ_1-potential value is influenced by the cation which is the nearest neighbor of the reacting anion (5, 6, 7, 8, 9), and might be markedly different from the average potential, $\bar{\psi}_1$, at a distance from the electrode equal to the radius of the reacting particle. The rate of the electrode process depends therefore not only on the interaction between the charge of the anion with the charges on the metal surface, but on its interaction with the charge of the neighboring cation, which facilitates its approach to the negatively charged surface as well. In this sense we can use the concept of the formation of cationic bridges between the negatively charged surface and the reacting anion (Fig. 1). We shall not discuss here the question of the role played by the adjacent cation in the elementary act of the electron transfer itself.
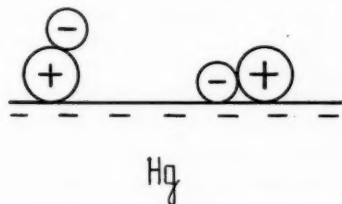
FIG. 1. Schematic representation of the adsorption of anions on a negatively charged metallic surface. The decrease of the absolute value of the negative charge of the mercury surface on anion adsorption shows that the configuration represented to the right is the preponderant one.

The object of this communication is to describe some characteristic features of the electroreduction of the $S_2O_8^{2-}$ anion, which might be considered as an example of the dependence of the kinetics of this reaction upon the details of the double layer structure.

Kalish and Frumkin found that the rate of the persulphate electroreduction on positively charged mercury strongly decreases in the presence of surface active anions (10). Thus, the half-wave potential of this reaction is *ca.* 0.6 v more negative in N KBr than in N Na$_2$SO$_4$. Qualitatively, this can be easily accounted for by the building up of a negative ψ_1-potential, when Br$^-$ anions are adsorbed on mercury, which decreases the surface concentration of the $S_2O_8^{2-}$ ions (and shifts the effective potential difference

$\phi-\psi_1$ between the electrode surface and the center of the reacting particle in an un-
favorable direction too). However, a quantitative comparison of the rates of the process
at different potentials shows that the decrease of the reaction velocity caused by the
negative ψ_1-potential at equal $\bar{\psi}_1$-values is smaller when the ψ_1-potential arises from a
specific anion adsorption than in the case of a negative ψ_1-potential build-up in the
neighborhood of a negatively charged metal surface, which attracts cations by coulombic
forces only, that is in a double layer with a "normal" structure. Although a quantitative
explanation of this discrepancy cannot be given at the present moment, it is probable
that the discrepancy is connected with the difference between the average and the local
(effective) ψ_1-potential values. In an electric field with localized negative charges, which
arise from the specific adsorption of anions, the distribution of the potential parallel
to the electrode surface must be much more inhomogeneous than in a "normal" double
layer with negative electrical charges smeared on the equipotential metal surface.

Kalish and Frumkin came to another, somewhat unexpected, conclusion. They found
that with a negatively charged surface at potentials at which the repulsion between the
electrode and the reacting anion manifests itself and a minimum on the current–voltage
curve is observed, the sequence of the action of halogen anions is reversed. Thus, when
10^{-4} N $K_2S_2O_8$ is reduced in the presence of potassium halogenides at a concentration
of 10^{-2} N, the current strength increases in the sequence $Cl^- < Br^- < I^-$. The small
adsorption of anions which occurs on a negatively charged surface therefore exerts on
the kinetics of the process an influence opposite to that observed in the case of their
strong adsorption on a positively charged surface. The cause of this inversion has not
been completely elucidated until now and we shall not consider it here in detail.*

Differential capacity measurements as well as determinations of the zero-charge
potential in solutions of fluorides, chlorides, and iodides of sodium, potassium, and
cesium showed that the adsorption of surface active anions on a negatively charged
surface is strongly influenced by the nature of the cations (8, 11). Thus, the increase
of the differential capacity at negative potentials and the shift of the zero charge poten-
tial to more negative values is much more pronounced in the case of a transition from a
CsCl solution to a CsI solution of equal concentration than in the case of a transition
from a NaCl solution to a NaI solution. Apparently, the adsorption of anions on a
negatively charged mercury depends to a large extent on the formation of cationic
bridges, although, as follows from other considerations, the $\bar{\psi}_1$-potential in the cationic
Helmholtz layer is also more positive in the presence of Cs^+ cations than in the presence
of Na^+ cations.

On comparing these results with those obtained earlier by Kalish and Frumkin, the
conclusion could be drawn that the acceleration of the $S_2O_8^{2-}$ electroreduction by iodide
ions described in (10) must depend on the nature of the cation, increasing in the sequence
$Na^+ < K^+ < Cs^+$. To check this conclusion some measurements with a dropping elec-
trode were carried out. Current–voltage curves obtained with 2.10^{-4} N solutions of
$K_2S_2O_8$ in the presence of fluorides, chlorides, bromides, and iodides of sodium, potassium,

---

*At any rate, an effect of that kind would be impossible, if the average ψ-potential would determine the rate, as
the specific adsorption of anions will always cause a shift of ψ_1 to more negative values, and must therefore
decrease the reaction rate. It appears that by taking into account the inhomogeneity of the potential distribution
in the double layer in the case of specific anion adsorption and the decrease of the absolute value of the negative
charge of the metal surface, caused by the appearance of this double layer, it can be understood that local ψ_1-potential
values (in points lying sufficiently far from adsorbed anions) at a given ϕ might be, in fact, more positive in this
case than in a "normal" double layer. In the paper of Kalish and Frumkin a schematic picture of the double
layer was given with the purpose of explaining the kinetic effects observed, but a more detailed consideration
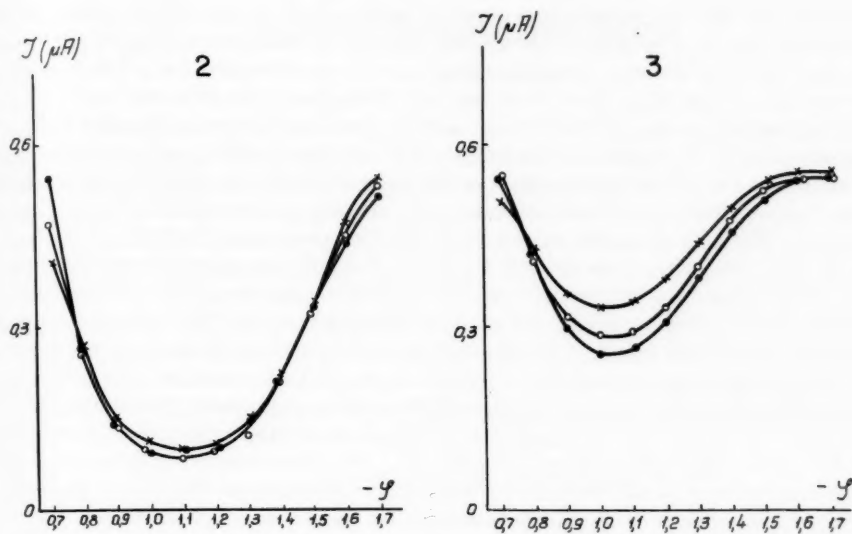showed that this scheme is incorrect and must be abandoned.

Fig. 2. Current–voltage curves for the electroreduction of 2.10^{-4} N $K_2S_2O_8$ in the presence of sodium salts. ● 10^{-2} N NaF; ○ 10^{-2} N NaCl; × 10^{-2} N NaI.

Fig. 3. Current–voltage curves for the electroreduction of 2.10^{-4} N $K_2S_2O_8$ in the presence of potassium salts. ● 10^{-2} N KCl; ○ 10^{-2} N KBr; × 10^{-2} N KI.
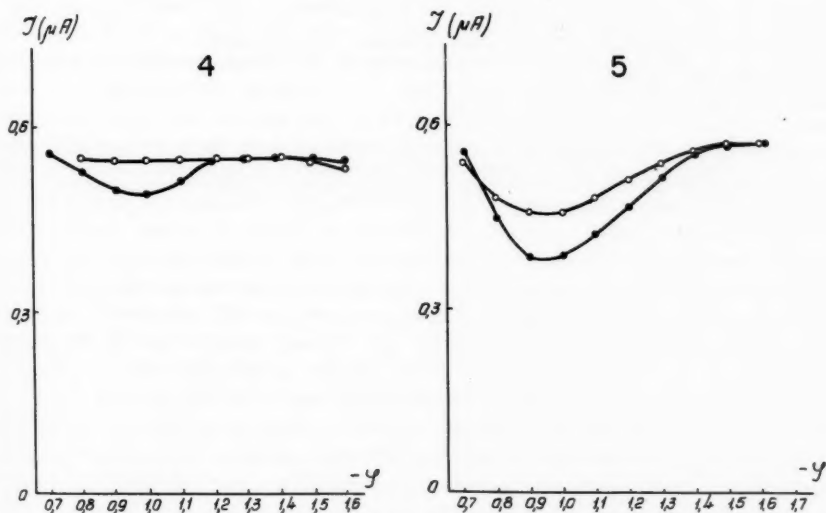

Fig. 4. Current–voltage curves for the electroreductions of 2.10^{-4} N $K_2S_2O_8$ in the presence of cesium salts. ● 10^{-2} N CsCl; ○ 10^{-2} N CsI.

Fig. 5. Current–voltage curves for the electroreduction of 2.10^{-4} N $K_2S_2O_8$ in the presence of cesium. ● 5.10^{-3} N CsCl; ○ 5.10^{-3} N CsI.

and cesium in a $10^{-2} N$ concentration are given on Figs. 2, 3, 4, and 5. The potentials are referred to a N.C.E. The parts of the current–voltage curves corresponding to potentials more positive than the zero-charge potential, which are deformed by a polarographic maximum of the first kind, have been omitted throughout. No difference between the current strength $\bar{J}$ in the presence of F^- and Cl^- can be observed within the limits of experimental error in sodium salts solutions (Fig. 2); the transition to a sodium iodide solution causes an increase of the reaction rate amounting to some 20%. On substituting K^+ for Na^+ we observe a marked increase of the velocity of the reaction (Fig. 3), which was already discussed in earlier papers (3, 8, 12) (primary cationic effect); at the same time the difference between the rates in the presence of different anions strongly increases. Thus on transition from $10^{-2} N$ KCl to $10^{-2} N$ KI the quantity $\bar{J}/(\bar{J}_d - \bar{J})$ increases ca. 1.6 times. In the presence of $10^{-2} N$ CsI (Fig. 4) the rate of the $S_2O_8^{2-}$ electroreduction on negatively charged mercury becomes so large that the minimum on the current-voltage curve disappears altogether. In order to obtain a quantitative estimate of the I^- anion efficiency in the presence of Cs^+, we have carried out measurements with $5.10^{-3} N$ solutions of CsCl and CsI. The quantity $\bar{J}/(\bar{J}_d - \bar{J})$ increases in this case on transition from Cl^- to I^- approximately twice* (Fig. 5). The experiments thus confirm the expected dependence of the influence of surface active anions on the rate of the $S_2O_8^{2-}$ electroreduction at negatively charged mercury on the nature of the cation.

<div align="center">REFERENCES</div>

1. KRJUKOVA, T. Compt. rend. acad. sci. U.R.S.S. **65**, 57 (1949).
2. FRUMKIN, A. and FLORIANOVICH, G. M. Compt. rend. acad. sci. U.R.S.S. **80**, 907 (1951); J. Phys. Chem. (U.S.S.R.), **29**, 1827 (1955).
3. FRUMKIN, A. Z. Elektrochem. **59**, 807 (1955).
4. FRUMKIN, A. Proc. Second Congr. Surface Activity (London), **III**, 58 (1957).
5. FRUMKIN, A. and NIKOLAJEVA-FEDOROVICH, N. J. Chem. Phys. **26**, 1552 (1957).
6. FRUMKIN, A. Actualités sci. et ind. **373** (1936).
7. FRUMKIN, A. Proc. Acad. Sci. U.S.S.R., Sect. Chem. (English Translation), 1429 (1957).
8. FRUMKIN, A. and NIKOLAJEVA-FEDOROVICH, N. Vestnik Moskov. Univ. Chem. Ser. 169 (1957).
9. FRUMKIN, A. Trans. Faraday Soc. (In press).
10. KALISH, A. and FRUMKIN, A. J. Phys. Chem. (U.S.S.R.), **28**, 1473 (1954).
11. FRUMKIN, A., DAMASKIN, A., and NIKOLAJEVA-FEDOROVICH, N. Compt. rend. acad. sci. U.R.S.S. **115**, 751 (1957); **121**, 129 (1958).
12. ZEZULA, I. Chem. Listy, **47**, 492, 969 (1953).

*At a potential $\phi = 0.75 v$ the current strength is always somewhat smaller in the presence of I^- as in the presence of Cl^-. This effect is caused by the superposition of the current of the anodic dissolution of mercury on the current of the $S_2O_8^{2-}$ electroreduction. The former becomes noticeable in iodide solutions at the given potential on account of complex formation with mercury.

CATHODIC ORGANIC PROCESSES[1]

M. J. ALLEN

The investigation of cathodic organic processes has been handicapped by two factors: the physical chemist who is qualified to indulge in this work but who feels organic systems too complex to ever be decipherable, and the organic chemist who being aware of the complexity of his medium is generally fearful of a pair of wires, a voltmeter, ammeter, and the other physical accessories, both real and mathematical, required to accomplish an electrochemical investigation. Thus investigations of this type have been left to those too few physical–organic chemists who understand the underlying physical principles and who are not overcome by the thought of working with an organic system.

As the organic electrochemist deals mainly with irreversible systems he must be content with a more empirical approach than his colleagues the inorganic electrochemists, who can readily obtain the potential of their system by application of the thermodynamic expression for a reversible electrochemical reaction:

$$E = E - RT/nF \ln(\text{Ox})/(\text{Red}).$$

The organic electrochemist is at a further disadvantage in that his reactions usually cannot be studied in purely aqueous systems and he must be concerned with the possible side reactions associated with the medium and/or the temperature used in the experiment. However, despite these difficulties, many problems involving cathodic processes have been more readily solved by use of a methodical approach which I admit is somewhat empirical, but still superior to a grossly haphazard attack on the problem which generally results in discouraging negative results. I should like to illustrate my point by a brief discussion followed by a few examples.

The first concern in the performance of a cathodic process is the choice of a medium which will serve as a suitable solvent for the organic compound, and still when mixed with an electrolyte offer as low a resistance as possible to the passage of an electric current. These conditions are far superior to the use of an excellent electrolyte medium but a poor solvent medium. The consequence of the latter is that one has essentially a suspension of the organic compound in the catholyte which leads to low process efficiency. Within this category also lies the choice of electrode material, and the current density or reference potential required to achieve the desired end result. Constant current density electrolysis is suitable so long as it is used in conjunction with an electrode whose potential is such that it will give the desired reduction product and will not further reduce this product. Under these circumstances it must be remembered that maximum efficiency is impossible, for as the depolarizer (the organic compound being reduced) diminishes in concentration as a result of the cathodic process, the limiting reaction current should also diminish. Generally a polarographic or voltammetric investigation prior to a mass electrolysis study will give the desired information as to the optimum reference potential to use when controlled potential electrolysis is being considered, or the ideal electrode material to consider for the process. When controlled potential conditions are to be used the electrode material is generally not a problem as one chooses a high overpotential electrode such as mercury or lead and adjusts its reductive ability by the potential at the electrode

surface vs. a standard reference electrode. When using constant current density conditions, one can obtain an arbitrary focal point for initial experimentation by application of the limiting current equation, i.e. $L_i = 0.0223DCn$ in which D is the diffusion coefficient, C the concentration of the organic species in g-moles per liter, and n the number of electrons exchanged in the process. By performing experiments at multiples or fractions of this arbitrary calculated limiting reaction current, and by examination of the reaction products, one can then choose those constant current density conditions which will yield maximum results.

Having decided on the aforementioned conditions the next item is the choice of a cell to be used for the actual experiment. Beyond the fact that the electrolysis cell consists of a cathode, anode, a low porosity membrane to separate the catholyte from the anolyte, a stirrer, a thermometer, and a reference electrode if controlled potential conditions are to be employed, the investigator may permit free reign to his imagination in the design of these cells. Two such cells are illustrated in Figs. 1 and 2.
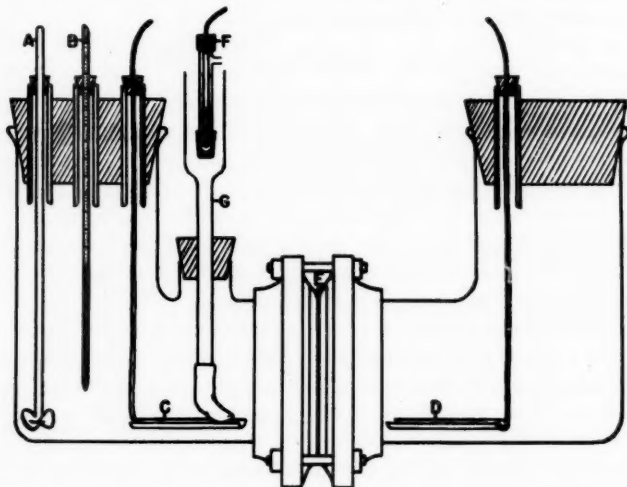
Fig. 1.   Electrolysis cell for solid type electrode. A, stirrer; B, thermometer; C, lead cathode; D, platinum, lead, nickel, or stainless steel anode; E, gasketed ion-exchange or cellophane membrane; F, reference electrode; G, salt bridge.

Last but by no means the least important item in performing the electrolysis is the electrical equipment required for this operation. A simple circuit will consist of a variable d-c. voltage supply, a voltmeter, ammeter, and if one desires to investigate the possibilities of controlled potential conditions a reference electrode, and a vacuum tube voltmeter. Such a simple circuit is described in Fig. 3.

The literature, of course, abounds with descriptions of devices for automatic controlled potential electrolysis (1). Each of these devices has its respective advantages and disadvantages. The prime prerequisite for an instrument which is to be used for organic electrochemical investigations is that it have an output of approximately 10 amp and 60 v. The circuit of an apparatus of this type recently designed in our laboratories is illustrated in Figs. 4 and 5.
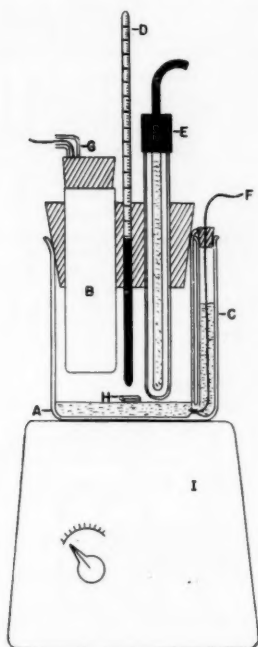
FIG. 2.   Electrolysis cell for mercury cathode. A, pyrex beaker; B, porous porcelain membrane (Alundum); C, side-arm contact to the mercury pool consisting of a piece of glass tubing through which is sealed a piece of platinum wire; D, thermometer; E, reference electrode; F, cathode lead wire; G, nitrogen inlet and outlet tubes (for removal of peroxides from anode compartment); H, glass-covered magnetic bar; I, magnetic stirrer.
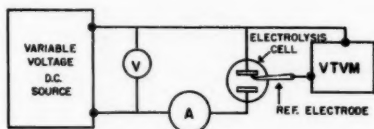
FIG. 3. Simple electrolysis circuit.
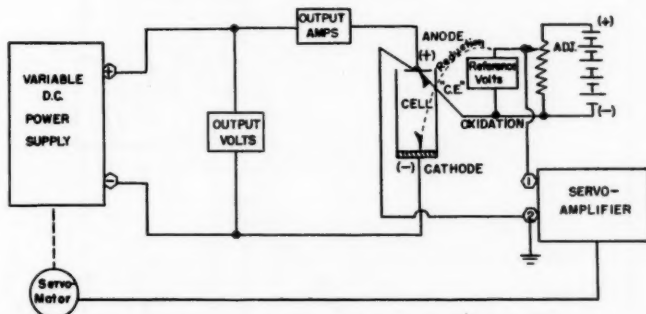
FIG. 4.   Function diagram—Redox-o-trol Mark IV.

FIG. 5. Redox-o-trol Mark IV.
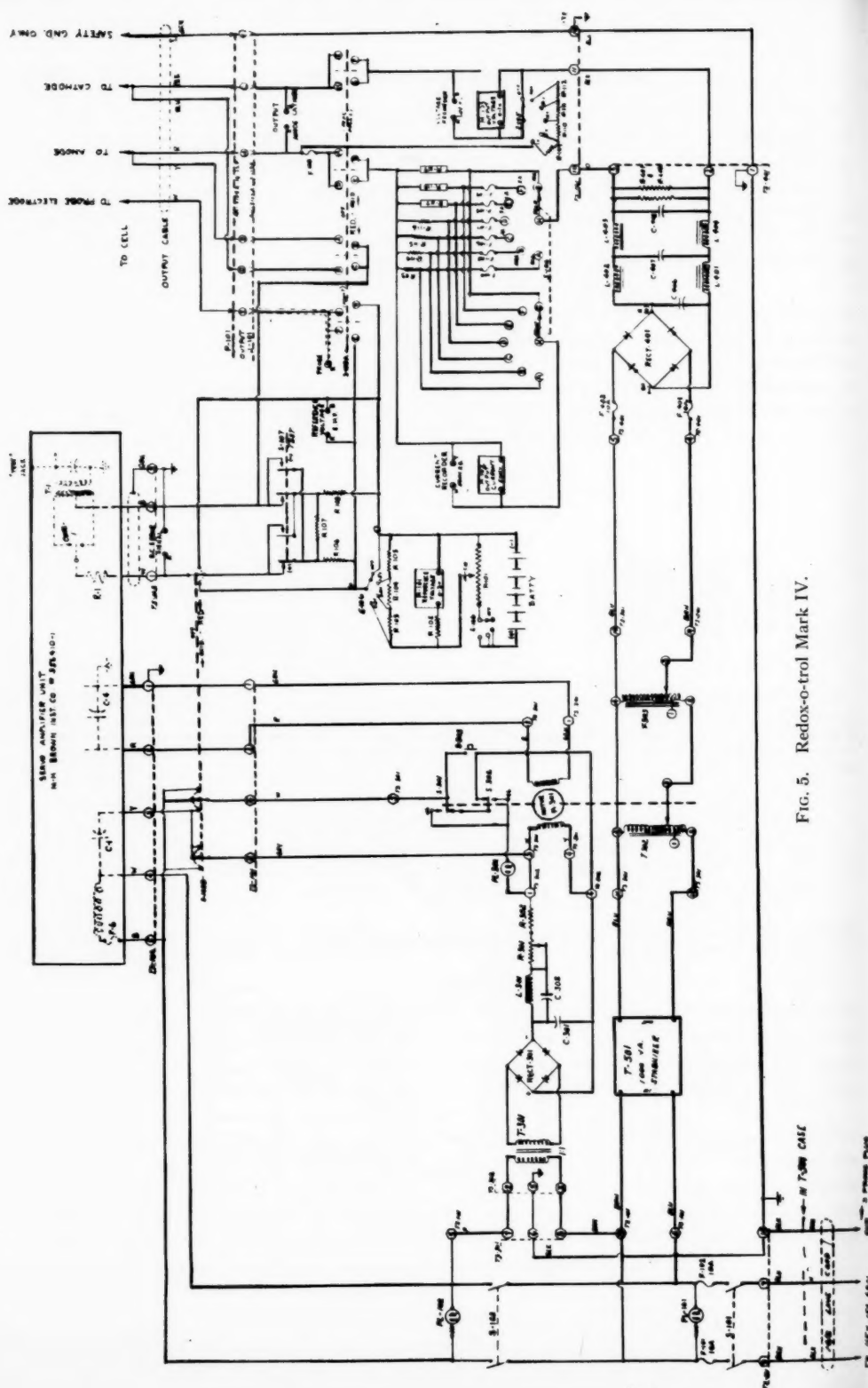
Components list:
  Amplifier   M.H.-Brown No. 356410-1
  *Conv.-1   M.H.-Brown No. 75829-1 (Part of above)
  *M-301   M.H.-Brown No. 76750-3

  Capacitors
  C-1, 4   1.0 mf, 600 v (Part of Brown Amplifier)
  C-301   20 mf, 250 v Sprague TVL-1509
  C-302   0.5 mf, 600 v Sprague No. BP-506
  *C-406   500 mf, 125 v, d-c. Mallory No. NP1255
  *C-407, 408   1000 mf, 150 v, d-c. Mallory No. HC-15010

  Fuses
  *F-6   1/2 amp Slo-Blo   3 AG (Part of amplifier)
  *F-101, 102, 103   10 amp   3 AG Little-Fuse No. 314010
  *F-104   1/100 amp   8 AG ”   ”   No. 361010
  *F-105   1/16 amp   8 AG ”   ”   No. 361062
  *F-106   1/8 amp   8 AG ”   ”   No. 361125
  *F-107   1/2 amp   8 AG ”   ”   No. 361500
  *F-108   1 amp   8 AG ”   ”   No. 361001
  *F-109   5 amp   8 AG ”   ”   No. 361005
  F-401, 402   10 amp 250 v   (Renewable links)
                                         Chase-Shawmutt “Shurlag” No. 1007

  Connectors
  J-101   No. AN-3102A-18-125 Amphenol Co.
  P-101   No. AN-3108A-18-12P Amphenol Co.
  All other Jacks   “5 Way” Binding Posts—H. H. Smith No. 257, or
                       Johnson No. 108-900 Series.

  Chokes
  L-301   8 Hys., 40 ma, Stancor No. C-1333
  L-401, 402, 403, 404 Special .04 Hys., 2 ohms, 10 amp
                       (Virgina Electronics Products Company, Bethesda, Maryland)

  Lamps
  PL-101 115 v, Neon, Clear Jewel, NE 51 Bulb, Dial Company No. 91408-930
  PL-102 115 v, Neon, Yellow Jewel, NE 51 Bulb, Dial Company No. 91408-936
  PL-301 115 v, Neon, Red Jewel, NE 51 Bulb, Dial Company No. 91408-931

  Resistors
  R-1   47 kohm, 10%, 1/2 W. Carbon IRC No. BTS
  R-101   1000 ohm, Potentiometer, 4 w, W.W., Mallory No. MIMPK
  R-102, 103   3 kohm, 1%, 1/2 w, W. W., IRC No. WW3J
  R-104, 105   1.5 kohm, 1%, 1/2 w, W. W., IRC No. WW3J
  R-106, 108   10 kohm, 10%, 1/2 w, Carbon IRC BTS
  R-107   2 ohm, 10%, 1/2 w, Carbon IRC BTS
  R-109   4 kohm, 1%, 1/2 w, W. W., IRC No. WW3J
  R-110   5 kohm, 1%, 1/2 w, W. W., IRC No. WW3J
  R-111   40 kohm, 1%, 1/2 w, W. W., IRC No. WW3J
  R-112   50 kohm, 1%, 1/2 w, W. W., IRC No. WW3J
  R-113   25 ohm, 1/2% (consists of four 100 ohm selected W.W.)
  R-114   1/2 ohm, 1% (made of 1.0, 1%, and 0.2, 1% IRC No. WW3J)
  R-115   .545 ohm, 1%, 1/2 w, W. W. IRC No. WW3J
  R-116   .102 ohm, 1%, 1/2 w, W. W. IRC No. WW3J
  R-117   SHUNT 1.0 amp, 50 mv Westinghouse No. 936938
  R-118   SHUNT 5.0 amp, 50 mv Westinghouse No. 724755
  R-119   SHUNT 10.0 amp, 50 mv Westinghouse No. 724756
  R-301   5000 ohm Adj., 10 w, Ohmite No. 1033
  R-302   2500 ohm, 5 w, Ohmite “Brown Devil”
  R-401, 402   3000 ohm, 20%, 10 w, Ohmite “Brown Devil”

  Rectifiers
  RECT-301   Four (4) 75 ma, 115 v Federal No. 1003A
  RECT-401   10 amp, 100 v, Full Wave Bridge, Sarkes No. D35

  Switches
  S-101   D.P.S.T. 15 amp, 250 v, Toggle, C-H No. 7561
  S-102   D.P.S.T. 12 amp, 250 v, Toggle, C-H No. 7565
  S-103A   4.P., 3 Pos. 10 amp, 250 v, Electro-Switch Corporation
  S-103B   4.P., 3 Pos. Centralab No. 2515
                       (Note: S-103A and 103B are ganged to operate together)
  S-104   2.P., 7 Pos., 10 amp, 250 v, Electro-Switch Corporation
  S-105   1.P., 6 Pos., 10 amp, 250 v, General Electric Company
  S-106   2 Pole, 5 Pos. Centralab No. 1405

R-107	4 Pole, 3 Pos. Lever Switch, Switchcraft No. 6038
S-301, 302	S.P.D.T. 10 amp, 115 v, Roller Arm, Microswitch No. BZ-2RW22-A2
S-303	P.B. (open) 5 amp, 115 v, Grayhill No. 4001

Batteries
*Five (5) required	Mercury Cells (1.34 to 1.4 v)
	Mallory No. RM-12-R
	RCA No. VS313

Meters
M-101	3 volts d-c., 1000 ohms/volt, 2%, Triplett No. 420
M-102	50 mv., d-c. (10 amp scale), 2%, Triplett No. 420
M-103	1 volt d-c., 1000 volt ohms, 2%, Triplett No. 420

Transformers
T-301	Isolation, 115 v to 115 v, Triad No. N-51X
T-302	Variable Voltage, "Variac", General Radio No. V-10
T-303	Variable Voltage, "Variac", General Radio No. V-20H
T-501	Stabilizer, 1000 va, Sola No. 20–13–210

Notes:

5 inside ⬡ TS-301 denotes 5th terminal, 1st strip, 300 series unit.

A or 2 inside ○ denotes terminal number on particular component.
Unit series numbers are servo amp unit.
100 series numbers are control chassis and panel.
200 series numbers are monitor panel.
300 series numbers are variac chassis and panel.
400 series numbers are rectifier chassis and panel.
500 series numbers are stabilizers.

Indicates recommended spare part item.

Essentially this instrument consists of a d-c. power rectifier, the magnitude of whose output is controlled by a motor-driven rheostat on the a-c. side of the power supply. The rheostat receives its activating signal from the amplifier, which in turn receives its signal from the cathode in conjunction with the reference electrode. In Fig. 6 will be seen the front and rear views of the instrument mentioned.
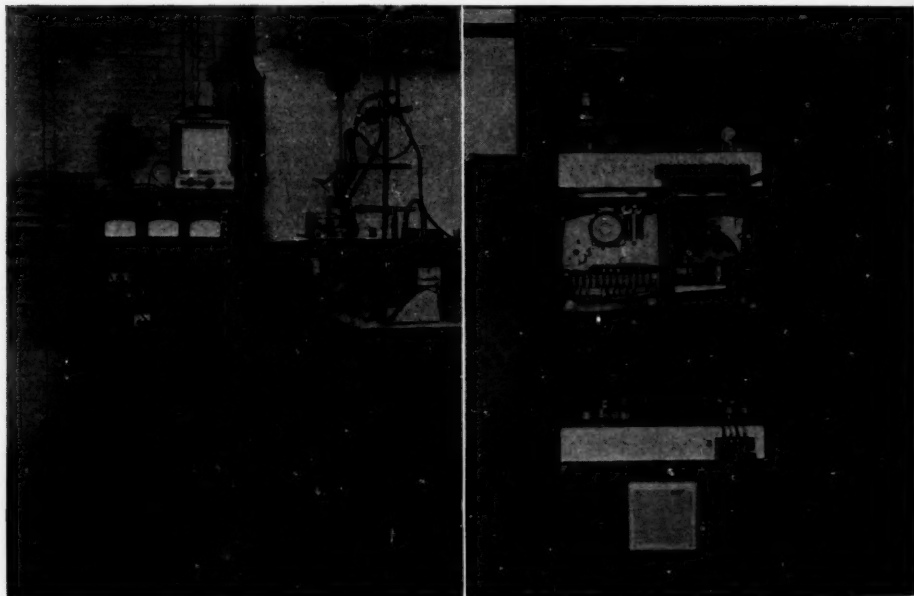
FIG. 6.   Redox-o-trol Mark IV: left, front view; right, rear view.

The ammeter of this instrument has seven ranges of 100 divisions each, so that one can obtain a minimum of 0.01 amp to a maximum of 10 amp full scale. The voltmeter indicating total applied voltage has a range of 1 volt to 100 volts full scale. Reference potentials as high as 3 volts can be imposed from a separate voltage supply. In addition the instrument is also suitable for oxidations under controlled potential conditions as well as constant current density electrolysis by the use of a suitable resistor built into the instrument.

I shall now briefly illustrate by a few examples the approach generally taken in the solution of a problem. The first example involves the cathodic reduction of 3,4,5,6-tetrachloro-N-(2-dimethylaminoethyl)phthalimide (I) to the fully reduced isoindoline (IV), an intermediate in the preparation of a potent ganglionic blocking agent used in the treatment of hypertension.
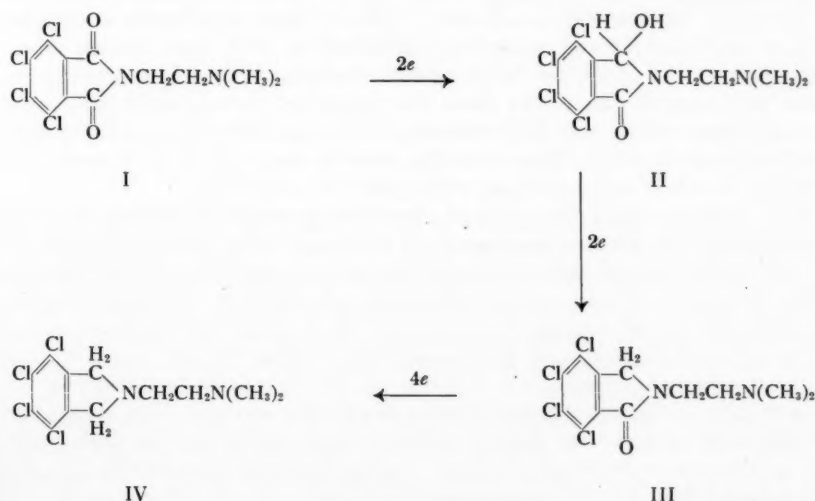
Previous investigators in their studies on phthalimides found that in an aqueous sulphuric acid medium at a copper cathode the phthalimide underwent a 2-electron change to yield the hydroxyphthalimidine. The use of a lead electrode yielded the fully reduced isoindoline via an 8-electron change (a). This indicated that in our case a lead electrode would be the most desirable one to use. It was obvious that the media used in the past which gave a suspension of the starting material accounted, together with the reported excessive current densities, for the low current efficiencies obtained. Therefore, as we in the solution of our particular problem desired improved efficiency, we firstly had to choose a medium which would enable us to perform our reactions on a solution, and secondly determine the optimum current density for the reactions. The former was solved by using an aqueous acetic sulphuric acid medium. By application of the limiting current equation in which D was 0.6 cm^2 day^{-1} and C, 0.2435 g-moles/liter we found our arbitrary current density to be 0.0493 amp/cm^2 when corrected for an electrolysis temperature of 50°. As the process at best was not too efficient we found it necessary to run the reaction twice the theoretical time in order to obtain suitable yields.

The results obtained using multiples and fractions thereof are illustrated in Table I.

TABLE I

Effect of current density on yield of isoindoline

	Current density (amp/cm^2)	% yield isoindoline	% current efficiency
	0.1950	39.6	19.8
↑	0.1540	52.0	26.0
	0.1190	53.9	27.0
H$_2$	0.0770	56.4	28.2
	0.0493	91.1	45.6
	0.0243	90.5	45.2

At current densities of 0.0770 amp/cm^2 and higher, considerable gas evolution was observed initially and throughout the course of the electrolysis which accounted to a great extent for the low current efficiency. Also in these experiments a considerable amount of partially reduced tetrachlorophthalimidine (III) was isolated from the reaction mixture. Use of the two lower current densities resulted in practically no gas evolution until approximately 1.25 times the theoretical current had been passed. In these cases, if there was any partially reduced tetrachlorophthalimidine (III), its quantity was too small to be detected. Thus we see that even the empirical use of an exact physical equation can be useful as an arbitrary focal point for a beginning.

In order to demonstrate the value of controlled potential electrolysis in obtaining maximum current efficiency an experiment was performed using a lead cathode previously treated by Tafel's method and a catholyte, the same as used in previous experiments, consisting of 6.5 g of the tetrachlorophthalimide (I) dissolved in a solution of 30 ml glacial acetic acid, 36 ml distilled water, and 90 ml concentrated sulphuric acid. The anolyte consisted of a solution of 9 ml concentrated sulphuric acid in 66 ml distilled water. At a reference potential of −1.10 v vs. S.C.E. previously determined from a voltammetric curve, the initial current density was 0.0589 amp/cm^2. After 80 minutes the current plateaued at a current density of 0.0143 amp/cm^2. From the area under the current vs. time curve the total number of coulombs passed was 15,280. The desired tetrachloroisoindoline (IV) was isolated from the catholyte in a 84.3% yield with a 77.7% current efficiency. Thus we see in this instance the advantage of the use of controlled potential in obtaining greater current efficiency than obtained under constant current density conditions.

Of interest is an experiment performed at a potential of −0.68 v vs. S.C.E. The initial current density was 0.0189 amp/cm^2. After 70 minutes the current plateaued at 0.0107 amp/cm^2. From the catholyte was isolated 4,5,6,7-tetrachloro-2-(2-dimethylaminoethyl)-3-hydroxyphthalimidine (II) in 86% yield. Thus we also see here another advantage of controlled potential electrolysis, i.e. the selective reduction of a particular group in a molecule containing more than one reducible center.

I shall now illustrate another type approach to the solution of an electrochemical problem. Perhaps a brief history of the general problem might be of interest at this point. Some years ago in the course of studying the electrochemical mechanism of bimolecular reductions, one of the compounds studied was p-aminoacetophenone (V). The pinacol, 2,3-bis-(p-aminophenyl)-2,3-butanediol (VI), obtained from this ketone by cathodic bimolecular reduction was found to be an active anti-estrogen. Further pursuit of the biological aspects of the problem indicated that the animals under test with this compound tended toward demonstration of other biological responses. However, perhaps
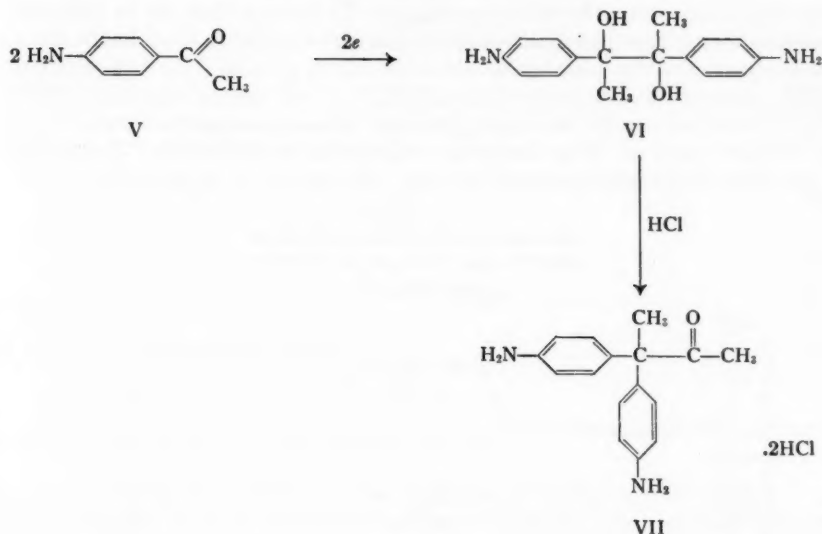
because of the lack of proper bodily reagents the animal could not quite accomplish the necessary transformation. Therefore it was decided to perform a pinacol–pinacone type reaction which resulted in the compound 3,3-di(p-aminophenyl)-butanone-2-dihydrochloride (VII), commonly referred to as Amphenone and which was found to have interesting adrenal inhibiting effects (3). Unfortunately, however, despite the widespread use of this compound its undesirable side effect precluded general usefulness for this drug. This naturally led us to search for more specific adrenal inhibitory compounds in the Amphenone series. One of the compounds which seemed interesting, but only moderately active, was the pinacol of 3-acetylpyridine (4). This pinacol (VIII) upon being subjected to a pinacol–pinacone type rearrangement gave, as the major product, 2-methyl-1,2-bis-(3-pyridyl)-1-propanone (IX) (5), which has been found to be a potent adrenocortical inhibitor (6).
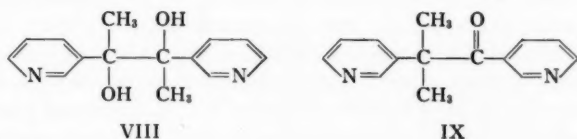
To return to the electrochemical aspects of this problem I should mention that the acidic medium used in the previously reported preparation of the pinacol of 3-acetyl-pyridine (4) made isolation of the desired pinacol extremely difficult. Therefore it became necessary for us to find a practical medium for this preparation. As a result of our previous experience it was decided that a basic medium of some type was probably desirable. Preliminary investigations in this direction indicated a solution of potassium acetate in aqueous ethanol at reflux temperature (82.5° C) to be a suitable medium. Analysis of the voltammetric curve indicated two processes occurring, the first at a potential of -1.5 to -1.64 v vs. S.C.E. and the other at a potential of -2.0 to -2.2 v vs. S.C.E.

As it has been demonstrated by other investigators (7) that pyridine can be fully reduced to piperidine under high potential conditions, it was decided that probably the lower potentials represented the bimolecular reduction to the pinacol. This was confirmed by controlled potential electrolysis at −1.6 v vs. S.C.E. It was further decided to determine the effect of constant current density on yield and efficiency using the calculated current density of 0.378 amp/cm². This electrolysis was run for approximately 1.75 times theory and a plot made of reference potential vs. time. The results are shown in Fig. 7.

REDUCTION OF 6g 3-ACETYLPYRIDINE AT REFLEX
Hg | KETONE, KOAc, EtOH, H_2O||K_2CO_3 (40% aq.) | Ni
c.d.=0.378amp/cm²
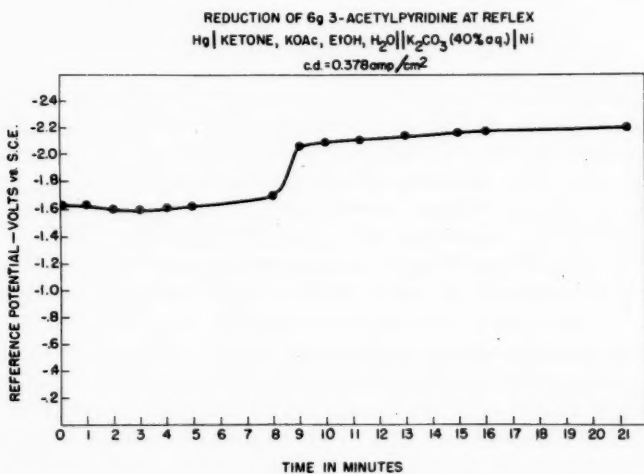
FIG. 7.   Reference potential vs. time curve for reduction of 3-acetylpyridine at constant current density.

From this curve it can be seen that at 6 minutes (65.3% of theoretical time) the potential begins to rapidly increase from −1.6 v to −2.05 v vs. S.C.E. At 12.25 minutes (theoretical time) the potential is already at the point known to give a secondary product. It was difficult to isolate more than a small quantity of the desired pinacol from this experiment. Experiments performed for the theoretical time (12.25 minutes) gave satisfactory yields and current efficiencies. In order to try to approach results obtained at controlled potential, experiments were performed using a higher current density for approximately 49% of the theoretical time and then lowering the current density to another fixed value with the object of maintaining the reference potential throughout the course of the electrolysis at −1.5 to −1.64 v vs. S.C.E. This gave yields and current efficiencies approaching that obtained under controlled potential conditions. Finally, as it was observed that the pinacol began to precipitate during the reaction using the original aqueous ethanolic potassium acetate medium, and as it was thought that in so doing the precipitate might occlude the electrode surface and thus prevent maximum efficiency, the alcohol content of the medium was increased with the net result being an increase in yield and efficiency. The results of the various mentioned experiments are tabulated in Table II.

It has been the objective in this presentation to illustrate that it is possible without strict mathematical treatment to arrive at information which can give the organic chemist the desired results. If we few investigators in the field of electroorganic chemistry can reduce the subject from an art to a science as we are rapidly doing it may be in time

TABLE II

Catholyte	Mode of operation	% yield	% current efficiency
Ketone, 6 g EtOH, 25 ml KOAc, 15 g H_2O, 17 ml	Reference potential −1.6 v vs. S.C.E. 0.408 to 0.051 amp/cm²	58.3	61.4
	0.378 amp/cm² 6 minutes 0.2034 amp/cm² 11.6 minutes 1 × theory	52.0	52.0
	0.378 amp/cm² 1 × theory	43.1	43.1
Ketone, 6 g EtOH, 35 ml KOAc, 15 g H_2O, 17 ml	Reference potential −1.6 v vs. S.C.E. 0.403 to 0.029 amp/cm²	68.3	80.3
	0.378 amp/cm² 6 minutes 0.2034 amp/cm² 11.6 minutes 1 × theory	60.2	60.2

NOTE: The anolyte in the above experiments consisted of 40% K_2CO_3.

that organic chemists will begin to look upon the electrochemical technique as a vital tool in his armentarium of reagents. The future lies in the hands of those physical and organic chemists who choose to collaborate to achieve this common goal.

REFERENCES

1. ALLEN, M. J. Organic electrode processes. Reinhold Publishing Corp., New York. 1958.
2. SPÄTH, E. and BREUSCH, F. Monatsh. **50**, 349 (1928). SAKURAI, B. Bull. Chem. Soc. Japan, **5**, 184 (1930); **7**, 155 (1932). CLEMO, G. R., RAPER, R., and TENNISWOOD, C. R. S. J. Chem. Soc. 429 (1931). COOK, E. W. and FRANCE, W. G. J. Phys. Chem. **36**, 2383 (1932).
3. ALLEN, M. J. and CORWIN, A. H. J. Am. Chem. Soc. **72**, 114, 117 (1950). ALLEN, M. J., HERTZ, R., and TULLNER, W. W. Proc. Soc. Exptl. Biol. Med. **74**, 632 (1950). HERTZ, R., ALLEN, M. J., and TULLNER, W. W. Proc. Soc. Exptl. Biol. Med. **75**, 627 (1950). HERTZ, R., TULLNER, W. W., and ALLEN, M. J. Proc. Soc. Exptl. Biol. Med. **77**, 480 (1951). HERTZ, R., ALLEN, M. J., TULLNER, W. W., and WESTFALL, B. B. Proc. Soc. Exptl. Biol. Med. **79**, 42 (1952). THORN, G. W. *et al.* New Engl. J. Med. **254**, 547 (1956). RENOLD, A. E. *et al.* New Engl. J. Med. **256**, 16 (1957). BENCZE, W. L. and ALLEN, M. J. J. Org. Chem. **22**, 352 (1957).
4. ALLEN, M. J. J. Org. Chem. **15**, 435 (1950).
5. ALLEN, M. J. and BENCZE, W. L. Unpublished results.
6. CHART, J. J., SHEPPARD, H., ALLEN, M. J., BENCZE, W. L., and GAUNT, R. Experientia, **14**, 151 (1958).

THE ANODIC PASSIVATION OF IRON[1]

Earl S. Snavely, Jr. and Norman Hackerman

ABSTRACT

A study was made of the anodic passivation of iron in solutions of 0.1 M sodium sulphate at a pH of 3.0. A mass balance of iron equivalent to coulombs required for passivation and iron found in solution after passivation showed that approximately 0.002 coulomb/cm² is involved in the passive layer. A Flade arrest does not appear in decay traces of anodic potential unless a potential of at least 1.2 v (E_H) is achieved on charging the electrode, indicating incomplete coverage by the passive layer below 1.2 v. Partial cathodic reduction followed by anodic reformation of the passive layer at the Flade arrest showed that the first charging current involved in reformation is highly efficient even when as much as 70% of the Flade arrest is reduced. These results support the view that only a fraction of the passive layer is represented by coulombs involved in the Flade arrest and that after partial reduction the remainder of the passive layer disintegrates spontaneously. Addition of chelating agents to the electrolyte has an adverse effect on passivation by chelation of ferrous ion.

INTRODUCTION

Experimental conditions necessary to achieve passivity of iron are well known; however, the nature of the passive layer is less familiar and has been the subject of many recent investigations. The theories which have been advanced can, in general, be divided into categories of oxide film theories and adsorption theories. The former are concerned with an iron oxide, rich in oxygen and hydrated, which requires specific conditions to form in such a manner as to give a high degree of protection to the base metal. The adsorption theories maintain that passivity is the result of adsorption of chemical species such as hydroxyl ions or molecular and atomic oxygen. Films of either type, oxide or adsorbed, can be similar once formed because of migration of iron atoms or ions through the passive film, and their chief difference lies in their means of formation. An oxide film formed by anodic polarization requires nucleation and lateral growth with a necessary consumption of coulombs, while an adsorbed film forms rapidly and completely on a properly prepared surface.

This paper presents the results of experiments to determine the quantity of electricity involved in the formation of a passive layer by anodic treatment. Other results concerning the phenomena observed on cathodic reduction of the passive layer are presented.

EXPERIMENTS

The iron electrodes used in all experiments were made from stock supplied by the Armco Steel Corporation and were reported to be 99.9% Fe containing 0.04% copper, 0.01% carbon, and traces of manganese, phosphorus, and silicon.

Circular coupons about 3.5 cm in diameter were vacuum-annealed and mounted in bakelite so that one face of the iron disk was exposed. This face was ground flush with the bakelite by means of a surface grinder and polished with 4/0 emery paper. The bakelite-iron junction at the periphery of the electrode, as well as all exposed bakelite, was covered with clean Ucilon or Glyptal to prevent imbibition of solution.

Electrical connection to the iron was accomplished by a tapped hole in the bakelite through which a metal rod could be screwed against the iron. The metal rod was protected with Myva wax.

All solutions were 0.1 M in Na_2SO_4. They were made from recrystallized salt and triple-distilled water and adjusted to a pH of 3.0 with c.p. H_2SO_4.

The polarization cell was a Pyrex vessel equipped with a large platinum electrode and a fritted gas-dispersion tube through which helium was bubbled to rid the cell and its contents of oxygen. The helium was purified by passage through a tube filled with hot copper followed by a drying tube containing $Mg(ClO_4)_2$. The cell and the electrical circuit are shown in Fig. 1.
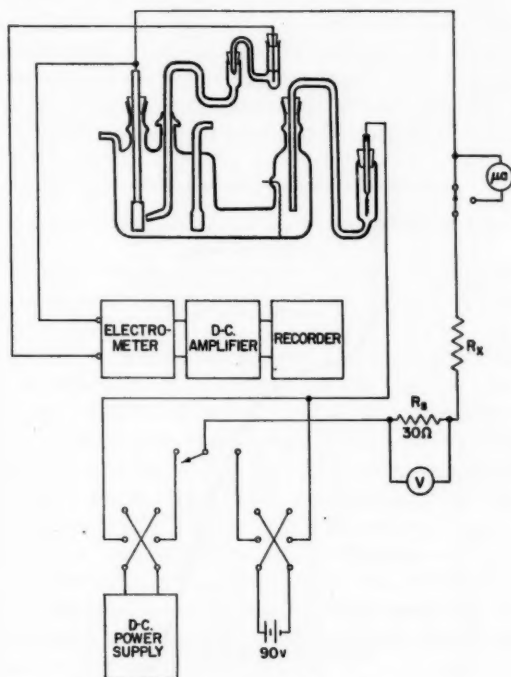
FIG. 1. Passivation cell and circuit.

Potential measurements were made with reference to a Hg, Hg_2SO_4 electrode. All potentials reported here are given with respect to the standard hydrogen electrode. The surface of the electrode is treated as a projected area and results are presented on that basis.

As shown in Fig. 1, the potential measuring circuit consisted of a Keithley Model 210 electrometer having an input impedance of 10^{14} ohms. The output of the electrometer supplied a d-c. amplifier which drove a Brush Recorder equipped for chart speeds of 25, 10, and 5 cm/second.

Analytical Experiments

To determine the amount of electricity required to passivate iron, a material balance was made on the amount of iron actually present in the cell solution after passivation was achieved and the amount of iron equivalent to the coulombs passed during the passivating process.

In these experiments the cleaned electrode was placed in the cell about 3 inches above the solution, while the latter was degassed by bubbling He. The iron was then lowered into the solution under an applied cathodic current of 12.5 ma/cm² to prevent corrosion. The recorder was then set on high speed and when the electrode had been in the cell solution 15 seconds an anodic current of 50 to 70 ma/cm² was applied. This passivated the iron and the electrode was then withdrawn from the cell while still passive and while oxygen was being evolved. The exact volume of solution was determined by weighing the cell, and the concentration of iron was then measured by the o-phenanthroline method. Cell solution in which iron had been only cathodically treated was used as a blank.

In these experiments the potential changes during passivation were recorded as shown in Fig. 2. The number of coulombs required for passivation was calculated from the constant current applied and the time interval from point A to the reversible oxygen potential or point B. This interval was used for reasons which are pointed out later.
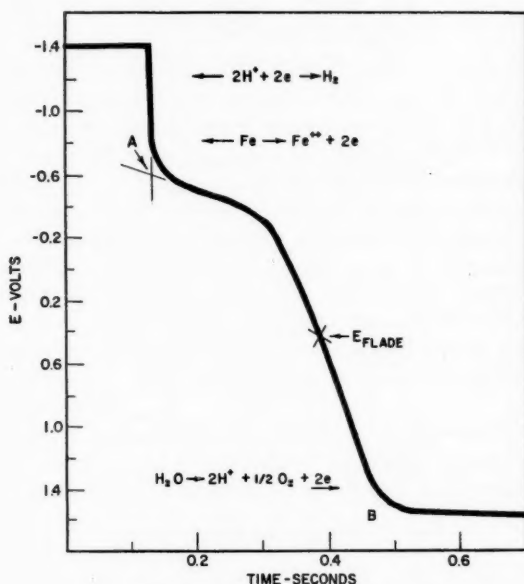
FIG. 2.   Typical passivating curve.

Typical results for these analytical experiments are shown in Table I. The column titled "Equivalent Fe++" gives the amount of ferrous ion equivalent to the coulombs passed during passivation. The next column lists the amount of ferrous ion which was found in the cell solution after passivation. The average of all values in the last column of Table I yields a value of 1 γ of Fe or 0.003 coulombs, which approaches the value reported by Kabanov (1). This is the amount of ferrous ion, as coulombs in the passivating process, in excess over the amount of iron determined in solution and per square centimeter of electrode surface. The results have an average deviation of 0.25 γ or about 30%.

The value of 0.003 coulomb/cm² required for passivation is far in excess of the quantity of electricity which is observed at the Flade region on reduction of the passive layer. For example, reduction of the passive layer in the 3.0 pH 0.1 M Na₂SO₄ solution at 14.5 μa/cm² requires 0.00016 coulomb/cm² or less than $\frac{1}{10}$ that required for passivation. It

TABLE I

Excess coulombic iron at the reversible oxygen potential

Anodic c.d. (ma/cm^2)	Time to rev. O_2 potential	Coulombs $\times 10^3$/cm^2	Equivalent Fe^{++} (γ/cm^2)	Fe^{++} det'd. (γ/cm^2)	Excess coulombic Fe^{++} (γ/cm^2)
71.6	0.20	14.3	4.1	3.2	0.9
53.0	0.23	12.2	3.5	2.5	1.0
53.0	0.22	11.7	3.4	2.9	0.5
54.0	0.20	10.8	3.1	2.6	0.5
51.9	0.21	10.9	3.2	2.8	0.4
53.5	0.22	11.8	3.4	2.7	0.7
54.8	0.22	12.1	3.5	3.1	0.4
46.3	0.24	11.1	3.2	2.7	0.5
46.3	0.24	11.1	3.2	2.8	0.4
45.3	0.40	18.1	5.2	2.6	2.6
46.3	0.26	12.1	3.5	2.1	1.4
46.3	0.26	12.1	3.5	2.8	0.7
40.2	0.43	17.3	5.0	2.5	2.5
40.6	0.32	13.0	3.8	2.6	1.2
				Average	0.98

is known that the iron passive layer is anodic to iron, and exposure of bare iron during the reduction process most certainly increases local cell action which leads to spontaneous decay of the passive layer (2).

To determine the extent to which the passive layer could be reduced without exposing iron, the current efficiency for formation of the passive layer was determined. This was done by repeatedly reducing and reforming the passive layer until a constant value for the number of coulombs involved at the Flade region was obtained. Care was taken to apply anodic current just at the end of the arrest so that excessive currents would not be required for repassivation. When a constant value was obtained, a small reducing current was applied until a fraction of the Flade arrest was passed. The current was then reversed and a small anodic current applied for a short period. The current was reversed again and reduction allowed to proceed until the end of the arrest was reached. The difference between the constant coulomb numbers necessary to pass through the Flade region, and the number of coulombs initially passed cathodically gives the charge remaining in the surface at any point in the region.
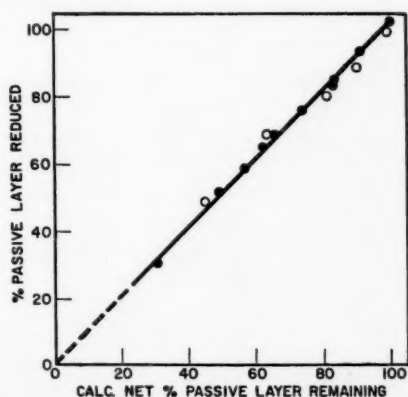
FIG. 3.   Relative anodic current efficiencies at Flade arrest.
● 0.1 M Na$_2$SO$_4$, pH 3.0; ○ 0.1 M Na$_2$SO$_4$, pH 3.0, 0.05% o-phenanthroline.

For a 100% efficient anodic current the number of coulombs actually required to pass the remainder of the arrest should be greater by an amount equal to the number of coulombs added anodically after the initial reduction. Figure 3 shows the results of an experiment in which 14.5 $\mu c/cm^2$ was added to the passive layer after various fractions of the arrest had been passed. The curve clearly shows the anodic current to be highly efficient up to a reduction of 70% of the Flade region. The open circles of Fig. 3 are results of the same experiment in which 0.05% o-phenanthroline was added to the cell solution. This treatment had no effect on efficiency of the anodic current.

Figure 4 shows the effect of additions of o-phenanthroline on the time required to achieve passivity when the passive layer is completely reduced. Presumably o-phenanthroline increases the time required for passivation due to chelation of the ferrous ions which are necessary to achieve the high potentials required for passivity (3). The high potentials are the result of precipitation of ferrous hydroxide on a ferrous salt. A cleaned coupon was used for each point of Fig. 4 so that equivalent roughness factors were involved for each passivation. Since 0.003 coulomb/cm² are involved in a formed passive layer but only 0.00016 coulomb/cm² are involved in the Flade region, the Flade region should be evident on reduction *only* if the passive layer is about 90% complete. If the Flade arrest is considered to involve a 1-electron process and passivation a 3-electron process, then the arrest should appear only if the passive layer is about 70% complete.
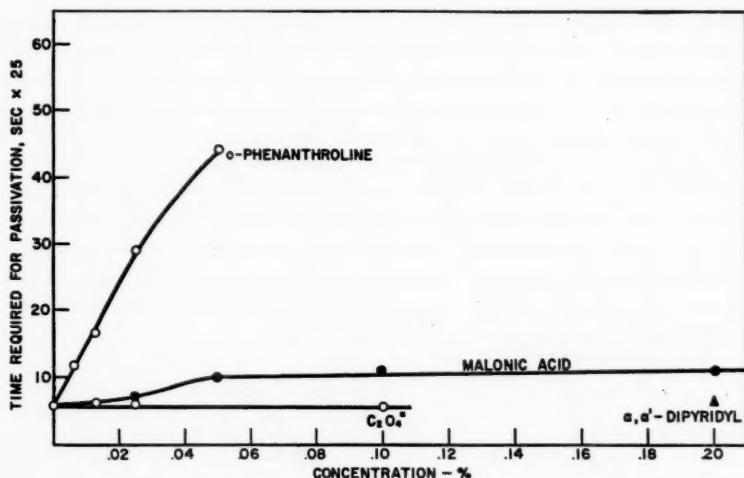
FIG. 4. Concentration chelating agent versus time required for passivation.

Additional evidence that the Flade region represents only a fraction of the passive layer is shown by the results in Fig. 5. This curve was obtained by plotting the anodic coulombs required to attain the reversible oxygen potential versus the fraction of Flade region achieved by cathodic reduction. When approximately 95% of the Flade region was passed passivity could no longer be attained by an anodic current of 14.5 $\mu a/cm^2$. When about 70% of the Flade region was passed the time required to reach the reversible oxygen potential increased, indicating that some iron was exposed and that local cell current began to increase. The flat portion of the curve in Fig. 5 is in accordance with the view that the thickness of the passive layer is proportional to the anodic potential
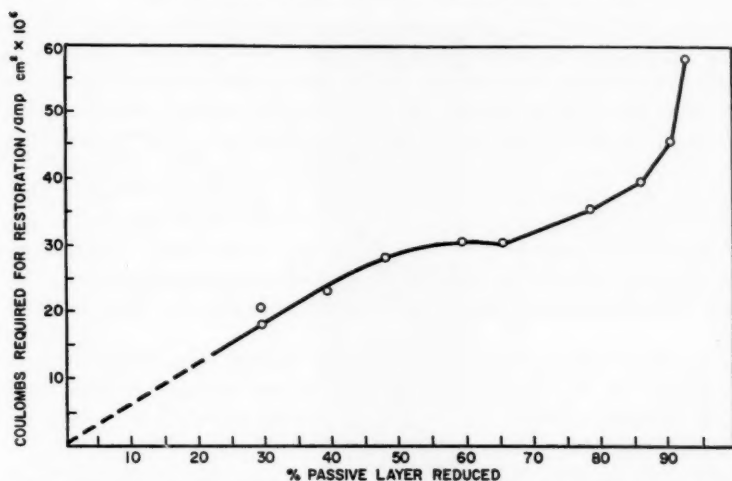
FIG. 5.   Restoration of passive layer. Anodic c.d. = 12.9 $\mu a/cm^2$; cathodic c.d. = 14.2 $\mu a/cm^2$.

achieved. If only a small part of the passive layer is reduced at the Flade region, then a nearly constant number of coulombs is required to attain the oxygen potential after various fractions of the arrest have been passed. In these experiments the total number of coulombs involved in the arrest was calculated from the time at which the current was made cathodic to the end of the flat portion. For the low currents used, concentration polarization was very small and any resistance drop at the electrode surface was not detectable.

In constant current experiments such as these, the only arrest which appears in the charging curve is found at a potential corresponding to the Fe, Fe^{++} potential. Even if the Flade region represents the formation potential of the passive layer it is not surprising that a detectable arrest does not appear in this region during charging because of the high current involved. For example, the results of the previously described analytical experiments yielded a value of $0.003/cm^2$ for the coulombs involved in the passive layer. For a passivating current of 70 ma/cm^2 only 1/35 second is required to pass 0.003 coulomb/cm^2 and, since some of the passive layer forms at potentials more anodic than that of the Flade region, only a portion of this short time would be involved in this arrest. To determine the potential at which a nearly complete passive layer had formed, the charging current was interrupted at various times and the potential then achieved was allowed to undergo open-circuit decay. Figure 6 shows the results of this experiment and indicates that a potential near the reversible oxygen potential must be achieved before a complete passive layer is formed. The Flade arrest on decay is visible only in the lower two charts where the potential achieved was 1.4 v. This result is in agreement with calculations made with the figures reported in Table I. Calculation of the time required, at the anodic current density employed, to account for all iron found in solution after passivation yields an average value corresponding to the achievement of 1.2 v. These results indicate that iron dissolution slows appreciably only on attainment of potentials more anodic than the Flade region.

To determine if the excess iron in solution after passivation was due to local cell action or if iron dissolution is necessary to achieve passivation, several chelating agents were
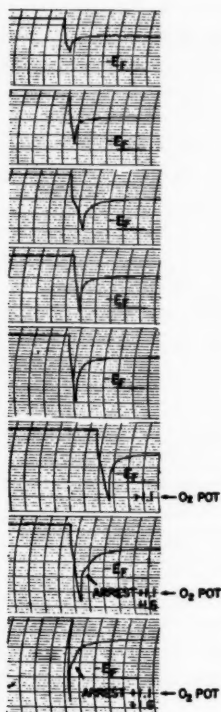
FIG. 6.   Appearance of the Flade arrest in open-circuit decay. Anodic c.d. = 70.0 ma/cm²; chart speed = 2.5 cm/second.

added to the cell solution prior to passivation. These included *o*-phenanthroline, malonic acid, and α, α′-bipyridyl. As shown in Fig. 4 none had a significant effect except *o*-phenanthroline. In the first case the time required to achieve passivation is proportional to the *o*-phenanthroline concentration. The instability constant of the ferrous–*o*-phenanthroline complex is very small, i.e., approximately 10^{-21}. As pointed out by a previous experiment, additions of *o*-phenanthroline to the cell solution after the passive layer was formed had no effect on its reduction or reformation from a partially reduced state. Thus, oxidation of the chelating agent does not play a major role in the increased consumption of electricity during the passivating process. Apparently at least a portion of the iron dissolved in the anodic treatment of iron is necessary to achieve passivity.

DISCUSSION

Suitable corrections must be applied to the results of the analytical experiments in order to arrive at an exact figure for the coulombs involved in formation of the passive layer. Presence of hydrogen in the metal has an inhibiting effect on passivity as shown by others (4). Introduction of hydrogen by the initial cathodic treatment may be responsible for instability of the passive layer at potentials more cathodic than the oxygen potential during the passivating process. Also, the number of coulombs involved in competing electrode processes such as oxidation of ferrous ion or ferrous hydroxide is

not known; however, the absence of arrests in the charging curve indicates that they do not take place to any notable extent. It was not possible to remove the iron electrode from the cell solution at the instant passivity was achieved and it is quite likely that the coupon, even though passive, corroded slightly, contributing to the amount of iron in solution, thereby making the results too small. Also, open-circuit decay of the electrode potential during the charging process indicates that some growth of the passive layer takes place after the beginning of oxygen evolution so that the number of coulombs · involved in a complete passive layer is slightly larger than that obtained in the analytical experiments. If the Flade region represents only 10% of the passive layer as concluded from other experiments presented here, then growth of the passive layer above the oxygen potential should add this amount to the 0.003 coulombs obtained from the analytical experiments.

A complete passive layer is very stable and passivity in acid solutions can be maintained by anodic currents of less than 1 μa/cm^2 (5). Very few changes are involved at the Flade region on cathodic reduction of a passive layer maintained by such a low current. These results indicate that passivity can be achieved by less than a monolayer. The monolayer is probably composed of sorbed ions and dipoles held in place by appreciable force fields. An alternative explanation is the stabilization of a primary passive film by an adsorbed species (6). The role of adsorption in maintaining passivity is indicated by the rapid potential changes associated with the application of small currents at the Flade region, the absence of effect of a chelating agent on current efficiencies at the Flade region, and the small number of coulombs involved in formation of a passive layer.

CONCLUSIONS

Anodic dissolution of iron at a rapid rate is necessary to achieve passivity, and passivity can be deferred or prevented by the addition of a suitable chelating agent. Approximately 0.003 coulomb/cm^2 is involved in the passive layer; this amount of electricity is equivalent to a thickness of 15 Å of Fe$_2$O$_3$ based on projected areas. Coulombs involved at the Flade region represent only 10% of the passive layer and the remainder decays spontaneously when iron is exposed. Small anodic currents applied at the Flade region are completely efficient, indicating absence of local cell action and a passive film consisting of at least a monolayer.

ACKNOWLEDGMENTS

REFERENCES

1. KABANOV, B. Discussions Faraday Soc. 1, 259 (1947).
2. BONHOEFFER, K. F. Corrosion, 11, No. 7, 32 (1955).
3. EVANS, U. R. Metallic corrosion, passivity and protection. Edward Arnold & Co., London. 1948. p. 51.
4. UHLIG, H. H., CARR, N. E., and SCHNEIDER, P. H. Trans. Electrochem. Soc. 79, 111 (1941).
5. WADE, W. H. and HACKERMAN, N. Trans. Faraday Soc. 53, 1636 (1957).
6. HACKERMAN, N. Z. Elektrochem. 61, 632 (1958).

THE THEORY OF FORMATION OF HIGH RESISTANCE ANODIC OXIDE FILMS[1]

L. YOUNG

ABSTRACT

Various models are considered for the growth of anodic oxide films (metal ions mobile). In general, a transition is expected, as the thickness of the film is increased, from control by the metal/oxide interface (Cabrera and Mott) with very thin films to control by the movement of ions through the body of the film (Verwey), with the concentration of mobile ions taking up the value (p, say) which gives electroneutrality. The field strength only varies with thickness in the transition region of thickness. Dewald's theory is the special case of p zero, which gives a field increasing continuously to infinite thickness. The high field production of Frenkel defects (with the vacant cation sites immobile and the interstitial ions mobile) as postulated by Bean, Fisher, and Vermilyea, and a slight mobility of oxygen ions are two processes which would allow p to vary with the field strength, and which would, therefore, give rise to "overshoot" in the transients in the field strength which occur when the applied current is suddenly changed. However, if the field strength is sufficiently great to produce Frenkel defects it would be expected to be sufficiently great to cause the vacancies to be mobile. This case is considered. Finally, it is noted that in an amorphous oxide it is difficult to maintain a distinction between lattice and interstitial ions, and, in fact, a range of site energies and jump distances would be expected. Some of the observed features (including "overshoot", and Tafel slope anomalies) of the kinetics for tantalum may, therefore, be due simply to the fact that the oxide is amorphous.

INTRODUCTION

This paper is concerned with developing the consequences of various models intended to represent the formation of the high ionic resistance type of anodic film in order to find crucial differences for experimental test. This type of film is formed on tantalum and niobium in most electrolytes and on aluminum, titanium, zirconium, hafnium, tungsten, uranium, silicon, germanium, and other metals or intermetallic compounds in certain electrolytes. It is distinguished from the type of anodic film used in storage batteries by the characteristic that electric field strengths of the order of 10^6 v cm^{-1} are produced in the oxide by anodic polarization, the resulting current being predominantly ionic. Part of the interest in the formation process lies in the connection with the formation of oxide films by reaction with oxygen ("tarnishing reaction"). The essential difference between the two processes is that in anodic oxidation only ions need cross the film for growth to occur,* but in the tarnishing reaction electrons must also move, since otherwise macroscopic separation of large electric charges would occur. In effect, the electrical circuit is closed within the oxide in the tarnishing reaction and externally in the anodic reaction. This means that the anodic kinetics should in principle be easier to interpret, in that there is no question, as there is in some tarnishing reactions (1), as to whether the ionic or the electronic current is rate determining. The anodic system is easier to investigate experimentally, since it has an extra degree of freedom: at a given temperature and concentration of reactants the rate of formation may still be varied (and, in fact, exactly controlled) by controlling the current through the oxide. In practice, it is only

A "leakage" current is usually observed. This is due partly to an electronic current through the oxide and partly to ionic discharge in pores. However, this current has invariably been tacitly assumed to be independent of (that is, in parallel with) the ionic current, though, admittedly, ultraviolet irradiation, which would be expected to produce only an electronic current, also causes film growth.

possible to discuss in a very provisional way whether a given metal behaves like a given model, since the experimental data are very restricted, and, even with the metals—tantalum, niobium, and zirconium—which have been at all extensively investigated, are incomplete or in dispute.

Basic Equations for the Ionic Current

All present theories treat ionic movement using models which are strictly applicable only to crystalline material. Thus they assume that either vacant anion or cation sites, or interstitial ions, are mobile, and that one vacancy or interstitial ion is exactly equivalent to another. Now, at least as far as X-ray diffraction is concerned, this type of film is normally amorphous. (Crystalline films can be produced, but detailed kinetic studies have not been made.) In an amorphous solid, it would seem difficult to make a distinction between interstitial and lattice ions. In fact, it may be necessary to abandon this distinction, and to consider the oxide as consisting of two random lattices (oxygen and metal), probably with a large concentration of vacancies in each lattice. There will be a distribution of mobilities because of the varying local environment of each ion. In other words, a given ion will encounter a range of jump distances and activation energies along its path through the oxide. Against this argument, there is, of course, the point that, even in an apparently amorphous lattice, there will be some degree of local order. For example, the detailed structures of tantalum and niobium pentoxide have not been worked out, but, if the structure reported (2) for one form of vanadium pentoxide is any guide, the lattice of the amorphous oxide may consist essentially of oxygen tetrahedra randomly linked to neighboring tetrahedra at an average of three points and with an average of one metal ion per tetrahedron.

The conventional equations, which are used to describe the ionic movement, apply only to either a few ions moving in a large number of empty sites, or a few vacancies moving in a nearly full lattice. This is because no allowance is made for the possibility that one carrier may block the path of another. It seems quite possible that this assumption of a very low concentration of the mobile species may fail. In particular, some theories postulate an exponential variation of carrier concentration with the field strength, with a large value appearing at accessible fields.

The same equations have been used to describe the movement both of interstitial ions and of vacant lattice sites. They were first applied to anodic oxide films by Verwey (3), who was, as it happens, considering specifically the movement of aluminum ions in the spinel structure γ-alumina, which has a large concentration of vacant cation sites at electroneutrality when the oxygen lattice is full. The conventional assumption is that the current at a given point x may be written

[1] $\qquad i = 2an\nu \exp{-(W-qaE)/kT} - 2a[n+2a(\partial n/\partial x)]\nu \exp{-(W+qaE)/kT},$

where a = (mean) half jump distance for the ions, n = concentration of ions, ν = vibration frequency of ions, W = activation energy at zero field, q = charge on the ions, and E = the field strength. The first term refers to the ions moving with the field, and the second term refers to ions moving against the field. The magnitudes of W and aq are such that, for the range of currents which is experimentally accessible at present, the second term is negligible (high field approximation). The concentration gradient needed to give a diffusion current comparable with the migration term is so large as to have little physical significance. The remaining term

[2] $i = 2an\nu \exp-(W-qaE)/kT$

gives a relation between field strength and current density which is of the form

$$i = i_0 \exp \beta E.$$

The kinetic expressions 1 and 2 apply to an ion vibrating in simple harmonic motion in one dimension with a frequency ν, so that the chance of acquiring sufficient energy to jump the barrier on a given vibration is given by the Boltzmann factor. This treatment is, of course, an oversimplification. In particular, one would expect that success in jumping the barrier would depend on the correct phase relation with the vibration of neighboring atoms, and, perhaps, on sufficiently great amplitudes of their vibration. Unfortunately, even to allow for the accumulation of a critical energy in several degrees of freedom leads to cumbersome expressions, and still does not represent much greater correspondence with reality. The significance of ν and the possibilities of multiple jumps have been discussed recently by Ubbelohde (4) for ordinary diffusion. Multiple jumps are more likely in the present systems, since the ion continues to gain energy from the field so long as it moves. The transition state theory either provides the same final expressions by a more circuitous route, or leaves one with expressions, involving free energies and activity coefficients of imprecisely defined transition states, and these expressions, though of great generality, are not very amenable to experimental verification.

We have so far formulated equations for the ionic current at a point where the concentration of ions and the field strength are specified. A complete account of a given model is obtained when it is determined how these two quantities vary through the thickness of the oxide.

The present discussion will be chiefly restricted to the model in which metal ions carry most of the current. The alternative single carrier model in which oxygen ions carry most of the current gives analogous equations when treated using the conventional equations, but the two models differ in that adsorption effects may occur at the oxide/solution interface and structural effects (discussed below) may occur at the metal/oxide interface.

The discussion is confined to the rather idealized case that pores and fissures are not present in the oxide.

Interface Control

The interfaces were first taken into account by Mott and Cabrera (5), who considered (apparently intuitively) that the first barrier which metal ions have to surmount to enter the film will be higher than subsequent barriers encountered during passage through the film. The passage over this first barrier was treated in the same way as the jumps over the barriers within the film, but with the vital difference that the concentration of metal ions facing the barrier was assumed to be a constant, determined by the concentration of metal ions on the metal surface. Space charge was neglected so that the field strength was assumed to be constant through the film. The current over the entrance barrier is given by

[3] $i = m_s\nu_s \exp-(W'-qa'E)/kT,$

where m_s = surface concentration of metal ions, ν_s = their vibration frequency, W' = activation energy required to jump the first barrier with zero field, and a' = the half jump distance for this barrier. The concentration n_0 say of ions within the oxide adjusts itself so that the current given by 2 is equal to that given by 3, giving

[4]
$$n_0 = \frac{(m_s \nu_s)^{a/a'}}{2a\nu} \exp\left(\frac{W - aW'/a'}{kT}\right) \cdot i^{1-a/a'}.$$

The kinetics are therefore determined by the entrance barrier. We may attempt to generalize the conditions under which the entrance barrier controls the kinetics. The required conditions are that space charge be negligible and that no upper limit be placed on n_0. The kinetics will then be controlled by the first barrier at which the backwards current is negligible (6). We introduce here an important parameter, the concentration (p, say) of mobile ions in the electrically neutral oxide. Apart from the improbable case that $n_0 \simeq p$, both n_0 and p must be small or the film must be very thin if the space charge is to be negligible. n_0 is certainly small in the original model, in which the first barrier is higher than later barriers. The significance of "small" will be clarified later.

Metal Ions Mobile, Space Charge Due to These Only

The theory proposed by Cabrera and Mott predicts that the Tafel slope $\partial E/\partial \log i$ is given by kT/qa', so that it should be proportional to the absolute temperature. This was reported not to be the case with tantalum (7, 6), niobium (8), and zirconium (9, 10), though it should be noted that the details of the behavior of tantalum as reported in recent investigations do not agree (6, 11, 12). Dewald (13) showed that an almost temperature-independent Tafel slope could appear if, as he claimed to be the case, the mobile metal ions were the only source of space charge. Actually, this assumption must be regarded as being made because it gives simple equations rather than because it would be expected to be true, as may be seen by putting it in the form that the concentration of the mobile ion near the interface given by 4 is assumed to be much greater than the critical value p which corresponds to electroneutrality. Poisson's equation gives

[5]
$$\partial E/\partial x = 4\pi \, nq/\epsilon,$$

where ϵ is the dielectric constant of the oxide. The continuity equation for the current is

[6]
$$\partial i/\partial x = \partial n/\partial t,$$

where $t =$ time. Dewald puts $\partial i/\partial x = 0$. (The final result that $n(x)$ is not a function of the total thickness is derived directly from this initial assumption.) From [1] to [6], after two integrations,

[7]
$$E = \frac{1}{\beta'} \log[i/m_s \, \nu_s \exp(-W'/kT)] + \frac{1}{\beta} \log(1 + \beta 4\pi \, qn_0x/\epsilon),$$

where

$$\beta = qa/kT \qquad \text{and} \qquad \beta' = qa'/kT.$$

This model exhibits a Tafel slope nearly independent of temperature over a certain region of temperature provided that certain conditions are fulfilled. Essentially, the space charge due to the ions causes a transition from control by the entrance barrier to control by the barriers within the oxide. However, the model also gives a field strength increasing with thickness. This has not been observed with tantalum or niobium though it is difficult to be sure that the small amount of variation required by the theory is absent. For example, the data given by Vermilyea (11, 14) for tantalum are inconclusive, because the ionic current was not shown to be constant, variations of surface area with thickness had not been shown to be absent, and the capacity had not been shown to measure thickness to the required accuracy. Some of these difficulties have been removed in subsequent work (15). When the integral rather than the differential field strength is

considered, a certain degree of uncertainty is caused by our lack of knowledge of the inner potential differences between phases of different chemical composition. This point is not always recognized. The uncertainty may be conservatively reckoned as corresponding to about one volt, i.e. 1% in the field strength at 100 volts overpotential, and proportionately more for thinner films.

It may be noted that when (below) we introduce the more realistic assumption that the concentration of ions p corresponding to electroneutrality is not negligible, the transition occurs between Cabrera and Mott's case and Verwey's case (control by movement of metal ions through the electrically neutral oxide) with the field strength independent of thickness except in the transition region.

Dewald (12) has recently shown that his model—when treated using the conventional equations—does not predict the "overshoot" which is observed in the transients in the field strength when the current is suddenly changed. This would invalidate its application to tantalum and niobium. However, Willis, Adams, and van Rysselberghe (9) have suggested that these transients could be due to the sluggish opening and closing of growth spirals, which, effectively, is equivalent to a variation of m_s.

The evidence is thus fairly conclusively against the application of this model to tantalum and niobium, either with $p = 0$ (Dewald) or with p constant and not zero. By contrast, recent work (10) has shown that zirconium in addition to Tafel slope variations exhibits a marked increase in field strength with thickness, and fails to exhibit the overshoot in the transients, in agreement with the predicted behavior for $p \ll n_0$.

The effect that, with a non-zero concentration of carriers, the next site in the path of a given carrier may be already occupied may be allowed for by multiplying the right of (2) and (3) by $(1 - n/N)$, where N is the total concentration of available sites. Variations of vibration frequencies and of the activation energies would remain to be taken into account. This modification introduces considerable complication, but does not explain the transients.

Field Production of Frenkel Defects

Bean, Fisher, and Vermilyea (16) have proposed for tantalum pentoxide films that Frenkel defects (lattice vacancy plus interstitial ion) are produced in the metal lattice by the high fields. They assume *ad hoc* that the interstitial ions are mobile and the vacancies are immobile. The idea that the field might produce lattice defects was considered as improbable in older work on conventional ionic conduction (17), but the greater field strengths in the present systems make it more feasible. In view of the amorphous nature of the oxide it can only represent an approximation to a real process. These authors appear to assume that the defect-producing process directly determines the concentration of interstitial ions. A more correct view is that the process creates a certain concentration of immobile negative space charge (associated with the vacant cation sites), and that any control of the concentration of mobile metal ions is due to this, in the way which is discussed in the next section.

Bean, Fisher, and Vermilyea postulated in addition that there is a quite sudden transition with increasing field strength in the half barrier width for the production of interstitial ions.* This gave an explanation for the sudden change from a half barrier width of 2.4 Å to one of 4.8 Å which Vermilyea (11) found in his second investigation of the kinetics. They seem to envisage that several barriers are taken at one jump,

---

Unless the maxima and minima in the potential energy curve of an ion in transit are mirror images there will, of course, be a second-order variation of the half jump distance with field strength. Further sources of gradual variation of "a" with field strength are discussed later.

though this is not stated explicitly. There is some disagreement on the experimental issues, and Dewald (12) has suggested that Vermilyea allowed insufficient time for the transients to decay. The present author's results (unpublished) suggest that the (apparent) jump distance (derived in a similar way) does vary with the field, but that there is no evidence for any sudden transition from a value a to $2a$. As a result of the variation of "a" with E, $(\partial E/\partial \log i)_E$ varies correctly with temperature, but $(\partial E/\partial \log i)_t$ is almost independent of temperature.

Both Vermilyea (18) and Dewald (12) have shown that this model can give "overshoot". The essential reason for this is that the concentration of carriers lags behind the field when the current is suddenly changed. More precisely, the concentration of negative charge (and hence the concentration of mobile ions) increases sluggishly with the field strength. The treatments given by these authors are, of course, not exact because they assume $n = p$ at all times.

Production of Frenkel Defects with Both Vacancies and Interstitial Ions Mobile

It seems reasonable to assume that if the field strength is sufficiently great to pull a lattice ion out of its position and place it in an interstitial position, it should also be able to move a lattice ion to an adjacent empty site. The assumption made by Bean, Fisher, and Vermilyea that vacant cation sites are immobile seems, therefore, inconsistent with the assumption of the creation of Frenkel defects. The more consistent model in which the vacancies are allowed to be mobile gives some interesting limiting cases. The equation for the rate of change of vacancy concentration at a given point acquires an extra term and becomes (in the form used by Dewald (12) in considering Bean, Fisher, and Vermilyea's model),

$$\partial m/\partial t = \partial i_m/\partial x + (N_0 - m)\gamma'' \exp - (W'' - Eqa'')/kT - i\sigma_m,$$

where m = concentration of vacancies; i_m = vacancy current (in ions); N_0 = total concentration of lattice sites; W'', ν'', and a'' the activation energy at zero field, vibration frequency, and half jump distance for the production of a Frenkel defect; and σ_m is the cross section for the capture of an interstitial ion by a vacancy. i_m is given by a term of the usual type.

If vacancies are not produced at the interface, $i_m(x = 0) = 0$. If the mobility of vacancies is sufficiently great with respect to their rate of production, their concentration falls to zero throughout. If not, m varies with x, and the field varies with thickness.

If vacancies are produced at the metal interface, as well as in the oxide, both constant and varying m and field are possible, according to the parameters, and the interface partly controls the kinetics over the range of fields where the vacancy current is important.

The Model in which Metal Ions Move in a Uniform Immobile Negative Space Charge

The significance of this model has been indicated in previous sections. We consider an immobile, uniform negative space charge given by $-pq$ where q is the charge on the *metal* ion. Poisson's equation is now

$$\partial E/\partial x = 4\pi q(n-p)/\epsilon,$$

where n, as before, is the concentration of metal ions. Using the continuity equation

$$\partial i/\partial x = 0$$

we obtain

$$(\partial n/\partial x) + n\beta(\partial E/\partial x) = 0.$$

After integrating as in Dewald's theory, we obtain

[8] $$n = p/\{1-(1-p/n_0)\exp(-\beta 4\pi\,qpx/\epsilon)\}$$

and, after a second integration,

[9] $$E = E_0+\frac{1}{\beta}\log\{[n_0-(n_0-p)\exp(-\beta 4\pi\,qpx/\epsilon)]/p\}$$

where n_0 and E_0 are the values of n and E at $x = 0$, and are given by equations [4] and [3] respectively.

For large x, the field is given by

[10] $$E = E_0+(1/\beta)\log(n_0/p).$$

On substituting for E_0,

[11] $$E = \frac{1}{\beta}\{\log(i/2a\nu\,p)+W/kT\}.$$

The field then becomes independent of the interface and is determined by whatever determines p. This is the result which Verwey (3), Bean, Fisher, and Vermilyea (16), and Dewald (12) assume implicitly or, in Dewald's case, explicitly, to apply at all x. The validity of their assumption depends on p/n_0 and on the value of p, since this controls the characteristic length l (say) $= \epsilon/\beta 4\pi\,qp$ in equation [8]. For $l \simeq 10$ Å, $p \simeq 10^{21}$ metal ion equivalents per cm^3, assuming a typical value for a in $\beta = qa/kT$ of 3 Å. The total concentration of metal ions in the oxide is $2\rho L/M \simeq 10^{22}$, where ρ = density, L = Avogadro's number, and M = the molecular weight of the oxide. Thus for $l \simeq 10$ Å, a fraction of the order of 1 in 10 ions must be mobile and so on. In the theory of Bean, Fisher, and Vermilyea p varies exponentially with the field, so that it appears that at low fields when p is small, the space charge region should become important, and the assumption of no net space should break down. At high fields p will become rather large. In contrast with Dewald's model, the concentration of mobile metal ions may either fall below or rise above the value corresponding to electroneutrality. The possibility of the net space charge being either positive or negative means that the field strength in the interfacial region may either rise or fall in passing from the interfacial region towards the center of the oxide.

Consequences of the Amorphous Nature of the Oxide

It has been noted that in the amorphous oxide one would expect a range of types of site. Thus as the field is increased an increasing proportion of sites will stop acting as traps for the mobile ions. In particular, sites which have a short "a" for the exit of ions will become active as the contribution of the field (qaE) increases. The effect is, therefore, that p is expected to increase with the field strength so that "overshoot" will occur and in addition, changes in "a" and W with field strength are to be expected. The experimental observation of these features may need no further explanation than the fact that the oxide is amorphous. However, another source of variation in "a" with field strength is due to the obvious but never-mentioned fact that jumps occur in a cone of solid angle along the field direction. This cone will open as the field increases. The expectation that n and "a" change instantaneously with field strength seems to invalidate Vermilyea's method of obtaining "a" by transient studies (18), in which "a" is assumed to be independent of field strength.

Both Ions Mobile

It appears fairly certain that for the usual experimental conditions most of the current is carried through the films on tantalum and niobium by metal ions (19, 20). However, this does not exclude the occurrence of a slight mobility of oxygen ions, and this could be important because it provides another mechanism causing the concentration of negative ions (and hence p) to vary sluggishly with the field strength.

The steady-state condition is discussed first.

It is assumed that the oxygen ion current may be described by an equation of the same form as that which is used to describe the metal ion current. The limitations in this assumption have already been discussed. The subscripts $+$ and $-$ refer to metal and to oxygen ions, respectively. The current is now given as a charge flow rather than as ion flow:

$$i_+ = q_+ 2a_+ n_+ \nu_+ \exp(-W_+/kT) \exp \beta_+ E,$$

where

[12]
$$\beta_+ = q_+ a_+/kT,$$

and similarly (with i_- and q_- as positive quantities)

[13]
$$i_- = q_- 2a_- n_- \nu_- \exp(-W_-/kT) \exp \beta_- E,$$
$$= q_+ 2a_- p\nu_- \exp(-W_-/kT) \exp \beta_- E.$$

As before, Poisson's equation gives

[14]
$$\partial E/\partial x = 4\pi \, q_+(n-p)/\epsilon.$$

In the steady state, the continuity equation becomes

[15]
$$(\partial i_+/\partial x) = (\partial i_-/\partial x) = 0.$$

Hence from [12] to [15],

[16]
$$n_+ = n_+{}^0 \exp-\beta_+(E-E^0)$$

and

[17]
$$p = p^0 \exp-\beta_-(E-E^0),$$

where n^0, p^0, and E^0 refer to values at $x = 0$.
From [14], [16], and [17]

[18]
$$x = \int_0^x dE/\{(4\pi \, q/\epsilon)(n_+{}^0 \exp-\beta_+(E-E^0)-p \exp-\beta_-(E-E^0)\}.$$

Since $q_+ = 5e$ and $q_- = 2e$ it is probable that for tantalum $\beta_+ > \beta_-$. Hence, if the space charge near the metal is negative, so that E decreases with increasing x, both n_+ and n_- will increase with x, but n_+ will increase more rapidly, so that eventually the space charge must fall to zero. Conversely, if the space charge is initially positive, then the field at first increases, both n_+ and n_- decrease with distance but n_+ decreases more than n_- so that the space charge eventually becomes very small. Thus for large x we have n_+, n_-, and the field strength all constant. The model behaves essentially the same as that with p constant throughout the film. The difference is that p is determined by the field strength in the outer part of the oxide, since this field strength determines the rate of entry of negative ions into the oxide, and their rate of movement through the oxide.

The reaction at the oxide/solution interface by which O'' enters the oxide must be

essentially $H_2O = O''(\text{oxide}) + 2H^+$. The experimental data for tantalum show (1) that the kinetics are independent of the pH and of the electrolyte in dilute aqueous solutions, but (2) that the kinetics are affected by a variation of composition large enough to vary the activity of the H_2O species.

The entry of O'' may be described using equations similar in form to those used to describe the entry of metal ions at the other interface:

$$i_-(D) = q_- m_l \nu_l \exp(-W_l/kT) \exp \beta_l E$$
$$= q_- 2a_- n_-(D) \, \nu_- \exp(-W_-/kT) \exp \beta_-/kT,$$

in which D = thickness of oxide, the subscript l refers to the oxide/solution boundary, and the field across the oxide/solution boundary is put equal to the field just inside the oxide. Hence,

$$n_-(D) = \frac{m_l \nu_l}{2a_- \nu_-} \exp\left(\frac{W_- - W_l}{kT}\right) \exp\left(\frac{Eq_-(a_l - a_-)}{kT}\right).$$

The measured current is nearly equal to the metal ion current from equation [12] with n_+ put equal to $p(D)$.

$$i_+ = q_- 2a_+ \nu_+ \left(\frac{m_l \nu_l}{2a_- \nu_-}\right) \exp\left(\frac{W_- - W_l - W_+}{kT}\right) \exp E(\beta_+ + \beta_l - \beta_-).$$

This model has the peculiar characteristic that the kinetics are controlled by the metal/oxide interface when the film is very thin and space charge effects are negligible, and by migration through the oxide (with the concentration of mobile ions controlled by the oxide/solution interface) when the film is thick enough for space charge effects to have isolated the bulk of the film from the effects of the metal/oxide interface.

The mathematics of the non-steady state are complex, and only a qualitative discussion will be attempted.

The concentration of oxygen ions will either increase or decrease with increasing $E(D)$ according to whether β_l is greater or smaller than β_-. The first case will be assumed. Since it is assumed that the metal ions are far more mobile than oxygen ions, the metal ion distribution at each stage will be nearly in the steady-state condition appropriate to the instantaneous distribution of negatively charged ions. Suppose that after the system has come to a steady state at an applied current $I_1 \simeq i_+$, the current is suddenly increased to a new value I_2. The average field will first rise to a new value given by equation [11] with almost the same value of p as existed before I was increased. The process is that of charging a condenser with a leakage given by $i = i_0 \exp \beta E$, where $E \simeq V/D$. If V = voltage across the condenser of capacity C,

$$I(t) = CdV/dt + i_0 \exp(\beta V/D),$$

where $I(t) = I_1$ for $t \leqslant 0$ and $I = I_2$ for $t > 0$,

we obtain $I_2 t = (DC/\beta) \log\{(1 - I_2/I_1)/[1 - I_2/i_0 \exp(\beta V/D)]\}$.

The time t for the condenser to charge up to a given fraction of its final charge is inversely proportional to the current density and independent of D.

As the field in the oxide increases, the rate of entry of oxygen ions also increases. As the concentration of oxygen ions builds up the field decreases and levels out at the new steady-state value. The decay of the overshoot should depend on the thickness of oxide, since the decay involves the movement across the oxide of something in the nature of a step function

in the concentration of both ions, and the velocity of movement will tend to be independent of thickness. According to Dewald (12), with tantalum the decay does not depend on the thickness, so that the above model would appear (if our qualitative treatment is correct) not to apply to this metal.

Structural Effects at the Metal/Oxide Interface

Each time that a metal ion leaves the metal to enter the oxide it leaves a vacancy in the metal lattice and some degree of local misfit. This may cause the outer two or three layers of metal to become effectively amorphous. The effect will depend on the current density, since the diffusion within the metal surface will tend to repair the damage. The degree of directional bonding within the metal, and the presence of impurities will also affect this process. When the disarrangement is present, it will tend to remove the differences between the kinetics on different crystal faces that might be expected when the Cabrera–Mott theory applies.

SUMMARY

A great many different special cases are possible—movement by metal or oxygen, vacancies or interstitial ions, creation of defects by the field, interfacial barriers important or not important according to the relative values of various parameters, and so on. A few essential principles may, however, be formulated. In the first place, for metal ion movement the metal/oxide interface will control the kinetics unless sufficient space charge can accumulate near this interface to permit the field strength at the boundary to differ appreciably from the field strength further into the oxide. If the interface is, so to speak, isolated by space charge effects, the concentration of carriers in the main body of the film is controlled by whatever determines the net space charge density due to the non-mobile species. The field production of Frenkel defects, the movement of oxygen ions, and the range of sites due to the amorphous nature of the oxide could cause this background charge to vary with the field strength. When the background charge varies with the field strength, it becomes possible to have "overshoot" in the field transients. Variation of jump distance and hence of Tafel slope with field strength may be due to the variation of sites to be expected in an amorphous oxide, and to the fact that jumps occur at greater angles to the field direction as the field strength increases.

REFERENCES

1. UHLIG, H. U.   Acta Met. **4**, 541 (1956).
2. KETELAAR, J. A. A.   Nature, **137**, 316 (1936).
3. VERWEY, E. J. W.   Physica, **2**, 1059 (1935).
4. UBBELOHDE, A. R.   Discussions Faraday Soc. **23**, 128 1957.
5. CABRERA, N. and MOTT, N. F.   Repts. Progr. in Phys. **12**, 163 (1948–1949).
6. JACOBS, P. W. M., BRAY, A. R., and YOUNG, L.   Proc. Phys. Soc. **71**, 405 (1958).
7. VERMILYEA, D. A.   Acta Met. **1**, 282 (1956).
8. YOUNG, L.   Trans. Faraday Soc. **52**, 502 (1956).
9. WILLIS, G. C., ADAMS, G. B., and VAN RYSSELBERGHE, P.   Private communication. (1958).
10. YOUNG, L.   Unpublished.
11. VERMILYEA, D. A.   J. Electrochem. Soc. **102**, 655 (1955).
12. DEWALD, J. F.   Phys. and Chem. Solids, **2**, 55 (1957).
13. DEWALD, J. F.   J. Electrochem. Soc. **102**, 1 (1955).
14. VERMILYEA, D. A.   J. Electrochem. Soc. **104**, 140 (1957).
15. YOUNG, L.   Proc. Roy. Soc. A, **244**, 41 (1958).
16. BEAN, C. P., FISHER, J. C., and VERMILYEA, D. A.   Phys. Rev. **101**, 551 (1956).
17. TOMPKINS, F. C. and JACOBS, P. W. M.   Quart. Revs. **6**, 238 (1952).
18. VERMILYEA, D. A.   J. Electrochem. Soc. **104**, 427 (1957).
19. VERMILYEA, D. A.   Acta Met. **2**, 482 (1954).
20. YOUNG, L.   Trans. Faraday Soc. **53**, 841 (1957).

THE FORMATION AND PROPERTIES OF PASSIVE FILMS ON IRON[1]

Morris Cohen

ABSTRACT

A unified mechanism for the formation of passive films on iron in aqueous solutions is presented. The effects of water, oxygen, and oxidizing and non-oxidizing ions are considered. The γ-Fe$_2$O$_3$ film is formed first by the oxidation of water-formed magnetite and further thickening of the film takes place by the oxidation of diffusing Fe^{++} ion at the water surface of the oxide film. The main force leading to diffusion is the field set up by the adsorbed negative ion and the positive Fe^{++} ions at the surface of the metal. Some of the properties of the protective γ-Fe$_2$O$_3$ film and factors leading to its destruction are discussed.

When iron is exposed to aqueous solutions containing certain oxidizing ions such as chromate or nitrite, or buffering agents and oxygen, it becomes passive. Electron diffraction measurements and film stripping experiments indicate that the iron is covered by a thin film, composed mainly of γ-Fe$_2$O$_3$ (1, 2).

Although much has been published concerning the behavior and possible physical and chemical structure of these passive films on iron (3, 4, 5), very little data has been presented or possible mechanisms proposed to account for the formation of the films.

Since the behavior of passive films on iron is much the same, independent of the solution in which they are formed, there is probably a common general mechanism of formation. In this paper such a mechanism for the formation process and composition of passive films is developed and used to explain the build-up and break-down of the films.

1. Reactions of Iron with Water

(a) In the Absence of Oxygen

This reaction has been reviewed recently by V. J. Linnenbom (6). At room temperature he found evidence for ferrous hydroxide only. At higher temperatures some Fe$_3$O$_4$ was also found. In earlier work Schikorr (7) reports that Fe(OH)$_2$ converted slowly to magnetite at room temperature but this was not confirmed by Linnenbom. It is thermodynamically possible for iron to react with water to form either Fe(OH)$_2$ or Fe$_3$O$_4$.

When film-free iron is exposed to water, in all probability a film is formed which separates the iron from the water. If this film is formed by a heterogeneous reaction between the iron and the water then the composition of the film will probably approximate that of an anhydrous oxide. FeO is not stable below a temperature of 500° C, so that the most likely film is Fe$_3$O$_4$. This persists as a very thin film and the iron remains bright and silvery in appearance.

The rate of reaction of iron with oxygen-free water is very slow, of the order of 20 μg/cm^2 in 5 days (3). This rate is about the same in the presence of chloride ion. The reaction rate corresponds to the reaction of 56 Å of metal/day or a current of $2\times10^{-1}/$ μa cm^2. The potential of the specimen, which corresponds to the equilibrium potential of iron in a saturated solution of Fe(OH)$_2$, indicates high hydrogen polarization. The mechanism of the reaction is probably that of diffusion of both Fe^{++} and electrons through a thin magnetite film of the order of 1 or 2 unit cells (8–16 Å) thick with the

rate of the reaction being controlled by the rate of formation of hydrogen. The very thin film of magnetite acts as a separator rather than a diffusion barrier and is stabilized by being in contact with the metal.

The reactions can be expressed as:

$$Fe \longrightarrow Fe^{++} + 2e,$$

$$\frac{2e + 2H_2O \longrightarrow 2OH^- + H_2}{Fe + 2H_2O \longrightarrow Fe(OH)_2 + H_2}.$$
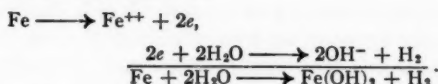
The rapidly formed magnetite film is formed by the reaction:

$$3Fe + 4H_2O \longrightarrow Fe_3O_4 + 4H_2.$$

The magnetite thickens and becomes visible at higher temperatures or by the addition of certain other chemicals—that is when the rate of the reaction of $Fe^{++} \longrightarrow Fe_3O_4$ in contrast to $Fe^{++} \longrightarrow Fe^{++}$ hydrated is increased.

A diagram of the reactions of iron in oxygen-free water is shown in Fig. 1.
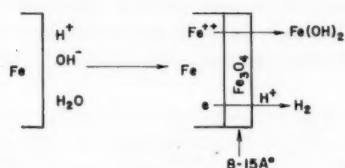
FIG. 1. Development of steady-state corrosion of iron in water. A thin film of magnetite is formed by direct reaction with water. Reaction continues by diffusion of ferrous ion into the solution and hydrogen formation.

(b) Absence of Oxygen but Presence of Oxidizing Anions

Four oxidizing ions—namely nitrite, chromate, molybdate, and tungstate—have been found to form films on iron in oxygen-free water. Of these, chromate forms a passive film at the lowest concentration. This film is of the order of 50–75 Å thick and contains both $\gamma\text{-}Fe_2O_3$ and Cr_2O_3 (8).

With nitrite solutions, at low concentrations thick films of Fe_3O_4 are formed. When the concentration of nitrite is increased to about 0.1 N a thin film of $\gamma\text{-}Fe_2O_3$, possibly containing some $\gamma\text{-}FeO(OH)$, is formed (1).

Of the four oxidizing inhibitors the strongest oxidizing agent with respect to ferrous ion in neutral solution is chromate. The others react relatively slowly. All four inhibitors are poor cathodic depolarizers: nitrite ion is not reduced when exposed to cathodically polarized iron, while the reaction rate of iron with water, which is controlled by cathodic depolarization, is the same irrespective of the presence of low concentrations of molybdate and tungstate (3).

As in the presence of water alone, the instantaneous surface reaction of film-free iron is a heterogeneous one to form Fe_3O_4. Adsorption of the oxidizing anions on the films during the formation of the film leads to further oxidation to $\gamma\text{-}Fe_2O_3$. In the case of the chromate ion, where the reduction product is insoluble Cr_2O_3, this leads to the build-up of a film containing both Cr_2O_3 and $\gamma\text{-}Fe_2O_3$ in a ratio of about 1:3. The amount of chromium found in the film would correspond to a film about 50–75 Å thick (8).

In the case of nitrite the reduction products are soluble and at sufficiently high concentrations a film consisting mainly of $\gamma\text{-}Fe_2O_3$ is formed. At low concentrations (0.001 N) magnetite films of sufficient thickness to be visible are formed (9).

With molybdate and tungstate visible magnetite films are also formed. However, if the iron is made anodic, γ-Fe_2O_3 films of a protective nature are formed. This may be due to an increase in oxidation rate by the discharge of hydroxyl ion to form oxygen and/ or discharge of the anions at the metal oxide – solution interface.

This order of efficiency of the formation of passive films is probably related to the oxidizing power of the anions with respect to the oxidation of Fe^{++} to Fe^{+++}. The reaction of chromate ion with ferrous ion is very rapid, while that of nitrite, molybdate, and tungstate is relatively slow.

The γ-Fe_2O_3 which forms the main part of all the passive films is formed as the film grows. The first formed unit cell of Fe_3O_4 is oxidized to γ-Fe_2O_3 and further diffusion of Fe^{++} takes place through this γ-Fe_2O_3 film. The ferrous ion which reaches the oxide-solution interface is oxidized to ferric ion by the adsorbed oxidizing agent, thus leading to further thickening of the film. Although there is no direct contact between the iron and the solution the iron is oxidized to Fe^{++} by water in that the electrons are neutralized by H^+. The main force responsible for the diffusion of Fe^{++} through the γ-Fe_2O_3 is supplied by the electrostatic attraction between the adsorbed negative anion and positive metal ions in the lattice. This force is sufficient to allow a film of about 50–75 Å thick to form. The geometry of these reactions is shown in Fig. 2.
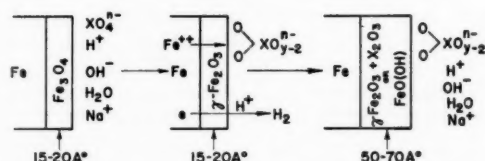
FIG. 2. Conversion of Fe_3O_4 to γ-Fe_2O_3 and further thickening of γ-Fe_2O_3 to form passive film. The attractive force between the anion and Fe^{++} depends on charge and thickness.

If the concentration of the passivating oxidizing agent is too low, oxidation of the ferrous ion takes place to magnetite only and a proportion of ferrous ion escapes into the solution. The magnetite film thickens considerably, probably because the cationic diffusion rate through magnetite is greater than that through γ-Fe_2O_3.

A number of oxidizing anions such as permanganate do not form passive films on iron. This could be due to either the physical nature of the reduction product and/or their ability to depolarize the cathodic reaction. The former is probably the more important in that a gelatinous reduction product interferes with the growth of the protective passive film. Because of depolarization of the hydrogen formation reaction some oxidizing anions may act as corrosion accelerators rather than passivating agents.

(c) Presence of Oxygen

Iron reacts rapidly with dry oxygen at room temperature to form a film of γ-Fe_2O_3 15–20 Å thick (10). At this thickness the reaction essentially ceases. If iron is exposed to water saturated with oxygen at normal pressures and temperatures the reaction continues at a relatively constant rate, the main products of the reaction being hydrated ferric oxides. If the specimen becomes covered with hydrated reaction product, so that there is a decrease in the oxygen concentration at the oxide–precipitate interface, visible films of magnetite are formed. The corrosion rate is very much higher than the rate in oxygen-free water, being of the order of 1.3 mg/cm² 5 days or 13 μa/cm², or 65 times the rate in oxygen-free water.

The initial reaction is the formation of a thin layer of magnetite as in the case of oxygen-free water. This thin layer of magnetite can then be oxidized to γ-Fe_2O_3 by reaction with adsorbed oxygen. At room temperature and pressure the solubility of oxygen in water is only 8 parts per million and owing to incomplete coverage by oxygen both the rate of oxidation to γ-Fe_2O_3 and further thickening of the γ-Fe_2O_3 film is slow. Fe^{++} ions continue to diffuse through the oxide into the solution where they are oxidized by dissolved oxygen to $FeO(OH)$. These hydrated oxides are precipitated on the metal surface and form a diffusion barrier for the movement of oxygen to the metal surface. As in the case of the oxidizing anions, the lowered concentration of oxygen at the metal oxide – solution interface allows further growth of magnetite but does not oxidize the magnetite to γ-Fe_2O_3. The precipitate, being laid down unevenly, will tend to allow the formation of separate anodic and cathodic areas on the surface and the over-all corrosion current is sufficiently high and the pH sufficiently low to cathodically reduce any already formed γ-Fe_2O_3 (11). The above sequence of formation of Fe_3O_4, etc., will then be repeated. As well as oxidizing magnetite to γ-Fe_2O_3 the oxygen can also react with ($e + H^+$) to form OH^- ions. This both accelerates the rate of corrosion and, at the normally low concentrations of oxygen in the solution, decreases the per cent of the surface area covered by oxygen. This lowered coverage leads to a decreased probability of the formation of a protective γ-Fe_2O_3 film.

At sufficiently high concentrations of oxygen it is possible to obtain protective passive films. This is related to a more rapid replenishment of the cathodically removed oxygen which leads to γ-Fe_2O_3 film growth rather than corrosion. The formation of a protective film thicker than 15–20 Å may be due in part to the field set up by the adsorption of some OH^- ions.

(d) Presence of Oxygen and Oxidizing Ion

In general the presence of oxygen decreases the concentration of oxidizing anion required to give passivity. Because of the presence of the anion the film still thickens to 50–75 Å. The main function of the oxygen in the case of the nitrite, molybdate, and tungstate is probably the oxidation to γ-Fe_2O_3 of some of the magnetite formed by the oxidation of ferrous ion by the anion.

(e) Presence of Oxygen and Non-oxidizing Buffering Ion

Iron is passive in air-saturated solutions containing relatively high concentrations of alkaline buffering agents such as Na_2CO_3, Na_3PO_4, and C_6H_5COONa. The passive film is mainly composed of γ-Fe_2O_3 with some hydrated oxide, and in the case of the phosphate, hydrated ferric phosphate (12). Most of the hydrated material appears to be located in rather thick inclusions which protrude above the oxide film (9). The salts would appear to serve two purposes. Firstly adsorption of the negative ion, by increasing the field strength across the oxide, leads to a sufficient thickening of the γ-Fe_2O_3 film formed by the reaction of O_2 with Fe_3O_4 to prevent further diffusion of iron ions. Secondly, where the film has not thickened, so that Fe^{++} ions continue to escape into the solution, the anodic pores are kept on the basic side. This decreases the rate of cathodic reduction and consequent thinning of the adjacent oxide. Since diffusion of ferrous ions through the porous precipitated plug of hydrated material is probably more rapid than through the oxide the plugs grow relatively thick before the reaction stops.

2. Reactions in the Presence of the Air-formed Film

As mentioned above, the air-formed film is γ-Fe_2O_3 of the order of 20 Å thick. In the presence of the passivating agent this film thickens, by the formation of more γ-Fe_2O_3

and possibly other hydrated products. Under borderline passivating conditions some of the film may be removed by cathodic reduction and either new film or plugs are formed in the manner outlined above.

3. Effect of an Applied Current

If the iron is made cathodic the γ-Fe_2O_3 film is reduced. At low cathodic current densities corrosion continues, probably through a layer of magnetite. At higher cathodic currents corrosion essentially ceases, probably with some redeposition of iron.

At low anodic currents the corrosion of iron is increased. At higher current densities passivity is often observed. This can be explained by a combination of the suppression of the cathodic reaction with its possibility of cathodic reduction of the γ-Fe_2O_3 and the direct discharge of oxygen on the metal surface. Because of the high overvoltage for oxygen evolution the equivalent pressure of oxygen at the metal surface is high and conditions for the formation of γ-Fe_2O_3 favorable. Oxidizing ions such as tungstate and molybdate will also be discharged at the anodic areas with a similar effect of apparent increased activity.

4. Properties of the Passive Film

Passive films have been stripped from iron by both chemical (13) and electrochemical (14) dissolution of the underlying metal. They are found to be mainly anhydrous γ-Fe_2O_3. They are chemically inert and dissolve in acid only with difficulty. The hydrated parts of the film are less inert than the anhydrous oxide. The film may be cathodically reduced to Fe^{++} ion which, at neutral and low pH's, is quite soluble. The film is a relatively good electronic conductor but a poor cationic conductor and the growth of the film appears to be controlled by the rate of cationic conduction.

The breakdown of the passive film probably takes place through the breakdown of pores in the anhydrous oxide film. Electron microscope and diffraction studies indicate that most of the passive films have discontinuities in the anhydrous oxide films which contain the less inert hydrated ferric oxides or other insoluble ferric salts. Diffusion of the solution through these rather porous precipitated plugs leads to the formation of acidity in the pores—particularly in the presence of such ions as chloride or sulphate. The ferric salts can be removed by the formation of soluble complexes with many ions. The combination of anodic current and acid conditions leads to undermining or cathodic reduction of the protective γ-Fe_2O_3 film.

It is rather surprising that there is such a large difference in the cationic diffusion properties of magnetite and γ-Fe_2O_3 as indicated by possible thicknesses of the two types of film. It is generally assumed that γ-Fe_2O_3 has essentially the Fe_3O_4 structure with cation vacancies (15). The diffraction patterns of the two oxides are very similar. The two oxides, however, behave quite differently chemically. Fe_3O_4 dissolves in acid very easily, while γ-Fe_2O_3 dissolves only with difficulty. On cathodic reduction γ-Fe_2O_3 is reduced completely to the ferrous state with high current efficiency, while magnetite is reduced with difficulty and very low current efficiency. In some X-ray diffraction studies in this laboratory it has been found that γ-Fe_2O_3 produced in several ways has d-values greater than 6 Å as well as two lines which do not appear in the Fe_3O_4 patterns. This would point to a somewhat different kind of ordered structure and may account for the different chemical and diffusional behaviors of the two oxides. This would also indicate that some recrystallization takes place in the conversion of Fe_3O_4 to γ-Fe_2O_3.

A second factor which may contribute to a difference in the growth rate and hence final thickness of the two oxides could be a difference in the rate of transfer of Fe^{++} ions

across the metal–oxide interface. This would be partly related to a difference in the crystallographic arrangement of the oxides on the metal. Thin films of Fe_3O_4 show preferred orientation on iron, while γ-Fe_2O_3 films do not. The bulk of evidence shows that γ-Fe_2O_3, the main constituent of the passive film, is an inert material which in passivating solutions grows to a maximum thickness of 50–75 Å.

REFERENCES

1. COHEN, M.   J. Phys. Chem. **56**, 451 (1952).
2. MAYNE, J. E. O. and PRYOR, M. J.   J. Chem. Soc. 1831 (1949).
3. PRYOR, M. J. and COHEN, M.   J. Electrochem. Soc. **100**, 203 (1953).
4. WADE, W. H. and HACKERMAN, N.   Trans. Faraday Soc. **53**, 1636 (1957).
5. HOAR, T. P. and EVANS, U. R.   J. Electrochem. Soc. **99**, 212 (1952).
6. LINNENBOM, V. J.   J. Electrochem. Soc. **105**, 322 (1958).
7. SCHIKORR, G.   Z. anorg. u. allgem. Chem. **212**, 33 (1933).
8. COHEN, M. and BECK, A. F.   Z. Elektrochem. (In press).
9. MELLORS, G. W., COHEN, M., and BECK, A. F.   J. Electrochem. Soc. **105**, 332 (1958).
10. GULBRANSEN, E. A.   J. Electrochem. Soc. **81**, 327, 1942.
11. OSWIN, H. G. and COHEN, M.   J. Electrochem. Soc. **104**, 9 (1957).
12. PRYOR, M. J., COHEN, M., and BROWN, F.   J. Electrochem. Soc. **99**, 542 (1952).
13. VERNON, W. H. J., WORMWELL, F., and NURSE, J. T.   J. Chem. Soc. 621 (1939).
14. EVANS, U. R.   Nature, **126**, 130 (1930).
15. WELLS, A. F.   Structural inorganic chemistry. Oxford University Press, London. 1950. p. 381.

THE ELECTROCHEMICAL BEHAVIOR OF THE NICKEL – NICKEL OXIDE ELECTRODE

PART I. KINETICS OF SELF-DISCHARGE[1]

B. E. CONWAY AND P. L. BOURGAULT

ABSTRACT

The nickel – nickel oxide electrode forms the positive plate in the charged nickel–cadmium battery. After "charging" the electrode to a chemical state represented by the non-structural formula NiO_x, where x can vary from about 1.4 to 1.8 depending on the current density and temperature, loss of oxygen and a fall of potential on open circuit occurs. In the present work this "self-discharge" effect has been examined by study of (i) the rate of decay of e.m.f. on open circuit, (ii) rate of oxygen evolution on open circuit, (iii) the electrochemical capacity of the electrode, and (iv) the build-up or charging curves for the electrode. The decay behavior has been studied in aqueous KOH solutions from 0.0015 to 15 M. Tafel slopes are obtained from the plots of e.m.f. vs. log (time of decay), and abrupt changes occur at certain electrode potentials which indicate changes of rate-determining mechanism in the self-discharge process. The slopes observed are interpreted in terms of a new scheme of consecutive reactions for anodic oxygen evolution by deducing, by means of the Christiansen method, the relevant Tafel slopes. It is shown that the scheme proposed uniquely accounts for the experimental behavior and that the change of mechanism observed in the self-discharge can only be explained if two consecutive and not alternative processes are involved. The dependence of the rates of self-discharge upon OH^- ion and water activity is deduced and the significance of these results is discussed.

INTRODUCTION

Interest in the behavior of the nickel – nickel oxide electrode arises from its use as the positive plate in the nickel–cadmium and nickel–iron batteries; at the same time, study of the system affords further insight into the fundamental kinetics of anodic processes, which in the case of the nickel system are complex owing to the existence of several possible oxidation states of the metal in corresponding hydrated oxides (1, 2). One of the features of interest is the loss of charge of the nickel oxide electrode when it is left standing in pure alkaline solution on open circuit. The loss of charge is accompanied by oxygen evolution and decay of e.m.f. of the electrode (e.g., measured with respect to the Hg/HgO electrode in the same solution). Hitherto, studies of the kinetics of decay have not been made rigorously and only somewhat arbitrary rate measurements have been obtained (i) by determining the total time required for the e.m.f. of the electrode to decay over about 0.6 v (3), and (ii) by determining the *total* volume of oxygen liberated from an electrode at the end of a period of 13 hours (4). Since it is clear that over the potential range studied (3) more than one process is involved in the decay, because the e.m.f.–time curve passes through an inflection, and since in the oxygen evolution process (4) the rate of oxygen evolution depends on the electrode potential, it must be concluded that the kinetic significance of "rates" measured by these procedures is unclear. Furthermore, the "rates" of self-discharge thus measured by these two procedures are found to be dependent in *opposite* senses upon the KOH or water activities in the solutions used. In the present work we have therefore attempted to make a more rigorous kinetic analysis of the self-discharge process by obtaining the decay of e.m.f. as a function of the theoretically significant *logarithm* of the time of decay, and relating this to the volume of

oxygen evolved, measured frequently during an over-all period of 10^5 to 10^6 seconds. Electrochemical capacities of the electrodes studied are obtained by several different methods involving the kinetics of the decay and charging processes.

EXPERIMENTAL

Electrodes

The electrodes used were similar to those utilized in the nickel–cadmium battery. Porous sintered pure nickel plaques having an average pore size of 1 μ (5) were impregnated under vacuum with a saturated solution of cobalt-free nickel nitrate prepared by recrystallization from A.C.S. analytical reagent grade material. The nickel hydroxide, $Ni(OH)_2$, was then precipitated in the sinter by immersion in 20% aqueous KOH solution purified as described below. The electrodes were then treated cathodically as described previously (6) and then washed in 10 changes of conductance water. The electrodes were finally charged anodically in the experimental solution (see below) until oxygen evolution occurred. The weight of oxide formed in the electrode was determined from the difference of the weights of the dry unimpregnated sinter and the oxide-impregnated one after drying at 80° C; under these conditions the oxide in the sinter is $Ni(OH)_2$. From this weight, the theoretical electrochemical capacity for a given degree of subsequent oxidation can be calculated.

Solutions

Conductance water was redistilled in CO_2-free nitrogen passed through liquid air traps containing charcoal. The steam was passed up a column of hard glass chips heated to 450° C. The water was then condensed into a second distillation vessel from which it was redistilled into a vessel containing solid A.C.S. analytical reagent grade KOH. This vessel was provided with a sintered glass bottom for filtering, and suitable exit and entry tubes for gas and solution. The KOH solution thus prepared was then recrystallized by immersion of the vessel in a refrigerated bath at $-20°$ C; the mother liquor was forced out of the tube leaving crystals of the dihydrate of KOH. Further water was then distilled on to the recrystallized KOH from the second distillation stage. The solution thus obtained was then used to prepare potassium amalgam which was then reacted with more of the redistilled water until a suitable concentration of aqueous KOH was obtained. This solution was then passed into the experimental cell where it was pre-electrolyzed with a nickel anode, purified oxygen being bubbled through the solution. The pre-electrolysis current of 10^{-2} amp per apparent cm^2 was passed for 12 hours between the nickel anode and a charged nickel – nickel oxide electrode as cathode. This procedure was adopted in order that no hydrogen could be evolved cathodically and diffuse subsequently to the experimental charged nickel electrode, which might thereby be depolarized. Experiments were also made, in order to simulate battery conditions, in ordinarily purified solutions, i.e., without KOH regeneration by means of potassium amalgam. These experiments were carried out mainly in the higher range of concentrations of KOH as used in the nickel battery.

Cells

In dilute solutions (< 0.1 N) it was found that use of the usual two-limb cell (7) with reference electrode and Luggin capillary lead to non-uniform charging* of the electrode, owing to asymmetry of the position of the electrode with regard to current

*By "charging" we signify the process of conversion of the initially precipitated $Ni(OH)_2$ to the non-stoichiometric higher hydrated oxide often referred to as nickel peroxide or NiO_2.

lines from the cathode. In order to overcome this difficulty, e.m.f. and oxygen volume measurements were made on electrodes charged in the cell shown in Fig. 1. The apparatus consisted in a central anodic compartment provided with two Hg/HgO reference electrodes and Luggin capillaries. The test electrode was situated at the center of two conical side limbs each communicating with a charged nickel – nickel oxide electrode used as a cathode. The field in which the test electrode was charged was thus relatively uniform, and uniform oxidation on both sides of the electrode was observed to occur. For stronger solutions it was found that an ordinary two-compartment cell with reference electrode and Luggin capillary could be satisfactorily used.
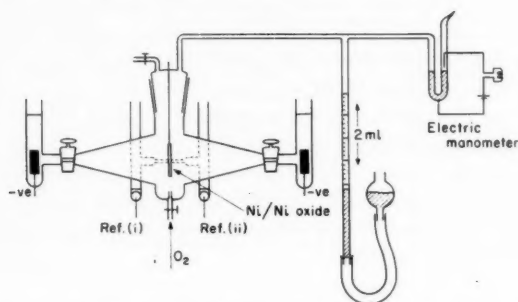
FIG. 1.   Uniform field cell for oxygen evolution measurements.

Measurements of Oxygen Evolution

The rates of oxygen evolution on open circuit were measured after termination of charging, by closing off the cathode compartment by means of a stopcock, closing off the oxygen supply used for stirring the solution, and allowing the system to come into communication with a 2-ml gas pipette calibrated in 0.01-ml marks, readable to 0.003 ml and connected to a variable head of mercury. The pipette was also joined to one side of a constant-pressure manometer with an electrical device capable of indicating constancy of pressure to 0.2 mm Hg. Capillary tubing was used between the cell, the pipette, and the manometer in order to minimize dead space, which was about 7 ml; in oxygen volume measurements the cell was filled, within a few milliliters, up to the top of the glass cap. The oxygen volume could be measured to 0.003 ml. The whole apparatus was maintained in an air thermostat at 25° C constant to 0.05° C. The total oxygen volumes measured over periods of 2 to 3 days were from 2 to 5 ml. Volumes above 2 ml were determined as follows: 2 ml were initially collected and measured up to a certain time; the cell was closed off and the mercury brought back up to the zero volume mark, the 2 ml being rejected out of another stopcock. Communication was then remade to the cell and further oxygen collected; the total volume at various times was then calculated. Volumes were corrected to n.t.p. allowing for the vapor pressure of water over the various solutions used (8).

Electrical Measurements

Potential measurements were made by means of a high impedance Doran pH-millivoltmeter and in some cases with a Tinsley potentiometer. Direct-current charging curves were obtained by manual potentiometric measurements and also in some cases by means of a high impedance recording electronic potentiometer. Short period e.m.f. decay curves were obtained by means of a Hewlett–Packard cathode ray oscillograph.

In these measurements in dilute solutions ($< 0.01\ N$), a flow technique was used (flow rates up to 15 ml sec^{-1} past the electrode could be attained in a 2-cm diameter cell) in order to eliminate concentration polarization effects which otherwise influence the open-circuit decay behavior in the most dilute solutions during the first several seconds of decay.

RESULTS

Electromotive force decay curves were obtained at 25° C for the charged nickel – nickel oxide electrode at the following concentrations: 0.0015, 0.015, 0.145, 0.93, 2.9, 7.0, 9.4, and 14.6 M, and are shown in Figs. 2, 4, and 5, where the e.m.f. is plotted (see below) against logarithmic time plus a correction factor θ which is the time required for the electrode to decay from infinite positive potential to the potential at zero time, i.e., at the moment of beginning of the open-circuit decay measurements. Figures 3 and 6 show the corresponding oxygen volume measurements obtained at various times and plotted against the corresponding values of e.m.f. Figure 3 shows the dependence of volume of oxygen evolved in 7.1 M KOH solutions as a function of logarithmic time. At other
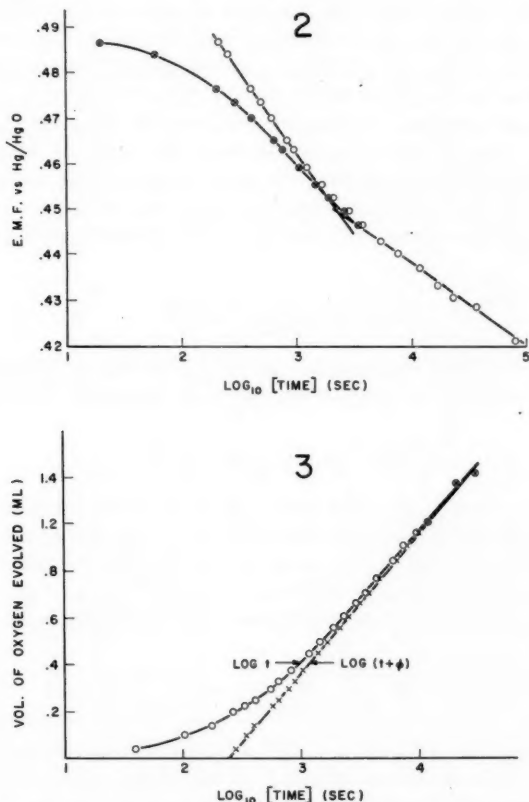
Fig. 2.   Typical e.m.f. – log (time) relationship in 0.72 M KOH showing θ correction and corresponding electrode capacity.

Fig. 3.   Oxygen evolution as a function of log (time) or log (time + ϕ) where ϕ is analogous to θ in Fig. 2.

concentrations the oxygen evolution rates follow from the data in the Figs. 4 and 6. The decay curves show two linear regions having different Tafel slopes; the upper region has a slope of 0.039 ± 0.003 whilst that of the lower region is 0.021 ± 0.002. These values closely correspond, at 25° C, with Tafel slopes having values of 2.3 $(2RT/3F)$ and 2.3 $(2RT/5F)$, respectively, although the lower slope observed could correspond to the value 2.3 $RT/3F$. It is seen that the potential or time at which the change of slope occurs depends markedly upon the concentration of the KOH (Figs. 4, 5). The e.m.f. at the inflection point of the e.m.f. – log (time) lines is shown in Fig. 7 as a function of KOH concentration.

DISCUSSION

The results show that the self-discharge process occurs on open circuit with change of e.m.f. of the electrode and simultaneous evolution of oxygen. The self-discharge must hence proceed by an electrochemical mechanism analogous to that of corrosion, i.e., anodic and cathodic reactions are occurring simultaneously at a mixed potential. Usually either the cathodic or the anodic process is rate-determining and a potential corresponding to the rate of one or other of the processes, whichever is the faster, is set up. We have, therefore, to decide from the observed kinetics: (a) whether the anodic or the cathodic type of process is rate-determining and (b) having established this, what individual mechanism(s) in the net anodic or cathodic process determines its rate.

For an ordinary metal electrode for which the activation polarization behavior can be represented by the Tafel equation, it follows quite generally (9) that the decay of e.m.f. is logarithmic in the time of decay measured from the moment of cessation of the polarizing current. This relationship holds over wide ranges of time, except at very short times after interrupting the polarizing current or near the reversible potential for the process concerned. It has been shown (10) that the e.m.f., E, depends on the time of decay, t, according to

$$[1] \qquad dE/dt = -\frac{b}{2.303} \bigg/ (t + \theta),$$

where b is the slope of the Tafel equation for the rate-determining process in decay and θ is as defined above, assuming a constant double-layer capacity. The integral form of equation [1] is

$$[2] \qquad E = E' - b \log (t + \theta),$$

where E' is the initial potential at $t = 0$ plus $b \log \theta$. E is thus logarithmic in $(t + \theta)$. θ can then be evaluated semiempirically from the e.m.f. – log (time) plots as that value of time which when added to the time, t, gives an initially linear e.m.f. – log $(t + \theta)$ plot, collinear with the relationship directly observed at higher times, e.g., for $t > ca.$ 10 θ. When θ has been evaluated as above, the capacitance C of the double layer at the electrode can be obtained from

$$[3] \qquad \theta = \frac{b}{2.303} C/i,$$

where i is the polarizing current passing at the moment of commencement of the decay.

It may be expected that the decay of e.m.f. of the nickel oxide electrode should be analogous to that for the discharge of the double-layer condenser at a polarized metal electrode, except that the capacitance involved probably has a different origin and order of magnitude. We have therefore plotted the decay of e.m.f. as a function of log t and log
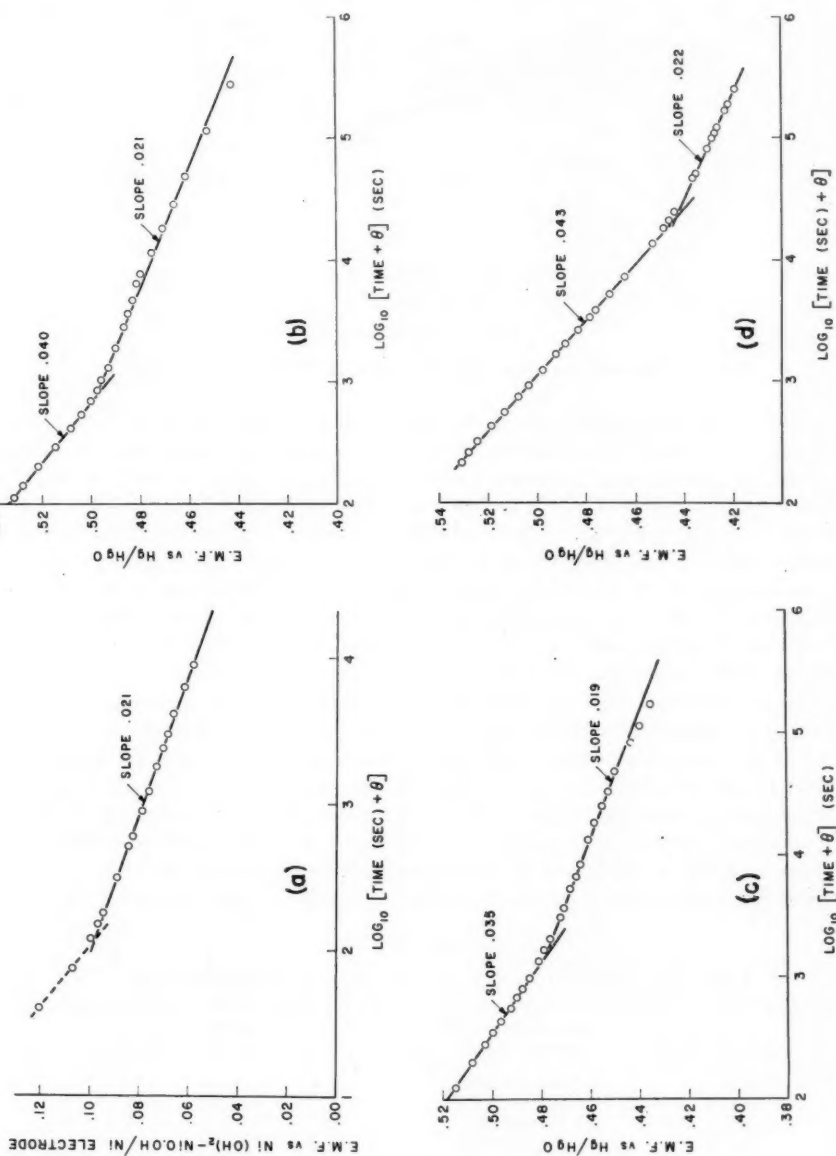
FIG. 4. Electromotive force decay lines at four low KOH concentrations. (a) 0.0015 M; (b) 0.015 M; (c) 0.145 M; (d) 0.93 M.
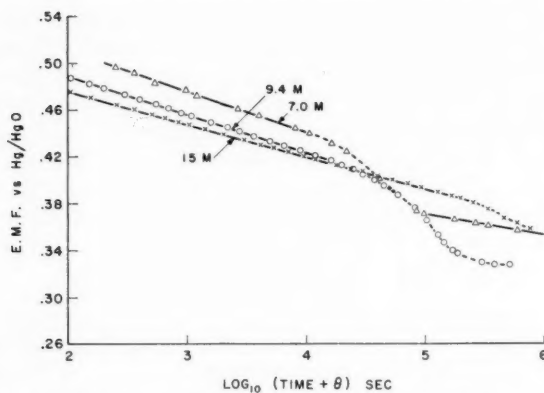
FIG. 5.   Electromotive force decay lines at high KOH concentrations.

$(t+\theta)$ in Fig. 2 (see also Figs. 4 and 5) for the electrode in 0.72 M KOH. The plots of log t and log $(t+\theta)$ are identical beyond about $10^{3.4}$ seconds. A unique value of θ exists, which gives the theoretically expected linear behavior; its value for 0.72 M KOH in Fig. 2 is 200 seconds. In this figure it is clear that there are two linear–logarithmic regions and it must be emphasized that in this and other cases (see Fig. 4), no value of θ can be found which gives a *single* straight line for the e.m.f. – log (time) plots except in the one case of the behavior in 15 M KOH solution (Fig. 5). Any arbitrariness in the value of θ derived semiempirically and any consequent uncertainty in the slope of the decay line can be avoided by plotting the e.m.f., E, as a function of log Δt for constant decrements of E during decay intervals Δt. Tafel b values, the same as these calculated semi-empirically, are obtained. (We are indebted to Dr. R. Parsons for this suggestion.) The e.m.f. – log $(t+\theta)$ lines shown in Fig. 4 and Fig. 5, for a wide range of concentrations from 0.0015 to 15 M, indicate a complex behavior in which more than one rate-determining mechanism in the self-discharge is involved. The slopes of the e.m.f. – log (time) line (see Figs. 4 and 5) have the values given in Table I and are characteristic of several steps in processes previously discussed (11) for the anodic evolution of oxygen. The higher slope of 0.038 is also found in direct polarization measurements (12).

The plots of oxygen evolved during decay as a function of e.m.f. shown in Fig. 6 also

TABLE I

Tafel slopes observed in the decay of e.m.f. of the nickel oxide electrode

Concn. of KOH	Mean slope in high potential region	Mean slope in low potential region	No. runs
14.6	0.028±0.0005	—	3
9.4	0.032±0.0005	—	2
9.0	0.032±0.001	—	2
7.1	0.038±0.0002	0.020±0.0003	9
2.9	0.034	0.016	1
0.93	0.040±0.0003	0.023±0.0005	4
0.327	0.038	0.019	1
0.145	0.037±0.0015	0.024±0.0004	2
0.077	0.040	0.021	1
0.015	0.039±0.002	0.020±0.000	2
0.0015	0.040±0.002	0.023±0.002	2
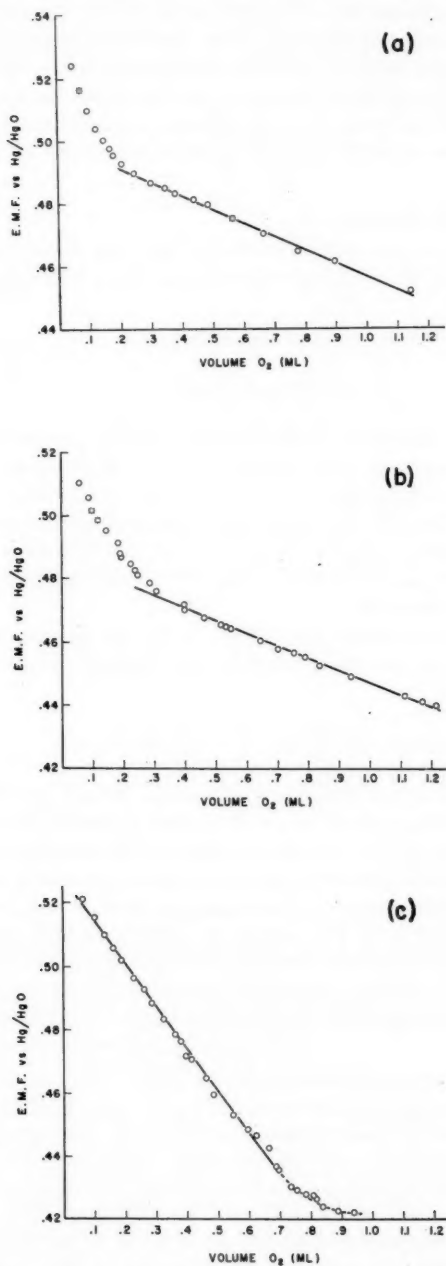
FIG. 6.   Volumes of oxygen evolved on open circuit as a function of e.m.f. during decay. (a) 0.015 M KOH; (b) 0.145 M KOH; (c) 0.93 M KOH.

indicate changes of the potential-determining species during the self-discharge process. Thermodynamic investigations of this aspect of the behavior of the electrodes are in progress. It is apparent that both in the e.m.f. decay and in the corresponding oxygen evolution behavior, the process which comes in at later times (or lower e.m.f.'s) is more dependent upon KOH activity than the first process at earlier times. The first process, however, gives Tafel slopes of 0.038 in dilute solution but in the strongest solutions the value changes to 0.029.

Evaluation of Rates of Self-discharge

Comparison of the rates of the two processes at high and low e.m.f.'s can be made if we can obtain a measure of the exchange currents for these processes.

(*i*) *From E.M.F. Decay*

The rate of decay of the e.m.f., E, is given (10) by

[4] $$dE/dt = -\frac{i_0}{C} 10^{\eta/b},$$

where i_0 is the exchange current for the rate-determining process in decay, C is the electrochemical capacity involved, η the oxygen overpotential,* and b the Tafel slope for the decay process obtained from the e.m.f. – log (time) plots. The values of η can be obtained from the values of e.m.f. experimentally measured with respect to the Hg/HgO electrode, since the reversible oxygen electrode is at 0.303 v more positive than the Hg/HgO electrode and its e.m.f. depends upon OH^- ion activity in the same way as does that of the Hg/HgO electrode.

From the logarithmic e.m.f. decay lines (Figs. 4, 5), we can obtain dE/d log (time) $(= -b)$; hence for a time t of decay required for the electrode to reach an overpotential η_t, equation [4] gives

[5] $$i_0 = -C\frac{dE}{dt} 10^{-\eta/b} = \frac{Cb}{2.3t} 10^{-\eta_t/b}.$$

The exchange current, and hence rate of self-discharge at any potential, is determined by the reciprocal of the time required to reach a given potential during decay.

From Figs. 4 and 5, values of t for various solutions can be obtained for chosen constant e.m.f. values and i_0 evaluated. The rates of self-discharge measured by $1/t_\eta$, for constant η, are shown in Fig. 8 for the range of concentrations studied and for the upper region of the decay lines. It is clear from Fig. 8 that the process at high positive potentials is much less dependent upon KOH activity than that at low potentials; at long times or low potentials the rate of self-discharge is approximately proportional to $(a_{OH^-})^2$; at shorter times or higher potentials the rate is proportional to a power of a_{OH^-} between $\frac{1}{2}$ and $\frac{1}{3}$.

(*ii*) *From Oxygen Evolution on Self-discharge*

From Figs. 2 and 6, the oxygen evolution rate, dV_{O_2}/dt, can be obtained from the slopes of the oxygen volume – e.m.f. lines and those of the e.m.f. – log (time) lines, since

[6] $$\frac{dV_{O_2}}{dt} = \left(\frac{dE}{dt}\right) \bigg/ \left(\frac{dE}{dV_{O_2}}\right) = \frac{1}{2.3t} \cdot \frac{dE}{d\log t} \bigg/ \frac{dE}{dV_{O_2}},$$

where t is again the time required to reach a given e.m.f. during oxygen evolution resulting from the self-discharge.† dV_{O_2}/dt can now be expressed as the anodic current, i_a, in

---

*We are here assuming that anodic processes are rate-determining in the self-discharge. That this is so, is indicated by the dependence of the rates upon OH^- and H_2O activity discussed below.

†dV_{O_2}/dt can, of course, be obtained directly by taking tangents to the oxygen volume – time curve; this procedure gives similar results to those obtained by means of equation [6], using appropriate values of the time, t.
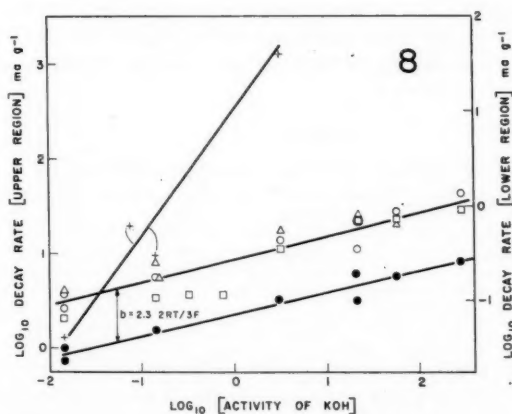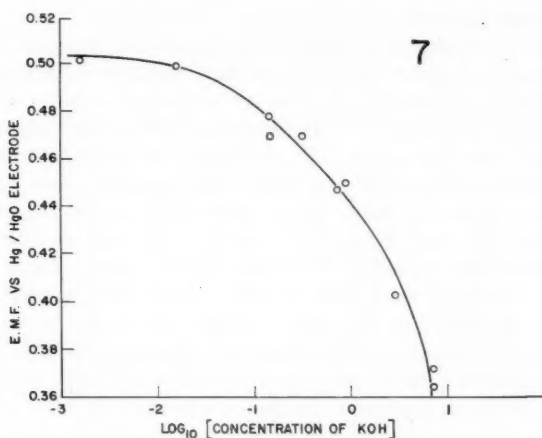
FIG. 7.   Electromotive force at the inflection point in decay as a function of KOH concentration.

FIG. 8.   Self-discharge rates from oxygen volume and e.m.f.–time measurements as a function of KOH activity; rates for high and low potential regions are shown.

+   Lower potential region, from $(1/2.3t)\ (dE/d \log t)/(dE/dV_{O_2})$. $E = 0.44$ v.

O   Upper potential region, from $(1/2.3t)\ (dE/d \log t)/(dE/dV_{O_2})$. $E = 0.48$ v.

□   Upper potential region, from $Cb/2.3t$. $E = 0.48$ v.

△   Upper potential region, from dV_{O_2}/dt. $E = 0.48$ v.

●   Upper potential region, from $(1/2.3t)\ (dE/d \log t)/(dE/dV_{O_2})$. $E = 0.46$ v.

self-discharge at the oxygen overpotential η, since $4F$ are required to evolve 22.4 l. of oxygen gas. Since the Tafel slope is found directly from the e.m.f. – log (time) plots, i_0 may readily be evaluated from the value of i_a at any suitable potential. The rates of self-discharge for the upper and lower potential regions may be expressed as current per unit weight of active material $(Ni(OH)_2)$ in the electrode. Values thus calculated are also shown in Fig. 8 as a function of KOH activity and for two electrode potentials; the dependence of the rates of self-discharge (from oxygen evolution measurements) upon KOH activity for the two regions is seen to be similar to that calculated for e.m.f. decay rates, as would be expected.

(iii) Values of Exchange Current

From the above considerations, the values of i_0 for the self-discharge process, expressed with respect to unit weight of active material, are then obtained and are given in Table II for unit activity of KOH in solution. Agreement between the values obtained by the two methods is satisfactory and as good as the reproducibility usually obtained in other kinds of electrode–kinetic measurements (13). Owing to the nature of the impregnated electrodes, it is not possible to specify the total real interfacial area exposed to the solution; hence i_0 values cannot be stated in the usual way, i.e., in amperes per square centimeter. An upper estimate may, however, be made of the area available per gram of active material. The electrodes consist of sintered particles having a size of about 1 μ with 80% free space between them (5). If we regard the particles as spherical for the purposes of the calculation of the order of magnitude of the real accessible area, a value of 6000 cm^2 per cm^3 of sinter may be calculated. An electrode plate 3 in. $\times$ 1.0 in. $\times$ 0.04 in. can be impregnated with about 1 g of Ni(OH)$_2$; we can then calculate that there are about 10^4 cm^2 per gram of oxide. i_0 values per cm^2 are then about 10^{-11} and 10^{-13} amp cm^{-2} for the process occurring in the upper and lower potential regions, respectively. The main interest in the present determinations of i_0 and the rates of self-discharge is not their absolute magnitude but their *relative* values, which indicate that the process appearing at lower potentials has a lower electrochemical rate constant than that at higher potentials; the rate of the slower process is also more affected by electrode potential and by OH$^-$ ion concentration than is that of the process occurring at more positive potentials.

TABLE II

Rates of self-discharge (i_0) at the reversible oxygen potential

Method	From e.m.f. decay	From O$_2$ evolution
Upper potential region	11.8×10^{-8} a.g.$^{-1}$	7.0×10^{-8} a.g.$^{-1}$
Lower potential region	3.5×10^{-10} a.g.$^{-1}$	4.3×10^{-10} a.g.$^{-1}$

Electrode Capacity

The electrochemical capacity involved in the self-discharge processes may be calculated in three ways: (i) from the θ correction in the determination of decay of e.m.f. using equation [3], (ii) from the volume of oxygen evolved as a function of e.m.f., i.e., from dV_{O_2}/dE, and (iii) from studies of d-c. charging on electrodes at which the self-discharge had virtually terminated (i.e. on electrodes still having a degree of oxidation approximately represented by the formula NiO$_{1.5}$). Values of electrode capacity obtained by the various methods are listed in Table III together with the ratios of "active" oxygen to nickel measured from the total charge which can be withdrawn from the electrode through an external circuit. From the active oxygen – nickel ratios in column 3 of Table III it is seen that the electrode is oxidized to the formal state NiO$_{1.57}$ in the strongest solution and to a smaller extent in more dilute solutions. The degrees of oxidation achieved with the present type of electrodes are thus somewhat less than that found by Wynne-Jones et al. (2, 3) for oxide films formed directly on nickel electrodes. The capacitance values calculated from θ, and oxygen evolution in the initial part of the decay are comparable as expected, since θ refers to this decay region. At longer times, the lower decay region (Fig. 2) gives higher capacities indicating that a different process

TABLE III
Electrode capacity and charge

Concn. of KOH, M	No. of results averaged	Active oxygen/nickel	Capacity, farads/equiv. $\times 10^{-3}$			
			From θ	O_2/e.m.f.		D-c. charging
				I	II	
14.6	3	0.57	17.8	21	41	—
9.4	2	0.51	26	32	64.6	—
7.0	8	0.48	33.4	41	62.5	—
2.9	1	0.45	31.9	39.5	70.3	37
0.93	4	0.43	47.5	57	—	39
0.145	2	0.39	25.1	44	170	25
0.015	2	0.36	21	33	140	20

Notes: (i) In columns 5 and 6, I and II signify the upper and lower regions, respectively, of oxygen evolution shown in Fig. 6.
(ii) Direct-current charging capacities in column 7 are given for the *initial* build-up of potential. At higher potentials in stronger solutions a more complex behavior is observed (Fig. 9).
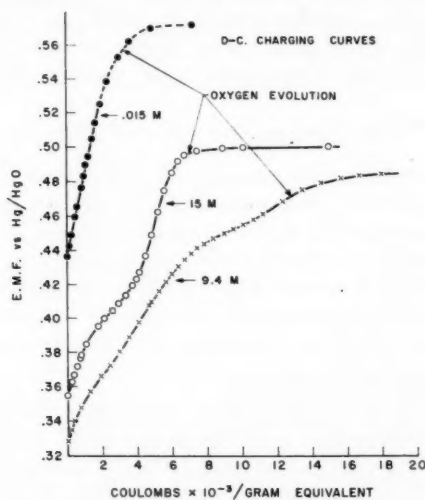
FIG. 9.   Direct-current charging curves for the nickel oxide electrode at three KOH concentrations.

is probably involved. The d-c. charging capacities for dilute solutions are recorded for comparison.

Reaction Mechanisms in the Self-discharge Process

The electrode capacities measured under various conditions, including those from the θ constant in e.m.f. decay, are clearly several orders of magnitude too large to be identifiable with the interfacial double-layer capacity of the electrode. However, the kinetics of the discharge process are formally analogous to those observed (9) for decay of e.m.f. of a polarized electrode through discharge of the double-layer condenser. A mechanism must therefore be proposed whereby the active material in the bulk of the electrode can be involved in self-discharge and be electrically accessible to the solution, yet the kinetics of the process can be formally similar to those observed in the discharge

of the double-layer condenser on open circuit. The following general scheme involving a mixed Ni^{III} and Ni^{IV} non-stoichiometric hydrated oxide lattice* (1, 3, 14) meets these requirements:

$$Ni^{4+}.2O^{--}{}_{(surface)} + OH^- \rightarrow Ni^{4+}.2O^{--}{}_{(surface)} + OH_{(ads)} + e_{(lattice)} \qquad [7]$$

$$Ni^{4+}.2O^{--}{}_{(surface)} + e_{(lattice)} \xrightarrow{\text{electron transfer}} Ni^{3+}.2O^{--}{}_{(surface)} \qquad [8]$$

$$Ni^{3+}.2O^{--}{}_{(surface)} + H_2O \xrightarrow{\text{proton transfer}} Ni^{3+}.O^{--}.OH^-. \qquad [9]$$
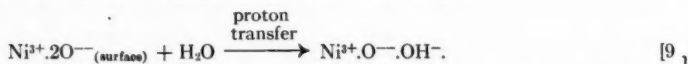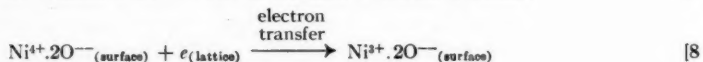
If there is electronic and protonic mobility in the lattice (3), $Ni^{4+}.2O^{--}$ can be regenerated in the surface of the oxide, since we can then write

$$Ni^{3+}.O^{--}.OH^-{}_{(surface)} + Ni^{4+}.2O^{--}{}_{(bulk)} \xrightarrow{e, H^+} Ni^{4+}.2O^{--}{}_{(surface)} + Ni^{3+}.O^{--}.OH^-{}_{(bulk)}. \qquad [10]$$
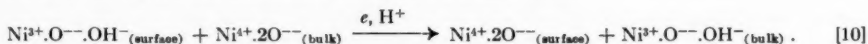
Process [7] can then continue to occur by discharge of OH^- ions in the double layer until all Ni^{4+} is converted to Ni^{3+}; similar self-discharge of the $Ni^{3+}.O^{--}.OH^-$ phase to $Ni^{++}.2OH^-$ could also occur if the potential of the electrode remained positive to that of the reversible oxygen electrode.† Oxygen evolution through process [7] then proceeds by the *over-all* reaction

$$2OH_{(ads)} \longrightarrow H_2O + \tfrac{1}{2}O_2. \qquad [11]$$
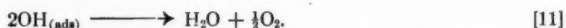
The rate-determining step in the anodic oxygen evolution process [7] with [11] is discussed below. Processes [8] and [10] involve electron shifts in the lattice and are likely to be very fast. The self-discharge rates are *increased* substantially by increasing KOH activity (Figs. 8, 9); hence process [9] is unlikely to be rate-determining, since with increasing KOH activity from 0 to 15 M, the water activity *falls* from unity to about 0.2 (8). Some step in the anodic oxygen evolution process in self-discharge is therefore rate-determining (cf. p. 300).

Rate-determining Steps in the Anodic Process

Two processes are likely to be involved, since two distinct slopes in the decay lines and in the e.m.f. – oxygen evolution plots are found (Figs. 2, 4, 5). These processes could be either consecutive or alternative; the one which is observed at lower electrode potentials has an exchange current of about 4×10^{-10} a.g^{-1} and a Tafel b value of about 0.021, whilst the other, observed at higher potentials, has an exchange current of about 9×10^{-8} a.g^{-1} and a Tafel b value of about 0.038. Since for two consecutive reactions, the slower determines the rate of the over-all reaction, whilst for two alternative reactions, it is the faster which predominates and hence kinetically characterizes the reaction, it follows from the above values of i_0 and b for the two processes concerned that they are *consecutive*. We therefore have to find a scheme of consecutive reactions which give amongst other possible slopes two leading to values of the Tafel b constant of 0.038 ($2.3\ 2RT/3F$) and

---

The constitution of the highest oxide of nickel is still under dispute (2, 15). It may be a peroxide of Ni^{II}(15) but this is hardly likely in view of the fact that the better characterized compound, β–NiO.OH, is formed as the electrode is charged, the highest state of oxidation being subsequently reached upon "overcharge". The higher oxides appear to be electrically conducting (2) otherwise the oxide electrode in the battery could hardly function in the necessary "reversible" manner. Such electronic conductivity would not be expected in a true peroxide lattice containing only Ni^{II} ions. In other kinds of compound the Ni^{IV} state is known to exist (16, 17).

†*In the studies of Wynne-Jones (3) on the nickel oxide electrode it appears that self-discharge occurred down to a potential of about zero volts with respect to the Hg/HgO electrode, i.e., 0.3 v negative to the oxygen reversible potential. In the present experiments the self-discharge of the electrode never continued below the reversible oxygen potential even after a period of a month. If depolarizers are, however, present, e.g., hydrogen, then further discharge can occur to lower potentials.*

0.021 (2.3 $RT/3F$ and 2.3 $2RT/5F$ are both close to the experimental value). Inspection of the schemes given by Bockris (11) and Hackerman (18) shows that none gives both slopes in the *same* reaction scheme; but in different schemes (i.e., alternative pathways) processes leading to one or other of these slopes occur (11). We may examine, however, the following consecutive reaction schemes for anodic oxygen evolution, which have not previously been considered:

$$M + OH^- \rightarrow MOH + e, \tag{12}$$

$$MOH + OH^- \rightarrow MO + H_2O + e, \tag{13}$$

$$MO + MOH \rightarrow MHO_2, \tag{14}$$

$$MHO_2 + MOH \rightarrow M + H_2O + O_2; \tag{15}$$

here M signifies the electronically conducting bulk oxide phase rather than the base metal as previously considered (11), since the electrochemical oxygen evolution occurs at the surface of the oxide (19) rather than at that of the metal. The present treatment differs only from previous approaches in that we regard the transient radical species as adsorbed at the oxide–solution interphase rather than at the metal–solution interphase. At the same time, the OH^- ion being discharged may be adsorbed (see 18 and below).

For the series of consecutive reactions [12] to [15], the rates v are given by

$$v_{12} = k_{12}\, C_{OH^-}(1 - k'\, C_{MOH} - k''\, C_{MO})e^{\Delta\phi F/2RT},$$
$$v_{-12} = k_{-12}\, C_{MOH}\, e^{-\Delta\phi F/2RT},$$
$$v_{13} = k_{13}\, C_{MOH}\, C_{OH^-}\, e^{\Delta\phi F/2RT},$$
$$v_{-13} = k_{-13}\, C_{MO}\, e^{-\Delta\phi F/2RT},$$
$$v_{14} = k_{14}\, C_{MOH}\, C_{MO},$$
$$v_{-14} = k_{-14}\, C_{MHO_2},$$
$$v_{15} = k_{15}\, C_{MHO_2}\, C_{MOH},$$

where C_{OH^-} is the concentration of hydroxyl ions in the double layer and $\Delta\phi$ is the potential difference between the electrode and the outer Helmholtz layer, k' and k'' are constants relating fractional surface coverage by intermediates to their surface concentrations (or activities). The symmetry factor for the charge-transfer steps is taken as 0.5 (cf. 13). In order to obtain the Tafel slopes for various rate-determining steps in the above scheme, we calculate the Christiansen coefficients w for each step as

$$w_{12} = k_{12}\, C_{OH^-}\, e^{\Delta\phi F/2RT},$$
$$w_{-12} = k_{12}k'\, C_{OH^-}\, e^{\Delta\phi F/2RT} + k_{12}k''\, C_{OH^-}{}^2\, K_{13}\, e^{3\Delta\phi F/2RT} + k_{-12}\, e^{-\Delta\phi F/2RT},$$

if C_{MOH} and C_{MO} are both appreciable, i.e., if [14] is rate-determining; or as

$$w_{-12} = k_{12}k'\, C_{OH^-}\, e^{\Delta\phi F/2RT} + k_{-12}\, e^{-\Delta\phi F/2RT},$$

if only C_{MOH} is appreciable, i.e., if [13] is rate-determining. K_{13} is the quasi-equilibrium constant for [13] in the steady state if [14] is rate-determining. Other w values are

$$w_{13} = k_{13}\, C_{OH^-}\, e^{\Delta\phi F/2RT},$$
$$w_{-13} = k_{-13}\, e^{-\Delta\phi F/2RT},$$
$$w_{14} = k_{14}\, C_{MOH},$$
$$w_{-14} = k_{-14},$$

and

$$w_{15} = k_{15}\, C_{MOH}.$$

If step [13] is rate-determining, the over-all velocity is then

$$v = \frac{k_{12}k_{13}\,C_{OH}\text{-}2\;e^{\Delta\phi F/RT}}{k_{12}k'\,C_{OH}\text{-}\,e^{\Delta\phi F/2RT}+k_{-12}\,e^{\Delta\phi F/2RT}}\;,$$

which at relatively low potentials gives

[16] $$v = K_{12}k_{13}\,C_{OH}\text{-}^2\,e^{3\Delta\phi F/2RT};$$

and if [14] is rate-determining, and at relatively low potentials

[17] $$v = K_{12}{}^2 K_{13}k_{14}\,C_{OH}\text{-}^3\,e^{3\Delta\phi F/RT}$$

where K_{13} is the quasi-equilibrium constant for [13] when [14] is rate-determining. Equations [16] and [17] give the Tafel b constants as

$$b_{13} = 2.3\,(2RT/3F) \text{ and } b_{14} = 2.3RT/3F.$$

For [12] as the rate-determining step, b has the usual value of $2.3\,(2RT/F)$. The slopes for the decay in the low potential region could also be close to the value $2.3\,(2RT/5F)$ which differs from $2.3\,RT/3F$ by only 4 mv. The scheme in equations [12] to [15] could be modified by changing process [14] to a charge-transfer reaction as follows:

$$M + OH^- \rightarrow MOH + e, \tag{12}$$

$$MOH + OH^- \rightarrow MO + H_2O + e, \tag{13}$$

$$MO + OH^- \rightarrow MHO_2 + e, \tag{14a}$$

$$MHO_2 + MOH \rightarrow M + H_2O + O_2. \tag{15}$$

The mathematical analysis then gives the Tafel slope for process [14a], if it were rate-determining, as $b = 2.3\,(2RT/5F)$, with b for process [13] still as $2.3\,(2RT/3F)$.

The schemes in equations [12] to [15] through [14] or [14a] are the only ones which can be formulated (cf. 13, 21) in which there are *two consecutive* steps in a single reaction path having Tafel slopes in agreement with those observed in the present work, and from which the correct *sequence* of slopes (viz. 0.038 at higher potentials followed by 0.021 at lower potentials, if [14] becomes rate-determining) can be deduced. The reactions in either of the schemes [12] to [15] hence appear to offer a satisfactory explanation of the experimental results at present available. Distinction between [14] and [14a] as mechanisms for the low potential process must await a rather more accurate determination of the slopes. With decreasing electrode potential on decay, [14] can tend to become slower than [13], and hence rate-determining, since the rate of [14] is more strongly dependent $(e^{3\Delta\phi F/RT})$ on potential than of that of [13].

In very strong solutions the Tafel slope for the high potential process changes towards the value 0.029; this could occur (11, 18) if recombination desorption of adsorbed OH radicals replaced the discharge process indicated in reaction [13].

In the absence of excess electrolyte, e.g., K_2SO_4, not participating in the discharge reaction, all mechanisms should lead to rates independent of activity of OH^- ions (11). In the present work, however, the observed rates of both steps in the self-discharge are increased with increasing KOH activity. This effect probably arises from specific adsorption of OH^- ions on the surface of the polar oxide lattice, as has been indicated in the case of anodic processes at the iron electrode (18).

ACKNOWLEDGMENTS

REFERENCES

1. GLEMSER, O. and EINERHAND, J.   Z. anorg. Chem. **261**, 26 (1950).
2. BRIGGS, G. W. D. and WYNNE-JONES, W. F. K.   Trans. Faraday Soc. **52**, 1272 (1956).
3. JONES, E. and WYNNE-JONES, W. F. K.   Trans. Faraday Soc. **52**, 1260 (1956).
4. PITMAN, A. L. and WORK, G. W.   Naval Research Lab. Rept. 4844 (1956); 4845 (1956).
5. CASEY, E. J., BOURGAULT, P. L., and LAKE, P. E.   Can. J. Technol. **34**, 95 (1956).
6. FLEISCHER, A.   Trans. Electrochem. Soc. **94**, 289 (1948).
7. AZZAM, A. M., BOCKRIS, J. O'M., CONWAY, B. E., and ROSENBERG, H.   Trans. Faraday Soc. **46**, 918 (1950).
8. AKERLOF, G. C. and BENDER, P.   J. Am. Chem. Soc. **70**, 2366 (1948).
9. ARMSTRONG, G. and BUTLER, J. A. V.   Trans. Faraday Soc. **29**, 1261 (1933).
10. MORLEY, H. B. and WETMORE, F. E. W.   Can. J. Chem. **34**, 359 (1956).
11. BOCKRIS, J. O'M.   J. Chem. Phys. **24**, 817 (1956).
12. ELINA, C. M., BORISOVA, T. K., and ZALKIND, T. I.   Zhur. Fiz. Khim. **28**, 785 (1953).
13. BOCKRIS, J. O'M. and POTTER, E. C.   J. Chem. Phys. **20**, 614 (1952).
14. FOERSTER, F.   Z. Elektrochem. **13**, 414 (1907); **14**, 17 (1908). ZEDNER, J.   Z. Elektrochem. **11**, 809 (1905); **12**, 463 (1906).
15. SIDGWICK, N. V.   Chemical elements and their compounds. Vol. II. Oxford University Press, London. 1950. p. 1451.
16. KLEMM, W.   Angew. Chem. **66**, 468 (1954). BESSON, J.   Compt. rend. **222** (No. 7), 390 (1946).
17. BESSON, J.   Compt. rend. **220** (No. 7), 320 (1945).
18. WADE, W. H. and HACKERMAN, N.   Trans. Faraday Soc. **53**, 1636 (1957).
19. KUCHINSKII, E. and ERSCHLER, B. V.   Zhur. Fiz. Khim. **14**, 985 (1940).

THERMODYNAMICS OF ADSORPTION IN IONIC SYSTEMS[1]

Roger Parsons

1. INTRODUCTION

Recently we have made measurements of the electrocapillary curve of mercury in aqueous solutions of potassium iodide at different temperatures (1). The object of this work was to increase our knowledge of the behavior of specifically adsorbed ions by determining the heat of adsorption. In the interpretation of these results, we drew an analogy between the mercury-solution system and the adsorption of a gas on a condensed phase. This enabled us to use the equations developed by Everett (2) for the calculation of the thermodynamic functions accompanying the adsorption process. A similar analogy has been used by Pethica (3) and his co-workers in considering adsorption of long-chain compounds at the air–solution interphase.

In the present paper we attempt to develop the thermodynamics of interphases between two phases containing charged particles in order to find out to what extent this analogy is justified.

2. THE COMPOSITION TERM IN THE CHARACTERISTIC EQUATION

The total differential of the energy (E) of any phase of c components is given by

$$[1] \qquad dE = TdS - pdV + \sum_{i=1}^{i=c} \mu_i \, dn_i$$

where T, p, S, and V are the temperature, pressure, entropy, and volume of the phase, and n_i is the number of moles of species i whose chemical potential in the phase is μ_i. For a plane interphase the corresponding equation is

$$[2] \qquad dE^\sigma = TdS^\sigma - pdV^\sigma + \gamma dA + \sum_{i=1}^{i=c} \mu_i \, dm_i,$$

where γ is the interfacial tension, A the area of the interphase, and m_i the number of moles of i in the interphase. We regard the interphase as a region of finite thickness comprising all the inhomogeneous region between the two phases (4).

Similar equations may be written for the other thermodynamic potentials, but at present we wish to concentrate attention on their common feature: the term

$$[3] \qquad \sum_{i=1}^{i=c} \mu_i \, dm_i.$$

For an ionic interphase the summation over all components is subject to the restriction that the interphase as a whole must remain electrically neutral. This condition may readily be incorporated in expression [3] so that [2] remains a complete differential. The form of expression [3] then, however, depends upon the nature of the interphase. For a perfectly non-polarizable interphase in which there is chemical equilibrium of one or more ionic species throughout the interphase, we may simply redefine our system in terms of $c-1$ components, each of which is a neutral complex of ions, i.e., a 'salt molecule'.

Thus, in the interphase between a zinc amalgam and an aqueous solution of zinc

chloride containing hydrochloric acid, there are six components which may be chosen as: Zn^{++}, Cl^-, H^+, H_2O, Hg^+, and e. For the total differential, we may choose the five $\mu\, dm$ terms corresponding to $ZnCl_2$, HCl, H_2O, Zn, and Hg. The electroneutrality condition is then automatically satisfied. The thermodynamics of such an interphase is then precisely of the same form as that for an interphase consisting of non-ionic components only (5).

On the other hand, this form is not obtained for an interphase in which there is no ionic equilibrium between one side of it and the other, such as in the perfectly polarized electrode. In order to study such an electrode it is necessary to combine it with a second electrode, which for thermodynamic convenience is reversible to one of the ions present in the interphase of the perfectly polarized electrode. The independent components can then be chosen, as before, as 'salt molecules', of which there will be $c-2$, leaving two ionic species, one on either side of the interphase. It is usually convenient to choose electrons as one of these, since one phase is normally a metal. The amount of each of these species in the interphase is then proportional to the charge on either side of the interphase (and may be positive or negative). Thus, we may write

[4]
$$z_{c-1} F\, m_{c-1} = Q^\alpha$$

and

[5]
$$z_c F\, m_c = Q^\beta,$$

where the $(c-1)$th component of valency z_{c-1} is left on the side of the interphase adjoining phase α and the cth on that adjoining phase β. Q^α is the electrical charge on the α side of the interphase and Q^β that on the β side. Since the interphase as a whole is electrically neutral,

[6]
$$Q^\alpha + Q^\beta = 0.$$

Thus, for a perfectly polarized electrode the sum [3] becomes

[7]
$$\left(\frac{\bar\mu_{c-1}}{z_{c-1}} - \frac{\bar\mu_c}{z_c} \right) \frac{dQ^\alpha}{F} + \sum_{i=1}^{i=c-2} \mu_i\, dm_i.$$

We note, by comparing the expression [3] for perfectly polarized and non-polarized electrodes, that for each the electroneutrality condition results in the loss of one degree of freedom.

It is convenient to express the coefficient of dQ^α in [7] in terms of more readily accessible quantities. It is here that the second electrode plays its part, since (if α is the metallic phase) we can find a relation between $\bar\mu_c$ and the electrochemical potential of the electrons in the reversible electrode. In general this coefficient, which we abbreviate as ϵ, is related to the measured e.m.f. E between these two electrodes through a constant K;

[8]
$$\left(\frac{\bar\mu_{c-1}}{z_{c-1}} - \frac{\bar\mu_c}{z_c} \right) \frac{1}{F} = \epsilon = E + K,$$

where K is a sum of chemical potentials of neutral substances. For example, in the cell

[9]
$$\text{Hg}' \mid \text{Hg}_2\text{Cl}_2 \mid \text{BaCl}_2, \text{HCl}, \text{H}_2\text{O} \mid e \mid \text{Hg}''$$
$$\text{(sat)}$$
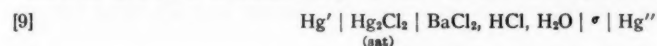
we have six components in the interphase: Ba^{++}, H^+, Cl^-, H_2O, Hg^+, and e^-. One choice of independent components would be $BaCl_2$, HCl, H_2O, Hg with Cl^-, and e^- regarded as constituting the charge. The constant K in [8] thus becomes

[10] $$K = \frac{\mu_{Hg} - \mu_{HgCl}}{(-1)F}.$$

3. CHARACTERISTIC EQUATIONS

In view of equations 2.7 and 2.8 we can write the analogue of 2.1 for a perfectly polarized electrode as

[1] $$dE^\sigma = TdS^\sigma - PdV^\sigma + \gamma dA + \epsilon dQ^\alpha + \sum_{i=1}^{i=c-2} \mu_i \, dm_i.$$

From equation [1] we may derive in the usual way complete differentials for the other characteristic thermodynamic potentials H^σ, F^σ, and G^σ. It has been pointed out by Guggenheim and by Everett (2) that, unlike a bulk phase, which has these four characteristic equations, a surface phase has eight. The additional four are defined in terms of the thermodynamic potentials $\mathfrak{E}$, $\mathfrak{H}$, $\mathfrak{F}$, and $\mathfrak{G}$ which are defined by equations such as*

[2] $$\mathfrak{E} = E^\sigma - \gamma A,$$
$$\vdots \qquad \vdots$$
$$\mathfrak{G} = G^\sigma - \gamma A.$$

The presence of the electrical energy term ϵdQ^α in the characteristic equation for a perfectly polarized electrode means that the number of characteristic equations is doubled again, since we can write equations for the thermodynamic potentials E_e, H_e, F_e, G_e, $\mathfrak{E}_e$, $\mathfrak{H}_e$, $\mathfrak{F}_e$, and $\mathfrak{G}_e$ which are defined by equations such as

[3] $$E_e = E^\sigma - \epsilon Q^\alpha$$
$$\vdots \qquad \vdots$$
$$\mathfrak{G}_e = \mathfrak{G} - \epsilon Q^\alpha.$$

For example,

[4] $$d\mathfrak{G}_e = -S^\sigma dT + V^\sigma dp - Ad\gamma - Q^\alpha d\epsilon + \sum_{i=1}^{i=c-2} \mu_i \, dm_i.$$

We may contrast [4] with the characteristic equations for the perfectly non-polarized electrode, since for the latter there is no term in Q^α and ϵ. Consequently, there are only eight characteristic equations which are the same as for a non-ionic interphase. The same is true if we restrict consideration of a perfectly polarized electrode to the condition $Q^\alpha = 0$ (the point of zero charge), since again the Q^α, ϵ term vanishes. This may be regarded as the state of affairs at an air–solution interphase.

4. HEATS OF ADSORPTION

It follows from Section 3 that just as there are four different heats of adsorption for a gas on a solid, there will be eight if the interphase is perfectly polarized. There is, however, a further complication due to the fact that we are necessarily dealing with a system of more than one adsorbed component. In dealing with a one-component system, Everett (2) was able to consider the adsorbed phase as a pure component and effectively to use in place of 3.1

[1] $$dE^\sigma = TdS^\sigma - PdV^\sigma + \gamma dA, \text{ etc.}$$

*To avoid confusion it must be noted that the quantities represented by 'German' capitals without subscripts are the same as those for which Everett (2) used 'Script' capitals.

From equations of this type, we obtain heats of adsorption in two classes: at constant surface pressure and at constant amount adsorbed. There are no exact analogues for a multicomponent system.

We consider as an example the heat of adsorption related to 4.4. By cross-differentiating, we obtain

[2]
$$\left(\frac{\partial \mu_j}{\partial T}\right)_{m_i, p, \gamma, \epsilon} = -\left(\frac{\partial S}{\partial m_j}\right)_{T, p, \gamma, \epsilon, m_i \neq m_j}.$$

Solving for dS the characteristic equation for $\mathfrak{H}_e$ and differentiating with respect to m_j while keeping T, p, γ, ϵ, and the other m_i constant, we obtain

[3]
$$\left(\frac{\partial S}{\partial m_j}\right)_{T, p, \gamma, \epsilon, m_i \neq m_j} = \frac{1}{T}\left[\left(\frac{\partial \mathfrak{H}_e}{\partial m_j}\right)_{T, p, \gamma, \epsilon, m_i \neq m_j} - \mu_j\right],$$

whence

[4]
$$\left[\frac{\partial(\mu_j/T)}{\partial T}\right]_{m_i, p, \gamma, \epsilon} = -\frac{\bar{\mathfrak{H}}_e}{T^2},$$

where $\bar{\mathfrak{H}}_{e,j} = (\partial \mathfrak{H}_e/\partial m_j)_{T, p, \gamma, \epsilon, m_i \neq m_j}$ is the interfacial partial molar electrochemical heat content of species j. The Clausius–Clapeyron equation is obtained from [4] by subtracting the corresponding equation for j in its standard state in the bulk phase. A complete analysis (which is too lengthy to present here) shows that all the Clausius–Clapeyron equations involve differentiating the chemical potential with respect to temperature at constant surface composition* and so all the corresponding heats are 'isosteric', although they differ according to which of three other pairs of variables are kept constant: (p, V), (γ, A), and (Q, ϵ). It must be emphasized that this conclusion applies to any type of interphase. Thus, it is only when we have a rather complete knowledge of the interfacial composition that we can determine heats of adsorption by means of the Clausius–Clapeyron equations.

5. THE GIBBS–DUHEM EQUATION

We can obtain the interfacial analogue of the Gibbs–Duhem equation from any of the characteristic equations by the usual methods

[1]
$$S^\sigma dT - V^\sigma dp + A d\gamma + Q \alpha d\epsilon + \sum_{i=1}^{i=c-2} m_i d\mu_i = 0.$$

This equation is well known as the basic electrocapillary equation (6). However, there is one feature by which [1] differs from the equation normally employed: the term $Q d\epsilon$. This is usually written with the cell e.m.f. E in place of ϵ. These quantities are related by 2.8 and it is clear that while $d\epsilon$ can be equated to dE at constant temperature (cf. 2.10), this assumption is not correct where temperature variations are to be considered.

It is possible to eliminate two variables from [1] by taking into account the Gibbs–Duhem equations for the adjoining phases. We write these in the form:

[2]
$$d\mu_1 = -\frac{S^\alpha}{n_1{}^\alpha} dT + \frac{V^\alpha}{n_1{}^\alpha} dp - \sum_{i \neq 1} \frac{n_i{}^\alpha}{n_1{}^\alpha} d\mu_i,$$

[3]
$$d\mu_2 = -\frac{S^\beta}{n_2{}^\beta} dT + \frac{V^\beta}{n_2{}^\beta} - \sum_{i \neq 2} \frac{n_i{}^\beta}{n_2{}^\beta} d\mu_i,$$

*We have ignored here the effect of the neighboring phases on the number of degrees of freedom in equations like 3.4. For a perfectly polarized electrode this reduces the number of independent composition variables by two.

and substitute in [1] the values of $d\mu_1$ and $d\mu_2$ the changes in the chemical potentials of the reference substances 1 and 2. If at the same time we divide through equation [1] by the area of the interphase A, we obtain:

[4]
$$sdT - vdp + d\gamma + qd\epsilon + \sum_{i=3}^{i=c-2} \Gamma_i d\mu_i = 0,$$

where

[5]
$$s = \left(S^\sigma - \frac{m_1}{n_1^\alpha} S^\alpha - \frac{m_2}{n_2^\beta} S^\beta \right) \Big/ A,$$

[6]
$$v = \left(V^\sigma - \frac{m_1}{n_1^\alpha} V^\alpha - \frac{m_2}{n_2^\beta} V^\beta \right) \Big/ A,$$

[7]
$$q = Q^\alpha / A,$$

[8]
$$\Gamma_i = \left(m_i - \frac{m_1}{n_1^\alpha} n_i^\alpha \right) \Big/ A,$$

or

[9]
$$\left(m_i - \frac{m_2}{n_2^\beta} n_i^\beta \right) \Big/ A.$$

It is frequently convenient to consider the adsorption of one substance taking as a starting point the system in the absence of this substance at the same T, p, ϵ, and μ_i for other components. If we consider the adsorption of component 3, then for the base system, equation [4] becomes

[10]
$$s^\circ dT - v^\circ dp + d\gamma^\circ + q^\circ d\epsilon + \sum_{i=4}^{i=c-2} \Gamma_i^\circ d\mu_i = 0.$$

Subtracting [4] from [10], we obtain

[11] $$(s^\circ - s)dT - (v^\circ - v)dp + d\pi + (q^\circ - q)d\epsilon + \sum_{i=4}^{i=c-2} (\Gamma_i^\circ - \Gamma_i)d\mu_i - \Gamma_3 d\mu_3 = 0,$$

where $\pi = \gamma^\circ - \gamma$ is the surface pressure associated with component 3. We can use [11] to calculate the effect of component 3 on various properties of the interphase, e.g.,

[12]
$$(\partial\pi/\partial\mu_3)_{T,p,\epsilon,\mu_i \neq \mu_3} = \Gamma_3,$$

[13]
$$(\partial\pi/\partial T)_{p,\epsilon,\mu_i} = s - s^\circ,$$

[14]
$$(\partial\mu_3/\partial T)_{p,\pi,\epsilon,\mu_i \neq \mu_3} = -(s - s^\circ)/\Gamma_3,$$

etc.

6. CHANGE OF VARIABLE TO ξ

In previous work we have argued that it is useful to consider changes in the composition of the interphase of a perfectly polarized electrode at a constant value of q. For convenience in calculation we have defined a new variable

[1]
$$\xi = \gamma + qE.$$

However, it is evident from the foregoing that when temperature variation is to be considered, a better definition would be

[2]
$$\xi = \gamma + q\epsilon.$$

Equation 5.4 then becomes

[3]
$$sdT - vdp + d\xi - \epsilon dq + \sum_{i=3}^{i=c-2} \Gamma_i d\mu_i,$$

and the analogue of 4.11, if we consider introducing component 3 to the base system, this time keeping q and not ϵ constant, is

[4]
$$(s^\circ - s)dT - (v^\circ - v)dp + d\Phi + (\epsilon^\circ - \epsilon)dq + \sum_{i=4}^{i=c-2} (\Gamma_i^\circ - \Gamma_i)d\mu_i - \Gamma_3 d\mu_3 = 0,$$

where
$$\Phi = \xi^\circ - \xi.$$

Again we can calculate the effect of component 3 on various properties of the interphase and obtain analogues of 5.12, 5.13, 5.14, etc.

[5]
$$(\partial \Phi / \partial \mu_3)_{T,p,q,\mu_i \neq \mu_3} = \Gamma_3,$$

[6]
$$(\partial \Phi / \partial T)_{p,q,\mu_i} = s - s^\circ,$$

[7]
$$(\partial \mu_3 / \partial T)_{p,\Phi,q,\mu_i \neq \mu_3} = -(s - s^\circ)/\Gamma_3.$$

Thus, we find that the same quantities may be calculated by two different routes. It is also evident that there is no advantage in principle in using [4] rather than 5.11, since the same quantities may be obtained from either. However, there may be practical advantages in a particular problem which would lead one to use one equation rather than the other.

It may be remarked here that our previous use of [1] in calculations from electrocapillary curves at different temperatures, which is incorrect in principle, has in fact led to no error because even with temperature varying

[8]
$$E^\circ - E = \epsilon^\circ - \epsilon$$

and we have used equations based on equation [4] in which only $\epsilon^\circ - \epsilon$ appears.

7. APPLICATION TO EXPERIMENT

The systems used up to now consist of an aqueous electrolyte CA in contact either with air (3) or with mercury (1). Provided that the electrolyte has no tendency to hydrolyze so that the effect of the ionization of water may be neglected, the terms under the summation sign in 5.11 and 6.4 vanish. We identify component 3 with the electrolyte CA. Under these conditions 5.14 reduces, for the air–solution interphase to

[1]
$$(\partial \mu_{CA} / \partial T)_{p,\pi} = -(s - s^\circ)/\Gamma_{CA},$$

while 6.7 for the mercury–solution interphase becomes

[2]
$$(\partial \mu_{CA} / \partial T)_{p,\Phi,q} = -(s - s^\circ)/\Gamma_{CA}.$$

[1] and [2] are identical if $q = 0$, so that we need only consider [2]. The so-called integral or isotensile heats of adsorption, which have been obtained for these interphases, have been calculated from the expression

[3]
$$\left[\frac{\partial (\mu_{CA} - \mu_{CA}^\circ)/T}{\partial T} \right]_{p,\Phi,q} = -\frac{\Delta h}{T^2}$$

where μ_{CA}° is the standard chemical potential of CA and

[4]
$$\Delta h = h - H_{CA}^\circ.$$

$H_{CA}°$ is the heat content of CA in its standard state. Since it is well known that

[5]
$$\left[\frac{\partial(\mu_{CA}°/T)}{T}\right]_p = -\frac{H_{CA}°}{T^2}$$

we need only investigate the meaning of the remaining part of [3] involving μ_{CA} and h. From [2] it follows that

[6]
$$\left[\frac{\partial(\mu_{CA}/T)}{\partial T}\right]_{p,\Phi,q} = -\frac{1}{T^2}\left\{\frac{T(s-s°)}{\Gamma_{CA}} + \mu_{CA}\right\} = -\frac{h}{T^2}.$$

It is evident from [6] that h is none of the thermodynamic potentials defined above. Therefore, in general, the heat of adsorption obtained from [3] has no simple significance. However, if it is assumed that the change in the interfacial entropy when CA is adsorbed can be ascribed entirely to CA and also that it is a linear function of the amount adsorbed, then we can put

[7]
$$\frac{s-s°}{\Gamma_{CA}} = \left(\frac{\partial S\sigma}{\partial m_{CA}}\right)_{T,p},$$

and

[8]
$$h = \bar{H}\sigma = \bar{\mathfrak{H}} = \bar{H}_e = \bar{\mathfrak{H}}_e,$$

i.e., the distinction between the various partial heat contents of the adsorbed phase vanishes. Thus, under these rather specialized conditions Δh has a satisfactory interpretation in terms of the change of a thermodynamic potential. For other conditions it would seem preferable to calculate the change in entropy of the interphase from 5.7 or 6.6 first, before attempting an interpretation in terms of a model.

On the other hand the isosteric heat of adsorption can be calculated from the rate of change of chemical potential with respect to temperature, if as well as the surface composition, one of each of the conjugate pairs of variables (γ, A), (q, ϵ) is kept constant (cf. 4.4). These conditions can be attained in practice, but if the surface concentration is obtained from interfacial tension measurements it is difficult to obtain accurate results.

Results of measurements of the Hg/KI(aq) system have previously been presented (1) in the form of curves of $-\Delta h$ and $[(s-s°) - \bar{S}_{KI}°]/\Gamma_{KI}$ against Γ_{KI}, although they were originally interpreted as isotensile heat and differential entropy curves. At higher coverages it was found that the entropy was approximately independent of coverage. In this region, it follows from the above that the heats of adsorption are simply differences of heat content in the two states. At lower coverages the interpretation is more complex; consequently, it appears that no thermodynamic error has been made in the discussion of these results except at the low coverages.

A further important result of the above analysis is that the thermodynamic quantities, in particular the entropy, can be calculated for any point on the electrocapillary curve, whereas the previous method was in practice limited to the region of a negative charge on the mercury surface. We hope to present some of these results for specifically adsorbed systems in the near future.

REFERENCES

1. ANDERSON, W. and PARSONS, R.   Proc. 2nd Intern. Congr. Surface Activity, III, 45 (1957).
2. EVERETT, D. H.   Trans. Faraday Soc. 46, 453 (1950).
3. ANDERSON, P. J. and PETHICA, B. A.   Trans. Faraday Soc. 52, 1080 (1956). BETTS, J. J. and PETHICA, B.A.   Proc. 2nd Intern. Congr. Surface Activity, I, 152 (1957).
4. GUGGENHEIM, E. A.   Trans. Faraday Soc. 36, 397 (1940).
5. GUGGENHEIM, E. A.   Thermodynamics. North-Holland Pub. Co., Amsterdam. 1949. p. 326.
6. PARSONS, R.   Modern aspects of electrochemistry. Edited by Bockris, J. O'M. Butterworth Scientific Publications, London, 1954. Chap. III.

THE ADSORPTION OF METHYLENE BLUE ON A POSITIVELY CHARGED MERCURY SURFACE[1]

J. M. Los and C. K. Tompkins

ABSTRACT

Direct measurement of the surface concentration Γ of methylene blue, adsorbed from a phosphate buffer solution onto an ideally polarized mercury electrode, has produced a Langmuir-type isotherm. The maximum value of Γ, Γ_m, was found to be dependent on the potential applied (E). Surface tension measurements showed that the rate-controlling process is not diffusion, but, presumably, the exchange of methylene blue cation (MB^+) with phosphate ions. A model for this process has been proposed. This allowed the calculation of the rate constant of adsorption (k_a) from the surface tension values as a function of time ($k_a \sim 5 \times 10^{-5}$ cm/sec; $dk_a/dE \sim 30 \times 10^{-5}$). There is some evidence for the occurrence of a consecutive process, most likely the combination of adsorbed MB^+ to dimers.

INTRODUCTION

It is well known that the presence of organic substances that will adsorb on mercury may change the characteristics of polarographic current–voltage waves of depolarizers. Even "reversible" waves can be affected. Much less is known about the effect on half-wave potential and limiting current that inorganic ions, mostly anions, may have. This problem should become interesting when the depolarizer is a big organic molecule, if it has to occupy a relatively large area of the electrode surface before electron transfer can take place. Alternatively, no adsorption of the compound may be needed for the latter, if only the electrons could be transferred by way of the Helmholtz part of the double layer. It is, therefore, of interest to find a compound which adsorbs more slowly than is required for reversibility (the rate constant of the electrode reaction at the latter's standard potential must be at least 10^{-2} cm sec^{-1} (1)). The experimental correlation between adsorption and reduction should thus enable one to decide upon the above-mentioned question of the mode of electron transfer.

The present paper will be concerned with an approach to this problem, namely a study of the kinetic parameters of adsorption of the compound methylene blue (MB^+Cl^-) on an ideally polarized mercury electrode, the solution being buffered by phosphate ($C_{HPO_4^=} = 0.05$; $C_{H_2PO_4^-} = 0.05$ moles/liter; pH is about 7).

The range of potentials available for ideal polarization is rather narrow. A polarogram shows that this range lies between anodic mercury dissolution, starting at $+0.2$ v (due to insolubility of Hg_2HPO_4, not of Hg_2Cl_2) and methylene blue reduction ($E_{\frac{1}{2}} \sim -0.2$ v; actually there is a small prewave, which, according to Brdicka (2), is due to the strong adsorption of reduced or leuco methylene blue). It was desirable to do measurements at more than one potential. The work presented here was done at -0.024 and $+0.076$ v (with respect to S.C.E.), i.e., 0.1 v apart.

MEASUREMENTS

Two types of measurements were performed, at 25° C.

(1) *Direct measurement of the surface concentration (excess) of methylene blue.*—This was achieved by means of an apparatus based on the principle of allowing the surface of many successive mercury drops at constant potential, to come to equilibrium with the

surrounding methylene blue solution before the drops are dislodged and separated from the solution (together with their adhering double layer). Finally all unite and reject their skins of solution into a common pool. The concentration difference between this collected solution and the original one is then directly related to the actual surface excess. Although the essential features of this apparatus have been described previously (3), a few additional remarks need to be made concerning its operation (see Experimental Section).

(2) *Measurements of the surface tension by the drop-weight method, as a function of time, potential, and concentration.*—Craxford and McKay (4) have shown that this method yields values as precise as the capillary electrometer. Surface tension and surface concentration are, of course, related to each other by the Gibbs adsorption equation,

$$[1] \qquad\qquad d\gamma = - \sum_i \Gamma_i d\mu_i{}^\alpha - qdE,$$

where α is the solution phase. This equation may only be applied if equilibrium has been attained.

RESULTS

The experimental points of Fig. 1, which shows the results of the surface concentration (Γ) measurements, bear out that we have a Langmuir-type isotherm. Each point is an average of three to six measurements. This number was taken in order to test for differences with change in radius of the mercury drops, curvature of the solution–nitrogen interface, and drop time. Values of the latter around 3.6, 25, and 50 seconds were usually taken. Taking into account that the average deviation of a single measurement from the mean value was about 3–5%, no dependence on drop radius and interface curvature could be established. Apparently, at the lowest concentrations ($c \sim 10^{-8}$ moles/cm³) the influence of the drop time has made itself felt (see Fig. 1). These particular points have, therefore, not been included in the least-square evaluation of the straight line.

Results of the surface tension (γ) measurements have been given as γ vs. t plots for five different concentrations in Fig. 2A (for -0.024 v) and Fig. 3A (for $+0.076$ v).
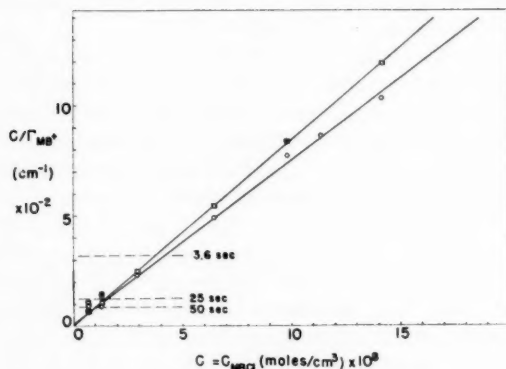
Fig. 1.   The constants of the lines $c/\Gamma = a + bc$ are:
Lower line at -0.024 v: $b = (7.40\pm0.11)\times10^9$ cm³/mole; $a = 10\pm9$ cm^{-1}.
Upper line at $+0.076$ v: $b = (8.37\pm0.03)\times10^9$ cm³/mole; $a = 5\pm2$ cm^{-1}.
(Deviations are probable errors.) For broken lines see text.

DISCUSSION

Surface Concentration Measurements

At first glance (Fig. 1) these measurements seem to provide ample proof that equilibrium with the solution has been approached quite closely, except for the low concentration points with drop time around 3.6 seconds. Since the c/Γ vs. c lines go nearly through the origin (according to the surface tension measurements even more so than indicated by the intercept (a) values in the caption to Fig. 1), the isotherm must have a very steep ascending branch and for all concentrations measured Γ_e should be closely equal to Γ_m (Γ_e is the equilibrium value, Γ_m is the maximum value of the surface concentration). This means that the minimum time necessary to reach equilibrium may be calculated from the Ilkovic equation (5),

$$[2] \qquad \Gamma_t = \frac{6}{7}(7/3)^{\frac{1}{2}}(D^{\frac{1}{2}}t^{\frac{1}{2}}/\pi^{\frac{1}{2}})c ,$$

where Γ_t is the maximum possible surface concentration at time t and D is the diffusion coefficient, here taken as 5×10^{-6} cm^2 sec^{-1}. The c/Γ_t values calculated from equation [2] for the drop times 3.6, 25, and 50 seconds, respectively, have been indicated in Fig. 1 by three horizontal broken lines. Measured points could not have reached equilibrium within 3.6, etc., seconds if they should fall below the corresponding line, and the reverse of this statement is approximately true as well. Whereas the low concentration points *included* in the calculation of the line had been taken at drop times 25 or 50 seconds, the corresponding 3.6-second points should have been at the level of the upper line. Of course, stirring of the solution by the falling drop invalidates equation [2] and speeds up the diffusion process. Such points, however, are of no value, since the potential of a falling drop changes rapidly if equilibrium has not been attained before it is released from the electrode.*

However, the surface tension measurements show clearly that a much slower process than diffusion must be rate-controlling, since γ continues to decrease for c/Γ values much in excess of the critical c/Γ values indicated by the horizontal lines in Fig. 1. From the analysis of the γ vs. t plots it follows that Γ_e would apply for drop times of 50 seconds and $c > 10\times10^{-8}$ moles/cm^3. The isotherm lines in Fig. 1 must therefore have the correct slope, while their intercepts could hardly be less within experimental error. Again considering the fact that the 3.6-second points are much lower than they should be, it follows that a mechanism other than stirring must be operating while the drops fall, so as to accelerate the surface adsorption.

Since $b = 1/\Gamma_m$ it follows that Γ_m (-0.024 v) $= 1.35\times10^{-10}$ and Γ_m ($+0.076$ v) $= 1.20\times10^{-10}$ moles/cm^2. These values have a precision of about 1%, and are in the sequence expected: the phosphate ions, in particular HPO$_4^-$, are more strongly held and the ions MB$^+$ more strongly repelled by the surface at the higher potential.

The Γ_m values correspond to an area/molecule of 1.22 Å^2 at -0.024 v and 1.39 Å^2 at $+0.076$ v, which values indicate that there is still phosphate left on the surface at "complete" coverage with MB$^+$. (A value of 90 Å^2 would probably be closer to the true area of a molecule.)

*The apparatus constructed by Kalousek and Blahnik (6), which is quite analogous to ours, has rapid dropping combined with a very long path of the drops through the solution. In principle, this long path should not be necessary.

Surface Tension Measurements

Gibb's adsorption equation does not apply to non-equilibrium cases, such as the γ vs. t plots of Figs. 2A and 3A. In order to find the change of γ with time we must treat the adsorption layer as a separate phase (σ), theoretically in equilibrium with the surrounding solution (α) at infinite time only. For the surface phase then, we have at constant potential,

$$[3] \qquad\qquad d\gamma = -\sum_i \Gamma_i d\mu_i^\sigma,$$

Γ_i being the surface concentration of species i and $\Gamma_i = \Gamma_i^\sigma(t,c,E)$.
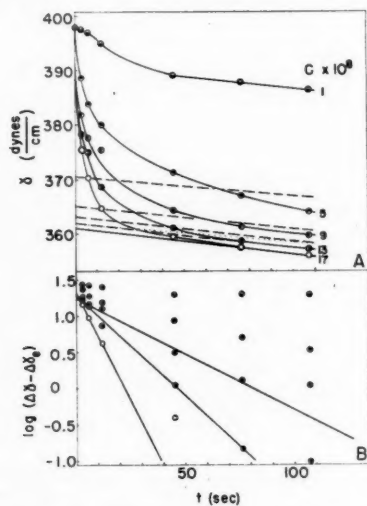
FIG. 2.   A. γ vs. t plots for -0.024 v (S.C.E.). For broken and dotted lines see text.
B. Plot of points from 2A according to equation [12].

We now shall postulate the following model:

(*a*) If σ is considered as an ordinary phase, only differing from the latter in its property of surface tension, we may write,

$$[4] \qquad\qquad \mu_i^\sigma = \mu_i^{\sigma,0} + R^*T \ln \Gamma_i/\Gamma_{i,e},$$

where

$$[5] \qquad\qquad \mu_i^{\sigma,0} = \mu_i^{\alpha,0} + RT \ln a_{i,e}.$$

Equation [5] assures that $\mu_i^\sigma = \mu_i^\alpha$ for $\Gamma_i = \Gamma_{i,e}$. It can be shown quite generally that $R^* = Rd \ln a_i/d \ln \Gamma_i$. As a first approximation R^* will be taken as independent of Γ_i.

(*b*) Chloride ions do not adsorb in significant quantity. The only species entering into equation [3] is MB$^+$. Although these cations are known to dimerize to some extent in solution (the dimer concentration is about 1.2×10^{-8} at a total concentration of 10^{-7} moles/cm^3 (7)), we shall assume monomers (M) only.

(*c*) The rate of reaching equilibrium at the surface is entirely determined by the interchange of MB$^+$ with phosphate ions. Consequently, the volume concentration of

MB^+ is constant up to the surface $(c_M = c)$ and the equilibrium to be established is
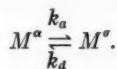
$$M^\alpha \underset{k_d}{\overset{k_a}{\rightleftharpoons}} M^\sigma.$$

(d) A Langmuir-type isotherm applies to the adsorption of M, as suggested by Fig. 1,

[6] $c/\Gamma_e = a+bc,$

where

$$a = a'/\Gamma_m = k_d/k_a\Gamma_m$$

and

$$b = 1/\Gamma_m.$$

(e) No surface activity coefficients will be considered. Constant ionic strength of the solution α does not guarantee the same in the surface phase.

(f) Expansion of the mercury drops, as used in the drop-weight method, will be neglected in the first analysis.

From (a), equation [4], we obtain

[7] $d\mu_M{}^\sigma = R^*T\, d\ln\Gamma_M.$

Substitution of equation [7] into equation [3] gives, considering (b) and (c),

[8] $d\gamma = -R^*T\, d\Gamma_M.$

Now we must find $\Gamma_M(t)$. According to (c),

$$\left(\frac{\partial\Gamma_M}{\partial t}\right)_{E,c} = k_ac(1-\theta)-k_d\theta.$$

Putting $\theta = \Gamma_M/\Gamma_m$, and substituting equation [6],

$$\left(\frac{\partial\Gamma_M}{\partial t}\right)_{E,c} = k_ac\left(1-\frac{\Gamma_M}{\Gamma_{M,e}}\right).$$

Upon integration:

[9] $\Gamma_M = \Gamma_{M,e}(1-e^{-k_act/\Gamma_{M,e}}).$

Now, substituting equation [9] into equation [8] and integrating:

[10] $\Delta\gamma = -R^*T\Gamma_{M,e}(1-e^{-k_act/\Gamma_{M,e}}).$

For $t \to \infty$, $\Delta\gamma \to \Delta\gamma_e$, and this establishes

[11] $R^*T = -\Delta\gamma_e/\Gamma_e.$

From equation [10] and equation [11] we derive,

[12] $\log(\Delta\gamma-\Delta\gamma_e) = \log(-\Delta\gamma_e)-(k_ac/2.303\,\Gamma_e)t.$

The surface tension falls off very rapidly at first, especially for the higher concentrations, but then it appears to decrease at a uniform rate. Rough calculations may show that this descent is too large to be caused by our postulate (f). We suggest that there may be a secondary process, slow compared with the one treated above. As a matter of fact, if we plot equation [12] as a straight line plot (Figs. 2B and 3B), we find that the best straight line can be obtained by correcting the experimental points of Figs. 2A and 3A
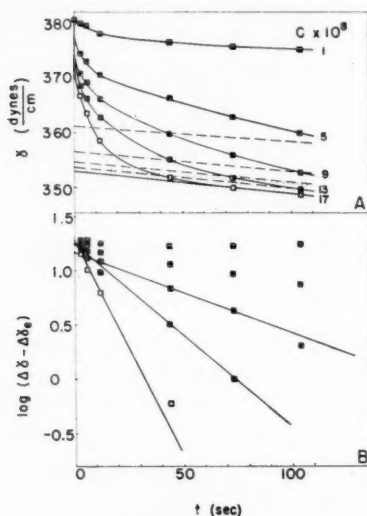
FIG. 3. A. γ vs. t plots for $+0.076$ v (S.C.E.). For broken and dotted lines see text.
B. Plot of points from 3A according to equation [12].

for this secondary process as indicated for the γ vs. t lines of $c = 17 \times 10^{-8}$. The extrapolation to $t = 0$ is not quite legitimate (see below), but this should not cause a large error. If one does not wish to admit that a consecutive process occurs, no correction is then made and $(\Delta\gamma_e) <$ smallest $\Delta\gamma$ measured. A plot according to equation [12] was found to deviate very much from a straight line in that case.

The following model would seem most logical in dealing with this secondary process:

(i) Dimers are produced on the surface in either one of two ways:

$$2\,M^\sigma \rightleftharpoons D^\sigma \text{ (homogeneous) or } M^\alpha + M^\sigma \rightleftharpoons D^\sigma \text{ (heterogeneous).}$$
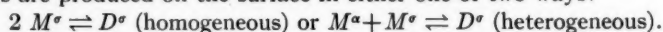
(ii) This process is so slow with respect to the first one, that at times $t > t_1$, the equilibrium under (c) remains established.

(iii) Analogous to equation [4] we have,

[13] $\mu^\sigma_D = \mu_D{}^{\sigma,0} + R^*T \ln \Gamma_D / \Gamma_{D,e},$

where

$$\mu_D{}^{\sigma,0} = 2\mu_M{}^{\sigma,0}.$$

Also, the postulates (b), (e), and (f) remain relevant.

The significance of (ii) and (e) is that $\Gamma_M = \Gamma_{M,e}$ and $\mu_M{}^\sigma = \mu_M{}^\alpha$, $(d\ \mu_M{}^\sigma = 0)$ for constant c and E, so that equation [3] now becomes

$$d\gamma = -\Gamma_D\, d\mu_D{}^\sigma$$
[14] $$= -R^*T\, d\Gamma_D \text{ (postulate (iii)).}$$

For the processes mentioned under (i) we obtain, respectively,

[15] $$d\Gamma_D = k_2 \Gamma_{M,e}{}^2\, dt,$$

or

[16] $$d\Gamma_D = k_2'\ \Gamma_{M,e} c\, dt.$$

Note that these processes are pseudo-zeroth order for $t > t_1$. Substitution of equation [16] and equation [11] into equation [14] finally gives

[17]
$$\left(\frac{\partial \gamma}{\partial t}\right)_{c,E} = -k_2 \Delta \gamma_e \Gamma_{M,e},$$

if the process is homogeneous. Alternatively, substituting equation [16] instead of equation [15], we obtain

[18]
$$(\partial \gamma / \partial t)_{c,E} = -k_2' \Delta \gamma_e c,$$

if the process is heterogeneous ($\Delta \gamma_e$ is the equilibrium value for the first process).

In Figs. 2A and 3A we have assumed that the correct slope is given by the solid straight line through the lowest two points of $c = 17 \times 10^{-8}$. Since

[19]
$$\Delta \gamma_e = -\frac{RT}{b} \ln \frac{a+bc}{a}$$

(substituting equation [6] into equation [1]), values of a may be calculated if the b values, previously given, are substituted. This yields

$$a(-0.024 \text{ v}) = 0.02 \quad \text{and} \quad a(+0.076 \text{ v}) = 0.11 \text{ cm}^{-1}.$$

These a values should be free from the systematic error to which the pair obtained from the surface concentration measurements was subjected, although the precision is certainly very poor in both cases.

The other (broken) straight lines in Figs. 2A and 3A have been calculated: their intercepts from [19] and their slopes from [17] (the ratio of the slopes of a broken and a solid line equals the ratio of the corresponding $\Delta \gamma_e$ values, $\Gamma_{M,e} \cong \Gamma_m$). By doing this we see from Figs. 2A and 3A that the points of longest drop time for $c = 13 \times 10^{-8}$ may have reached equilibrium with the monomer, but none of the other points have.

If, on the other hand, equation [18] had been used for the calculation of the same slopes, the latter would have been much larger (i.e., less negative; see dotted line for $c = 13 \times 10^{-8}$) and certain experimental points would have fallen below the dotted lines, which makes no physical sense. Of course more experimental points are needed to establish the conclusion definitely, but pending the production of this evidence, we tentatively conclude that the dimerization process—if it occurs at all, i.e., if our second model is correct—must be the *homogeneous* one.

The straight-line plots of Figs. 2B and 3B according to equation [12] have intercepts ($\log - \Delta \gamma_e$) which are somewhat less than the ones calculated from the $\Delta \gamma_e$ values of Figs. 2A and 3A. Also, the k_a values calculated from the slopes seem to increase somewhat with concentration causing the rather large individual deviations in the values quoted below. Taking the straight lines for the three highest concentrations for each potential, these values of k_a are:

$$k_a(-0.024 \text{ v}) = (7.5 \pm 2.5) \, 10^{-5} \text{ cm sec}^{-1},$$
$$k_a(+0.076 \text{ v}) = (4.2 \pm 1.8) \, 10^{-5} \text{ cm sec}^{-1}.$$

The lower concentrations cannot be expected to follow equation [12], especially at small values of the drop time; their γ values must be high because of diffusion control, as is clearly shown in the figures.

The k_a values given above certainly would agree with the anticipated trend: higher for the smaller potential. It would seem, then, that methylene blue is a compound which might show irreversible features in its polarographic current–voltage wave (see Introduction).

Values of $k_d = a\Gamma_m k_d$ are necessarily extremely inaccurate, but if the a values obtained from the surface tension measurements are used, these values are:

$$k_d(-0.024 \text{ v}) = 2 \times 10^{-15} \quad \text{and} \quad k_d(+0.076 \text{ v}) = 6 \times 10^{-16} \text{ mole cm}^{-2} \text{ sec}^{-1}.$$

EXPERIMENTAL

Surface Concentration Measurements

Reference will be made to Fig. 1 of ref. 3 throughout this section, which deals with further details on the operation of the apparatus used. The three sections, A, B, and C, which fit together with wide ground-glass joints, are assembled and the whole apparatus is placed in the thermostated water bath, as indicated in Fig. 1 (3). The connection to the Erlenmeyer flask outside the bath is made by way of a three-way stopcock (just above section A). The syphon (c) has a polyethylene section for flexibility. Connected to and vertically above the stopcock is a pear-shaped vessel, not shown. The Erlenmeyer flask contains sufficient solution to fill all the "dropping section" B, the siphon, and the flask itself to a height of about 1 cm. Before transferring the solution, the latter and the remainder of the glass apparatus are thoroughly washed with oxygen-free nitrogen by manipulating a set of stopcocks (not shown) in such a way that the nitrogen will pass through the tubular section in downward and upward directions alternatingly (the "head" A contains an extra outlet tube with stopcock, not shown). All but a small volume of the solution is next forced into the pear-shaped vessel above the apparatus, from which it can then flow into section B by gravity and extra nitrogen pressure. Simultaneously, a rather powerful stream of nitrogen is passed upward through capillary d in order to prevent any solution from entering this capillary. Both stopcocks above A are then closed and the nitrogen is shut off. The nitrogen overpressure in the small gas pocket above the solution in B will now force the solution downward into the capillary if the overpressure in C is slowly released through a stopcock on the side tube. Since the solution should not flow past the flare e it is necessary to open, simultaneously and carefully, the three-way stopcock toward the Erlenmeyer flask. The latter has been lowered a small distance to facilitate the operation, but after the solution has reached the flare e, it is raised till the surface of the solution in it is at the level of the bottom of the flare. It must be noticed that such a siphon is stable over a few (4–8) millimeters distance only, by virtue of the fact that the changing radius of the flare provides a balancing force of capillary "rise". Without the flare, the siphon would be completely unstable. An equally important function of the flare is that it allows the individual mercury drops to pass through the interface without difficulty.

The reference electrode ($Pt/Hg/Hg_2HPO_4/HPO_4^-$, $H_2PO_4^-$) had a fairly large mercury surface. It was filled to the top and then sealed, so that no liquid could flow into the methylene blue solution through the sintered glass disk. Its potential ($+0.3105$ v at $25°$ C with respect to S.C.E.) never changed more than a few ten thousandths of a volt throughout its period of use (many months).

The surface concentration, Γ_{MB^+}, is simply related to the concentration difference, Δc, between c_{MB^+} in the solution collected and the average in the dropping section B (before and after the period of dropping) by the equation

$$\Gamma_{MB^+} = v\Delta c/4\pi r^2_{Hg},$$

where Γ_{MB^+} is in moles/cm² and Δc in moles/cm³. The volume of solution entrained per drop (v) is found from the total volume of solution collected (determined by weighing) over the total number of mercury drops (calculated from the drop time, which was

usually quite constant, and the total duration of dropping), and the radius per drop (r_{Hg}) from the total weight of mercury collected. In order to collect 4 ml of solution in the tube f, ten to twenty thousand drops were required, depending on the radius of the dropping electrode and on the curvature of the solution–nitrogen interface at the flare (the more the interface was bulging downward, the larger v). There was no danger that part of the double layer should be stripped off when the mercury drops pierced the interface, since the value of v corresponds to a thickness of the entrained layer of 0.01 mm or so.

The determination of Δc was done with a Beckman D.U. spectrophotometer. At 620 mμ there is a strong absorption shoulder, but unfortunately Beer's law is known not to be obeyed (8), so before and after each analysis a calibration curve was determined by plotting $-\Delta \log T/\Delta c$ vs. Δc for four other methylene blue solutions, made at the same time as the solution used in the experiment.

Three runs could be done simultaneously in the same bath.

Surface Tension Measurements

These were generally performed under the same circumstances as described under "Surface Concentration Measurements". The mercury drops were collected in a little cup below the dropping electrode, from where they could be removed by suction without opening the apparatus. A 20-cm long capillary, diameter of bore $\sim$50 μ, could be used for the measurements up to 120 seconds drop time, without putting in any constrictions. This is a much longer drop time than the Poiseuille equation would give. It is known (9) that solution can penetrate between mercury and a glass wall and that at certain heights in the capillary this film of solution can become quite thick, so as to form a natural constriction somewhere along the tube. Drop times are not very constant this way, but the results are just as reproducible as those of short drop times.

Materials

The methylene blue (Merck, reagent grade) was recrystallized from alcohol and dried *in vacuo* (not in an oven, because of slight decomposition at 110° C). The sodium phosphate salts were recrystallized from water and dried *in vacuo* over P_2O_5. Water redistilled from a quartz still was used throughout.

<div align="center">REFERENCES</div>

1. DELAHAY, P.   J. Am. Chem. Soc. **75**, 1430 (1953).
2. BRDICKA, R.   Collection Czechoslov. Chem. Communs. **12**, 522 (1947).
3. LOS, J. M. and TOMPKINS, C. K.   J. Chem. Phys. **24**, 630 (1956).
4. CRAXFORD, S. R. and McKAY, H. A. C.   J. Phys. Chem. **39**, 545 (1935).
5. DELAHAY, P. and TRACHTENBERG, I.   J. Am. Chem. Soc. **79**, 2355 (1957).
6. KALOUSEK, M. and BLAHNIK, R.   Collection Czechoslov. Chem. Communs. **20**, 782 (1955).
7. VETTER, K. J. and BARDELEBEN, J.   Z. Elektrochem. **61**, 135 (1957).
8. MICHAELIS, L.   J. Phys. & Colloid Chem. **54**, 1 (1950).
9. JOHNSTON, R. J. and UBBELOHDE, A. R.   Proc. Roy. Soc. (London), A, **206**, 275 (1951).

Contents